frontiers | Research Topics

Advances in CNS tumors treatment and diagnosis: Obstacles, challenges, and opportunities

Edited by
Sheng Zhong, Peichen Pan, Ye Cheng and Wei Wang

Published in
Frontiers in Neuroscience
Frontiers in Pharmacology
Frontiers in Oncology

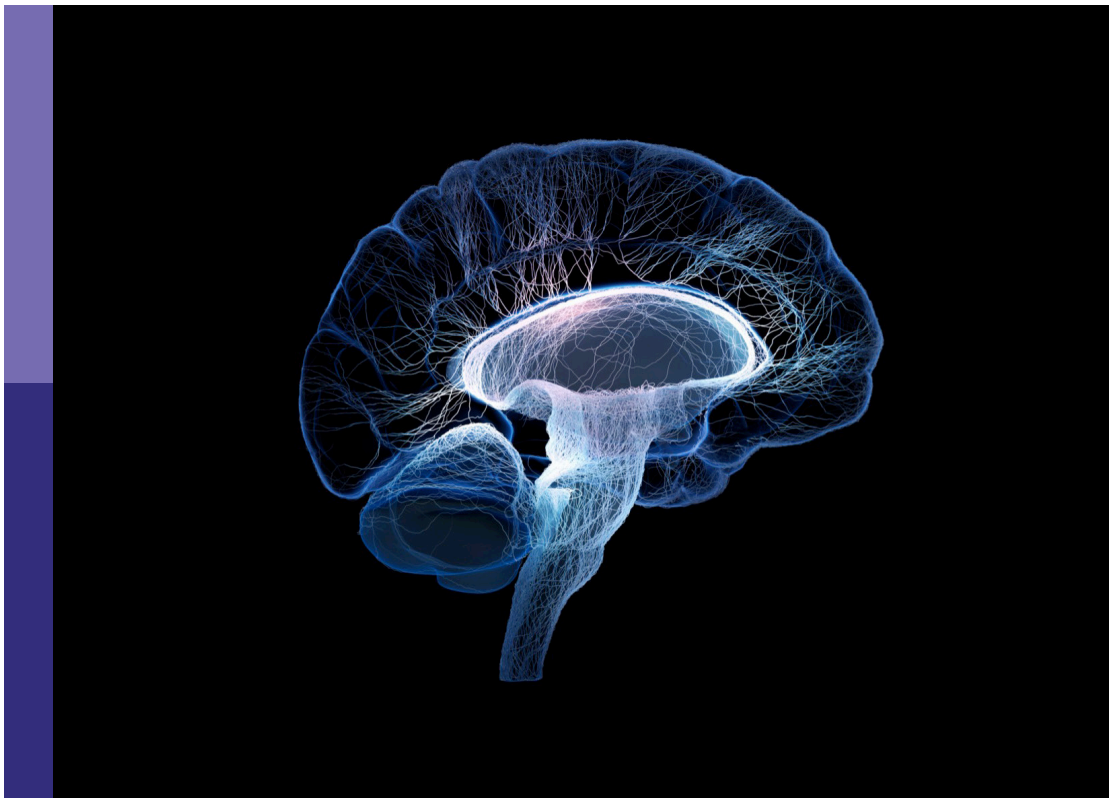

ISSN 1664-8714
ISBN 978-2-8325-4617-8
DOI 10.3389/978-2-8325-4617-8

About Frontiers

Frontiers is more than just an open access publisher of scholarly articles: it is a pioneering approach to the world of academia, radically improving the way scholarly research is managed. The grand vision of Frontiers is a world where all people have an equal opportunity to seek, share and generate knowledge. Frontiers provides immediate and permanent online open access to all its publications, but this alone is not enough to realize our grand goals.

Frontiers journal series

The Frontiers journal series is a multi-tier and interdisciplinary set of open-access, online journals, promising a paradigm shift from the current review, selection and dissemination processes in academic publishing. All Frontiers journals are driven by researchers for researchers; therefore, they constitute a service to the scholarly community. At the same time, the *Frontiers journal series* operates on a revolutionary invention, the tiered publishing system, initially addressing specific communities of scholars, and gradually climbing up to broader public understanding, thus serving the interests of the lay society, too.

Dedication to quality

Each Frontiers article is a landmark of the highest quality, thanks to genuinely collaborative interactions between authors and review editors, who include some of the world's best academicians. Research must be certified by peers before entering a stream of knowledge that may eventually reach the public - and shape society; therefore, Frontiers only applies the most rigorous and unbiased reviews. Frontiers revolutionizes research publishing by freely delivering the most outstanding research, evaluated with no bias from both the academic and social point of view. By applying the most advanced information technologies, Frontiers is catapulting scholarly publishing into a new generation.

What are Frontiers Research Topics?

Frontiers Research Topics are very popular trademarks of the *Frontiers journals series*: they are collections of at least ten articles, all centered on a particular subject. With their unique mix of varied contributions from Original Research to Review Articles, Frontiers Research Topics unify the most influential researchers, the latest key findings and historical advances in a hot research area.

Find out more on how to host your own Frontiers Research Topic or contribute to one as an author by contacting the Frontiers editorial office: frontiersin.org/about/contact

Advances in CNS tumors treatment and diagnosis: Obstacles, challenges, and opportunities

Topic editors

Sheng Zhong — Sun Yat-sen University Cancer Center, China
Peichen Pan — Zhejiang University, China
Ye Cheng — Capital Medical University, China
Wei Wang — Massachusetts General Hospital, Harvard Medical School, United States

Citation

Zhong, S., Pan, P., Cheng, Y., Wang, W., eds. (2024). *Advances in CNS tumors treatment and diagnosis: Obstacles, challenges, and opportunities*. Lausanne: Frontiers Media SA. doi: 10.3389/978-2-8325-4617-8

Table of contents

frontiers | Frontiers in Neuroscience

TYPE Original Research
PUBLISHED 30 November 2022
DOI 10.3389/fnins.2022.1076530

OPEN ACCESS

EDITED BY
Ye Cheng,
Xuanwu Hospital, Capital Medical University, China

REVIEWED BY
Qingtang Lin,
Xuanwu Hospital, Capital Medical University, China
Junpu Wang,
Xiangya Hospital, Central South University, China

*CORRESPONDENCE
Wanming Hu
huwm@sysucc.org.cn
Xia Yang
yangxia1@sysucc.org.cn

†These authors have contributed equally to this work

SPECIALTY SECTION
This article was submitted to Translational Neuroscience, a section of the journal Frontiers in Neuroscience

RECEIVED 21 October 2022
ACCEPTED 14 November 2022
PUBLISHED 30 November 2022

CITATION
Zeng J, Sun L, Huang J, Yang X and Hu W (2022) Enhancer of zeste homolog 2 is a negative prognostic biomarker and correlated with immune infiltrates in meningioma. *Front. Neurosci.* 16:1076530. doi: 10.3389/fnins.2022.1076530

Enhancer of zeste homolog 2 is a negative prognostic biomarker and correlated with immune infiltrates in meningioma

Jing Zeng[1,2†], Lu Sun[1,2†], Jiaming Huang[1,2], Xia Yang[1,2*] and Wanming Hu[1,2*]

[1]Department of Pathology, Sun Yat-sen University Cancer Center, Guangzhou, China, [2]State Key Laboratory of Oncology in Southern China, Sun Yat-sen University Cancer Center, Guangzhou, China

Background: Enhancer of zeste homolog 2 (EZH2), an important epigenetic regulator, that mainly regulates histone H3 lysine 27 trimethylation (H3K27me3) through histone methyltransferase, and participates in promoting the development of tumors. At present, the loss of H3K27me3 expression in meningioma is a poor prognostic factor, but the research of EZH2 in meningioma is rare. Therefore, we aim to explore the expression of EZH2 in the meningioma and its correlation with the prognosis and immune microenvironment and lay the foundation for the subsequently potential targeted therapy and immunotherapy for meningioma.

Methods: Tissue microarray immunohistochemistry staining was performed on 276 meningioma samples from Sun Yat-sen University Cancer Center. Expression levels of EZH2, H3K27me3, Ki67, programmed cell death protein 1 (PD-1), programmed cell death 1 ligand 1 (PD-L1), CD4, CD8, CD20, FOXP3, CD68, and CD163 were evaluated. Cox regression analyses were performed, and the Kaplan–Meier (KM) method was used to construct survival curves. In addition, we use biological information methods to analyze the mRNA expression of EZH2 and its relationship with the prognosis and immune microenvironment in the gene expression omnibus (GEO) database.

Results: Enhancer of zeste homolog 2 expression is concentrated in World Health Organization (WHO) grades 2 and 3 meningiomas (8.3+ and 33.3%+). We found that EZH2 expression was associated with a worse prognosis in meningioma ($P < 0.001$), the same results were confirmed in the GEO database ($P < 0.001$). Both EZH2 expression and H3K27me3 deletion ($P = 0.035$) predicted a worse prognosis, but EZH2 has no correlation with H3K27me3 expression. EZH2 expression was closely associated with increased Ki67 index ($P < 0.001$). In addition, EZH2 was associated with the immune microenvironment and positively correlated with PD-L1 expression ($P < 0.001$).

Conclusion: Enhancer of zeste homolog 2 is a new prognostic biomarker in meningioma. It correlates with PD-L1 expression and closely related to tumor immunosuppression. Our research can provide a reference for the potential targeted therapy and immunotherapy of meningioma in the future.

KEYWORDS

EZH2, meningioma, H3K27me3, GEO, PD-L1, immune infiltrates

Introduction

Meningioma is one of the most common primary tumors of the human central nervous system, accounting for 26.2–38.3% of all intracranial tumors, and arises from the arachnoid cap cells of the leptomeninges (Ostrom et al., 2019). According to the 5th edition of the World Health Organization (WHO) classification, meningiomas can be classified into three grades and 15 subtypes. Approximately 80% of meningiomas enrich for WHO grade 1 (such as meningothelial, fibrous, and transitional meningiomas, etc.), and they are considered to be benign meningiomas with benign histological behavior (Louis et al., 2021). The other 20% of meningiomas [such as atypical meningioma (WHO grade 2) and anaplastic (malignant) meningioma (WHO grade 3), etc.] have an aggressive behavior and a much higher recurrence and mortality rate (Dalle Ore et al., 2019). At present, the treatment of malignant meningiomas still relies on traditional surgery combined with radiotherapy (Gousias et al., 2016; Huntoon et al., 2020). More attention should be paid to further exploring the prognostic and treatment-related biomarkers and novel therapeutic approaches in malignant meningiomas.

Enhancer of zeste homolog 2 (EZH2) is a member of the polycomb genes (PcGs) family, a group of important epigenetic regulators that repress transcription (Cao and Zhang, 2004). It is the catalytic subunit of polycomb repressor complex 2 (PRC2), an enzyme that regulates gene expression through H3 lysine 27 trimethylation (H3K27me3) (Viré et al., 2006). The absence of H3K27me3 expression in meningiomas is currently considered to be a poor prognostic factor (Katz et al., 2018; Nassiri et al., 2021), but studies on EZH2 in meningiomas are still rare (Samal et al., 2020). It has been shown that the combination of EZH2 inhibitors and immunotherapy may be effective in tumor therapy such as EZH2 mutant lymphoma (McCabe et al., 2012; Kim and Roberts, 2016). Therefore, it is significant to explore the expression of EZH2, its prognosis value, its relationship with H3K27me3 in meningiomas and the immune microenvironment for subsequent potential targeting and immunotherapy of meningiomas.

Abbreviations: CXCR, CXC chemokine receptors; DEGs, differentially expressed genes; EZH2, enhancer of zeste homolog 2; ENKTL, extranodal NK/T-cell lymphoma; ER, estrogen receptor; FDA, food and drug administration; GEO, gene expression omnibus; GO, gene ontology; H3K27me3, histone H3 lysine 27 trimethylation; IHC, immunohistochemistry; KEGG, Kyoto encyclopedia of gene and genomes; KM survival curves, Kaplan–Meier survival curves; MHC I/II, major histocompatibility complex I/II; PD-1, programmed cell death protein 1; PD-L1, programmed cell death 1 ligand 1; ROC curve, receiver operating characteristic curve; TERT, telomerase reverse transcriptase; WHO, World Health Organization.

Materials and methods

Patient samples and clinical data

A total of 286 meningioma samples were included in this retrospective single-center study. All the tissue samples were resected at Sun Yat-sen University Cancer Center (SYSUCC, Guangzhou, China) from June 2008 to June 2018. Follow-up was last done in June 2022. The clinical data sets included gender, age at diagnosis, histopathological diagnosis (Goldbrunner et al., 2016), tumor location, time of death, time to radiographic tumor recurrence, and radiotherapy treatment between surgery and tumor recurrence. Hematoxylin and eosin (H&E) slides were reviewed from each case to confirm the diagnosis of meningioma by two pathologists (an experienced senior neuropathologist and a resident pathologist). The outcomes of each sample depend on tumor recurrence and time to recurrence. Recurrence was defined as tumor growth following the time of operation, and the time to recurrence was determined by calculating the duration from the date of surgery to the first post-operative imaging documenting tumor recurrence. The extent of resection was extracted from the surgeon's operative report and checked with post-operative magnetic resonance imaging (MRI). All samples were ethically approved for use based on informed consent and the Ethics Committee of SYSUCC.

Tissue microarray construction and immunohistochemistry

Archived formalin-fixed and paraffin-embedded tissue samples were used for the extraction of two biopsy punches of 2 mm diameter each to construct tissue microarrays with a conventional tissue microarrayer (Beecher Instruments, Sun

10.3389/fnins.2022.1076530

TABLE 1 Expression of enhancer of zeste homolog 2 (EZH2), H3 lysine 27 trimethylation (H3K27me3), and clinicopathologic parameters in meningioma.

Parameter	Subcategory	Total	Loss H3 lysine 27 trimethylation	*P*	Enhancer of zeste homolog 2 positive	*P*
n (%)	276	276	39 (14.1)		26 (9.4)	
Age	49.58 ± 13.076 (12–86)					
Sex	Male	97 (35.1)	15 (15.5)	0.64	11 (11.3)	0.275
	Female	179 (64.9)	24 (13.4)		15 (8.4)	
WHO grade	1	129 (46.7)	11 (8.5)	0.031	4 (3.1)	<0.001
	2	108 (39.1)	19 (17.6)		9 (8.3)	
	3	39 (14.1)	9 (23.1)		13 (33.3)	
Subtype	Meningothelial	76	4 (10.3)		1 (1.3)	
	Transitional	22	2 (5.1)		2 (9.1)	
	Secretory	2	1 (2.6)		0	
	Fibrous	16	1 (2.6)		1 (6.3)	
	Psammomatous	4	0		0	
	Angiomatous	5	2 (5.1)		0	
	Microcystic	4	1 (2.6)		0	
	Atypical	106	19 (48.7)		10 (9.4)	
	Choroid	2	0		0	
	Clear cell	1	0		0	
	Anaplastic	34	8 (20.5)		10 (29.4)	
	Papillary	3	0		2 (66.7)	
	Rhabdoid	1	1 (100)		0	
Location	Skull base	127 (46)	17 (43.6)	0.743	11 (7.4)	0.147
	Not skull base	149 (54)	22 (56.4)		15 (11.8)	
Ki67	<5%	120 (43.5)	13 (33.3)	0.168	2 (1.7)	<0.001
	≥5%	156 (56.5)	26 (66.7)		24 (15.4)	

P-value: Chi-square test.

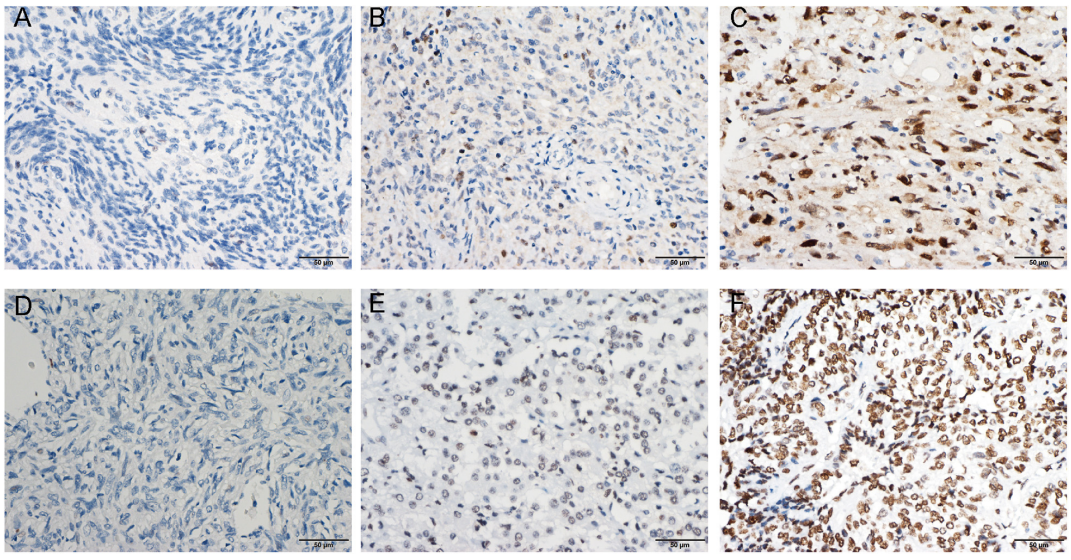

FIGURE 1
Enhancer of zeste homolog 2 (EZH2) protein expression was detected by immunohistochemistry (IHC). Representative images of negative **(A)**, low expression **(B)**, and high expression **(C)** staining of EZH2 are shown. Representative images of the high density of H3 lysine 27 trimethylation (H3K27me3) **(D)** in loss, moderate **(E)**, and strong **(F)** staining meningioma tissues are shown.

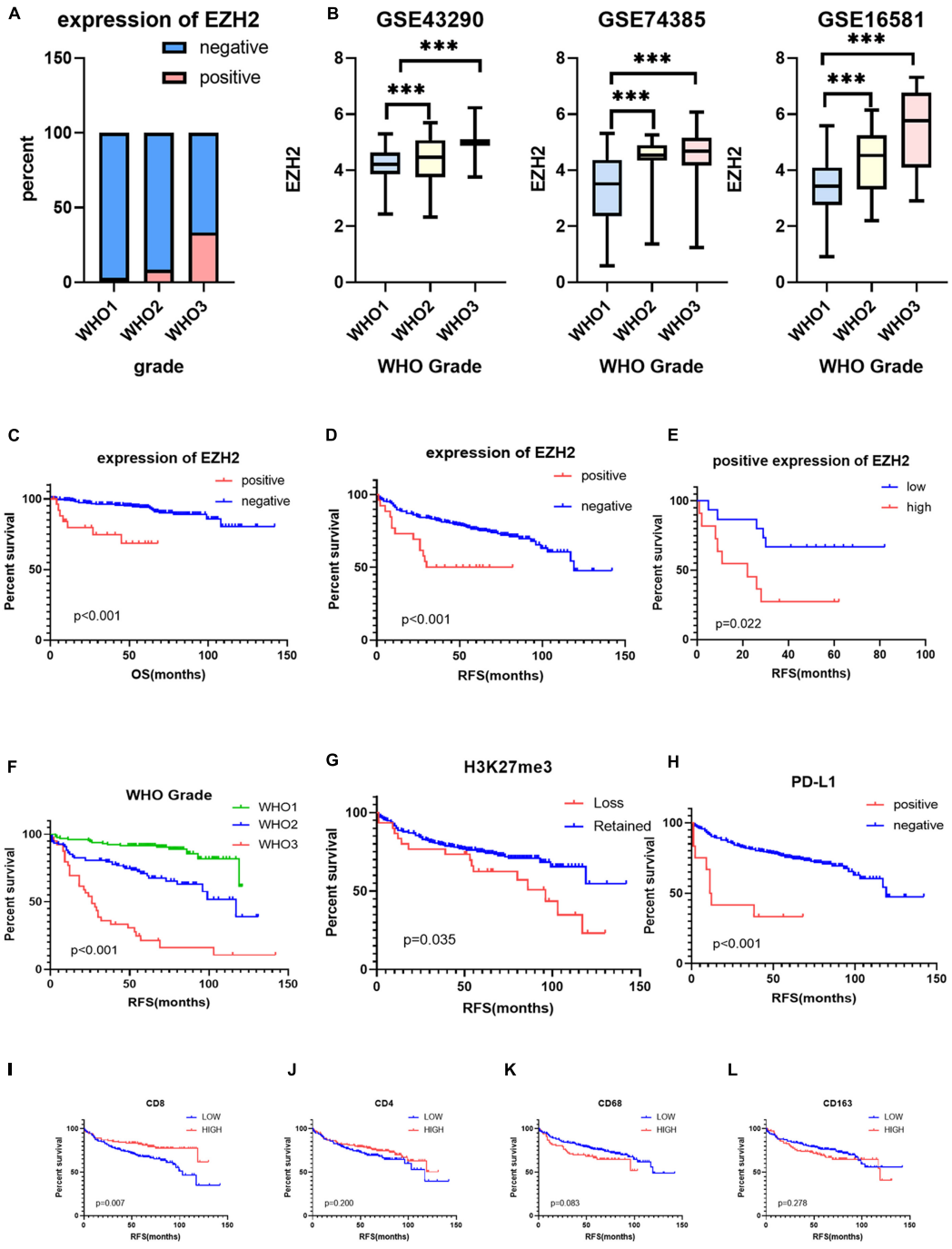

FIGURE 2
(A) The protein expression levels of enhancer of zeste homolog 2 (EZH2) in different World Health Organization (WHO) grades of meningioma. **(B)** The mRNA expression levels of EZH2 in meningioma in gene expression omnibus (GEO) datasets (***$P < 0.001$). **(C,D)** The prognostic impact of EZH2 expression in meningioma, Kaplan–Meier (KM) curves reveal expression of EZH2 predicts short overall survival (OS) time and short recurrence-free survival (RFS) in meningioma. **(E)** The prognostic impact of EZH2 high expression in meningioma, KM curves reveal expression of EZH2 predicts short RFS in meningioma. **(F–L)** KM survival curves for WHO grade and expression of H3 lysine 27 trimethylation (H3K27me3), programmed cell death 1 ligand 1 (PD-L1), CD4, CD8, CD68, and CD163.

Prairie, WI, USA). Tumor cylinder extraction was done after evaluation of H&E slides for suitable areas. The newly formed tissue blocks were cut into 4 μm slices with a microtome. After subsequent drying at 80°C for 15 min, subsequent immunohistochemical staining for H3K27me3 (1:200, rabbit monoclonal antibody C36B11, Cell Signaling, Danvers, MA,

USA) and EZH2 (1:100, rabbit monoclonal antibody D2C9, Cell Signaling, Danvers, MA, USA) were done with a Ventana BenchMark immunostainer (Ventana Medical Systems, Tucson, AZ, USA). Analysis of immunohistochemical staining were scored independently by two pathologists.

Immunohistochemical analyses

H3 lysine 27 trimethylation staining was assessed for nuclear expression on tumor cells. At least 1,000 tumor cells were counted under ×400 magnifications starting with the hot spot. The vascular endothelial cells and inflammatory cells were carefully excluded while counting morphologically. We calculate the cutoff value by the receiver operating characteristic (ROC) curve, and the labeling index of EZH2 was further sub-grouped as 0 for no positive cells, 1 for ≤25% of positive cells, and 2 for >25% of positive cells. In the case of heterogeneity of coloring intensity, the intensity of the major proportion of cells was considered. For EZH2, score 1 and 2 were considered low expressions and high expressions, and both score 1/2 were considered positive expressions. The expression of H3K27me3 was scored according to the positive proportion of the tumor cells. The percentage of positively stained tumor cells was scored as follows: 0 (<20% positive tumor cells) (Schaefer et al., 2016), 1 (≥20 and <50% positive tumor cells), and 2 (>50% positive tumor cells). The detailed protocol and assessment standard of other antibody markers including programmed cell death protein 1 (PD-1), programmed cell death 1 ligand 1 (PD-L1), CD4, CD8, CD20, FOXP3, CD68, and CD163 were described in a previous study (Du et al., 2015). We assessed and counted all immunohistochemical profiles of immune cell expression and divided them into two groups of high and low expression using the mean value (**Table 1**) as the cut-off value. The only difference was PDL1, which we divided it into expression and non-expression (<1%) groups by TPS (tumor cell proportion score), where the expression/positive group was divided into low expression (≥1–49%) and high expression group (≥50%) (Han et al., 2016).

Bioinformatic analysis in cancer datasets

The meningioma RNA-seq data were downloaded from https://www.ncbi.nlm.nih.gov/geo/. We analyzed 181 gene expression omnibus (GEO) RNA-seq cohorts of meningioma, ranging from WHO grade 1–3. The meningioma and meningeal RNA-seq data were from GEO datasets, including GSE43290, GSE74385, and GSE16581. Limma package in R software was conducted to screen out the differentially expressed genes (DEGs) with the cut-off criterion of adjusted $P < 0.05$ and $|\log2FC| > 1$. The dataset GSE16581 with survival information we used to perform survival scores, compare the survival differences between high and low expression groups, and Kaplan–Meier (KM) plot survival curves by the Survival package and Survminer package in R. We divided all meningioma data into high and low expression groups based on the cutoff value of the median EZH2 mRNA expression, and compared and analyzed the differences in immune cell expression between high and low expression groups and plotted the graphs. To explore the functions and pathways of related genes, we performed gene ontology (GO) and Kyoto encyclopedia of genes and genomes (KEGG) analyses on ClueGo and Metascape websites.

Statistical analysis

GraphPad Prism 8 and SPSS 25 software were performed for statistical analyses. The measurement data was represented as mean ± SD. The Chi-square test was conducted to explore the correlations between the expression of EZH2, H3K27me3, and clinicopathological or immune features. Categorical factors between EZH2 groups were compared using Fisher's exact tests. Survival distributions of groups were compared using KM estimates and log-rank tests. The Cox proportional hazards regression model was used for univariate and multivariate analyses to evaluate the independence of EZH2, H3K27me3, and other markers in predicting prognosis. A P-value < 0.05 was considered to be statistically significant.

Results

The expression of enhancer of zeste homolog 2 in meningiomas and its correlation with clinicopathological parameters

We collected clinical information from 286 meningioma patients and 10 were lost of follow-up. Finally, 276 meningioma patients were included in our retrospective study. Out of the 276 cases, 129 (47%) cases were WHO grade 1, 108 (39%) cases were WHO grade 2, and the remaining 39 (14%) cases were WHO grade 3. The mean age of the patients was 49.58 ± 13.08, with a median age of 50.50, and the majority was the elderly, and only three patients being underage. A total of 179 cases (65%) of patients were women. We also counted Ki67 expression, and based on previous reports in the literature that high Ki67 expression correlates with poor prognosis, we divided the Ki67 expression into low and high expression groups (<5 vs. ≥5%) (Olar et al., 2015) based on immunohistochemical results. In addition, we divided into two groups (Skull base vs. not skull base) according to the location of tumorigenesis. The details were showed in **Table 1**. By evaluating the expression of EZH2 (**Figures 1A–C**) and H3K27me3 (**Figures 1D,F**) by immunohistochemistry, we found some correlations between expression and clinical information. Most H3K27me3 positive

TABLE 2 Multivariate analysis of prognostic variables of recurrence-free survival (RFS).

Variables	HR	95% CI	*P*-value
WHO grade			
2 vs. 1	1.934	0.965–3.879	0.063
3 vs. 1	4.911	2.214–10.893	<0.001
H3 lysine 27 trimethylation			
Retain vs. loss	0.570	0.341–0.952	0.032
Enhancer of zeste homolog 2			
Positive vs. negative	1.080	0.537–2.170	0.829
Programmed cell death 1 ligand 1			
Positive vs. negative	2.147	0.885–5.205	0.091
Location			
Skull base vs. not skull base	0.938	0.593–1.485	0.786
Sex			
Male vs. female	1.552	0.992–2.430	0.054
Age	1.015	0.998–1.032	0.085
MIB-1			
≥5% vs. <5%	2.093	1.063–4.118	0.033

CI, confidence interval; HR, hazard ratio.

cases showed a low level of EZH2 expression, and strong expression of EZH2 was detected in only 11 cases, 4 of which were WHO grade 2 and 6 of which were WHO grade 3 (Table 1 and Figure 2A). EZH2 expression was correlated with increased Ki67 index ($p < 0.001$), for immunohistochemical positive expression was more prominent in areas of high proliferative activity. To further explore the mRNA expression of EZH2 in meningiomas, we analyzed three datasets of meningioma cases from the GEO database and found that mRNA expression of EZH2 was higher in WHO grade 2–3 meningiomas than in WHO grade 1. This is consistent with our results of the immunohistochemical exploration of EZH2 expression (Figure 2B).

Impact of enhancer of zeste homolog 2 expression on the prognosis of meningioma

The samples included in this cohort showed the expected distribution patterns of recurrence-free survival (RFS) when stratified by WHO grade, with WHO grade 2–3 tumors showed significantly shorter times to recurrence when compared to WHO grade 1 tumors (Figure 2A, log-rank test $P < 0.001$). Mean RFS was 108 months (95% CI 102.5−114.2), 88 months (95% CI 77.6−99.1), and 42 months (95% CI 28.2−56.6) for WHO grade 1–3 tumors (Figure 2F), respectively. We analyzed the survival analysis of two groups of meningioma patients with EZH2 positive and negative, and we found that there was a statistically significant difference in the RFS, demonstrating that expression of EZH2 was associated with poorer RFS in meningioma [Mean RFS 48.9 (95% CI 35.9−62.0) months vs. 102.1 (95% CI 94.1−110.1) months, $P < 0.001$, Figure 2D]. Similarly, we found that there was a worse prognosis in the high EZH2 expression groups than low EZH2 expression groups which divided into two groups by cutoff value (>25 vs. ≤25%) [Mean RFS 26.6 (95% CI 12.9−40.4) months vs. 61.3 (95% CI 46.1−76.4) months, $P = 0.022$, Figure 2E]. In addition, although meningioma patients have a lower mortality rate, we still did overall survival (OS) survival analysis and the result also showed EZH2 expression predicted a worse prognosis (Figure 2C). However, we cannot yet consider it as an independent prognostic factor (Table 2). The dataset GSE16581 in the GEO database contains survival information, and the OS prognostic analysis also showed EZH2 high expression group had a shorter survival time (Figure 3A).

Both enhancer of zeste homolog 2 expression and H3 lysine 27 trimethylation deletion predicted a worse prognosis, but enhancer of zeste homolog 2 has no correlation with H3 lysine 27 trimethylation expression in meningiomas

We analyzed the survival analysis of two groups of meningioma patients with H3K27me3 loss and retained, we found that there was a statistically significant difference in the RFS, demonstrating that loss of trimethylation was associated with poorer RFS in meningioma (Figure 2G). In addition, we also analyzed the EZH2 expression positive and negative groups and we found a statistically significant difference in RFS, demonstrating that EZH2 positive expression is associated with poorer RFS in meningiomas (Figure 2D). However, there was no connection between EZH2 expression and the deletion of H3K27me3. Only two cases expressed EZH2 with concomitant deletion of H3K27me3, and both were EZH2 low expression.

Lower CD8 expression and higher programmed cell death 1 ligand 1 expression in the immune microenvironment of meningiomas predicted a worse prognosis

Infiltrating immune cells are important components of the tumor microenvironment and are frequently associated with tumor behavior and patient outcomes. Since several studies and GO analysis revealed that EZH2 was related to the immune response, we further explored the infiltration of immune cells in meningioma (Figure 3D). In addition, we evaluated several immune cell markers, including CD4, CD8, CD20, CD68,

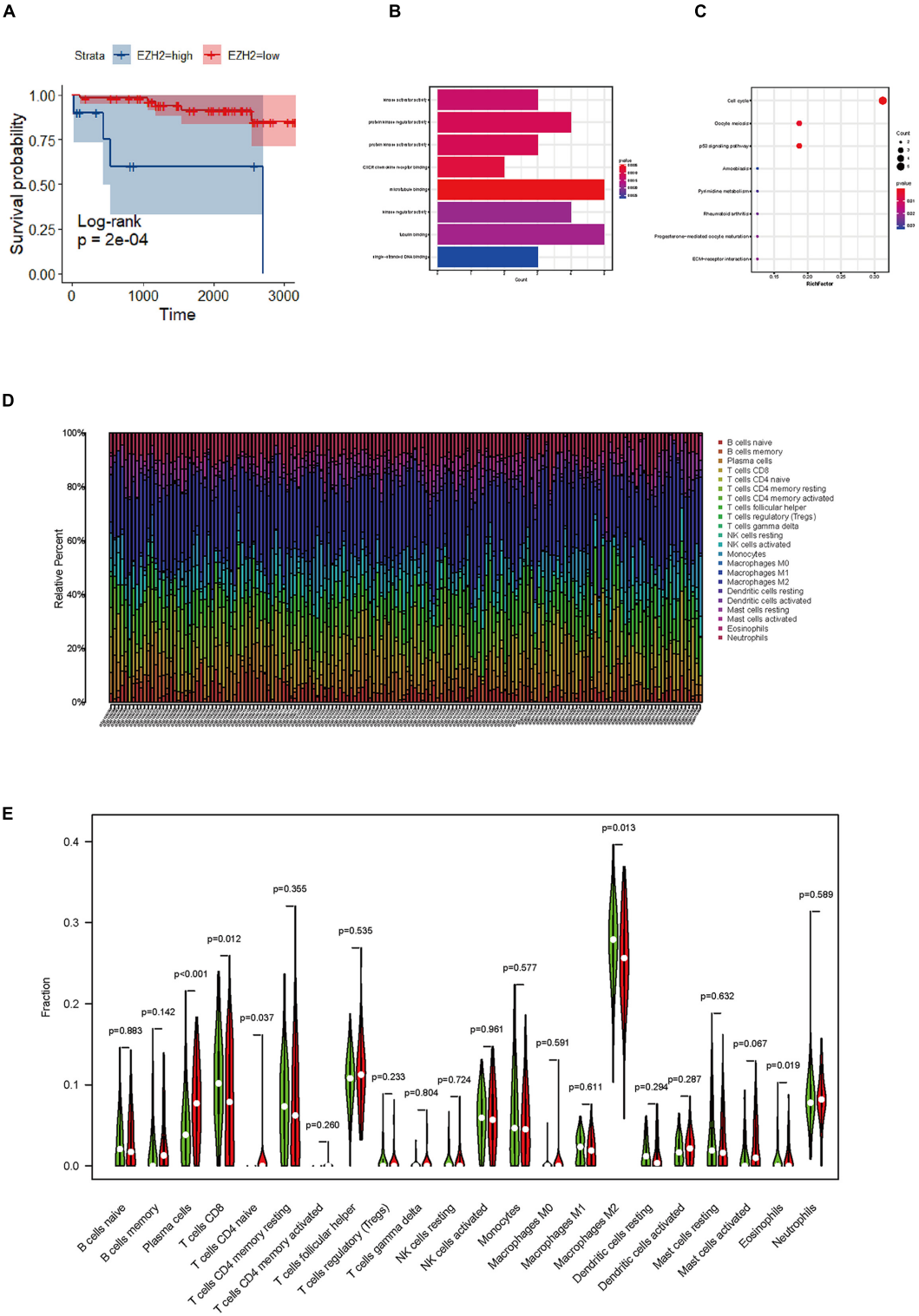

FIGURE 3
Identification of functions, and pathways in meningioma. **(A)** The prognostic impact of enhancer of zeste homolog 2 (EZH2) mRNA levels in meningioma in gene expression omnibus (GEO) datasets. KM curves reveal high EZH2 mRNA levels predict short overall survival (OS) time in meningioma. **(B)** Gene ontology (GO) analysis shows multiple biological processes of overlapping differentially expressed genes (DEGs). **(C)** Several pathways of overlapping DEGs are identified by Kyoto encyclopedia of genes and genomes (KEGG) analysis. **(D)** The graph of immune cell expression in meningioma after merging data from GEO databases. **(E)** The level of EZH2 mRNA expression correlates with sets of immune cells in meningioma.

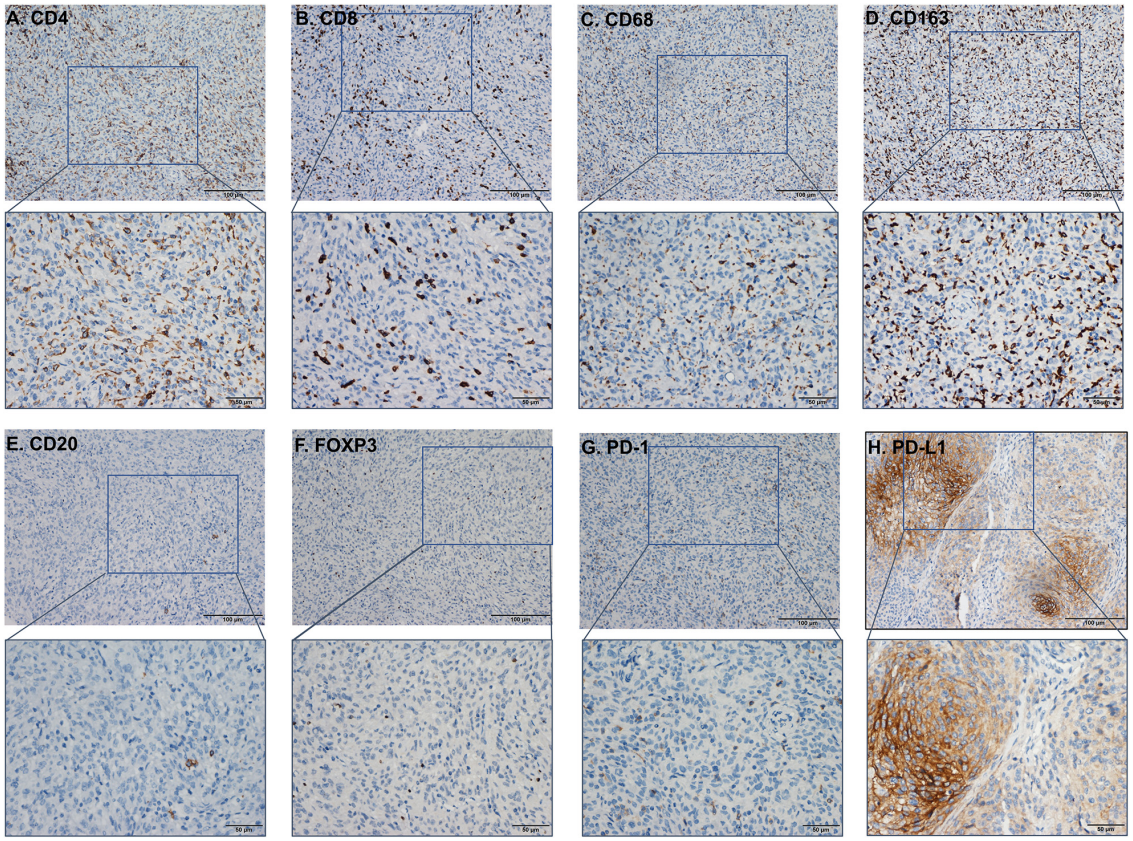

FIGURE 4
The immunohistochemistry (IHC) figure of various immune cells. **(A)** CD4, **(B)** CD8, **(C)** CD163, **(D)** CD68, **(E)** CD20, **(F)** FOXP3, **(G)** programmed cell death protein 1 (PD-1), and **(H)** PD-L1 (under ×100 and ×400 magnification).

CD163, PD-1, PD-L1, and FOXP3 in meningioma samples (Figures 4A–H), and found that the lymphocyte infiltrates in the meningioma tissue was comprised predominantly of T cells with infrequent B cells (Table 3).

Based on the scores for microarray immunohistochemistry, with a mean cutoff value, we divided the expression of each maker into two groups, high and low expression. We found that the density of immunohistochemical expression of infiltrating lymphocytes was significantly different in WHO grade 2–3 meningiomas compared to WHO grade 1 meningiomas. CD4 and CD8 lymphocytes were all more highly expressed in WHO grade 1 meningiomas, compared to WHO grade 2–3 (Figures 5A–H). This is also consistent with previous studies of reduced T-cell infiltration in WHO grade 2–3 meningiomas. CD20, PD1, and FOXP3 expressions were not found to be different between the different grades of meningioma (Table 3). In addition, we counted the differences in survival analysis between high and low expression of each immune cells (Figures 2J–L) and found that the prognosis of the CD8 low expression group was significantly worse than that of the high expression group (p = 0.003; Figure 2I). We further counted the expression pattern of PD-L1+/CD68− and divided into positive and negative groups in this way. Although the overall positive rate of PD-L1 was not high, the PD-L1 positive group was mostly distributed in WHO grade 2–3 meningiomas, especially grade 3 cases, and was statistically significantly different ($p < 0.001$). Survival analyses of the positive and negative groups were counted according to group expression and were found to be statistically significantly different ($p < 0.001$). Positive expression of PD-L1 represented a poorer prognosis (Figure 2H).

The correlation between enhancer of zeste homolog 2, H3 lysine 27 trimethylation, and markers of immune infiltrates in meningiomas

To study the correlation between EZH2, H3K27me3, and different markers of immune infiltrates in meningioma, we counted the expression of immune cells in the H3K27me3-loss samples and found that the expression of CD8 was lower in the H3K27me3-loss samples compared to H3K27me3-preserved samples. However, there was no significant difference in the expression of CD4, CD20, CD68, CD163, and PD-L1 (Table 4).

TABLE 3 Correlation analysis between World Health Organization (WHO) grade and markers of immune cells in meningioma.

Parameter	Mean/mm^2		Total	WHO 1	WHO 2	WHO 3	*P*-value
CD4	11.43 ± 0.82 (0–75.00)	Low	131 (47.5)	53 (41.1)	54 (50.0)	24 (61.5)	0.065
		High	145 (52.5)	76 (58.9)	54 (50.0)	15 (38.5)	
CD8	16.26 ± 1.16 (0–133.33)	Low	168 (60.9)	65 (50.4)	74 (68.5)	29 (74.4)	0.003
		High	108 (39.1)	64 (49.6)	34 (31.5)	10 (25.6)	
CD163	37.91 ± 1.68 (0–133.33)	Low	173 (62.7)	86 (66.7)	70 (64.8)	17 (43.6)	0.028
		High	103 (37.3)	43 (33.3)	38 (35.2)	22 (56.4)	
CD68	9.62 ± 0.85 (0–83.33)	Low	200 (72.5)	90 (69.8)	85 (78.7)	25 (64.1)	0.139
		High	76 (27.5)	39 (30.2)	23 (21.3)	14 (35.9)	
CD20	0.36 ± 0.12 (0–20.83)	Low	260 (94.2)	122 (94.6)	100 (92.6)	38 (97.4)	0.524
		High	16 (5.8)	7 (5.4)	8 (7.4)	1 (2.6)	
FOXP3	0.06 ± 0.03 (0–4.17)	Low	272 (98.6)	129 (100)	107 (99.1)	36 (92.3)	0.002
		High	4 (1.4)	0	1 (0.9)	3 (7.7)	
Programmed cell death protein 1	0.11 ± 0.04 (0–4.17)	Low	269 (97.5)	124 (96.1)	106 (98.1)	39 (100)	0.340
		High	7 (2.5)	5 (3.9)	2 (1.9)	0	
Programmed cell death 1 ligand 1		Negative	264 (95.7)	128 (99.2)	104 (96.3)	32 (82.1)	<0.001
		Positive	12 (4.3)	1 (0.8)	4 (3.7)	7 (17.9)	

Interestingly, in the comparison of EZH2 positive and negative, we were surprised to find a significant correlation between EZH2 positive samples and PD-L1 positive samples (<0.001; **Figure 5P**). In addition, CD68 expression was higher in EZH2-positive specimens compared to EZH2-negative specimens (p = 0.010; **Figure 5L**) and no correlation has been found in other immune cell groups (**Figures 5I–K**, **5M–O** and **Table 4**).

To further verify the results of our study, we collected a total of 181 samples from the GEO dataset. We identified overlapping DEGs between EZH2 high expression group and low expression group. The top hub genes were screened *via* the plug-in molecular complex detection and cytoHubba of Cytoscape. GO analysis was performed to show the overlapping DEGs were involved in several biological processes, including kinase activator activity, and CXC chemokine receptors (CXCR) chemokine receptor binding, etc. (**Figure 3B**). The KEGG pathways are enriched in several classic signaling pathways, such as cell cycle pathway (**Figure 3C**). We analyzed the difference in the proportion of immune cells according to the gene EZH2 into high and low expression groups and determined the correlation between the expression of the target gene and the content of immune cells. We found that T cells CD4 naive and plasma cells had a higher proportion in the EZH2 high expression group, while T cells CD8 and macrophages M2 had a lower proportion (**Figure 3E**).

Discussion

Enhancer of zeste homolog 2 is the catalytic subunit of histone methyltransferase and PRC2. EZH2 catalyzes the H3K27me3 and histone marks, associated with tight chromatin and transcriptional repression, which lead to tumor progression (Kim and Roberts, 2016; Wang et al., 2022). However, there are limited studies on EZH2 expression in meningiomas. We note that Samal explored the prognostic relevance of EZH2 immunohistochemistry in 149 meningioma cases (Samal et al., 2020), but it was limited to WHO grades 1 and 2 meningiomas. Another study enrolled 138 meningiomas and reported EZH2 gene expression was upregulated in atypical samples (Harmancı et al., 2017). In this study, we included 276 meningioma cases of all the grade (129 cases of WHO 1, 108 cases of WHO 2, and 39 cases of WHO 3), enriching as much as possible cases for all tissue subtypes of meningioma. In addition, we screened three datasets through the GEO database to further validate our study. We found that there was a higher EZH2 expression in WHO grade 2–3 meningiomas compared to WHO grade 1 meningioma according to the results of immunohistochemistry. We also further validated higher proportion of EZH2 mRNA in WHO grade 2–3 meningiomas in the GEO database, which is consistent with the immunohistochemical protein results. Moreover, patients with positive EZH2 expression have a shorter time to RFS and a relatively shorter survival time, indicated expression of EZH2 might be a potential prognostic factor.

H3 lysine 27 trimethylation is catalyzed by EZH2, which is involved in the formation of the PRC2 that aggregates to the promoter region and leads to transcriptional repression of the target gene. Methylation of H3K27 is associated with gene repression and plays a notable role in mediating the expression of genes involved in lineage commitment and differentiation (Margueron and Reinberg, 2011). The deletion of H3K27me3 in meningiomas has been considered as an important prognostic factor, but its relationship with EZH2 expression remains unknown. Although the canonical function of EZH2 is

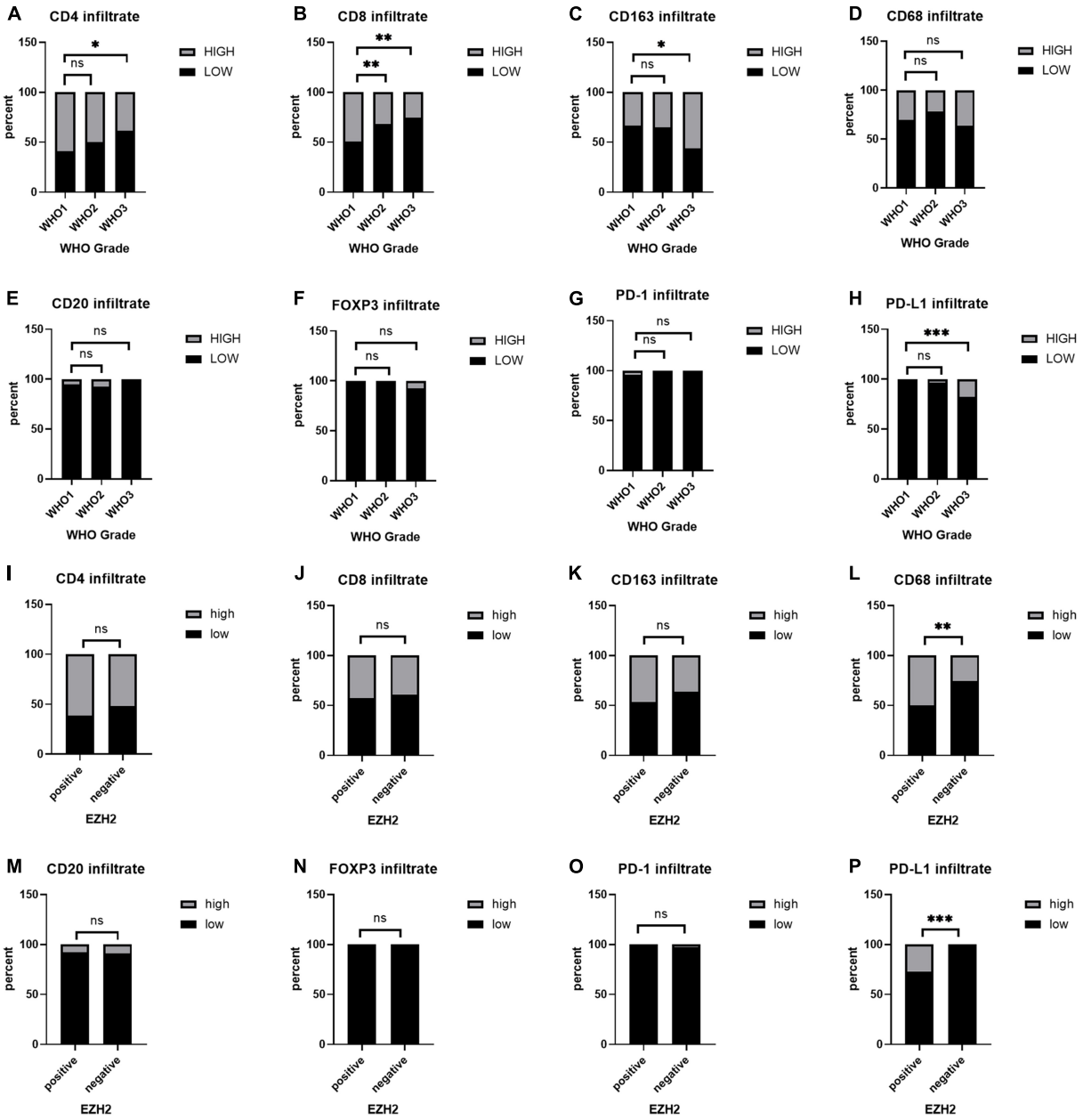

FIGURE 5
(A–H) Immunohistochemical expression of immune cells at different World Health Organization (WHO) levels. **(I–P)** Differences in the expression of immune cell infiltration between the positive and negative groups in enhancer of zeste homolog 2 (EZH2). $^{*}P < 0.05$, $^{**}P < 0.01$, and $^{***}P < 0.001$.

gene repression through H3K27 methylation, EZH2 can also act independently of H3K27me3. Hitherto, multiple studies have produced contradictory results. In extranodal NK/T-cell lymphoma (ENKTL), nasal type, aberrant differential expression of EZH2 and H3K27me3 is associated with disease progression and prognosis, EZH2 and H3K27me3 were overexpressed in the majority of ENKTL samples, but EZH2 and H3K27me3 showed an inverse correlation in ENKTL (Liu et al., 2019). In breast cancer, although high EZH2 and low H3K27me3 correlate with poor prognosis of estrogen receptor-positive (ER+) breast cancers, the methyltransferase EZH2 is not required for mammary cancer development (Bae et al., 2015). In mantle cell lymphoma, EZH2 expression is associated with inferior OS and EZH2 expression shows a weak correlation with other PRC2 complex molecules, but no correlation with H3K27me3 expression, or loss of major histocompatibility complex (MHC) I/II (Martinez-Baquero et al., 2021). In contrast, our findings are

TABLE 4 Correlation analysis between expression of enhancer of zeste homolog 2 (EZH2), H3 lysine 27 trimethylation (H3K27me3), and markers of immune cells in meningioma.

Parameter		H3 lysine 27 trimethylation			Enhancer of zeste homolog 2		
		Loss	Retain	*P*	Positive	Negative	*P*
CD4	Low	24 (61.5)	107 (45.1)	0.057	10 (38.5)	121 (48.4)	0.334
	High	15 (38.5)	130 (54.9)		16 (61.5)	129 (51.6)	
CD8	Low	31 (79.5)	137 (57.8)	0.010	15 (57.7)	153 (61.2)	0.727
	High	8 (20.5)	100 (42.2)		11 (42.3)	97 (38.8)	
CD163	Low	25 (64.1)	148 (62.4)	0.843	14 (51.4)	159 (63.6)	0.328
	High	17 (35.9)	89 (37.6)		12 (46.2)	91 (36.4)	
CD68	Low	30 (76.9)	170 (71.7)	0.501	13 (50.0)	187 (74.8)	0.007
	High	9 (23.1)	67 (28.3)		13 (50.0)	63 (25.2)	
CD20	Low	36 (92.3)	224 (94.5)	0.585	24 (92.3)	236 (94.4)	0.664
	High	3 (7.7)	13 (5.5)		2 (7.7)	24 (5.6)	
FOXP3	Low	37 (94.9)	235 (99.2)	0.097	26 (100)	246 (98.4)	0.672
	High	2 (5.1)	2 (0.8)		0	4 (1.6)	
Programmed cell death protein 1	Low	38 (97.4)	231 (97.5)	0.990	26 (100)	243 (97.2)	0.387
	High	1 (2.6)	6 (2.5)		0	7 (2.8)	
Programmed cell death 1 ligand 1	Negative	38 (97.4.7)	226 (95.4)	0.556	19 (73.1)	245 (99.8)	<0.001
	Positive	1 (2.6)	11 (4.6)		7 (26.9)	5 (0.02)	

consistent with the study of mantle cell lymphoma, that there is no correlation between the two markers.

Enhancer of zeste homolog 2 plays a role in the normal biology of many cell types, including immune cells. Dysfunctional EZH2 is associated with the development of multiple cancer types in humans and can promote immune evasion by inhibiting intra-tumoral antigen presentation, immune cell migration, and enhancing CD4+ T regulatory cell (Treg) suppressive activity (Kang et al., 2020; Kim et al., 2020). EZH2 overexpressed tumors often exhibit immunosuppressive tumor microenvironment and immunotherapy resistance (Guo et al., 2020). In prostate cancer, the EZH2 inhibitors combined with PD-1 immunotherapy further improved patient prognosis (Morel et al., 2021). In addition, studies have shown that PD-L1 may be a risk factor for poor prognosis of meningoma, and the PD-1 inhibitor can improve the prognosis of meningoma patients in small samples. This reveals that immunotherapy may be the direction of meningoma therapy in the future. We have investigated the expression of meningiomas with multiple immune-related cells and markers (including PD-1 and PD-L1), and additionally explored their relationship using datasets from the GEO database, and found that high expression of EZH2 have multiple immune-related pathways and associated with several immune cell expression. In prostate cancer, the EZH2 inhibitors combined with PD-1 immunotherapy further improved patient prognosis (Morel et al., 2021). Our study demonstrates that WHO grade 2–3 meningiomas tend to have low CD4, and CD8 expression, which has been confirmed in other studies (Fang et al., 2013; Turner et al., 2022). In previous studies, high CD8 expression was shown to be associated with a better prognosis in meningiomas (Turner et al., 2022). In our study, we also found that high expression of CD8 predicted a better prognosis, but there is no correlation has been found between EZH2 expression and CD8 expression. However, in analysis of immune cell differences in GEO databases, we found that the meningioma EZH2 high expression group had relatively lower CD8 T lymphocytes than the EZH2 low expression group, and it was statistically significant. Interestingly, we found that 12 cases with PD-L1 expression had a worse prognosis, while PD-L1 expression was concentrated in WHO grade 2–3 meningiomas, and PD-L1 expression correlated positively with EZH2-positive cases.

Although we have not been able to demonstrate that immunohistochemical expression of EZH2 in meningiomas correlates with immunosuppression, we found a higher tendency of PD-L1 positivity in EZH2-expressing case. Recently, several studies explored the relationship of EZH2 and PD-L1 in lung cancers. EZH2-expressing lung adenocarcinomas were more frequently to show PD-L1 protein expression than EZH2-negative cases (Toyokawa et al., 2019). Böttcher et al. (2021) found a novel Notch-c-Myc-EZH2 signaling axis which might be controlled PD-L1 upregulation. Zhao et al. (2019) reported EZH2 regulated the immunosuppressive molecule PD-L1 expression *via* HIF-1α in non-small cell lung cancer cells. However, there was no study in meningioma and we will keep studying the potential molecular regulatory mechanism in the future. At present, EZH2 inhibitors including tazemetostat, which has been approved by the Food and Drug Administration (FDA) for use in epithelioid sarcoma (Gounder et al., 2020) and follicular lymphoma (Morschhauser et al., 2020). EZH2

inhibitors in combination with PD-1 inhibitors have been used as a chemotherapy regimen in clinical treatment (Morel et al., 2021). We hold the opinion that the contribution of EZH2 to lymphocyte subpopulation differentiation and function suggested that inhibition of EZH2 has the potential to enhance anti-cancer immunity in certain neoplastic diseases, however, the specific mechanisms involved are yet to be investigated and need to be explored further.

There are still several limitations in our study. First of all, immunohistochemistry is performed by tissue microarray, which restricts our evaluation, for those samples were mainly selected from the central part of the tumor and lacked peripheral tumor tissue. Secondly, our cases were selected before 2018, which lacked molecular testing and markers such as telomerase reverse transcriptase (TERT) and CDKN2A. In addition, our sample size was not large enough.

In conclusion, our study explored the expression of EZH2 and its relationship with H3K27me3 and the immune microenvironment in meningiomas. EZH2 may be a potential prognostic factor and therapeutic target for meningiomas. Our research indicates a direction of EZH2 inhibitors combined with PD-1 immunotherapy for malignant meningiomas in the future.

Data availability statement

The datasets presented in this study can be found in online repositories RDD (https://www.researchdata.org.cn/), which will be shared by request from any qualified investigator upon approval by the SYSUCC data request committee. The accession number and the data is available from the corresponding authors on reasonable request.

Ethics statement

The studies involving human participants were reviewed and approved by the Sun Yat-sen University Cancer Center Ethics Committee (B2022-305-01). The patients/participants provided their written informed consent to participate in this study.

Author contributions

JZ, LS, and WH were designed the study and wrote the manuscript. JH acquired the data. LS and XY were provided help for the IHC test and performed the data analysis. XY, JZ, and WH were reviewed the manuscript. All authors read and approved the final manuscript.

Funding

This work was funded by the National Natural Science Foundation of China (82102877). The funders had no role in study design, data collection and analysis, decision to publish, or preparation of the manuscript.

Conflict of interest

The authors declare that the research was conducted in the absence of any commercial or financial relationships that could be construed as a potential conflict of interest.

Publisher's note

All claims expressed in this article are solely those of the authors and do not necessarily represent those of their affiliated organizations, or those of the publisher, the editors and the reviewers. Any product that may be evaluated in this article, or claim that may be made by its manufacturer, is not guaranteed or endorsed by the publisher.

References

Bae, W. K., Yoo, K. H., Lee, J. S., Kim, Y., Chung, I.-J., Park, M. H., et al. (2015). The methyltransferase EZH2 is not required for mammary cancer development, although high EZH2 and low H3K27me3 correlate with poor prognosis of ER-positive breast cancers. *Mol. Carcinog.* 54, 1172–1180.

Böttcher, M., Bruns, H., Völkl, S., Lu, J., Chartomatsidou, E., Papakonstantinou, N., et al. (2021). Control of PD-L1 expression in CLL-cells by stromal triggering of the Notch-c-Myc-EZH2 oncogenic signaling axis. *J. Immunother. Cancer* 9:e001889. doi: 10.1136/jitc-2020-001889

Cao, R., and Zhang, Y. (2004). The functions of E(Z)/EZH2-mediated methylation of lysine 27 in histone H3. *Curr. Opin. Genet. Dev.* 14, 155–164. doi: 10.1016/j.gde.2004.02.001

Dalle Ore, C. L., Magill, S. T., Yen, A. J., Shahin, M. N., Lee, D. S., Lucas, C. G., et al. (2019). Meningioma metastases: Incidence and proposed screening paradigm. *J. Neurosurg.* 132, 1447–1455. doi: 10.3171/2019.1.JNS181771

Du, Z., Abedalthagafi, M., Aizer, A. A., McHenry, A. R., Sun, H. H., Bray, M. A., et al. (2015). Increased expression of the immune modulatory molecule PD-L1 (CD274) in anaplastic meningioma. *Oncotarget* 6, 4704–4716.

Fang, L., Lowther, D. E., Meizlish, M. L., Anderson, R. C. E., Bruce, J. N., Devine, L., et al. (2013). The immune cell infiltrate populating meningiomas is composed of mature, antigen-experienced T and B cells. *Neuro Oncol.* 15, 1479–1490. doi: 10.1093/neuonc/not110

Goldbrunner, R., Minniti, G., Preusser, M., Jenkinson, M. D., Sallabanda, K., Houdart, E., et al. (2016). EANO guidelines for the diagnosis and treatment of meningiomas. *Lancet Oncol.* 17, e383–e391.

Gounder, M., Schöffski, P., Jones, R. L., Agulnik, M., Cote, G. M., Villalobos, V. M., et al. (2020). Tazemetostat in advanced epithelioid sarcoma with loss of INI1/SMARCB1: An international, open-label, phase 2 basket study. *Lancet Oncol.* 21, 1423–1432. doi: 10.1016/S1470-2045(20)30451-4

Gousias, K., Schramm, J., and Simon, M. (2016). The Simpson grading revisited: Aggressive surgery and its place in modern meningioma management. *J. Neurosurg.* 125, 551–560. doi: 10.3171/2015.9.JNS15754

Guo, B., Tan, X., and Cen, H. (2020). EZH2 is a negative prognostic biomarker associated with immunosuppression in hepatocellular carcinoma. *PLoS One* 15:e0242191. doi: 10.1371/journal.pone.0242191

Han, S. J., Reis, G., Kohanbash, G., Shrivastav, S., Magill, S. T., Molinaro, A. M., et al. (2016). Expression and prognostic impact of immune modulatory molecule PD-L1 in meningioma. *J. Neurooncol.* 130, 543–552. doi: 10.1007/s11060-016-2256-0

Harmancı, A. S., Youngblood, M. W., Clark, V. E., Coşkun, S., Henegariu, O., Duran, D., et al. (2017). Integrated genomic analyses of de novo pathways underlying atypical meningiomas. *Nat. Commun.* 8:14433.

Huntoon, K., Toland, A. M. S., and Dahiya, S. (2020). Meningioma: A review of clinicopathological and molecular aspects. *Front. Oncol.* 10:579599. doi: 10.3389/fonc.2020.579599

Kang, N., Eccleston, M., Clermont, P.-L., Latarani, M., Male, D. K., Wang, Y., et al. (2020). EZH2 inhibition: A promising strategy to prevent cancer immune editing. *Epigenomics* 12, 1457–1476. doi: 10.2217/epi-2020-0186

Katz, L. M., Hielscher, T., Liechty, B., Silverman, J., Zagzag, D., Sen, R., et al. (2018). Loss of histone H3K27me3 identifies a subset of meningiomas with increased risk of recurrence. *Acta Neuropathol.* 135, 955–963.

Kim, H.-J., Cantor, H., and Cosmopoulos, K. (2020). Overcoming immune checkpoint blockade resistance via EZH2 inhibition. *Trends Immunol.* 41, 948–963. doi: 10.1016/j.it.2020.08.010

Kim, K. H., and Roberts, C. W. M. (2016). Targeting EZH2 in cancer. *Nat. Med.* 22, 128–134.

Liu, J., Liang, L., Huang, S., Nong, L., Li, D., Zhang, B., et al. (2019). Aberrant differential expression of EZH2 and H3K27me3 in extranodal NK/T-cell lymphoma, nasal type, is associated with disease progression and prognosis. *Hum. Pathol.* 83, 166–176. doi: 10.1016/j.humpath.2018.08.025

Louis, D. N., Perry, A., Wesseling, P., Brat, D. J., Cree, I. A., Figarella-Branger, D., et al. (2021). The 2021 WHO classification of tumors of the central nervous system: A summary. *Neuro Oncol.* 23, 1231–1251.

Margueron, R., and Reinberg, D. (2011). The Polycomb complex PRC2 and its mark in life. *Nature* 469, 343–349.

Martinez-Baquero, D., Sakhdari, A., Mo, H., Kim, D. H., Kanagal-Shamanna, R., Li, S., et al. (2021). EZH2 expression is associated with inferior overall survival in mantle cell lymphoma. *Mod. Pathol.* 34, 2183–2191. doi: 10.1038/s41379-021-00885-9

McCabe, M. T., Ott, H. M., Ganji, G., Korenchuk, S., Thompson, C., Van Aller, G. S., et al. (2012). EZH2 inhibition as a therapeutic strategy for lymphoma with EZH2-activating mutations. *Nature* 492, 108–112. doi: 10.1038/nature11606

Morel, K. L., Sheahan, A. V., Burkhart, D. L., Baca, S. C., Boufaied, N., Liu, Y., et al. (2021). EZH2 inhibition activates a dsRNA-STING-interferon stress axis that potentiates response to PD-1 checkpoint blockade in prostate cancer. *Nat. Cancer* 2, 444–456. doi: 10.1038/s43018-021-00185-w

Morschhauser, F., Tilly, H., Chaidos, A., McKay, P., Phillips, T., Assouline, S., et al. (2020). Tazemetostat for patients with relapsed or refractory follicular lymphoma: An open-label, single-arm, multicentre, phase 2 trial. *Lancet Oncol.* 21, 1433–1442.

Nassiri, F., Wang, J. Z., Singh, O., Karimi, S., Dalcourt, T., Ijad, N., et al. (2021). Loss of H3K27me3 in meningiomas. *Neuro Oncol.* 23, 1282–1291.

Olar, A., Wani, K. M., Sulman, E. P., Mansouri, A., Zadeh, G., Wilson, C. D., et al. (2015). Mitotic index is an independent predictor of recurrence-free survival in meningioma. *Brain Pathol.* 25, 266–275.

Ostrom, Q. T., Cioffi, G., Gittleman, H., Patil, N., Waite, K., Kruchko, C., et al. (2019). CBTRUS statistical report: Primary brain and other central nervous system tumors diagnosed in the United States in 2012-2016. *Neuro Oncol.* 21(Suppl. 5), v1–v100. doi: 10.1093/neuonc/noz150

Samal, S., Patnaik, A., Sahu, F., and Purkait, S. (2020). Altered expression of epigenetic modifiers EZH2, H3K27me3, and DNA methyltransferases in meningiomas–prognostic biomarkers for routine practice. *Folia Neuropathol.* 58, 133–142. doi: 10.5114/fn.2020.96970

Schaefer, I. M., Fletcher, C. D., and Hornick, J. L. (2016). Loss of H3K27 trimethylation distinguishes malignant peripheral nerve sheath tumors from histologic mimics. *Mod. Pathol.* 29, 4–13.

Toyokawa, G., Takada, K., Tagawa, T., Hamamoto, R., Yamada, Y., Shimokawa, M., et al. (2019). A positive correlation between the EZH2 and PD-L1 expression in resected lung adenocarcinomas. *Ann. Thorac. Surg.* 107, 393–400. doi: 10.1016/j.athoracsur.2018.08.056

Turner, C. P., McLay, J., Hermans, I. F., Correia, J., Bok, A., Mehrabi, N., et al. (2022). Tumour infiltrating lymphocyte density differs by meningioma type and is associated with prognosis in atypical meningioma. *Pathology* 54, 417–424. doi: 10.1016/j.pathol.2021.10.002

Viré, E., Brenner, C., Deplus, R., Blanchon, L., Fraga, M., Didelot, C., et al. (2006). The Polycomb group protein EZH2 directly controls DNA methylation. *Nature* 439, 871–874.

Wang, J., Yu, X., Gong, W., Liu, X., Park, K.-S., Ma, A., et al. (2022). EZH2 noncanonically binds cMyc and p300 through a cryptic transactivation domain to mediate gene activation and promote oncogenesis. *Nat. Cell Biol.* 24, 384–399. doi: 10.1038/s41556-022-00850-x

Zhao, Y., Wang, X.-X., Wu, W., Long, H., Huang, J., Wang, Z., et al. (2019). EZH2 regulates PD-L1 expression via HIF-1α in non-small cell lung cancer cells. *Biochem. Biophys. Res. Commun.* 517, 201–209. doi: 10.1016/j.bbrc.2019.07.039

frontiers | Frontiers in Neuroscience

TYPE Original Research
PUBLISHED 04 January 2023
DOI 10.3389/fnins.2022.1060012

OPEN ACCESS

EDITED BY
Ye Cheng,
Capital Medical University, China

REVIEWED BY
Shunchao Bao,
Second Affiliated Hospital of Jilin University, China
Feng Lin,
Jilin University, China
Zhenluan Tian,
Sun Yat-sen Memorial Hospital, China

*CORRESPONDENCE
Yinghao Gu
✉ gyh1787@126.com

†These authors have contributed equally to this work and share first authorship

SPECIALTY SECTION
This article was submitted to Translational Neuroscience, a section of the journal Frontiers in Neuroscience

RECEIVED 02 October 2022
ACCEPTED 01 December 2022
PUBLISHED 04 January 2023

CITATION
Yang W, Wang S, Zhang X, Sun H, Zhang M, Chen H, Cui J, Li J, Peng F, Zhu M, Yu B, Li Y, Yang L, Min W, Xue M, Pan L, Zhu H, Wu B and Gu Y (2023) New natural compound inhibitors of PDGFRA (platelet-derived growth factor receptor α) based on computational study for high-grade glioma therapy.
Front. Neurosci. 16:1060012.
doi: 10.3389/fnins.2022.1060012

New natural compound inhibitors of PDGFRA (platelet-derived growth factor receptor α) based on computational study for high-grade glioma therapy

Wenzhuo Yang[1,2†], Shengnan Wang[3†], Xiangmao Zhang[1], Hu Sun[1], Menghan Zhang[4], Hongyu Chen[2], Junxiang Cui[5], Jinyang Li[5], Fei Peng[6], Mingqin Zhu[3], Bingcheng Yu[7], Yifan Li[7], Liu Yang[8], Wanwan Min[3], Mengru Xue[3], Lin Pan[9], Hao Zhu[10], Bo Wu[11] and Yinghao Gu[1]*

[1]Department of Neurosurgery, Zibo Central Hospital, Zibo, China, [2]Department of Neurosurgery, Cancer Hospital of Sun Yat-sen University, Guangzhou, China, [3]Department of Neurology, The First Hospital of Jilin University, Changchun, China, [4]Department of Clinical Laboratory, The Fifth Affiliated Hospital of Xinxiang Medical College, Xinxiang, China, [5]School of Clinical Medicine, Weifang Medical University, Weifang, China, [6]Division of Endocrinology, Diabetes and Metabolism, Department of Medicine, Baylor College of Medicine, Houston, TX, United States, [7]Zhongshan School of Medicine, Sun Yat-sen University, Guangzhou, China, [8]Department of Neurosurgical Oncology, The First Hospital of Jilin University, Changchun, China, [9]School of Clinical Medicine, Jilin University, Changchun, China, [10]Department of Hepatology, The First Hospital of Jilin University, Changchun, China, [11]Department of Orthopaedics, The First Hospital of Jilin University, Changchun, China

Background: High-grade glioma (HGG) is a malignant brain tumor that is common and aggressive in children and adults. In the current medical paradigm, surgery and radiotherapy are the standard treatments for HGG patients. Despite this, the overall prognosis is still very bleak. Studies have shown that platelet-derived growth factor receptor α (PDGFRA) is an essential target to treat tumors and inhibiting the activity of PDGFRA can improve the prognosis of HGG. Thus, PDGFRA inhibitors are critical to developing drugs and cancer treatment.

Objective: The purpose of this study was to screen lead compounds and candidate drugs with potential inhibitors against platelet-derived growth factor receptor α (PDGFRA) from the drug library (ZINC database) in order to improve the prognosis of patients with high-grade glioma (HGG).

Materials and methods: In our study, we selected Imatinib as the reference drug. A series of computer-aided technologies, such as Discovery Studio 2019 and Schrodinger, were used to screen and assess potential inhibitors of PDGFRA. The first step was to calculate the LibDock scores and then analyze the pharmacological and toxicological properties. Following this, we docked the small molecules selected in the previous steps with PDGFRA to study their docking mechanism and affinity. In addition, molecular dynamics simulation was used to determine whether the ligand-PDGFRA complex was stable in nature.

Results: Two novel natural compounds 1 and 2 (ZINC000008829785 and ZINC000013377891) from the ZINC database were found binding to PDGFRA with more favorable interaction energy. Also, they were predicted with less Ames mutagenicity, rodent carcinogenicity, non-developmental toxic potential, and tolerant with cytochrome P450 2D6 (CYP2D6). The dynamic simulation analysis demonstrated that ZINC000008829785-PDGFRA and ZINC000013377891-PDGFRA dimer complex had more favorable potential energy compared with Imatinib, and they can exist in natural environments stably.

Conclusion: ZINC000008829785 and ZINC000013377891 might provide a solid foundation for drugs that inhibit PDGFRA in HGG. In addition to being safe drug candidates, these compounds had important implications for improving drugs targeting PDGFRA.

KEYWORDS

high-grade glioma, PDGFRA, natural products, Imatinib, virtual screening

1 Introduction

High-grade glioma (HGG) is a malignant brain tumor that is common and aggressive in children and adults. In the current medical paradigm, surgery, and radiotherapy are the standard treatments for HGG patients. Temozolomide or Carmustine chips are also administered as part of the treatment regimen. Despite this, the overall prognosis is still very bleak. In general, patients survive 18 months on average, 30 percent survive 2 years, and ten percent survive 3 years or more. Because of its heterogeneity and instability, HGG is susceptible to multiple resistance to radiation and chemical treatment (Weller, 2011), and patients frequently consider targeted therapies after up-front radiation and at recurrence (Miklja et al., 2020).

Platelet-derived growth factor receptor α(PDGFRA) is one of the hot-spot targets in HGG. It is one of the most frequently altered genes in HGG. In 12% of adults with HGGs and 21% of kids with HGGs, PDGFRA is mutated or amplified. The PDGFRA receptor subunit interacts with four PDGF ligands out of two subunits in the receptor (Farahani and Xaymardan, 2015). It regulates normal glial cell proliferation and oligodendrocyte differentiation in the central nervous system (CNS) during normal development (Alentorn et al., 2012). As a result of the amplification of PDGFRA, the PI3K/mTOR signaling pathway or MAPK signaling pathway is commonly activated in HGG (Qu et al., 2010; Paugh et al., 2011; Schwartzentruber et al., 2012). Multiple cellular activities are induced, including proliferation, transformation, migration, and survival of cells (Farahani and Xaymardan, 2015). These mutations are connected to aggressive behaviors in gliomas (Koschmann et al., 2016; Mackay et al., 2018). It is therefore crucial to select PDGFRA inhibitors that are effective in cancer treatment.

Currently, the most studied PDGFRA inhibitors include Dasatinib, Avapritinib, Imatinib, and so on. Imatinib was the first tyrosine kinase inhibitor and received approval from the Food and Drug Administration (FDA) for the treatment of chronic myelogenous leukemia (Mansilla et al., 2012) and gastrointestinal stromal tumors (Gronwald et al., 1988). Imatinib is also a potent inhibitor of wild-type PDGFR family members (Wilson et al., 2018). Imatinib can induce PDGFRA phosphorylation and exert a growth inhibitory effect on glioma cells. Its efficacy against HGG had been demonstrated both *in vitro* and *in vivo* (Holtkamp et al., 2006). The drug used in the treatment of HGG has also entered the clinical trial stage. We selected Imatinib as the reference drug in this study. However, prolonged Imatinib treatment may cause mutations in PDGFRA which are Imatinib-resistant (Helbig et al., 2008). Intratumoral hemorrhage was observed in 84 recurrent pHGG patients treated with Imatinib in a phase I trial (Pollack et al., 2007). The aim of this study was to screen natural compounds from natural drugs that are more effective in treating HGG than Imatinib.

Through structural modification, natural products, such as lead compounds, can be converted into new drugs in the pharmaceutical industry (Yarla et al., 2016). To identify compounds that may have potential regulatory

Abbreviations: HGG, high-grade glioma; PDGFRA, platelet-derived growth factor receptor α; DS 2019, Discovery Studio 2019; PDB, the protein database; ADME, absorption, distribution, metabolism, and excretion; BBB, blood-brain barrier penetration; PPB, plasma protein binding levels; DTP, developmental toxicity potential; AMES, Ames mutagenicity; OS, overall survival; GBM, glioblastoma; TMZ, temozolomide.

functions for PDGFRA from Natural Products Database, structural biological and chemical methods (including virtual screening, molecular docking, etc.) were utilized in this study. These compounds were also predicted to be absorbed, distributed, metabolized, excreted, and toxic. To develop PDGFRA inhibitors, we present a list of drug candidates and their pharmacological properties.

2 Materials and methods

2.1 Software and ZINC15 database

Discovery Studio 2019 (DS 2019) is a comprehensive modeling and simulation tool used widely in molecular biology and environmental science. Among others, it displays chemical/biological data, performs simulations/analyses, constructs three-dimensional molecules, simulates dynamic changes, and provides three-dimensional mapping. DS 2019 has been applied to a variety of life science research fields, including drug discovery, bioinformatics, structural biology, and tumor research. To screen for potential PDGFRA inhibitors, DS 2019 was applied in this study. In the first step, we screened small molecules that docked with PDGFRA using the LibDock module. The pharmacological and toxicological properties of selected compounds were also analyzed using the ADME and TOPKAT modules. We then used CDOCKER module to achieve more accurate docking between proteins and molecules. The molecular docking results were refined by using Schrodinger's equation. In addition, small molecules were downloaded from the ZINC15 database (developed by Irwin and Shoichet Laboratories, Department of Pharmaceutical Chemistry, University of California, San Francisco, CA, USA). The ZINC15 database contains 17,931 natural, purchasable, for-sale molecules.

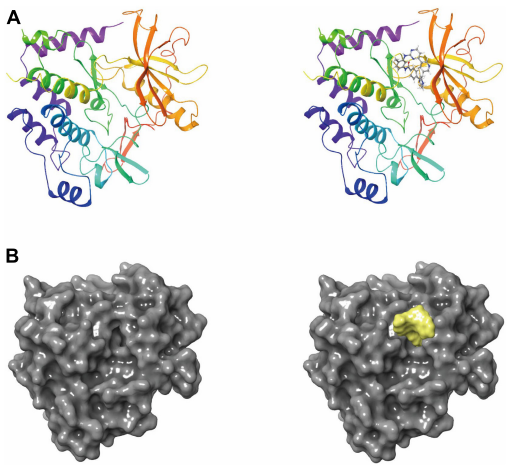

FIGURE 1
(A) The molecular structure of platelet-derived growth factor receptor α (PDGFRA), as well as the complex structure of PDGFRA combined with imatinib. **(B)** A molecular structure of PDGFRA and a complex structure of PDGFRA with Imatinib. Yellow represents Imatinib and gray represents PDGFRA.

2.2 LibDock-based virtual screening

Discovery Studio 2019's LibDock module performed a rigidity-based virtual screening (Rao et al., 2007). To make proteins, hydrogen, protonation, ionization, and energy minimization are used to remove crystalline water and other heteroatoms (Chamberlain, 2010). The first step of this procedure was to calculate hotspots that characterized where the ligand interacts with PDGFRA. After the ligand formed multiple conformations, docking was performed and then the docking was optimized and scored. These conformations were docked into the receptor's binding pocket using the principle of matching the conformation of small molecules with the receptor's hotspot. Its main advantages were speed, parallelism, and large-scale virtual filtering. Molecule positions were ranked according to the LibDock score (Li et al., 2021a). To screen Imatinib for its ability to bind to PDGFRA, we chose the binding pocket region where it binds to PDGFRA. Crystal structures of human PDGFRA and inhibitor have been downloaded from PDB (the protein database ID: 6JOK). **Figure 1** shows PDGFRA and Imatinib-PDGFRA complex's chemical structure. Protein preparation involves removing the water of crystallization and other heteroatoms and hydrogenating, protonating, ionizing, and minimizing energy consumption. The active docking site was generated by binding the ligand Imatinib to the binding site determined by the prepared protein. LibDock then performs virtual filtering to dock molecules at the defined region. Next, all docking positions were sorted and grouped according to Lidock scores.

2.3 Calculation of ADME (absorption, distribution, metabolism, and excretion) and toxicity

Absorption, distribution, metabolism, and excretion module of DS 2019 was used to evaluate blood-brain barrier penetration (BBB), hepatotoxicity, CYP2D6 inhibition, plasma protein binding levels (PPB), aqueous solubility, and human intestinal absorption of molecules. We calculated molecules' toxicological properties using DS's TOPKAT module, including rodent carcinogenicity, developmental toxicity potential (DTP), and Ames mutagenicity (AMES) (Li et al., 2021b). When selecting potential inhibitors of PDGFRA, all of the above calculations were taken into account.

2.4 An analysis of CDOCKER and assessment of pharmacophores

Discovery Studio's CDOCKER module was used for high-precision docking using the CHARMM force field. The docking conformation of LibDock's ligand-PDGFRA is precisely re-docked by CDOCKER. Both receptors and ligands have been enhanced with CHARMM force fields. PDGFRA remains rigid in docking, whereas ligands are flexible. During the CDOCKER process, each ligand displayed ten docking postures, and the interaction energies were calculated for each pose. We selected the ligand with the highest docking score and the most appropriate direction. A CDOCKER interaction energy was calculated for each complex posture, which indicates ligand-PDGFRA affinity. Each molecule can adopt as many as 255 conformations, but only those within the energy threshold of 10 kcal/mol can survive. To further visualize the optimal binding state of the ligand and protein, Schrodinger software was used. To display compound pharmacophores, the pharmacophore formation module of 3D-QSAR was used.

2.5 Molecular dynamic simulation

On account of the importance of evaluating the stability of the ligand-PDGFRA complex in the natural environment, a molecular dynamics simulation module was designed. Following the above analysis, the best conformation of the ligand was further evaluated in the molecular dynamic simulation module. As a first step, we placed the ligand-receptor complex in an orthogonal box and developed a transparent periodic boundary solvated water model. Our next step is to simulate the physiological environment by adding sodium chloride with an ionic strength of 0.145. CHARMM's force field was added to energy minimization (the steepest descent and conjugate gradient were 500 steps). For a balanced simulation of 2 ps, the system's temperature rose slowly from 50 to 300 K. Equilibrium simulation and production module were run separately for 5 and 100 ps (Zhong et al., 2021). Production module time step was 1 fs. A particle mesh Ewald algorithm was also used to evaluate the long-range electrostatic field. In this case, the constant temperature was set at 300 K. As a result of the linear constraint solver algorithm, all hydrogen

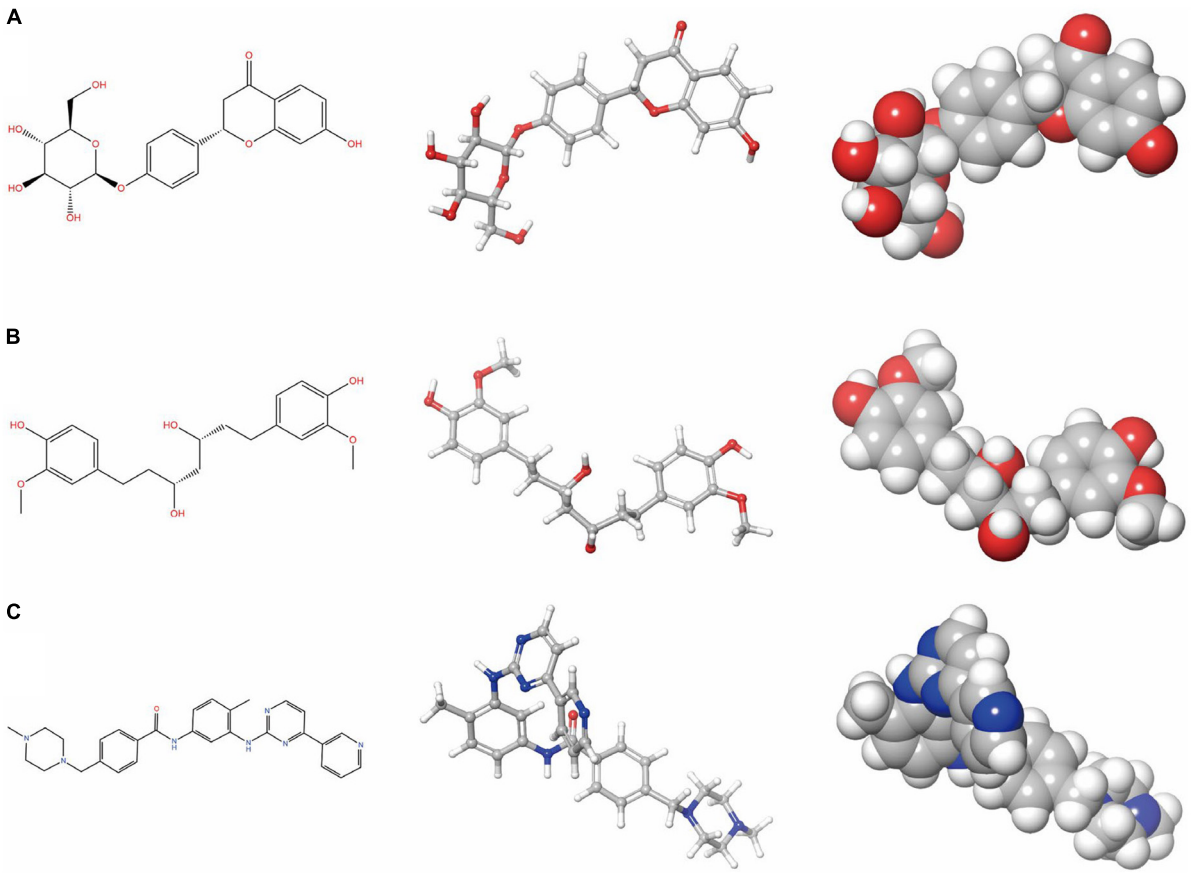

FIGURE 2
Schrodinger selected the 2D and 3D structures of Imatinib and novel compounds from virtual screening. **(A)** ZINC000008829785; **(B)** ZINC000013377891; and **(C)** Imatinib.

TABLE 1 Top 20 ranked compounds with LibDock scores.

Number	Compounds	LibDock score
1	ZINC000044086691	170.604
2	ZINC000004016719	157.336
3	ZINC000014780845	151.788
4	ZINC000014767731	149.908
5	ZINC000033970417	147.87
6	ZINC000004654958	145.269
7	ZINC000005762784	145.253
8	ZINC000008829785	142.413
9	ZINC000002509755	141.302
10	ZINC000004655035	141.216
11	ZINC000014658378	140.124
12	ZINC000028817821	140.061
13	ZINC000014883348	139.94
14	ZINC000013377891	139.898
15	ZINC000032840901	139.368
16	ZINC000014657833	139.198
17	ZINC000027646086	138.897
18	ZINC000003791929	138.273
19	ZINC000004557101	137.478
20	ZINC000001916008	137.366
	Imatinib	103.14

bonds were fixed. In accordance with DS's trajectory protocol, structural characteristics, potential energy, and root-mean-square deviation's (RMSD's) trajectory were drawn based on the initial complex setup. The original confirmation has been obtained by molecular docking with the CDOCKER module.

3 Results

3.1 Screening inhibitors of PDGFRA virtually

Platelet-derived growth factor receptor α's ligand-binding pocket played an important role in its regulation. Therefore, this pocket area is used as the reference. PDB was used to select PDGFRA as the receptor protein. Furthermore, Imatinib was selected as the reference ligand (Figure 2C). The purpose of this study was to virtually screen PDGFRA-favorable small molecules using LibDock. There were 17,931 compounds that met the conditions of stable binding to PDGFRA, among which 3,229 compounds scored higher than Imatinib (103.14) on the LibDock test. Following are the top 20 ranked compounds (Table 1).

3.2 Prediction of pharmacological and toxicological effects

We first calculated the pharmacological properties of Imatinib and 20 ligands using the DS's ADME module, including PPB, human intestinal absorption, BBB, hepatotoxicity, CYP2D6 inhibition, and aqueous solubility (Table 2). At 25°C, 13 compounds are predicted to be soluble in water by aqueous solubility predictions. Among them, ZINC000004654958, ZINC000008829785, ZINC000013377891, and ZINC000027646086 has improved water-solubility. CYP2D6 is an essential enzyme in drug metabolism. Except for ZINC000004016719, ZINC000014780845, ZINC000032840901, and ZINC000002509755, most compounds have no inhibitory effect on CYP2D6. In addition, in predictive hepatotoxicity, we found that 18 compounds were non-hepatotoxicity, and 2 compounds were similar in toxicity to Imatinib. 13 compounds were predicted to be higher than Imatinib in human intestinal absorption levels. Finally, 14 of the compounds were shown to have high binding to plasma proteins, while the others did not.

To ensure the safety of these compounds, this study also conducted comprehensive research. To predict the toxicity indicators of the selected compounds and Imatinib, the TOPKAT module of DS was applied. As part of this module, three indicators were predicted, including rodent carcinogenicity, DTP, and AMES (Table 3). The results showed that 13 molecules were not mutagenic, and 9 molecules were not developmental toxic. Several studies have found that Imatinib had developmental toxicity properties and higher rodent carcinogenicity in the mouth of male rats. Two compounds were identified as potentially ideal lead compounds based on all of the above results: ZINC000008829785 (compound 1) and ZINC000013377891 (compound 2) due to lack of hepatotoxicity, CYP2D6 inhibition, AMES, rodent carcinogenicity, and developmental toxicity potential. Therefore, ZINC000008829785 and ZINC000013377891 proved safe candidates for subsequent studies (Figures 2A, B).

3.3 Analyses of ligand binding and ligand pharmacophores

In conjunction with the CHARMm36 force field, the CDOCKER module docked the ligand precisely into the PDGFRA. We studied the interaction mechanism of Imatinib, ZINC000008829785, and ZINC000013377891 with PDGFRA, including bond type, bond length, and CDOCKER potential energy. CDOCKER potential energy is shown in Table 4. Compared with the reference ligand Imatinib (−34.6412 kcal/mol), the CDOCKER potential energy of ZINC000008829785 and ZINC000013377891 was lower, indicating that the binding ability of these two molecules

TABLE 2 Absorption, distribution, metabolism, and excretion properties of compounds.

Number	Compounds	Solubility level	BBB level	CYP2D6	Hepatotoxicity	Absorption level	PPB level
1	ZINC000044086691	1	4	0	0	3	1
2	ZINC000004016719	2	4	1	0	3	0
3	ZINC000014780845	2	4	0	1	0	1
4	ZINC000014767731	0	4	0	0	3	1
5	ZINC000033970417	1	4	0	0	3	1
6	ZINC000004654958	3	4	0	0	1	0
7	ZINC000005762784	2	1	0	0	0	1
8	ZINC000008829785	3	4	0	0	2	0
9	ZINC000002509755	2	2	1	1	0	1
10	ZINC000004655035	0	4	0	0	3	1
11	ZINC000014658378	2	0	0	0	0	1
12	ZINC000028817821	2	2	0	0	0	1
13	ZINC000014883348	0	4	0	0	3	1
14	ZINC000013377891	3	4	0	0	0	1
15	ZINC000032840901	3	4	1	0	1	0
16	ZINC000014657833	2	0	0	0	1	1
17	ZINC000027646086	4	1	0	0	0	0
18	ZINC000003791929	0	4	0	0	3	1
19	ZINC000004557101	3	4	0	0	1	0
20	ZINC000001916008	1	4	0	0	3	1
21	Imatinib	2	2	0	1	0	0

BBB, blood-brain barrier; CYP2D6, cytochrome P-450 2D6; PPB, plasma protein binding. Aqueous-solubility level: 0, extremely low; 1, very low, but possible; 2, low; 3, good. BBB level: 0, very high penetrant; 1, high; 2, medium; 3, low; 4, undefined. CYP2D6 level: 0, non-inhibitor; 1, inhibitor. Hepatotoxicity: 0, non-toxic; 1, toxic. Human-intestinal absorption level: 0, good; 1, moderate; 2, poor; 3, very poor. PPB: 0, absorbent weak; 1, absorbent strong.

TABLE 3 Toxicities of compounds.

Number	Compounds	Mouse NTP		Rat NTP		Ames	DTP
		Female	Male	Female	Male		
1	ZINC000044086691	0.004	0.998	0.987	0	1	1
2	ZINC000004016719	0.265	0.05	1	1	0	1
3	ZINC000014780845	0	0.975	1	1	0.113	1
4	ZINC000014767731	1	0	1	1	0	1
5	ZINC000033970417	0	0.021	0	0	1	0
6	ZINC000004654958	0	0	0	0	0	0
7	ZINC000005762784	0	0.001	0	0.001	1	0
8	ZINC000008829785	0	0	0	0	0	1
9	ZINC000002509755	0.996	0.535	0	0.001	0.603	0.019
10	ZINC000004655035	1	0	1	1	0	1
11	ZINC000014658378	0	0	1	1	0	1
12	ZINC000028817821	0	0	0	0	1	0.265
13	ZINC000014883348	0	0.968	0	0	1	0
14	ZINC000013377891	0.017	0.971	0	0.008	0.122	1
15	ZINC000032840901	0.448	0.001	0	0.047	0	0
16	ZINC000014657833	1	0	1	1	0.04	1
17	ZINC000027646086	0	0	0	0	0	0
18	ZINC000003791929	1	0	1	1	0	1
19	ZINC000004557101	0	0	0	0.006	0	0
20	ZINC000001916008	1	0	1	1	0	1
21	Imatinib	0.03	0	0	1	0.102	1

NTP, U.S. national toxicology program; DTP, developmental toxicity potential. NTP <0.3 (non-carcinogen); >0.8 (carcinogen). Ames <0.3 (non-mutagen); >0.8 (mutagen). DTP <0.3 (non-toxic); >0.8 (toxic).

TABLE 4 CDOCKER Potential energy of compounds with platelet-derived growth factor receptor α (PDGFRA).

Compound	-CDOCKER potential energy (kcal/mol)
ZINC000008829785	44.7761
ZINC000013377891	45.2444
imatinib	34.6412

to PDGFRA was superior to that of Imatinib. In addition, we applied structural calculation methods to analyze the interaction relationships formed by ligand-PDGFRA complexes (Figure 3), such as hydrogen bonds, and hydrophobic interactions (Alkyl interactions, Pi-Alkyl interactions, and Pi-Sigma interactions). The results are described below, 11 pair of hydrogen bonds was formed between ZINC000013377891 and PDGFRA, by the O9 of the compound with A: LYS627:HZ1 of 6JOK, O27 of the compound with A: CYS677:HN of 6JOK, O9 of the compound with A: LYS627:HE2 of 6JOK, et al. Also, five pairs of Pi-Alkyl interactions were presented in the complex. For ZINC000008829785, there were five pairs of Pi-Alkyl interactions and a pair of Pi-Pi T-shaped interactions with PDGFRA. There were also eight pairs of hydrogen bonds in the complex (A:LYS627:HZ–ZINC000008829785:O23, A:CYS814:HG–ZINC000008829785:O18, A:ASP836:HN–ZINC000008829785:O23, ZINC000008829785:H40–A:ASP836:OD1, ZINC000008829785:H42–A:VAL815:O, ZINC000008829785:H44–A:VAL815:O, ZINC000008829785:H37–A:ASP836:OD1, and ZINC000008829785:H50–A:PHE837). About the reference compound Imatinib, it formed three pairs of hydrogen

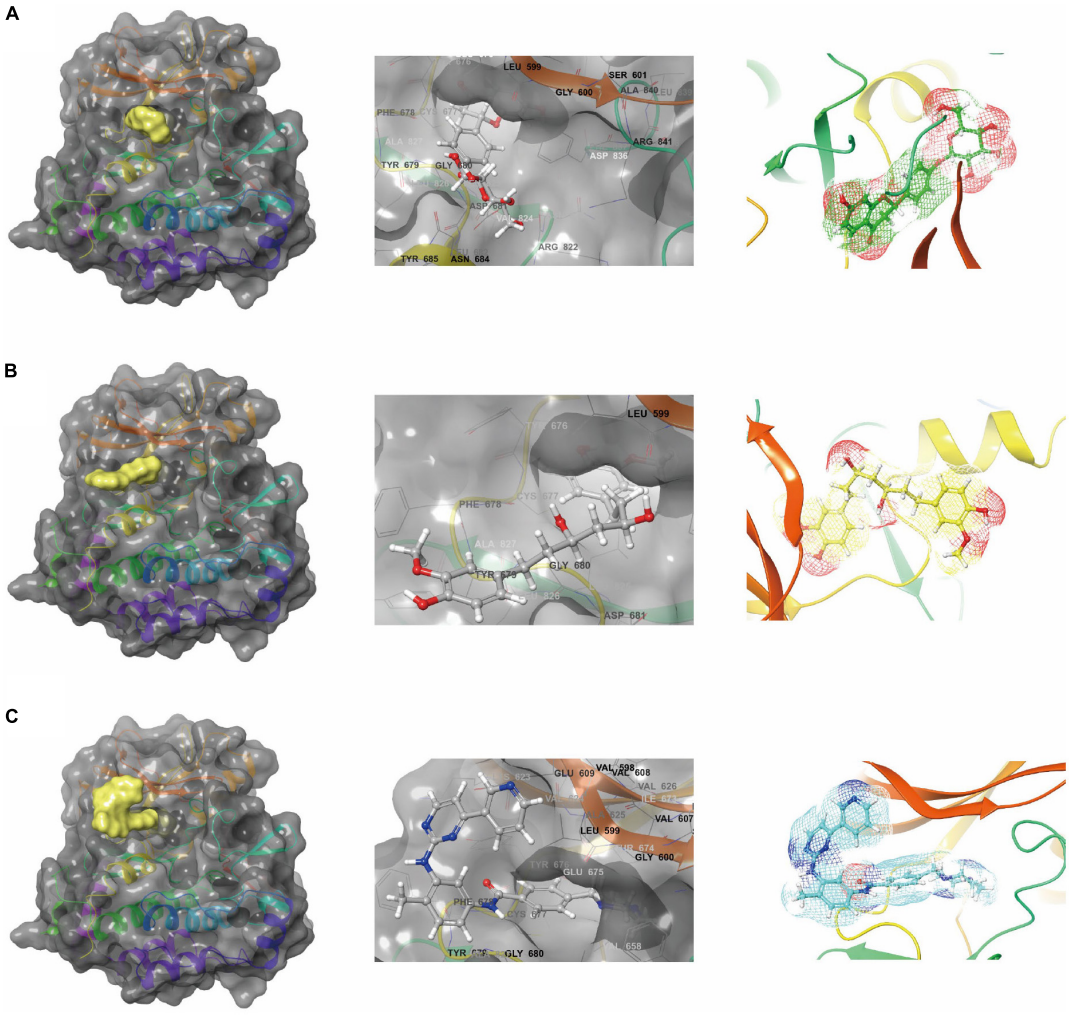

FIGURE 3
Schematic drawing of interactions between ligands and platelet-derived growth factor receptor α (PDGFRA) by Schrodinger.
(A) ZINC000008829785-PDGFRA complex: structures and net electron cloud structures of ZINC000008829785 are shown in purple sticks.
(B) ZINC000013377891-PDGFRA complex: structures and net electron cloud structures of ZINC000013377891 are shown in yellow sticks.
(C) Imatinib-PDGFRA complex: structures and net electron cloud structures of Imatinib are shown in green sticks.

bonds with PDGFRA (Molecular:H38–A:TYR676:OH, Molecular:H51–A:GLU675:O, and Molecular:H52–A:THR674 :OG1). A total of two pairs of Pi-Alkyl interaction, 1 Pi-Sigma interaction, 1 Pi-Pi T-shaped interaction, and 5 Alkyl interactions were also formed with PDGFRA (Tables 5, 6). These binding interactions were further analyzed using Schrodinger (Figure 4). The green dashed line represents hydrogen bonds, and the more hydrogen bonds, the higher the binding affinity. In conclusion, these results imply that ZINC000008829785 and ZINC000013377891 may have a better binding affinity with PDGFRA than Imatinib, indicating the promising application of these two compounds.

In addition, with the help of other virtual docking software (Schrodinger software), the conformation of ligand binding pocket in PDGFRA and the 2D and 3D structure of ligand interaction with PDGFRA amino acid residues were further demonstrated and analyzed (Figure 5). We can intuitively find that the posture of the three small molecules in the binding pocket has certain similarities. Interestingly, we found the same amino acid in the bond with PDGFRA in all three drugs. ZINC000008829785 and Imatinib form bonds with the same amino acids in protein binding pockets, including VAL-607 and ALA-625. Similarly, ZINC000013377891 and Imatinib have the same bonds in the protein binding pocket, including VAL-607, ALA-625, CYS-677, LEU-825, and LEU-599. Notably, all three molecules form the same bond with the amino acids VAL-607 and ALA-625 in the binding pocket. This phenomenon partly supports the similar inhibition of PDGFRA by the two selected small molecules and Imatinib because of their similar binding and interaction patterns. Furthermore, amino acid residues VAL-607 and ALA-625 play an important structural and functional role in the PDGFRA binding pocket domain.

As for the pharmacophore of these two compounds, the results showed 58 characteristic pharmacophores in ZINC000008829785 and 42 characteristic pharmacophores in ZINC000013377891 (Table 7). In addition, Figures 6A–C shows the hydrogen bond receptor, hydrogen bond donor, and hydrophobic center in ZINC000008829785 and ZINC000013377891.

3.4 Molecular dynamics simulation

Root-mean-square deviation and the potential energy of these ligand-PDGFRA complexes were analyzed and used as

TABLE 5 Hydrogen bond interaction parameters for each compound with platelet-derived growth factor receptor α (PDGFRA).

Receptor	Compound	Donor atom	Receptor atom	Distances (Å)
6JOK	ZINC000013377891	A:LYS627:HZ1	ZINC000013377891:O9	2.11092
		A:CYS677:HN	ZINC000013377891:O27	1.93733
		ZINC000013377891:H37	A:ASP836:O	2.88582
		ZINC000013377891:H41	A:GLU644:OE1	2.0075
		ZINC000013377891:H41	A:MET648:SD	2.74568
		A:LYS627:HE2	ZINC000013377891:O9	2.73758
		ZINC000013377891:H40	A:GLU644:OE1	2.61332
		ZINC000013377891:H40	A:ASP836:O	2.62855
		ZINC000013377891:H49	A:HIS816:O	2.49461
		ZINC000013377891:H50	A:ASP836:OD1	2.61296
		ZINC000013377891:H51	A:ASP836:OD1	3.07523
		A:LYS627:HZ1	ZINC000008829785:O23	2.88712
	ZINC000008829785	A:CYS814:HG	ZINC000008829785:O18	2.19944
		A:ASP836:HN	ZINC000008829785:O23	2.47838
		ZINC000008829785:H40	A:ASP836:OD1	2.63525
		ZINC000008829785:H42	A:VAL815:O	2.88983
		ZINC000008829785:H44	A:VAL815:O	1.83837
		ZINC000008829785:H37	A:ASP836:OD1	2.46762
		ZINC000008829785:H50	A:PHE837	2.69054
		Imatinib:H38	A:TYR676:OH	2.81239
	Imatinib	Imatinib:H51	A:GLU675:O	2.30423
		Imatinib:H52	A:THR674:OG1	2.89619

TABLE 6 Hydrophobic interaction parameters for each compound with platelet-derived growth factor receptor α (PDGFRA).

Compound	Hydrophobic bond type	Donor atom	Receptor atom	Distances (Å)
	Pi-Alkyl	ZINC000013377891	A:LEU599	5.48452
	Pi-Alkyl	ZINC000013377891	A:VAL607	5.25537
ZINC000013377891	Pi-Alkyl	ZINC000013377891	A:ALA625	3.58356
	Pi-Alkyl	ZINC000013377891	A:CYS677	5.19166
	Pi-Alkyl	ZINC000013377891	A:LEU825	4.45943
	Pi-Pi T-shaped	A:PHE837	ZINC000008829785	5.50749
	Pi-Alkyl	ZINC000008829785	A:MET648	4.4137
	Pi-Alkyl	ZINC000008829785	A:VAL607	4.4684
ZINC000008829785	Pi-Alkyl	ZINC000008829785	A:ALA625	5.34806
	Pi-Alkyl	ZINC000008829785	A:VAL658	5.22524
	Pi-Alkyl	ZINC000008829785	A:CYS835	4.66191
	Pi-Sigma	A:LEU599:CD1	Molecule	3.72166
	Pi-Pi T-shaped	A:PHE678	Molecule	4.43744
	Alkyl	A:LEU599	Molecule	4.74205
	Alkyl	A:VAL607	Molecule	5.18751
Imatinib	Alkyl	A:ALA625	Molecule	4.5518
	Alkyl	A:CYS677	Molecule	4.94212
	Alkyl	A:LEU825	Molecule	4.48423
	Pi-Alkyl	A:PHE678	Molecule:C28	5.15591
	Pi-Alkyl	Imatinib	A:LYS688	3.92448

parameters to evaluate their stability. The results show that the RMSD and potential energy of compound 1, 2-PDGFRA complex reach an equilibrium trajectory at 100 ps and remain stable over time after that. It is proved that these two complexes can exist stably in the natural environment (**Figures 6D, E**).

4 Discussion

High-grade gliomas are common and aggressive pediatric and adult brain tumors. It is estimated that the median overall survival (OS) of adult patients with glioblastoma (GBM), a grade IV glioma, is 12.6 months (Liu et al., 2018) and that for pediatrics with HGG it is 14.1 months (Mackay et al., 2017). It is usually treated with surgery, combined radiotherapy and chemotherapy, and adjuvant temozolomide (TMZ) 6 months after surgery (Stupp et al., 2005). Patients always relapse after adjuvant therapy protocols, which only extend survival by 3 months (Stupp et al., 2009). Around 90% of cases recur, and the prognosis is poorer when HGG recurs (Weller et al., 2013). Most recurrences occur within 2 cm of the margin of the initial tumor, are usually inaccessible by surgery, and respond less well to therapy (Audureau et al., 2018; Aldaz and Arozarena, 2021). Therefore, it is vital to research targeted therapy and develop more targeted drugs to treat HGG.

Targeted therapy is still in the exploratory stage. It is shown that most HGGs demonstrated amplification of PDGFRA-driven signal (Paugh et al., 2011). The ATP-binding site of PDGFRA can be occupied when the PDGFRA inhibitor is in the inactive conformation, preventing substrate phosphorylation and inhibiting downstream signaling (Bauer et al., 2021). Currently, the most studied PDGFRA inhibitors include Dasatinib, Avapritinib, Imatinib, and so on. Moreover, preclinical studies have shown that Imatinib can prevent the PI3K/mTOR signaling pathway or MAPK signaling pathway by docking with PDGFRA. It can effectively inhibit tumor growth, exert anti-tumor activity, and be proven effective in pediatric HGG with PDGF pathway alterations (Schwark et al., 2022). In line with this, a small RCT study found that patients with glioblastoma responded frequently to the combination of hydroxyurea and imatinib (Joensuu et al., 2005; Mantica et al., 2018). This study selected Imatinib as the reference drug. However, Imatinib has significant therapeutic limitations, with developmental toxicity and the risk of intratumoral hemorrhage as side effects (Schwark et al., 2022). The screening of more desirable inhibitors of PDGFRA is therefore essential for the treatment of HGG.

Our study used DS 2019's six modules (LibDock, ADME, TOPKAT, CDOCKER, 3D-QSAR, and molecular dynamics simulation) to screen and identify ideal inhibitors

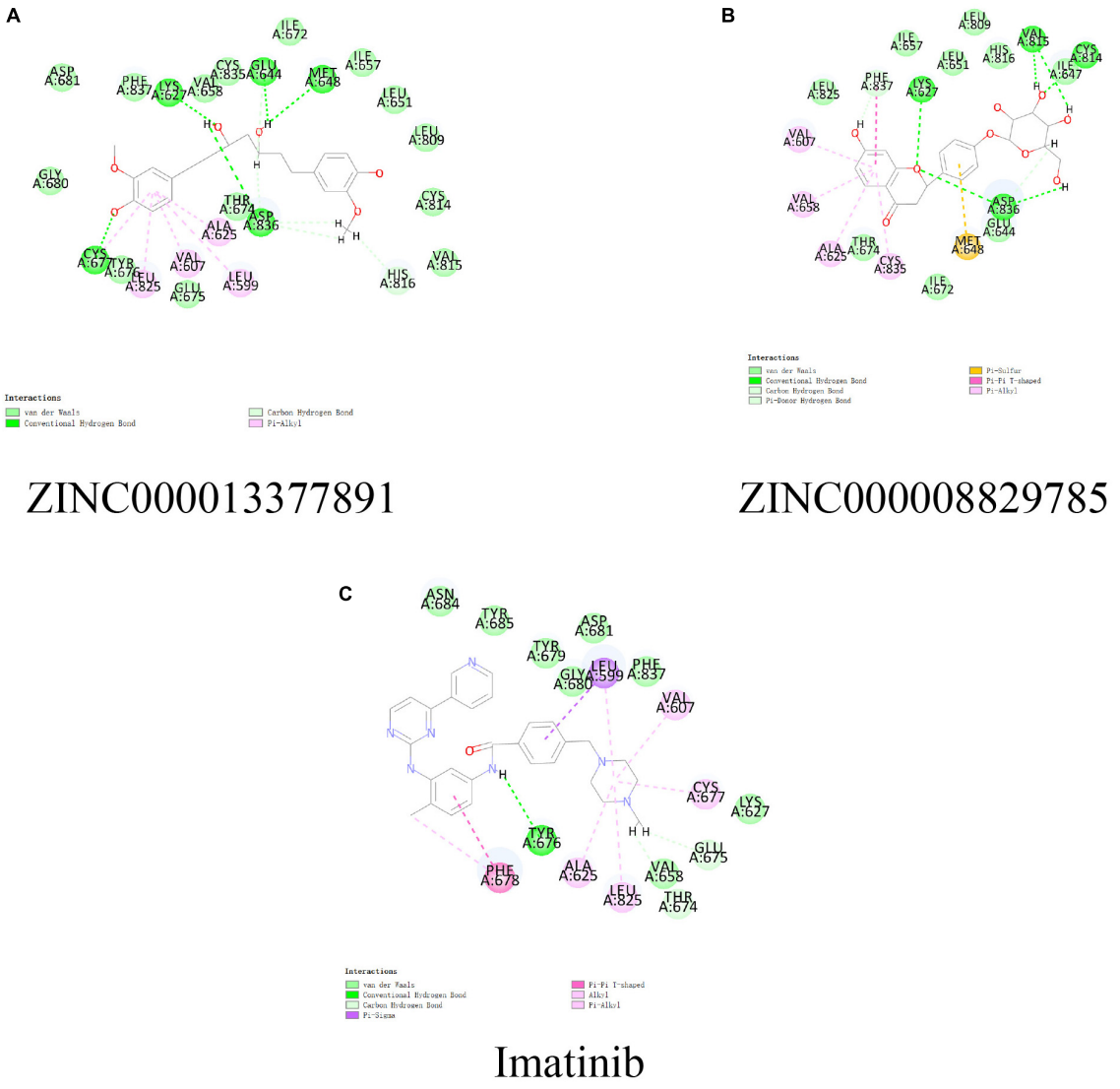

FIGURE 4
Schematic of intermolecular interaction in the binding pockets by DS of the predicted binding modes of **(B)** ZINC000008829785 with platelet-derived growth factor receptor α (PDGFRA), **(A)** ZINC000013377891 with PDGFRA, and **(C)** Imatinib with PDGFRA.

of PDGFRA. The molecular conformation, pharmacological and toxicological properties, binding affinity, and stability were analyzed. And several potential superior inhibitors of PDGFRA were found with reasonable pharmacological and toxicological properties compared with Imatinib, which lays a solid foundation for drug development of PDGFRA inhibitors and HGG therapy.

For virtual screening, 17,931 named, natural, and purchasable compounds were downloaded from the ZINC15 database. Energy optimization and conformational stability were evaluated using the LibDock score. LidDock's score is influenced by energy optimization and conformational stability, so the higher the score, the better. Using DS 2019's LibDock module, we selected 9,842 compounds that were considered to have a high affinity for PDGFRA. Additionally, 3,229 compounds had higher LibDock scores than the reference inhibitor Imatinib (LibDock score: 103.104). In addition, the top 20 compounds scored by the LibDock module were selected for further research.

To evaluate pharmacological properties and toxicology of molecules, ADME and TOPKAT modules were applied. The results indicate that compounds 1 (ZINC000008829785) and 2 (ZINC000013377891) are ideal inhibitors of PDGFRA. Compounds 1 and 2 dissolve well in water, indicating that they can be readily absorbed by the body. Additionally, they show no hepatotoxicity or inhibition of CYP2D6, an enzyme that plays a key role in drug metabolism. Furthermore, three toxicity indices, including Ames mutagenicity, rodent carcinogenicity,

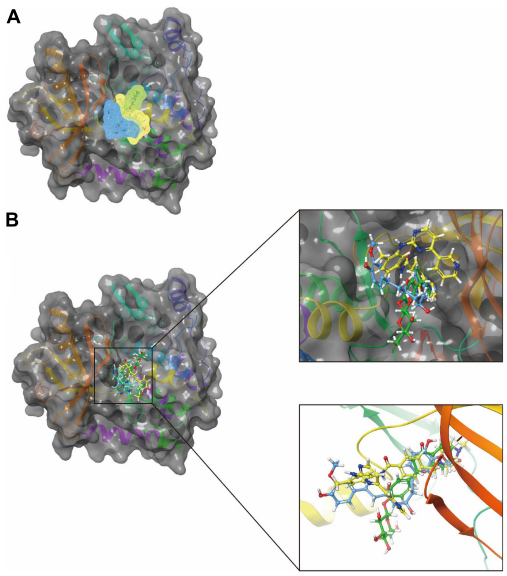

FIGURE 5
A comparison of the spatial conformation of small molecules in protein binding pockets with the gray surface of platelet-derived growth factor receptor α (PDGFRA). **(A)** In yellow, green, and red, respectively, are the structures and net electron cloud structures of ZINC000008829785, ZINC000013377891, and Imatinib. **(B)** Structures of ZINC000008829785, ZINC000013377891, and Imatinib are shown in yellow, green, and red sticks, respectively.

and developmental toxicity potential, are within reasonable safety limits. This indicates that they may be used in drug development. However, we cannot assume categorically that the other compounds do not have potential drug development applications as PDGFRA inhibitors. It is possible to design specific groups and atoms in order to alter pharmacological and toxicological properties. In some cases, these compounds may also show their potential value in drug development when designed in a certain way. The compounds 1 and 2 were found to be potential inhibitors of PDGFRA. We also analyzed the precise interaction and combination between compounds 1, 2, and PDGFRA.

Additionally, the CDOCKER module was applied to evaluate the chemical bonding and interaction mechanisms of the ligand- PDGFRA complex. In this procedure, CDOCKER interaction energy of complex of PDGFRA with compounds 1, 2, and Imatinib was calculated separately. The higher absolute value of CDOCKER interaction energy means higher stability and affinity of ligand -PDGFRA complex. Compound 1, 2 -PDGFRA complex was proved to be more stable and tighter for their higher absolute value of CDOCKER interaction energy than the reference ligand Imatinib (−34.6412 kcal/mol). Moreover, the interactions and combinations between compounds 1, 2, Imatinib, and PDGFRA were also shown in two-dimensional and three-dimensional structures (Figures 2, 3). In this step, Schrodinger was also used to illustrate the interaction between the ligand and amino acid residues in the protein binding pocket (Figure 3). It is interesting to note that these selected molecules as well as Imatinib overlap a lot at the location of the PDGFRA binding pocket and form bonds with identical amino acid residues (Figure 5). For example, compound 1 and Imatinib form bonds with the identical amino residues VAL-607, ALA-625, and compound 2 and Imatinib form bonds with VAL-607, ALA-625, CYS-677, LEU-825, and LEU-599. The essentially identical binding and interaction patterns suggest that they may have the same inhibitory effect on PDGFRA. Furthermore, VAL-607 and ALA-625 bond in the protein-binding pocket in binding all three small molecules to PDGFRA, which may play a vital role in the structural, and functional domain. Moreover, the binding of amino acids in the binding pocket may be our new criterion for assessing binding capacity. In addition, pharmacophore is the physical and chemical characteristics and spatial arrangement of ligands required for molecular recognition by biomacromolecules. These pharmacodynamic signatures are the active sites of ligand and receptor interactions. Compounds 1 and 2 showed several hydrogen acceptors, hydrophobic centers, and hydrogen donors with the 3D-QSAR module, which indicated that these two molecules are pharmacologically active and have the potential to be developed as inhibitors of PDGFRA. In future research, diverse specific groups can be added to the two compounds to optimize the drug, thus enhancing its efficacy, and making it a perfect PDGFRA inhibitor.

Finally, the molecular dynamics simulation module appraised the stability of ligand-PDGFRA in the natural environment. As parameters for evaluating the stability of these ligand-PDGFRA complexes, RMSD and potential energy were analyzed. The results show that the RMSD and potential energy of compound 1, 2-PDGFRA complex reach an equilibrium trajectory at 100 ps and remain stable over time after that. These two complexes can exist in the natural environment stably.

TABLE 7 The analysis of feature pharmacophores.

	Total	HB_acceptor	HB_donor	Hydrophobic	Ring_aromatic	Pos_ionizable
ZINC000013377891	42	18	16	4	4	0
ZINC000008829785	58	29	23	2	4	0
Imatinib	18	2	0	6	8	2

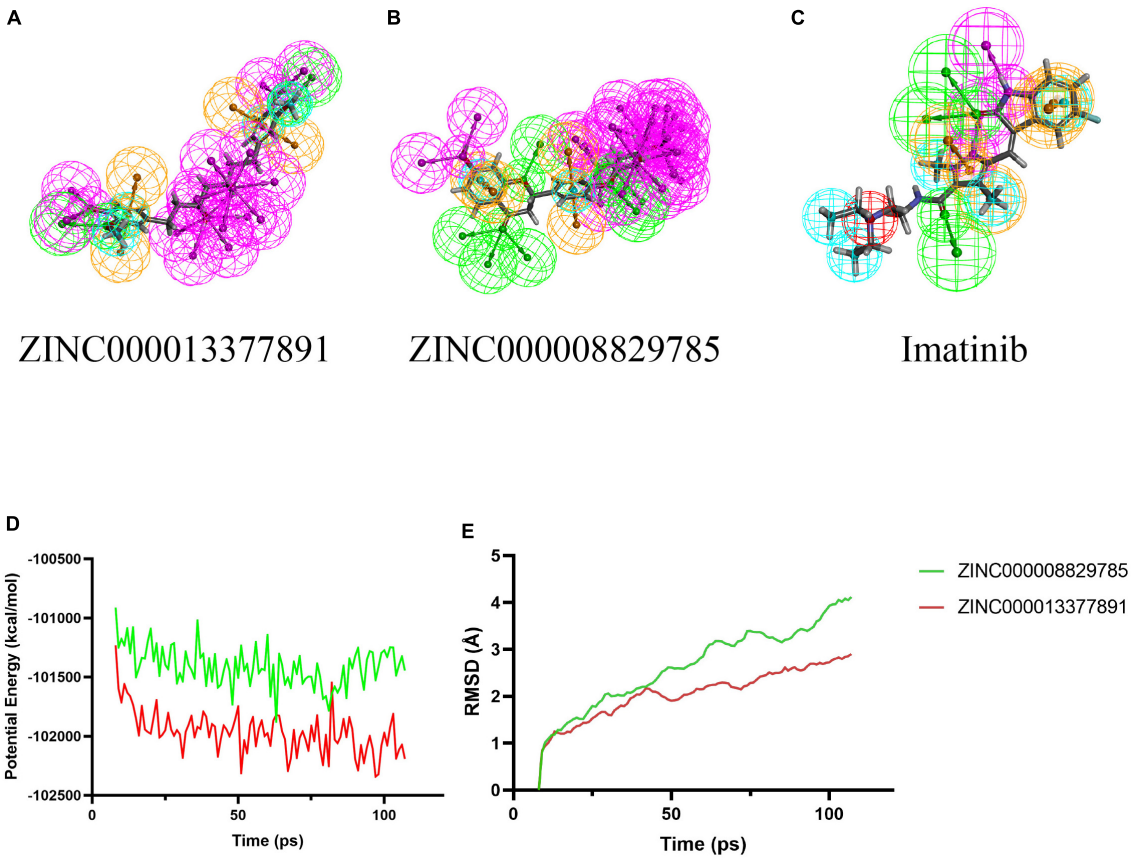

FIGURE 6
3D-QSAR module of DS used for pharmacophore prediction. By DS, green represents hydrogen acceptor; blue represents hydrophobic center; purple represents hydrogen donor; yellow represents aromatic ring. **(B)** ZINC000008829785; **(A)** ZINC000013377891; and **(C)** Imatinib. **(D,E)** Results of molecular dynamics simulation of the compounds ZINC000008829785 and ZINC000013377891. **(D)** Potential energy. **(E)** Average backbone root-mean-square deviation. RMSD, root-mean-square deviation.

Even though this study was carefully designed and accurately measured, some limitations remain. There is no literature report on ZINC000008829785 and ZINC000013377891 in the treatment of glioma. As a result, subsequent studies can directly focus on refining and improving the lead compounds chosen in this study. Further prospective studies are needed to validate our findings since the nomogram is based on retrospective studies.

5 Conclusion

This study is significant for screening ideal lead compounds and is a critical step in PDGFRA inhibitor drug design. It provides a solid foundation for future drug designation and development. Our calculations suggest these two molecules (ZINC000008829785 and ZINC000013377891) might serve as ideal inhibitors of cancer through a series of advanced technical calculations. Additionally, this study provides practical guidance and technical means for screening potential therapeutic compounds. Drug development could be aided by this advanced approach in the future. This study provides screening of targeted drugs for HGG patients and improves their prognosis.

Data availability statement

The original contributions presented in this study are included in the article/supplementary material, further inquiries can be directed to the corresponding author.

Author contributions

SW and WY drafted the manuscript and contributed to editing and revision. LY, MQZ, LP, WM, and MX downloaded datasets and conducted a bioinformatic analysis. FP, MHZ, and HZ performed the analysis of the results. BY, YL, XZ, HS, JC, and JL contributed to figures and tables. YG substantively edited

the manuscript. All authors read and agreed to the final version of this manuscript.

Conflict of interest

The authors declare that the research was conducted in the absence of any commercial or financial relationships that could be construed as a potential conflict of interest.

Publisher's note

References

Aldaz, P., and Arozarena, I. (2021). Tyrosine kinase inhibitors in adult glioblastoma: An (Un)closed chapter? *Cancers (Basel)* 13, 5799. doi: 10.3390/cancers13225799

Alentorn, A., Marie, Y., Carpentier, C., Boisselier, B., Giry, M., Labussière, M., et al. (2012). Prevalence, clinico-pathological value, and co-occurrence of PDGFRA abnormalities in diffuse gliomas. *Neuro Oncol.* 14, 1393–1403. doi: 10.1093/neuonc/nos217

Audureau, E., Chivet, A., Ursu, R., Corns, R., Metellus, P., Noel, G., et al. (2018). Prognostic factors for survival in adult patients with recurrent glioblastoma: A decision-tree-based model. *J. Neurooncol.* 136, 565–576. doi: 10.1007/s11060-017-2685-4

Bauer, S., Messinger, D., Cummings, J. R., Bradin, J., Kawakibi, A., Babila, C. M., et al. (2021). Early and next-generation KIT/PDGFRA kinase inhibitors and the future of treatment for advanced gastrointestinal stromal tumor. *Front. Oncol.* 11:672500. doi: 10.3389/fonc.2021.672500

Chamberlain, M. C. (2010). Anticancer therapies and CNS relapse: Overcoming blood-brain and blood-cerebrospinal fluid barrier impermeability. *Expert Rev. Neurother.* 10, 547–561. doi: 10.1586/ern.10.14

Farahani, R. M., and Xaymardan, M. (2015). Platelet-derived growth factor receptor alpha as a marker of mesenchymal stem cells in development and stem cell biology. *Stem Cells Int.* 2015:362753.

Gronwald, R. G., Grant, F. J., Haldeman, B. A., Hart, C. E., O'Hara, P. J., Hagen, F. S., et al. (1988). Cloning and expression of a cDNA coding for the human platelet-derived growth factor receptor: Evidence for more than one receptor class. *Proc. Natl. Acad. Sci. U.S.A.* 85, 3435–3439. doi: 10.1073/pnas.85.10.3435

Helbig, G., Stella-Hołowiecka, B., Majewski, M., Całbecka, M., Gajkowska, J., Klimkiewicz, R., et al. (2008). A single weekly dose of imatinib is sufficient to induce and maintain remission of chronic eosinophilic leukaemia in FIP1L1-PDGFRA-expressing patients. *Br. J. Haematol.* 141, 200–204. doi: 10.1111/j.1365-2141.2008.07033.x

Holtkamp, N., Okuducu, A. F., Mucha, J., Afanasieva, A., Hartmann, C., Atallah, I., et al. (2006). Mutation and expression of PDGFRA and KIT in malignant peripheral nerve sheath tumors, and its implications for imatinib sensitivity. *Carcinogenesis* 27, 664–671. doi: 10.1093/carcin/bgi273

Joensuu, H., Puputti, M., Sihto, H., Tynninen, O., and Nupponen, N. N. (2005). Amplification of genes encoding KIT, PDGFRalpha and VEGFR2 receptor tyrosine kinases is frequent in glioblastoma multiforme. *J. Pathol.* 207, 224–231. doi: 10.1002/path.1823

Koschmann, C., Zamler, D., MacKay, A., Robinson, D., Wu, Y. M., Doherty, R., et al. (2016). Characterizing and targeting PDGFRA alterations in pediatric high-grade glioma. *Oncotarget* 7, 65696–65706.

Li, H., Yang, W., Wang, Z., Wang, X., Hao, Y., Xi, J., et al. (2021a). Computational research of mTORC1 inhibitor on cerebral ischemia-reperfusion injury. *Aging (Albany NY)* 13, 19598–19613. doi: 10.18632/aging.203371

Li, H., Yang, W., Xi, J., Wang, Z., Lu, H., Du, Z., et al. (2021b). Computational study on new natural compound agonists of dopamine receptor. *Aging (Albany NY)* 13, 16620–16636. doi: 10.18632/aging.203180

Liu, J., Lichtenberg, T., Hoadley, K. A., Poisson, L. M., Lazar, A. J., Cherniack, A. D., et al. (2018). An integrated TCGA pan-cancer clinical data resource to drive high-quality survival outcome analytics. *Cell* 173, 400–416.e11. doi: 10.1016/j.cell.2018.02.052

Mackay, A., Burford, A., Carvalho, D., Izquierdo, E., Fazal-Salom, J., Taylor, K. R., et al. (2017). Integrated molecular meta-analysis of 1,000 pediatric high-grade and diffuse intrinsic pontine glioma. *Cancer Cell* 32, 520–537.e5. doi: 10.1016/j.ccell.2017.08.017

Mackay, A., Burford, A., Molinari, V., Jones, D. T. W., Izquierdo, E., Brouwer-Visser, J., et al. (2018). Molecular, pathological, radiological, and immune profiling of non-brainstem pediatric high-grade glioma from the HERBY Phase II randomized trial. *Cancer Cell* 33, 829–842.e5. doi: 10.1016/j.ccell.2018.04.004

Mansilla, S., Llovera, L., and Portugal, J. (2012). Chemotherapeutic targeting of cell death pathways. *Anticancer Agents Med. Chem.* 12, 226–238.

Mantica, M., Pritchard, A., Lieberman, F., and Drappatz, J. (2018). Retrospective study of nivolumab for patients with recurrent high grade gliomas. *J. Neurooncol.* 139, 625–631. doi: 10.1007/s11060-018-2907-4

Miklja, Z., Yadav, V. N., Cartaxo, R. T., Siada, R., Thomas, C. C., Cummings, J. R., et al. (2020). Everolimus improves the efficacy of dasatinib in PDGFRα-driven glioma. *J. Clin. Invest.* 130, 5313–5325. doi: 10.1172/JCI133310

Paugh, B. S., Broniscer, A., Qu, C., Miller, C. P., Zhang, J., Olson, J. M., et al. (2011). Genome-wide analyses identify recurrent amplifications of receptor tyrosine kinases and cell-cycle regulatory genes in diffuse intrinsic pontine glioma. *J. Clin. Oncol.* 29, 3999–4006. doi: 10.1200/JCO.2011.35.5677

Pollack, I. F., Jakacki, R. I., Blaney, S. M., Hancock, M. L., Kieran, M. W., Phillips, P., et al. (2007). Phase I trial of imatinib in children with newly diagnosed brainstem and recurrent malignant gliomas: A pediatric brain tumor consortium report. *Neuro Oncol.* 9, 145–160. doi: 10.1215/15228517-2006-031

Qu, H. Q., Jacob, K., Fatet, S., Ge, B., Barnett, D., Delattre, O., et al. (2010). Genome-wide profiling using single-nucleotide polymorphism arrays identifies novel chromosomal imbalances in pediatric glioblastomas. *Neuro Oncol.* 12, 153–163. doi: 10.1093/neuonc/nop001

Rao, S. N., Head, M. S., Kulkarni, A., and LaLonde, J. M. (2007). Validation studies of the site-directed docking program LibDock. *J. Chem. Inf. Model.* 47, 2159–2171. doi: 10.1021/ci6004299

Schwark, K., Messinger, D., Cummings, J. R., Bradin, J., Kawakibi, A., Babila, C. M., et al. (2022). Receptor tyrosine kinase (RTK) targeting in pediatric high-grade glioma and diffuse midline glioma: Pre-clinical models and precision medicine. *Front. Oncol.* 12:922928. doi: 10.3389/fonc.2022.922928

Schwartzentruber, J., Korshunov, A., Liu, X. Y., Jones, D. T., Pfaff, E., Jacob, K., et al. (2012). Driver mutations in histone H3.3 and chromatin remodelling genes in paediatric glioblastoma. *Nature* 482, 226–231. doi: 10.1038/nature10833

Stupp, R., Hegi, M. E., Mason, W. P., van den Bent, M. J., Taphoorn, M. J., Janzer, R. C., et al. (2009). Effects of radiotherapy with concomitant and adjuvant temozolomide versus radiotherapy alone on survival in glioblastoma in a randomised phase III study: 5-year analysis of the EORTC-NCIC trial. *Lancet Oncol.* 10, 459–466.

Stupp, R., Mason, W. P., van den Bent, M. J., Weller, M., Fisher, B., Taphoorn, M. J., et al. (2005). Radiotherapy plus concomitant and adjuvant temozolomide for glioblastoma. *N. Engl. J. Med.* 352, 987–996.

Weller, M. (2011). Novel diagnostic and therapeutic approaches to malignant glioma. *Swiss Med. Wkly.* 141:w13210.

Weller, M., Cloughesy, T., Perry, J. R., and Wick, W. (2013). Standards of care for treatment of recurrent glioblastoma–are we there yet? *Neuro Oncol.* 15, 4–27. doi: 10.1093/neuonc/nos273

Wilson, E. A., Russu, W. A., and Shallal, H. M. (2018). Preliminary in vitro and in vivo investigation of a potent platelet derived growth factor receptor (PDGFR) family kinase inhibitor. *Bioorg. Med. Chem. Lett.* 28, 1781–1784. doi: 10.1016/j.bmcl.2018.04.030

Yarla, N. S., Bishayee, A., Sethi, G., Reddanna, P., Kalle, A. M., Dhananjaya, B. L., et al. (2016). Targeting arachidonic acid pathway by natural products for cancer prevention and therapy. *Semin. Cancer Biol.* 40-41, 48–81.

Zhong, S., Wu, B., Yang, W., Ge, J., Zhang, X., Chen, Z., et al. (2021). Effective natural inhibitors targeting poly ADP-ribose polymerase by computational study. *Aging (Albany NY)* 13, 1898–1912.

frontiers | Frontiers in Neuroscience

TYPE Review
PUBLISHED 09 January 2023
DOI 10.3389/fnins.2022.1071314

OPEN ACCESS

EDITED BY
Sheng Zhong,
Sun Yat-sen University Cancer Center, China

REVIEWED BY
Fan Chen,
Universitätsmedizin Greifswald, Germany
Xiujian M. A.,
German Cancer Research Center (DKFZ), Germany
Alessandro Consales,
Giannina Gaslini Institute (IRCCS), Italy

*CORRESPONDENCE
Guoming Luan
✉ luangm@ccmu.edu.cn

SPECIALTY SECTION
This article was submitted to Translational Neuroscience, a section of the journal Frontiers in Neuroscience

RECEIVED 16 October 2022
ACCEPTED 12 December 2022
PUBLISHED 09 January 2023

CITATION
Xie M, Wang X, Duan Z and Luan G (2023) Low-grade epilepsy-associated neuroepithelial tumors: Tumor spectrum and diagnosis based on genetic alterations.
Front. Neurosci. 16:1071314.
doi: 10.3389/fnins.2022.1071314

Low-grade epilepsy-associated neuroepithelial tumors: Tumor spectrum and diagnosis based on genetic alterations

Mingguo Xie[1,2], Xiongfei Wang[1,2], Zejun Duan[3] and Guoming Luan[1,2,4,5]*

[1]Department of Neurosurgery, Epilepsy Center, Sanbo Brain Hospital, Capital Medical University, Beijing, China, [2]Beijing Key Laboratory of Epilepsy, Sanbo Brain Hospital, Capital Medical University, Beijing, China, [3]Department of Pathology, Sanbo Brain Hospital, Capital Medical University, Beijing, China, [4]Beijing Institute for Brain Disorders, Capital Medical University, Beijing, China, [5]Chinese Institute for Brain Research, Beijing, China

Brain tumors can always result in seizures when involving the cortical neurons or their circuits, and they were found to be one of the most common etiologies of intractable focal seizures. The low-grade epilepsy-associated neuroepithelial tumors (LEAT), as a special group of brain tumors associated with seizures, share common clinicopathological features, such as seizure onsets at a young age, a predilection for involving the temporal lobe, and an almost benign course, including a rather slow growth pattern and thus a long-term history of seizures. Ganglioglioma (GG) and dysembryoplastic neuroepithelial tumor (DNET) are the typical representatives of LEATs. Surgical treatments with complete resection of tumors and related epileptogenic zones are deemed the optimal way to achieve postoperative seizure control and lifetime recurrence-free survival in patients with LEATs. Although the term LEAT was originally introduced in 2003, debates on the tumor spectrum and the diagnosis or classification of LEAT entities are still confusing among epileptologists and neuropathologists. In this review, we would further discuss these questions, especially based on the updated classification of central nervous system tumors in the WHO fifth edition and the latest molecular genetic findings of tumor entities in LEAT entities.

KEYWORDS

brain tumor, neuroepithelial, diagnosis, pathology, epilepsy

Introduction

Actually, every brain tumor involving the neocortex or neuronal circuits thereof can result in seizures (Stone et al., 2018b). Brain tumors have been found to be the second most common histopathological diagnosis among the surgical specimens from patients with epilepsy, second to focal cortical dysplasia (FCD) in children and hippocampal sclerosis (HS) in adults (Blumcke et al., 2017). Some brain tumors, however, grow rather slowly and are specifically prone to occurring in young patients and primarily presenting

with seizures (Luyken et al., 2003; Blumcke et al., 2017). The term "long-term epilepsy-associated tumors (LEATs)" was thus originally introduced by Luyken et al. (2003), when recognizing that tumors were more commonly encountered in surgical series of patients who had been treated for drug-resistant epilepsy with such long-term seizure onsets as more than 2 years. Notably, ganglioglioma (GG) and dysembryoplastic neuroepithelial tumor (DNET) are the classical representatives of this category of tumors (Englot et al., 2012; Giulioni et al., 2017). Since then, more and more cases of brain tumors with epilepsy have been reported, and the concept of LEATs has been gradually recognized (Thom et al., 2012; Slegers and Blumcke, 2020). LEATs are the collective name of a group of tumors with different histological features in each entity (Luyken et al., 2003; Thom et al., 2012; Slegers and Blumcke, 2020). Despite the large morphological variability in LEATs, commonalities were also reported as follows: (1) seizure onsets begin at a young age (usually 12–15 years), without significant sex preference (Luyken et al., 2003; Wessling et al., 2015; Blumcke et al., 2017; Giulioni et al., 2017; Faramand et al., 2018); (2) tumors occur with preference of the temporal involvement (approximately 65–80%) of either left or right brain hemisphere (Giulioni et al., 2017; Ristić et al., 2020; Slegers and Blumcke, 2020); and (3) the majority of LEAT entities are mixed glioneuronal tumors (GNT), belonging to benign neoplasms and assigned to WHO grade 1, with rather slow growth patterns and very few cases of malignant progression, and thus accompanied by a long-term seizure history (usually > 2 years) (Luyken et al., 2003; Wessling et al., 2015; Ehrstedt et al., 2017; Pelliccia et al., 2017). Surgical treatments with complete resection of tumors and associated epileptogenic zones (EZ) are recognized as the optimal approach to achieve postoperative seizure control and lifetime recurrence-free survival for patients with LEATs (Luyken et al., 2003; Englot et al., 2012; Blumcke et al., 2017; Shan et al., 2018).

Although relevant in clinical practice, several aspects of the concept of LEATs have been questioned. First of all, the term was originally applied to brain tumors associated with long-term (>2 years) drug-resistant epilepsy (Luyken et al., 2003), but the definition of refractory epilepsy has become less strict since the term was proposed (Wessling et al., 2015; Radhakrishnan et al., 2016; Stone et al., 2018a; Ko et al., 2019). Particularly in children with epilepsy, the strategy of early neuroimaging screening and surgical intervention, if possible, has been encouraged to prevent abnormal brain development and future neurocognitive deficits caused by recurrent seizures (Blümcke et al., 2016; Pelliccia et al., 2017; Vogt et al., 2018). Thus, changing the phrase "long-term" in LEATs to "low-grade" has been proposed, as the majority of LEAT entities are truly low-grade neoplasms (Blümcke et al., 2016; Slegers and Blumcke, 2020). Recently, the term "low-grade developmental epilepsy-associated brain tumors" was also introduced among researchers in recognition of the fact that most LEAT entities belong to developmental glioneuronal tumors, such as GG and DNET, which are rather related to the occurrence of FCD (Palmini et al., 2013; Aronica and Crino, 2014). More specifically, as Blümcke et al. proposed, the definition of LEATs was changed to "low-grade epilepsy-associated neuroepithelial tumors" to indicate such distinguishable pathological features of LEATs as low-grade and neuroepithelial from other groups of tumors with epilepsy (Blumcke et al., 2014; Blümcke et al., 2016; Slegers and Blumcke, 2020). However, this term does not fit into the WHO concept of nosology in tumor classification, which is based on specific cell types, for instance, astrocytoma, pineocytoma, meningioma, etc. (Louis et al., 2016, 2021). In addition, debates on, in particular, the tumor spectrum and the diagnosis or classification of LEAT entities are still controversial and always confusing among epileptologists and neuropathologists (Thom et al., 2012; Blümcke et al., 2016; Slegers and Blumcke, 2020). In the review, we also quoted the nosology of "low-grade epilepsy-associated neuroepithelial tumors," with an abbreviation of LEATs, and we would like to further discuss these debatable aspects of LEATs mentioned above.

The spectrum of brain tumors in LEAT

Since the terminology of LEATs was proposed, a large number of brain tumors with neuroepithelial origination have been included in the tumor spectrum of LEATs (Thom et al., 2012; Phi and Kim, 2019; Slegers and Blumcke, 2020). The tumor spectrum of established LEAT entities is broad and has significantly increased according to the fourth WHO classification update (**Table 1**; Blümcke et al., 2016; Slegers and Blumcke, 2020; Louis et al., 2021). However, except for the established tumors of GG and DNET, other tumors in LEATs are not yet well-recognized due to their rather low incidences, especially from a single center report with limited cases (Blümcke et al., 2016; Blumcke et al., 2017), and thus they are variably reported in the surgical series of LEATs (Luyken et al., 2003; Wessling et al., 2015; Radhakrishnan et al., 2016; Giulioni et al., 2017; Vogt et al., 2018; Ristić et al., 2020), including angiocentric glioma (AG) (Ni et al., 2015; Wang et al., 2020), papillary glioneuronal tumor (PGNT) (Bridge et al., 2013; Pages et al., 2015; Hou et al., 2019), multinodular and vacuolating neuronal tumor (MVNT) (Gonzalez-Quarante et al., 2018; Pekmezci et al., 2018a; Thom et al., 2018; Choi et al., 2019; Gökçe, 2020), isomorphic astrocytoma/isomorphic diffuse glioma (IDG) (Wefers et al., 2020; Appay et al., 2021), pilocytic astrocytoma (PA) (Blümcke et al., 2016), and sometimes including pleomorphic xanthoastrocytoma (PXA) (Weber et al., 2007), diffuse low-grade gliomas (DLGGs) of diffuse astrocytoma (DA) and oligodendroglioma (d-OT) or oligoastrocytoma (d-OA) (Luyken et al., 2003; Vogt et al., 2018; Ius et al., 2020), and the newly diagnosed entity of "polymorphous low-grade neuroepithelial tumor of the young (PLNTY)" (Huse et al., 2017; Louis et al., 2021). Although shared

TABLE 1 The grouping of low-grade gliomas, glioneuronal/neuronal tumors based on the 2021 WHO classification of CNS tumors and the tumor spectrum of LEAT.

Gliomas, glioneuronal tumors, and neuronal tumors	Abbreviation	WHO grading	Traditional LEAT entities	Characteristic genes/Molecular profiles
Part 1. Diffuse glioma				
1. Adult-type diffuse gliomas				
Astrocytoma, IDH-mutant	DA	2/3/4†	N	IDH1, IDH2, ATRX, TP53, and CDKN2A/B
Oligodendroglioma, IDH-mutant, and 1p/19q-codeleted	d-OT	2/3†	N	IDH1, IDH2, 1p/19q, TERT promoter, CIC, FUBP1, and NOTCH1
2. Pediatric-type diffuse gliomas				
2.1 Pediatric-type diffuse low-grade gliomas				
Diffuse astrocytoma, MYB- or MYBL1-altered	p-DA/(IDG)*	1	Y	MYB and MYBL1
Angiocentric glioma	AG	1	Y	MYB
Polymorphous low-grade neuroepithelial tumor of the young	PLNTY	1	Y	BRAF and FGFR family
Diffuse low-grade glioma, MAPK pathway-altered	DLGG*	nd	nd	FGFR1 and BRAF
Part 2. Circumscribed astrocytic gliomas				
Pilocytic astrocytoma	PA	1	Y	KIAA1549-BRAF, BRAF, and NF1
High-grade astrocytoma with piloid features	HGAP	nd	N	BRAF, NF1, ATRX, and CDKN2A/B (methylome)
Pleomorphic xanthoastrocytoma	PXA	2/3†	N	BRAF and CDKN2A/B
Subependymal giant cell astrocytoma	SGCA	1	N	TSC1 and TSC2
Chordoid glioma	CG	2	N	PRKCA
Astroblastoma, MN1-altered	AB	nd	N	MN1
Part 3. Glioneuronal and neuronal tumors				
Ganglioglioma	GG	1/3†	Y	BRAF
Desmoplastic infantile ganglioglioma/astrocytoma	DIG/DIA	1	N	nd
Dysembryoplastic neuroepithelial tumor	DNET	1	Y	FGFR1
Diffuse glioneuronal tumor with oligodendroglioma-like features and nuclear clusters	DGONC	nd	nd	Chromosome 14 (methylome)
Papillary glioneuronal tumor	PGNT	1	Y	PRKCA
Rosette-forming glioneuronal tumor	RGNT	1	N	FGFR1, PIK3CA, and NF1
Myxoid glioneuronal tumor	MGNT	nd	N	PDFGRA
Diffuse leptomeningeal glioneuronal tumor	DLGNT	nd	N	KIAA1549-BRAF fusion, 1p (methylome)
Gangliocytoma	GC	1	N	BRAF
Multinodular and vacuolating neuronal tumor	MVNT	1	Y	MAPK pathway
Dysplastic cerebellar gangliocytoma (Lhermitte-Duclos disease)	DCG (LDD)	1	N	PTEN
Central neurocytoma	CN	2	N	nd
Extraventricular neurocytoma	EVN	2	N	FGFR (FGFR1-TACC1 fusion), IDH-wild-type
Cerebellar liponeurocytoma	CLN	2	N	nd

LEAT, low-grade epilepsy-associated neuroepithelial tumors; nd, not defined; Y, yes; N, no.

*IDG, isomorphic diffuse glioma with MYB or MYBL1 alterations, equally to the new tumor type of "diffuse astrocytoma, MYB- or MYBL1-altered" in Pediatric-type (p-DA) group classified by the 2021 WHO classification; DLGG, diffuse low-grade glioma, MAPK pathway-altered, which as a new tumor type was not defined by WHO panel with specific tumor grading.

†The high WHO grades of 3/4 indicate tumor subtype with anaplasia or malignancy in the new 2021 classification.

clinical features are found in these lesions, arguments still exist in the categorization of which tumor entities are true LEATs (Blümcke et al., 2016; Slegers and Blumcke, 2020). Reviewing the case reports in the literature, the less common tumor entities of AG, PGNT, MVNT, and PA, plus the classical representatives of GG and DNET, are gradually regarded as the traditional members of the LEAT family (Ko et al., 2019; Ristić et al., 2020). However, debates could be found on the remaining entities of PXA, IDG, PLNTY, and even low-grade DA and d-OT/OA, with inconsistent results of the tumor spectrum in the LEAT group from different surgical series (Thom et al., 2012; Phi and Kim, 2019; Slegers and Blumcke, 2020).

Pleomorphic xanthoastrocytomas are an astrocytic tumor that predominantly occurs in children and young adults and usually has a relatively favorable behavior when compared to diffuse glial tumors in adults (Louis et al., 2016; Vaubel et al., 2021). PXAs account for less than 1% of all astrocytic tumors and have a typical superficial meningocerebral location, often with the involvement of the temporal lobe, in nearly 70–80% of cases (Luyken et al., 2003; Blumcke et al., 2017; Giulioni et al., 2017). PXAs are semi-benign brain tumors that share molecular and morphological commonalities with traditional LEATs, such as CD34 immunoreactivity in 73% of cases of PXAs (Thom et al., 2012) and $BRAF^{V600E}$ mutation in 50–75% of analyzed PXAs (Schindler et al., 2011). Recently, a homozygous deletion of CDKN2A/B, corresponding to the loss of 9q21.3, was found as a rather distinctive molecular feature of PXA, regardless of tumor grade or BRAF mutation (Vaubel et al., 2018). Patients with PXAs often present with seizures and are thus frequently represented in epilepsy surgery series within the spectrum of LEATs, accounting for 2% of all brain tumors in epilepsy surgery (Blumcke et al., 2017; Qi et al., 2018). However, some authors did not treat PXA as a true LEAT entity, due to their semi-malignant nature and WHO tumor grading of grade 2 and grade 3 with anaplasia (Slegers and Blumcke, 2020; Vaubel et al., 2021). PXAs are always found with relatively high tumor recurrence and malignant transformation than other entities in LEATs, with 5-year progression-free and overall survival of 59.9–70.9 and 80.8–90.4%, respectively, in grade 2 cases, and with more aggressive behavior and decreased 5-year overall survival of 47.6–57.1% in tumor with anaplasia (Ida et al., 2015; Vaubel et al., 2018, 2021).

Diffuse low-grade gliomas usually refer to DA and d-OT in previous case reports, regardless of age grouping (Phi and Kim, 2019). These tumors are commonly found developing in young adults and involve large areas of the brain cortex and subcortical areas, most notably the frontal lobes (Roberts et al., 2018; Ius et al., 2020). Seizure onsets are the most common manifestation of DLGGs, and nearly 80–90% of patients with DLGGs had seizures (Pallud and McKhann, 2019; Ius et al., 2020). Frequently, however, DLGGs have been excluded from the discussion of epilepsy-associated tumors because the majority of DLGGs correspond to histopathological WHO grade 2 tumors with a far higher rate of infiltration, recurrence, and malignant progression than typical LEATs (Blümcke et al., 2016; Ko et al., 2019; Slegers and Blumcke, 2020). DLGGs are thus considered a true invasive neoplasm that should be dealt with in the oncology field (Duffau, 2018). However, many patients with DLGGs attain long-term survival and subsequently face the same problem of long-standing seizures as patients with LEATs. In fact, many surgical cohorts of epilepsy-associated tumors have included a number of patients with DLGGs in addition to the backbone of the traditional LEAT entities, especially when adolescents or young adults are included (Luyken et al., 2003; Wessling et al., 2015; Radhakrishnan et al., 2016; Vogt et al., 2018). The differences in clinicopathological features between DLGG in adults and children have been highlighted in a variety of surgical series (Luyken et al., 2003; Phi and Kim, 2019; Ius et al., 2020). Particularly, according to the 2021 WHO classification of central nervous system (CNS) tumors, the DLGG have been divided into adult and pediatric types (Louis et al., 2021), and the adult-type DLGG (Astrocytoma, IDH-mutant; Oligodendroglioma, IDH-mutant, and 1p/19q-codeleted) are recognized as truly invasive neoplasms with a higher risk of tumor progression and malignant transformation (Duffau and Taillandier, 2015; Jones et al., 2018; Lombardi et al., 2020). Furthermore, these tumors are more likely to present with symptoms of increased intracranial pressure and/or focal neurological deficits, or with a shorter history of seizures, and thus should be differently treated from tumor entities of LEATs (Phi and Kim, 2019; Lombardi et al., 2020; Young et al., 2020).

In contrast, the pediatric-type DLGG, which includes four tumor types, namely, DA (MYB/MYBL1-altered), AG, PLNTY, and DLGGs (MAPK pathway-altered), is considered benign tumors and assigned as WHO grade 1, and they have been found to be more related to the LEATs (**Table 1**; Slegers and Blumcke, 2020; Louis et al., 2021). For example, the PLNTY was described by Huse et al. (2017) in 2017 as a distinct epileptogenic neoplasm within the spectrum of pediatric, low-grade neuroepithelial tumors. This group of tumors presented in 10 patients with infiltrative growth patterns, a predominant oligodendroglioma-like glial cell component, and intense CD34+ as the most common features. All 10 patients were diagnosed at a young age, with a mean age of 17 years (4–32 years old), with 8/10 seizures, and with 7/10 temporal locations that are similar to LEAT entities (Huse et al., 2017). Molecular analysis revealed a $BRAF^{V600E}$ mutation, FGFR2 fusion, and FGFR3 fusion in 3/8, 3/8, and 1/8 tested tumors, respectively. This kind of tumor is recognized by the WHO panel of CNS tumor classification as a new tumor type, mainly because they represent a high proportion of low-grade oligodendroglial tumors in children and should be distinguished from other low-grade tumors with a distinct DNA analysis (Huse et al., 2017; Riva et al., 2018; Louis et al., 2021).

In addition, the pediatric-type DAs with MYB/MYBL1 alterations have also been reported to be closely related to the

LEATs that are quite different from DAs with IDH mutations in adults (Bergthold et al., 2014; Vogt et al., 2018; Ius et al., 2020). For instance, previous clinical neuropathological studies have found that postoperative tumor progression and recurrence are less often in patients with DAs with a long history of seizures than those with a very short history of seizures (Luyken et al., 2003; Schramm et al., 2004), indicating a tumor subtype presenting with better prognosis in patients with chronic epilepsy, the so-called "isomorphic astrocytoma" (Blümcke et al., 2004), which recently was renamed by Wefers et al. (2020) as "isomorphic diffuse glioma (IDG)," a group of tumors clearly distinct from other glial/glioneuronal brain tumors (Louis et al., 2021). These astrocytoma variants are characterized by a supratentorial, highly differentiated glioma with low cellularity, low proliferation, and focal diffuse brain infiltration. Patients typically had seizures since childhood and were operated on as adults, with excellent progression-free survival after resection (Blümcke et al., 2004; Thom et al., 2012). Interestingly, 77% of IDGs demonstrated MYM/MYBL1 alterations, and all (100%) were IDH-wild-type, which are closely related to pediatric MYB/MYBL1-altered diffuse astrocytomas, according to the WHO fifth edition of CNS tumor classification (Wefers et al., 2020; Louis et al., 2021). Thus, these pediatric-type MYB/MYBL1-altered DAs or IDGs probably represent a distinct group of genetically defined LEATs (Blümcke et al., 2016; Slegers and Blumcke, 2020).

In fact, based on the more biologically and molecularly defined entities of CNS tumors, the 2021 WHO fifth edition classification separated the low-grade neuroepithelial tumors from those with higher infiltration or WHO grading. Furthermore, most of the cortex-involved tumors in the subgroups of "Pediatric-type diffuse low-grade gliomas," "Circumscribed astrocytic gliomas" and "Glioneuronal and neuronal tumors" are regarded as benign entities with a rather slow growth pattern and thus can result in a long-term history of epilepsy that would much relate to the LEATs (**Table 1**; Blümcke et al., 2016; Slegers and Blumcke, 2020; Louis et al., 2021). Indeed, several tumor types have been reported in different surgical cohorts of epilepsy-associated neuroepithelial tumors, such as AG and PLNTY in the subgroup of "Pediatric-type diffuse low-grade gliomas" (Bandopadhayay et al., 2016; Huse et al., 2017; Han et al., 2020), PA and PXA in the subgroup of "Circumscribed astrocytic gliomas" (Wallace et al., 2011; Jones et al., 2013; Collins et al., 2015) and GG, DNET, PGNT, and MVNT in the subgroup of "Glioneuronal and neuronal tumors" (Blümcke et al., 2016; Slegers and Blumcke, 2020; Louis et al., 2021). Herein, we propose that the LEAT entities could be roughly grouped into the three subgroups mentioned above, and any new tumor types found in these subgroups in the future could be potential members of the LEAT family and thus be treated by epilepsy surgery in the neurosurgery department. However, for these tumors, further classification requires precise molecular analyses, notably based on the integration of histopathological and molecular information in a tiered diagnostic format as Louis et al. (2021) had recommended recently. Future studies, especially between multiple epilepsy therapeutic centers, are required to improve and standardize the terminology of LEATs and to extend the use of molecular genetic diagnostic tools over a histomorphology-based classification to specify clinically meaningful tumor entities that could be included in the LEAT spectrum.

Molecular genetic alterations and diagnoses in LEAT

Although the tumor spectrum of LEATs has been widely discussed since nosology was introduced, the histopathological diagnosis and classification of tumors in LEATs remain challenging due to their variable histopathological features (Qaddoumi et al., 2016; Stone et al., 2018a; Slegers and Blumcke, 2020), which include varieties of cellular components, such as astroglia, oligodendroglia, neoplastic or pre-existing neurons, and inflammatory cellular infiltrates, as well as multiple architectural growth patterns, including nodular or cyst growth and even diffuse infiltration of tumor cell clusters at sites distant from the tumor mass with or without calcification (Blümcke and Wiestler, 2002; Thom et al., 2011). In addition, many glioneuronal tumors lack specific histological features that are crucial for the diagnosis of GG or DNET or have mixed histological features in the same specimen. For example, 5–20% of case series have mixed GG and DNET or PXA histological components (Prayson and Napekoski, 2012; Qaddoumi et al., 2016; Faramand et al., 2018; Stone et al., 2018a). Furthermore, LEAT-associated FCD, namely FCD IIIb (Blumcke et al., 2011), is another complex issue in need of clarification, with highly variable proportions of 10–75% (Prayson, 2011; Giulioni et al., 2017; Pelliccia et al., 2017).

To make a more accurate diagnosis or classification of the LEATs, many ways have been tried to assist in tumor diagnosis by purely microscopic inspection of pathological tissue, especially for some tumors with limited tissue specimens from piece-meal resection or by biopsy (Thom et al., 2012; Blümcke et al., 2016). Immunohistochemistry with staining for CD34, P16, S100, MAP2, GFAP, NeuN, and synaptophysin is helpful, but these markers are not so specific (Thom et al., 2012). Recently, combined molecular pathological diagnosis is widely discussed in the LEAT group (**Table 2**; Qaddoumi et al., 2016; Stone et al., 2018a). Simultaneously, the current 2021 WHO classification of CNS tumors has also recommended some specific molecular genetic signatures for the neuropathological diagnosis of low-grade neuroepithelial tumors (**Table 1**; Louis et al., 2016). However, the genetic biomarkers that have been unraveled for LEATs have not yet been systematically reviewed in a large and consecutive cohort of LEATs due to their low

TABLE 2 The molecular genetic alterations in each tumor subtype of LEAT summarized from different case reports in the literature*.

Genetic alterations	$BRAF^{V600E}$ mutations (%)	FGFR1/(2/3) alterations (%)	MYB/MYBL1 (MYB-QKI fusion) (%)	SLC44A1-PRKCA fusion (%)	Other genetic alterations
GG	18.2–57.7% (Sievert et al., 2009; Dougherty et al., 2010; Schindler et al., 2011; Chappé et al., 2013; Dahiya et al., 2013; Koelsche et al., 2013; Ramkissoon et al., 2013; Zhang et al., 2013; Prabowo et al., 2014; Qaddoumi et al., 2016; Pekmezci et al., 2018b)	16% (Huse et al., 2017)	/	/	RAF1 (3%), KRAS (5%), NF1 (3%), FGFR1 (5%), FGFR2 (8%), ABL2 (3%), CDKN2A (8%), and PTEN (3%) (Pekmezci et al., 2018b)
DNET	29.8–51% (Chappé et al., 2013; Prabowo et al., 2014; Ross et al., 2014)	58.1–81.8% (Qaddoumi et al., 2016; Rivera et al., 2016)	/	/	/
AG	13.3% (Qaddoumi et al., 2016)	/	66–100% (Ramkissoon et al., 2013; Bandopadhayay et al., 2016; Qaddoumi et al., 2016)	/	MYB-ESR1 fusion, QKI rearrangement (Qaddoumi et al., 2016)
PGNT	/	/	/	39.3–100% (Pages et al., 2015; Hou et al., 2019)	NOTCH1-PRKCA fusion (Hou et al., 2019)
PXA	60.5–65.5% (Schindler et al., 2011; Ida et al., 2015; Vaubel et al., 2018)	/	/	/	CDKN2A/B (83 and 93%) (Weber et al., 2007)
MVNT	25% (BRAF not V600E) (Pekmezci et al., 2018a)	12.5–14.3% (FGFR2) (Pekmezci et al., 2018a; Choi et al., 2019)	/	/	MAP2K1,(Pekmezci et al., 2018a) DEPDC5, SMO, and TP53 (Thom et al., 2018)
IDG	/	/	77% (54%, MYBL1; 23%, MYB) (Wefers et al., 2020)	/	/
PLNTY	37.5% (Huse et al., 2017)	12.5–37.5% (12.5%, FGFR3; 37.5%, FGFR2) (Huse et al., 2017)	/	/	/
PA	9.3% (33%, extra-cerebellar) (Schindler et al., 2011)	/	/	/	NF1, KRAS, the NTRK family, and FGFR1 (Jones et al., 2013; Zhang et al., 2013)
DA	17–29% (Ramkissoon et al., 2013; Zhang et al., 2013; Cruz et al., 2014; Roth et al., 2014; Qaddoumi et al., 2016)	17% (Zhang et al., 2013)	26–41% (Ramkissoon et al., 2013; Zhang et al., 2013; Qaddoumi et al., 2016)	/	/
d-OT	8% (Zhang et al., 2013)	40–69% (Zhang et al., 2013; Qaddoumi et al., 2016)	8% (Zhang et al., 2013)	/	/

AG, angiocentric glioma; DA, diffuse astroglioma; DNET, dysembryoplastic neuroepithelial tumor; d-OT, diffuse oligodendroglioma; GG, ganglioglioma; IDG, isomorphic diffuse glioma; LEAT, low-grade epilepsy associated neuroepithelial tumors; MVNT, multinodular and vacuolated neuronal tumor; PA, pilocytic astrocytoma; PGNT, papillary glioneuronal tumor; PXA, pleomorphic xanthoastrocytoma; PLNTY, polymorphous low-grade neuroepithelial tumor of the young.

*The molecular genetic alterations with their incidences were found in each tumor entity of LEAT and DA/d-OT from different reports in the literature, and the DA and d-OT include tumors occurring both in pediatric and adult groups thus the real rates of genetic alteration might be compromised in previous reports.

incidences. Meanwhile, parts of the molecular genetic signatures are shared by more than one tumor type (**Table 2**). This dilemma finally contributes to the long-lasting challenge of achieving a reliable differential diagnosis of tumors in the LEAT group (Horbinski et al., 2011; Blümcke et al., 2016). Thus, as Louis et al. (2014, 2021) have recommended, it requires the integration of histopathological and molecular information in a tiered diagnostic format for precisely differentiating the diagnosis and classification of tumors, also in the LEAT group. Herein, we exclusively conclude the recent findings that are helpful to make a more accurate diagnosis or classification of LEATs, including the histological and molecular genetic aspects of each entity.

$BRAF^{V600E}$ mutations in GG

The GG is a well-differentiated, slowly growing neuroepithelial tumor, with its biphasic composition of glial and neuronal cell elements first introduced by Perkins OC in 1926 (Wolf et al., 1994; Blümcke et al., 2016). GGs are the most common epilepsy-associated neoplasms that account for 50–60% of brain tumors in epileptic patients but only 1–2% of all primary brain tumors, and they are recognized by the WHO as a grade 1 tumor or a grade 3 tumor with anaplasia (Louis et al., 2016; Blumcke et al., 2017).

The $BRAF^{V600E}$ mutation was found to be significantly related to GG, but different rates of $BRAF^{V600E}$ mutation were reported from previous series of GG in surgical specimens, ranging from 18 to 56% (Sievert et al., 2009; Dougherty et al., 2010; Schindler et al., 2011; Chappé et al., 2013; Dahiya et al., 2013; Koelsche et al., 2013; Ramkissoon et al., 2013; Zhang et al., 2013; Prabowo et al., 2014; Pekmezci et al., 2018b). Interestingly, Koh et al. (2018) further confirmed the pathogenic role of the $BRAF^{V600E}$ mutation in an animal model that $BRAF^{V600E}$ induced epileptogenesis in the neuronal lineage and tumorigenesis in the glial lineage. Since the first $BRAF^{V600E}$-specific antibody was reported in 2011 (clone VE1) (Capper et al., 2011), it has been widely used nowadays to screen for $BRAF^{V600E}$ mutations in the diagnostic work-up of tissue specimens. In particular, several clinicopathological features, such as seizure onset, tumor progression, and postoperative seizure outcome, have been investigated in relation to BRAF mutations. For example, Vornetti et al. (2017) found multiple seizure types were present in patients with LEATs and $BRAF^{V600E}$ mutation but none with the $BRAF^{V600E}$ wild type ($p = 0.035$); Dahiya et al. (2013) and Chen et al. (2017) found the worse recurrence-free survival was related to the $BRAF^{V600E}$ mutation in GG cohorts. Furthermore, Prabowo et al. (2015) investigated a cohort of GNTs with $BRAF^{V600E}$ mutations detected in 38/93 (40.8%) GGs and 23/77 (29.8%) DNETs by immunohistochemistry and found the expression of $BRAF^{V600E}$ was associated with a worse postoperative seizure outcome in GNTs ($p < 0.001$). However, other case reports did not find any significant associations of BRAF mutations with patient age, seizure onset, tumor progression or recurrence, and seizure outcome (Shen et al., 2017; Vornetti et al., 2017; Pekmezci et al., 2018b; Stone et al., 2018a). Thus, further studies are required to investigate the possible role of $BRAF^{V600E}$ mutations, such as being a prognostic marker of tumor behavior and seizure outcome, in epilepsy-associated tumors (Martinoni et al., 2015).

It is noteworthy that the $BRAF^{V600E}$ mutation is not much specific to GG. As reported by Pekmezci et al., the $BRAF^{V600E}$ mutation was screened in a cohort of 1320 nervous system tumors, and the mutation was found more frequently in PXA (66%) than WHO grade 1 GG (18%) and PA (9%) (Schindler et al., 2011). In addition, DNET (30–50%) (Chappé et al., 2013; Prabowo et al., 2014; Ross et al., 2014), AG (13%) (Qaddoumi et al., 2016), DA (17–29%) (Zhang et al., 2013; Cruz et al., 2014; Roth et al., 2014), and d-OT (8%) (Zhang et al., 2013) also share the $BRAF^{V600E}$ alteration (**Table 2**). In addition, many other genetic alterations, but without IDH1/2, have also been described in GG, among which genetic alterations of the MAP kinase signaling pathway are most prominent (Horbinski et al., 2011). In a study of 40 GGs by Pekmezci et al. (2018b), for example, RAF1 (3%), KRAS (5%), NF1 (3%), FGFR1 (5%), FGFR2 (8%), ABL2 (3%), CDKN2A (8%), and PTEN (3%) were detected. Although the $BRAF^{V600E}$ mutation could not be a such specific diagnostic marker in the genetic panel of brain tumors as GG, the differential diagnosis of GG can be established with the combination of its histological features with CD34 immunoreactive, $BRAF^{V600E}$ mutation and IDH1/2 wild type (Blümcke et al., 2016; Slegers and Blumcke, 2020).

FGFR1 alterations in DNET

The DNET was originally described by Daumas-Duport et al. (1988), and it is histologically composed of a simple form with a unique glioneuronal element or a complex form with both glial nodules and glioneuronal elements, corresponding to WHO grade 1 (Blümcke et al., 2016; Louis et al., 2016). DNETs are the second most prevalent tumors associated with chronic or drug-resistant epilepsy and are frequently represented in the LEAT series, approximately 30–50% (Radhakrishnan et al., 2016; Faramand et al., 2018; Slegers and Blumcke, 2020).

FGFR1 gene alterations in DNET were first reported by Zhang et al. (2013). A more comprehensive study revealed FGFR1 alterations in 18 of 22 DNETs (82%), including 9 tyrosine kinase domain duplications, 8 missense single nucleotide variants, and 8 FGFR1-TACC fusions (Qaddoumi et al., 2016). Rivera et al. (2016) confirmed the above findings and showed 12 FGFR1 tyrosine kinase domain duplications, 10 point mutations, and 3 breakpoints in 25 of 43 DNETs (58%). However, FGFR1 alterations are also shared by other neuroepithelial tumors in various proportions, such as GG (16%) (Stone et al., 2018a), DA (17%) (Zhang et al., 2013), and d-OT (40–69%) (Zhang et al., 2013; Qaddoumi et al., 2016). In addition, $BRAF^{V600E}$ alteration was also frequently documented in 30–51% of DNETs (**Table 2**), but without IDH1/2 mutation (Thom et al., 2011). Even so, the diagnosis of DNET, as with GG, can be established with the combination of its histological features with FGFR1 alterations, the $BRAF^{V600E}$ mutation, and IDH1/2 wild type (Thom et al., 2011; Blümcke et al., 2016; Slegers and Blumcke, 2020).

MYB fusions in AG

The AG represents a rare, slowly growing cerebral glial tumor that has been recognized by the WHO as a grade 1 tumor (Blümcke et al., 2016). AGs often occur in children and young adults and are more frequently identified in the setting of chronic epilepsy, but only account for 0.5% of all epileptic patients with brain tumors (Blumcke et al., 2017; Han et al., 2020). AGs often involve the frontoparietal

and temporal lobes and histopathologically are characterized by perivascular pseudorosettes with an ependymoma-like appearance (Bandopadhayay et al., 2016; Louis et al., 2016).

MYB fusions have been reported as rare events in pediatric low-grade gliomas and were first described in a total of 9 tumors of which two were AG (Zhang et al., 2013). This has been confirmed by Qaddoumi et al. (2016), who studied 15 AGs, and identified recurrent MYB alterations in all AGs assayed. Of the 15 cases analyzed, 13 (87%) possessed a MYB-QKI fusion, while the remaining 2 possessed a MYB-ESR1 fusion and a QKI rearrangement, respectively (Qaddoumi et al., 2016). The prevalence of MYB alterations in AG was repeated in a subsequent cohort of 19 tumors, all of which harbor MYB-QKI fusions (Bandopadhayay et al., 2016). This study also demonstrated that MYB-QKI fusion was able to drive tumorigenesis *via* simultaneous activation of MYB as a result of enhancer translocation combined with the loss of the tumor suppressor activity of QKI. Taken together, these data suggest that MYB abnormalities are sufficient as a specific and single-driver event in AG (Blümcke et al., 2016; Stone et al., 2018b). However, shared mutations of MYB/MYBL1 abnormalities can occur in other low-grade neuroepithelial tumors, including DA (26–41%) (Ramkissoon et al., 2013; Zhang et al., 2013; Qaddoumi et al., 2016), d-OT (8%) (Zhang et al., 2013), IDG (77%), MYBL1 (54%), MYB (23%) (Wefers et al., 2020), and DNET (in one case) (Zhang et al., 2013). In addition, Qaddoumi et al. (2016) found two tumors of AG with a MYB-QKI fusion also harbored a $BRAF^{V600E}$ mutation (2/15) (**Table 2**).

PRKCA translocations in PGNT

The PGNT is a rare glioneuronal tumor first described in 1997 and was recognized in the WHO 2007 classification as an entity distinct from GG (Komori et al., 1998; Blümcke et al., 2016). PGNTs tend to be tumors of young adults with a mean age at presentation of 25.9 years (ranging from 4 to 75 years) (Hou et al., 2019; Slegers and Blumcke, 2020). A history of seizures was recorded in 30–50% of the reported PGNTs, and they approximately account for 0.1% of the epilepsy-associated brain tumors (Blumcke et al., 2017). PGNTs are composed of GFAP-positive astrocytes, lining hyalinized vascular pseudopapillae, SYN-positive, interpapillary collections of sheets of neurocytes, neurons, and "ganglioid" cells, attributed to WHO grade 1 (Thom et al., 2012; Pages et al., 2015; Blümcke et al., 2016).

Recently, a fusion of SLC44A1 and PRKCA, which encodes a protein kinase C involved in the MAP kinase signaling pathway, has been described in several studies (Bridge et al., 2013; Pages et al., 2015; Hou et al., 2019). Bridge et al. (2013) identified a recurrent chromosomal translocation *t*(9;17)(q31;q24), with a resultant oncogenic fusion protein SLC44A1-PRKCA, in three PGNTs. Pages et al. (2015) analyzed 4 pediatric PGNTs and 15 PGNT mimics. SLC44A1-PRKCA fusion occurred in all PGNTs, but none of the PGNT mimics, and all PGNTs were negative for BRAF and FGFR1 mutations. More recently, Hou et al. (2019) looked at 28 PGNTs using DNA methylation analysis and revealed that 11/28 of the tumors were true PGNT with a canonical SLC44A1-PRKCA fusion and the remainder of 17/28 tumors were other types of tumors due to previous incorrect histological classification, but an alteration of NOTCH1-PRKCA fusion was also found in PGNT (**Table 2**). These results reported in previous studies suggest that SLC44A1-PRKCA fusion can be a specific characteristic of PGNT with a high diagnostic value and be detectable by fluorescence *in situ* hybridization (FISH). Notwithstanding, further studies with molecular genetic information analyzed in a large case series of PGNT are still necessary to identify these genetic alterations.

Genetic alterations in MVNT

The MVNT was originally described by Huse et al. (2013) in 10 patients, which was subsequently confirmed by Bodi et al. (2014) in two additional patients. MVNTs are defined currently by the WHO as benign tumors (WHO grade 1) associated with seizures, predominately in the temporal lobe (Blumcke et al., 2017; Louis et al., 2021). These tumors are featured by clustering in multiple small nodules of vacuolating neuronal tumor cells and lacking cell proliferation and infiltration (Blümcke et al., 2016; Pekmezci et al., 2018a; Thom et al., 2018).

In a cohort of 7 MVNTs, no $BRAF^{V600E}$ mutations were found, but one case showed a FGFR2 fusion (Choi et al., 2019). In another cohort of 8 MVNTs, genetic alterations were found in BRAF other than V600E, MAP2K1, and FGFR2 in 2/8, 5/8, and 1/8 of cases, respectively (Pekmezci et al., 2018a). Interestingly, all of these genetic alterations are converging on the activation of the MAP kinase signaling pathway and are found to be related to the tumorigenesis and the resultant epileptogenesis (Koh et al., 2018; Delev et al., 2020; Drosten and Barbacid, 2020). Particularly, all cases of MVNT in previous reports with the molecular analysis are absent in $BRAF^{V600E}$ mutations (**Table 2**; Thom et al., 2018; Choi et al., 2019). In addition, in a recent cohort of 10 MVNT cases, no mutations in FGFR1 or MYB were identified (Thom et al., 2018). Thus, given the prevalence of mutations affecting $BRAF^{V600E}$, FGFR1, and MYB in other entities of LEATs, the absence of these genetic alterations in MVNT may be helpful to differentiate these tumors (Stone et al., 2018b). However, due to the diverse and limited molecular findings reported in the literature, more studies are needed to further understand the molecular genetics and etiology of this rare neoplasm (Stone et al., 2018b; Slegers and Blumcke, 2020).

In summary, genetic alterations detected in LEAT entities involve and connect two major signaling pathways, namely, the mitogen-activated protein kinase (MAPK) pathway and the mammalian target of rapamycin (mTOR) pathway (**Figure 1**; Blümcke et al., 2016; Pernice et al., 2016; Delev et al., 2020). For example, FGFR1 as receptor signaling at upstream of both pathways has been identified in DNETs with FGFR1 alterations; BRAF as a substrate further downstream of the

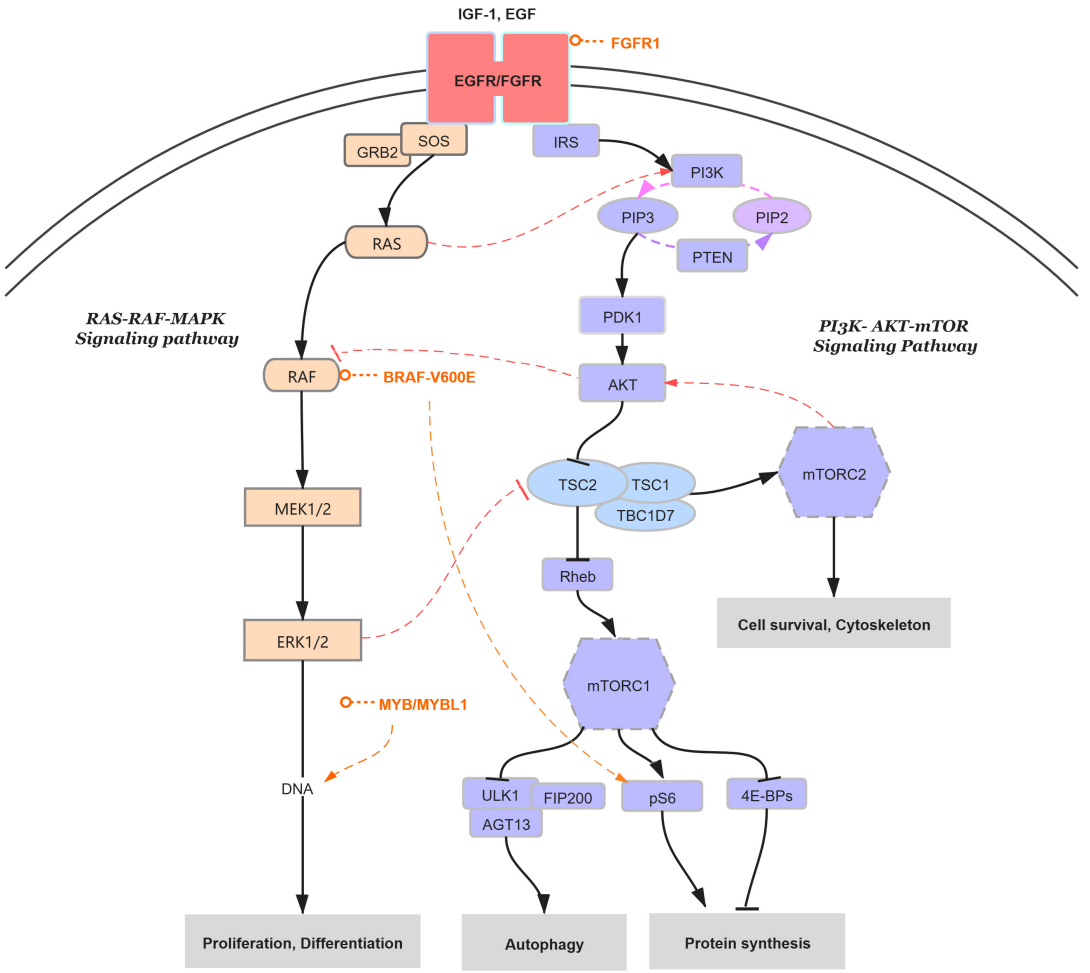

FIGURE 1
RAS-RAF-MAPK signaling pathway with molecular genetic alterations affected in LEATs. Genetic alterations detected in LEAT entities mainly involve two signaling cascades, namely, RAS-RAF-MAPK (left/pink) and PI3K-AKT-mTOR (right/blue). Signals begin at the insulin-like growth factor-1 (IGF-1) receptor at the cell surface, as well as the epidermal growth factor (EGF) receptor, and transmit to the downstream canonical cascades of the MAPK pathway (through RAS, RAF, and MEK1/2 to ERK1/2) and the mTOR pathway (through PI3K, PDK-1, AKT, and TSC1-TSC2-TBC1D7 complex to mTORC1/2). The specific genetic alterations are listed in the figure (light red), including the FGFR1 alteration and $BRAF^{V600E}$ mutation detected in GG and DNET and the MYB/MYBL1 fusions found in AG and IDG, with the activation of the RAS-RAF-MAPK signaling pathway to control DNA transcriptions for cell proliferation and differentiation. In particular, the MAPK pathway activation is regulated by substrates of the PI3K-AKT-mTOR signaling cascade, which, in turn, was controlled by the components from RAS-RAF-MAPK cascades to determine the protein synthesis (dashed lines).

RAS-RAF-MAPK signaling cascade have been described in GG and DNET with $BRAF^{V600E}$ mutations, which were always accompanied by the activation of mTOR signaling cascade with increased phosphorylated ribosomal S6 protein (pS6) (LaSarge and Danzer, 2014; Prabowo et al., 2014; Ehrstedt et al., 2020); in addition, c-MYB/MYBL1, as one of the regulated transcription factors of both signaling cascades, have also been demonstrated in IDG and AG with MYB-QKI fusion (Blümcke et al., 2016; Qaddoumi et al., 2016; Slegers and Blumcke, 2020). Particularly, the MAP kinase activation can be regulated by substrates of the PI3K-AKT-mTOR signaling cascade and vice versa, which have been identified as more related to focal malformations of cortical development (MCD), such as tuberous sclerosis complex (TSC), hemimegalencephaly, and FCD (Crino, 2015; Pernice et al., 2016). Interestingly, LEAT entities are also found to be closely related to the occurrence of MCD (Thom et al., 2012; Giulioni et al., 2017). In addition, molecular alterations of CD34 expression and BRAF mutation are often concurrently met in low-grade tumors, such as GG, DNT, and PXA. However, the relationships between CD34 expression and the BRAF mutation were still unknown in previous studies. Studies with molecular genetic information analyzed in a large case cohort of LEATs in the future are still required to further identify the genetic alterations and interactions of the two major signaling pathways (Blümcke et al., 2016), as well as the relationships between CD34 expression and the BRAF mutation.

The epileptogenesis and surgical management of LEATs

Brain tumors result in 6–15% of seizure onsets in patients with epilepsy and 24–27% of focal seizures (Blumcke et al., 2017; Ertürk Çetin et al., 2017). Although our knowledge of molecular pathways driving neoplastic cell growth and malignant progression has gradually matured, the issues of why and how a seizure occurs in a patient with a brain tumor still need to be clarified (Slegers and Blumcke, 2020; Natale et al., 2021). Two main hypotheses have been proposed previously, namely, the tumor-centric and the epilepsy-centric approaches (van Breemen et al., 2007; Pallud et al., 2013). The tumor-centric approach states that the epileptic activity derives from the tumor itself, which was recently confirmed by the experimental work of Koh et al. (2018) in neurons transfected with the $BRAF^{V600E}$ mutation *in vivo*. In addition, nearly half of patients would have seizure onsets completely controlled after the tumor resection alone (Englot et al., 2012; Bonney et al., 2015). The epilepsy-centric approach provides evidence that the infiltrated peritumoral neocortex is key for tumor-related epileptic activity, due to metabolic imbalances of glioma-related glutamatergic and γ-aminobutyric acid changes leading to epileptogenicity (Lee et al., 2007; Yuen et al., 2012; Pallud et al., 2013; Neal et al., 2016). In fact, many alterations have been found in human peritumoral brain tissue that has the potential to dramatically alter neuronal and glial homeostasis and the microenvironment and thus result in an epileptogenic state (Stone et al., 2018b; Maschio et al., 2019; Thomas and Pierson, 2020; Zhang et al., 2020).

These two epileptogenic hypotheses lead to another important issue of how to achieve complete seizure control after surgery (Stone et al., 2018b). However, LEATs were among the best candidates for complete postoperative seizure control, and approximately 75–90% of patients could get seizure-free after surgery (Luyken et al., 2003; Slegers and Blumcke, 2020). Planning for epilepsy surgery needs to take into consideration, therefore, any MRI-visible lesion as well as resecting of the ictal onset zone (Maschio et al., 2019). After all, a better seizure control was always documented in patients with the extensive resection of tumor and peritumoral EZ, which thus satisfies the surgical demands of both tumor-centric and epilepsy-centric approaches (Englot et al., 2012; Bonney et al., 2015; Shan et al., 2018).

Discussion

The LEATs, as a distinct group of epilepsy-associated brain tumors, share common clinicopathological characteristics. Although the GG, DNET, AG, PGNT, MVNT, and PA are deemed the typical tumor entities in the LEAT spectrum, other new tumor entities, especially in the 2021 WHO edition of CNS tumors, are gradually being recognized with close association with LEATs, such as PLGTY and IDG (or pediatric-type diffuse astrocytoma with MYB/MYBL1 alteration), which, however, should be further identified in large cohorts. The LEAT entities always have a rather slow growth pattern, thus accompanying a long-term history of seizures, and complete seizure control with lifetime recurrence-free survival can be achieved after surgical resection. However, the histopathological heterogeneities of both morphological and cellular elements in LEAT entities always confuse neuropathologists, and thus the diagnosis of a specific neoplasm needs to combine the histomorphological features with the specific molecular genetic markers in each tumor, such as $BRAF^{V600E}$, FGFR1, MYB, and PRKCA alterations. Notwithstanding, more collaborations, especially between multiple epilepsy therapeutic centers, should be underlined to improve and standardize the criteria and terminology of LEATs and to extend the use of molecular genetic diagnostic tools over a histomorphology-based classification to specify clinically meaningful tumor entities within the LEAT spectrum when considering the low incidence of these lesions. In addition, although several clinicopathological features, such as tumor progression and postoperative seizure outcome, have been reported related to molecular markers, especially, BRAF mutations, future studies are also needed to confirm these data in a larger, well-matched cohort of LEATs and to further investigate possible relationships between clinicopathological features and other molecular markers of LEAT entities as well.

Author contributions

MX and GL wrote the manuscript. MX, XW, and ZD analyzed and interpreted the patient data regarding epilepsy-associated neuroepithelial tumors from the literature and our institute. All authors read and approved the final manuscript.

Funding

This work was supported by the Chinese Institute for Brain Research (Beijing) Scientific Research Open Cooperation Program (2020-NKX-XM-02) and the Major Project of National Natural Science Foundation of China (81790654).

Conflict of interest

The authors declare that the research was conducted in the absence of any commercial or financial relationships that could be construed as a potential conflict of interest.

Publisher's note

References

Appay, R., Tauziède-Espariat, A., Silva, K., Fritih, R., Scavarda, D., Delteil, C., et al. (2021). [Low grade glioma with MYBL1 alteration: Case report of an uncommon pediatric neoplasm]. *Ann. Pathol.* 41, 129–133. doi: 10.1016/j.annpat.2020.07.003

Aronica, E., and Crino, P. B. (2014). Epilepsy related to developmental tumors and malformations of cortical development. *Neurotherapeutics* 11, 251–268. doi: 10.1007/s13311-013-0251-0

Bandopadhayay, P., Ramkissoon, L. A., Jain, P., Bergthold, G., Wala, J., Zeid, R., et al. (2016). MYB-QKI rearrangements in angiocentric glioma drive tumorigenicity through a tripartite mechanism. *Nat. Genet.* 48, 273–282. doi: 10.1038/ng.3500

Bergthold, G., Bandopadhayay, P., Bi, W. L., Ramkissoon, L., Stiles, C., Segal, R. A., et al. (2014). Pediatric low-grade gliomas: How modern biology reshapes the clinical field. *Biochim. Biophys. Acta* 1845, 294–307. doi: 10.1016/j.bbcan.2014.02.004

Blümcke, I., Aronica, E., Becker, A., Capper, D., Coras, R., Honavar, M., et al. (2016). Low-grade epilepsy-associated neuroepithelial tumours - the 2016 WHO classification. *Nat. Rev. Neurol.* 12, 732–740. doi: 10.1038/nrneurol.2016.173

Blumcke, I., Aronica, E., Urbach, H., Alexopoulos, A., and Gonzalez-Martinez, J. A. (2014). A neuropathology-based approach to epilepsy surgery in brain tumors and proposal for a new terminology use for long-term epilepsy-associated brain tumors. *Acta Neuropathol.* 128, 39–54. doi: 10.1007/s00401-014-1288-9

Blümcke, I., Luyken, C., Urbach, H., Schramm, J., and Wiestler, O. D. (2004). An isomorphic subtype of long-term epilepsy-associated astrocytomas associated with benign prognosis. *Acta Neuropathol.* 107, 381–388. doi: 10.1007/s00401-004-0833-3

Blumcke, I., Spreafico, R., Haaker, G., Coras, R., Kobow, K., Bien, C. G., et al. (2017). Histopathological findings in brain tissue obtained during epilepsy surgery. *N. Engl. J. Med.* 377, 1648–1656. doi: 10.1056/NEJMoa1703784

Blumcke, I., Thom, M., Aronica, E., Armstrong, D. D., Vinters, H. V., Palmini, A., et al. (2011). The clinicopathologic spectrum of focal cortical dysplasias: A consensus classification proposed by an ad hoc task force of the ILAE diagnostic methods commission. *Epilepsia* 52, 158–174. doi: 10.1111/j.1528-1167.2010.02777.x

Blümcke, I., and Wiestler, O. D. (2002). Gangliogliomas: An intriguing tumor entity associated with focal epilepsies. *J. Neuropathol. Exp. Neurol.* 61, 575–584. doi: 10.1093/jnen/61.7.575

Bodi, I., Curran, O., Selway, R., Elwes, R., Burrone, J., Laxton, R., et al. (2014). Two cases of multinodular and vacuolating neuronal tumour. *Acta Neuropathol. Commun.* 20, 2–7. doi: 10.1186/2051-5960-2-7

Bonney, P. A., Glenn, C. A., Ebeling, P. A., Conner, A. K., Boettcher, L. B., Cameron, D. M., et al. (2015). Seizure freedom rates and prognostic indicators after resection of gangliogliomas: A review. *World Neurosurg.* 84, 1988–1996. doi: 10.1016/j.wneu.2015.06.044

Bridge, J. A., Liu, X. Q., Sumegi, J., Nelson, M., Reyes, C., Bruch, L. A., et al. (2013). Identification of a novel, recurrent SLC44A1-PRKCA fusion in papillary glioneuronal tumor. *Brain Pathol.* 23, 121–128. doi: 10.1111/j.1750-3639.2012.00612.x

Capper, D., Preusser, M., Habel, A., Sahm, F., Ackermann, U., Schindler, G., et al. (2011). Assessment of BRAF V600E mutation status by immunohistochemistry with a mutation-specific monoclonal antibody. *Acta Neuropathol.* 122, 11–19. doi: 10.1007/s00401-011-0841-z

Chappé, C., Padovani, L., Scavarda, D., Forest, F., Nanni-Metellus, I., Loundou, A., et al. (2013). Dysembryoplastic neuroepithelial tumors share with pleomorphic xanthoastrocytomas and gangliogliomas BRAF(V600E) mutation and expression. *Brain Pathol.* 23, 574–583. doi: 10.1111/bpa.12048

Chen, X., Pan, C., Zhang, P., Xu, C., Sun, Y., Yu, H., et al. (2017). BRAF V600E mutation is a significant prognosticator of the tumour regrowth rate in brainstem gangliogliomas. *J. Clin. Neurosci.* 46, 50–57. doi: 10.1016/j.jocn.2017.09.014

Choi, E., Kim, S. I., Won, J. K., Chung, C. K., Kim, S. K., Choi, S. H., et al. (2019). Clinicopathological and molecular analysis of multinodular and vacuolating neuronal tumors of the cerebrum. *Hum. Pathol.* 86, 203–212. doi: 10.1016/j.humpath.2018.11.028

Collins, V. P., Jones, D. T., and Giannini, C. (2015). Pilocytic astrocytoma: Pathology, molecular mechanisms and markers. *Acta Neuropathol.* 129, 775–788. doi: 10.1007/s00401-015-1410-7

Crino, P. B. (2015). mTOR signaling in epilepsy: Insights from malformations of cortical development. *Cold Spring Harb. Perspect. Med.* 5:a022442. doi: 10.1101/cshperspect.a022442

Cruz, G. R., Dias Oliveira, I., Moraes, L., Del Giudice Paniago, M., de Seixas Alves, M. T., Capellano, A. M., et al. (2014). Analysis of KIAA1549-BRAF fusion gene expression and IDH1/IDH2 mutations in low grade pediatric astrocytomas. *J. Neurooncol.* 117, 235–242. doi: 10.1007/s11060-014-1398-1

Dahiya, S., Haydon, D. H., Alvarado, D., Gurnett, C. A., Gutmann, D. H., and Leonard, J. R. (2013). BRAF(V600E) mutation is a negative prognosticator in pediatric ganglioglioma. *Acta Neuropathol.* 125, 901–910. doi: 10.1007/s00401-013-1120-y

Daumas-Duport, C., Scheithauer, B. W., Chodkiewicz, J. P., Laws, E. R. Jr., and Vedrenne, C. (1988). Dysembryoplastic neuroepithelial tumor: A surgically curable tumor of young patients with intractable partial seizures. Report of thirty-nine cases. *Neurosurgery* 23, 545–556. doi: 10.1227/00006123-198811000-00002

Delev, D., Daka, K., Heynckes, S., Gaebelein, A., Franco, P., Pfeifer, D., et al. (2020). Long-term epilepsy-associated tumors: Transcriptional signatures reflect clinical course. *Sci. Rep.* 10:96. doi: 10.1038/s41598-019-56146-y

Dougherty, M. J., Santi, M., Brose, M. S., Ma, C., Resnick, A. C., Sievert, A. J., et al. (2010). Activating mutations in BRAF characterize a spectrum of pediatric low-grade gliomas. *Neurooncology* 12, 621–630. doi: 10.1093/neuonc/noq007

Drosten, M., and Barbacid, M. (2020). Targeting the MAPK pathway in KRAS-driven tumors. *Cancer Cell* 37, 543–550. doi: 10.1016/j.ccell.2020.03.013

Duffau, H. (2018). Diffuse low-grade glioma, oncological outcome and quality of life: A surgical perspective. *Curr. Opin. Oncol.* 30, 383–389. doi: 10.1097/cco.0000000000000483

Duffau, H., and Taillandier, L. (2015). New concepts in the management of diffuse low-grade glioma: Proposal of a multistage and individualized therapeutic approach. *Neurooncology* 17, 332–342. doi: 10.1093/neuonc/nou153

Ehrstedt, C., Ahlsten, G., Strömberg, B., Lindskog, C., and Casar-Borota, O. (2020). Somatostatin receptor expression and mTOR pathway activation in glioneuronal tumours of childhood. *Seizure* 76, 123–130. doi: 10.1016/j.seizure.2020.01.011

Ehrstedt, C., Moreira, N. C., Casar-Borota, O., Strömberg, B., and Ahlsten, G. (2017). Glioneuronal tumors in childhood - before and after surgery. A long-term follow-up study. *Epilepsy Behav.* 72, 82–88. doi: 10.1016/j.yebeh.2017.02.012

Englot, D. J., Berger, M. S., Barbaro, N. M., and Chang, E. F. (2012). Factors associated with seizure freedom in the surgical resection of glioneuronal tumors. *Epilepsia* 53, 51–57. doi: 10.1111/j.1528-1167.2011.03269.x

Ertürk Çetin, Ö., İşler, C., Uzan, M., and Özkara, Ç (2017). Epilepsy-related brain tumors. *Seizure* 44, 93–97. doi: 10.1016/j.seizure.2016.12.012

Faramand, A. M., Barnes, N., Harrison, S., Gunny, R., Jacques, T., Tahir, M. Z., et al. (2018). Seizure and cognitive outcomes after resection of glioneuronal tumors in children. *Epilepsia* 59, 170–178. doi: 10.1111/epi.13961

Giulioni, M., Marucci, G., Pelliccia, V., Gozzo, F., Barba, C., Didato, G., et al. (2017). Epilepsy surgery of "low grade epilepsy associated neuroepithelial tumors": A retrospective nationwide Italian study. *Epilepsia* 58, 1832–1841. doi: 10.1111/epi.13866

Gökçe, E. (2020). Magnetic resonance imaging findings of two cases with multinodular and vacuolating neuronal tumor. *Acta Neurol. Belg.* 120, 457–461. doi: 10.1007/s13760-017-0872-x

Gonzalez-Quarante, L. H., Ruiz-Juretschke, F., Sola Vendrell, E., Gil de Sagredo Del Corral, O. L., Agarwal, V., and Garcia-Leal, R. (2018). Multinodular and vacuolating neuronal tumor of the cerebrum. A rare entity. New case and review of the literature. *Neurocirugia* 29, 44–55. doi: 10.1016/j.neucir.2017.08.003

Han, G., Zhang, J., Ma, Y., Gui, Q., and Yin, S. (2020). Clinical characteristics, treatment and prognosis of angiocentric glioma. *Oncol. Lett.* 20, 1641–1648. doi: 10.3892/ol.2020.11723

Horbinski, C., Kofler, J., Yeaney, G., Camelo-Piragua, S., Venneti, S., Louis, D. N., et al. (2011). Isocitrate dehydrogenase 1 analysis differentiates gangliogliomas from infiltrative gliomas. *Brain Pathol.* 21, 564–574. doi: 10.1111/j.1750-3639.2011.00480.x

Hou, Y., Pinheiro, J., Sahm, F., Reuss, D. E., Schrimpf, D., Stichel, D., et al. (2019). Papillary glioneuronal tumor (PGNT) exhibits a characteristic methylation profile and fusions involving PRKCA. *Acta Neuropathol.* 137, 837–846. doi: 10.1007/s00401-019-01969-2

Huse, J. T., Edgar, M., Halliday, J., Mikolaenko, I., Lavi, E., and Rosenblum, M. K. (2013). Multinodular and vacuolating neuronal tumors of the cerebrum: 10 cases of a distinctive seizure-associated lesion. *Brain Pathol.* 23, 515–524. doi: 10.1111/bpa.12035

Huse, J. T., Snuderl, M., Jones, D. T., Brathwaite, C. D., Altman, N., Lavi, E., et al. (2017). Polymorphous low-grade neuroepithelial tumor of the young (PLNTY): An epileptogenic neoplasm with oligodendroglioma-like components, aberrant CD34 expression, and genetic alterations involving the MAP kinase pathway. *Acta Neuropathol.* 133, 417–429. doi: 10.1007/s00401-016-1639-9

Ida, C. M., Rodriguez, F. J., Burger, P. C., Caron, A. A., Jenkins, S. M., Spears, G. M., et al. (2015). Pleomorphic xanthoastrocytoma: Natural history and long-term follow-up. *Brain Pathol.* 25, 575–586. doi: 10.1111/bpa.12217

Ius, T., Pauletto, G., Tomasino, B., Maieron, M., Budai, R., Isola, M., et al. (2020). Predictors of postoperative seizure outcome in low grade glioma: From volumetric analysis to molecular stratification. *Cancers* 12:397. doi: 10.3390/cancers12020397

Jones, D. T., Hutter, B., Jäger, N., Korshunov, A., Kool, M., Warnatz, H. J., et al. (2013). Recurrent somatic alterations of FGFR1 and NTRK2 in pilocytic astrocytoma. *Nat. Genet.* 45, 927–932. doi: 10.1038/ng.2682

Jones, D. T. W., Kieran, M. W., Bouffet, E., Alexandrescu, S., Bandopadhayay, P., Bornhorst, M., et al. (2018). Pediatric low-grade gliomas: Next biologically driven steps. *Neurooncology* 20, 160–173. doi: 10.1093/neuonc/nox141

Ko, A., Kim, S. H., Kim, S. H., Park, E. K., Shim, K. W., Kang, H. C., et al. (2019). Epilepsy surgery for children with low-grade epilepsy-associated tumors: Factors associated with seizure recurrence and cognitive function. *Pediatr. Neurol.* 91, 50–56. doi: 10.1016/j.pediatrneurol.2018.10.008

Koelsche, C., Wöhrer, A., Jeibmann, A., Schittenhelm, J., Schindler, G., Preusser, M., et al. (2013). Mutant BRAF V600E protein in ganglioglioma is predominantly expressed by neuronal tumor cells. *Acta Neuropathol.* 125, 891–900. doi: 10.1007/s00401-013-1100-2

Koh, H. Y., Kim, S. H., Jang, J., Kim, H., Han, S., Lim, J. S., et al. (2018). BRAF somatic mutation contributes to intrinsic epileptogenicity in pediatric brain tumors. *Nat. Med.* 24, 1662–1668. doi: 10.1038/s41591-018-0172-x

Komori, T., Scheithauer, B. W., Anthony, D. C., Rosenblum, M. K., McLendon, R. E., Scott, R. M., et al. (1998). Papillary glioneuronal tumor: A new variant of mixed neuronal-glial neoplasm. *Am. J. Surg. Pathol.* 22, 1171–1183. doi: 10.1097/00000478-199810000-00002

LaSarge, C. L., and Danzer, S. C. (2014). Mechanisms regulating neuronal excitability and seizure development following mTOR pathway hyperactivation. *Front. Mol. Neurosci.* 7:18. doi: 10.3389/fnmol.2014.00018

Lee, H. H., Walker, J. A., Williams, J. R., Goodier, R. J., Payne, J. A., and Moss, S. J. (2007). Direct protein kinase C-dependent phosphorylation regulates the cell surface stability and activity of the potassium chloride cotransporter KCC2. *J. Biol. Chem.* 282, 29777–29784. doi: 10.1074/jbc.M705053200

Lombardi, G., Barresi, V., Castellano, A., Tabouret, E., Pasqualetti, F., Salvalaggio, A., et al. (2020). Clinical management of diffuse low-grade gliomas. *Cancers* 12:3008. doi: 10.3390/cancers12103008

Louis, D. N., Perry, A., Burger, P., Ellison, D. W., Reifenberger, G., von Deimling, A., et al. (2014). International society of neuropathology–haarlem consensus guidelines for nervous system tumor classification and grading. *Brain Pathol.* 24, 429–435. doi: 10.1111/bpa.12171

Louis, D. N., Perry, A., Reifenberger, G., von Deimling, A., Figarella-Branger, D., Cavenee, W. K., et al. (2016). The 2016 world health organization classification of tumors of the central nervous system: A summary. *Acta Neuropathol.* 131, 803–820. doi: 10.1007/s00401-016-1545-1

Louis, D. N., Perry, A., Wesseling, P., Brat, D. J., Cree, I. A., Figarella-Branger, D., et al. (2021). The 2021 WHO classification of tumors of the central nervous system: A summary. *Neurooncology* 23, 1231–1251. doi: 10.1093/neuonc/noab106

Luyken, C., Blümcke, I., Fimmers, R., Urbach, H., Elger, C. E., Wiestler, O. D., et al. (2003). The spectrum of long-term epilepsy-associated tumors: Long-term seizure and tumor outcome and neurosurgical aspects. *Epilepsia* 44, 822–830. doi: 10.1046/j.1528-1157.2003.56102.x

Martinoni, M., Marucci, G., de Biase, D., Rubboli, G., Volpi, L., Riguzzi, P., et al. (2015). BRAF V600E mutation in neocortical posterior temporal epileptogenic gangliogliomas. *J. Clin. Neurosci.* 22, 1250–1253. doi: 10.1016/j.jocn.2015.02.016

Maschio, M., Aguglia, U., Avanzini, G., Banfi, P., Buttinelli, C., Capovilla, G., et al. (2019). Management of epilepsy in brain tumors. *Neurol. Sci.* 40, 2217–2234. doi: 10.1007/s10072-019-04025-9

Natale, G., Cucchiara, F., and Bocci, G. (2021). Historical overview of the "Firing" liaison between brain tumors and epilepsy. *Neuroscientist* 28, 411–419. doi: 10.1177/1073858421992316

Neal, A., Yuen, T., Bjorksten, A. R., Kwan, P., O'Brien, T. J., and Morokoff, A. (2016). Peritumoural glutamate correlates with post-operative seizures in supratentorial gliomas. *J. Neurooncol.* 129, 259–267. doi: 10.1007/s11060-016-2169-y

Ni, H. C., Chen, S. Y., Chen, L., Lu, D. H., Fu, Y. J., and Piao, Y. S. (2015). Angiocentric glioma: A report of nine new cases, including four with atypical histological features. *Neuropathol. Appl. Neurobiol.* 41, 333–346. doi: 10.1111/nan.12158

Pages, M., Lacroix, L., Tauziede-Espariat, A., Castel, D., Daudigeos-Dubus, E., Ridola, V., et al. (2015). Papillary glioneuronal tumors: Histological and molecular characteristics and diagnostic value of SLC44A1-PRKCA fusion. *Acta Neuropathol. Commun.* 3:85. doi: 10.1186/s40478-015-0264-5

Pallud, J., Capelle, L., and Huberfeld, G. (2013). Tumoral epileptogenicity: How does it happen? *Epilepsia* 54(Suppl. 9), 30–34. doi: 10.1111/epi.12440

Pallud, J., and McKhann, G. M. (2019). Diffuse low-grade glioma-related epilepsy. *Neurosurg. Clin. N. Am.* 30, 43–54. doi: 10.1016/j.nec.2018.09.001

Palmini, A., Paglioli, E., and Silva, V. D. (2013). Developmental tumors and adjacent cortical dysplasia: Single or dual pathology? *Epilepsia* 54(Suppl. 9), 18–24. doi: 10.1111/epi.12438

Pekmezci, M., Stevers, M., Phillips, J. J., Van Ziffle, J., Bastian, B. C., Tsankova, N. M., et al. (2018a). Multinodular and vacuolating neuronal tumor of the cerebrum is a clonal neoplasm defined by genetic alterations that activate the MAP kinase signaling pathway. *Acta Neuropathol.* 135, 485–488. doi: 10.1007/s00401-018-1820-4

Pekmezci, M., Villanueva-Meyer, J. E., Goode, B., Van Ziffle, J., Onodera, C., Grenert, J. P., et al. (2018b). The genetic landscape of ganglioglioma. *Acta Neuropathol. Commun.* 6:47. doi: 10.1186/s40478-018-0551-z

Pelliccia, V., Deleo, F., Gozzo, F., Sartori, I., Mai, R., Cossu, M., et al. (2017). Early and late epilepsy surgery in focal epilepsies associated with long-term epilepsy-associated tumors. *J. Neurosurg.* 127, 1147–1152. doi: 10.3171/2016.9.jns161176

Pernice, H. F., Schieweck, R., Kiebler, M. A., and Popper, B. (2016). mTOR and MAPK: From localized translation control to epilepsy. *BMC Neurosci.* 17:73. doi: 10.1186/s12868-016-0308-1

Phi, J. H., and Kim, S. K. (2019). Clinical pearls and advances in molecular researches of epilepsy-associated tumors. *J. Korean Neurosurg. Soc.* 62, 313–320. doi: 10.3340/jkns.2019.0033

Prabowo, A. S., Iyer, A. M., Veersema, T. J., Anink, J. J., Schouten-van Meeteren, A. Y., Spliet, W. G., et al. (2014). BRAF V600E mutation is associated with mTOR signaling activation in glioneuronal tumors. *Brain Pathol.* 24, 52–66. doi: 10.1111/bpa.12081

Prabowo, A. S., Iyer, A. M., Veersema, T. J., Anink, J. J., Schouten-van Meeteren, A. Y., Spliet, W. G., et al. (2015). Expression of neurodegenerative disease-related proteins and caspase-3 in glioneuronal tumours. *Neuropathol. Appl. Neurobiol.* 41, e1–e15. doi: 10.1111/nan.12143

Prayson, R. A. (2011). Brain tumors in adults with medically intractable epilepsy. *Am. J. Clin. Pathol.* 136, 557–563. doi: 10.1309/ajcp0rbuqaqpzoue

Prayson, R. A., and Napekoski, K. M. (2012). Composite ganglioglioma/dysembryoplastic neuroepithelial tumor: A clinicopathologic study of 8 cases. *Hum. Pathol.* 43, 1113–1118. doi: 10.1016/j.humpath.2011.08.023

Qaddoumi, I., Orisme, W., Wen, J., Santiago, T., Gupta, K., Dalton, J. D., et al. (2016). Genetic alterations in uncommon low-grade neuroepithelial tumors: BRAF, FGFR1, and MYB mutations occur at high frequency and align with morphology. *Acta Neuropathol.* 131, 833–845. doi: 10.1007/s00401-016-1539-z

Qi, X. L., Yao, K., Duan, Z. J., Bian, Y., Ma, Z., Piao, Y. S., et al. (2018). [BRAF V600E mutation and clinicopathologic characteristics in 250 cases of brain tumors associated with epilepsy]. *Zhonghua Bing Li Xue Za Zhi* 47, 664–670. doi: 10.3760/cma.j.issn.0529-5807.2018.09.003

Radhakrishnan, A., Abraham, M., Vilanilam, G., Menon, R., Menon, D., Kumar, H., et al. (2016). Surgery for "Long-term epilepsy associated tumors (LEATs)": Seizure outcome and its predictors. *Clin. Neurol. Neurosurg.* 141, 98–105. doi: 10.1016/j.clineuro.2015.12.020

Ramkissoon, L. A., Horowitz, P. M., Craig, J. M., Ramkissoon, S. H., Rich, B. E., Schumacher, S. E., et al. (2013). Genomic analysis of diffuse pediatric low-grade gliomas identifies recurrent oncogenic truncating rearrangements in the transcription factor MYBL1. *Proc. Natl. Acad. Sci. U.S.A.* 110, 8188–8193. doi: 10.1073/pnas.1300252110

Ristić, A. J., Mindruta, I., Dimova, P., Kelemen, A., Grujičić, D., Ilić, R., et al. (2020). Low-grade epilepsy-associated tumour management with or without presurgical evaluation: A multicentre, retrospective, observational study of postsurgical epilepsy outcome. *Epileptic Disord.* 22, 555–562. doi: 10.1684/epd.2020.1195

Riva, G., Cima, L., Villanova, M., Ghimenton, C., Sina, S., Riccioni, L., et al. (2018). Low-grade neuroepithelial tumor: Unusual presentation in an adult without history of seizures. *Neuropathology* 38, 557–560. doi: 10.1111/neup.12504

Rivera, B., Gayden, T., Carrot-Zhang, J., Nadaf, J., Boshari, T., Faury, D., et al. (2016). Germline and somatic FGFR1 abnormalities in dysembryoplastic neuroepithelial tumors. *Acta Neuropathol.* 131, 847–863. doi: 10.1007/s00401-016-1549-x

Roberts, M., Northmore, T., Shires, J., Taylor, P., and Hayhurst, C. (2018). Diffuse low grade glioma after the 2016 WHO update, seizure characteristics, imaging correlates and outcomes. *Clin. Neurol. Neurosurg.* 175, 9–15. doi: 10.1016/j.clineuro.2018.10.001

Ross, J. S., Wang, K., Al-Rohil, R. N., Nazeer, T., Sheehan, C. E., Otto, G. A., et al. (2014). Advanced urothelial carcinoma: Next-generation sequencing reveals diverse genomic alterations and targets of therapy. *Mod. Pathol.* 27, 271–280. doi: 10.1038/modpathol.2013.135

Roth, J. J., Santi, M., Rorke-Adams, L. B., Harding, B. N., Busse, T. M., Tooke, L. S., et al. (2014). Diagnostic application of high resolution single nucleotide polymorphism array analysis for children with brain tumors. *Cancer Genet.* 207, 111–123. doi: 10.1016/j.cancergen.2014.03.002

Schindler, G., Capper, D., Meyer, J., Janzarik, W., Omran, H., Herold-Mende, C., et al. (2011). Analysis of BRAF V600E mutation in 1,320 nervous system tumors reveals high mutation frequencies in pleomorphic xanthoastrocytoma, ganglioglioma and extra-cerebellar pilocytic astrocytoma. *Acta Neuropathol.* 121, 397–405. doi: 10.1007/s00401-011-0802-6

Schramm, J., Luyken, C., Urbach, H., Fimmers, R., and Blümcke, I. (2004). Evidence for a clinically distinct new subtype of grade II astrocytomas in patients with long-term epilepsy. *Neurosurgery* 55, 340–347; discussion 347–348. doi: 10.1227/01.neu.0000129546.38675.1b

Shan, X., Fan, X., Liu, X., Zhao, Z., Wang, Y., and Jiang, T. (2018). Clinical characteristics associated with postoperative seizure control in adult low-grade gliomas: A systematic review and meta-analysis. *Neurooncology* 20, 324–331. doi: 10.1093/neuonc/nox130

Shen, C. H., Zhang, Y. X., Xu, J. H., Zhu, Q. B., Zhu, J. M., Guo, Y., et al. (2017). Autophagy-related protein expression was associated with BRAF V600E mutation in epilepsy associated glioneuronal tumors. *Epilepsy Res.* 135, 123–130. doi: 10.1016/j.eplepsyres.2017.06.006

Sievert, A. J., Jackson, E. M., Gai, X., Hakonarson, H., Judkins, A. R., Resnick, A. C., et al. (2009). Duplication of 7q34 in pediatric low-grade astrocytomas detected by high-density single-nucleotide polymorphism-based genotype arrays results in a novel BRAF fusion gene. *Brain Pathol.* 19, 449–458. doi: 10.1111/j.1750-3639.2008.00225.x

Slegers, R. J., and Blumcke, I. (2020). Low-grade developmental and epilepsy associated brain tumors: A critical update 2020. *Acta Neuropathol. Commun.* 8:27. doi: 10.1186/s40478-020-00904-x

Stone, T. J., Keeley, A., Virasami, A., Harkness, W., Tisdall, M., Izquierdo Delgado, E., et al. (2018a). Comprehensive molecular characterisation of epilepsy-associated glioneuronal tumours. *Acta Neuropathol.* 135, 115–129. doi: 10.1007/s00401-017-1773-z

Stone, T. J., Rowell, R., Jayasekera, B. A. P., Cunningham, M. O., and Jacques, T. S. (2018b). Review: Molecular characteristics of long-term epilepsy-associated tumours (LEATs) and mechanisms for tumour-related epilepsy (TRE). *Neuropathol. Appl. Neurobiol.* 44, 56–69. doi: 10.1111/nan.12459

Thom, M., Blumcke, I., and Aronica, E. (2012). Long-term epilepsy-associated tumors. *Brain Pathol.* 22, 350–379. doi: 10.1111/j.1750-3639.2012.00582.x

Thom, M., Liu, J., Bongaarts, A., Reinten, R. J., Paradiso, B., Jäger, H. R., et al. (2018). Multinodular and vacuolating neuronal tumors in epilepsy: Dysplasia or neoplasia? *Brain Pathol.* 28, 155–171. doi: 10.1111/bpa.12555

Thom, M., Toma, A., An, S., Martinian, L., Hadjivassiliou, G., Ratilal, B., et al. (2011). One hundred and one dysembryoplastic neuroepithelial tumors: An adult epilepsy series with immunohistochemical, molecular genetic, and clinical correlations and a review of the literature. *J. Neuropathol. Exp. Neurol.* 70, 859–878. doi: 10.1097/NEN.0b013e3182302475

Thomas, D. L., and Pierson, C. R. (2020). Neuropathology of surgically managed epilepsy specimens. *Neurosurgery* 88, 1–14. doi: 10.1093/neuros/nyaa366

van Breemen, M. S., Wilms, E. B., and Vecht, C. J. (2007). Epilepsy in patients with brain tumours: Epidemiology, mechanisms, and management. *Lancet Neurol.* 6, 421–430. doi: 10.1016/s1474-4422(07)70103-5

Vaubel, R., Zschernack, V., Tran, Q. T., Jenkins, S., Caron, A., Milosevic, D., et al. (2021). Biology and grading of pleomorphic xanthoastrocytoma-what have we learned about it? *Brain Pathol.* 31, 20–32. doi: 10.1111/bpa.12874

Vaubel, R. A., Caron, A. A., Yamada, S., Decker, P. A., Eckel Passow, J. E., Rodriguez, F. J., et al. (2018). Recurrent copy number alterations in low-grade and anaplastic pleomorphic xanthoastrocytoma with and without BRAF V600E mutation. *Brain Pathol.* 28, 172–182. doi: 10.1111/bpa.12495

Vogt, V. L., Witt, J. A., Delev, D., Grote, A., von Lehe, M., Becker, A. J., et al. (2018). Cognitive features and surgical outcome of patients with long-term epilepsy-associated tumors (LEATs) within the temporal lobe. *Epilepsy Behav.* 88, 25–32. doi: 10.1016/j.yebeh.2018.08.028

Vornetti, G., Marucci, G., Zenesini, C., de Biase, D., Michelucci, R., Tinuper, P., et al. (2017). Relationship among clinical, pathological and bio-molecular features in low-grade epilepsy-associated neuroepithelial tumors. *J. Clin. Neurosci.* 44, 158–163. doi: 10.1016/j.jocn.2017.06.022

Wallace, D. J., Byrne, R. W., Ruban, D., Cochran, E. J., Roh, D., and Whisler, W. W. (2011). Temporal lobe pleomorphic xanthoastrocytoma and chronic epilepsy: Long-term surgical outcomes. *Clin. Neurol. Neurosurg.* 113, 918–922. doi: 10.1016/j.clineuro.2011.06.001

Wang, Q., Xiong, Y., Chen, J., and Shao, Q. (2020). Cystic angiocentric glioma: A case report and literature review. *Childs Nerv. Syst.* 37, 2701–2705. doi: 10.1007/s00381-020-04882-2

Weber, R. G., Hoischen, A., Ehrler, M., Zipper, P., Kaulich, K., Blaschke, B., et al. (2007). Frequent loss of chromosome 9, homozygous CDKN2A/p14(ARF)/CDKN2B deletion and low TSC1 mRNA expression in pleomorphic xanthoastrocytomas. *Oncogene* 26, 1088–1097. doi: 10.1038/sj.onc.1209851

Wefers, A. K., Stichel, D., Schrimpf, D., Coras, R., Pages, M., Tauziède-Espariat, A., et al. (2020). Isomorphic diffuse glioma is a morphologically and molecularly distinct tumour entity with recurrent gene fusions of MYBL1 or MYB and a benign disease course. *Acta Neuropathol.* 139, 193–209. doi: 10.1007/s00401-019-02078-w

Wessling, C., Bartels, S., Sassen, R., Schoene-Bake, J. C., and von Lehe, M. (2015). Brain tumors in children with refractory seizures—a long-term follow-up study after epilepsy surgery. *Childs Nerv. Syst.* 31, 1471–1477. doi: 10.1007/s00381-015-2825-0

Wolf, H. K., Müller, M. B., Spänle, M., Zentner, J., Schramm, J., and Wiestler, O. D. (1994). Ganglioglioma: A detailed histopathological and immunohistochemical analysis of 61 cases. *Acta Neuropathol.* 88, 166–173. doi: 10.1007/bf00294510

Young, J. S., Gogos, A. J., Morshed, R. A., Hervey-Jumper, S. L., and Berger, M. S. (2020). Molecular characteristics of diffuse lower grade gliomas: What neurosurgeons need to know. *Acta Neurochir.* 162, 1929–1939. doi: 10.1007/s00701-020-04426-2

Yuen, T. I., Morokoff, A. P., Bjorksten, A., D'Abaco, G., Paradiso, L., Finch, S., et al. (2012). Glutamate is associated with a higher risk of seizures in patients with gliomas. *Neurology* 79, 883–889. doi: 10.1212/WNL.0b013e318266fa89

Zhang, J., Wu, G., Miller, C. P., Tatevossian, R. G., Dalton, J. D., Tang, B., et al. (2013). Whole-genome sequencing identifies genetic alterations in pediatric low-grade gliomas. *Nat. Genet.* 45, 602–612. doi: 10.1038/ng.2611

Zhang, W., Chen, J., Hua, G., Zhu, D., Tan, Q., Zhang, L., et al. (2020). Surgical treatment of low-grade brain tumors associated with epilepsy. *Int. Rev. Neurobiol.* 151, 171–183. doi: 10.1016/bs.irn.2020.03.021

frontiers | Frontiers in Neuroscience

TYPE Original Research
PUBLISHED 11 January 2023
DOI 10.3389/fnins.2022.1099019

OPEN ACCESS

EDITED BY
Sheng Zhong,
Department of Neurosurgery, Sun Yat-sen University Cancer Center, China

REVIEWED BY
Yibin Xi,
Fourth Military Medical University, China
Wan-Ming Hu,
Sun Yat-sen University Cancer Center (SYSUCC), China

*CORRESPONDENCE
Shuangshuang Song
songshuangshuang@qdu.edu.cn
Xuejun Liu
dr.liuxuejun@qdu.edu.cn

†These authors have contributed equally to this work

SPECIALTY SECTION
This article was submitted to Translational Neuroscience, a section of the journal Frontiers in Neuroscience

RECEIVED 15 November 2022
ACCEPTED 28 December 2022
PUBLISHED 11 January 2023

CITATION
Xie Z, Li J, Zhang Y, Zhou R, Zhang H, Duan C, Liu S, Niu L, Zhao J, Liu Y, Song S and Liu X (2023) The diagnostic value of ADC histogram and direct ADC measurements for coexisting isocitrate dehydrogenase mutation and O6-methylguanine-DNA methyltransferase promoter methylation in glioma. *Front. Neurosci.* 16:1099019. doi: 10.3389/fnins.2022.1099019

The diagnostic value of ADC histogram and direct ADC measurements for coexisting isocitrate dehydrogenase mutation and O6-methylguanine-DNA methyltransferase promoter methylation in glioma

Zhiyan Xie[1†], Jixian Li[1†], Yue Zhang[1], Ruizhi Zhou[1], Hua Zhang[1], Chongfeng Duan[1], Song Liu[1], Lei Niu[1], Jiping Zhao[1], Yingchao Liu[2], Shuangshuang Song[3*] and Xuejun Liu[1*]

[1]Department of Radiology, The Affiliated Hospital of Qingdao University, Qingdao, China, [2]Department of Neurosurgery, Shandong Provincial Hospital Affiliated to Shandong First Medical University, Jinan, China, [3]Department of Nuclear Medicine, The Affiliated Hospital of Qingdao University, Qingdao, China

Objectives: To non-invasively predict the coexistence of isocitrate dehydrogenase (IDH) mutation and O6-methylguanine-DNA methyltransferase (MGMT) promoter methylation in adult-type diffuse gliomas using apparent diffusion coefficient (ADC) histogram and direct ADC measurements and compare the diagnostic performances of the two methods.

Materials and methods: A total of 118 patients with adult-type diffuse glioma who underwent preoperative brain magnetic resonance imaging (MRI) and diffusion weighted imaging (DWI) were included in this retrospective study. The patient group included 40 patients with coexisting IDH mutation and MGMT promoter methylation (IDHmut/MGMTmet) and 78 patients with other molecular status, including 32 patients with IDH wildtype and MGMT promoter methylation (IDHwt/MGMTmet), one patient with IDH mutation and unmethylated MGMT promoter (IDHmut/MGMTunmet), and 45 patients with IDH wildtype and unmethylated MGMT promoter (IDHwt/MGMTunmet). ADC histogram parameters of gliomas were extracted by delineating the region of interest (ROI) in solid components of tumors. The minimum and mean ADC of direct ADC measurements were calculated by placing three rounded or elliptic ROIs in solid components of gliomas. Receiver operating characteristic (ROC) curve analysis and the area under the curve (AUC) were used to evaluate the diagnostic performances of the two methods.

Results: The 10th percentile, median, mean, root mean squared, 90th percentile, skewness, kurtosis, and minimum of ADC histogram analysis and minimum and mean ADC of direct measurements were significantly different between IDHmut/MGMTmet and the other glioma group ($P < 0.001$ to $P = 0.003$). In terms of single factors, 10th percentile of ADC histogram analysis had the best diagnostic efficiency (AUC = 0.860), followed by mean ADC obtained by direct measurements (AUC = 0.844). The logistic regression model combining ADC histogram parameters and direct measurements had the best diagnostic efficiency (AUC = 0.938), followed by the logistic regression model combining the ADC histogram parameters with statistically significant difference (AUC = 0.916) and the logistic regression model combining minimum ADC and mean ADC (AUC = 0.851).

Conclusion: Both ADC histogram analysis and direct measurements have potential value in predicting the coexistence of IDHmut and MGMTmet in adult-type diffuse glioma. The diagnostic performance of ADC histogram analysis was better than that of direct ADC measurements. The combination of the two methods showed the best diagnostic performance.

KEYWORDS

ADC histogram, isocitrate dehydrogenase mutation, O6-methylguanine-DNA methyltransferase promoter methylation, glioma, diffusion weighted imaging

Introduction

The guidelines for the molecular diagnosis of gliomas have continued to change over recent years. The 2016 WHO classification of tumors of the central nervous system inserted molecular characteristics into the diagnostic criteria of gliomas, which had previously relied on histological diagnosis, and the 2021 edition emphasized the importance of classifying tumors by the type of molecular feature (Louis et al., 2016, 2021; McNamara et al., 2022). Isocitrate dehydrogenase mutations (IDHmut) occur in a high proportion of grade II and III gliomas and secondary glioblastomas and a low proportion of primary glioblastomas (Yan et al., 2009; Chen et al., 2017). The overall survival of patients with grade III glioma and glioblastoma harboring IDHmut was significantly longer than that of patients with IDH wildtype (IDHwt) (Yan et al., 2009).

O6-methylguanine-DNA methyltransferase (MGMT) repairs the DNA damage induced by temozolomide, and therefore higher levels of MGMT lead to temozolomide resistance (Chen et al., 2017; Molinaro et al., 2019). Methylation of the MGMT promoter (MGMTmet) decreases MGMT protein expression, thereby increasing sensitivity to temozolomide (Chen et al., 2017). Previous studies showed that patients with MGMTmet with grade II or III glioma or glioblastoma have a longer overall survival compared with those with unmethylated MGMT promoter (MGMTunmet) (Binabaj et al., 2018; Schaff et al., 2020; Haque et al., 2021, 2022). Notably, previous studies showed that patients with the coexistence of IDHmut and MGMTmet (IDHmut/MGMTmet) with low-grade glioma or glioblastoma had the longest survival, followed by those with IDHmut or MGMTmet alone, while glioma patients with IDHwt and MGMTunmet (IDHwt/MGMTunmet) had the shortest survival (Molenaar et al., 2014; Tanaka et al., 2015). The coexistence of IDHmut and MGMTmet thus indicates a better patient prognosis. Therefore, clarifying the status of IDH mutation and MGMT promoter methylation is critical to assess the prognosis of glioma patients. While genomic sequence analysis of surgical or biopsy specimens for IDH mutation status and MGMT promoter methylation status is accurate, this approach can be time consuming and is invasive. Furthermore, there is a risk that the specimens obtained by biopsy are too small to yield results. Therefore, a non-invasive method to predict the molecular status before surgery is ideal.

Magnetic resonance imaging (MRI) is a routine preoperative examination of gliomas. Diffusion-weighted imaging (DWI) is the most used MRI examination and provides important information on tumor proliferation by detecting the diffusion of water molecules in neoplastic tissues (Charles-Edwards and deSouza, 2006). Both direct apparent diffusion coefficient (ADC) measurements and ADC histogram analysis have been applied to predict the status of molecules, but the diagnostic performances vary widely. Several studies have used direct ADC values to predict IDH mutation or MGMT promoter methylation status of gliomas, and the area under the curve (AUC) varied from 0.686 to 0.870 (Xing et al., 2017, 2019, 2022; Cindil et al., 2022). Other studies have applied ADC histogram

to predict the molecular status of gliomas. Lee et al. (2015) used ADC histogram parameters to predict IDH1 mutation of high-grade gliomas; however, the diagnostic value was limited (AUC 0.707). Direct ADC measurement is simple to performed, but only a few voxels are obtained. Histogram analysis is time-consuming, but it can capture subtle differences that are not visible to the naked eye. Therefore, it is meaningful and worthful to compare the diagnostic performances of the two methods, which may help researchers select a better method to maximize the value of DWI.

The goal of our study was to use ADC histogram analysis and direct ADC measurements to non-invasively predict the coexistence of IDHmut and MGMTmet in adult-type diffuse gliomas. We then compared the diagnostic performances of the two methods.

Materials and methods

Subjects

This retrospective study was approved by the medical ethics committee of the Affiliated Hospital of Qingdao University, and the requirement for informed consent was waived. The study included 211 patients with histopathologically proved diffuse glioma who underwent preoperative brain MRI and DWI between January 2017 and April 2022. None of the patients had received any brain treatment before the MRI scans. All patients underwent surgery within 2 weeks of the MRI scan. Exclusion criteria were as follows: (1) patients without information on IDH mutation and MGMT promoter methylation status; (2) patients with lost MR images or poor-quality images; and (3) patients younger than 18 years old. Finally, 118 patients (56 females and 62 males; mean age: 53.3 years; range: 21–75 years) with adult-type diffuse glioma were enrolled in the present study (**Figure 1**). IDH mutation and MGMT promoter methylation status were assessed by genomic sequence analysis using Sanger method and fluorescence quantitative PCR method.

MR imaging protocols

Magnetic resonance imaging scans were performed using a 3.0 T or 1.5T MR scanner (Signa HDXt 3.0T, GE Healthcare, Milwaukee, WI, USA; Signa HDx 1.5T, GE Healthcare), using an eight-channel array coil. The MRI protocol included pre-contrast T1-weighted imaging (T1WI), T2-weighted imaging (T2WI), T2WI-fluid attenuated inversion recovery imaging (T2WI-FLAIR), and DWI. The repetition time (TR)/echo time (TE) of magnetic resonance sequences at the 3.0 T GE MR system were as follows: (1) T1WI: TR/TE = 2761/9 ms; (2) T2WI: TR/TE = 3040/99 ms; (3) T2WI-FLAIR: TR/TE = 8000/154 ms; and (4) DWI: TR/TE = 5100/76 ms. The TR/TE of magnetic resonance sequences at the 1.5 T GE MR system were as follows: (1) T1WI: TR/TE = 2612/20 ms; (2) T2WI: TR/TE = 3460/109 ms; (3) T2WI-FLAIR: TR/TE = 6004/126 ms; and (4) DWI: TR/TE = 4600/82 ms. DWI was performed with effective b values of 0 and 1000 s/mm^2. ADC maps were reconstructed by DWI on the GE workstation.

MR data processing

For ADC histogram analysis, tumor segmentation and feature extraction were implemented on 3D Slicer 4.11 software.[1] Patient DICOM data were imported into 3D Slicer software by a radiologist with 3 years of neuroradiology experience. The radiologist was blinded to patient-related information and the histopathological and molecular results. ROIs were manually delineated in solid components of tumors layer by layer on ADC maps, and the necrotic, hemorrhagic, and cystic regions were avoided with reference to T1WI, T2WI, and T2WI-FLAIR (**Figure 2**). After the tumor was segmented, the pyradiomics module was applied to extracted ADC histogram parameters, including 10th percentile, mean, median, entropy, 90th percentile, interquartile range, minimum, kurtosis, maximum, skewness, mean absolute deviation, range, robust mean absolute deviation, uniformity, root mean squared, and variance.

The neuroradiologist measured minimum and mean ADC in solid components of tumors on the basis of the direct measurement method on AW workstation. Three rounded or elliptic ROIs were placed in solid components that were dark on ADC maps avoiding the necrotic, hemorrhagic, and cystic regions; the areas of ROIs ranged from 15–40 mm^2 (**Figure 2**). The minimum and mean ADC of the three measurements were calculated.

After 2 months, the ROIs of all tumors on the basis of histogram analysis and direct measurement method were drawn again, and intraobserver agreement was assessed.

Statistical analysis

The intraclass correlation coefficient (ICC) was used to evaluate intraobserver agreement; an ICC value more than 0.75 was considered as good consistency.

Statistical analyses were performed using the statistical package SPSS for Windows (Version 26.0, Chicago, IL, USA). Categorical variables such as gender and pathological grade were expressed as frequencies. Mean ADC, minimum ADC, kurtosis, skewness, and other continuous variables were expressed as mean and standard deviations (normal distribution) or median

1 Available at https://www.slicer.org.

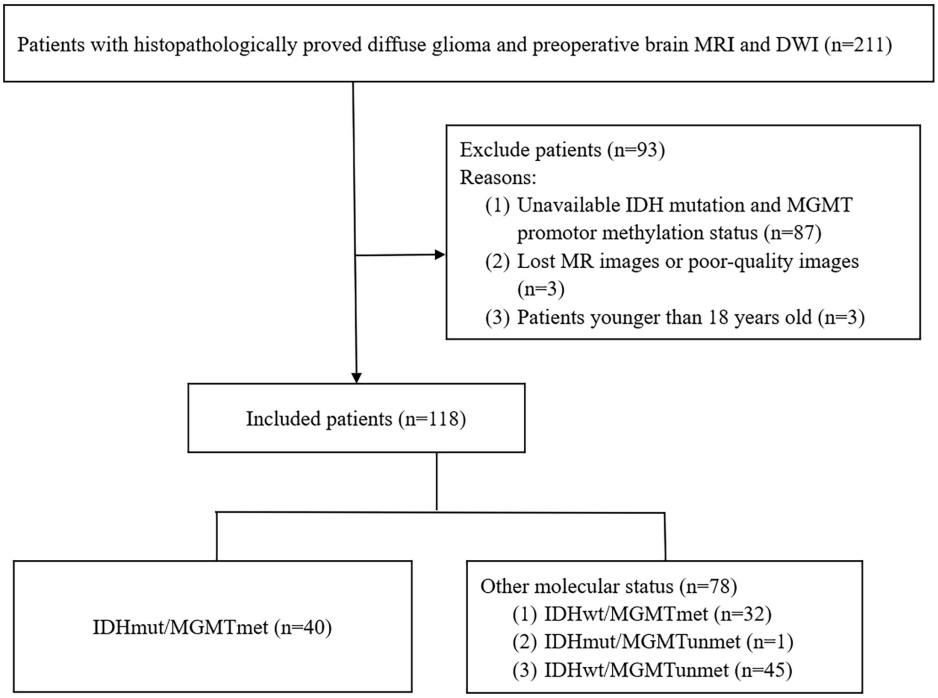

FIGURE 1
Flowchart of the collection of patients.

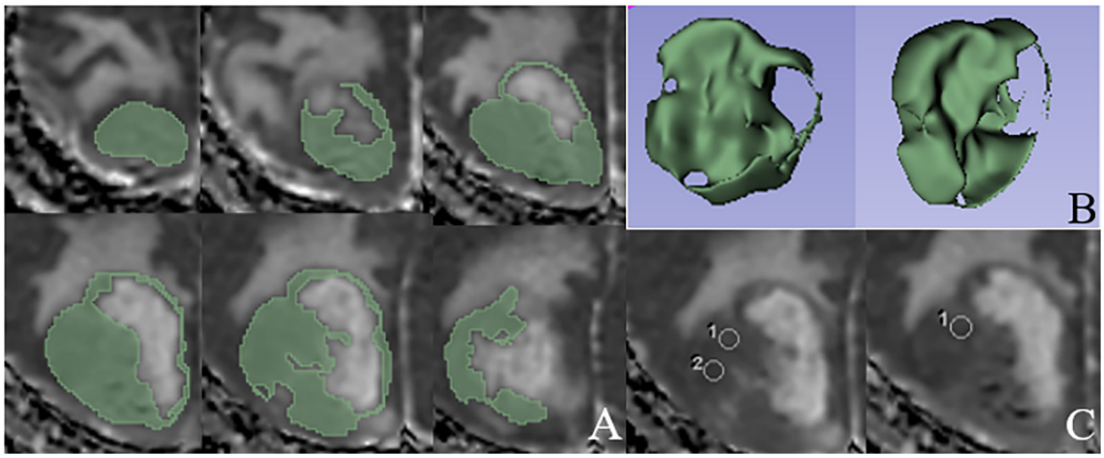

FIGURE 2
An example of ROIs delineated based on ADC histogram analysis and direct measurements, respectively. **(A)** ROIs manually delineated in solid components layer by layer on ADC map. **(B)** Three-dimensional stereogram generated by 3D Slicer software after the tumor segmentation. **(C)** Three rounded ROIs in solid components of the tumor based on the direct ADC measurements.

and quartiles (skewed distribution). The normal distribution of continuous data was assessed using Shapiro–Wilk test. The *t*-test (normal distribution) or Wilcoxon–Mann–Whitney test (heavily skewed distribution) was used to compare continuous variables between IDHmut/MGMTmet and gliomas with different mutation status, and the χ^2 test was used to compare categorical variables. The variables that were statistically different between the two sets were included in the multivariate binary logistic regression analysis. Receiver operating characteristic (ROC) curve analysis and AUC were used to evaluate the diagnostic performances of the two methods. The cut-off value and the corresponding sensitivity and specificity were calculated by ROC curves. A P-value < 0.05 was considered statistically significant.

Results

ICC evaluation

The intraobserver agreement of ADC histogram parameters obtained from the two measurements was good (ICCs: 0.751–0.942). The minimum and mean ADC obtained from two direct measurements also showed good consistency (ICC: 0.934 and ICC: 0.945).

Patient characteristics and pathological diagnosis of tumors

A total of 118 patients with adult-type diffuse glioma were enrolled in the present study. Among the 118 tumors, 40 tumors exhibited IDHmut/MGMTmet status. In the other 78 tumors, 32 tumors were IDHwt/MGMTmet, one tumor was IDHmut/MGMTunmet, and 45 tumors were IDHwt/MGMTunmet. Due to the lack of the results of EGFR gene amplification, +7/−10 chromosome copy number changes and CDKN2A/B homozygous deletion, the pathological diagnosis of tumors were carried out according to the 2016 WHO classification of tumors of CNS, including 5 diffuse astrocytoma, IDH-mutant (WHO II), 4 anaplastic astrocytoma, IDH-mutant (WHO III), 5 glioblastoma, IDH-mutant (WHO IV), 18 oligodendroglioma, IDH-mutant and 1p19q codeleted (WHO II), 9 anaplastic oligodendroglioma, IDH-mutant and 1p19q codeleted (WHO III), 4 diffuse astrocytoma, IDH-wildtype (WHO II), 8 anaplastic astrocytoma, IDH-wildtype (WHO III) and 65 glioblastoma, IDH-wildtype (WHO IV) (Louis et al., 2016, 2021).

There was no statistically significant difference in sex between the IDHmut/MGMTmet group and the other group (P = 0.995). Patients with IDHmut/MGMTmet gliomas were younger than patients with other molecular status (49.03 ± 11.77 vs. 55.53 ± 11.44 years, P = 0.005). The difference in the distribution of glioma grades between the IDHmut/MGMTmet group and the other group was statistically significant (P < 0.001). Lower grade gliomas (II + III) were the majority in IDHmut/MGMTmet gliomas, while glioblastoma (IV) was the majority in gliomas of other status. Comparison of sex, age, and pathological grade between the two groups is shown in Table 1.

Diagnostic performance of the ADC histogram

Comparison of ADC histogram parameters between IDHmut/MGMTmet and the other glioma group is shown in Table 2 and Figure 3. The 10th percentile, median, minimum, 90th percentile, mean, and root mean squared of IDHmut/MGMTmet gliomas were higher than those of the other glioma group, and the difference was statistically significant (P < 0.001 to P = 0.002). Kurtosis and skewness of IDHmut/MGMTmet gliomas were lower than those of the other group, and the difference was statistically significant (P = 0.003 and P < 0.001). The remaining ADC histogram parameters including maximum, uniformity, entropy, mean absolute deviation, range, interquartile range, variance, and robust mean absolute deviation showed no statistically significant differences between IDHmut/MGMTmet and gliomas with other molecular status.

The diagnostic performances of the ADC histogram parameters are shown in Table 3. The 10th percentile had the highest diagnostic efficiency (AUC: 0.860, 95% CI: 0.787–0.934), and the optimal cut-off value was 937.50 × 10^{-6} mm^2/s with 80.0% sensitivity and 83.3% specificity. The AUC of median was 0.824 (95% CI: 0.748–0.900), followed by mean (AUC: 0.823, 95% CI: 0.748–0.899) and root mean squared (AUC: 0.818, 95% CI: 0.742–0.893). The AUC of 90th percentile, skewness, kurtosis, and minimum were 0.759, 0.726, 0.666, and 0.655, respectively.

Diagnostic performance of direct ADC measurements

Comparison of minimum ADC and mean ADC between IDHmut/MGMTmet and the other group is shown in Table 2 and Figure 3. The minimum ADC and mean ADC of

TABLE 1 Comparison of sex, age, and pathological grade between IDHmut/MGMTmet and the other glioma group.

Demographics	IDHmut/MGMTmet, N = 40	Other molecular status (IDHwt/MGMTmet, n = 32; IDHmut/MGMTunmet, n = 1; IDHwt/MGMTunmet, n = 45), N = 78	P-value
Age (years)	49.03 ± 11.77	55.53 ± 11.44	0.005*
Sex [male, n (%)]	21 (52.5%)	41 (52.6%)	0.995
Grade, n (%)			
Lower grade (II + III)	36 (90.0%)	12 (15.4%)	< 0.001*
Glioblastoma (IV)	4 (10.0%)	66 (84.6%)	

*P < 0.05.

TABLE 2 Comparison of ADC histogram parameters and minimum ADC and mean ADC between IDHmut/MGMTmet and the other glioma group.

Variable[#]	IDHmut/MGMTmet, $N = 40$	Other molecular status (IDHwt/MGMTmet, $n = 32$; IDHmut/MGMTunmet, $n = 1$; IDHwt/MGMTunmet, $n = 45$), $N = 78$	*P*-value
ADC histogram parameters			
10th percentile	1022.81 ± 152.53	803.55 ± 134.00	< 0.001*
90th percentile	1451.00 (1309.00, 1679.75)	1273.50 (1135.00, 1439.28)	< 0.001*
Entropy	4.89 (4.55, 5.14)	4.82 (4.57, 5.15)	0.695
Interquartile range	237.84 ± 79.60	232.37 ± 84.94	0.736
Kurtosis	3.89 (3.24, 4.65)	4.63 (3.66, 6.95)	0.003*
Maximum	2251.84 ± 508.33	2231.36 ± 532.18	0.841
Mean absolute deviation	147.18 ± 46.96	146.89 ± 51.14	0.976
Mean	1248.80 ± 165.37	1023.07 ± 171.02	< 0.001*
Median	1238.63 ± 177.84	1002.16 ± 170.87	< 0.001*
Minimum	556.75 ± 228.17	432.44 ± 186.38	0.002*
Range	1695.09 ± 664.53	1798.92 ± 604.99	0.395
Robust mean absolute deviation	99.81 ± 32.83	97.81 ± 35.11	0.766
Root mean squared	1264.64 ± 164.74	1042.41 ± 175.67	< 0.001*
Skewness	0.30 ± 0.66	0.89 ± 0.68	< 0.001*
Uniformity	0.040 (0.035, 0.051)	0.043 (0.036, 0.051)	0.481
Variance	36408.81 (20943.50, 53342.96)	34819.11 (22237.20, 57707.43)	0.887
Direct ADC measurements			
Minimum ADC	971.63 ± 226.79	719.32 ± 162.30	< 0.001*
Mean ADC	1146.96 ± 218.15	870.15 ± 157.31	< 0.001*

[#]Continuous variables with normal distribution were described as mean and standard deviations, and continuous variables with skewed distribution were described as median and quartiles. *$P < 0.05$.

IDHmut/MGMTmet gliomas were higher than those of other gliomas, and the difference was statistically significant ($P < 0.001$).

The diagnostic performances of minimum ADC and mean ADC are shown in Table 3. The AUC of mean ADC was 0.844 (95% CI: 0.770–0.918), and the optimal cut-off value was 1073.17×10^{-6} mm^2/s with 67.5% sensitivity and 89.7% specificity. The AUC of minimum ADC was 0.810 (95% CI: 0.721–0.899), and the optimal cut-off value was 945.50×10^{-6} mm^2/s with 65.0% sensitivity and 91.0% specificity.

The diagnostic performance of the combination of the two methods

The diagnostic performances of multivariate logistic regression models are shown in Table 3 and Figure 4. The logistic regression model combining ADC histogram parameters and direct measurements had the best diagnostic efficiency (AUC: 0.938, CI: 0.896–0.980), followed by the logistic regression model combining the ADC histogram parameters with statistically significant difference (AUC: 0.916, CI: 0.868–0.964), and the logistic regression model combining minimum ADC and mean ADC (AUC: 0.851, CI: 0.780–0.921).

Discussion

In this study, we demonstrated the value of DWI in predicting the coexistence of IDHmut and MGMTmet in adult-type diffuse glioma. Both ADC histogram and direct ADC values had good diagnostic performance, and the combination of the two methods had the best predictive value. Previous studies showed that the coexistence of IDHmut and MGMTmet significantly prolonged the overall survival of glioblastoma patients who received temozolomide and radiation therapy (Yang et al., 2015; Li et al., 2016), and IDH mutation and MGMT promoter methylation were independent predictive factors for pseudoprogression disease (Li et al., 2016). Additionally, Tanaka et al. (2015) reported that combined IDH1 mutation and MGMT promoter methylation was associated with a better

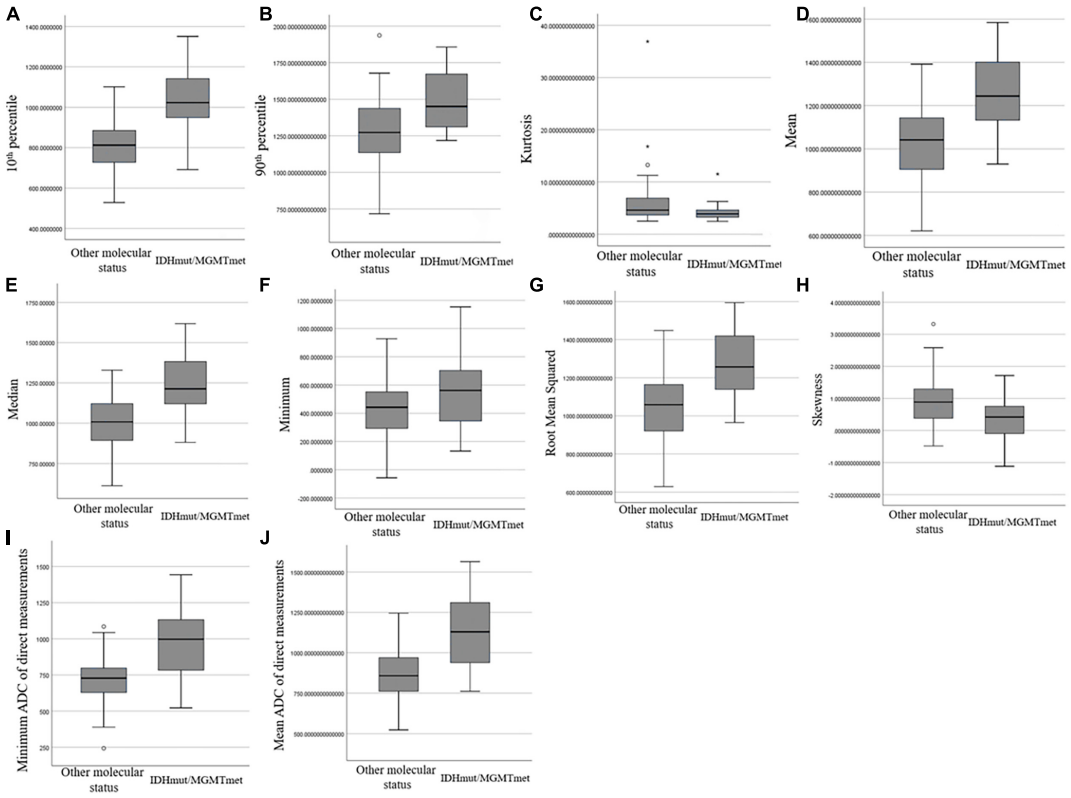

FIGURE 3
Box and whisker plot graphs showing comparison of ADC histogram parameters that were statistically different **(A–H)** and minimum ADC **(I)** and mean ADC **(J)** of direct measurements between IDHmut/MGMTmet and the other glioma group.

prognosis in low-grade glioma. Therefore, the status of IDH mutation and MGMT promoter methylation are important prognostic factors for glioma. A previous study used mean relative ADC to differentiate IDH wild-type and IDH-mutant gliomas with an AUC of 0.790 (Wu et al., 2018). In the current study, the combination of ADC histogram and direct ADC measurements showed the highest value of DWI (AUC = 0.938), which contributed to predicting the prognosis of glioma patients.

In our study, the diagnostic performance of ADC histogram was better than direct ADC measurement in predicting the coexistence of IDHmut and MGMTmet in gliomas. Several studies have compared the diagnostic performance of ADC histogram analysis with direct measurements in tumor grading or differentiating benign from malignant tumors. Han et al. (2017) found that the diagnostic performance of whole-volume histogram analysis was not better than single-slice methods in glioma grading. Another study reported that whole-lesion ADC histogram analysis and single-slice ADC measurement had a similar diagnostic performance in differentiating benign and malignant soft tissue tumors (Ozturk et al., 2021). The reason why our results differed from those of previous studies may be that we selected variables with statistically significant differences to establish the multivariate logistic regression models. The results indicated that the AUC of the logistic regression model combining ADC histogram parameters was higher than that of the model combining parameters obtained by direct measurements.

Apparent diffusion coefficient histogram analysis uses descriptive parameters to characterize and compare distributions of ADC values in a quantitative manner (Just, 2014). In the current study, the ADC histogram parameter of 10th percentile, mean, median, 90th percentile, and minimum described distributions of ADC values of gliomas and the ADC values of IDHmut/MGMTmet gliomas were higher than those of other gliomas. Since lower cellular density led to higher ADC values, we concluded that the cellular density in IDHmut/MGMTmet gliomas was lower than that of other gliomas. The ADC histogram parameter of maximum of IDHmut/MGMTmet gliomas was not statistically significantly different from that of the other group. The reason may be that small cystic and necrotic areas were manually delineated into the ROIs, which was inevitable, even with conscious efforts to avoid cystic and necrotic areas.

Skewness of ADC histogram represents a measure of asymmetrical distribution of ADC value, and an ADC histogram

TABLE 3 The diagnostic performances of ADC histogram parameters that were statistically different between IDHmut/MGMTmet and the other glioma group, minimum ADC and mean ADC of direct measurements and multivariate logistic regression models.

Variable	AUC	95% CI	Cut-off value	Sensitivity	Specificity
ADC histogram parameters					
10th percentile	0.860	0.787–0.934	937.50	80.0%	83.3%
90th percentile	0.759	0.673–0.846	1216.00	100.0%	42.3%
Mean	0.823	0.748–0.899	1108.79	85.0%	69.2%
Median	0.824	0.748–0.900	1085.50	85.0%	67.9%
Minimum	0.655	0.545–0.766	553.50	57.5%	75.6%
Root mean squared	0.818	0.742–0.893	1111.21	85.0%	67.9%
Kurtosis	0.666	0.567–0.765	5.07	87.5%	41.0%
Skewness	0.726	0.632–0.821	0.78	85.0%	59.0%
Direct ADC measurements					
Minimum ADC	0.810	0.721–0.899	945.50	65.0%	91.0%
Mean ADC	0.844	0.770–0.918	1073.17	67.5%	89.7%
Multivariate logistic regression models					
ADC histogram parameters	0.916	0.868–0.964		82.5%	85.9%
Direct ADC measurements	0.851	0.780–0.921		67.5%	88.5%
ADC histogram parameters + direct ADC measurements	0.938	0.896–0.980		87.5%	87.2%

AUC, area under the ROC curve; CI, confidence interval.

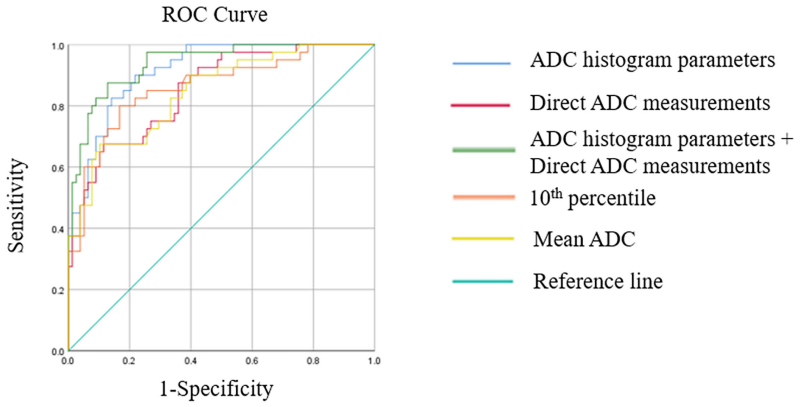

FIGURE 4
This figure shows receiver operating characteristics (ROC) curves of multivariate logistic regression models, the best ADC histogram parameter, and the best parameter of direct ADC measurements.

is generally considered positively skewed if it has an elongated tail on the right side of the mean (Just, 2014). In our study, the skewness value of gliomas with other molecular status was positive and higher than that of IDHmut/MGMTmet gliomas; the difference was statistically significant. Therefore, the skewness of gliomas with other molecular status was more positive than IDHmut/MGMTmet gliomas and the shape of ADC histogram of the former was more asymmetric than the latter. A previous study reported that the change in ADC histogram skewness may be associated with early treatment response to anti-angiogenic therapy in patients with recurrent high-grade glioma (Nowosielski et al., 2011). Our results showed that skewness was predictive of IDHmut/MGMTmet in gliomas.

Kurtosis of ADC histogram represents the peakedness of the distribution of ADC value. In our study, kurtosis was significantly different between IDHmut/MGMTmet and the other group, but its diagnostic value was limited. Root mean square refers to the standard deviation of ADC values of all voxels in the ROI. Our results showed that root mean square of IDHmut/MGMTmet gliomas was higher than that of the other group, and the root mean square had good diagnostic value.

Patients with IDHmut/MGMTmet gliomas were younger than patients with other molecular status in the current study, which was consistent with a previous study (Zhang et al., 2021). In addition, lower grade gliomas were the majority in IDHmut/MGMTmet gliomas, while glioblastoma was the majority in gliomas with other molecular status. This result was consistent with a previous study that reported that a high percentage of lower grade gliomas harbors mutations in IDH1 and IDH2 (Cohen et al., 2013).

Furthermore, the data were collected from MR scanners different field strength (1.5T and 3.0T). However, we compared age, sex, pathological grade, ADC histogram parameters and direct ADC values between 1.5T and 3.0T scanner group. The results were provided in **Supplementary Tables 1, 2**. All parameters with statistically difference between IDHmut/MGMTmet and the other glioma group showed no statistically difference between 1.5T and 3.0T scanner group. We concluded that scanners with different field strengths did not affect the results of the current study. In addition, a previous study reported that ADC is a field strength-independent parameter (Chawla et al., 2009). Another study scanned submandibular glands of three healthy volunteers at both 1.5 and 3.0 T scanners, and there was no statistical difference between ADC values measured on 1.5 and 3.0 T scanners (Kim et al., 2009).

This study has several limitations. First, it was a retrospective study with possible biases in patient selection. Second, the sample size of this single-center study was relatively small, and multicenter studies may be needed to obtain a larger sample size for future analysis. Third, due to the lack of the results of EGFR gene amplification, +7/−10 chromosome copy number changes and CDKN2A/B homozygous deletion (Louis et al., 2021), the pathology of tumors was diagnosed according to the 2016 WHO classification of tumors of CNS. However, gliomas were grouped according to the status of IDH mutation and MGMT promoter methylation in this study, and the results of WHO grade of tumors did not affect the main results of this study.

Conclusion

Both ADC histogram analysis and direct measurements have potential value in predicting the coexistence of IDHmut and MGMTmet in adult-type diffuse gliomas. The diagnostic performance of ADC histogram analysis was better than that of direct ADC measurements. Furthermore, the combination of the two methods showed the best diagnostic performance.

Data availability statement

The raw data supporting the conclusions of this article will be made available by the authors, without undue reservation.

Ethics statement

The studies involving human participants were reviewed and approved by the Medical Ethics Committee of the Affiliated Hospital of Qingdao University. Written informed consent for participation was not required for this study in accordance with the national legislation and the institutional requirements.

Author contributions

ZX and XL designed the idea and framework of the manuscript. CD, SL, LN, and JZ collected the data. SS, YZ, RZ, and HZ conducted a statistical analysis of the data. ZX and JL wrote the manuscript. YL, SS, and XL put forward revisions. All authors contributed to the article and approved the final version of the manuscript.

Funding

This study was funded by National Natural Science Foundation of China (82202113).

Acknowledgments

We thank Gabrielle White Wolf, Ph.D., from Liwen Bianji (Edanz) (www.liwenbianji.cn) for editing the English text of a draft of this manuscript.

Conflict of interest

The authors declare that the research was conducted in the absence of any commercial or financial relationships that could be construed as a potential conflict of interest.

Publisher's note

Supplementary material

The Supplementary Material for this article can be found online at: https://www.frontiersin.org/articles/10.3389/fnins.2022.1099019/full#supplementary-material

References

Binabaj, M. M., Bahrami, A., Shahidsales, S., Joodi, M., Joudi Mashhad, M., Hassanian, S. M., et al. (2018). The prognostic value of Mgmt promoter methylation in glioblastoma: A meta-analysis of clinical trials. *J. Cell Physiol.* 233, 378–386. doi: 10.1002/jcp.25896

Charles-Edwards, E. M., and deSouza, N. M. (2006). Diffusion-weighted magnetic resonance imaging and its application to cancer. *Cancer Imaging* 6, 135–143. doi: 10.1102/1470-7330.2006.0021

Chawla, S., Kim, S., Wang, S., and Poptani, H. (2009). Diffusion-weighted imaging in head and neck cancers. *Future Oncol.* 5, 959–975. doi: 10.2217/fon.09.77

Chen, R., Smith-Cohn, M., Cohen, A. L., and Colman, H. (2017). Glioma subclassifications and their clinical significance. *Neurotherapeutics* 14, 284–297. doi: 10.1007/s13311-017-0519-x

Cindil, E., Sendur, H. N., Cerit, M. N., Erdogan, N., Celebi, F., Dag, N., et al. (2022). Prediction of Idh mutation status in high-grade gliomas using Dwi and High T1-weight Dsc-Mri. *Acad. Radiol.* 29 Suppl 3, S52–S62. doi: 10.1016/j.acra.2021.02.002

Cohen, A. L., Holmen, S. L., and Colman, H. (2013). Idh1 and Idh2 mutations in gliomas. *Curr. Neurol. Neurosci. Rep.* 13:345. doi: 10.1007/s11910-013-0345-4

Han, X., Suo, S., Sun, Y., Zu, J., Qu, J., Zhou, Y., et al. (2017). Apparent diffusion coefficient measurement in glioma: Influence of region-of-interest determination methods on apparent diffusion coefficient values, interobserver variability, time efficiency, and diagnostic ability. *J. Magn. Reson. Imaging* 45, 722–730. doi: 10.1002/jmri.25405

Haque, W., Teh, C., Butler, E. B., and Teh, B. S. (2022). Prognostic and predictive impact of Mgmt promoter methylation status in high risk grade Ii glioma. *J. Neurooncol.* 157, 137–146. doi: 10.1007/s11060-022-03955-3

Haque, W., Thong, E., Andrabi, S., Verma, V., Brian Butler, E., and Teh, B. S. (2021). Prognostic and predictive impact of Mgmt promoter methylation in grade 3 gliomas. *J. Clin. Neurosci.* 85, 115–121. doi: 10.1016/j.jocn.2020.12.028

Just, N. (2014). Improving tumour heterogeneity Mri assessment with histograms. *Br. J. Cancer* 111, 2205–2213. doi: 10.1038/bjc.2014.512

Kim, S., Loevner, L., Quon, H., Sherman, E., Weinstein, G., Kilger, A., et al. (2009). Diffusion-weighted magnetic resonance imaging for predicting and detecting early response to chemoradiation therapy of squamous cell carcinomas of the head and neck. *Clin. Cancer Res.* 15, 986–994. doi: 10.1158/1078-0432.CCR-08-1287

Lee, S., Choi, S. H., Ryoo, I., Yoon, T. J., Kim, T. M., Lee, S. H., et al. (2015). Evaluation of the microenvironmental heterogeneity in high-grade gliomas with Idh1/2 gene mutation using histogram analysis of diffusion-weighted imaging and dynamic-susceptibility contrast perfusion imaging. *J. Neurooncol.* 121, 141–150. doi: 10.1007/s11060-014-1614-z

Li, H., Li, J., Cheng, G., Zhang, J., and Li, X. (2016). Idh mutation and Mgmt promoter methylation are associated with the pseudoprogression and improved prognosis of glioblastoma multiforme patients who have undergone concurrent and adjuvant temozolomide-based chemoradiotherapy. *Clin. Neurol. Neurosurg.* 151, 31–36. doi: 10.1016/j.clineuro.2016.10.004

Louis, D. N., Perry, A., Reifenberger, G., Von Deimling, A., Figarella-Branger, D., Cavenee, W. K., et al. (2016). The 2016 world health organization classification of tumors of the central nervous system: A summary. *Acta Neuropathol.* 131, 803–820. doi: 10.1007/s00401-016-1545-1

Louis, D. N., Perry, A., Wesseling, P., Brat, D. J., Cree, I. A., Figarella-Branger, D., et al. (2021). The 2021 Who classification of tumors of the central nervous system: A summary. *Neuro Oncol.* 23, 1231–1251. doi: 10.1093/neuonc/noab106

McNamara, C., Mankad, K., Thust, S., Dixon, L., Limback-Stanic, C., D'arco, F., et al. (2022). 2021 Who classification of tumours of the central nervous system: A review for the neuroradiologist. *Neuroradiology* 64, 1919–1950. doi: 10.1007/s00234-022-03008-6

Molenaar, R. J., Verbaan, D., Lamba, S., Zanon, C., Jeuken, J. W., Boots-Sprenger, S. H., et al. (2014). The combination of Idh1 mutations and Mgmt methylation status predicts survival in glioblastoma better than either Idh1 or Mgmt alone. *Neuro Oncol.* 16, 1263–1273. doi: 10.1093/neuonc/nou005

Molinaro, A. M., Taylor, J. W., Wiencke, J. K., and Wrensch, M. R. (2019). Genetic and molecular epidemiology of adult diffuse glioma. *Nat. Rev. Neurol.* 15, 405–417. doi: 10.1038/s41582-019-0220-2

Nowosielski, M., Recheis, W., Goebel, G., Güler, O., Tinkhauser, G., Kostron, H., et al. (2011). Adc histograms predict response to anti-angiogenic therapy in patients with recurrent high-grade glioma. *Neuroradiology* 53, 291–302. doi: 10.1007/s00234-010-0808-0

Ozturk, M., Polat, A. V., and Selcuk, M. B. (2021). Whole-lesion Adc histogram analysis versus single-slice Adc measurement for the differentiation of benign and malignant soft tissue tumors. *Eur. J. Radiol.* 143:109934. doi: 10.1016/j.ejrad.2021.109934

Schaff, L. R., Yan, D., Thyparambil, S., Tian, Y., Cecchi, F., Rosenblum, M., et al. (2020). Characterization of Mgmt and Egfr protein expression in glioblastoma and association with survival. *J. Neurooncol.* 146, 163–170. doi: 10.1007/s11060-019-03358-x

Tanaka, K., Sasayama, T., Mizukawa, K., Takata, K., Sulaiman, N. S., Nishihara, M., et al. (2015). Combined Idh1 mutation and Mgmt methylation status on long-term survival of patients with cerebral low-grade glioma. *Clin. Neurol. Neurosurg.* 138, 37–44. doi: 10.1016/j.clineuro.2015.07.019

Wu, C. C., Jain, R., Radmanesh, A., Poisson, L. M., Guo, W. Y., Zagzag, D., et al. (2018). Predicting genotype and survival in glioma using standard clinical mr imaging apparent diffusion coefficient images: A pilot study from the cancer genome atlas. *AJNR Am. J. Neuroradiol.* 39, 1814–1820. doi: 10.3174/ajnr.A5794

Xing, Z., Huang, W., Su, Y., Yang, X., Zhou, X., and Cao, D. (2022). Non-invasive prediction of p53 and Ki-67 labelling indices and O-6-methylguanine-Dna methyltransferase promoter methylation status in adult patients with isocitrate dehydrogenase wild-type glioblastomas using diffusion-weighted imaging and dynamic susceptibility contrast-enhanced perfusion-weighted imaging combined with conventional Mri. *Clin. Radiol.* 77, e576–e584. doi: 10.1016/j.crad.2022.03.015

Xing, Z., Yang, X., She, D., Lin, Y., Zhang, Y., and Cao, D. (2017). Noninvasive Assessment of idh mutational status in world health organization grade Ii and Iii Astrocytomas Using Dwi and Dsc-Pwi combined with conventional Mr Imaging. *AJNR Am. J. Neuroradiol.* 38, 1138–1144. doi: 10.3174/ajnr.A5171

Xing, Z., Zhang, H., She, D., Lin, Y., Zhou, X., Zeng, Z., et al. (2019). Idh genotypes differentiation in glioblastomas using Dwi and Dsc-Pwi in the enhancing and peri-enhancing region. *Acta Radiol.* 60, 1663–1672. doi: 10.1177/0284185119842288

Yan, H., Parsons, D. W., Jin, G., Mclendon, R., Rasheed, B. A., Yuan, W., et al. (2009). Idh1 and Idh2 mutations in gliomas. *N Engl. J. Med.* 360, 765–773. doi: 10.1056/NEJMoa0808710

Yang, P., Zhang, W., Wang, Y., Peng, X., Chen, B., Qiu, X., et al. (2015). Idh mutation and Mgmt promoter methylation in glioblastoma: Results of a prospective registry. *Oncotarget* 6, 40896–40906. doi: 10.18632/oncotarget.5683

Zhang, S., Sun, H., Su, X., Yang, X., Wang, W., Wan, X., et al. (2021). Automated machine learning to predict the co-occurrence of isocitrate dehydrogenase mutations and O(6) -methylguanine-Dna methyltransferase promoter methylation in patients with gliomas. *J. Magn. Reson. Imaging* 54, 197–205. doi: 10.1002/jmri.27498

frontiers | Frontiers in Neuroscience

TYPE Case Report
PUBLISHED 13 April 2023
DOI 10.3389/fnins.2023.1158601

OPEN ACCESS

EDITED BY
Peichen Pan,
Zhejiang University,
China

REVIEWED BY
Sheng Zhong,
Sun Yat-sen University Cancer Center,
China
Lifen Duan,
Kunming Children's Hospital,
China

*CORRESPONDENCE
Hao Xue
✉ xuehao@sdu.edu.cn
Gang Li
✉ dr.ligang@sdu.edu.cn

SPECIALTY SECTION
This article was submitted to Translational Neuroscience, a section of the journal Frontiers in Neuroscience

RECEIVED 04 February 2023
ACCEPTED 23 March 2023
PUBLISHED 13 April 2023

CITATION
Han Z, Chi H, Li X, Jia D, Li H, Ni S, Zhang K, Feng Z, Wang Q, Xue H and Li G (2023) The first prospective application of AIGS real-time fluorescence PCR in precise diagnosis and treatment of meningioma: Case report. *Front. Neurosci.* 17:1158601. doi: 10.3389/fnins.2023.1158601

The first prospective application of AIGS real-time fluorescence PCR in precise diagnosis and treatment of meningioma: Case report

Zhe Han[1,2,3], Huizhong Chi[1,2,3], Xueen Li[1], Deze Jia[1], Haiyan Li[1], Shilei Ni[1], Kailiang Zhang[1], Zichao Feng[1], Qingtong Wang[1,2,3], Hao Xue[1,2,3]* and Gang Li[1,2,3]*

[1]Department of Neurosurgery, Qilu Hospital, Cheeloo College of Medicine, Shandong University, Jinan, Shandong, China, [2]Institute of Brain and Brain-Inspired Science, Shandong University, Jinan, Shandong, China, [3]Shandong Key Laboratory of Brain Function Remodeling, Jinan, Shandong, China

Background: The emergence of the new WHO classification standard in 2021 incorporated molecular characteristics into the diagnosis system for meningiomas, making the diagnosis and treatment of meningiomas enter the molecular era.

Recent findings: At present, there are still some problems in the clinical molecular detection of meningioma, such as low attention, excessive detection, and a long cycle. In order to solve these clinical problems, we realized the intraoperative molecular diagnosis of meningioma by combining real-time fluorescence PCR and AIGS, which is also the first known product applied to the intraoperative molecular diagnosis of meningioma.

Implications for practice: We applied AIGS to detect and track a patient with TERTp mutant meningioma, summarized the process of intraoperative molecular diagnosis, and expounded the significance of intraoperative molecular diagnosis under the new classification standard, hoping to optimize the clinical decision-making of meningioma through the diagnosis and treatment plan of this case.

KEYWORDS

TERTp, PCR, intraoperative, surgery, molecular diagnosis, meningioma

Introduction

Meningiomas have the highest incidence rate (39%) among all primary intracranial and central nervous system tumors. According to a report released in 2021 by the Central Brain Tumor Registry of the United States, the annual age-adjusted incidence rate of meningiomas in the United States (US) was 9.49 per 100,000 population in 2014–2018. The incidence increases with age, with a strong increase after the age of 65 years (Ostrom et al., 2021). The WHO classification of central nervous system tumors, published in 2021, confirmed that any meningioma with a telomerase reverse transcriptase gene promoter (TERTp) mutation and/or CDKN2A or B homozygous deletion, regardless of its histological characteristics, was classified as WHO grade 3 (Louis et al., 2021). This means that some meningiomas with histological diagnoses of grades 1 and 2 are degraded in treatment due to a lack of molecular diagnostic information, which affects the progression-free survival and overall survival of patients. At present, there are only a few molecular markers that are proven to be related to the prognosis of

meningiomas and have diagnostic significance. Therefore, in the actual clinical diagnosis and treatment process, many neurosurgeons and pathologists have a low understanding of molecular diagnosis and still use the diagnostic criteria of histology, resulting in many patients being unable to achieve an accurate diagnosis and individualized treatment. However, due to the differences in the degree of development of various regions, the popularity of molecular testing is high in some regions, but we found that there are many detection sites with less significance under the commercialized detection package, which not only wastes medical resources but also increases the economic burden on patients. At present, the common detection method is postoperative sequencing, which takes a long time, and the average result feedback time is 10 days. Therefore, based on the above clinical problems, we designed a set of products for intraoperative molecular diagnosis. Through the automatic integrated gene detection system (AIGS) and real-time fluorescence PCR technology, the product can feed back the TERTp mutation information of patients within 1 h, realizing individualized and accurate intraoperative diagnosis and treatment under the new classification standard. In this paper, we describe the diagnosis and treatment of a patient with TERTp mutant meningioma and hope to optimize the clinical decision-making process for meningioma.

Case summary

Diagnosis and treatment process

On 23 March 2022, a 54-year-old male patient was treated for half a year due to paroxysmal headache. MRI and MRV examinations were performed on the same day, which showed that there were solid space-occupying lesions near the right frontal midline that were closely related to the superior sagittal sinus, mild compression of brain tissue, and local skull invasion (Figures 1A–E). According to previous experience, considering that meningioma invaded the skull, a CT plain scan and three-dimensional reconstruction were carried out to determine the invasion location and plan the skull repair area (Figures 1F–I). On 29 March 2022, the patient underwent resection of the right frontal tumor. The scalp was cut layer by layer. The skull at the lesion site was slightly raised. After milling the bone flap, the inner plate of the skull was involved and proliferated. After cutting the dura mater along the edge of the tumor, the tumor was gray, the boundary was clear, and there was a small amount of adhesion with the brain tissue. The dura mater of the tumor and surrounding lesions was completely removed, and the affected skull was removed at the same time, and the skull was remodeled with PEEK material (Figures 2A–D). Three days after the operation, we performed a CT scan and three-dimensional reconstruction to observe the intracranial condition and skull repair (Figures 2E–G). The histopathological examination 4 days after the operation revealed that meningioma, WHO grade 2, was absent and no lesion was found at the cutting edge (Figures 2H,I). That is, the operation reached the Simpson I resection. The patient recovered well after the operation and was discharged on 15 April 2022.

Intraoperative molecular diagnosis

Since it is clearly pointed out in the 2021 WHO classification standard for meningiomas, regardless of its histological diagnosis of grade 1, grade 2, or grade 3, as long as there is a TERTp mutation and/or CDKN2A/BB homozygous deletion, it is defined as WHO grade 3 (Louis et al., 2021). Therefore, in order to clarify the mutation status, we used AIGS real-time fluorescence PCR to detect the TERTp mutation during operation (Figure 3A). Take a 2.5–5 mg isolated meningioma sample, add it to the lysis tube, shake it, centrifuge it for 4 min, take the homogenate, add it to the self-designed integrated detection kit, and insert it into the AIGS card slot. The results are given after 50 min. The FAM curve is the C250T mutation (Figure 3B), ROX is the C228T mutation (Figure 3C), and the patient is the C250T mutation. After feeding back the results to the surgeon, he consciously expanded the resection scope of the dura mater based on the original resection and provided a theoretical basis for skull remodeling rather than electrocautery. Patients underwent NGS after surgery to demonstrate the accuracy of detection, and the results indicated the presence of the TERT C250T mutation (Figure 3D). According to the molecular mutation of this patient, the final integrated diagnosis result is: meningioma, TERTp mutation, WHO grade 3. Therefore, at the time of discharge, we provided patients with a more active follow-up adjuvant treatment scheme. Although Simpson I resection was achieved, fractionated radiotherapy (RT) was still necessary, and reexamination should be more frequent. On 9 May 2022, the patient came to the clinic for reexamination, and the imaging examination showed a normal postoperative state. The patient was generally in good condition and was preparing for radiotherapy. The case study was approved by the ethics committee of Qilu Hospital of Shandong University, and the patient provided written, informed consent.

Discussions

Meningiomas are mostly benign tumors and grow slowly. However, some meningiomas relapse, often accompanied by an improvement in grade; most of these meningiomas have specific gene mutations (Saraf et al., 2011). Many studies have shown that the TERTp mutation is associated with poor prognosis and the invasiveness of tumors in meningiomas (Sahm et al., 2016; Mirian et al., 2020). The meta-analysis of Lu et al. found that the TERTp mutation occurred in 8% of meningiomas, and the incidence rates in WHO grade 1, 2, and 3 meningiomas were 1%, 6%, and 14%, respectively. Mortality increased by 3.79 times in the mutant population, and overall survival was cut by 5 years (Lu et al., 2019). Therefore, the revision of molecular markers in the 2021 WHO classification standard replaces the histological classification and grading standards of many brain tumors. For meningiomas, TERTp mutation and/or CDKN2A/B homozygous deletion are regarded as the independent standards for grading grade 3 meningiomas (Louis et al., 2021). There were significant differences in survival and prognosis between WHO grade 3 meningiomas and grade 1 and grade 2 meningiomas. Among 7,811 WHO grade 2 patients and 1936 WHO grade 3 meningiomas obtained from the national cancer database from 2004 to 2014, the 5-year overall survival rate (OS) of grade 2 patients was 75.9% and that of grade 3 meningiomas was 55.4% ($P < 0.0001$; Rydzewski et al., 2018).

As a result, understanding how to accurately grade meningiomas using molecular detection is critical, as it not only affects patients' follow-up adjuvant treatment plans but also predicts their survival and prognosis. At present, the mainstream detection method in the market is NGS, but in the actual clinical work, it is found that the average time

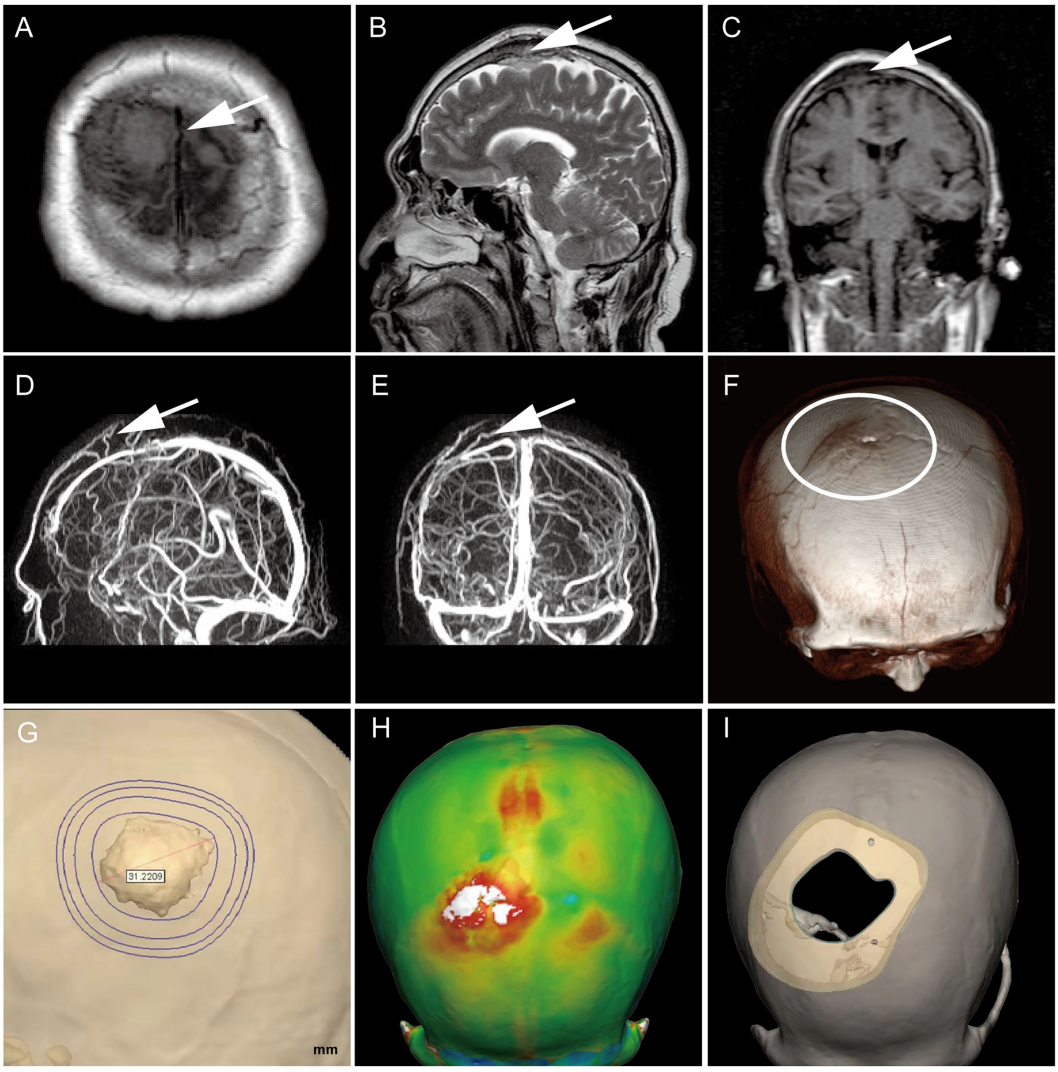

FIGURE 1
Preoperative MRI confirmed the tumor's location (white arrow), with T1 low signal and T2 equal high signal, invading the skull and compressing brain tissue locally **(A–C)**.MRV suggests that it is closely related to the branches of the sagittal sinus **(D,E)**; Preoperative CT three-dimensional reconstruction showed a slight skull bulge at the lesion site **(F)**; Determine the skull repair scheme by three-dimensional modeling **(G–I)**.

of this detection is 10 days, and the results cannot play a role in the intraoperative surgical decision-making. In the guidelines for the diagnosis and treatment of meningiomas issued by the European Association of Neuro-Oncology (EANO; Goldbrunner et al., 2021), it is suggested that for WHO grade 1 meningiomas with high surgical risk, some residual tumors are allowed after weighing, and the residual tumors may not need immediate radiotherapy. Because the recurrence time of WHO grade 3 meningiomas is short and the survival prognosis is poor, radical surgery should be performed as soon as possible. Simpson I resection should be performed as far as possible after it is determined to be WHO grade 3 meningioma during operation to prolong the recurrence time and avoid reoperation. At the same time, in clinical work, we also found that many gene points in commercial NGS detection have little relationship with the typing and prognosis of meningiomas, which not only wastes detection resources but also increases the economic burden of patients. Based on the current research, among many mutation sites, the KLF4/TRAF7 mutation can be used to diagnose secretory meningiomas (Clark et al., 2013; Williams et al., 2019; Youngblood et al., 2021). AKT1 and SMO mutations are related to a better prognosis for meningiomas (Yuzawa et al., 2016; von Spreckelsen et al., 2020). But only TERTp and/or CDKN2A or B can be used for meningioma grading. Therefore, based on the many clinical problems listed above, we have successfully transformed laboratory technology into clinical application by combining AIGS and real-time fluorescence PCR detection and designing the TERT mutation detection kit. In the preliminary study (Chinese Clinical Trial Registry: ChiCTR2100048172), we have evaluated the sensitivity, specificity, and accuracy of the detection technology, and the detection results are completely consistent with the results of the NGS. It can complete the automatic interpretation of the results within 1 h, and the accuracy rate is up to 100%,which can be applied in the operation (Xue et al., 2022). In our case, it is precisely because of the TERTp mutation information provided by AIGS that we can diagnose WHO grade 3 meningioma during operation. Therefore, we consciously performed an extended resection of the dura mater based on the original resection and decisively removed the

10.3389/fnins.2023.1158601

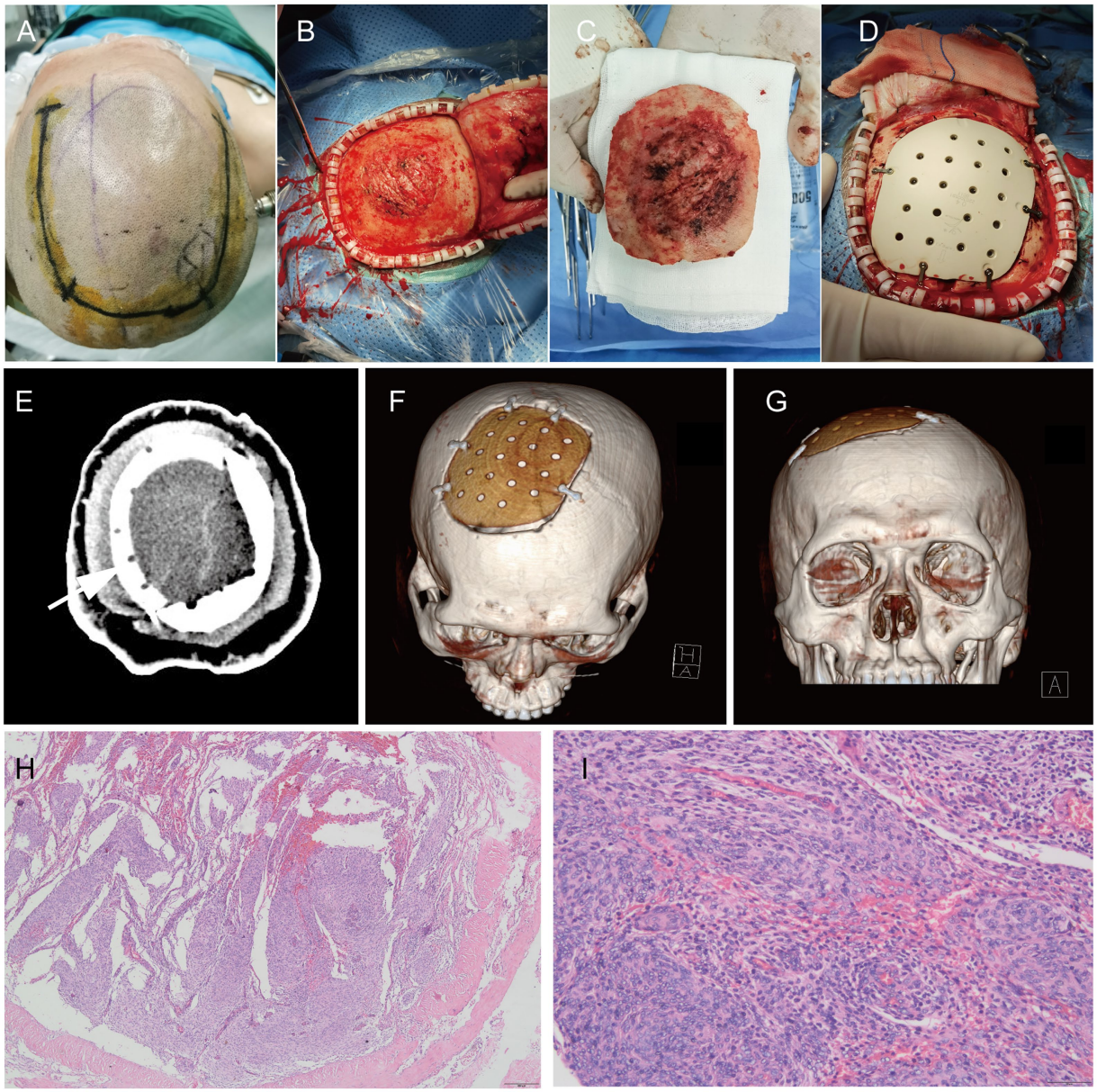

FIGURE 2
During the operation, the scalp incision range was planned **(A)**. After cutting the periosteum, the outer plate of the skull was rough and convex **(B)**. After removing the bone flap, the inner plate of the skull was severely eroded **(C)**. PEEK material was used for repair **(D)**; CT plain scan **(E)** and three-dimensional reconstruction **(F,G)** were performed after operation; H&E staining pictures of pathological tissues of meningiomas after operation: 40x **(H)** and 200X **(I)**.

invading skull and remolded it. Although no obvious histological features of grade 3 meningioma were found in postoperative histopathology, which was more inclined to grade 2, this did not hinder the diagnosis of WHO grade 3 meningioma.

EANO clearly stated in the guidelines for the diagnosis and management of meningiomas that molecular diagnosis of meningiomas is strongly recommended, which is not only related to accurate classification but also plays an important role in the treatment decision of meningiomas (Goldbrunner et al., 2021). At present, intraoperative molecular diagnosis has been applied to breast cancer, gastric cancer, lung cancer, etc. (Tamaki et al., 2009; Shimizu et al., 2012; Namba et al., 2022) providing a theoretical basis for optimizing the operation plan, determining the resection scope, and defining the subtype. However, the concept of intraoperative molecular diagnosis of central nervous system tumors has not been deepened. In the currently known research, we are the first team to develop intraoperative molecular diagnosis of meningiomas, and we have realized the transformation from basic to clinical research through early research. Therefore, due to the realization of intraoperative rapid molecular diagnosis technology, we believe that during the operation of meningioma resection, some tumor tissues should be taken for molecular diagnosis. When the detected tumor contains the TERTp mutation, the operation strategy should be adjusted and a more active resection scheme should be adopted. The bone tissue and dura that

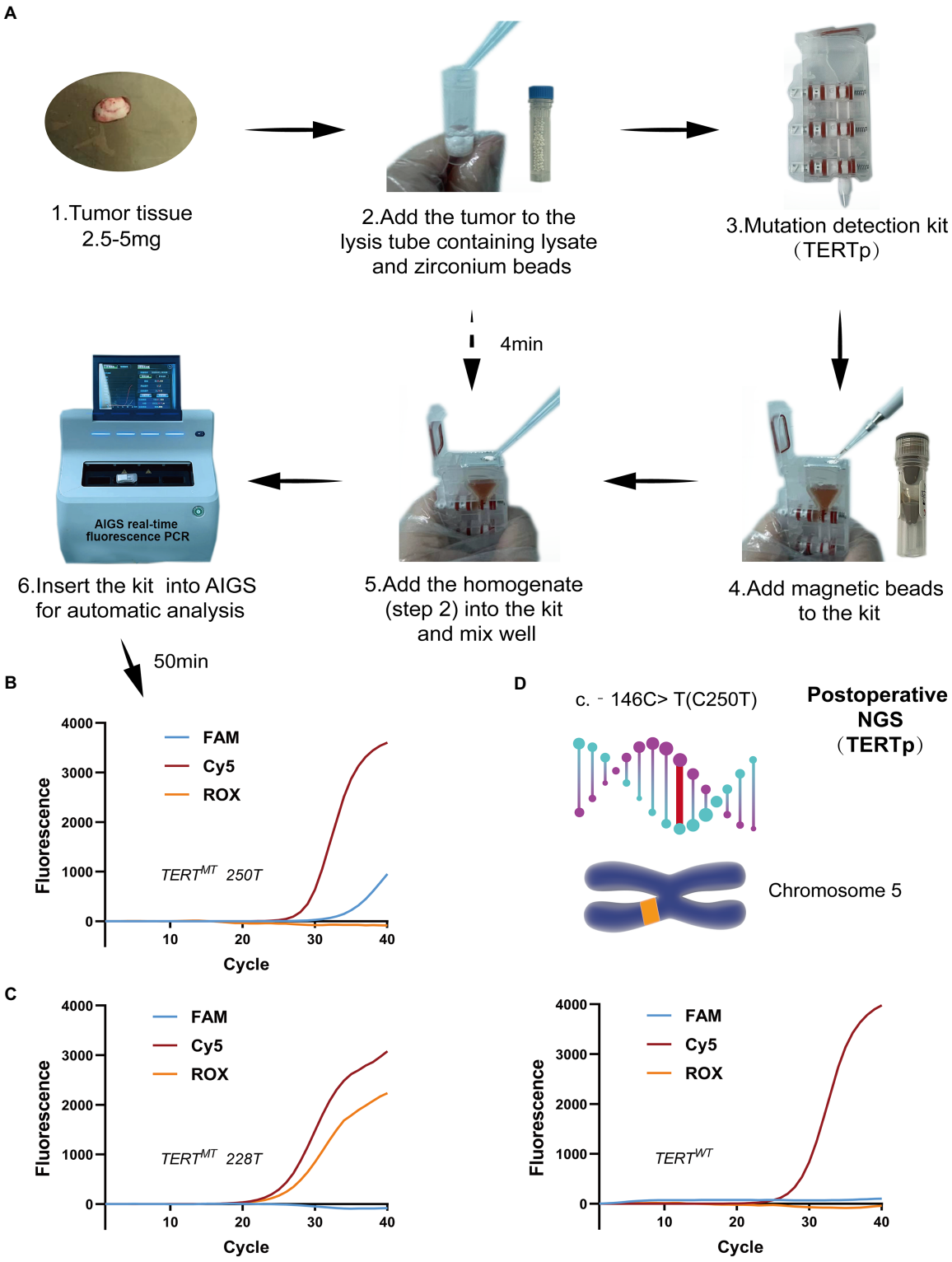

FIGURE 3
AIGS real-time fluorescence PCR was used for intraoperative molecular diagnosis **(A)**. Real-time fluorescence curve **(B)** represents TERTp C250T mutation (FAM and Cy5 showed S-type amplification). NGS was performed at the same time after operation. The results showed that the patient had TERTp C250T mutation **(C)**; Panel **(D)** represents the meaning of the other two curves detected by AIGS. (Left): TERTp C228T mutation (ROX and Cy5 showed S-type amplification), (Right): TERTp wild type (Cy5 showed S-type amplification). FAM is the C250T probe, Cy5 is the GAPDH internal reference probe, and ROX is the C228T probe.

could have been retained should be removed together, and the resection scope should be expanded as much as possible. When it adheres to brain tissue, part of the brain tissue should be removed.

AIGS real-time fluorescence PCR detection can be applied not only to meningiomas but also to gliomas, because our detection kit also includes the detection of the most important IDH mutation in gliomas.

We believe that soon, the popularization of intraoperative molecular diagnosis technology will optimize the intraoperative treatment strategies for meningiomas, gliomas, and other brain tumors.

Limitations

The detection time is a critical factor in the surgical process. Even though we can complete the detection in 1 h, strict surgical procedures may have an effect on the process. As a result, we have upgraded the next generation of AIGS products to further reduce detection time (within 35 min), and the sample size for synchronous detection has been expanded (16 detection channels) to meet different surgical needs while minimizing the impact on the surgical process. As a case report, this study cannot provide a clear conclusion on the level of evidence-based medicine, which would necessitate increasing the sample size and conducting long-term follow-up to assess prognosis. In addition, our team is conducting research in this area.

Conclusion

In this case study, AIGS real-time fluorescence PCR was used for intraoperative molecular diagnosis of TERTp mutant meningioma. As the first product applied to intraoperative molecular diagnosis of meningioma, it has important pioneering significance. Through this technology, TERTp mutation can be accurately judged during operation, allowing us to adjust the operation plan in real time, optimize the treatment strategy, and provide important evidence support for intraoperative targeted treatment in the future. Finally, we strive to improve the survival and prognosis of patients.

Patient perspective

Now is the 10th month after the operation. The patient came to the clinic for re-examination. From the imaging performance, the patient recovered well without any sign of recurrence. The patient was very satisfied with the surgical results and expressed his affirmation on the application of intraoperative molecular diagnosis and judgment technology to the determination of meningioma nature. Finally, the patient was also very happy to help more people with his diagnosis and treatment through case sharing.

Data availability statement

The original contributions presented in the study are included in the article/supplementary material, further inquiries can be directed to the corresponding authors.

Ethics statement

Ethical approval was not provided for this study on human participants because this study does not interfere with the normal diagnosis and treatment of patients. As a case report, it is important to record the whole diagnosis and treatment process of patients. The patients/participants provided their written informed consent to participate in this study. Written informed consent was obtained from the individual(s) for the publication of any potentially identifiable images or data included in this article.

Author contributions

HX and GL designed and concepted of the study. ZH drafted the manuscript. HX revised the manuscript. HL, XL, DJ, KZ, and SN analyzed and interpreted of the data. ZH, HC, QW, and ZF played the role in the acquisition of data. All authors contributed to the article and approved the submitted version.

Funding

This work was supported by the research on the future application prospect of classical gene marker Kit (contract no. 6010122006), Key Clinical Research Project of Clinical Research Center of Shandong University (2020SDUCRCA011), and Taishan Pandeng Scholar Program of Shandong Province (no. tspd20210322).

Acknowledgments

The authors thank the patient for agreeing to participate in the case report.

Conflict of interest

The authors declare that the research was conducted in the absence of any commercial or financial relationships that could be construed as a potential conflict of interest.

Publisher's note

References

Clark, V. E., Erson-Omay, E. Z., Serin, A., Yin, J., Cotney, J., Ozduman, K., et al. (2013). Genomic analysis of non-NF2 meningiomas reveals mutations in TRAF7, KLF4, AKT1, and SMO. *Science* 339, 1077–1080. doi: 10.1126/science.1233009

Goldbrunner, R., Stavrinou, P., Jenkinson, M. D., Sahm, F., Mawrin, C., Weber, D. C., et al. (2021). EANO guideline on the diagnosis and management of meningiomas. *Neuro Oncol.* 23, 1821–1834. doi: 10.1093/neuonc/noab150

Louis, D. N., Perry, A., Wesseling, P., Brat, D. J., Cree, I. A., Figarella-Branger, D., et al. (2021). The 2021 WHO classification of tumors of the central nervous system: a summary. *Neuro Oncol.* 23, 1231–1251. doi: 10.1093/neuonc/noab106

Lu, V. M., Goyal, A., Lee, A., Jentoft, M., Quinones-Hinojosa, A., and Chaichana, K. L. (2019). The prognostic significance of TERT promoter mutations in meningioma: a systematic review and meta-analysis. *J. Neurooncol* 142, 1–10. doi: 10.1007/s11060-018-03067-x

Mirian, C., Duun-Henriksen, A. K., Juratli, T., Sahm, F., Spiegl-Kreinecker, S., Peyre, M., et al. (2020). Poor prognosis associated with TERT gene alterations in meningioma is independent of the WHO classification: an individual patient data meta-analysis. *J. Neurol. Neurosurg. Psychiatry* 91, 378–387. doi: 10.1136/jnnp-2019-322257

Namba, K., Suzawa, K., Shien, K., Miura, A., Takahashi, Y., Miyauchi, S., et al. (2022). One-step nucleic acid amplification for intraoperative diagnosis of lymph node metastasis in lung cancer patients: a single-center prospective study. *Sci. Rep.* 12:7297. doi: 10.1038/s41598-022-11064-4

Ostrom, Q. T., Cioffi, G., Waite, K., Kruchko, C., and Barnholtz-Sloan, J. S. (2021). CBTRUS statistical report: primary brain and other central nervous system tumors diagnosed in the United States in 2014-2018. *Neuro Oncol.* 23, iii1–iii105. doi: 10.1093/neuonc/noab200

Rydzewski, N. R., Lesniak, M. S., Chandler, J. P., Kalapurakal, J. A., Pollom, E., Tate, M. C., et al. (2018). Gross total resection and adjuvant radiotherapy most significant predictors of improved survival in patients with atypical meningioma. *Cancer* 124, 734–742. doi: 10.1002/cncr.31088

Sahm, F., Schrimpf, D., Olar, A., Koelsche, C., Reuss, D., Bissel, J., et al. (2016). TERT promoter mutations and risk of recurrence in meningioma. *J. Natl. Cancer Inst.* 108:djv377. doi: 10.1093/jnci/djv377

Saraf, S., McCarthy, B. J., and Villano, J. L. (2011). Update on meningiomas. *Oncologist* 16, 1604–1613. doi: 10.1634/theoncologist.2011-0193

Shimizu, Y., Takeuchi, H., Sakakura, Y., Saikawa, Y., Nakahara, T., Mukai, M., et al. (2012). Molecular detection of sentinel node micrometastases in patients with clinical N0 gastric carcinoma with real-time multiplex reverse transcription-polymerase chain reaction assay. *Ann. Surg. Oncol.* 19, 469–477. doi: 10.1245/s10434-011-2122-4

Tamaki, Y., Akiyama, F., Iwase, T., Kaneko, T., Tsuda, H., Sato, K., et al. (2009). Molecular detection of lymph node metastases in breast cancer patients: results of a multicenter trial using the one-step nucleic acid amplification assay. *Clin. Cancer Res.* 15, 2879–2884. doi: 10.1158/1078-0432.CCR-08-1881

von Spreckelsen, N., Waldt, N., Poetschke, R., Kesseler, C., Dohmen, H., Jiao, H. K., et al. (2020). KLF4(K409Q)-mutated meningiomas show enhanced hypoxia signaling and respond to mTORC1 inhibitor treatment. *Acta Neuropathol. Commun.* 8:41. doi: 10.1186/s40478-020-00912-x

Williams, S. R., Juratli, T. A., Castro, B. A., Lazaro, T. T., Gill, C. M., Nayyar, N., et al. (2019). Genomic analysis of posterior fossa meningioma demonstrates frequent AKT1 E17K mutations in foramen magnum Meningiomas. *J Neurol Surg B Skull Base* 80, 562–567. doi: 10.1055/s-0038-1676821

Xue, H., Han, Z., Li, H., Li, X., Jia, D., Qi, M., et al. (2022). Application of intraoperative rapid molecular diagnosis in precision surgery for Glioma: mimic the World Health Organization CNS5 integrated diagnosis. *Neurosurgery* 92, 762–771. doi: 10.1227/neu.0000000000002260

Youngblood, M. W., Miyagishima, D. F., Jin, L., Gupte, T., Li, C., Duran, D., et al. (2021). Associations of meningioma molecular subgroup and tumor recurrence. *Neuro Oncol.* 23, 783–794. doi: 10.1093/neuonc/noaa226

Yuzawa, S., Nishihara, H., Yamaguchi, S., Mohri, H., Wang, L., Kimura, T., et al. (2016). Clinical impact of targeted amplicon sequencing for meningioma as a practical clinical-sequencing system. *Mod. Pathol.* 29, 708–716. doi: 10.1038/modpathol.2016.81

frontiers | Frontiers in Neuroscience

TYPE Case Report
PUBLISHED 17 May 2023
DOI 10.3389/fnins.2023.1174309

OPEN ACCESS

EDITED BY
Ye Cheng,
Capital Medical University, China

REVIEWED BY
Xinyu Wang,
Jilin University, China
Liang Zhang,
The First Affiliated Hospital of China Medical University, China

*CORRESPONDENCE
Run Cui
✉ cuir@gd2h.org.cn

†These authors have contributed equally to this work and share first authorship

RECEIVED 26 February 2023
ACCEPTED 27 April 2023
PUBLISHED 17 May 2023

CITATION
Wang S, Yang W, Zhu M, Wang X, Pan L, Jin T, Chen Y, Xi J, Yang L and Cui R (2023) Cerebrospinal fluid protein levels are elevated 100 times in a Leptomeningeal metastasis patient: a case report and literature review. *Front. Neurosci.* 17:1174309. doi: 10.3389/fnins.2023.1174309

Cerebrospinal fluid protein levels are elevated 100 times in a Leptomeningeal metastasis patient: a case report and literature review

Shengnan Wang[1,2†], Wenzhuo Yang[3†], Mingqin Zhu[2†], Xiaochuang Wang[3†], Lin Pan[4†], Tao Jin[2], Youqi Chen[4], Jianxin Xi[4], Laiyu Yang[4] and Run Cui[1*]

[1]Department of Neurosurgery, Guangdong Second Provincial General Hospital, Guangzhou, China, [2]Department of Neurology, The First Hospital of Jilin University, Changchun, China, [3]Department of Neurosurgery, Cancer Hospital of Sun Yat-sen University, Guangzhou, China, [4]Clinical College, Jilin University, Changchun, China

Leptomeningeal metastasis (LM) has a high degree of malignancy and high mortality. We describe a patient admitted to hospital with acute lower extremity weakness, dysuria, and high intracranial pressure. Enhanced magnetic resonance imaging (MRI) showed extensive enhancement of the leptomeningeal and spinal meninges with multiple nodular changes and extensive fusion. His cerebrospinal fluid (CSF) was yellow and cloudy, the Pandy test was strongly positive (++++), the protein was 46 g/L (normal range 0.15–0.45 g/L), which attracted our attention. Initially, miliary TB with associated tuberculous meningitis (TBM) was diagnosed, and neurosarcoidosis cannot be ruled out. After poor therapeutic effect of standard antituberculosis (anti-TB) therapy, further inspection found that malignant cells were detected by cerebrospinal fluid (CSF) cytology. PET/CT suggested the diagnosis of LM. The purpose of this paper is to describe the characteristics of atypical diffuse LM. In conclusion, when patient with unexplained high levels of CSF protein, it is necessary to be alert to the diagnosis of LM. Multiple examinations of fresh CSF are helpful to increase the positive detection rate of tumor cells. Early diagnosis and active treatment are conducive to improving survival rate.

KEYWORDS

leptomeningeal metastasis, tuberculous meningitis, CSF protein, cytology, CNS tumor

1. Introduction

Leptomeningeal metastasis (LM) or leptomeningeal carcinomatosis, is characterized by the spread of tumor cells to the leptomeninges and the subarachnoid space (Mack et al., 2016). When LM is diagnosed, it is usually late in the disease process, and it is usually associated with a high level of systemic tumor burden (Wasserstrom et al., 1982; Balm and Hammack, 1996). Patients can present with a wide range of symptoms related to the involvement of various sites in the craniospinal axis. It is not always easy to diagnose, and clinicians need to always have a high level of suspicion.

Protein levels in cerebrospinal fluid (CSF) are one of the most sensitive indicators of pathology in the central nervous system. CSF protein levels are elevated in infections,

intracranial hemorrhages, multiple sclerosis, Guillain Barré syndrome, malignancies, some endocrine abnormalities, certain medication use, and a variety of inflammatory conditions (Talati et al., 2008).

Non-tuberculous mycobacteria (NTM) infections of the CNS are extremely rare. Neurosurgery, trauma, intracranial implants, otomastoiditis, and disseminated infection are important modes of acquisition (Maniu et al., 2001). Infections due to Mycobacterium abscessus complex are rare among NTM CNS diseases, and only four case reports have been published in English-language literature (Liebeskind et al., 2001; Maniu et al., 2001; Seehusen et al., 2003; Lee et al., 2012).

Here, we present a case of a patient without a history of systemic malignancy, who was diagnosed with LM after a delay. The patient's CSF protein was extremely high (46.17 g/L, normal range 0.15–0.45 g/L) and glucose was extremely low (0.28 mmol/L, normal range 2.3–4.1 mmol/L), which attracted our attention. Since no cancer cells were found in the CSF, and the MRI features were similar to those of tuberculous meningitis, the patient was diagnosed as tuberculous meningitis at an early stage of onset. The patient did not improve after standard antituberculosis (anti-TB) treatment. After repeated CSF examinations, heteromorphic cells were discovered, and the patient was eventually diagnosed with LM.

2. Case report

A 33-year-old male who had been experiencing neck pain for a month and dysuria for a week was admitted to a local hospital for examination. Cervical MRI plain scan and enhanced scan done at the local hospital revealed multiple abnormal signals in the central canal of spinal cord on November 28, 2021 (Figure 1). Primary lumbar puncture (LP) was performed, and his CSF suggested high protein (2.95 g/L, normal range 0.15–0.45 g/L), high white blood cells (WBC) count ($243*10^6$/L, normal range 0–$8*10^6$/L), low glucose level (0.88 mmol/L, normal range 2.3–4.1mmol/L) and low chloride level (113 mmol/L, normal range 119–129 mmol/L). Color Doppler sonography of urinary system suggested right renal cyst, turbid urine in the bladder, prostate calcifications and prostate cyst. Ceftazidime was given anti-inflammatory treatment during local hospitalization, but he did not show improvement and had trouble defecating after 2 days. On the third day the patient was transferred to our hospital for further treatment.

The patient had dizziness, headache, nausea and vomiting occasionally, however, no physical activity disorder and no fever was present during the early stage. The patient was previously healthy and had occasional neck pain a year ago, which resolved spontaneously. Neurological exam showed right lower limb muscle strength grade 4, Kernig sign (+), neck rigidity (+), and a bilateral Babinski sign, all other neurological examination were otherwise normal. The brain MRI were conducted on the second day following admission, shows abnormal signal and nodular enhancement of medulla oblongata and cervical medulla. Considering the patient's long spinal cord lesion, mannitol Q6H dehydration treatment was given at once. Upon admission, based on the clinical symptoms, the possibility of myelitis was considered. Levels of AQP4, MOG, MBP and GFAP antibodies in serum and CSF were measured and negative.

We performed LP to collect CSF on the third day following admission and yielded a surprising result. CSF routine test showed high intracranial pressure (240 mmH_2O, normal range: 80–180 mmH_2O). CSF was yellow and cloudy (Figure 2B), the Pandy test was strongly positive (++++), the protein was 46 g/L (normal range 0.15–0.45 g/L), which was an unbelievable result. His CSF glucose was also extremely low (0.28 mmol/L, normal range 2.3–4.1 mmol/L), which was a significant deterioration compared to the last test performed a week ago. Cytology was not possible due to rapid coagulation of the patient's cerebrospinal fluid.

The patient's condition deteriorated rapidly. Combined with the imaging findings and extremely elevated cerebrospinal fluid protein levels, tuberculous meningitis cannot be ruled out. Standard antituberculosis (anti-TB) therapy was given, including isoniazid 0.6 g 1/day intravenously, rifampicin 0.6 g 1/day intravenously, pyrazinamide 1.5 g 1/day orally and ethambutol 0.75 g 1/day orally. At the same time, liver protection treatment was carried out. Two days later, he had vision and restlessness at night, which was relieved by risperidone. The next morning, the patient developed severe headache and projectile vomiting. Neurological exam showed double lower limb muscle strength down to grade 3. We performed the third LP to collect CSF. His intracranial pressure was over 400 mmH_2O. CSF routine test showed the protein was 34.12 g/L, the glucose was 0.15 mmol/L, the WBC count was $202*10^6$/L and the Chloride level was 102.4 mmol/L. Metagenomic next-generation sequencing (NGS) of viral and bacterial genomes from the CSF was performed, which was positive exclusively for the normal skin flora DNA and was not significant. Xpert MTB/RIF prior, rpoB sequencing and Brucella serology were also performed, but no significant results were detected. A day later, the patient was transferred to the infectious disease hospital for further treatment.

CSF cytology specimens were performed twice and were finally positive for malignant cells (Figure 2A). We performed whole genome sequencing for MTB&NTM and full-length resistance genes sequencing by the third generation nanopore sequencing technology. Subsequently, mycobacterium abscessus have been sequenced, the number of which was 7,940. He subsequently underwent the whole-body 18F-FDG positron emission tomography/computed tomography (PET/CT) scanning. It revealed multiple hypermetabolic foci in leptomeningeal and the whole spinal cord, indicating primary meningeal malignancy with spinal cord spread. The patient was eventually diagnosed with LM and admitted to the Radiotherapy Department of our hospital on December 24, 2021. Although we actively contacted neurosurgery department of our hospital to prepare the spinal cord biopsy, the patient had a fever and died after 2 days.

3. Discussion

We present a 33-year male patient, who manifested as acute episode of dysuria and lower limb weakness with marked inhomogeneous enhanced nodules in the meninges. Tuberculous meningitis was initially considered, anti-TB and dehydration therapy were given. However, the symptoms of

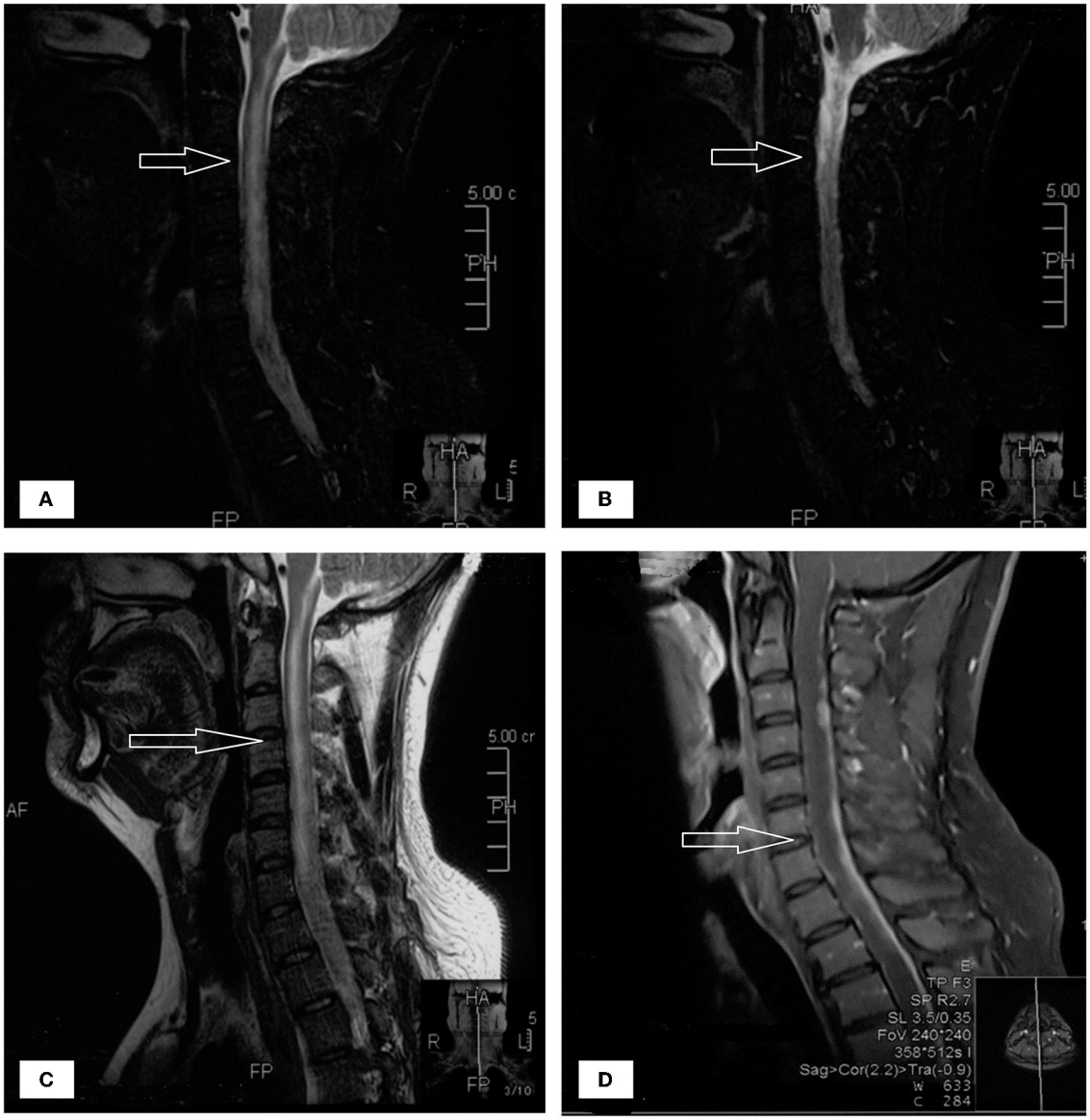

FIGURE 1
(A–D) The patient's spinal MRI showed multiple abnormal signals in the central canal of spinal cord, as shown by the arrow.

the patient progressively deteriorated. Afterwards, malignant cells were found in his CSF, and mycobacterium abscessus 7,940 infection was detected, LM and CNS Mycobacterium abscessus infection was diagnosed. Unfortunately, the patient died without further diagnosis.

The patient presented with acute episode of dysuria and lower limb weakness with marked inhomogeneous enhanced nodules in the meninges. CSF protein levels are elevated up to over 100 times. Neuromyelitis optica spectrum disorders (NMOSD) scans may occasionally show a cloud-like pattern of gadolinium enhancement with an inhomogeneous appearance and poorly defined margins; also, enhancements of the peripendyma and leptomeninges are common (Pekcevik et al., 2016). A variety of infectious diseases can also cause cerebral enhancement, including Lyme disease, Candida albicans, Cryptococcus, neurotuberculosis, and histoplasmosis (Bot et al., 2020). Combined with the results of several routine examinations of CSF (Table 1), the patient was critically ill at that time, with a rapid progression of his condition. Thus, tuberculous meningitis was initially considered and the patient was treated with anti-TB and dehydration therapy while awaiting the return of NGS for viral and bacterial genomes results, however, the patient's symptom deteriorated with the above treatment and NGS results came back negative. Although NGS provides a substantial improvement in accurate diagnosis of TBM, it still had a negative predictive value of 90.1% for definite TBM, which does not represent a perfect rule-out test. Therefore, the diagnosis of tuberculous meningitis cannot be excluded, and we continued with LP examination to collect CSF for further diagnose.

Symptoms of LM include cranial nerve palsies, radicular symptoms, and signs of increased intracranial pressure, such as

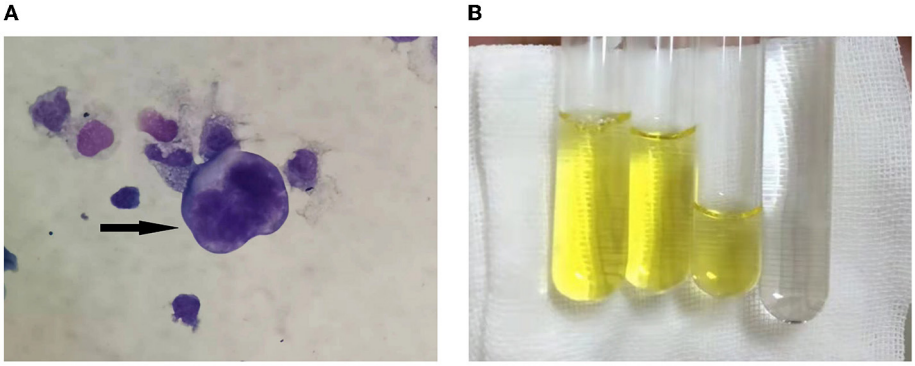

FIGURE 2
(A) Cerebrospinal fluid cytology showed atypical tumor cells, as shown by the arrow. **(B)** The CSF aspired was yellowish and viscous compared with the clear water.

TABLE 1 Cytological examination of CSF.

	Protein (normal range 0.15–0.45 g/L)	WBC count (normal range 0–8*10^6/L)	Glucose level (normal range 2.3–4.1 mmol/L)	Chloride level (normal range 119–129 mmol/L)
December 1, 2021	2.95 ↑	243 ↑	0.88 ↓	113 ↓
December 7, 2021	46.17 ↑	106 ↑	0.28 ↓	105.5 ↓
December 9, 2021	34.12 ↑	202 ↑	0.15 ↓	102.4 ↓

↑, increase; ↓, decrease.

headaches, nausea, vomiting, and cognitive dysfunction (Mack et al., 2016). Due to the rapid progression of the patient's disease, the possibility of tumor was considered. Meningeal metastases commonly present as arachnoidal, subependymal, or dural enhancement; superficial cerebral lesions; and communicating hydrocephalus (Bot et al., 2020). Therefore, LM may be the primary lesion in patients with malignant tumor, although the patient has no history of tumor. In addition to clinical manifestations of neurologic involvement and tumor history, LM diagnosis relies more on CSF cytology and imaging (especially MRI enhanced scanning). At present, finding tumor cells in CSF is the gold standard for LM diagnosis, but there is a certain false negative rate. Therefore, withdrawing a sufficient amount of CSF or repeating the procedure multiple times were recommended in order to avoid false-negative results (Glantz et al., 2015). Afterwards, malignant cells were found in his CSF, connecting with his PET/CT results, the diagnosis of LM was excluded.

Non-tuberculous mycobacteria (NTM) refer generally to mycobacteria other than Mycobacterium tuberculosis complex (MTB) and Mycobacterium leprae. Moreover, MTB and NTM infections often cause indistinguishable clinical symptoms, but their treatment can be vastly different (Peng et al., 2021). Clinically, the low prevalence of NTM infections puts them rarely in the differential diagnosis of CNS infections, which occurs more frequently in patients with immunosuppression. Mycobacterium abscessus is an acid-fast NTM, which can cause the most drug-resistant NTM infections (Kasperbauer and Groote, 2015), and there is an urgent need for new drug development to improve the treatment outcomes for NTM diseases (Koh, 2011; Choules et al., 2019). Antimicrobial susceptibility testing should be performed whenever possible to guide therapy selection. Therefore, additional attention should be paid to the screening and identification of patients with unexplained CNS infection in clinical practice.

Under normal circumstances, CSF protein levels are much lower than those in the blood, and in healthy people CSF protein levels are about 0.5% of plasma protein concentrations (normal range 35–55 g/L). The patient's CSF protein concentration reached an astonishing 46 g/L, which has never been reported in the literature before. We analyzed that the increased CSF protein content in patients with meningeal carcinomatosis is due to the massive proliferation of cancer cells infiltrating meningeal, which further destroys the blood-brain barrier, elevates vascular permeability, and leads to a large amount of exudation of WBC and proteins. The blood-CSF-barrier dysfunction in leptomeningeal metastasis is most likely caused by reduced CSF absorption due to obstruction by malignant cells (Chamberlain, 2008; Djukic et al., 2017). At the same time, the patient was complicated with NTM infection, which further aggravated the damage and increased permeability of BBB. Although the patient had a significant increase in CSF protein concentration, it did not lead to a definitive diagnosis of meningeal carcinomatosis, and CSF cytology remained irreplaceable. Unfortunately, the patient died too early, and we didn't have time to perfect the biopsy to determine the nature of the tumor, which was a limitation of our study.

LM is an advanced malignant tumor with poor prognosis. Untreated patients cannot relieve symptoms and the course of disease is irreversible. At present, the treatment effect of LM is not ideal, there is no clear treatment method, and there are still no standard treatment guidelines. The main purpose

of the treatment of LM is to reduce and improve the patient's clinical neurological symptoms and signs, prolong the survival period, and improve the quality of life. Current treatment methods include surgery, radiotherapy, systemic chemotherapy, intrathecal chemotherapy, targeted therapy, immunotherapy and support therapy.

In conclusion, LM has a variety of manifestations, and the possibility of LM should be considered in patients with increased intracranial pressure, cranial nerve palsy, or spinal nerve root involvement accompanied by abnormal white matter signals in the spinal cord. Further enhanced cerebral spinal MR scan and CSF cytology are required to confirm the diagnosis. For patients with diagnosis difficulties, enhanced spinal membrane or nerve root biopsy is feasible when necessary to avoid delayed diagnosis and treatment and affect the prognosis.

Data availability statement

The original contributions presented in the study are included in the article/supplementary material, further inquiries can be directed to the corresponding author.

Ethics statement

Written informed consent was obtained from the individual(s) for the publication of any potentially identifiable images or data included in this article.

Author contributions

SW drafted the article. LP, WY, and XW contributed to editing and revision. TJ contributed to patient follow-up. MZ and RC has substantively edited the manuscript. JX, YC, and LY collected clinical data for us. All author has made substantial contributions to the manuscript. All authors have read and agreed to the final version of this manuscript.

Funding

This study was supported by grants from the Guangdong Yiyang Healthcare Charity Foundation (No. JZ2022005).

Conflict of interest

The authors declare that the research was conducted in the absence of any commercial or financial relationships that could be construed as a potential conflict of interest.

Publisher's note

References

Balm, M., and Hammack, J. (1996). Leptomeningeal carcinomatosis: presenting features and prognostic factors. *Arch. Neurol.* 53, 626–632 doi: 10.1001/archneur.1996.00550070064013

Bot, J. C. J., Mazzai, L., Hagenbeek, R. E., Ingala, S., van Oosten, B., Sanchez-Aliaga, E., et al. (2020). Brain miliary enhancement. *Neuroradiology* 62, 283–300. doi: 10.1007/s00234-019-02335-5

Chamberlain, M. C. (2008). Neoplastic Meningitis. *World J Gastrointestinal Oncology* 8, 249–258. doi: 10.1016/B978-012370863-2.50010-5

Choules, M. P., Wolf, N. M., Lee, H., Anderson, J. R., Grzelak, E. M., Wang, Y., et al. (2019). Rufomycin targets ClpC1 proteolysis in *Mycobacterium tuberculosis* and *M. abscessus*. *ASM J.* 63:e02204-18. doi: 10.1128/AAC.02204-18

Djukic, M., Trimmel, R., Nagel, I., Spreer, A., Lange, P., Stadelmann, C., et al. (2017). Cerebrospinal fluid abnormalities in meningeosis neoplastica: a retrospective 12-year analysis. *Fluids Barriers CNS* 14, 7. doi: 10.1186/s12987-017-0057-2

Glantz, M. J., Cole, B. F., Glantz, L. K., Cobb, J., Mills, P., Lekos, A., et al. (2015). Cerebrospinal fluid cytology in patients with cancer: minimizing false-negative results. *Cancer* 82, 733–7393. doi: 10.1002/(SICI)1097-0142(19980215)82:4<733::AIDCNCR17>3.0.CO;2-Z

Kasperbauer, S. H., and Groote, M. A. (2015). The treatment of rapidly growing mycobacterial infections. *Clin Chest Med* 36, 67–78. doi: 10.1016/j.ccm.2014.10.004

Koh, W. J. (2011). Diagnosis and treatment of nontuberculous mycobacterial lung disease. *J Korean Med Assoc* 54, 1053–1058. doi: 10.5124/jkma.2011.54.10.1053

Lee, M.-R., Cheng, A., Lee, Y.-C., Yang, C.-Y., Lai, C.-C., Huang, Y.-T., et al. (2012). CNS infections caused by *Mycobacterium abscessus* complex: clinical features and antimicrobial susceptibilities of isolates. *J. Antimicrob. Chemother.* 67, 222–225. doi: 10.1093/jac/dkr420

Liebeskind, D. S., Ostrzega, N., Wasterlain, C. G., and Buttner, E. A. (2001). Neurologic manifestations of disseminated infection with *Mycobacterium abscessus*. *Neurology* 56, 810–813. doi: 10.1212/WNL.56.6.810

Mack, F., Baumert, B. G., Schäfer, N., Hattingen, E., Scheffler, B., Herrlinger, U., et al. (2016). Therapy of leptomeningeal metastasis in solid tumors. *Cancer Treat. Rev.* 43, 83–91 doi: 10.1016/j.ctrv.2015.12.004

Maniu, C. V., Hellinger, W. C., Chu, S. Y., Palmer, R., and Alvarez-Elcoro, S. (2001). Failure of treatment for chronic *Mycobacterium abscessus* meningitis despite adequate clarithromycin levels in cerebrospinal fluid. *Clin. Infect. Dis.* 33, 745–748. doi: 10.1086/322633

Pekcevik, Y., Orman, G., Lee, I. H., Mealy, M. A., Levy, M., Izbudak, I. (2016). What do we know about brain contrast enhancement patterns in neuromyelitis optica? *Clin Imaging.* 40, 573–580. doi: 10.1016/j.clinimag.2015.07.027

Peng, J., Song, J., Wang, F., Zuo, P., Lu, Y., Liu, W., et al. (2021). harnessing big data to optimize an algorithm for rapid diagnosis of pulmonary tuberculosis in a real-world setting. *Front. Cell Infect. Microbiol.* 11, 650163. doi: 10.3389/fcimb.2021.650163

Seehusen, D. A., Reeves, M. M., and Fomin, D. A. (2003). Cerebrospinal fluid analysis. *Am Fam Physician.* 68, 1103–1108.

Talati, N. J., Rouphael, N., Kuppalli, K., and Franco-Paredes, C. (2008). Spectrum of CNS disease caused by rapidly growing mycobacteria. *Lancet Infect. Dis.* 8, 390–398. doi: 10.1016/S1473-3099(08)70127-0

Wasserstrom, W. R., Glass, J. P., and and. Posner, J. B. (1982). Diagnosis and treatment of leptomeningeal metastases from solid tumors: experience with 90 patients. *Cancer* 49, 7593. doi: 10.1002/1097-0142(19820215)49:4andlt;759::AID-CNCR2820490427andgt;3.0.CO;2-7

frontiers | Frontiers in Pharmacology

TYPE Systematic Review
PUBLISHED 01 June 2023
DOI 10.3389/fphar.2023.1191480

OPEN ACCESS

EDITED BY
Sheng Zhong,
Sun Yat-sen University Cancer Center, China

REVIEWED BY
Yao Liu,
Daping Hospital, China
Fusheng Liu,
Capital Medical University, China

*CORRESPONDENCE
Zhigang Zhao,
1022zzg@sina.com

RECEIVED 22 March 2023
ACCEPTED 22 May 2023
PUBLISHED 01 June 2023

CITATION
Xu Y, Guan H, Yu K, Ji N and Zhao Z (2023), Efficacy and safety of pharmacotherapy for recurrent high-grade glioma: a systematic review and network meta-analysis.
Front. Pharmacol. 14:1191480.
doi: 10.3389/fphar.2023.1191480

Efficacy and safety of pharmacotherapy for recurrent high-grade glioma: a systematic review and network meta-analysis

Yanan Xu[1,2], Haijing Guan[1], Kefu Yu[1], Nan Ji[3] and Zhigang Zhao[1,2]*

[1]Department of Pharmacy, Beijing Tiantan Hospital, Capital Medical University, Beijing, China, [2]School of Pharmacy, Capital Medical University, Beijing, China, [3]Department of Neurosurgery, Beijing Tiantan Hospital, Capital Medical University, Beijing, China

Objective: To compare the efficacy and safety of treatments for patients with recurrent high-grade gliomas.

Methods: Electronic databases including Pubmed, Embase, Cochrane Library and ClinicalTrials.gov were searched for randomized controlled trials (RCT) related to high-grade gliomas. The inclusion of qualified literature and extraction of data were conducted by two independent reviewers. The primary clinical outcome measures of network meta-analysis were overall survival (OS) while progression-free survival (PFS), objective response rate (ORR) and adverse event of grade 3 or higher were secondary measures.

Results: 22 eligible trials were included in the systematic review, involving 3423 patients and 30 treatment regimens. Network meta-analysis included 11 treatments of 10 trials for OS and PFS, 10 treatments of 8 trials for ORR, and 8 treatments of 7 trials for adverse event grade 3 or higher. Regorafenib showed significant benefits in terms of OS in paired comparison with several treatments such as bevacizumab (hazard ratio (HR), 0.39; 95% confidence interval (CI), 0.21–0.73), bevacizumab plus carboplatin (HR, 0.33; 95%CI, 0.16–0.68), bevacizumab plus dasatinib (HR, 0.44; 95%CI, 0.21–0.93), bevacizumab plus irinotecan (HR, 0.4; 95%CI, 0.21–0.74), bevacizumab plus lomustine (90 mg/m^2) (HR, 0.53; 95%CI, 0.33–0.84), bevacizumab plus lomustine (110 mg/m^2) (HR, 0.21; 95%CI, 0.06–0.7), bevacizumab plus vorinostat (HR, 0.42; 95%CI, 0.18–0.99), lomustine (HR, 0.5; 95%CI, 0.33–0.76), and nivolumab (HR, 0.38; 95%CI, 0.19–0.73). For PFS, only the hazard ratio between bevacizumab plus vorinostat and bevacizumab plus lomustine (90 mg/m^2) was significant (HR,0.51; 95%CI, 0.27–0.95). Lomustine and nivolumab conferred worse ORR. Safety analysis showed fotemustine as the best and bevacizumab plus temozolomide as the worst.

Conclusion: The results suggested that regorafenib and bevacizumab plus lomustine (90 mg/m^2) provide improvements in terms of survival but may have poor ORR in patients with recurrent high-grade glioma.

KEYWORDS

high-grade glioma, recurrent, pharmacotherapy, network meta-analysis, systematic review, efficacy, safety

Introduction

According to the latest criteria of World Health Organization classification in 2021 (Louis et al., 2021), high-grade gliomas encompass various types, including grade 3 and 4 astrocytoma, grade 3 oligodendroglioma, and grade 4 glioblastomas (GBM), with GBM being the most common. Despite the fact that high-grade gliomas account for approximately 25% of all brain tumors, they are characterized by high aggression and malignancy, with an inevitable tendency for recurrence (Ostrom et al., 2018). The median progression-free survival (PFS) after recurrence is only 1.8 months (McKinnon et al., 2021), and the median overall survival (OS) ranges between 7.1 and 9.8 months, with a 5-year survival rate of only about 5% (Ostrom et al., 2018).

Surgical resection remains a viable option for treating recurrent high-grade gliomas, particularly in the case of symptomatic or large lesions. Nonetheless, successful outcomes are largely dependent on complete resection (Wen et al., 2020). Due to the extensive and invasive nature of tumor tissue, often infiltrating into healthy surrounding tissue, the success rate of re-operation is limited by factors such as tumor location and structural complexities (Ma et al., 2021).

In cases where radiotherapy is repeated, careful consideration must be given to variables such as the initial radiation dose, time interval since treatment, and the location and volume of the recurrent tumor (Cabrera et al., 2016). However, there are few randomized trials to definitively prove whether radiotherapy prolongs survival time (Wen et al., 2020).

Alternatively, drug therapies have relatively fewer limitations and are often the primary choice for relapsed patients. The drugs currently available for high-grade glioma include bevacizumab, lomustine, temozolomide, regorafenib, PCV (procarbazine, lomustine, and vincristine), and relative drug combinations. However, the clinical benefit of these therapies is limited, as evidenced by the results of numerous clinical trials (Nabors et al., 2020; Weller et al., 2021). With the abundance of clinical trials with inconclusive results (Omuro and DeAngelis, 2013), it becomes perplexing for clinicians to make informed decisions. Therefore, performing a network meta-analysis that compares treatments from varying clinical trials becomes pivotal.

An analysis focusing on recurrent GBM has been previously conducted, (McBain et al., 2021), while it lacked a collection of evidence on grade 3 glioma treatment. Furthermore, fresh clinical study outcomes have emerged that necessitate evaluation. Hence, we performed this systematic review and Bayesian network meta-analysis to amass and summarize the treatment evidence for both grade 3 and 4 gliomas. Additionally, we reconstruct data from published Kaplan-Meier survival curves to include as much clinical evidence as possible and enable comprehensive results. The results of direct and indirect comparisons were integrated to evaluate the efficacy and safety of various drug therapies. We also ranked the clinical measures of each therapeutic regimen to provide a comprehensive assessment for clinical decision-making and to improve prognosis for patients experiencing tumor recurrence.

Methods

This study was conducted in accordance with Preferred Reporting Items for Systematic Reviews and Meta-analyses (PRISMA) statement (Supplementary Table S1) (Page et al., 2021). The protocol was registered with the international prospective register of systematic reviews (PROSPERO CRD42022383881).

Data sources and search strategy

A thorough search of PubMed, Embase, Cochrane Central Register, China National Knowledge Infrastructure, WanFang Data Knowledge Service Platform and China Science and Technology Journal Database was conducted for published randomized controlled trials (RCTs) with the inclusion of an additional search of ClinicalTrials.gov for

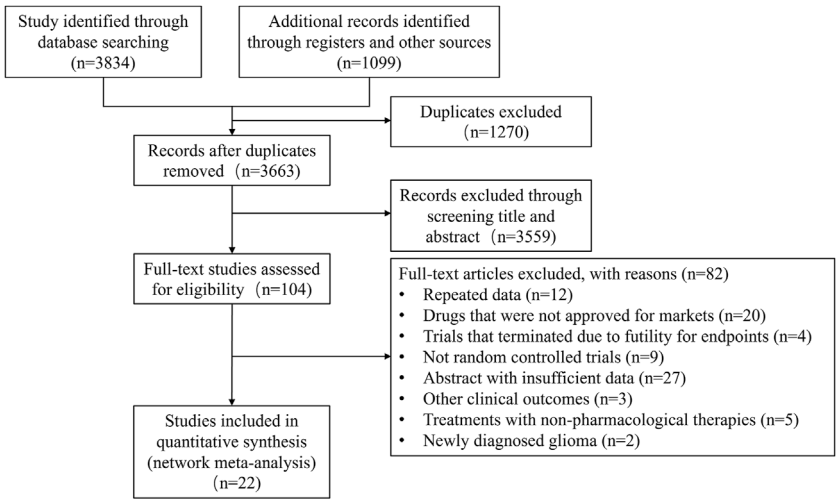

FIGURE 1
Study selection.

TABLE 1 Baseline characteristic of included studies of patients with high-grade glioma.

Study id	Tumor types	Number of relapses	Number of patients	Female (%)	Median age	KPS ≥ 80 (%)	Regimens	Reported outcomes
Boiardi et al, 1992	GBM	NM	19	NM	56	NM	Vincristine 2 mg; lomustine 75 mg/m^2; procarbazine75 mg/m^2; hydroxyurea 1500 mg/m^2; cisplatin 90 mg/m^2; algocytidine 300 mg/m^2; dacarbazine 150 mg/m^2 and methylprednisolone 300 mg/m^2 were administered every 6 h for 3 does.	ORR
			16		61	NM	Lomustine 110 mg/m^2 was administered on day 1, procarbazine 60 mg/m^2 was administered daily for 14 days beginning on day 8, and vincristine 1.4 mg/m^2 was administered on day 8 and 29 of each 6 weeks cycle of therapy.	
Brada et al, 2010	AA, GBM, gliosarcoma, oligoastrocytoma, gliosarcoma	1	112	35.7	53	NM	TMZ 200 mg/m^2 on day 1–5 every 28 days.	OS, PFS, Grade ≥3 AEs
			111	36.9	53	NM	TMZ 100 mg/m^2 on day 1–21 every 28 days.	
			224	34.8	53	NM	lomustine 110 mg/m^2 on day 1, procarbazine 60 mg/m^2 once a day on day 8–21 and vincristine 1.4 mg/m^2 on day 8 and 29 every 6 weeks.	
Brandes et al, 2016	GBM	1	32	28.1	56	NM	Fotemustine 75 mg/m^2 on days 1, 8, and 15. After a 35-day break, fotemustine 100 mg/m^2 every 3 weeks.	OS, PFS, Grade ≥3 AEs
			59	33.9	59	NM	Bevacizumab 10 mg/kg every 2 weeks.	
Brandes et al, 2019	GBM	1	61	27.9	56	90	Lomustine 90 mg/m^2 every 6 weeks. Bevacizumab 10 mg/kg every 2 weeks.	OS, PFS, Grade ≥3 AEs
			62	27.4	58.5	92	Lomustine 110 mg/m^2 every 6 weeks.	
Dresemann et al, 2010	GBM	1, 2	120	41.7	52	NM	Imatinib 600 mg once a day. Hydroxyurea 500 mg twice a day.	OS, PFS, Grade ≥3 AEs
			120	31.7	51	NM	Hydroxyurea 500 mg 3 times a day.	
Duerinck et al, 2018	GBM	1, 2	29	37.9	56	NM	Axitinib 5 mg twice a day. Lomustine 90 mg/m^2 every 6 weeks.	OS, PFS, ORR, Grade ≥3 AEs
			50	34.0	55	NM	Axitinib 5 mg twice a day.	
Field et al, 2015	GBM	1, 2	60	43.3	55	82	Carboplatin AUC 5 every 4 weeks. Bevacizumab 10 mg/kg every 2 weeks.	OS, PFS, ORR, Grade ≥3 AEs
			62	46.8	55	84	Bevacizumab 10 mg/kg every 2 weeks.	
Friedman et al, 2009	GBM	1, 2	82	30.5	57	100	Irinotecan 125 mg/m^2 every 2 weeks. Bevacizumab 10 mg/kg every 2 weeks.	OS, PFS, ORR, Grade ≥3 AEs
			85	31.8	54	100	Bevacizumab 10 mg/kg every 2 weeks	

(Continued on following page)

TABLE 1 (*Continued*) Baseline characteristic of included studies of patients with high-grade glioma.

Study id	Tumor types	Number of relapses	Number of patients	Female (%)	Median age	KPS ≥ 80 (%)	Regimens	Reported outcomes
Galanis et al, 2019	GBM	NM	83	33.7	58	NM	Dasatinib 100 mg twice a day. Bevacizumab 10 mg/kg every 2 weeks.	OS, PFS, ORR, Grade ≥3 AEs
			38	42.1	56.5	NM	Bevacizumab 10 mg/kg every 2 weeks.	
Gilbert et al, 2017	GBM or Gliosarcoma	NM	60	43.3	58	100	TMZ 75 mg/m^2 on day 1–21 every 28 days. Bevacizumab 10 mg/kg every 2 weeks.	OS, PFS, ORR, Grade ≥3 AEs
			57	40.4	55	100	Irinotecan 125 mg/m^2 every 2 weeks. Bevacizumab 10 mg/kg every 2 weeks.	
Lombardi et al, 2019	GBM	1	59	30.5	54.8	NM	Regorafenib 160 mg once a day for the first 3 weeks of each 4-week.	OS, PFS, ORR, Grade ≥3 AEs
			60	28.3	58.9	NM	Lomustine 110 mg/m^2 every 6 weeks.	
Nayak et al, 2021	GBM	1, 2	50	30.0	52	100	Pembrolizumab 200 mg every 3 weeks. Bevacizumab 10 mg/kg every 2 weeks.	OS, PFS, ORR
			30	36.7	55	100	Pembrolizumab 200 mg every 3 weeks.	
Patil et al, 2022	GBM	NM	44	25.0	40.5	NM	Mebendazole 1600 mg 3 times a day. TMZ 200 mg/m^2 on day 1–5 every 28 days.	OS, PFS, Grade ≥3 AEs
			44	27.3	41	NM	Mebendazole 800 mg 3 times a day. Lomustine 110 mg/m^2 on day 1 every 6 weeks.	
Puduvalli et al, 2020	Grade IV glioma	1, 2, 3	47	36.2	NM	94	Vorinostat 400 mg on day 1–7 and 15–21 every 4 weeks. Bevacizumab 10 mg/kg every 2 weeks.	OS, PFS, Grade ≥3 AEs
			38	26.3		97	Bevacizumab 10 mg/kg every 2 weeks.	
Reardon et al, 2015	Grade IV glioma	1	41	34.1	56.6	100	Afatinib 40 mg once a day.	OS, PFS, ORR, Grade ≥3 AEs
			39	46.2	55.4	100	Afatinib 40 mg once a day. TMZ 75 mg/m^2 on day 1–21 every 28 days.	
			39	35.9	56.9	100	TMZ 75 mg/m^2 on day 1–21 every 28 days.	
Reardon et al, 2020	GBM or Gliosarcoma	1	184	37.0	55.5	99	Nivolumab 3 mg/kg every 2 weeks.	OS, PFS, ORR, Grade ≥3 AEs
			185	35.7	55	100	Bevacizumab 10 mg/kg every 2 weeks.	
Song et al, 2010	GBM	NM	23	NM	NM	NM	Hydroxycamptothecin 6 mg/m^2 on day 1–7 every 28 days.	OS, PFS, ORR
			24	NM	NM	NM	TMZ 150 mg/m^2 on day 1–5 every 28 days.	
Sun et al, 2013	GBM	NM	65	40.0	45.1	NM	Semustine 150 mg/m^2 on day 1 every 28 days.	ORR
			79	30.4	44.3	NM	TMZ 150 or 200 mg/m^2 on day 1–5 every 28 days.	

(Continued on following page)

TABLE 1 (*Continued*) Baseline characteristic of included studies of patients with high-grade glioma.

Study id	Tumor types	Number of relapses	Number of patients	Female (%)	Median age	KPS ≥ 80 (%)	Regimens	Reported outcomes
Taal et al, 2014	GBM	1	50	38.0	58	NM	Bevacizumab 10 mg/kg every 2 weeks.	OS, PFS, ORR
			46	43.5	56	NM	Lomustine 110 mg/m^2 every 6 weeks.	
			8	62.5	53	NM	Lomustine 110 mg/m^2 every 6 weeks. Bevacizumab 10 mg/kg every 2 weeks.	
			44	31.8	58	NM	Lomustine 90 mg/m^2 every 6 weeks. Bevacizumab 10 mg/kg every 2 weeks.	
Twelves et al, 2021	GBM	1	12	58.3	59	91	TMZ 85 mg/m^2 on day 1–21 every 28 days. Nabiximols 3–12 sprays daily.	Grade ≥3 AEs
			9	11.1	57	100	TMZ 85 mg/m^2 on day 1–21 every 28 days.	
Wick et al, 2017	GBM	1	149	38.9	59.8	NM	Lomustine 110 mg/m^2 every 6 weeks.	OS, PFS, ORR, Grade ≥3 AEs
			288	39.6	57.1	NM	Lomustine 90 mg/m^2 every 6 weeks. Bevacizumab 10 mg/kg every 2 weeks.	
Yung et al, 2000	GBM or Gliosarcoma	1	112	31.3	52	100	TMZ 150 or 200 mg/m^2 on day 1–5 every 28 days.	OS, PFS, ORR, Grade ≥3 AEs
			113	36.3	52	99	Procarbazine 125 or 150 mg/m^2 on day 1–28 every 56 days.	

AA, anaplastic astrocytoma; GBM, glioblastoma; NM, not mentioned; ORR, objective response rate; OS, overall survival; PFS, progression-free survival; TMZ, temozolomide.

unpublished RCTs. The search terms included "high-grade gliomas," "anaplastic astrocytoma," "glioblastoma," "anaplastic oligoastrocytoma," "recurren*," "relapse," and drug names. Details of the literature search strategy can be found in Supplementary Table S2, with the search results collected up until 3 August 2022. The listing status of drugs was confirmed through the U.S. Food and Drug Administration (FDA) and drug-approval agencies in other countries.

Selection criteria

RCTs were included based on the following criteria:

1) Adult patients (≥18 years) with histologically confirmed recurrent high-grade gliomas, including GBM and anaplastic gliomas.
2) Trials that compared two or more arms of drug therapies, such as chemotherapy, immunotherapy and targeted therapy.
3) Trials that reported at least one of the following outcomes:
   (i) OS, defined as the time from randomization to death;
   (ii) PFS, defined as the time from randomization to first progression (local or distant) or death;
   (iii) Objective response rate (ORR), defined as the proportion of patients achieving an objective response;
   (iv) The incidence of grade 3 or higher adverse events (AE), determined according to the common terminology criteria for adverse events.

Duplicate studies and trials that were terminated or closed, along with trials in which drugs had not been approved for marketing by any nation were excluded. Furthermore, study arms that included operation or radiotherapy were disallowed.

Xu and Guan independently excluded irrelevant results by screening titles and abstracts, and included eligible articles by browsing through full texts. Any divergences during selection were resolved through arbitration by all reviewers.

Data extraction and quality evaluation

The details of the included articles were extracted to a pre-designed form, including publication information (title, first author, year of publication, journal of publication, country, etc.), trial information (trial start and cut-off time, disease, patient inclusion criteria, number of enrolled patients, baseline characteristics of the population, follow-up time), treatment regimens, and outcomes. If the OS and PFS were incomplete, missing data were estimated based on Kaplan-Meier curves following the methods provided by Tierney et al. (2007).

The Cochrane Risk of Bias 2 tool (Cumpston et al., 2019) assessed the individual study's risk of bias in five areas: randomization process, deviations from intended interventions, missing outcome data, measurement of the outcome and selection of the reported result. Trials were

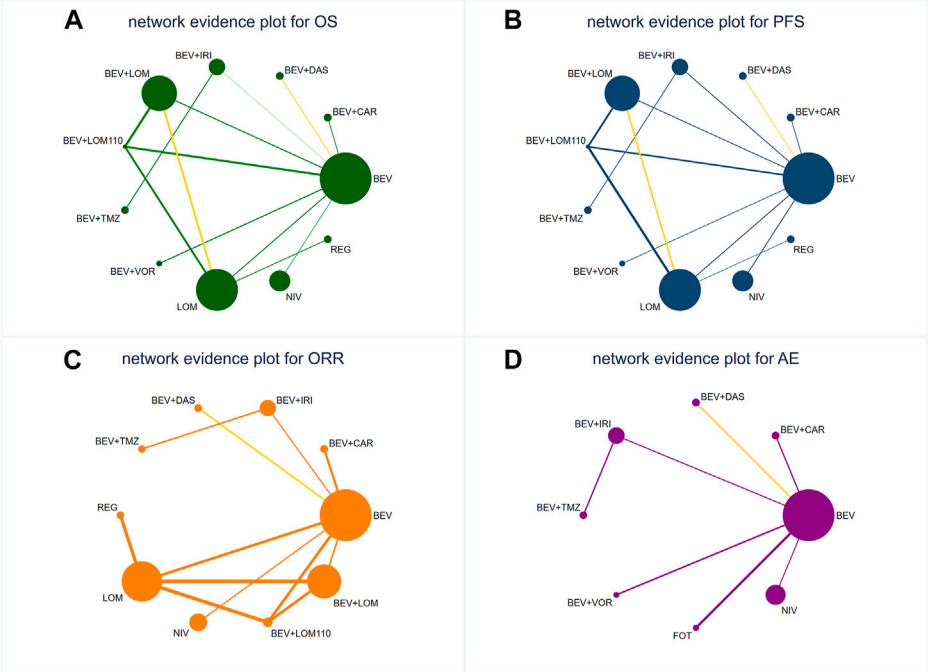

FIGURE 2
Network diagrams of comparisons on different outcomes of treatments s in different groups for patients with recurrent high-grade glioma. The yellow line indicates that there are studies in this comparison group that implemented a blinded approach. **(A)** Comparison of network diagrams for OS in high-grade glioma. **(B)** Comparison of network diagrams for PFS in high-grade glioma. **(C)** Comparison of network diagrams for ORR in high-grade glioma. **(D)** Comparison of network diagrams for grade 3 or higher AEs in high-grade glioma. BEV, bevacizumab; CAR, carboplatin; DAS, dasatinib; IRI, irinotecan; LOM, lomustine (90 mg/m^2); LOM110, lomustine (110 mg/m^2); TMZ, temozolomide; VOR, vorinostat; NIV, nivolumab; REG, regorafenib; FOT, fotemustine.

categorized as low risk, high risk, or unclear concern of bias based on the above criteria.

Data extraction was conducted by Xu and Guan, and quality evaluation was conducted independently by Xu and Yu. Any discrepancies that emerged during the evaluation process were resolved through consensus among all reviewers.

Data synthesis and statistical analysis

The primary study outcome in this study was OS, with secondary outcomes being PFS, ORR, and grade 3 or higher AE. Survival data were presented as the hazard ratio (HR) with corresponding 95% confidence interval (CI), while categorical variables were expressed as the odds ratio (OR) with corresponding 95% CI.

Bayesian network meta-analysis was conducted due to its adaptability with complicated situations and its ability to explain the effects of study-specific covariates, leading to accurate estimates with limited information. Additionally, it provides a straightforward approach to carry out probabilistic statements and treatment effect predictions (Salanti et al., 2011). Network diagrams were generated for different treatment outcomes using Stata (version 17) (Chaimani et al., 2013). Fixed-effects and random-effects models were established separately through a Markov Chain Monte Carlo simulation technique in R (version 4.2.2) with 150000 iterations, 30000 burn-ins and a thinning interval of 1, based on the Bayesian framework (Salanti et al., 2011). The final appropriate analytical model was chosen based on the model parameters. Convergence was assessed through visual inspection of trace plots, density plots and Brooks-Gelman Rubin diagnosis plots (Supplementary Figure S1). Heterogeneity was evaluated using I^2 statistics, with values categorized as low, medium and high heterogeneity for I^2 values < 25%, 25%–50% and >50%, respectively, (Higgins et al., 2003). Global consistency was assessed by comparing the consistent and inconsistent models (Dias et al., 2010). The inconsistency of the models was assessed using the node splitting method (Higgins et al., 2003). Probability plots and surface under the cumulative ranking curve (SUCRA) were used to predict and evaluate the efficacy and safety of each treatment.

A sensitivity analysis was conducted to evaluate the reliability and stability of network meta-analysis results, with articles causing greater heterogeneity excluded for sensitive analysis.

Results

Systematic review and characteristics

In this study, a total of 104 out of 4933 records for full-text reading and 22 RCTs (Boiardi et al., 1992; Yung et al., 2000; Friedman et al., 2009; Brada et al., 2010; Dresemann et al., 2010; Song et al., 2010; Sun et al.,

A

Progression-free survival \ Overall survival	BEV	BEV+CAR	BEV+DAS	BEV+IRI	BEV+LOM	BEV+LOM110	BEV+TMZ	BEV+VOR	LOM	NIV	REG
BEV		1.18 (0.83, 1.69)	0.89 (0.59, 1.34)	0.99 (0.92, 1.07)	0.74 (0.46, 1.19)	1.87 (0.59, 5.96)	0.88 (0.51, 1.5)	0.93 (0.52, 1.68)	0.78 (0.49, 1.25)	1.04 (0.84, 1.29)	**0.39 (0.21, 0.73)**
BEV+CAR	1.08 (0.37, 3.22)		0.75 (0.44, 1.29)	0.84 (0.58, 1.2)	0.62 (0.34, 1.13)	1.58 (0.47, 5.3)	0.74 (0.39, 1.4)	0.79 (0.4, 1.56)	0.66 (0.37, 1.18)	0.88 (0.58, 1.33)	**0.33 (0.16, 0.68)**
BEV+DAS	1.27 (0.43, 3.76)	1.17 (0.25, 5.37)		1.12 (0.73, 1.7)	0.83 (0.44, 1.56)	2.11 (0.62, 7.25)	0.99 (0.5, 1.94)	1.05 (0.51, 2.15)	0.88 (0.47, 1.64)	1.17 (0.74, 1.87)	**0.44 (0.21, 0.93)**
BEV+IRI	1.18 (0.39, 3.57)	1.09 (0.23, 5.14)	0.93 (0.2, 4.34)		0.75 (0.46, 1.21)	1.89 (0.59, 6.03)	0.89 (0.52, 1.5)	0.94 (0.52, 1.7)	0.79 (0.49, 1.26)	1.05 (0.84, 1.32)	**0.4 (0.21, 0.74)**
BEV+LOM	1.45 (0.52, 4.01)	1.33 (0.3, 5.9)	1.14 (0.26, 4.99)	1.23 (0.27, 5.59)		2.53 (0.81, 7.92)	1.19 (0.58, 2.43)	1.26 (0.59, 2.7)	1.06 (0.86, 1.29)	1.41 (0.84, 2.37)	**0.53 (0.33, 0.84)**
BEV+LOM110	1.3 (0.34, 4.97)	1.19 (0.22, 6.6)	1.02 (0.19, 5.62)	1.1 (0.2, 6.31)	0.9 (0.25, 3.17)		0.47 (0.13, 1.68)	0.5 (0.14, 1.81)	0.42 (0.13, 1.29)	0.56 (0.17, 1.8)	**0.21 (0.06, 0.7)**
BEV+TMZ	1.33 (0.28, 6.32)	1.23 (0.18, 8.13)	1.05 (0.16, 6.95)	1.13 (0.37, 3.39)	0.92 (0.14, 5.95)	1.03 (0.13, 7.82)		1.06 (0.48, 2.35)	0.89 (0.44, 1.81)	1.18 (0.67, 2.11)	0.45 (0.2, 1.02)
BEV+VOR	1.58 (0.53, 4.73)	1.46 (0.31, 6.85)	1.24 (0.27, 5.76)	1.34 (0.28, 6.39)	1.09 (0.25, 4.83)	1.22 (0.22, 6.71)	1.19 (0.18, 8.01)		0.84 (0.39, 1.77)	1.12 (0.6, 2.09)	**0.42 (0.18, 0.99)**
LOM	0.74 (0.26, 2.04)	0.69 (0.15, 3.01)	0.59 (0.13, 2.56)	0.63 (0.14, 2.84)	**0.51 (0.27, 0.95)**	0.57 (0.16, 2)	0.56 (0.08, 3.61)	0.47 (0.1, 2.05)		1.33 (0.8, 2.23)	**0.5 (0.33, 0.76)**
NIV	0.51 (0.17, 1.55)	0.47 (0.1, 2.23)	0.4 (0.08, 1.87)	0.43 (0.09, 2.08)	0.35 (0.08, 1.58)	0.39 (0.07, 2.19)	0.38 (0.06, 2.63)	0.32 (0.07, 1.52)	0.68 (0.15, 3.14)		**0.38 (0.19, 0.73)**
REG	1.14 (0.25, 4.88)	1.05 (0.17, 6.39)	0.9 (0.14, 5.48)	0.97 (0.15, 6.11)	0.79 (0.22, 2.67)	0.88 (0.17, 4.43)	0.86 (0.1, 7.32)	0.72 (0.11, 4.44)	1.54 (0.53, 4.47)	2.25 (0.35, 14.17)	

B

Grade ≥3 adverse events \ Objective response rate	BEV	BEV+CAR	BEV+DAS	BEV+IRI	BEV+LOM	BEV+LOM110	BEV+TMZ	BEV+VOR	LOM	FOT	NIV	REG
BEV		2.33 (0.67, 9.46)	0.52 (0.2, 1.36)	1.55 (0.81, 3.01)	0.73 (0.32, 1.69)	2.95 (0.61, 16.77)	0.88 (0.29, 2.63)		**0.15 (0.06, 0.36)**		**0.28 (0.13, 0.55)**	0.24 (0.03, 2.52)
BEV+CAR	0.86 (0.53, 1.38)		0.22 (0.04, 1.08)	0.66 (0.14, 2.73)	0.31 (0.06, 1.41)	1.26 (0.15, 10.67)	0.38 (0.06, 1.97)		**0.06 (0.01, 0.29)**		**0.12 (0.02, 0.49)**	**0.1 (0.01, 1.48)**
BEV+DAS	0.74 (0.39, 1.33)	0.86 (0.39, 1.83)		3 (0.94, 9.51)	1.41 (0.4, 5.02)	5.71 (0.9, 41.13)	1.7 (0.39, 7.25)		0.28 (0.07, 1.04)		0.53 (0.16, 1.72)	0.47 (0.04, 5.81)
BEV+IRI	**0.62 (0.4, 0.94)**	0.71 (0.38, 1.35)	0.83 (0.4, 1.79)		0.47 (0.16, 1.36)	1.9 (0.35, 12.18)	0.57 (0.23, 1.36)		**0.09 (0.03, 0.29)**		**0.18 (0.07, 0.46)**	0.16 (0.02, 1.77)
BEV+LOM						4.01 (0.84, 23.02)	1.19 (0.3, 4.81)		**0.2 (0.12, 0.33)**		0.38 (0.12, 1.12)	0.33 (0.04, 3.07)
BEV+LOM110							0.3 (0.04, 2.04)		**0.05 (0.01, 0.25)**		**0.09 (0.01, 0.52)**	0.08 (0.01, 1.21)
BEV+TMZ	**0.37 (0.19, 0.69)**	**0.43 (0.19, 0.94)**	0.49 (0.21, 1.22)	**0.6 (0.37, 0.95)**					**0.17 (0.04, 0.69)**		0.31 (0.08, 1.16)	0.28 (0.02, 3.65)
BEV+VOR	1.14 (0.66, 1.95)	1.32 (0.64, 2.71)	1.54 (0.69, 3.53)	1.85 (0.93, 3.69)			**3.11 (1.35, 7.22)**					
LOM											1.89 (0.6, 5.99)	1.64 (0.24, 14.62)
FOT	2.44 (0.75, 11.26)	2.85 (0.79, 14.06)	3.33 (0.88, 17.24)	3.98 (1.13, 19.38)			**6.72 (1.74, 34.8)**	2.15 (0.58, 10.76)				
NIV	0.85 (0.5, 1.42)	0.98 (0.48, 1.98)	1.14 (0.52, 2.58)	1.38 (0.7, 2.68)			**2.31 (1.02, 5.24)**	0.74 (0.35, 1.57)		0.35 (0.07, 1.26)		0.87 (0.09, 10.12)
REG												

FIGURE 3
Pooled estimates of the network meta-analysis. **(A)** Pooled HRs (95% credible intervals) for OS in the upper triangle and PFS in the lower triangle. **(B)** Pooled ORs (95% credible intervals) for ORR in the upper triangle and 3 or higher AEs in the lower triangle. BEV, bevacizumab; CAR, carboplatin; DAS, dasatinib; IRI, irinotecan; LOM, lomustine (90 mg/m^2); LOM110, lomustine (110 mg/m^2); TMZ, temozolomide; VOR, vorinostat; NIV, nivolumab; REG, regorafenib; FOT, fotemustine.

2013; Taal et al., 2014; Field et al., 2015; Reardon et al., 2015; Brandes et al., 2016; Gilbert et al., 2017; Wick et al., 2017; Duerinck et al., 2018; Brandes et al., 2019; Galanis et al., 2019; Lombardi et al., 2019; Puduvalli et al., 2020; Reardon et al., 2020; Nayak et al., 2021; Twelves et al., 2021; Patil et al., 2022) were included for analysis (Figure 1). The study population consisted of 3423 patients who received 30 different treatments. Bevacizumab, lomustine and temozolomide were the most commonly studied. The characteristics of the tumor types, number of tumor recurrences, sex ratio, age, Karnofsky performance status (KPS), and specific treatment regimens were summarized in Table 1. The risk of bias assessment in the literature was evaluated and presented in Supplementary Figure S2.

Network meta-analysis

Network evidence plots

A network meta-analysis was conducted to assess the efficacy and safety of the different treatment regimens. A total of 11 treatment regimens from 10 studies (Friedman et al., 2009; Taal et al., 2014; Field et al., 2015; Gilbert et al., 2017; Wick et al., 2017; Brandes et al., 2019; Galanis et al., 2019; Lombardi et al., 2019; Puduvalli et al., 2020; Reardon et al., 2020) constituted the analysis network for OS and PFS (Figures 2A, B), and 10 treatment regimens from 8 studies (Friedman et al., 2009; Taal et al., 2014; Field et al., 2015; Gilbert et al., 2017; Wick et al., 2017; Galanis et al., 2019; Lombardi et al., 2019; Reardon et al., 2020) constituted the analysis network for ORR (Figure 2C). Furthermore, 8 treatment regimens from 7 studies (Friedman et al., 2009; Field et al., 2015; Brandes et al., 2016; Gilbert et al., 2017; Galanis et al., 2019; Puduvalli et al., 2020; Reardon et al., 2020) constituted the analysis network for AEs (Figure 2D).

Heterogeneity and inconsistency assessment

A fixed-effects model was used for the analysis of OS, ORR and AEs ($I^2 < 25\%$) and a random-effects model for the analysis of PFS ($I^2 > 50\%$). The results of heterogeneity test were presented

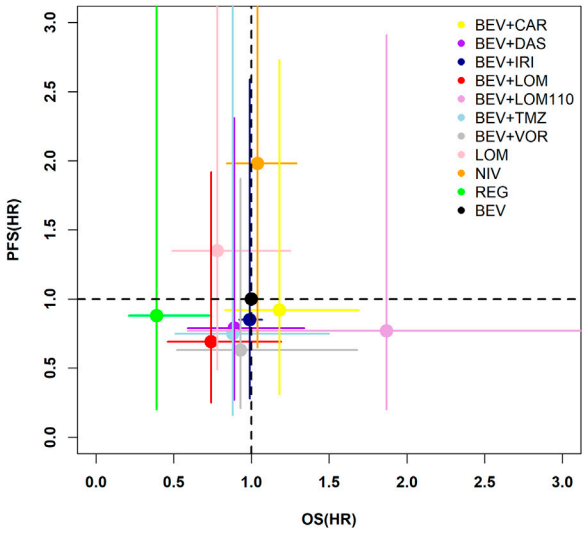

FIGURE 4
Two-dimensional plot of OS and PFS for difference treatments. The horizontal coordinate indicates the risk ratio for OS of the study regimen with bevacizumab as the control, and the vertical coordinate indicates the risk ratio for PFS of the study regimen with bevacizumab as the control. The dots indicate the estimated risk ratios for the study regimens, and the horizontal line indicates the 95% confidence interval for HR. BEV, bevacizumab; CAR, carboplatin; DAS, dasatinib; IRI, irinotecan; LOM, lomustine (90 mg/m^2); LOM110, lomustine (110 mg/m^2); TMZ, temozolomide; VOR, vorinostat; NIV, nivolumab; REG, regorafenib.

in Supplementary Figure S3. The heterogeneity of the comparison group of lomustine and bevacizumab plus lomustine was high (I^2 = 69.6%), which was mainly due to the Brandes2019 study. After removing this trial, the I^2 decreased to 32.4% (Supplementary Figure S3E). A closed-loop structure was present in the network of OS, PFS, and ORR, but since the arms that comprised the loop were from one literature, (Taal et al., 2014), there was no need to check the consistency of the direct evidence (van Valkenhoef et al., 2016).

Comparison of efficacy and safety

The direct and indirect evidence of different treatments in terms of survival and binary outcomes were synthesized and reported as HR and OR, respectively.

Regorafenib was found to have the best benefit for OS (Figure 3A), compared to other treatment regimens. In terms of PFS (Figure 3A), only bevacizumab plus lomustine (90 mg/m^2) was significantly effective than lomustine alone (HR = 0.51, 95% CI 0.27-0.95). The HR of bevacizumab plus lomustine (90 mg/m^2) was less than 1, which had a therapeutic advantage compared to the other nine regimens, though the confidence interval spanned 1.

Lomustine and nivolumab performed poorly on ORR (Figure 3B). The range of ORs were from 0.05 to 0.28 for lomustine compared to bevacizumab, bevacizumab plus carboplatin, bevacizumab plus dasatinib, bevacizumab plus irinotecan, bevacizumab plus lomustine (including 90 mg/m^2 and 110 mg/m^2) and bevacizumab plus temozolomide. The range of ORs were from 0.09 to 0.53 for nivolumab compared to the above regimens.

For grade 3 or higher AE (Figure 3B), bevacizumab plus temozolomide suffered the worst safety. The primary adverse event of bevacizumab plus temozolomide was myelotoxicity (Gilbert et al., 2017).

A two-dimensional graph was drawn to visualize the effect of different treatments on OS and PFS, taking bevacizumab as control (Figure 4). The diagram showed that regorafenib, bevacizumab plus lomustine (90 mg/m^2), bevacizumab plus temozolomide, bevacizumab plus dasatinib, and bevacizumab plus vorinostat had better efficacy than bevacizumab in terms of OS and PFS, athough the confidence interval for HR of most regimens crossed 1 with no significant difference.

Rank probabilities

The ranking and SUCRA of comparable treatments for patients with high-grade glioma obtained by network meta-analysis (Figures 5, 6) were consistent with HR and OR.

Patients with recurrent high-grade glioma treated with regorafenib are likely to experience the longest OS (94% probability). The SUCRA of regorafenib was much higher than other regimens. Patients treated with bevacizumab plus vorinostat may attain the longest PFS (24% probability). However, the SUCRA of bevacizumab plus lomustine (90 mg/m^2) and bevacizumab plus vorinostat were similar. Patients treated with bevacizumab plus lomustine (110 mg/m^2) may have better ORRs (54% probability). Lomustine and nivolumab performed poorly for ORR. Patients treated with lomustine were minimally at risk for a grade ≥3 AEs (84% probability), whereas bevacizumab-based regimens tended to have higher toxicity than bevacizumab alone.

Sensitivity analysis

There was a large heterogeneity of PFS after combining various trials. Therefore, a sensitivity analysis was conducted, excluding each trial in turn. As a result, it was identified that Brandes2019 was the primary source of heterogeneity in the PFS network. With this information in mind, sensitivity analyses of PFS outcomes were performed using the remaining studies, excluding Brandes 2019. Supplementary Figure S4 display the results of pairwise comparison, probability ranking, and the SUCRA.

The sensitivity analysis outcomes aligned with those yielded by the Bayesian network meta-analysis. In the pairwise comparison, it remained that bevacizumab plus lomustine (90 mg/m^2) achieved a significantly enhanced PFS, as compared to lomustine. The HRs of other comparisons were not found to be significant.

Similarly, in the ranking of PFS, the curves followed the same pattern as the network meta-analysis. Additionally, there was a slight increase in the probability that bevacizumab plus lomustine (90 mg/m^2) would rank in the top four. Global results obtained from the network meta-analysis were robust.

Discussion

In this systematic review and Bayesian network meta-analysis, we present a comprehensive summary and comparison of the efficacy and safety profiles of various interventions for high-grade gliomas, including bevacizumab monotherapy, bevacizumab-based

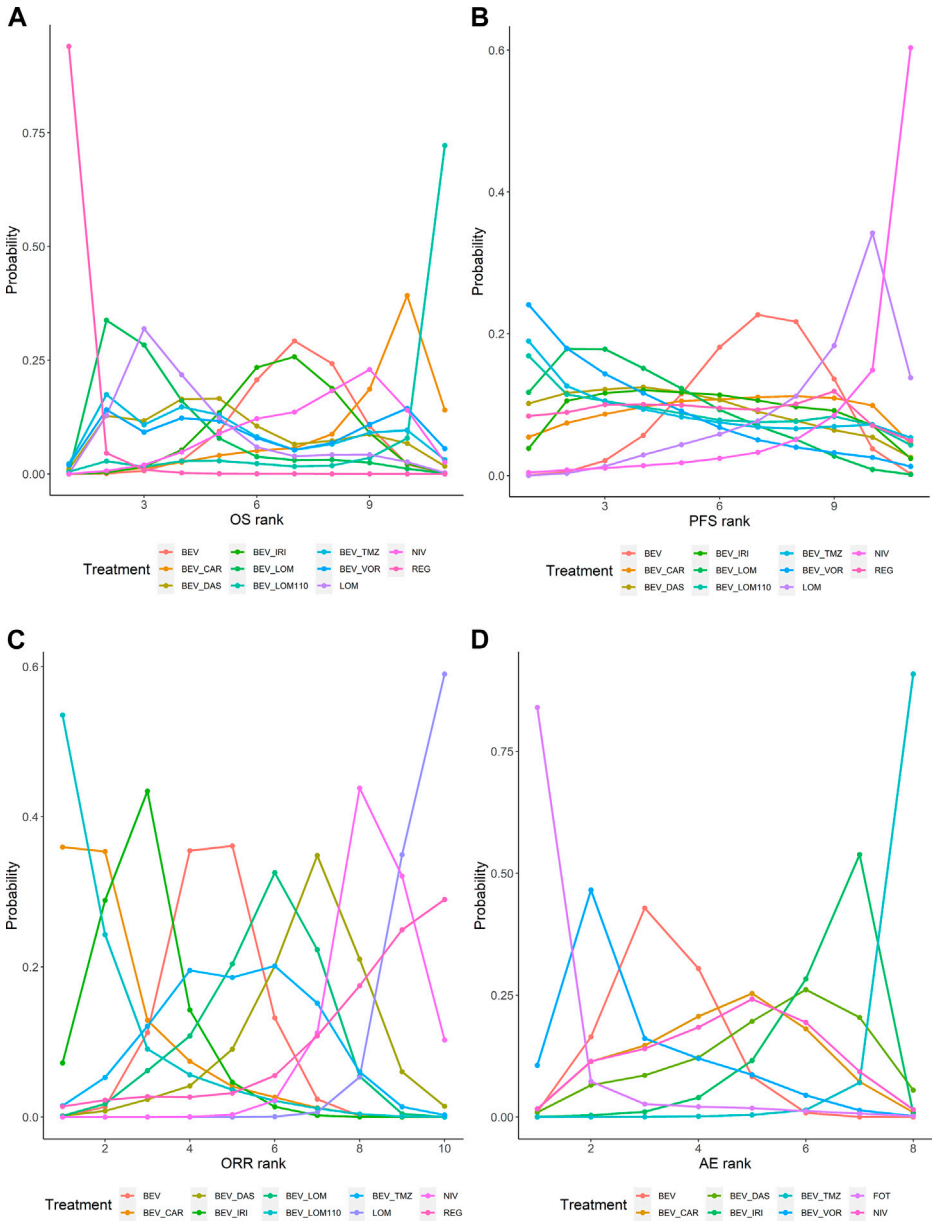

FIGURE 5
Bayesian ranking profiles of comparable treatments on efficacy and safety for patients with high-grade gliomas. Profiles indicate the probability of each treatment being ranked from first to last on OS **(A)**, PFS **(B)**, ORR **(C)**, and grade 3 or higher AEs **(D)**. Ranking curves are described according to the Bayesian ranking results presented in Supplementary Table S3. BEV, bevacizumab; CAR, carboplatin; DAS, dasatinib; IRI, irinotecan; LOM, lomustine (90 mg/m^2); LOM110, lomustine (110 mg/m^2); TMZ, temozolomide; VOR, vorinostat; NIV, nivolumab; REG, regorafenib; FOT, fotemustine.

therapies, nitrosoureas, PD-1 inhibitors, and multi-targeted kinase inhibitors. To bolster the study's clinical utility in real-world practice, we excluded investigations on experimental drugs that remain unavailable commercially.

The results of the study suggest that regorafenib is likely to be the most effective treatment for improving survival outcomes in patients with longer OS and PFS, although the options may not provide the same benefit in terms of ORR. The efficacy of the combination therapy of bevacizumab and lomustine (90 mg/m^2) was inferior to that of regorafenib. Nevertheless, it outperformed other treatment options in terms of survival outcomes and is recommended as the second option according to our findings. However, the ORR was unsatisfactory as well. Notably, bevacizumab plus lomustine (110 mg/m^2) ranked high in ORR outcomes, which may be attributed to the dose administered. However, the limited sample size of patients in original studies may have introduced some bias into our results.

In terms of safety, no drug had an absolutely good safety profile. Regorafenib and bevacizumab plus lomustine (90 mg/m^2) were not included in the safety evaluation network due to incomplete safety data. Grade 3 or higher AEs for regorafenib were dominated by elevated lipase and hand-foot skin reactions (both incidences were over 10%)

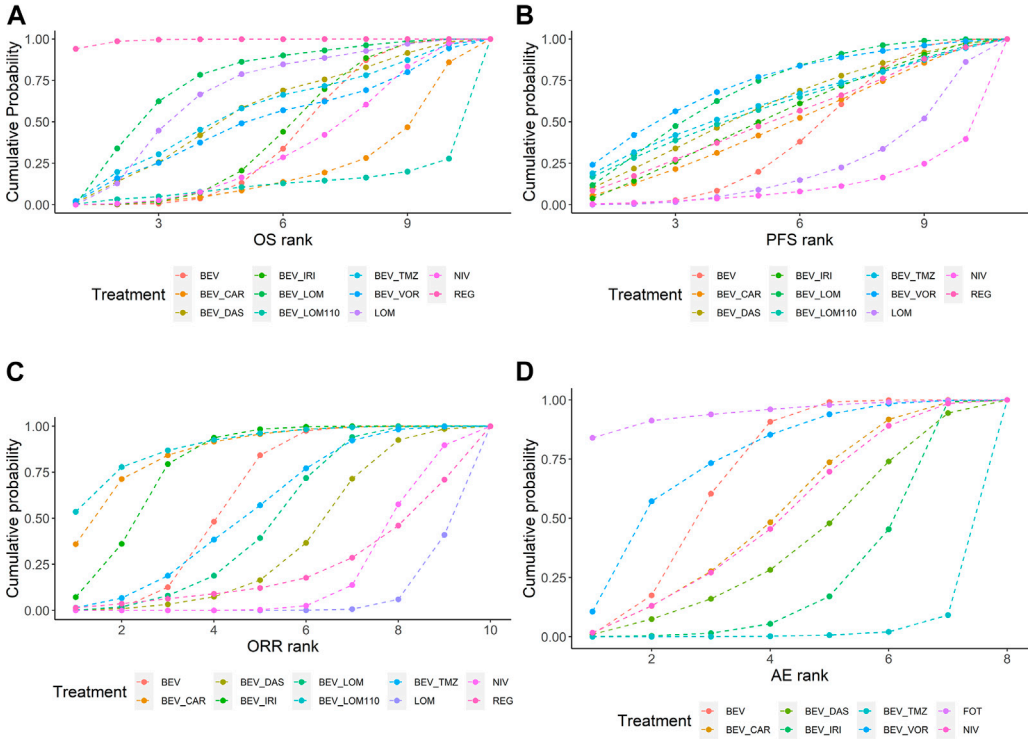

FIGURE 6
SUCRA ranking of comparable treatments on efficacy and safety for patients with high-grade gliomas. Profiles indicate the cumulative probability of each treatment being ranked in the top on OS **(A)**, PFS **(B)**, ORR **(C)**, and grade 3 or higher AEs **(D)**. SUCRA are described according to the Bayesian cumulative ranking results presented in Supplementary Table S4. BEV, bevacizumab; CAR, carboplatin; DAS, dasatinib; IRI, irinotecan; LOM, lomustine (90 mg/m^2); LOM110, lomustine (110 mg/m^2); TMZ, temozolomide; VOR, vorinostat; NIV, nivolumab; REG, regorafenib; FOT, fotemustine.

(Lombardi et al., 2019). Main AEs for bevacizumab plus lomustine (90 mg/m2) were hypertension, hematologic effects, and fatigue (Taal et al., 2014; Wick et al., 2017). Our investigation revealed that fotemustine exhibited the most favorable safety profile. Given that it belongs to the same class of nitrosourea as lomustine, it appears reasonable to assert that nitrosourea drugs may generally confer a measure of therapeutic advantage in terms of safety.

The study by Brandes in 2019 exhibited a greater degree of heterogeneity in contrast to the research conducted by Taal in 2014 and Wick in 2017 in paired comparison of lomustine and bevacizumab plus lomustine (90 mg/m^2). This may be attributed to the ratio of O-6-methylguanine-DNA methyltransferase (MGMT) methylation and unmethylation, which was approximately 1/2 in the Brandes2019 study, compared to a near 1:1 ratio seen in the other two studies. A multitude of investigations have demonstrated an association between MGMT unmethylation and resistance to chemotherapeutic agents (Oldrini et al., 2020). This may plausibly account for the observed larger HR for PFS in the Brandes2019 study, in contrast to the Taal2014 and Wick2017 studies, where the HR values were quite similar. However, we are reassured that our final results were not impacted by heterogeneity through sensitivity analyses.

The study enrolled predominantly patients with recurrent GBM. The National Comprehensive Cancer Network (NCCN) clinical practice guidelines for central nervous system cancers (Nabors et al., 2020) recommend preferential use of bevacizumab, temozolomide, lomustine or carmustine, PCV and regorafenib for recurrent GBM. The European Association of Neuro-Oncology (EANO) guidelines of diffuse glioma in adults (Weller et al., 2021) endorse nitrosoureas, temozolomide and bevacizumab for progression or relapse of GBM. The findings of our analysis support the use of regorafenib for recurrent GBM based on its association with significant survival benefits. However, experience with regorafenib in recurrent GBM is limited compared with other recommended therapeutic options in the guidelines. Regorafenib is a multi-kinase inhibitor. Its anti-tumor mechanism remains elusive despite several clinical trials. A recent investigation delving into its mode of action has unearthed regorafenib's ability to stabilize the critical enzyme PSAT1 (phosphoserine aminotransferase 1) involved in serine synthesis. This unfavorable activity in GBM cells leads to fatal autophagy arrest and tumor suppression (Jiang et al., 2020). The promising results suggest that the levels of PSAT1 play a key regulatory role in the success of regorafenib-induced GBM therapy. Additional research has identified molecular features correlated with prolonged survival rate in regorafenib-treated GBM patients. These features include EGFR mutations (Chiesa et al., 2022), gene transcripts such as HIF1A and CDKN1A, miRNAs like miR-3607–3p, miR-301a-3p, miR-93–5p (Santangelo et al., 2021), and MAPK pathway mutations that may associate with a poor prognosis (Chiesa et al., 2022). However, limited evidence restricts the scope of individualized dosing of regorafenib, hence, greater evidence is required to increase its widespread acceptance.

The Chinese guidelines (Jiang et al., 2021) recommended bevacizumab plus lomustine (90 mg/m^2), while it is not a preferred regimen in NCCN(7) and EANO(8) guidelines. Clinicians need to carefully consider the AEs and patient status when selecting this combination. Additionally, cost effectiveness is also an important factor to consider (Cagney and Alexander, 2017), but there is a paucity of evidence in this area at present.

There are commendable aspects to our review, particularly the emphasis placed on high-grade glioma, as opposed to recurrent GBM, although the latter still featured prominently in the final analysis. We established a comprehensive network pertaining to all drug treatments, and judiciously applied analytical methods to estimate hazard ratios founded upon Kaplan-Meier curves, yielding the added benefit of integrating studies that did not report hazard ratios, thus allowing for a more comprehensive evaluation of the many treatments evaluated. Our review presents valuable information for clinical decision-making, which we achieved by carefully scrutinizing and assessing the outcomes of various treatments, and performing rigorous analyses, including sensitivity analysis of network heterogeneity and consistency, thus ensuring robust and dependable results.

Our research, though valuable, still presents some limitations. Firstly, the scope of this study was limited to patients with recurrent high-grade glioma. However, upon examining relevant literature, we discovered a dearth of randomized controlled trials pertaining to grade 3 glioma or anaplastic glioma. Furthermore, we were unable to perform a comprehensive subgroup analysis of grade 3 glioma due to insufficient data. It is thus imperative to acknowledge that the results of our work may not fully represent the ideal treatment strategies for grade 3 recurrent glioma. Another shortcoming of the study was incomplete reporting of results, which prevented the integration of certain guidelines-recommended treatments, such as temozolomide and PCV, into the network. Despite these limitations, pertinent data of clinical trials can be gleaned from Table 1. Language bias may also have some impact on the results. The literature in this article is from English and Chinese databases and may miss potential and qualified studies from other language databases.

As per our research findings, conventional drugs appear to be ineffective in producing significant impacts towards recurrent high-grade glioma. The large molecular phenotype heterogeneity is likely a contributing factor (Nicholson and Fine, 2021). Targeting specific pathways may be a more effective approach (Le Rhun et al., 2019). Among the targeted agents analyzed in this study, both bevacizumab and regorafenib interact with vascular endothelial growth factor (VEGF), which inhibits neoangiogenesis and thus exerts anti-tumor effects. In addition, regorafenib targets multiple gene and kinase such as BRAF, KIT, and RET, which may be potential therapeutic targets but need to be confirmed by further studies. The latest study has found that patients presenting a BRAF-V600E mutation showed improved ORR with dabrafenib and trametinib, providing a clear indication of the potential benefits of individualized treatment strategies (Wen et al., 2022). Likewise, a phase 3 clinical trial of a vaccine has shown promising results in the treatment of recurrent glioma. As demonstrated by Liah et al.'s study, the addition of an autologous tumor lysate-loaded dendritic cell vaccine has resulted in significant clinical benefits resulting in a statistically significant increase in survival time for patients with relapsed GBM (Liau et al., 2023). Whether by targeting specific molecules, pathways, or through autologous tumor lysates, individualized therapy holds significant promise for the treatment of recurrent high-grade gliomas. However, current advancements in this critical area have been insufficient to fully realize the potential of personalized medicine in this setting. In the present context, emerging data emphasizes that regorafenib and bevacizumab in combination with lomustine, represents the most promising therapeutic alternative for high-grade glioma.

Data availability statement

The original contributions presented in the study are included in the article/Supplementary Material, further inquiries can be directed to the corresponding author.

Author contributions

ZZ conceived and designed the study, and revised the manuscript. YX searched and screened the literature, evaluated the quality of random controlled trials, extracted and processed the data, and completed the first draft. HG screened the literature and extracted the data. KY evaluated the quality of trials and processed the data. NJ made the final decisions for the disagreements in the study. All authors contributed to the article and approved the submitted version.

Funding

This work was supported by Capital Health Development Research Special Project: research on precision treatment of recurrent high-grade glioma based on PTC drug screening technology (No. SF 2022-2-2047).

Conflict of interest

The authors declare that the research was conducted in the absence of any commercial or financial relationships that could be construed as a potential conflict of interest.

The reviewer FL declared a shared parent affiliation with the author(s) to the handling editor at the time of review.

Publisher's note

Supplementary material

The Supplementary Material for this article can be found online at: https://www.frontiersin.org/articles/10.3389/fphar.2023.1191480/full#supplementary-material

References

Boiardi, A., Silvani, A., Milanesi, I., Broggi, G., and Fariselli, L. (1992). Efficacy of '8-drugs-in-one-day' combination in treatment of recurrent GBM patients. *J. Neurooncol* 12 (2), 153–158. doi:10.1007/bf00172666

Brada, M., Stenning, S., Gabe, R., Thompson, L. C., Levy, D., Rampling, R., et al. (2010). Temozolomide versus procarbazine, lomustine, and vincristine in recurrent high-grade glioma. *J. Clin. Oncol.* 28 (30), 4601–4608. doi:10.1200/JCO.2009.27.1932

Brandes, A. A., Finocchiaro, G., Zagonel, V., Reni, M., Caserta, C., Fabi, A., et al. (2016). Avareg: A phase II, randomized, noncomparative study of fotemustine or bevacizumab for patients with recurrent glioblastoma. *Neuro-oncology* 18 (9), 1304–1312. doi:10.1093/neuonc/now035

Brandes, A. A., Gil-Gil, M., Saran, F., Carpentier, A. F., Nowak, A. K., Mason, W., et al. (2019). A randomized phase II trial (TAMIGA) evaluating the efficacy and safety of continuous bevacizumab through multiple lines of treatment for recurrent glioblastoma. *Oncologist* 24 (4), 521–528. doi:10.1634/theoncologist.2018-0290

Cabrera, A. R., Kirkpatrick, J. P., Fiveash, J. B., Shih, H. A., Koay, E. J., Lutz, S., et al. (2016). Radiation therapy for glioblastoma: Executive summary of an American society for radiation oncology evidence-based clinical practice guideline. *Pract. Radiat. Oncol.* 6 (4), 217–225. doi:10.1016/j.prro.2016.03.007

Cagney, D. N., and Alexander, B. M. (2017). The cost and value of glioblastoma therapy. *Expert Rev. Anticancer Ther.* 17 (8), 657–659. doi:10.1080/14737140.2017.1351355

Chaimani, A., Higgins, J. P., Mavridis, D., Spyridonos, P., and Salanti, G. (2013). Graphical tools for network meta-analysis in STATA. *PLoS One* 8 (10), e76654. doi:10.1371/journal.pone.0076654

Chiesa, S., Mangraviti, A., Martini, M., Cenci, T., Mazzarella, C., Gaudino, S., et al. (2022). Clinical and NGS predictors of response to regorafenib in recurrent glioblastoma. *Sci. Rep.* 12 (1), 16265. doi:10.1038/s41598-022-20417-y

Cumpston, M., Li, T., Page, M. J., Chandler, J., Welch, V. A., Higgins, J. P., et al. (2019). Updated guidance for trusted systematic reviews: A new edition of the Cochrane handbook for systematic reviews of interventions. *Cochrane database Syst. Rev.* 10, Ed000142. doi:10.1002/14651858.Ed000142

Dias, S., Welton, N. J., Caldwell, D. M., and Ades, A. E. (2010). Checking consistency in mixed treatment comparison meta-analysis. *Statistics Med.* 29 (7-8), 932–944. doi:10.1002/sim.3767

Dresemann, G., Weller, M., Rosenthal, M. A., Wedding, U., Wagner, W., Engel, E., et al. (2010). Imatinib in combination with hydroxyurea versus hydroxyurea alone as oral therapy in patients with progressive pretreated glioblastoma resistant to standard dose temozolomide. *J. Neuro-Oncology* 96 (3), 393–402. doi:10.1007/s11060-009-9976-3

Duerinck, J., Du Four, S., Bouttens, F., Andre, C., Verschaeve, V., Van Fraeyenhove, F., et al. (2018). Randomized phase II trial comparing axitinib with the combination of axitinib and lomustine in patients with recurrent glioblastoma. *J. Neuro-Oncology* 136 (1), 115–125. doi:10.1007/s11060-017-2629-z

Field, K. M., Simes, J., Nowak, A. K., Cher, L., Wheeler, H., Hovey, E. J., et al. (2015). Randomized phase 2 study of carboplatin and bevacizumab in recurrent glioblastoma. *Neuro-oncology* 17 (11), 1504–1513. doi:10.1093/neuonc/nov104

Friedman, H. S., Prados, M. D., Wen, P. Y., Mikkelsen, T., Schiff, D., Abrey, L. E., et al. (2009). Bevacizumab alone and in combination with irinotecan in recurrent glioblastoma. *J. Clin. Oncol.* 27 (28), 4733–4740. doi:10.1200/JCO.2008.19.8721

Galanis, E., Anderson, S. K., Twohy, E. L., Carrero, X. W., Dixon, J. G., Tran, D. D., et al. (2019). A phase 1 and randomized, placebo-controlled phase 2 trial of bevacizumab plus dasatinib in patients with recurrent glioblastoma: Alliance/north central cancer treatment group N0872. *Cancer* 125 (21), 3790–3800. doi:10.1002/cncr.32340

Gilbert, M. R., Pugh, S. L., Aldape, K., Sorensen, A. G., Mikkelsen, T., Penas-Prado, M., et al. (2017). NRG oncology RTOG 0625: A randomized phase II trial of bevacizumab with either irinotecan or dose-dense temozolomide in recurrent glioblastoma. *J. Neuro-Oncology* 131 (1), 193–199. doi:10.1007/s11060-016-2288-5

Higgins, J. P., Thompson, S. G., Deeks, J. J., and Altman, D. G. (2003). Measuring inconsistency in meta-analyses. *BMJ Clin. Res. ed)* 327 (7414), 557–560. doi:10.1136/bmj.327.7414.557

Jiang, J., Zhang, L., Chen, H., Lei, Y., Zhang, T., Wang, Y., et al. (2020). Regorafenib induces lethal autophagy arrest by stabilizing PSAT1 in glioblastoma. *Autophagy* 16 (1), 106–122. doi:10.1080/15548627.2019.1598752

Jiang, T., Nam, D. H., Ram, Z., Poon, W. S., Wang, J., Boldbaatar, D., et al. (2021). Clinical practice guidelines for the management of adult diffuse gliomas. *Cancer Lett.* 499, 60–72. doi:10.1016/j.canlet.2020.10.050

Le Rhun, E., Preusser, M., Roth, P., Reardon, D. A., van den Bent, M., Wen, P., et al. (2019). Molecular targeted therapy of glioblastoma. *Cancer Treat. Rev.* 80, 101896. doi:10.1016/j.ctrv.2019.101896

Liau, L. M., Ashkan, K., Brem, S., Campian, J. L., Trusheim, J. E., Iwamoto, F. M., et al. (2023). Association of autologous tumor lysate-loaded dendritic cell vaccination with extension of survival among patients with newly diagnosed and recurrent glioblastoma: A phase 3 prospective externally controlled cohort trial. *JAMA Oncol.* 9 (1), 112–121. doi:10.1001/jamaoncol.2022.5370

Lombardi, G., De Salvo, G. L., Brandes, A. A., Eoli, M., Rudà, R., Faedi, M., et al. (2019). Regorafenib compared with lomustine in patients with relapsed glioblastoma (REGOMA): A multicentre, open-label, randomised, controlled, phase 2 trial. *lancet Oncol.* 20 (1), 110–119. doi:10.1016/S1470-2045(18)30675-2

Louis, D. N., Perry, A., Wesseling, P., Brat, D. J., Cree, I. A., Figarella-Branger, D., et al. (2021). The 2021 WHO classification of tumors of the central nervous system: A summary. *Neuro Oncol.* 23 (8), 1231–1251. doi:10.1093/neuonc/noab106

Ma, R., Taphoorn, M. J. B., and Plaha, P. (2021). Advances in the management of glioblastoma. *J. neurology, Neurosurg. psychiatry* 92 (10), 1103–1111. doi:10.1136/jnnp-2020-325334

McBain, C., Lawrie, T. A., Rogozińska, E., Kernohan, A., Robinson, T., and Jefferies, S. (2021). Treatment options for progression or recurrence of glioblastoma: A network meta-analysis. *Cochrane Database Syst. Rev.* 2021 (12), 2020. doi:10.1002/14651858.CD013579.pub2

McKinnon, C., Nandhabalan, M., Murray, S. A., and Plaha, P. (2021). Glioblastoma: Clinical presentation, diagnosis, and management. *BMJ Clin. Res. ed)* 374, n1560. doi:10.1136/bmj.n1560

Nabors, L. B., Portnow, J., Ahluwalia, M., Baehring, J., Brem, H., Brem, S., et al. (2020). Central nervous system cancers, version 3.2020, NCCN clinical practice guidelines in oncology. *J. Natl. Compr. Cancer Netw. JNCCN* 18 (11), 1537–1570. doi:10.6004/jnccn.2020.0052

Nayak, L., Molinaro, A. M., Peters, K., Clarke, J. L., Jordan, J. T., de Groot, J., et al. (2021). Randomized phase II and biomarker study of pembrolizumab plus bevacizumab versus pembrolizumab alone for patients with recurrent glioblastoma. *Clin. cancer Res.* 27 (4), 1048–1057. doi:10.1158/1078-0432.CCR-20-2500

Nicholson, J. G., and Fine, H. A. (2021). Diffuse glioma heterogeneity and its therapeutic implications. *Cancer Discov.* 11 (3), 575–590. doi:10.1158/2159-8290.Cd-20-1474

Oldrini, B., Vaquero-Siguero, N., Mu, Q., Kroon, P., Zhang, Y., Galán-Ganga, M., et al. (2020). MGMT genomic rearrangements contribute to chemotherapy resistance in gliomas. *Nat. Commun.* 11 (1), 3883. doi:10.1038/s41467-020-17717-0

Omuro, A., and DeAngelis, L. M. (2013). Glioblastoma and other malignant gliomas: A clinical review. *Jama* 310 (17), 1842–1850. doi:10.1001/jama.2013.280319

Ostrom, Q. T., Gittleman, H., Truitt, G., Boscia, A., Kruchko, C., and Barnholtz-Sloan, J. S. (2018). CBTRUS statistical report: Primary brain and other central nervous system tumors diagnosed in the United States in 2011-2015. *Neuro Oncol.* 20, iv1–iv86. doi:10.1093/neuonc/noy131

Page, M. J., McKenzie, J. E., Bossuyt, P. M., Boutron, I., Hoffmann, T. C., Mulrow, C. D., et al. (2021). The PRISMA 2020 statement: An updated guideline for reporting systematic reviews. *BMJ Clin. Res. ed)* 372, n71. doi:10.1136/bmj.n71

Patil, V. M., Menon, N., Chatterjee, A., Tonse, R., Choudhari, A., Mahajan, A., et al. (2022). Mebendazole plus lomustine or temozolomide in patients with recurrent glioblastoma: A randomised open-label phase II trial. *EClinicalMedicine* 49, 101449. doi:10.1016/j.eclinm.2022.101449

Puduvalli, V. K., Wu, J., Yuan, Y., Armstrong, T. S., Vera, E., Wu, J., et al. (2020). A Bayesian adaptive randomized phase II multicenter trial of bevacizumab with or without vorinostat in adults with recurrent glioblastoma. *Neuro-oncology* 22 (10), 1505–1515. doi:10.1093/neuonc/noaa062

Reardon, D. A., Brandes, A. A., Omuro, A., Mulholland, P., Lim, M., Wick, A., et al. (2020). Effect of nivolumab vs bevacizumab in patients with recurrent glioblastoma: The CheckMate 143 phase 3 randomized clinical trial. *JAMA Oncol.* 6 (7), 1003–1010. doi:10.1001/jamaoncol.2020.1024

Reardon, D. A., Nabors, L. B., Mason, W. P., Perry, J. R., Shapiro, W., Kavan, P., et al. (2015). Phase I/randomized phase II study of afatinib, an irreversible ErbB family blocker, with or without protracted temozolomide in adults with recurrent glioblastoma. *Neuro-Oncology* 17 (3), 430–439. doi:10.1093/neuonc/nou160

Salanti, G., Ades, A. E., and Ioannidis, J. P. (2011). Graphical methods and numerical summaries for presenting results from multiple-treatment meta-analysis: An overview and tutorial. *J. Clin. Epidemiol.* 64 (2), 163–171. doi:10.1016/j.jclinepi.2010.03.016

Santangelo, A., Rossato, M., Lombardi, G., Benfatto, S., Lavezzari, D., De Salvo, G. L., et al. (2021). A molecular signature associated with prolonged survival in glioblastoma patients treated with regorafenib. *Neuro Oncol.* 23 (2), 264–276. doi:10.1093/neuonc/noaa156

Song, W. G., Wang, Y. F., Liu, R., Yang, Z. H., Fang, F., Wang, R. L., et al. (2010). Efficacy comparison of hydroxycamptothecine and temozolomide for recurrent high-grade gliomas. *Chin. J. Cancer Prev. Treat.* 17 (20), 1676–1678.

Sun, J., Yang, X. J., and Yang, S. Y. (2013). Multicenter randomized controlled study of temozolomide versus semustine in the treatment of recurrent malignant glioma. *Natl. Med. J. China* 93 (3), 165–168. doi:10.3760/cma.j.issn.0376-2491.2013.03.003

Taal, W., Oosterkamp, H. M., Walenkamp, A. M., Dubbink, H. J., Beerepoot, L. V., Hanse, M. C., et al. (2014). Single-agent bevacizumab or lomustine versus a

combination of bevacizumab plus lomustine in patients with recurrent glioblastoma (BELOB trial): A randomised controlled phase 2 trial. *Lancet Oncol.* 15 (9), 943–953. doi:10.1016/s1470-2045(14)70314-6

Tierney, J. F., Stewart, L. A., Ghersi, D., Burdett, S., and Sydes, M. R. (2007). Practical methods for incorporating summary time-to-event data into meta-analysis. *Trials* 8, 16. doi:10.1186/1745-6215-8-16

Twelves, C., Sabel, M., Checketts, D., Miller, S., Tayo, B., Jove, M., et al. (2021). A phase 1b randomised, placebo-controlled trial of nabiximols cannabinoid oromucosal spray with temozolomide in patients with recurrent glioblastoma. *Br. J. Cancer* 124 (8), 1379–1387. doi:10.1038/s41416-021-01259-3

van Valkenhoef, G., Dias, S., Ades, A. E., and Welton, N. J. (2016). Automated generation of node-splitting models for assessment of inconsistency in network meta-analysis. *Res. synthesis methods* 7 (1), 80–93. doi:10.1002/jrsm.1167

Weller, M., van den Bent, M., Preusser, M., Le Rhun, E., Tonn, J. C., Minniti, G., et al. (2021). EANO guidelines on the diagnosis and treatment of diffuse gliomas of adulthood. *Nat. Rev. Clin. Oncol.* 18 (3), 170–186. doi:10.1038/s41571-020-00447-z

Wen, P. Y., Stein, A., van den Bent, M., De Greve, J., Wick, A., de Vos, F., et al. (2022). Dabrafenib plus trametinib in patients with BRAF(V600E)-mutant low-grade and high-grade glioma (ROAR): A multicentre, open-label, single-arm, phase 2, basket trial. *Lancet Oncol.* 23 (1), 53–64. doi:10.1016/s1470-2045(21)00578-7

Wen, P. Y., Weller, M., Lee, E. Q., Alexander, B. M., Barnholtz-Sloan, J. S., Barthel, F. P., et al. (2020). Glioblastoma in adults: A society for neuro-oncology (SNO) and European society of neuro-oncology (EANO) consensus review on current management and future directions. *Neuro Oncol.* 22 (8), 1073–1113. doi:10.1093/neuonc/noaa106

Wick, W., Gorlia, T., Bendszus, M., Taphoorn, M., Sahm, F., Harting, I., et al. (2017). Lomustine and bevacizumab in progressive glioblastoma. *N. Engl. J. Med.* 377 (20), 1954–1963. doi:10.1056/NEJMoa1707358

Yung, W. K., Albright, R. E., Olson, J., Fredericks, R., Fink, K., Prados, M. D., et al. (2000). A phase II study of temozolomide vs. procarbazine in patients with glioblastoma multiforme at first relapse. *Br. J. cancer* 83 (5), 588–593. doi:10.1054/bjoc.2000.1316

frontiers | Frontiers in Neuroscience

TYPE Original Research
PUBLISHED 22 June 2023
DOI 10.3389/fnins.2023.1186312

OPEN ACCESS

EDITED BY
Peichen Pan,
Zhejiang University, China

REVIEWED BY
Zhisheng Wei,
The First Affiliated Hospital of Guangdong Pharmaceutical University, China
Feng Lin,
Jilin University, China

*CORRESPONDENCE
Yang Bai
✉ baiyang0221@jlu.edu.cn

†These authors have contributed equally to this work and share first authorship

RECEIVED 14 March 2023
ACCEPTED 02 June 2023
PUBLISHED 22 June 2023

CITATION
Zhang Z, Wang S, Ren F, Yang L, Xie H, Pan L, Li Y, Yu B, Yang Y, Su H, Chen Y, Zhang C, Chen H, Yang W, An N and Bai Y (2023) Inflammatory factors and risk of meningiomas: a bidirectional mendelian-randomization study. *Front. Neurosci.* 17:1186312. doi: 10.3389/fnins.2023.1186312

Inflammatory factors and risk of meningiomas: a bidirectional mendelian-randomization study

Zhiyun Zhang[1,2†], Shengnan Wang[3†], Fei Ren[4], Laiyu Yang[2], Haoqun Xie[4], Lin Pan[3], Yifan Li[5], Bingcheng Yu[5], Yifan Yang[4], Haoyi Su[1], Youqi Chen[1], Chuyi Zhang[1], Hongyu Chen[6], Wenzhuo Yang[6], Nan An[5] and Yang Bai[1*]

[1]Department of Neurosurgery, The First Hospital of Jilin University, Changchun, China, [2]Department of Plastic and Reconstructive Surgery, The First Hospital of Jilin University, Changchun, China, [3]Department of Neurology, The First Hospital of Jilin University, Changchun, China, [4]The Second Hospital of Jilin University, Changchun, Jilin, China, [5]Zhongshan School of Medicine, Sun Yat-sen University, Guangzhou, China, [6]Department of Neurosurgery, Sun Yat-sen University Cancer Center, Guangzhou, China

Background: Meningiomas are one of the most common intracranial tumors, and the current understanding of meningioma pathology is still incomplete. Inflammatory factors play an important role in the pathophysiology of meningioma, but the causal relationship between inflammatory factors and meningioma is still unclear.

Method: Mendelian randomization (MR) is an effective statistical method for reducing bias based on whole genome sequencing data. It's a simple but powerful framework, that uses genetics to study aspects of human biology. Modern methods of MR make the process more robust by exploiting the many genetic variants that may exist for a given hypothesis. In this paper, MR is applied to understand the causal relationship between exposure and disease outcome.

Results: This research presents a comprehensive MR study to study the association of genetic inflammatory cytokines with meningioma. Based on the results of our MR analysis, which examines 41 cytokines in the largest GWAS datasets available, we were able to draw the relatively more reliable conclusion that elevated levels of circulating TNF-β, CXCL1, and lower levels of IL-9 were suggestive associated with a higher risk of meningioma. Moreover, Meningiomas could cause lower levels of interleukin-16 and higher levels of CXCL10 in the blood.

Conclusion: These findings suggest that TNF-β, CXCL1, and IL-9 play an important role in the development of meningiomas. Meningiomas also affect the expression of cytokines such as IL-16 and CXCL10. Further studies are needed to determine whether these biomarkers can be used to prevent or treat meningiomas.

KEYWORDS

meningioma, inflammation, risk, Mendelian randomization (MR), cytokines

Introduction

Meningiomas are brain tumors that occur in the meninges surrounding the brain and spinal cord (Brastianos et al., 2019). They are one of the most common primary intracranial tumors of the central nervous system (CNS) and are second only to glioma in incidence. The vast majority of meningiomas are benign and are classified as World Health Organization (WHO) grade I;

those of WHO grade II are more aggressive; and a very small percentage are malignant (only 1 to 3%) and they belong to WHO grade III (Buerki et al., 2018). Benign meningiomas can be completely cured by surgery and radiotherapy, while malignant meningiomas have a higher frequency of local invasion, recurrence, and metastasis, and the treatment options are extremely limited (Maggio et al., 2021).

The majority of meningiomas are located outside the blood–brain barrier (BBB), rendering them more vulnerable to systemic immunology and inflammation compared to structures within the BBB (von Spreckelsen et al., 2022). A retrospective study revealed elevated levels of TNF-α in meningioma patients, which induces inflammatory damage, triggers inflammatory responses, and promotes the release of pro-inflammatory factors like IL-6 (Zheng et al., 2022). Earlier investigations have demonstrated that increased IL-10 within the tumor microenvironment, including meningiomas, is associated with a poorer prognosis (Singh et al., 2019; Manjunath et al., 2022), highlighting the crucial role of inflammatory factor regulation in the pathophysiology of meningioma. Cytokines have been identified as reliable screening targets for inflammation and pain in meningiomas, with potential diagnostic and therapeutic applications (Shamsdin et al., 2019). However, these studies have focused on a limited number of inflammatory factors and have not accounted for the influence of other physical factors on altered inflammatory factor levels. Hence, it is essential to ascertain whether changes in inflammatory factors contribute to tumorigenesis or if the tumor itself modifies the microenvironment, leading to variations in inflammatory factors. Given the incomplete understanding of the etiology of malignant meningiomas, investigating the precise nature of the interaction between inflammatory factors and meningiomas holds significant clinical importance.

To establish a causal relationship between exposure to inflammatory cytokines and the development of meningiomas, we can employ Mendelian randomization (MR). MR is an observational study design that leverages genetic variants as instrumental variables to estimate the causal effect of risk factors on health outcomes. Unlike traditional multivariable observational analyses, MR is less susceptible to confounding variables and measurement errors, and avoids bias arising from reverse causality. As a result, MR has become a reliable method to obtain robust estimates for the causal impact of various risk factors on health outcomes, often yielding results similar to those obtained from randomized controlled trials (RCTs) when available (Davey Smith and Hemani, 2014).

In our study, we conducted a bidirectional Mendelian randomization analysis using genetic variations as instrumental variables to assess the causal relationship between alterations in inflammatory cytokine levels and the risk of developing meningiomas (Bouras et al., 2022). We found no evidence of a link between genetically predicted inflammatory variables and levels of potential confounders. Thus, by assuming that the connection between genetic variants and meningiomas exclusively operates through exposure, Mendelian randomization analysis can be employed to ascertain the causal influence of inflammatory factors on the risk of developing meningiomas.

Methods

MR is based on three hypotheses: (1) the genetic instrumental variable (s) should be strongly associated with the exposure (risk factor of interest); (2) there should be no confounding variables that influence both the risk factor and the outcome, and these variables should not be associated with the genetic instrument associated with risk factor and outcome either; and (3) there should be no other pathways from the genetic instrument to the outcome other than through the risk factor of interest (Bowden and Holmes, 2019; Figure 1).

Summary statistics source

In this bidirectional Mendelian randomization study, the first step was to select appropriate genetic variants from publicly available genome-wide association study (GWAS) databases. SNPs were selected as IVs from GWAS databases for exposure and outcome. The SNPs associated with inflammatory factors were obtained from a study of 8,293 individuals that included 41 cytokines and growth factors (Ahola-Olli et al., 2017). Summary statistics for meningiomas were obtained from the UK Biobank, which included 307 cases and 456,041 controls of European ancestry, and a generalized linear mixed model (GLMM)-based method named (fastGWA-GLMM) was utilized with adjustments for covariates (Rusk, 2018). To prevent population stratification bias from confounding the findings, all SNPs and their accompanying pooled data were restricted to populations of European ancestry in this study (Jiang et al., 2021). Table 1 summarizes details about cytokines based on summary-level data from genome-wide association studies (GWAS).

Instrumental variables selection

We selected SNPs strongly associated with inflammatory factors, with genome-wide significance (P-value $< 5 \times 10^{-8}$), as potential IVs (Burgess and Thompson, 2011). After that, we need to remove linkage disequilibrium (LD). Setting the threshold as r2 < 0.001, kb = 5,000, and removing the SNPs with r2 greater than 0.001 with the most significant SNP within 5,000 kb. Only 10 inflammatory cytokines had more than two independent SNPs at the P-value $< 5 \times 10^{-8}$ level after reconciling the selected SNPs with the resulting data. Therefore, we widen the threshold to P-value $< 5 \times 10^{-6}$ to select eligible instrumental variables. Through the above steps, we obtained 41 kinds of inflammatory factors. Due to the lowered significance threshold, IVs with F-statistics less than 10 were considered weak instrumental variables and would be excluded from our study. To comply with the law of Mendelian randomization, we will also screen the target SNPs to exclude SNPs associated with the results. Finally, the effect alleles of the genetic variants were coordinated in the exposure and outcome of GWAS, Supplementary Tables S1–S42.

Data analysis

In this study, we primarily used the inverse variance weighting (IVW) method to estimate the causal effect of exposure on the outcome, which required SNPs to fully comply with the three principles of MR studies to obtain correct causal estimates (Wang et al., 2022). And the method will provide the most accurate results when the selected SNPs are all valid IVs. We also applied several

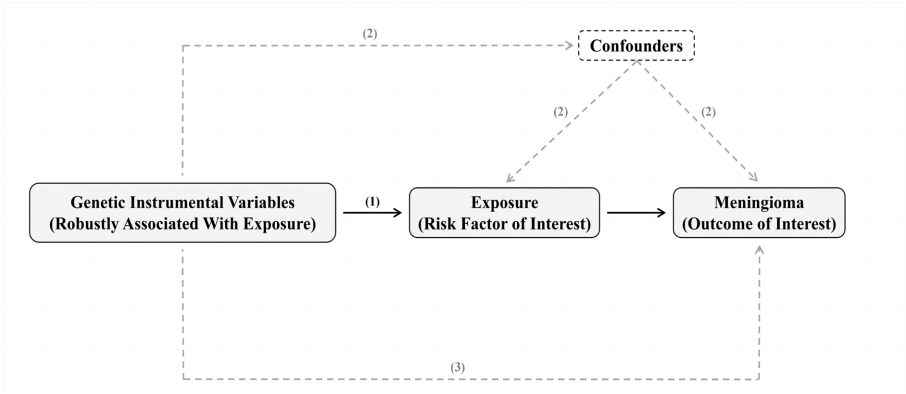

FIGURE 1
Summary of Mendelian randomization and its assumptions. The assumptions underlying Mendelian randomization (MR) analysis are as follows: (1) the genetic instrumental variable(s) should be strongly associated with the exposure (risk factor of interest); (2) there should be no confounding variables that influence both the risk factor and the outcome, and these variables should not be associated with the genetic instrument associated with risk factor and outcome either; and (3) there should be no other pathways from the genetic instrument to the outcome other than through the risk factor of interest. In practice, the last assumption is often violated due to horizontal pleiotropy, where the genetic instruments affect other factors that independently influence the outcome. This can result in biased MR estimates, either overestimating or underestimating the true effect of the risk factor on the outcome. There are various statistical methods available for estimating causal MR effects. The most intuitive method involves taking the ratio of "the association of genetic instruments with the outcome" and "the association of genetic instruments with the risk factor." Valid MR estimates can be obtained using two independent samples, where one sample is used to assess the association of the genetic instrument with the outcome and the other sample is used to assess the association of the genetic instrument with the risk factor. The advantage of this two-sample approach is the potential to use publicly available genome-wide data to obtain large sample sizes and apply novel methods to test for horizontal pleiotropy. Please refer to the Methods section and the ESM for a detailed explanation of these methods.

complementary methods, including the weighted median (WM) method, and MR Egger regression, to estimate the causal associations under different conditions (Bowden et al., 2016). The WM method uses the median MR estimate as the causal estimate and has some advantages over MR Egger regression because it provides lower type I error and higher causal estimation power. MR Egger uses the reciprocal of the resulting variances as the weights for the analysis. Different from IVW, MR Egger considers the presence of an intercept term in the regression analysis. The intercept of the MR Egger regression model reveals the presence or absence of horizontal pleiotropy (P-value < 0.05 is considered significant) (Burgess and Thompson, 2011). When horizontal pleiotropy is present, it indicates that IVs affect outcomes independently of exposure factors, which is inconsistent with the definition of IVs. Sensitivity analyses were also performed to ensure the stability of the findings, Table 2. The Cochran Q test was used to assess heterogeneity between SNPs, Table 2. When heterogeneity was present (P-value < 0.05), certain SNPs with small p-values needed to be excluded or a random-effects model was used directly to assess the MR effect. Finally, we performed the "leave-one-out" analysis to test the stability of the results, Supplementary Figures S1–S5. The packages 'TwoSampleMR' in R version 4.2.2 were used for the analysis.

Results

Genetically predicted systemic inflammatory regulators are associated with meningiomas, as evidenced by the following results. The higher tumor necrosis factor-beta (TNF-β) (OR = 1.351, 95% CI = 1.015–1.797) and CXCL1 (Growth regulated oncogene-α) (OR = 1.291, 95% CI = 1.002–1.663) levels are associated with an increased risk of meningiomas using IVW methods, Table 3. MR-Egger Intercept did not detect potential horizontal pleiotropy (P-value > 0.05). Furthermore, MR-Egger and IVW heterogeneity tests showed that there was no obvious heterogeneity (P-value > 0.05). Leave-one-out studies were used for sensitivity analysis and demonstrated no influence, Supplementary Figures S1, S3. Moreover, we found that higher interleukin-9 (IL-9) levels can reduce meningioma risk (OR = 0.544, 95% CI = 0.322–0.918) using IVW methods. There was no heterogeneity or horizontal pleiotropy in the results (P-value > 0.05). The above results are listed in Tables 2, 3.

Similarly, we found an association between genetically predicted meningiomas and cytokine levels. Genetically predicted meningiomas were associated with levels of interleukin-16 (IL-16) (BETA = −0.037, 95% CI = −0.069 ~ −0.004) and interferon gamma-induced protein 10 (IP10) (BETA = 0.036, 95% CI = 0.003–0.068) using IVW methods. There was no evidence of pleiotropy and heterogeneity observed in these results. The above results are summarized in Tables 2, 3. The Figures of Leave-one-out Analysis, Scatter Plot, Funnel Plot, and Forest Plot are listed in Supplementary material.

Discussion

Meningiomas are one of the most common intracranial tumors. Most meningiomas occur intracranially, and a small proportion occurs in the spinal cord. Meningiomas usually grow gradually, with many tumors appearing in inaccessible places (Buerki et al., 2018; Hou et al., 2021). This sporadic behavior creates a therapeutic challenge for clinicians, as it makes it difficult to achieve complete and complete tumor removal, which in turn often leads to postoperative recurrences (Maggio et al., 2021). Inflammation in meningioma is an important part of the pathogenesis and progression. Studies have shown that in response to various stimuli and signals, circulating (systemic) immune

TABLE 1 The sample size for each cytokine analyzed in this study acquired from the GWAS.

Cytokines	Abbreviation	Sample size	Number
Cutaneous T-cell attracting (CCL27)	CTACK	3,631	GCST004420
Beta nerve growth factor	βNGF	3,531	GCST004421
Vascular endothelial growth factor	VEGF	7,118	GCST004422
Macrophage migration inhibitory factor (glycosylation-inhibiting factor)	MIF	3,494	GCST004423
TNF-related apoptosis inducing ligand	TRAIL	8,186	GCST004424
Tumor necrosis factor-beta	TNFβ	1,559	GCST004425
Tumor necrosis factor-alpha	TNFα	3,454	GCST004426
Stromal cell-derived factor-1 alpha (CXCL12)	SDF1α	5,998	GCST004427
Stem cell growth factor beta	SCGFβ	3,682	GCST004428
Stem cell factor	SCF	8,290	GCST004429
Interleukin-16	IL-16	3,483	GCST004430
Regulated on activation, normal T cell expressed and secreted (CCL5)	RANTES	3,421	GCST004431
Platelet derived growth factor BB	PDGFbb	8,293	GCST004432
Macrophage inflammatory protein-1β (CCL4)	MIP1β	8,243	GCST004433
Macrophage inflammatory protein-1α (CCL3)	MIP1α	3,522	GCST004434
Monokine induced by interferon-gamma (CXCL9)	MIG	3,685	GCST004435
Macrophage colony-stimulating factor	MCSF	840	GCST004436
Monocyte specific chemokine 3 (CCL7)	MCP3	843	GCST004437
Monocyte chemotactic protein-1 (CCL2)	MCP1	8,293	GCST004438
Interleukin-12p70	IL-12p70	8,270	GCST004439
Interferon gamma-induced protein 10 (CXCL10)	IP10	3,685	GCST004440
Interleukin-18	IL-18	3,636	GCST004441
Interleukin-17	IL-17	7,760	GCST004442
Interleukin-13	IL-13	3,557	GCST004443
Interleukin-10	IL-10	7,681	GCST004444
Interleukin-8 (CXCL8)	IL-8	3,526	GCST004445
Interleukin-6	IL-6	8,189	GCST004446
Interleukin-1 receptor antagonist	IL1ra	3,638	GCST004447
Interleukin-1-beta	IL-1β	3,309	GCST004448
Hepatocyte growth factor	HGF	8,292	GCST004449
Interleukin-9	IL-9	3,634	GCST004450
Interleukin-7	IL-7	3,409	GCST004451
Interleukin-5	IL-5	3,364	GCST004452
Interleukin-4	IL-4	8,124	GCST004453
Interleukin-2 receptor, alpha subunit	IL2rα	3,677	GCST004454
Interleukin-2	IL-2	3,475	GCST004455
Interferon-gamma	IFN-γ	7,701	GCST004456
Growth regulated oncogene-α (CXCL1)	GROα	3,505	GCST004457
Granulocyte colony-stimulating factor	GCSF	7,904	GCST004458
Basic fibroblast growth factor	bFGF	7,565	GCST004459
Eotaxin (CCL11)	Eotaxin	8,153	GCST004460

cells can migrate out of the cerebral vasculature and into the perivascular space and brain parenchyma (Domingues et al., 2016). Most meningiomas occur outside the blood–brain barrier (BBB) and can be infiltrated by different cell types, mainly immune cells, making them more susceptible to systemic immunity and inflammation than structures inside the BBB. Some meningioma variants have also been shown to be associated with systemic inflammatory syndromes (Polyzoidis et al., 2015). Other studies have shown that the proportion of immune cells changes significantly during the development of meningiomas, suggesting that meningiomas also affect the immune

TABLE 2 Heterogeneity test of the IVW and MR egger analyses and pleiotropy test (egger intercept).

Exposure	Outcome	Methods	Cochran's Q	*Q*-value	*P*-value (Pleiotropy test)
TNF-β (Tumor necrosis factor-β)	Meningiomas	MR egger	1.952	0.377	0.452
		Inverse variance weighted	2.809	0.422	
Interleukin-9	Meningiomas	MR egger	1.033	0.905	0.949
		Inverse variance weighted	1.038	0.959	
CXCL1 (Growth regulated oncogene-α)	Meningiomas	MR egger	7.452	0.383	0.617
		Inverse variance weighted	8.686	0.369	
Meningiomas	Interleukin-16	MR egger	2.796	0.947	0.102
		Inverse variance weighted	6.208	0.719	
Meningiomas	Interferon gamma-induced protein 10 (CXCL10)	MR egger	7.491	0.485	0.628
		Inverse variance weighted	7.745	0.560	

TABLE 3 Bidirectional Mendelian randomization estimates of cytokines and meningiomas (IVW, MR-egger, weighted median, MR-PRESSO).

Exposure	Outcome	Methods	Number of SNPs	OR (95% CI)	*P*-value
TNF-β (Tumor necrosis factor-β)	Meningiomas	Inverse variance weighted	4	1.351 (1.015–1.797)	0.039
		MR egger	4	1.181 (0.789–1.767)	0.503
		Weighted median	4	1.267 (0.931–1.724)	0.132
Interleukin-9	Meningiomas	Inverse variance weighted	6	0.544 (0.322–0.918)	0.023
		MR egger	6	0.567 (0.156–2.064)	0.438
		Weighted median	6	0.576 (0.294–1.131)	0.109
CXCL1 (Growth regulated oncogene-α)	Meningiomas	Inverse variance weighted	10	1.291 (1.002–1.663)	0.048
		MR egger	10	1.127 (0.636–1.997)	0.693
		Weighted median	10	1.291 (0.950–1.753)	0.102
				BETA (95% CI)	
Meningiomas	Interleukin-16	Inverse variance weighted	10	−0.037 (−0.069 ~ −0.004)	0.027
		MR egger	10	−0.078 (−0.133 ~ −0.023)	0.023
		Weighted median	10	−0.039 (−0.084 ~ 0.005)	0.082
Meningiomas	Interferon gamma-induced protein 10 (CXCL10)	Inverse variance weighted	10	0.036 (0.003–0.068)	0.033
		MR egger	10	0.024 (−0.030–0.079)	0.402
		Weighted median	10	0.031 (−0.014–0.076)	0.182

response process (Sahab-Negah and Gorji, 2020). However, reverse causality and residual confounding are common biases in these traditional observational studies. Whether these changes in inflammatory modulators cause meningiomas or are a response to meningiomas remains to be investigated. Therefore, there is an urgent need for a more comprehensive understanding of the pathogenesis of meningioma, which could lead to greater advances in therapeutic approaches.

Meanwhile, by using genetic variation as an instrumental variable that can alter exposure to instrumental variables, MR studies can overcome the limitations of observational studies by examining the independent conventional biases associated with observational studies (Davey Smith and Hemani, 2014). This research presents a comprehensive MR study to study the association of genetic inflammatory cytokines with meningioma. Based on the results of our MR analysis, which examines 41 cytokines in the largest GWAS datasets available, we were able to draw the relatively more reliable conclusion that elevated levels of circulating TNF-β, CXCL1, and lower levels of IL-9 were associated with a high risk of meningioma.

TNF-β is involved in regulating tumor cell proliferation, invasion, and apoptosis, and influencing the formation of the tumor microenvironment. TNF-β activates multiple signaling pathways, including NF-κB and MAPK, promoting inflammatory responses and cell survival. Additionally, TNF-beta can induce angiogenesis, providing nutrients and oxygen to the tumor (Buhrmann et al., 2019; Zhong et al., 2022). However, there is a lack of definitive research evidence regarding the association between TNF-beta and the prognosis of meningioma patients. Some studies have shown higher levels of TNF-beta in the peripheral blood of meningioma patients compared to normal individuals (Boyle-Walsh et al., 1996), which may be associated with increased tumor invasiveness, higher risk of recurrence, and enhanced resistance to treatment. Increased expression of CXCL1 is associated with tumor development and progression in meningiomas. CXCL1 is a chemokine that attracts

leukocytes and other immune cells to sites of inflammation or tumors (Acharyya et al., 2012). Research has demonstrated that CXCL1 can promote the proliferation of human meningioma cells (Barbieri et al., 2006). In our study, using a Mendelian randomization approach, we also found that elevated levels of CXCL1 are associated with an increased risk of developing meningiomas. This finding supports the role of CXCL1 in meningioma pathogenesis and suggests its potential as a risk factor for the development of this tumor. The ability of CXCL1 to enhance cell proliferation provides a mechanistic explanation for its involvement in meningioma development. These findings highlight the importance of CXCL1 as a potential therapeutic target and underscore the need for further investigations to explore its precise mechanisms of action in meningioma tumorigenesis. IL-9 activates downstream signaling pathways, such as JAK/STAT and MAPK, by binding to its receptor IL-9R. In certain tumor types, IL-9 may promote tumor growth and metastasis (Angkasekwinai and Dong, 2021). In contrast, our study found that elevated levels of IL-9 in peripheral blood are associated with a decreased risk of developing meningiomas. However, the specific mechanisms of IL-9 in meningiomas require further investigation. Overall, TNF-beta may promote tumor growth and metastasis in meningiomas, while CXCL1 may be involved in tumor invasiveness and resistance to treatment. The role of IL-9 in meningiomas requires further investigation. These research findings provide an important foundation for gaining a deeper understanding of the mechanisms underlying meningioma development and for developing corresponding therapeutic strategies.

The bilateral MR analysis in this study also showed that meningiomas may not be correlated with changes in blood cytokine levels. IL-16, as a multifunctional cytokine, plays a role in regulating immune cell functions in cancer. It enhances the activity of natural killer (NK) cells and promotes cytotoxicity of T cells, thereby inhibiting tumor cell proliferation and dissemination. Additionally, IL-16 has been associated with poor prognosis in cancers such as gastric cancer, possibly due to its ability to attract other immune cells into the tumor microenvironment, including regulatory T cells, influencing tumor growth and progression (Liu et al., 2016; Xiong et al., 2022). Our research findings indicate that meningiomas lead to a decrease in IL-16 levels, although the evidence regarding the relationship between meningiomas and IL-16 is limited. We speculate that the decrease in IL-16 levels may suggest the presence of similar immunosuppressive mechanisms in the meningioma microenvironment, which contribute to tumor growth and evasion of immune surveillance. On the other hand, IP-10 (also known as CXCL10) is a chemokine involved in recruiting and activating immune cells. Elevated levels of IP-10 have been observed in various cancers and are associated with tumor progression, angiogenesis, and immune cell infiltration (Karin and Razon, 2018; Chen et al., 2020; Wu et al., 2021; Limagne et al., 2022). The increased levels of IP-10 in the blood of meningioma patients may reflect inflammatory responses to the tumor or aggregation of immune cells. In summary, the alterations in IL-16 and IP-10 levels in the blood of meningioma patients indicate complex interactions between tumors and the immune system. These findings support the importance of cytokine dysregulation and immune modulation in the pathogenesis of meningiomas. Further research is needed to elucidate the precise mechanisms underlying these cytokine changes and their impact on the development, progression, and therapeutic strategies for meningiomas.

There are several limitations to our study. Firstly, in the GWAS data for cytokines, we used a significance cut-off of P-value $< 5 \times 10^{-6}$ because only 10 had at least one genome-wide significant SNP at a cut-off of P-value $< 5 \times 10^{-8}$. Secondly, the result of our MR-Egger and Weight Median estimates were not significant. As the statistical power of the IVW method was significantly higher than other MR methods, especially MR-Egger, and the fact that we followed the strengthened requirement in the consistent β-direction of MR methods in our study, our result can also be considered significant. The third issue is that all GWAS data are from European populations and there is a shortcoming of whether our findings will be consistent across populations, which remains to be seen. The results of these studies may be influenced by other measured and unmeasured confounders, and cytokine production may be influenced by many other factors, including the cytokine network system, rather than the disease itself.

Data availability statement

The original contributions presented in the study are included in the article/Supplementary material, further inquiries can be directed to the corresponding author.

Author contributions

ZZ and SW conceived the ideas, designed the experiments, and wrote the manuscript. FR, LY, HX, LP, YL, BY, YY, HS, YC, CZ, HC, WY, and NA carried out experiments and analyzed experiments results. YB revised the manuscript, figures, and tables. All authors contributed to the article and approved the submitted version.

Funding

This work was supported by the Natural Science Foundation of Jilin Province to Xing Su (YDZJ202301ZYTS081).

Conflict of interest

The authors declare that the research was conducted in the absence of any commercial or financial relationships that could be construed as a potential conflict of interest.

Publisher's note

Supplementary material

The Supplementary material for this article can be found online at: https://www.frontiersin.org/articles/10.3389/fnins.2023.1186312/full#supplementary-material

References

Acharyya, S., Oskarsson, T., Vanharanta, S., Malladi, S., Kim, J., Morris, P. G., et al. (2012). A CXCL1 paracrine network links cancer chemoresistance and metastasis. *Cells* 150, 165–178. doi: 10.1016/j.cell.2012.04.042

Ahola-Olli, A. V., Würtz, P., Havulinna, A. S., Aalto, K., Pitkänen, N., Lehtimäki, T., et al. (2017). Genome-wide association study identifies 27 loci influencing concentrations of circulating cytokines and growth factors. *Am. J. Hum. Genet.* 100, 40–50. doi: 10.1016/j.ajhg.2016.11.007

Angkasekwinai, P., and Dong, C. (2021). IL-9-producing T cells: potential players in allergy and cancer. *Nat. Rev. Immunol.* 21, 37–48. doi: 10.1038/s41577-020-0396-0

Barbieri, F., Bajetto, A., Porcile, C., Pattarozzi, A., Massa, A., Lunardi, G., et al. (2006). CXC receptor and chemokine expression in human meningioma: SDF1/CXCR4 signaling activates ERK1/2 and stimulates meningioma cell proliferation. *Ann. N. Y. Acad. Sci.* 1090, 332–343. doi: 10.1196/annals.1378.037

Bouras, E., Karhunen, V., Gill, D., Huang, J., Haycock, P. C., Gunter, M. J., et al. (2022). Circulating inflammatory cytokines and risk of five cancers: a Mendelian randomization analysis. *BMC Med.* 20:3. doi: 10.1186/s12916-021-02193-0

Bowden, J., Davey Smith, G., Haycock, P. C., and Burgess, S. (2016). Consistent estimation in Mendelian randomization with some invalid instruments using a weighted median estimator. *Genet. Epidemiol.* 40, 304–314. doi: 10.1002/gepi.21965

Bowden, J., and Holmes, M. V. (2019). Meta-analysis and Mendelian randomization: a review. *Res. Synth. Methods* 10, 486–496. doi: 10.1002/jrsm.1346

Boyle-Walsh, E., Birch, M., Gallagher, J. A., Speirs, V., White, M. C., Shenkin, A., et al. (1996). RT-PCR detection of cytokine transcripts in a series of cultured human meningiomas. *J. Pathol.* 178, 442–446. doi: 10.1002/(SICI)1096-9896(199604)178:4<442::AID-PATH521>3.0.CO;2-I

Brastianos, P. K., Galanis, E., Butowski, N., Chan, J. W., Dunn, I. F., Goldbrunner, R., et al. (2019). Advances in multidisciplinary therapy for meningiomas. *Neurooncology* 21, i18–i31. doi: 10.1093/neuonc/noy136

Buerki, R. A., Horbinski, C. M., Kruser, T., Horowitz, P. M., James, C. D., and Lukas, R. V. (2018). An overview of meningiomas. *Fut. Oncol.* 14, 2161–2177. doi: 10.2217/fon-2018-0006

Buhrmann, C., Yazdi, M., Popper, B., Shayan, P., Goel, A., Aggarwal, B. B., et al. (2019). Evidence that TNF-β induces proliferation in colorectal cancer cells and resveratrol can down-modulate it. *Exp. Biol. Med.* 244, 1–12. doi: 10.1177/1535370218824538

Burgess, S., and Thompson, S. G. (2011). CRP CHD genetics collaboration. Avoiding bias from weak instruments in Mendelian randomization studies. *Int. J. Epidemiol.* 40, 755–764. doi: 10.1093/ije/dyr036

Chen, J., Chen, Q.-L., Wang, W.-H., Chen, X.-L., Hu, X.-Q., Liang, Z.-Q., et al. (2020). Prognostic and predictive values of CXCL10 in colorectal cancer. *Clin. Transl. Oncol.* 22, 1548–1564. doi: 10.1007/s12094-020-02299-6

Davey Smith, G., and Hemani, G. (2014). Mendelian randomization: genetic anchors for causal inference in epidemiological studies. *Hum. Mol. Genet.* 23, R89–R98. doi: 10.1093/hmg/ddu328

Domingues, P., González-Tablas, M., Otero, Á., Pascual, D., Miranda, D., Ruiz, L., et al. (2016). Tumor infiltrating immune cells in gliomas and meningiomas. *Brain Behav. Immun.* 53, 1–15. doi: 10.1016/j.bbi.2015.07.019

Hou, Y., Xie, H., Dou, G., Yang, W., Ge, J., Zhou, B., et al. (2021). Computational study on novel natural inhibitors targeting c-MET. *Medicine* 100:e27171. doi: 10.1097/MD.0000000000027171

Jiang, L., Zheng, Z., Fang, H., and Yang, J. (2021). A generalized linear mixed model association tool for biobank-scale data. *Nat. Genet.* 53, 1616–1621. doi: 10.1038/s41588-021-00954-4

Karin, N., and Razon, H. (2018). Chemokines beyond chemo-attraction: CXCL10 and its significant role in cancer and autoimmunity. *Cytokine* 109, 24–28. doi: 10.1016/j.cyto.2018.02.012

Limagne, E., Nuttin, L., Thibaudin, M., Jacquin, E., Aucagne, R., Bon, M., et al. (2022). MEK inhibition overcomes chemoimmunotherapy resistance by inducing CXCL10 in cancer cells. *Cancer Cell* 40, 136–152.e12. doi: 10.1016/j.ccell.2021.12.009

Liu, F.-T., Zhu, P.-Q., Ou, Y.-X., Liu, W.-W., Xia, G.-F., and Luo, H.-L. (2016). Positive association between IL-16 rs1131445 polymorphism and cancer risk: a meta-analysis. *Minerva Med.* 107, 84–91.

Maggio, I., Franceschi, E., Tosoni, A., Nunno, V. D., Gatto, L., Lodi, R., et al. (2021). Meningioma: not always a benign tumor. A review of advances in the treatment of meningiomas. CNS. *Oncologia* 10:CNS72. doi: 10.2217/cns-2021-0003

Manjunath, N., Mishra, S., Garg, K., Suri, V., Sharma, M. C., Tandon, V., et al. (2022). Is there any relationship between systemic inflammatory markers and meningioma grade? *Neurol. India* 70, 223–230. doi: 10.4103/0028-3886.338647

Polyzoidis, S., Koletsa, T., Panagiotidou, S., Ashkan, K., and Theoharides, T. C. (2015). Mast cells in meningiomas and brain inflammation. *J. Neuroinflammation* 12:170. doi: 10.1186/s12974-015-0388-3

Rusk, N. (2018). The UK biobank. *Nat. Methods* 15:1001. doi: 10.1038/s41592-018-0245-2

Sahab-Negah, S., and Gorji, A. (2020). Meningioma tumor microenvironment. *Adv. Exp. Med. Biol.* 1296, 33–48. doi: 10.1007/978-3-030-59038-3_3

Shamsdin, S. A., Mehrafshan, A., Rakei, S. M., and Mehrabani, D. (2019). Evaluation of VEGF, FGF and PDGF and serum levels of inflammatory cytokines in patients with glioma and meningioma in southern Iran. *Asian Pac. J. Cancer Prev.* 20, 2883–2890. doi: 10.31557/APJCP.2019.20.10.2883

Singh, N., Baby, D., Rajguru, J. P., Patil, P. B., Thakkannavar, S. S., and Pujari, V. B. (2019). Inflammation and cancer. *Ann. Afr. Med.* 18, 121–126. doi: 10.4103/aam.aam_56_18

von Spreckelsen, N., Kesseler, C., Brokinkel, B., Goldbrunner, R., Perry, A., and Mawrin, C. (2022). Molecular neuropathology of brain-invasive meningiomas. *Brain Pathol.* 32:e13048. doi: 10.1111/bpa.13048

Wang, J., Liu, D., Tian, E., Guo, Z.-Q., Chen, J.-Y., Kong, W.-J., et al. (2022). Is hearing impairment causally associated with falls? Evidence from a two-sample Mendelian randomization study. *Front. Neurol.* 13:876165. doi: 10.3389/fneur.2022.876165

Wu, B., Zhang, Z., Dou, G., Lv, X., Ge, J., Wang, H., et al. (2021). Novel natural inhibitors targeting B-RAF(V600E) by computational study. *Bioengineered* 12, 2970–2983. doi: 10.1080/21655979.2021.1943113

Xiong, J., Hu, H., Kang, W., Shao, X., Li, Y., Jin, P., et al. (2022). Association of sarcopenia and expression of interleukin-16 in gastric cancer survival. *Nutrients* 14:14. doi: 10.3390/nu14040838

Zheng, Z., Jia, L., Zhang, P., Tian, Y., and Chen, X. (2022). Effectiveness of super-selective embolization for parasagittal meningiomas and its effect on the level of inflammatory factors. *Evid. Based Complement. Alternat. Med.* 2022, 1–6. doi: 10.1155/2022/2466007

Zhong, S., Zhang, Z., Guo, Z., Yang, W., Dou, G., Lv, X., et al. (2022). Identification of novel natural inhibitors targeting AKT serine/threonine kinase 1 (AKT1) by computational study. *Bioengineered* 13, 12003–12020. doi: 10.1080/21655979.2021.2011631

frontiers | Frontiers in Neuroscience

TYPE Review
PUBLISHED 29 June 2023
DOI 10.3389/fnins.2023.1189606

OPEN ACCESS

EDITED BY
Sheng Zhong,
Sun Yat-sen University Cancer Center, China

REVIEWED BY
Rashmi Rana,
Sir Ganga Ram Hospital, India
Kristin Huntoon,
University of Texas MD Anderson Cancer Center, United States

*CORRESPONDENCE
Konstantinos Gousias
✉ kostasgousias@yahoo.com

RECEIVED 19 March 2023
ACCEPTED 12 June 2023
PUBLISHED 29 June 2023

CITATION
Gousias K, Trakolis L and Simon M (2023) Meningiomas with CNS invasion. *Front. Neurosci.* 17:1189606. doi: 10.3389/fnins.2023.1189606

Meningiomas with CNS invasion

Konstantinos Gousias[1,2,3]*, Leonidas Trakolis[1] and Matthias Simon[4]

[1]Department of Neurosurgery, St. Marien Academic Hospital Lünen, KLW St. Paulus Corporation, Luenen, Germany, [2]Medical School, Westfaelische Wilhelms University of Muenster, Muenster, Germany, [3]Medical School, University of Nicosia, Nicosia, Cyprus, [4]Department of Neurosurgery, Bethel Clinic, Medical School, Bielefeld University, Bielefeld, Germany

CNS invasion has been included as an independent criterion for the diagnosis of a high-grade (WHO and CNS grade 2 and 3) meningioma in the 2016 and more recently in the 2021 WHO classification. However, the prognostic role of brain invasion has recently been questioned. Also, surgical treatment for brain invasive meningiomas may pose specific challenges. We conducted a systematic review of the 2016–2022 literature on brain invasive meningiomas in Pubmed, Scopus, Web of Science and the Cochrane Library. The prognostic relevance of brain invasion as a stand-alone criterion is still unclear. Additional and larger studies using robust definitions of histological brain invasion and addressing the issue of sampling errors are clearly warranted. Although the necessity of molecular profiling in meningioma grading, prognostication and decision making in the future is obvious, specific markers for brain invasion are lacking for the time being. Advanced neuroimaging may predict CNS invasion preoperatively. The extent of resection (e.g., the Simpson grading) is an important predictor of tumor recurrence especially in higher grade meningiomas, but also – although likely to a lesser degree – in benign tumors, and therefore also in brain invasive meningiomas with and without other histological features of atypia or malignancy. Hence, surgery for brain invasive meningiomas should follow the principles of maximal but safe resections. There are some data to suggest that safety and functional outcomes in such cases may benefit from the armamentarium of surgical adjuncts commonly used for surgery of eloquent gliomas such as intraoperative monitoring, awake craniotomy, DTI tractography and further advanced intraoperative brain tumor visualization.

KEYWORDS

invasive meningioma, CNS invasion, Simpson grade of resection, functional outcome, surgery

Introduction

Meningiomas account for approximately 32% of the primary brain tumours (Ostrom et al., 2021). They are usually associated with a favorable prognosis after routine surgical treatments, since the vast majority are assigned to WHO ° (or CNS grade) 1 and the convexity represent their most predominant location (Sun et al., 2020; Louis et al., 2021; Ostrom et al., 2021). However, their treatment may become challenging and their prognosis more complicated in cases with deep seated lesions of the skull base, or of meningiomas infiltrating venous sinuses, or tumors with brain invasion. The surgical management of those lesions is somewhat controversial. Some consider a radical tumor removal, when safely possible, as the gold standard, while others find the Simpson grading obsolete (Sughrue et al., 2010; Gousias et al., 2016), i.e.,

there is no general agreement if treatment of more complex meningiomas should be guided by the concept of complete excision or cytoreduction only.

More than 60 years ago, Simpson published his classification describing the degree of meningioma resection (Simpson, 1957). According to radicality, resections are categorized in 5 groups. The oncological benefit of more radical resections was clear; better resected patients showed lower rates of recurrence. More recently, the prognostic value of the Simpson grading has been questioned (Perry et al., 1997; Sughrue et al., 2010; Chotai and Schwartz, 2022). Many surgeons decide for an incomplete resection of the tumor in order to prevent intraoperative complications and postoperative morbidity, since serial neuroimaging follow-up may allow for staged treatment aiming a tumor control rather than cure. Also, adjuvant radiotherapy and – importantly – radiosurgery may help to achieve acceptable local control rates in cases with residual tumor.

In this paper we will systematically review the recent literature on meningiomas with CNS invasion. We will specifically focus on prognostic issues. We will also investigate the relationship between extent of resection and recurrence in these tumors, as well as their surgical management and recent advances in meningioma invasion imaging.

Methods

We performed a systematic review of English language original articles, reviews or meta-analyses registered in the Pubmed, Scopus, Web of Science and Cochrane Library databases (1st January 2016 to 31th May 2023) according to the PRISMA guidelines using the following search terms: 'meningioma' and'CNS invasion' or 'brain invasion' (Page et al., 2021). 2016 was chosen as the starting time in order to include only studies published after the release of the revised 4th edition of WHO brain tumor classification in 2016. No studies on the prognostic relevance of CNS invasion based on new 5th WHO edition have been identified (Figure 1). We also provide a narrative review of radiological advances and the surgical aspects of meningioma brain invasion.

Definition and prognostic relevance of CNS invasion. A systematic review

Meningiomas that invade the skull, venous sinuses as well as the neighboring soft tissue show an aggressive clinical course and should be aggressively treated, accordingly (Gousias et al., 2016; Goldbrunner et al., 2021; Ostrom et al., 2022). High grade invasive meningiomas, in particular those with infiltration of the venous sinuses or scalp invasion, may even demonstrate, in addition to their high recurrence rate, extremely rare distant metastasis (Kessler et al., 2017; Dalle Ore et al., 2019; Bailey et al., 2023).

However, the term of invasive meningiomas refers mainly to CNS invasion.The latter has been identified as an unfavorable prognostic factor for recurrence already some decades ago (Perry et al., 1997, 1999). As a consequence, brain invasion has been included in the revised 4th edition of the WHO classification for CNS tumours in 2016 and still remains in the newest 2021 release as a stand-alone criterion for assigning a meningioma to the CNS grade 2.

It should nevertheless be noted, that brain invasive meningiomas most often demonstrate additional malignant features. Behling et al. assessed retrospectively 1718 meningiomas, 6.7% of which showed CNS invasion, and found a positive correlation between invasion and higher Ki67 proliferation rate (Behling et al., 2021). A medical history of radiation exposure may be associated with invasive growth and a higher histological grade (Goto et al., 2014; Carr et al., 2021). Radiation-induced meningiomas demonstrate higher rates of recurrence after surgery and radiotherapy, and develop in relatively younger patients at the site of previous radiation (Goto et al., 2014; Carr et al., 2021).

More recently, the prognostic relevance of a sole CNS invasion without further characteristics of atypia or malignancy (BIOBM, brain invasive but otherwise benign meningiomas) has been questioned (Baumgarten et al., 2016; Spille et al., 2016; Nakasu and Nakasu, 2021; Kim et al., 2022). Spille et al. reviewed retrospectively their institutional cohort of 467 primary meningiomas of all grades according to the 2007/2016 WHO criteria and reported a twice as high recurrence rate of brain invasive vs. noninvasive meningiomas after gross total resection. However, brain invasive but otherwise benign meningiomas WHO ° 2 showed better progression free survival (PFS), similar to benign WHO ° 1, when compared to atypical WHO ° 2 meningiomas (Spille et al., 2016). Baumgarten et al. investigated the recurrence rate in a cohort of 229 patients WHO ° 2 treated in two different brain tumor centers in Germany and also found a significant better PFS in BIOBM when compared to atypical meningiomas WHO ° 2 (Baumgarten et al., 2016). A strong limitation of the aforementioned study, though, was the short follow up (median 22 months). Kim et al. analyzed their cohort consisting of 292 meningiomas WHO ° 2 treated between 2001 and 2020, and carried out an additional meta-analysis of the available literature including 3,590 meningiomas. These authors found no consistent association between CNS invasion and PFS. However, this study did not include a central neuropathological review and the histological evaluation reported was according to the WHO criteria at the time of treatment (Kim et al., 2022). Another meta-analysis of the prognostic relevance of CNS invasion was conducted by Nakasu et al. and included studies published after 2000. CNS invasion was identified as a predictor of a shorter PFS in the combined cohort, i.e., meningiomas WHO ° 1–3, whereas BIOBM in particular showed similar recurrence rates to meningiomas WHO ° 1 (Nakasu and Nakasu, 2021). Similarly, Garcia-Segure et al. identified brain invasion as a predictor of tumor recurrence in meningioma WHO ° 2 only in cases with additional histological signs of necrosis in their cohort comprising 181 meningiomas WHO ° 2 treated between 1995 and 2015 (Garcia-Segura et al., 2020).

Studies allowing direct comparisons of BIOBM vs. remaining meningiomas WHO ° I are definitely more appropriate to analyze the prognostic relevance of sole CNS invasion. Biczok et al. investigated retrospectively a bi-institutional cohort comprising 875 meningiomas WHO ° 1 diagnosed according to the 2007 WHO criteria and treated between 2005 and 2014, and found shorter PFS in patients with BIOBM compared to the remaining population (50 vs. 68 months), which however did not reach statistical significance. Importantly, similar results were obtained in 170 patients for which tissue samples could be made available for a neuropathological review of the brain/meningioma interface. Noteworthy, brain invasion without further signs of atypia was suspiciously frequent in these specimens (16.5%)

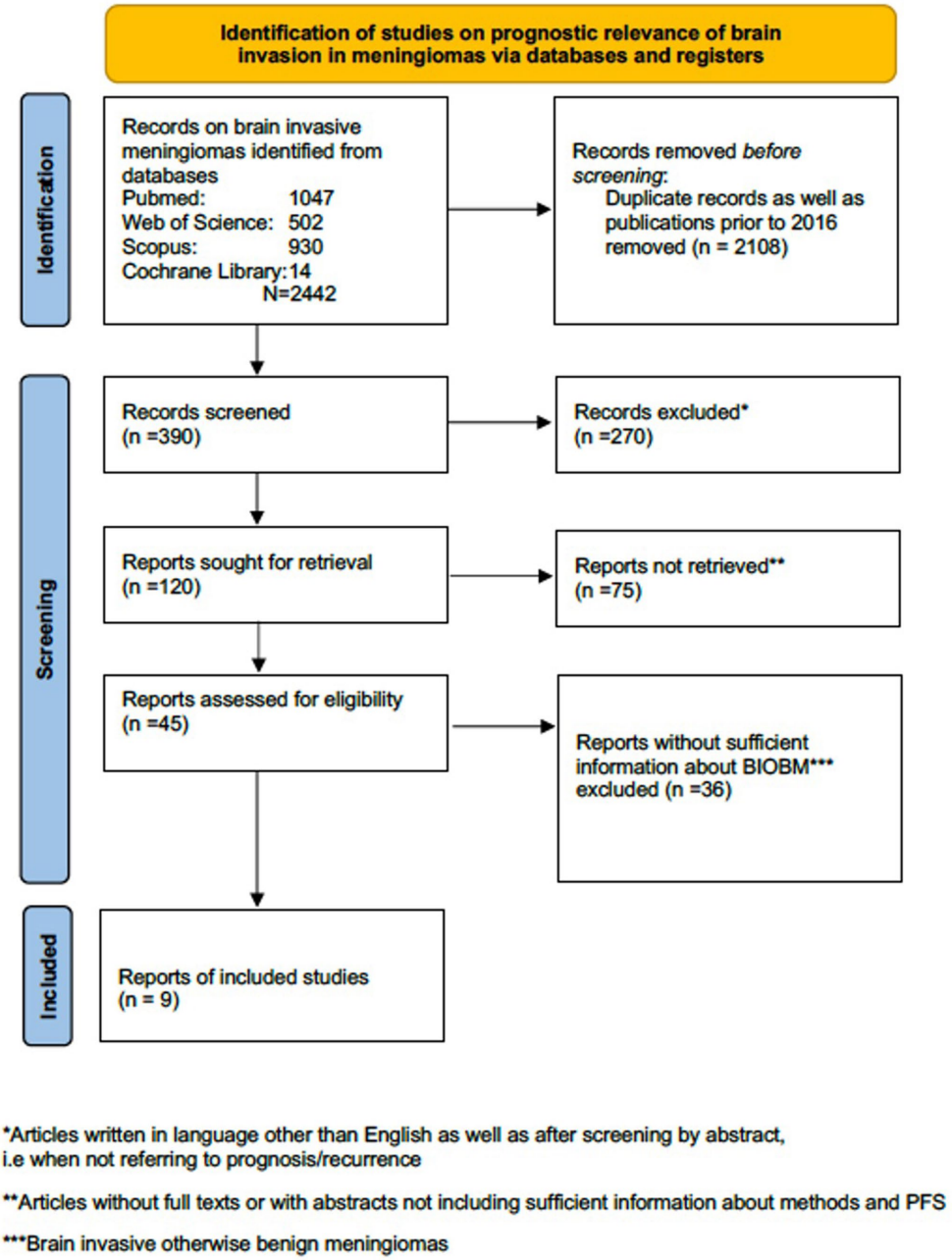

FIGURE 1
PRISMA flow diagram regarding studies on prognostic relevance of brain invasive meningioma.

(Biczok et al., 2019). Traylor et al. reviewed a series of 543 meningiomas (339 WHO ° 1, 200 WHO °2 and 4 WHO ° 3 after neuropathological review according to WHO 2016 criteria) treated surgically in Texas Southwestern Medical Center between 1994 and 2005 and found no significant increase of recurrence risk for BIOBM vs. WHO grade ° 1. Similar to the previous study, this study includes a very high rate of WHO ° 2 (37%) and BIOBM (26.5%) (Traylor et al., 2023). Banan et al. compared the recurrence rates between 243 benign WHO ° 1 meningiomas without CNS invasion and 25 BIOBM (i.e., 9.3% of the overall cohort) treated between 2004 and 2012 and found significantly higher rates (28% vs. 4%) in BIOBM vs. remaining WHO °1 tumors. Strengths of the study design include a central neuropathological reevaluation according to the WHO criteria of 2016 as well as the use of additional immunohistochemical staining against GFAP (Banan et al., 2021). Table 1 lists all relevant meningioma studies on the prognostic relevance of CNS invasion with specific consideration of BIOBM.

The lack of large (prospective) studies with long follow up after complete resections definitely hinders far reaching conclusions regarding the prognostic relevance of brain invasion. However, another possible source of bias, which may contribute to controversial results has been pointed out by Perry, namely the ill-defined criteria for diagnosing brain invasion (Perry, 2021). This may well result in distinctly different rates of CNS invasion reported by different

TABLE 1 Prognostic relevance of invasion in brain invasive otherwise benign meningiomas WHO ° 2 (BIOBM, studies since 2016 included).

Author	No of patients with meningiomas	WHO edition	Follow-up in months	Degree of resection and recurrence*	Association of CNS invasion with recurrence
Spille et al. (2016)	401 WHO ° 1, 60 WHO ° 2 (incl. 20 BIOBM) 6 WHO ° 3	4th/rev.4th, 2007/2016 (neuropathological re-evaluation)	91	Longer PFS after GTR vs. STR, $p = 0.025$	Brain invasive vs. noninvasive meningiomas showed twice as high recurrence rates after GTR BIOBM showed better prognosis than atypical meningiomas WHO ° 2 and similar prognosis as benign WHO ° 1 meningiomas
Baumgarten et al. (2016)	141 WHO ° 2 (incl. 20 BIOBM) (Frankfurt series)	Rev.4th, 2016 (neuropathological re-evaluation)	22	No data on degree of resection	BIOBM showed longer PFS vs. atypical meningiomas WHO ° 2
Biczok et al. (2019)	142 WHO ° 1 28 BIOBM	4th, 2007	66	Longer PFS after GTR vs. STR, $p = 0.001$	Shorter PFS of BIOBM than WHO ° I (50 vs. 68 months) however difference did not reach significance
Garcia-Segura et al. (2020)	181 WHO ° 2	Rev. 4th, 2016 (neuropathological re-evaluation)	>48	Longer PFS after GTR vs. STR, $p = 0.001$ GTR defined as Simpson grade I and II	BIOBM showed better prognosis than remaining WHO ° 2 Combination of necrosis and CNS invasion identified as strong predictor of meningioma recurrence
Nakasu and Nakasu (2021)	Meta-analysis (8 studies)	3rd, 2000 4th, 2007 rev.4th, 2016	Unknown	Meta-analysis, thus no data on degree of resection	Brain invasion was a significant predictor of PFS only when both low and high-grade meningiomas have been considered Brain invasion was not prognostic for BIOBM
Banan et al. (2021)	243 WHO ° 1 65 WHO ° 2 (incl. 25 BIOBM)	Rev. 4th, 2016 (neuropathological re-evaluation)	38,2	Degree of resection was not significant for PFS	25 patients with BIOBM showed shorter PFS vs. 243 patients with benign meningiomas WHO grade 1
Behling et al. (2021)	1,412 WHO ° 1 285 WHO ° 2 21 WHO ° 3	3rd, 2000 4th, 2007 (BIOBM outlined as WHO ° 1)	39,6	No data on prognostic role of degree of resection	Positive correlation of CNS invasion and Ki67 proliferation rate
Kim et al. (2022)	Own cohort of 292 meningiomas WHO ° 2 (BIOBM = 7), Meta-analysis (25 studies, 3,590 patients)	3rd, 2000, 4th, 2007 rev.4th, 2016 no central neuropathological review	54 unknown	Longer PFS for own cohort after GTR vs. STR, $p < 0.001$	No consistent association with PFS
Traylor et al. (2023)	339 WHO ° 1 200 WHO ° 2 4 WHO ° 3 (incl. 90 BIOBM)	Rev. 4th, 2016 (neuropathological re-evaluation)	48	Longer PFS after GTR vs. STR, $p < 0.01$	Similar risk of recurrence between BIOBM and WHO grade 1

*The prognostic role of degree of resection refers to the general series and not specific to BIOBM; GTR has been defined as Simpson grade I-III.

neurosurgical centers (Timme et al., 2020). Indeed, as detailed above the studies reported by Biczok et al., and Banan and co-workers detail a 16.5% vs. 9.3% incidence of BIOBM among otherwise histologically benign meningiomas (Biczok et al., 2019; Banan et al., 2021). While only a slight effect of the classification modification in 2016 on clinical practice had been expected, the increase of cases diagnosed as BIOBM and therefore WHO ° 2 was reported as overwhelming (Timme et al., 2020). Perry described a mini-epidemic of BIOBM in his personal consults, whereas he rejected a sizable number of BIOBM diagnoses during his central review, and discourages neuropathologists from interpretating only focal brain invasion without any additional high-grade features as a criterion for assigning tumors to WHO ° 2. Spreckelsen et al. confirmed Perry's observation of a large interobserver variability and use of somewhat varying criteria among neuropathologists (Baumgarten et al., 2016). Picart und Spreckelsen et al. point out that precise assessment of CNS invasion is mandatory (Picart et al., 2022; von Spreckelsen et al., 2022). The 5th edition of WHO classification of CNS tumours in 2021 has recognized this issue and suggested more uniformed criteria for the diagnosis of CNS invasion. According to the new classification system, CNS invasion is defined as 'irregular, tongue-like protrusions of tumour cells into underlying GFAP-positive parenchyma, without intervening leptomeninges. Extension along perivascular Virchow-Robin spaces is not considered to constitute brain invasion because the pia is not breached' (Timme et al., 2020). Another important aspect of the problem is surgical sampling error (Biczok et al., 2019). Brain invasion may be missed by the neuropathologist because the brain tumor interface has not been or has not been sufficiently sampled during the surgery (Jenkinson et al., 2017; Picart et al., 2022). To this end, Timme et al. reviewed the histological reports of the Neuropathological Institute in Münster, which diagnosed meningioma samples from different Neurosurgical Departments of the region. Since the rate of CNS invasion differed among some neurosurgical departments, he concluded that surgical sampling nuances may impact the accuracy of recognition of CNS invasion (Timme et al., 2020).

TABLE 2 Criteria for histological grade classification of WHO 5th Edition 2021 (Louis et al., 2021).

WHO grade	Description of criteria
Grade 1	Low mitotic rate, <4 per 10 HPFs*
Grade 2	Mitotic rate 4–19 per 10 HPF or Brain invasion** or ≥3 or 5 specific atypical features: • Spontaneous or geographic necrosis, • Patternless sheet-like growth • Prominent nucleoli • High cellularity • Small cells with high n:c ratio or specific morphology: chordoid or clear cell
Grade 3	Mitotic rate > 20 per 10 HPF or specific morphology: papillary or rhabdoid or specific molecular criteria: *TERT* promoter mutation or homozygous deletion of *CDKN2A/B*

Pathophysiology and molecular profile of CNS invasion

The 2021 WHO classification incorporated for the first-time molecular biomarkers into the diagnosis of grading, like *CDKN2A* homozygous deletion and *TERT* promoter mutation, allowing the assignment of the tumor to WHO/CNS ° 3 even in cases that appear histologically as lower grade (Louis et al., 2021; Table 2). The last edition of WHO classification recognizes also the importance of additional molecular profile analysis, like mutations of *SMARCE1* (clear cell architecture), *KLF4/TRAF7* (secretory meningiomas) and *BAP1* (rhabdoid or papillary morphology) or *H3K27ME3* loss of nuclear expression (potentially adverse prognosis) (Louis et al., 2021). It is now more than obvious, that translational/molecular neuroscience will soon play a key role in diagnosis but also estimation of prognosis and decision making for meningiomas.

CNS invasion has been associated with *AKT1* mutations as well as alterations of metalloproteases and adhesion molecule expression (Jalali et al., 2015; Barresi et al., 2021; Qin et al., 2021). The pathophysiology of CNS invasion seems to undergo different stages (Quintero-Fabian et al., 2019; Maggio et al., 2021; Furtak et al., 2023; Go and Kim, 2023). The crucial point for the initiation of meningioma cells invasion is the cleavage of the basement membrane and the following remodeling of the extracellular matrix (ECM) by specific matrix metalloproteinases (*MMPs*) (Quintero-Fabian et al., 2019; Maggio et al., 2021; Furtak et al., 2023; Go and Kim, 2023). Several activators of *MMPs*, like *uPA* have been linked to plasmin mediated matrix breakdown and cell adhesion (Fleetwood et al., 2014). Kandenwein et al. reported increased levels of plasminogen activator inhibitor-1 *(PAI-1)* in patients with brain invasive meningiomas (Kandenwein et al., 2011). *PAI-1* expression has been identified as a significant prognostic factor (Kandenwein et al., 2011). In a further step, the migration of meningioma cells within the loose environment of the degraded ECM is promoted by adhesion agents, like integrins (Wilisch-Neumann et al., 2013). Finally, well known growth factors, like *EGFR, VEGFR* or *HGF* contribute to neoangiogenesis and growth of the tumor cells (Fleetwood et al., 2014; Go and Kim, 2023). In this regard, Pei et al. reported lower expression of canstatin, an angiogenesis inhibitor, in WHO grade 3 brain invasive meningiomas (Pei et al., 2023). Several other pathways have also been implicated in the biology of meningioma invasion, i.e., *P13K/AKT, FAK, MAPK* and *Hippo* signaling (von Spreckelsen et al., 2022). Alterations in *TERT, BAP1* and *DMD* have been associated with higher histological grade and poorer prognosis (Shankar et al., 2017; Juratli et al., 2018; Samal et al., 2020; Williams et al., 2020; Pellerino et al., 2022).

Roehrkasse et al. (2022) have reported data supporting the concept that the analysis of the molecular background of meningiomas may hold superior prognostic power when compared to histological features. Nassiri et al. (2021) described four consensus molecular meningioma groups with distinct tumour behaviour. Comprehensive molecular profiling of meningiomas should probably include DNA methylation pattern and copy number aberration analyses,

investigating mRNA abundance, as well as driver mutations of oncogenes, such as *BAP1, CDKN2A/B*, and the *TERT* promoter (Louis et al., 2021; Nassiri et al., 2021; Roehrkasse et al., 2022). Maas et al. reviewed DNA methylation and copy number aberrations in 3031 meningiomas, and studied mutation data of 858 meningiomas. They merged the molecular and histological data into an integrated molecular-morphological classification score, which predicted more accurately the risk of recurrence than the WHO histological grading alone (Maas et al., 2021).

In summary, these latter studies may indicate that future meningioma grading schemes will increasingly rely on molecular parameters. Nevertheless, the overall number of cases investigated and published is not very large, molecular profiling strategies are complex and time consuming, and vary between investigators. Confirmatory studies are largely lacking. Finally, the quality of the clinic data used for correlations with molecular findings so far is limited, which somewhat precludes drawing robust clinical conclusions already at this point in time.

Imaging of CNS invasion

Predicting the grade of meningiomas and brain invasion preoperatively may be advantageous for surgical planning. Basic MR imaging may already help with the identification of brain invasion before the surgery. A higher volume of peritumoral edema as well as heterogeneity regarding tumor morphology and contrast enhancement may suggest an increased risk of brain invasion (Adeli et al., 2018; Joo et al., 2021; Ong et al., 2021). Hyperostosis and bony destruction have been associated with aggressive biological behaviour by some authors (Hanft et al., 2010). The aforementioned signs serve only as 'warning signs', though, and are definitely not robust enough to allow for a reliable preoperative diagnosis (Figures 2, 3). Recently, Luo et al. reviewed preoperative MRIs from 543 patients with meningioma WHO grade 1 and 123 with WHO grade 2 including 67 BIOBM and concluded that the imaging features of BIOBM are more similar to WHO grade 2 than 1 (Luo et al., 2023).

Noteworthy, brain invasion as well as meningioma grade may be better predicted prior to surgery by modern high-dimensional quantitative imaging analysis, the so-called radiomics (Zhang et al., 2020; Ugga et al., 2022). Radiomics is increasingly attracting attention in medical oncology, since radiomics-derived nomograms may predict the diagnosis and biological behaviour of different tumours (Lambin et al., 2017). Peng et al. employed radiomics to obtain data from preoperative MRI and cCT studies of 215 patients with benign or high grade meningiomas and established a diagnostic nomogram model for predicting tumor grade based on features like tumor-brain interface, bone invasion and tumor location (Peng et al., 2021). Li et al. (2021) acquired traditional semantic features like tumour volume, location or peritumoral edema as well as radiomic features from the tumour and from the tumour-to-brain interface in a series of 284 meningioma (173 with, 111 without brain invasion), and constructed an integrated nomogram to predict brain invasion. Similarly, Xiao et al. (2021) established a diagnostic nomogram for predicting brain invasion after obtaining radiomic features in 719 patients with meningiomas.

(Aggressive) surgery for brain invasive meningiomas?

Oncological benefit from aggressive meningioma surgery

Simpson identified already in 1957 an aggressive meningioma resection as a beneficial prognostic factor (Simpson, 1957). However, nowadays many neurosurgeons recommend more conservative surgeries under the premise that modern adjuvant therapies and imaging follow-up may compensate for incomplete resections. Although these arguments are valid, there is still a risk that patients may forego an oncological benefit that is easy to obtain. If we accept that recurrence rates of meningiomas do not differ significantly with the Simpson grade, resecting the tumor's dural attachment or bone infiltrations will no longer be rational. Leaving behind tumor tissue in a case with a benign growth may have no adverse midterm consequences, however this may be very different during long-term follow-up (Pettersson-Segerlind et al., 2011). Of note, clinical studies in patients with meningiomas commonly often report only limited follow up, i.e., less than 5 years.

E.g. Sughrue et al. questioned the relevance of Simpson grading of resection in modern neurosurgery, since he indeed found no significant difference in PFS between 373 patients following a Simpson Grade I, II, III, or IV resection for benign meningiomas. However, median follow up was only 3.7 years (Sughrue et al., 2010). A more recent and larger retrospective study on 1,571 patients with meningiomas WHO grade 1,2 or 3 concluded that Simpson grade IV resection was an unfavorable prognostic factor. PFS did not differ between patients with a Simpson grade I vs. grade II resection. Again, mean follow up was only 38 months (Behling et al., 2021). On the other hand, Brokinkel et al. studied 939 patients, who underwent surgery for meningioma of all WHO grades. Median follow-up was 37 months. They found a strong correlation between the Simpson grading and recurrence in general and importantly also between cases with a Simpson grades I vs. II resection. Dichotomizing extent of resection (e.g., gross total vs. subtotal resection) resulted in loss of predictive value (Brokinkel et al., 2021). We have retrospectively analysed 901 patients with meningiomas WHO grade 1 to 3. Median follow-up was 62 months. The estimated 10 years PFS was 91.8 and 81.2% after Simpson grade I and II resections, respectively (Gousias et al., 2016). Thus, coagulation instead of resection of the dural attachment more than doubled the recurrence rate at 10 years in our series. Some groups conducted retrospective cohort studies with a longer median follow up ranging from 85 to 123 months and found a prognostic relevance of the Simpson grades of resection, too (Alvernia et al., 2011; Hasseleid et al., 2012; Winther and Torp, 2017).

It should be noted, that the association between extent or resection (i.e., the Simpson grade) and recurrence seems to be much stronger in tumors with higher WHO grades. Simonetti et al. (2021) investigated 183 higher grade (i.e., WHO grades 2 and 3) meningiomas and found a 5-year survival rate of 95 and 67% after complete or partial resections, respectively. In our study we were able to analyze separately 172 patients with WHO ° 2 tumors. Estimated 10 years recurrence rates were 16% after a Simpson grade I and 50% after a Simpson grade II resection (Gousias et al., 2016). Masalha et al. analyzed retrospectively a cohort of 36 patients with anaplastic

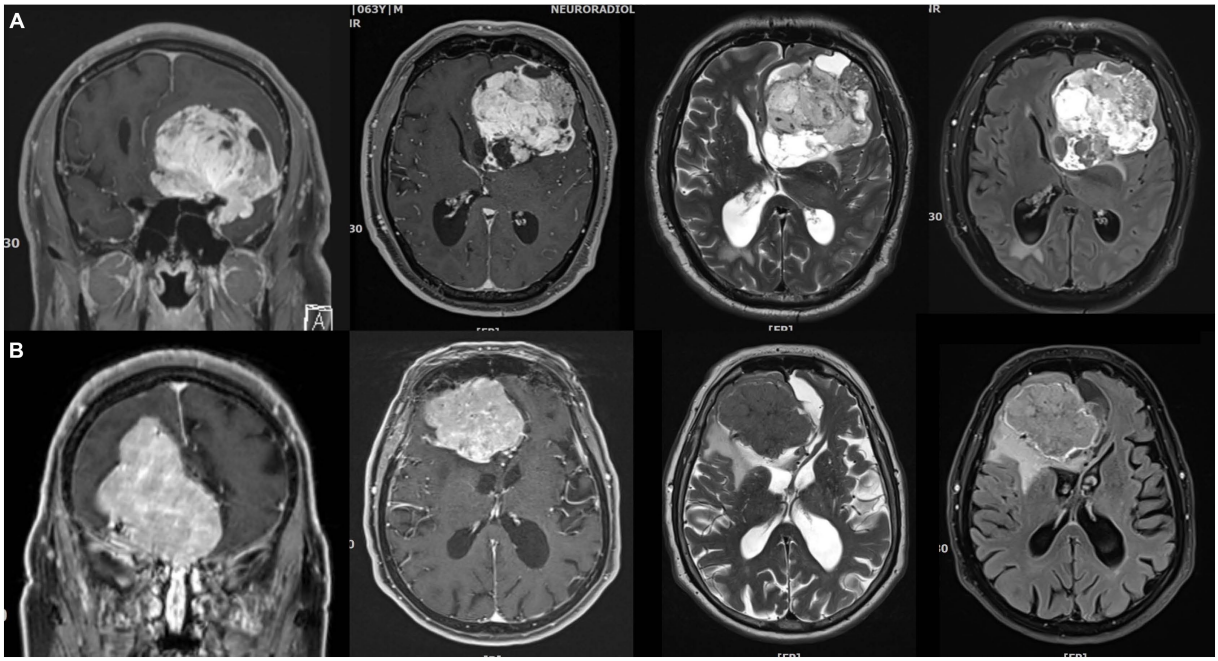

FIGURE 2
Imperfect correlations between imaging findings, histopathological atypia, and brain invasion (I). **(A)** 64 years old male patient with a very large left anterior clinoidal meningioma assigned to CNS grade 2 based on cytological atypia and an increased mitotic count. However, there was no brain invasion. Somewhat fittingly, MR imaging reveals cysts, a cleft sign and heterogenous contrast enhancement as well as FLAIR and T2 intratumoral heterogeneity, but there was only limited peritumoral edema. **(B)** 82 years old female patient with a large right>left olfactory groove meningioma CNS grade 2. The neuropathological evaluation revealed no atypia, but prominent brain invasion. There is surprisingly little edema. Contrast enhancement is somewhat heterogenous, but the tumor looks rather homogenous on the T2 and FLAIR weighted images.

WHO ° 3 meningiomas. A complete resection was associated with significantly longer PFS and OS (Masalha et al., 2019). Depei et al. retrieved data for 530 patients from the Surveillance Epidemiology and End Results database who had surgery between 2000 and 2015 and identified a prognostic relevance of a complete resection, in terms of longer PFS, for both cases with WHO ° 2 and 3 tumors (Li et al., 2019).

Since the Simpson grading of resection reflects the subjective intraoperative impression of the surgeon, external imaging-based validation is probably useful. Ueberschaer et al. (2021) validated prospectively the documented Simpson grading through postoperative MRI and 68Ga-DOTATATE/PET-CT and found in 40.5% of the cases unexpected tumour remnants. Along the same lines, Haslund-Vinding et al. (2022) proposed a new (the Copenhagen) grading system for the extent of resection of meningiomas based on a postoperative 68Ga-DOTATOC PET/MRI.

The Simpson grading may not properly account for tumor location (Voss et al., 2017). Schwartz and McDermott have recently reviewed the role of the Simpson grading and suggested to 'abandon the scale of Simpson grading of resection but preserve the message' (Schwartz and McDermott, 2020).

Quality of life and functional outcome after aggressive surgery

Although meningiomas do not always cause neurological deficits or other symptoms, patients with meningiomas demonstrate significant impaired quality of life compared to normative healthy controls even before surgery (van Nieuwenhuizen et al., 2013; Haider et al., 2021). This may be partially attributed to disease-related stress, when a patient realizes that he or she has got a brain tumour, or to preoperative anxiety (Wagner et al., 2019; Haider et al., 2021). Jakola et al. (2012) prospectively evaluated a cohort of 54 patients with meningiomas and found an improvement of the cases' health related quality of life (HRQOL) after surgery, which was mainly due to relief from anxiety. Miao et al. (2010) reported an improvement of the HRQOL score after treatment, which was nevertheless still worse than the baseline score of healthy controls in a larger cohort of 147 meningiomas. Neurocognitive scores tend to worsen after treatment (Constanthin et al., 2021). A large prospective cross-sectional study of 291 patients with meningiomas WHO ° 1 found a 'clinically meaningful' impairment in cognitive functioning after surgery (Nassiri et al., 2019). Sekely et al. reported neurocognitive impairments in 68% of 61 patients treated for a meningioma (surgery, radiation or both). 48% of the patients faced difficulties returning to work (Sekely et al., 2022). Unfortunately, the aforementioned studies have not specifically investigated the potential impact of the degree of resection or brain invasion upon HRQOL.

Methods of assessing of quality of life and neurocognition may differ between researchers and some degree of standardization is probably warranted (Gondar et al., 2021). Functional outcome are easier to study, e.g., in terms of new neurological deficits or performance status scales such as the Karnofsky index. Skull base location, larger tumour volume, but also invasive growth have been associated with and increased risk for postoperative deficits

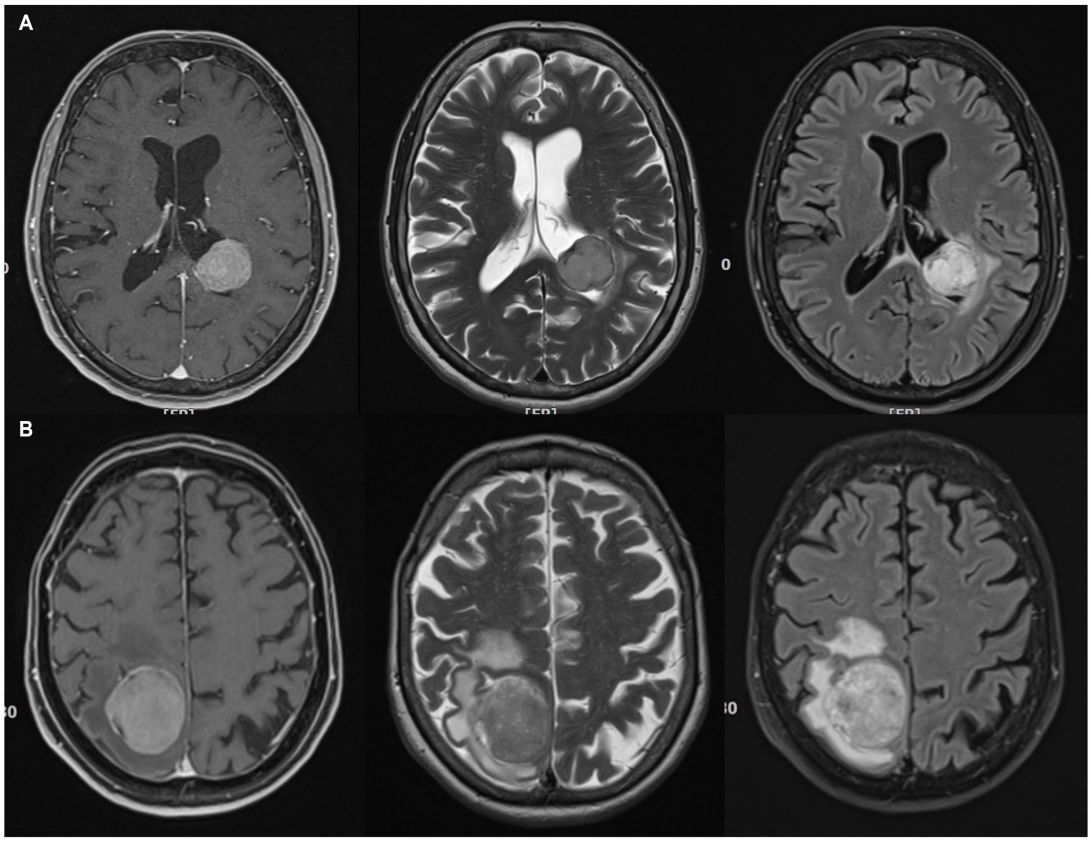

FIGURE 3
Imperfect correlations between imaging findings, histopathological atypia, and brain invasion (II). **(A)** 74 years old female patient with a left ventricular (trigonal) CNS grade 2 meningioma. This tumor had atypical histopathological features and was found to invade the brain. Possibly in contrast, the MR showed little edema. However, the actual zone of contact between the tumor and the brain parenchyma is very small. T2, FLAIR and contrast-enhanced T1 imaging reveals little heterogeneity. **(B)** 64 years old female patient right parietal parasagittal meningioma CNS grade 2. There was no brain invasion, however, histopathological atypia. Note, that there is substantial edema, while the tumor tissue looks otherwise inconspicuous on T2, FLAIR and contrast-enhanced T1 weighted MR images.

(Ehresman et al., 2019; Maschke et al., 2019; Przybylowski et al., 2020; Haider et al., 2021; Starnoni et al., 2021). The role of the degree of resection has been controversially discussed. Ehresman et al. report a Simpson grade IV rather than complete resection as a predictor of postoperative deficits in a series of 761 patients with meningioma (Ehresman et al., 2019). We similarly found a correlation between adverse Karnofsky outcomes and increasing Simpson grade (Gousias et al., 2016). It is likely that these findings largely reflect incomplete surgeries for more difficult to resect tumours. Along those lines, Schneider et al. described an increased risk for postoperative neurological deficits in patients undergoing radical resections in anterior and posterior skull fossa (Schneider et al., 2019, 2021). However, it is probably also fair to state that more aggressive surgery is not necessarily and always associated with worse functional outcomes (Gousias et al., 2016).

Surgery of meningiomas with CNS invasion

Only a small proportion of invasive meningiomas are characterized as BIOBM, while the vast majority of tumors with CNS invasion demonstrate additional features of malignancy, like atypia, necrosis and high proliferative capacity (Perry, 2021). As detailed above only few studies investigate specifically BIOBM, and these papers focus on the prognostic value of CNS invasion rather than surgical issues. In lieu of better data, surgical management strategies for these tumors and invasive meningiomas in general should therefore probably reflect the concept of maximal safe resection as well as the relatively strong correlation between extent of resection and recurrence in higher grade meningiomas.

The surgical management of brain invasive meningiomas may pose specific challenges. E.g. Brokinkel et al. (2018) have reported an increased risk of postoperative hemorrhage after surgery for brain invasive meningiomas. However, resection of an infiltrative brain tumor is nothing new for neurosurgeons. The experience gained during glioma surgery could be applied also to surgical cases with brain invasive meningiomas, even if the patterns of invasion are not comparable. Most cases of BIOBM or atypical meningiomas demonstrate slight invasion of pia and superficial cortex, whereas excessive brain parenchyma invasion may be apparent in malignant meningiomas (Perry et al., 1999).

The use of IONM has been reported by several authors. Paldor et al. reviewed forty cases with meningiomas in eloquent areas, mainly adjacent to the sulcus centralis and concluded that IONM

may guide the surgical technique and extent of resection in favor of a better postoperative functional outcome (Paldor et al., 2022). Policicchio et al. managed infiltrative lesions of the sulcus centralis, among others also anaplastic meningioma, by IONM but also 3D Ultrasound to identify the tumor-tissue interface. Awake craniotomies may also be helpful. Kumar et al. found awake surgery useful for resections of supratentorial meningiomas during pregnancy (Kumar et al., 2020). Awake craniotomies for meningioma resection may not only maximize the safety of the resection but also result in earlier patient recovery, a reduced length of the hospital stay, ands well as costs (Bakhshi et al., 2021). Shinoura et al. routinely use awake surgery not only for meningiomas compressing cranial nerves (Shinoura et al., 2019) but also in cases with perilolandic tumors and describe a beneficial effect of this technique in terms of less postoperative deficits (Shinoura et al., 2013).

Chakravarthi et al. (2021) routinely incorporate 3D tractography during surgery of anterior skull base meningiomas. Tractography has been used not only in skull base meningiomas, but also in eloquently located meningiomas (Kumar et al., 2014; Zhao et al., 2015). Zhao et al. (2015) reported gross total resection of 11 meningiomas located in the atrium of the lateral ventricle. Surgical planning included tractography. Kumar et al. (2014) confirmed the relevance of tractography use in the surgery of eloquent cortical lesions, among others also in meningiomas.

A more precise intraoperative visualization of tumor margins may also maximize the resections of invasive meningiomas. Advanced optical imaging techniques such as confocal microscopy, optical coherence tomography, and Raman spectroscopy have been used for "optical biopsies," i.e., intraoperative identification of tumor tissue (Shin et al., 2019). Reichert et al. report an increased glycolytic activity of meningiomas as a possible explanation for their extremely high autofluorescence capacities during a modern visualization technique, namely the flavin mononucleotide fluorescence (Reichert et al., 2023). Charalampaki et al. have recently described confocal laser endomicroscopy which combined with multispectral fluorescence microscopy as a novel technique for intraoperative tumor visualization. The authors report that their technique allows for the depiction of the cellular architecture of tumor margins with 400–1,000 fold magnification (Charalampaki et al., 2019). The ability of confocal microscopy in general to identify brain invasion of aggressive meningiomas has been reported in a mouse model (Peyre et al., 2013). Raman spectroscopy has been used for intraoperative differentiation between meningioma and healthy dura mater (Jelke et al., 2021). Fluorescence-guided microsurgery may also prove helpful when dealing with brain invasive meningiomas (Linsler et al., 2019; Jelke et al., 2021; Chotai and Schwartz, 2022). In order to further assess the benefit of 5-ALA fluorescence-guided meningioma surgery, the NXDC-MEN-301 phase 3 open-label single arm study is currently being conducted in 16 centers of USA, Germany and Austria (Stummer et al., 2022).

Conclusion

For this paper we have reviewed the more recent literature on meningiomas with histological CNS invasion. From a prognostic point of view brain invasive tumors with additional histological feature of atypia or malignancy are atypical or malignant meningiomas. The prognostic impact of brain invasion as a stand-alone criterion for the diagnosis of an aggressive tumor, however, is not clear. More investigations including larger cohorts of BIOBM will be key for answering this question. The histological analysis of CNS invasion remains the diagnostic gold standard, and more uniform and robust criteria as well as surgical sampling protocols are warranted especially in cases in which only a questionable local brain invasion is suspected (Perry, 2021). It is however not impossible that advanced neuroimaging and high-dimensional image analysis such as radiomics will eventually predict CNS invasion preoperatively (Li et al., 2021; Xiao et al., 2021). Specific molecular markers and correlates for brain invasion are lacking while on the other hand there is considerable progress toward a molecular tumor grading of meningiomas in general.

In lieu of better evidence surgical management of brain invasive meningiomas should follow the principles of a safe, but maximal resection. The extent of resection remains a major predictor of tumor recurrence, and this relation is much stronger in higher grade when compared to benign meningiomas (and by inference therefore quite likely also in brain invasive meningiomas). More conservative surgical attitudes may even be questionable in cases with completely benign tumors since most pertinent studies suffer from limited follow-up, while some nevertheless still provide evidence in favor of radical resections.

Technical adjuncts and techniques which are routinely used in glioma surgery such as intraoperative monitoring, awake craniotomy, DTI tractography, fluorescence-guided microsurgery and ultrasound may help to increase the safety of meningioma surgeries in general and of operations for brain invasive tumors in particular.

Author contributions

KG: conceptualization. KG and MS: methodology, writing—review and editing, and supervision. KG, LT, and MS: data curation and writing—original draft preparation. All authors have read and agreed to the published version of the manuscript and agreed to be accountable for the content of the work.

Conflict of interest

The authors declare that the research was conducted in the absence of any commercial or financial relationships that could be construed as a potential conflict of interest.

Publisher's note

References

Adeli, A., Hess, K., Mawrin, C., Streckert, E. M. S., Stummer, W., Paulus, W., et al. (2018). Prediction of brain invasion in patients with meningiomas using preoperative magnetic resonance imaging. *Oncotarget* 9, 35974–35982. doi: 10.18632/oncotarget.26313

Alvernia, J. E., Dang, N. D., and Sindou, M. P. (2011). Convexity meningiomas: study of recurrence factors with special emphasis on the cleavage plane in a series of 100 consecutive patients. *J. Neurosurg.* 115, 491–498. doi: 10.3171/2011.4.JNS101922

Bailey, D. D., Montgomery, E. Y., and Garzon-Muvdi, T. (2023). Metastatic high-grade meningioma: a case report and review of risk factors for metastasis. *Neurooncol. Adv.* 5:vdad014. doi: 10.1093/noajnl/vdad014

Bakhshi, S. K., Jawed, N., Shafiq, F., and Enam, S. A. (2021). Awake craniotomy for resection of intracranial meningioma: first case series from a low-and middle-income country. *Cureus* 13:e18716. doi: 10.7759/cureus.18716

Banan, R., Abbetmeier-Basse, M., Hong, B., Dumitru, C. A., Sahm, F., Nakamura, M., et al. (2021). The prognostic significance of clinicopathological features in meningiomas: microscopic brain invasion can predict patient outcome in otherwise benign meningiomas. *Neuropathol. Appl. Neurobiol.* 47, 724–735. doi: 10.1111/nan.12700

Barresi, V., Simbolo, M., Fioravanzo, A., Piredda, M. L., Caffo, M., Ghimenton, C., et al. (2021). Molecular profiling of 22 primary atypical meningiomas shows the prognostic significance of 18q heterozygous loss and CDKN2A/B homozygous deletion on recurrence-free survival. *Cancers (Basel)* 13:903. doi: 10.3390/cancers13040903

Baumgarten, P., Gessler, F., Schittenhelm, J., Skardelly, M., Tews, D. S., Senft, C., et al. (2016). Brain invasion in otherwise benign meningiomas does not predict tumor recurrence. *Acta Neuropathol.* 132, 479–481. doi: 10.1007/s00401-016-1598-1

Behling, F., Fodi, C., Hoffmann, E., Renovanz, M., Skardelly, M., Tabatabai, G., et al. (2021). The role of Simpson grading in meningiomas after integration of the updated WHO classification and adjuvant radiotherapy. *Neurosurg. Rev.* 44, 2329–2336. doi: 10.1007/s10143-020-01428-7

Behling, F., Fodi, C., Wang, S., Hempel, J. M., Hoffmann, E., Tabatabai, G., et al. (2021). Increased proliferation is associated with CNS invasion in meningiomas. *J. Neuro Oncol.* 155, 247–254. doi: 10.1007/s11060-021-03892-7

Biczok, A., Jungk, C., Egensperger, R., von Deimling, A., Suchorska, B., Tonn, J. C., et al. (2019). Microscopic brain invasion in meningiomas previously classified as WHO grade I is not associated with patient outcome. *J. Neuro Oncol.* 145, 469–477. doi: 10.1007/s11060-019-03312-x

Brokinkel, B., Sicking, J., Spille, D. C., Hess, K., Paulus, W., and Stummer, W. (2018). Letter to the editor. Brain invasion and the risk for postoperative hemorrhage and neurological deterioration after meningioma surgery. *J. Neurosurg.* 129, 849–851. doi: 10.3171/2018.5.JNS181287

Brokinkel, B., Spille, D. C., Brokinkel, C., Hess, K., Paulus, W., Bormann, E., et al. (2021). The Simpson grading: defining the optimal threshold for gross total resection in meningioma surgery. *Neurosurg. Rev.* 44, 1713–1720. doi: 10.1007/s10143-020-01369-1

Carr, C. M., Benson, J. C., DeLone, D. R., Diehn, F. E., Kim, D. K., Merrell, K. W., et al. (2021). Intracranial long-term complications of radiation therapy: an image-based review. *Neuroradiology* 63, 471–482. doi: 10.1007/s00234-020-02621-7

Chakravarthi, S. S., Fukui, M. B., Monroy-Sosa, A., Gonen, L., Epping, A., Jennings, J. E., et al. (2021). The role of 3D tractography in skull base surgery: technological advances, feasibility, and early clinical assessment with anterior skull base meningiomas. *J. Neurol. Surg. B Skull Base* 82, 576–592. doi: 10.1055/s-0040-1713775

Charalampaki, P., Nakamura, M., Athanasopoulos, D., and Heimann, A. (2019). Confocal-assisted multispectral fluorescent microscopy for brain tumor surgery. *Front. Oncol.* 9:583. doi: 10.3389/fonc.2019.00583

Chotai, S., and Schwartz, T. H. (2022). The Simpson grading: is it still valid? *Cancers (Basel)* 14:2007. doi: 10.3390/cancers14082007

Constanthin, P. E., Gondar, R., Fellrath, J., Wyttenbach, I. M., Tizi, K., Weman, L., et al. (2021). Neuropsychological outcomes after surgery for olfactory groove meningiomas. *Cancers (Basel)* 13:2520. doi: 10.3390/cancers13112520

Dalle Ore, C. L., Magill, S. T., Yen, A. J., Shahin, M. N., Lee, D. S., Lucas, C. G., et al. (2019). Meningioma metastases: incidence and proposed screening paradigm. *J. Neurosurg.* 132, 1447–1455. doi: 10.3171/2019.1.JNS181771

Ehresman, J. S., Garzon-Muvdi, T., Rogers, D., Lim, M., Gallia, G. L., Weingart, J., et al. (2019). Risk of developing postoperative deficits based on tumor location after surgical resection of an intracranial meningioma. *J Neurol Surg B Skull Base* 80, 59–66. doi: 10.1055/s-0038-1667066

Fleetwood, A. J., Achuthan, A., Schultz, H., Nansen, A., Almholt, K., Usher, P., et al. (2014). Urokinase plasminogen activator is a central regulator of macrophage three-dimensional invasion, matrix degradation, and adhesion. *J. Immunol.* 192, 3540–3547. doi: 10.4049/jimmunol.1302864

Furtak, J., Birski, M., Bebyn, M., Sledzinska, P., Krajewski, S., Szylberg, T., et al. (2023). Uncovering the molecular landscape of meningiomas and the impact of perioperative steroids on patient survival. *Acta Neurochir.* doi: 10.1007/s00701-023-05567-w [Epub ahead of print]

Garcia-Segura, M. E., Erickson, A. W., Jairath, R., Munoz, D. G., and Das, S. (2020). Necrosis and brain invasion predict radio-resistance and tumor recurrence in atypical meningioma: a retrospective cohort study. *Neurosurgery* 88, E42–E48. doi: 10.1093/neuros/nyaa348

Go, K. O., and Kim, Y. Z. (2023). Brain invasion and trends in molecular research on meningioma. *Brain Tumor Res. Treat.* 11, 47–58. doi: 10.14791/btrt.2022.0044

Goldbrunner, R., Stavrinou, P., Jenkinson, M. D., Sahm, F., Mawrin, C., Weber, D. C., et al. (2021). EANO guideline on the diagnosis and management of meningiomas. *Neuro Oncol.* 23, 1821–1834. doi: 10.1093/neuonc/noab150

Gondar, R., Patet, G., Schaller, K., and Meling, T. R. (2021). Meningiomas and cognitive impairment after treatment: a systematic and narrative review. *Cancers (Basel)* 13:1846. doi: 10.3390/cancers13081846

Goto, Y., Yamada, S., Yamada, S. M., Nakaguchi, H., Hoya, K., Murakami, M., et al. (2014). Radiation-induced meningiomas in multiple regions, showing rapid recurrence and a high MIB 1 labeling index: a case report and review of the literature. *World J. Surg. Oncol.* 12:123. doi: 10.1186/1477-7819-12-123

Gousias, K., Schramm, J., and Simon, M. (2016). The Simpson grading revisited: aggressive surgery and its place in modern meningioma management. *J. Neurosurg.* 125, 551–560. doi: 10.3171/2015.9.JNS15754

Haider, S., Taphoorn, M. J. B., Drummond, K. J., and Walbert, T. (2021). Health-related quality of life in meningioma. *Neurooncol. Adv.* 3:vdab089. doi: 10.1093/noajnl/vdab089

Hanft, S., Canoll, P., and Bruce, J. N. (2010). A review of malignant meningiomas: diagnosis, characteristics, and treatment. *J. Neuro-Oncol.* 99, 433–443. doi: 10.1007/s11060-010-0348-9

Haslund-Vinding, J., Skjoth-Rasmussen, J., Poulsgaard, L., Fugleholm, K., Mirian, C., Maier, A. D., et al. (2022). Proposal of a new grading system for meningioma resection: the Copenhagen Protocol. *Acta Neurochir.* 164, 229–238. doi: 10.1007/s00701-021-05025-5

Hasseleid, B. F., Meling, T. R., Ronning, P., Scheie, D., and Helseth, E. (2012). Surgery for convexity meningioma: Simpson grade I resection as the goal: clinical article. *J. Neurosurg.* 117, 999–1006. doi: 10.3171/2012.9.JNS12294

Jakola, A. S., Gulati, M., Gulati, S., and Solheim, O. (2012). The influence of surgery on quality of life in patients with intracranial meningiomas: a prospective study. *J. Neurooncol.* 110, 137–144. doi: 10.1007/s11060-012-0947-8

Jalali, S., Singh, S., Agnihotri, S., Wataya, T., Salehi, F., Alkins, R., et al. (2015). A role for matrix remodelling proteins in invasive and malignant meningiomas. *Neuropathol. Appl. Neurobiol.* 41, e16–e28. doi: 10.1111/nan.12166

Jelke, F., Mirizzi, G., Borgmann, F. K., Husch, A., Slimani, R., Klamminger, G. G., et al. (2021). Intraoperative discrimination of native meningioma and dura mater by Raman spectroscopy. *Sci. Rep.* 11:23583. doi: 10.1038/s41598-021-02977-7

Jenkinson, M. D., Santarius, T., Zadeh, G., and Aldape, K. D. (2017). Atypical meningioma-is it time to standardize surgical sampling techniques? *Neuro Oncol.* 19, 453–454. doi: 10.1093/neuonc/now245

Joo, L., Park, J. E., Park, S. Y., Nam, S. J., Kim, Y. H., Kim, J. H., et al. (2021). Extensive peritumoral edema and brain-to-tumor interface MRI features enable prediction of brain invasion in meningioma: development and validation. *Neuro-Oncology* 23, 324–333. doi: 10.1093/neuonc/noaa190

Juratli, T. A., McCabe, D., Nayyar, N., Williams, E. A., Silverman, I. M., Tummala, S. S., et al. (2018). DMD genomic deletions characterize a subset of progressive/higher-grade meningiomas with poor outcome. *Acta Neuropathol.* 136, 779–792. doi: 10.1007/s00401-018-1899-7

Kandenwein, J. A., Park-Simon, T. W., Schramm, J., and Simon, M. (2011). uPA/PAI-1 expression and uPA promoter methylation in meningiomas. *J. Neurooncol.* 103, 533–539. doi: 10.1007/s11060-010-0411-6

Kessler, R. A., Garzon-Muvdi, T., Yang, W., Weingart, J., Olivi, A., Huang, J., et al. (2017). Metastatic atypical and anaplastic meningioma: a case series and review of the literature. *World Neurosurg.* 101, 47–56. doi: 10.1016/j.wneu.2017.01.070

Kim, M. S., Chun, S. W., Dho, Y. S., Seo, Y., Lee, J. H., Won, J. K., et al. (2022). Histopathological predictors of progression-free survival in atypical meningioma: a single-center retrospective cohort and meta-analysis. *Brain Tumor Pathol.* 39, 99–110. doi: 10.1007/s10014-021-00419-w

Kumar, A., Chandra, P. S., Sharma, B. S., Garg, A., Rath, G. K., Bithal, P. K., et al. (2014). The role of neuronavigation-guided functional MRI and diffusion tensor tractography along with cortical stimulation in patients with eloquent cortex lesions. *Br. J. Neurosurg.* 28, 226–233. doi: 10.3109/02688697.2013.835370

Kumar, D., Siraj, S., Ahsan, K., and Shafiq, F. (2020). Utilization of awake craniotomy for supra-tentorial tumor resection during pregnancy: a technique useful for fetal-maternal wellbeing. *Pak. J. Med. Sci.* 36, 293–295. doi: 10.12669/pjms.36.2.1853

Lambin, P., Leijenaar, R. T. H., Deist, T. M., Peerlings, J., de Jong, E. E. C., van Timmeren, J., et al. (2017). Radiomics: the bridge between medical imaging and personalized medicine. *Nat. Rev. Clin. Oncol.* 14, 749–762. doi: 10.1038/nrclinonc.2017.141

Li, D., Jiang, P., Xu, S., Li, C., Xi, S., Zhang, J., et al. (2019). Survival impacts of extent of resection and adjuvant radiotherapy for the modern management of high-grade meningiomas. *J. Neuro-Oncol.* 145, 125–134. doi: 10.1007/s11060-019-03278-w

Li, N., Mo, Y., Huang, C., Han, K., He, M., Wang, X., et al. (2021). A clinical semantic and Radiomics nomogram for predicting brain invasion in WHO grade II meningioma based on tumor and tumor-to-brain Interface features. *Front. Oncol.* 11:752158. doi: 10.3389/fonc.2021.752158

Linsler, S., Ketter, R., Oertel, J., and Urbschat, S. (2019). Fluorescence imaging of meningioma cells with somatostatin receptor ligands: an in vitro study. *Acta Neurochir.* 161, 1017–1024. doi: 10.1007/s00701-019-03872-x

Louis, D. N., Perry, A., Wesseling, P., Brat, D. J., Cree, I. A., Figarella-Branger, D., et al. (2021). The 2021 WHO classification of tumors of the central nervous system: a summary. *Neuro Oncol.* 23, 1231–1251. doi: 10.1093/neuonc/noab106

Luo, X., Jiang, H., Liu, X. J., Zhang, Z., Deng, K., Lin, F., et al. (2023). Base MRI imaging characteristics of meningioma patients to discuss the WHO classification of brain invasion otherwise benign meningiomas. *Technol. Cancer Res. Treat.* 22. doi: 10.1177/15330338231171470

Maas, S. L. N., Stichel, D., Hielscher, T., Sievers, P., Berghoff, A. S., Schrimpf, D., et al. (2021). Integrated molecular-morphologic meningioma classification: a multicenter retrospective analysis, retrospectively and prospectively validated. *J. Clin. Oncol.* 39, 3839–3852. doi: 10.1200/JCO.21.00784

Maggio, I., Franceschi, E., di Nunno, V., Gatto, L., Tosoni, A., Angelini, D., et al. (2021). Discovering the molecular landscape of meningioma: the struggle to find new therapeutic targets. *Diagnostics* 11:1852. doi: 10.3390/diagnostics11101852

Masalha, W., Heiland, D. H., Delev, D., Fennell, J. T., Franco, P., Scheiwe, C., et al. (2019). Survival and prognostic predictors of anaplastic meningiomas. *World Neurosurg.* 131, e321–e328. doi: 10.1016/j.wneu.2019.07.148

Maschke, S., Martinez-Moreno, M., Micko, A., Millesi, M., Minchev, G., Mallouhi, A., et al. (2019). Challenging the osseous component of sphenoorbital meningiomas. *Acta Neurochir.* 161, 2241–2251. doi: 10.1007/s00701-019-04015-y

Miao, Y., Lu, X., Qiu, Y., Jiang, J., and Lin, Y. (2010). A multivariate analysis of prognostic factors for health-related quality of life in patients with surgically managed meningioma. *J. Clin. Neurosci.* 17, 446–449. doi: 10.1016/j.jocn.2009.07.111

Nakasu, S., and Nakasu, Y. (2021). Prognostic significance of brain invasion in meningiomas: systematic review and meta-analysis. *Brain Tumor Pathol.* 38, 81–95. doi: 10.1007/s10014-020-00390-y

Nassiri, F., Liu, J., Patil, V., Mamatjan, Y., Wang, J. Z., Hugh-White, R., et al. (2021). A clinically applicable integrative molecular classification of meningiomas. *Nature* 597, 119–125. doi: 10.1038/s41586-021-03850-3

Nassiri, F., Price, B., Shehab, A., Au, K., Cusimano, M. D., Jenkinson, M. D., et al. (2019). Life after surgical resection of a meningioma: a prospective cross-sectional study evaluating health-related quality of life. *Neuro Oncol.* 21, i32–i43. doi: 10.1093/neuonc/noy152

Ong, T., Bharatha, A., Alsufayan, R., Das, S., and Lin, A. W. (2021). MRI predictors for brain invasion in meningiomas. *Neuroradiol. J.* 34, 3–7. doi: 10.1177/1971400920953417

Ostrom, Q. T., Cioffi, G., Waite, K., Kruchko, C., and Barnholtz-Sloan, J. S. (2021). CBTRUS statistical report: primary brain and other central nervous system tumors diagnosed in the United States in 2014–2018. *Neuro Oncol.* 23, iii1–iii105. doi: 10.1093/neuonc/noab200

Ostrom, Q. T., Price, M., Neff, C., Cioffi, G., Waite, K. A., Kruchko, C., et al. (2022). CBTRUS statistical report: primary brain and other central nervous system tumors diagnosed in the United States in 2015–2019. *Neuro-Oncology* 24, v1–v95. doi: 10.1093/neuonc/noac202

Page, M. J., McKenzie, J. E., Bossuyt, P. M., Boutron, I., Hoffmann, T. C., Mulrow, C. D., et al. (2021). Updating guidance for reporting systematic reviews: development of the PRISMA 2020 statement. *J. Clin. Epidemiol.* 134, 103–112. doi: 10.1016/j.jclinepi.2021.02.003

Paldor, I., Doron, O., Peso, D., Jubran, M., and Sviri, G. E. (2022). Intraoperative neuromonitoring during resection of cranial meningiomas and its effect on the surgical workflow. *Neurosurg. Rev.* 45, 1481–1490. doi: 10.1007/s10143-021-01667-2

Pei, J., Li, P., Gao, Y. H., Tian, B. G., Wang, D. Y., Zheng, Y., et al. (2023). Type IV collagen-derived angiogenesis inhibitor: canstatin low expressing in brain-invasive meningiomas using liquid chromatography-mass spectrometry (LC-MS/MS). *J. Neuro-Oncol.* 161, 415–423. doi: 10.1007/s11060-023-04256-z

Pellerino, A., Bruno, F., Palmiero, R., Pronello, E., Bertero, L., Soffietti, R., et al. (2022). Clinical significance of molecular alterations and systemic therapy for meningiomas: where do we stand? *Cancers* 14:2256. doi: 10.3390/cancers14092256

Peng, S., Cheng, Z., and Guo, Z. (2021). Diagnostic nomogram model for predicting preoperative pathological grade of meningioma. *Transl. Cancer Res.* 10, 4057–4064. doi: 10.21037/tcr-21-798

Perry, A. (2021). The definition and role of brain invasion in meningioma grading: still controversial after all these years. *Free Neuropathol.* 2:8. doi: 10.17879/freeneuropathology-2021-3276

Perry, A., Scheithauer, B. W., Stafford, S. L., Lohse, C. M., and Wollan, P. C. (1999). "Malignancy" in meningiomas: a clinicopathologic study of 116 patients, with grading implications. *Cancer* 85, 2046–2056.

Perry, A., Stafford, S. L., Scheithauer, B. W., Suman, V. J., and Lohse, C. M. (1997). Meningioma grading: an analysis of histologic parameters. *Am. J. Surg. Pathol.* 21, 1455–1465. doi: 10.1097/00000478-199712000-00008

Pettersson-Segerlind, J., Orrego, A., Lonn, S., and Mathiesen, T. (2011). Long-term 25-year follow-up of surgically treated parasagittal meningiomas. *World Neurosurg.* 76, 564–571. doi: 10.1016/j.wneu.2011.05.015

Peyre, M., Clermont-Taranchon, E., Stemmer-Rachamimov, A., and Kalamarides, M. (2013). Miniaturized handheld confocal microscopy identifies focal brain invasion in a mouse model of aggressive meningioma. *Brain Pathol.* 23, 371–377. doi: 10.1111/bpa.12039

Picart, T., Dumot, C., Guyotat, J., Pavlov, V., Streichenberger, N., Vasiljevic, A., et al. (2022). Clinical and pathological impact of an optimal assessment of brain invasion for grade 2 meningioma diagnosis: lessons from a series of 291 cases. *Neurosurg. Rev.* 45, 2797–2809. doi: 10.1007/s10143-022-01792-6

Przybylowski, C. J., Hendricks, B. K., Frisoli, F. A., Zhao, X., Cavallo, C., Borba Moreira, L., et al. (2020). Prognostic value of the Simpson grading scale in modern meningioma surgery: barrow neurological institute experience. *J. Neurosurg.* 1-9, 1–9. doi: 10.3171/2020.6.JNS20374

Qin, C., Huang, M., Pan, Y., Li, Y., Long, W., and Liu, Q. (2021). Brain-invasive meningiomas: molecular mechanisms and potential therapeutic options. *Brain Tumor Pathol.* 38, 156–172. doi: 10.1007/s10014-021-00399-x

Quintero-Fabian, S., Arreola, R., Becerril-Villanueva, E., Torres-Romero, J. C., Arana-Argaez, V., Lara-Riegos, J., et al. (2019). Role of matrix metalloproteinases in angiogenesis and cancer. *Front. Oncol.* 9:1370. doi: 10.3389/fonc.2019.01370

Reichert, D., Wadiura, L. I., Erkkilae, M. T., Gesperger, J., Lang, A., Roetzer-Pejrimovsky, T., et al. (2023). Flavin fluorescence lifetime and autofluorescence optical redox ratio for improved visualization and classification of brain tumors. *Front. Oncol.* 13:1105648. doi: 10.3389/fonc.2023.1105648

Roehrkasse, A. M., Peterson, J. E. G., Fung, K. M., Pelargos, P. E., and Dunn, I. F. (2022). The discrepancy between standard histologic WHO grading of meningioma and molecular profile: a single institution series. *Front. Oncol.* 12:846232. doi: 10.3389/fonc.2022.846232

Samal, S., Patnaik, A., Sahu, F., and Purkait, S. (2020). Altered expression of epigenetic modifiers EZH2, H3K27me3, and DNA methyltransferases in meningiomas – prognostic biomarkers for routine practice. *Folia Neuropathol.* 58, 133–142. doi: 10.5114/fn.2020.96970

Schneider, M., Schuss, P., Guresir, A., Borger, V., Vatter, H., and Guresir, E. (2021). Surgery for posterior fossa meningioma: elevated postoperative cranial nerve morbidity discards aggressive tumor resection policy. *Neurosurg. Rev.* 44, 953–959. doi: 10.1007/s10143-020-01275-6

Schneider, M., Schuss, P., Guresir, A., Wach, J., Hamed, M., Vatter, H., et al. (2019). Cranial nerve outcomes after surgery for frontal skull base meningiomas: the eternal quest of the maximum-safe resection with the lowest morbidity. *World Neurosurg.* 125, e790–e796. doi: 10.1016/j.wneu.2019.01.171

Schwartz, T. H., and McDermott, M. W. (2020). The Simpson grade: abandon the scale but preserve the message. *J. Neurosurg.* 1-8, 1–8. doi: 10.3171/2020.6.JNS201904

Sekely, A., Zakzanis, K. K., Mabbott, D., Tsang, D. S., Kongkham, P., Zadeh, G., et al. (2022). Long-term neurocognitive, psychological, and return to work outcomes in meningioma patients. *Support Care Cancer* 30, 3893–3902. doi: 10.1007/s00520-022-06838-5

Shankar, G. M., Abedalthagafi, M., Vaubel, R. A., Merrill, P. H., Nayyar, N., Gill, C. M., et al. (2017). Germline and somatic BAP1 mutations in high-grade rhabdoid meningiomas. *Neuro Oncol.* 19, 535–545. doi: 10.1093/neuonc/now235

Shin, K. S., Francis, A. T., Hill, A. H., Laohajaratsang, M., Cimino, P. J., Latimer, C. S., et al. (2019). Intraoperative assessment of skull base tumors using stimulated Raman scattering microscopy. *Sci. Rep.* 9:20392. doi: 10.1038/s41598-019-56932-8

Shinoura, N., Midorikawa, A., Hiromitsu, K., Saito, S., and Yamada, R. (2019). Preservation of cranial nerve function following awake surgery for benign brain tumors in 22 consecutive patients. *J. Clin. Neurosci.* 61, 189–195. doi: 10.1016/j.jocn.2018.10.037

Shinoura, N., Midorikawa, A., Yamada, R., Hana, T., Saito, A., Hiromitsu, K., et al. (2013). Awake craniotomy for brain lesions within and near the primary motor area: a retrospective analysis of factors associated with worsened paresis in 102 consecutive patients. *Surg. Neurol. Int.* 4:149. doi: 10.4103/2152-7806.122003

Simonetti, G., Silvani, A., Tramacere, I., Farinotti, M., Legnani, F., Pinzi, V., et al. (2021). Long term follow up in 183 high grade meningioma: a single institutional experience. *Clin. Neurol. Neurosurg.* 207:106808. doi: 10.1016/j.clineuro.2021.106808

Simpson, D. (1957). The recurrence of intracranial meningiomas after surgical treatment. *J. Neurol. Neurosurg. Psychiatry* 20, 22–39. doi: 10.1136/jnnp.20.1.22

Spille, D. C., Hess, K., Sauerland, C., Sanai, N., Stummer, W., Paulus, W., et al. (2016). Brain invasion in meningiomas: incidence and correlations with clinical variables and prognosis. *World Neurosurg.* 93, 346–354. doi: 10.1016/j.wneu.2016.06.055

Starnoni, D., Tuleasca, C., Giammattei, L., Cossu, G., Bruneau, M., Berhouma, M., et al. (2021). Surgical management of anterior clinoidal meningiomas: consensus statement on behalf of the EANS skull base section. *Acta Neurochir.* 163, 3387–3400. doi: 10.1007/s00701-021-04964-3

Stummer, W., Holling, M., Bendok, B. R., Vogelbaum, M. A., Cox, A., Renfrow, S. L., et al. (2022). The NXDC-MEN-301 study on 5-ALA for meningiomas surgery: an innovative study design for the assessing the benefit of intra-operative fluorescence imaging. *Brain Sci.* 12:1044. doi: 10.3390/brainsci12081044

Sughrue, M. E., Kane, A. J., Shangari, G., Rutkowski, M. J., McDermott, M. W., Berger, M. S., et al. (2010). The relevance of Simpson Grade I and II resection in modern neurosurgical treatment of World Health Organization Grade I meningiomas. *J. Neurosurg.* 113, 1029–1035. doi: 10.3171/2010.3.JNS091971

Sun, C., Dou, Z., Wu, J., Jiang, B., Iranmanesh, Y., Yu, X., et al. (2020). The preferred locations of meningioma according to different biological characteristics based on voxel-wise analysis. *Front. Oncol.* 10:1412. doi: 10.3389/fonc.2020.01412

Timme, M., Thomas, C., Spille, D. C., Stummer, W., Ebel, H., Ewelt, C., et al. (2020). Brain invasion in meningiomas: does surgical sampling impact specimen characteristics and histology? *Neurosurg. Rev.* 43, 793–800. doi: 10.1007/s10143-019-01125-0

Traylor, J. I., Plitt, A. R., Hicks, W. H., Mian, T. M., Mickey, B. E., and Barnett, S. L. (2023). Evaluating risk of recurrence in patients with meningioma. *J. Neurosurg.* 138, 621–628. doi: 10.3171/2022.6.JNS221162

Ueberschaer, M., Vettermann, F. J., Forbrig, R., Unterrainer, M., Siller, S., Biczok, A. M., et al. (2021). Simpson grade revisited - intraoperative estimation of the extent of resection in meningiomas versus postoperative somatostatin receptor positron emission tomography/computed tomography and magnetic resonance imaging. *Neurosurgery* 88, 140–146. doi: 10.1093/neuros/nyaa333

Ugga, L., Spadarella, G., Pinto, L., Cuocolo, R., and Brunetti, A. (2022). Meningioma Radiomics: at the Nexus of imaging, pathology and biomolecular characterization. *Cancers (Basel).* 14:2605. doi: 10.3390/cancers14112605

van Nieuwenhuizen, D., Ambachtsheer, N., Heimans, J. J., Reijneveld, J. C., Peerdeman, S. M., and Klein, M. (2013). Neurocognitive functioning and health-related quality of life in patients with radiologically suspected meningiomas. *J. Neurooncol.* 113, 433–440. doi: 10.1007/s11060-013-1132-4

von Spreckelsen, N., Kesseler, C., Brokinkel, B., Goldbrunner, R., Perry, A., and Mawrin, C. (2022). Molecular neuropathology of brain-invasive meningiomas. *Brain Pathol.* 32:e13048. doi: 10.1111/bpa.13048

Voss, K. M., Spille, D. C., Sauerland, C., Suero Molina, E., Brokinkel, C., Paulus, W., et al. (2017). The Simpson grading in meningioma surgery: does the tumor location influence the prognostic value? *J. Neurooncol.* 133, 641–651. doi: 10.1007/s11060-017-2481-1

Wagner, A., Shiban, Y., Kammermeier, V., Joerger, A. K., Lange, N., Ringel, F., et al. (2019). Quality of life and emotional burden after transnasal and transcranial anterior skull base surgery. *Acta Neurochir.* 161, 2527–2537. doi: 10.1007/s00701-019-04062-5

Wilisch-Neumann, A., Kliese, N., Pachow, D., Schneider, T., Warnke, J. P., Braunsdorf, W. E., et al. (2013). The integrin inhibitor cilengitide affects meningioma cell motility and invasion. *Clin. Cancer Res.* 19, 5402–5412. doi: 10.1158/1078-0432.CCR-12-0299

Williams, E. A., Wakimoto, H., Shankar, G. M., Barker, F. G. 2nd, Brastianos, P. K., Santagata, S., et al. (2020). Frequent inactivating mutations of the PBAF complex gene PBRM1 in meningioma with papillary features. *Acta Neuropathol.* 140, 89–93. doi: 10.1007/s00401-020-02161-7

Winther, T. L., and Torp, S. H. (2017). Significance of the extent of resection in modern neurosurgical practice of World Health Organization grade I Meningiomas. *World Neurosurg.* 99, 104–110. doi: 10.1016/j.wneu.2016.11.034

Xiao, D., Zhao, Z., Liu, J., Wang, X., Fu, P., Le Grange, J. M., et al. (2021). Diagnosis of invasive meningioma based on brain-tumor Interface Radiomics features on brain MR images: a multicenter study. *Front. Oncol.* 11:708040. doi: 10.3389/fonc.2021.708040

Zhang, J., Yao, K., Liu, P., Liu, Z., Han, T., Zhao, Z., et al. (2020). A radiomics model for preoperative prediction of brain invasion in meningioma non-invasively based on MRI: a multicentre study. *EBioMedicine* 58:102933. doi: 10.1016/j.ebiom.2020.102933

Zhao, X., Shen, X., Chen, X., Zhang, J., Wang, X., Zhang, Y., et al. (2015). Integrated functional neuronavigation-guided resection of small meningiomas of the atrium via the paramedian parieto-occipital approach. *Clin. Neurol. Neurosurg.* 128, 47–52. doi: 10.1016/j.clineuro.2014.11.001

frontiers | Frontiers in Pharmacology

TYPE Original Research
PUBLISHED 19 July 2023
DOI 10.3389/fphar.2023.1162540

OPEN ACCESS

EDITED BY
Ye Cheng,
Capital Medical University, China

REVIEWED BY
Hongyu Chu,
Jilin University, China
Liang Zhang,
The First Affiliated Hospital of China Medical University, China
Sisi Wu,
China Three Gorges University, China

*CORRESPONDENCE
Hui Wu,
wuhui707@jlu.edu.cn

RECEIVED 09 February 2023
ACCEPTED 27 June 2023
PUBLISHED 19 July 2023

CITATION
Zhang A, Guo Z, Ren J-x, Chen H, Yang W, Zhou Y, Pan L, Chen Z, Ren F, Chen Y, Zhang M, Peng F, Chen W, Wang X, Zhang Z and Wu H (2023), Development of an MCL-1-related prognostic signature and inhibitors screening for glioblastoma. *Front. Pharmacol.* 14:1162540. doi: 10.3389/fphar.2023.1162540

Development of an MCL-1-related prognostic signature and inhibitors screening for glioblastoma

Ao Zhang[1], Zhen Guo[2], Jia-xin Ren[3], Hongyu Chen[4], Wenzhuo Yang[4], Yang Zhou[5], Lin Pan[5], Zhuopeng Chen[4], Fei Ren[5], Youqi Chen[5], Menghan Zhang[6], Fei Peng[7], Wanting Chen[5], Xinhui Wang[8], Zhiyun Zhang[9] and Hui Wu[10]*

[1]Department of Neurology, The First Hospital of Jilin University, Changchun, China, [2]Department of Cardiology, The First Affiliated Hospital of Sun Yat-sen University, Guangzhou, China, [3]Department of Neurology, Stroke Center, The First Hospital of Jilin University, Changchun, China, [4]Department of Neurosurgery, State Key Laboratory of Oncology in South China, Collaborative Innovation Center for Cancer Medicine, Sun Yat-sen University Cancer Center, Guangzhou, China, [5]Clinical College, Jilin University, Changchun, China, [6]Department of Clinical Laboratory, The Fifth Affiliated Hospital of Xinxiang Medical College, Xinxiang, China, [7]Department of Medicine, Division of Endocrinology, Diabetes and Metabolism, Baylor College of Medicine, Houston, TX, United States, [8]Department of Hematology, The First Clinical Medical School of Lanzhou University, Lanzhou, Gansu, China, [9]Department of Plastic Surgery, The First Hospital of Jilin University, Changchun, China, [10]Department of Ophthalmology, First Hospital of Jilin University, Changchun, China

Introduction: The effect of the conventional treatment methods of glioblastoma (GBM) is poor and the prognosis of patients is poor. The expression of MCL-1 in GBM is significantly increased, which shows a high application value in targeted therapy. In this study, we predicted the prognosis of glioblastoma patients, and therefore constructed MCL-1 related prognostic signature (MPS) and the development of MCL-1 small molecule inhibitors.

Methods: In this study, RNA-seq and clinical data of 168 GBM samples were obtained from the TCGA website, and immunological analysis, differential gene expression analysis and functional enrichment analysis were performed. Subsequently, MCL-1-associated prognostic signature (MPS) was constructed and validated by LASSO Cox analysis, and a nomogram was constructed to predict the prognosis of patients. Finally, the 17931 small molecules downloaded from the ZINC15 database were screened by LibDock, ADME, TOPKAT and CDOCKER modules and molecular dynamics simulation in Discovery Studio2019 software, and two safer and more effective small molecule inhibitors were finally selected.

Results: Immunological analysis showed immunosuppression in the MCL1_H group, and treatment with immune checkpoint inhibitors had a positive effect. Differential expression gene analysis identified 449 differentially expressed genes. Build and validate MPS using LASSO Cox analysis. Use the TSHR HIST3H2A, ARGE OSMR, ARHGEF25 build risk score, proved that low risk group of patients prognosis is better. Univariate and multivariate analysis proved that risk could be used as an independent predictor of patient prognosis. Construct a nomogram to predict the survival probability of patients at 1,2,3 years. Using a series of computer-aided techniques, two more reasonable lead compounds ZINC000013374322 and ZINC000001090002 were virtually selected. These compounds have potential inhibitory effects on MCL-1 and provide a basis for the design and further development of MCL-1 specific small molecule inhibitors.

Discussion: This study analyzed the effect of MCL-1 on the prognosis of glioblastoma patients from the perspective of immunology, constructed a new prognostic model to evaluate the survival rate of patients, and further screened 2 MCL-1 small molecule inhibitors, which provides new ideas for the treatment and prognosis of glioblastoma.

KEYWORDS

glioblastoma (GBM), MCL-1, nomogram, virtual screening, molecular docking

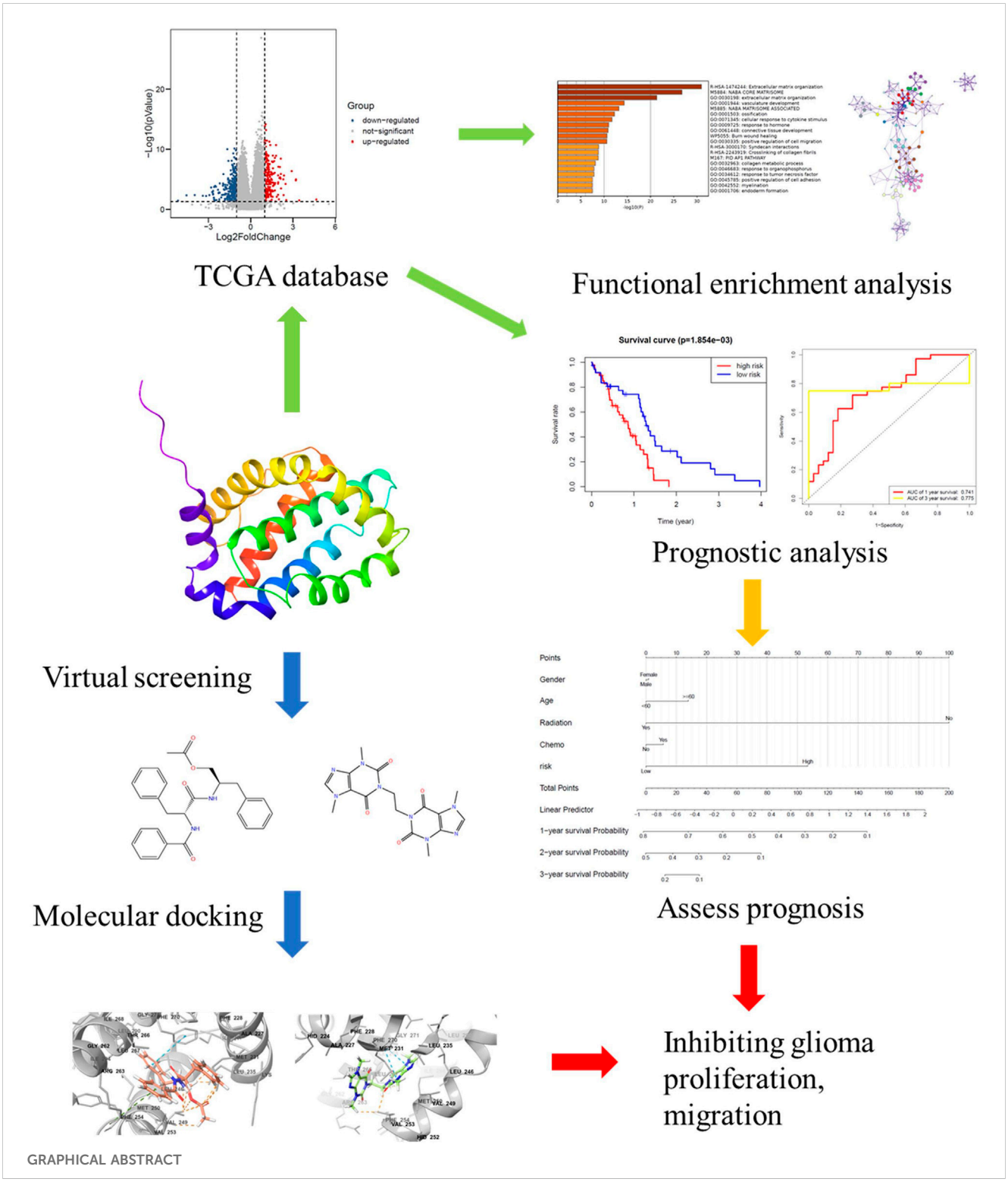

GRAPHICAL ABSTRACT

1 Introduction

Glioblastoma (GBM) is a brain tumor originating from glial progenitor cells and is the most common primary malignant tumor of the brain, accounting for 81% of malignant brain tumors (Ostrom et al., 2014; Xu et al., 2020; Li et al., 2023). Among them, glioblastoma has the highest and increasing incidence, but no curative treatment is available (Ostrom et al., 2019). The survival time of most patients is much lower than that of patients with other tumors, and the quality of life is very poor (Finch et al., 2021). At present, the conventional treatment methods for GBM include tumor resection, radiotherapy combined with temozolomide (TMZ) and targeted therapy with bevacizumab, etc., but these treatments have more or less obvious limitations (Allahyarzadeh Khiabani et al., 2023; Boongird et al., 2023; Hotchkiss et al., 2023; Jatyan et al., 2023; You et al., 2023). Therefore, how to predict the prognosis of GBM patients more accurately and intervene the factors affecting the prognosis, formulate more reasonable and effective treatment plans, and develop safer and more effective drugs are the key to treating glioblastoma patients.

Myeloid cell ischemia-1 (MCL-1), as a member of the B-cell lymphoma 2 (BCL-2) protein family, is one of the most frequently amplified genes in all human cancers including glioblastoma (Xiang et al., 2018). MCL-1 has three BH domains (BH1, BH2, and BH3), a C-terminal TM domain, and a large N-terminal region (Li S. et al., 2021). The four binding pockets (P1-P4) of MCL-1 interact with hydrophobic residues H1-H4 of only-BH3 protein, respectively, where the P2 and P3 pockets are the locations of "hot spot" residues for protein-protein interaction in MCL-1. This is different from anti-apoptotic proteins such as BCL2 (P4/P1 and P2) or BCL-XL (P2 and P4) and facilitates the design of specific MCL-1 inhibitors (Denis et al., 2020). Based on the structure of MCL-1, its role in apoptosis is promoting cell survival by interfering in the cascade of the events that cause trigger cell death and MOMP (Sancho et al., 2021). Numerous previous studies have demonstrated that MCL-1 is extremely important for glioblastoma, which can be used as a key target to inhibit the activity of glioblastoma cells. Downregulation of MCL-1 expression significantly induced apoptosis of tumor cells (Premkumar et al., 2013; Gratas et al., 2014; Jane et al., 2016; Juric et al., 2021). Therefore, there is great potential for the development of MCL-1 specific inhibitors for the treatment of glioblastoma, and it is crucial to create inhibitors that are both more efficient and less poisonous for the treatment of glioblastoma.

At present, the main strategies to design inhibitors against MCL-1 are based on the direct binding of BH3-mimetic to MCL-1, thereby releasing proapoptotic proteins and finally activating apoptosis (Li S. et al., 2021). Clinical studies for MCL-1 inhibitors have started for drugs such S64315, AZD5991, AMG 397, AMG 176, MIM1, etc. (Wei et al., 2020). These inhibitors have shown remarkable efficacy in the treatment of non-Hodgkin's lymphoma, multiple myeloma, acute myeloid leukemia, B-cell lymphoma, and other hematological malignancies (Wei et al., 2020; Liu et al., 2021). However, in the treatment of glioblastoma, most MCL-1 small molecule inhibitors are not applicable due to the existence of blood-brain barrier. Among them, MIM1, as an identified BH3-mimetic, has promising biological and biophysical properties such as low molecular weight, ideal solubility, and stability. MIM1 reduced the viability of glioblastoma cells in a dose and time-dependent manner (Respondek et al., 2018). However, for other types of glioblastoma, the role of MIM1 has not been investigated so far.

The aim of this study is to establish an MCL-1-based prognostic model and to screen safe and effective MCL-1 inhibitors. Firstly, the RNA-seq and clinical data of 168 glioblastoma samples were downloaded from the TCGA database. According to the expression level of MCL-1, the samples were divided into MCL-1_L and MCL-1_H groups, and the enrichment levels of 29 immune signals in the two groups were analyzed. Functional enrichment analysis of these differentially expressed genes was performed. The MCL-1-associated prognostic signature was then constructed using lasso cox regression analysis. Finally, a nomogram prediction model was established to estimate the survival rate of glioblastoma patients. In addition, two small molecule inhibitors of MCL-1 were screened by a series of computer-aided techniques. With the development of drug research, natural products are playing an increasingly important role in molecular biology and drug exploration, which provide structural patterns for target compounds of new drugs and are an important source of new drugs. MIM1 was used as a reference drug in this study. NP (natural products) database in the ZINC database was virtually screened to explore potential MCL-1 inhibitors. Secondly, the pharmacological and toxicological characteristics of the compounds were analyzed. Molecular docking was then performed to assess the interaction between the selected compounds and MCL-1. The pharmacophore of the compound was also predicted. Therefore, a more suitable small-molecule MCL-1 inhibitor is required for the treatment of glioblastoma. Natural products are becoming a more significant part of molecular biology and drug discovery as drug research progresses since they offer structural patterns for target molecules of new medications and are a significant source of such pharmaceuticals. In this study, MIM1 served as the reference medication. Virtual screening was done on the natural products database in the ZINC database to look for probable MCL-1 inhibitors. Secondly, the pharmacological and toxicological properties of the compounds were examined. Then, molecular docking was used to evaluate how well the chosen drugs interacted with MCL-1. Additionally anticipated was the compound's pharmacophore. Finally, using a molecular dynamics simulation, we examined the stability of the binding interaction. The study's findings are summarized in a list of potential MCL-1 small molecule inhibitors and their pharmacological characteristics, which can support and assist the research on MCL-1 inhibitors and give further leads for the creation and advancement of glioblastoma therapy medications.

2 Materials and methods

2.1 Immunogenomic analysis, differential gene expression and functional enrichment analysis

RNA-seq and clinical data of 168 GBM samples were downloaded from TCGA (Cancer Genome Atlas database) website, and they were divided into 2 groups according to the

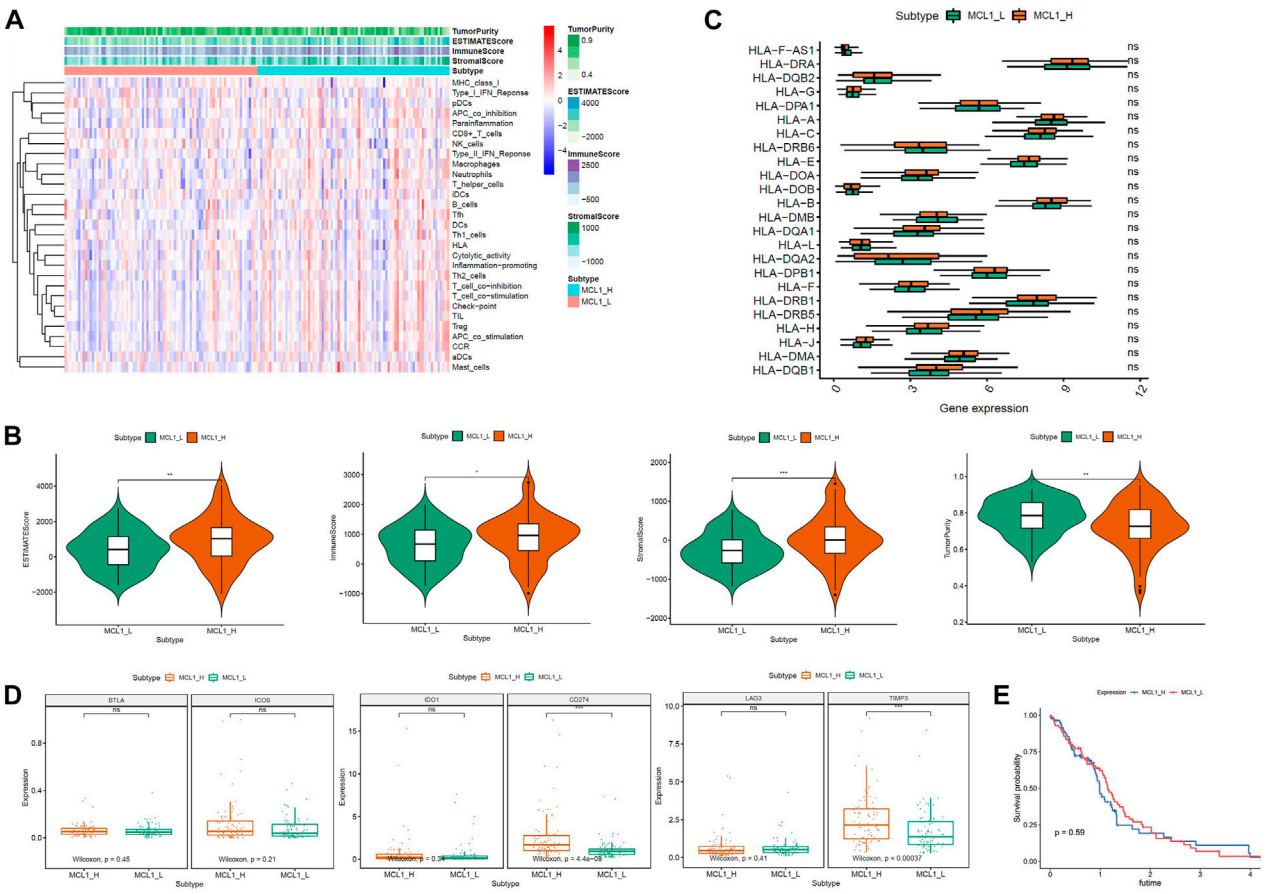

FIGURE 1
Immunogenomic analyses between MCL-1_H and MCL-1_L. **(A)** The enrichment levels of the 29-immune signature by ssGSEA score in each glioblastoma sample. ESTIMATE was used to evaluate Tumor purity, Stromal score and Immune score. **(B)** Comparison of the Immune score, Stromal score, ESTIMATE score, Tumor purity between MCL-1_H and MCL-1_L (Kruskal–Wallis test). **(C)** Comparison of the expression levels of HLA genes between MCL-1_H and MCL-1_L (ANOVA test). **(D)** Comparison of immune checkpoint gene expression levels between MCL-1_H and MCL-1_L (ANOVA test). **(E)** Survival curves of patients in MCL1_H group and MCL1_L group.

expression level of MCL-1: MCL-1_L (n = 84) and MCL-1_H (n = 84). First, 29 immune signal enrichment levels were quantified in all glioblastoma samples, and single-sample gene set enrichment analysis (ssGSEA) score was used in this analysis. ssGSEA scores were used to analyze the activity or enrichment levels of different immune cell functions in each glioblastoma sample. All glioblastoma samples were then evaluated for the level of immune cell infiltration (immunoscore), stromal content (stromal score), and tumor purity. Finally, the expression of HLA genes and immune checkpoint genes in MCL-1_H and MCL-1_L groups was tested by ANOVA.

Rstudio and Wilcoxon Rank Sum And Signed Rank Tests were used to analyze the differential expression between MCL-1_H and MCL-1_L. Using |log2 fold change (FC)|>1 and adjusted p values < 0.05 as the cutoff criterion, all genes were analyzed. "limma" package was used for analysis, and 449 differentially expressed genes were obtained. Then "ggpubr" and "ggthemes" packages were used to visualize the expression levels of all genes, and the differentially expressed genes in the MCL1_H and MCL1_L groups were shown in volcano maps. The Metascape website (https://metascape.org) features gene annotation and visualization. The differentially expressed genes were uploaded to this website, and the gene ontology and signal pathway enrichment of these genes were analyzed.

2.2 Construction and validation of MCL-1-associated prognostic signature (MPS)

To construct an immune prognostic signature, we randomly divided the TCGA_GBM data set into two groups: training set and verification set. LASSO Cox analysis is a widely used high-dimensional predictive regressive method. By selecting the optimal penalty parameter lambda and using 10-fold cross-verification, shrinkage and variable identification can be achieved at the same time to prevent overfitting. To establish immune prognostic characteristics, we put DEGs into LASSO Cox regression and use the "glmnet" R package to proceed to analysis. By weighting Cox regression coefficients to estimate the risk score of each patient, MPS was created. Patients are classified as low-risk and high-risk "survivor" R packages obtained based on the best cut-off value of the risk score. The "survival ROC" R package was used to describe the receiver

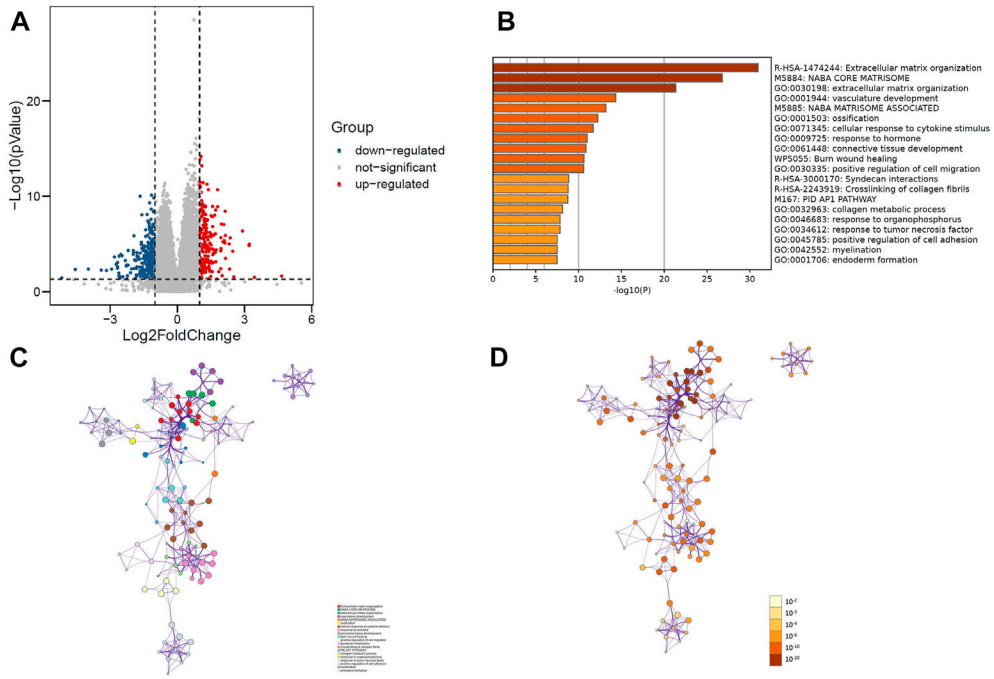

FIGURE 2
(A) Volcano plot of 449 genes differentially expressed between MCL-1_H and MCL-1_L. **(B)** Top 20 GO terms and KEGG pathways enrichment of DEGs. **(C)** Network plot colored by *p*-value, where terms containing more genes tend to have a more significant *p*-value in DEGs. **(D)** Network plot colored by cluster ID, where nodes that share the same cluster ID are typically close to each other in DEGs.

operating characteristic (ROC) curve to evaluate its sensitivity and specificity. Calculate the area under the curve (AUC) value according to the ROC curve. At the same time, the prognostic prediction ability of the MPS was further verified in the verification set.

2.3 Development of the nomogram

We assessed the independent prognostic power of MPS by univariate and multivariate Cox analyses. And based on the result of Cox analyses, we use the "rms" package to develop an innovative nomogram. Calibration charts for the probabilities of observing and predicting 1- year OS were performed to determine accuracy.

2.4 Virtual screening based on structure using Libdock, ADMT and TOPKAT

The Discovery Studio 2019 software, from BIOVIA in San Diego, California, United States, provides researchers with easy-to-use tools for protein simulation, modification, and precision medicine (Zhong et al., 2021; Zhong et al., 2022). In addition, we used the ZINC database, a free virtual screening database for commercial chemicals, as a ligand database. 3D molecular formats for 17,931 natural, named, and purchasable chemicals were initially obtained from the ZINC15 database. Both the 1.35 Å crystal structure of human MCL-1 (Protein Data Bank identifier: 6UDV) and the 3D structure of the positive reference medication MIM1 were imported into the LibDock working environment. To identify potential MCL-1 inhibitors, the ligand binding pocket domain of MCL-1 was selected as the binding site. The molecular docking between MIM1 and the treated MCL-1 was found to be successful. This site was therefore used as the active site for docking. All downloaded small molecule files were linked to this active site through the libdock module for preliminary virtual screening. All compounds' docking postures were graded based on their LibDock score. The ADME module of Discovery Studio 2019 was used to calculate the absorption, distribution, metabolism and excretion (ADME) levels of the top 30 compounds, and the TOPKAT module was used to analyze the toxicological characteristics of the compounds. Finally, two molecules were selected as candidates.

2.5 Molecular docking and pharmacological analysis

Studies on molecular docking of ligands and proteins were conducted using the CDOCKER module of Discovery Studio 2019. Using the CHARMm force field, CDOCKER is a method that generates very accurate molecular docking statistics (Wu et al., 2021; Yang et al., 2022). During docking, the CDOCKER algorithm is based on a simulated annealing protocol where the receptor remains rigid and the ligand is allowed to bend and dock with protein residues within the binding site to find the most suitable binding mode (Li H. et al., 2021). The section within a 13 Å radius of the ligand's geometric center is referred as the binding site spot.

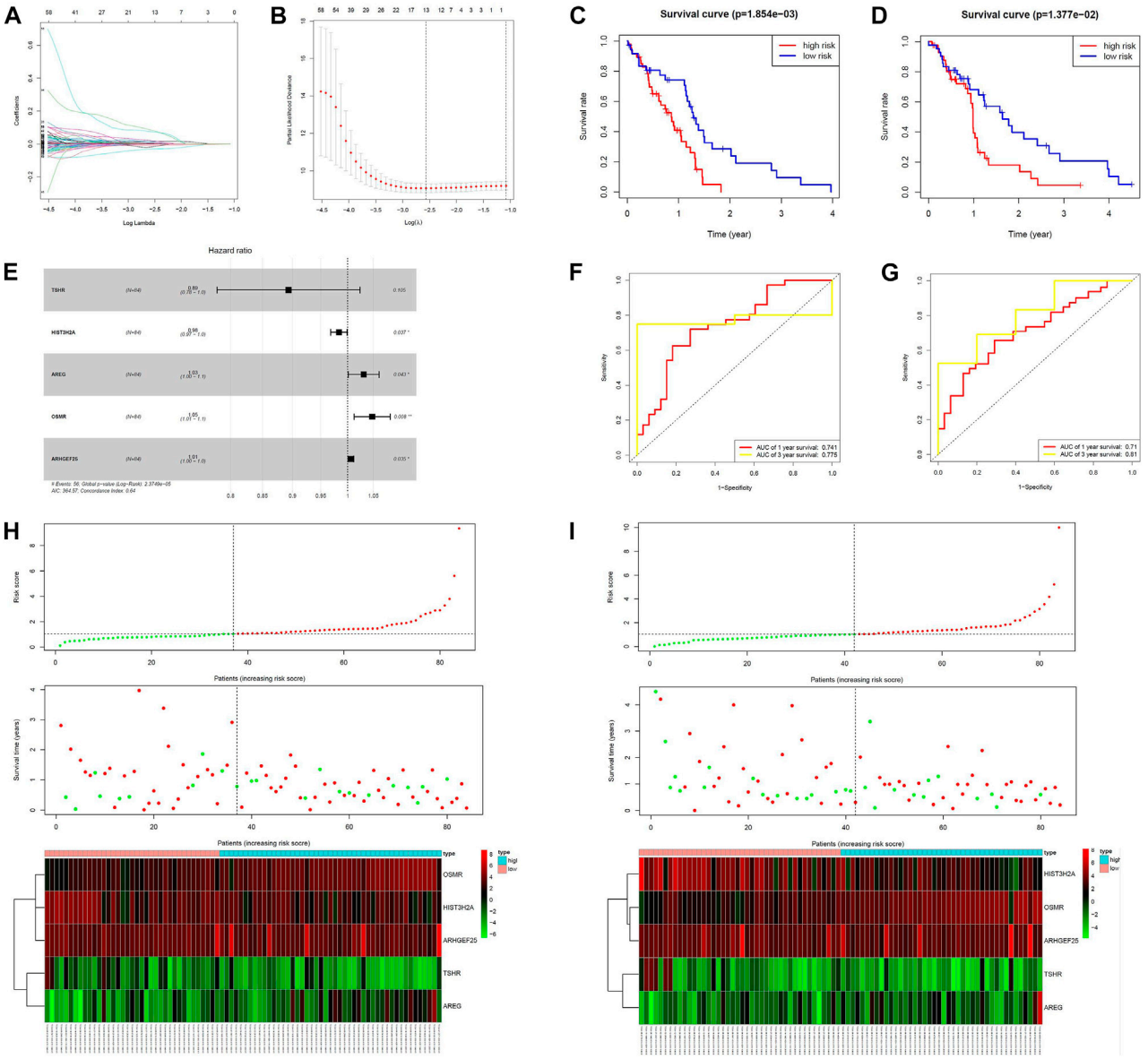

FIGURE 3
Construction of the MCL-1-related prognostic signature. **(A,B,E)** Kaplan–Meier curves of overall survival based on the MPS in the verification set and train set. **(C,D)** LASSO Cox analysis identified five genes most correlated to overall survival in the verification set and training set. **(F,G)** ROC curve analysis of the MPS. **(H,I)** Risk scores distribution, survival status of each patient, and heatmaps of prognostic five-gene signature in verification set and training set.

Therefore, according to the interaction energy analysis of CDOCKER, the most suitable compound was selected for the next study. In addition, the best binding pose of the selected compounds to the protein was demonstrated using the Schrodinger software.

2.6 Molecular dynamic simulation

The best binding conformation of the ligand-MCL-1 complex obtained from the previous molecular docking step was selected for molecular dynamics simulations. Using an explicit periodic boundary solvated water model, the ligand-receptor complex was contained in an orthogonal box and solvated. Sodium chloride was added to the solution with an ionic strength of 0.145 to mimic the physiological environment. The following simulation protocols were used for the system: 500 steps of steepest descent and conjugate gradient minimization; 5 ps-equilibration simulations in a normal pressure ensemble at a temperature of 300 K (slowly driven from an initial temperature of 50 K); and 50 ps-MD simulation (production module) at NPT (normal pressure and temperature) with a time step of 1 fs. Long-range electrostatics calculations were performed using the particle mesh Ewald (PME) technique, and all hydrogen-containing bonds were fixed using an adaptation of the linear constraint solver technique. The Discovery Studio 2019 analysis trajectory procedure was used to construct a trajectory for root-

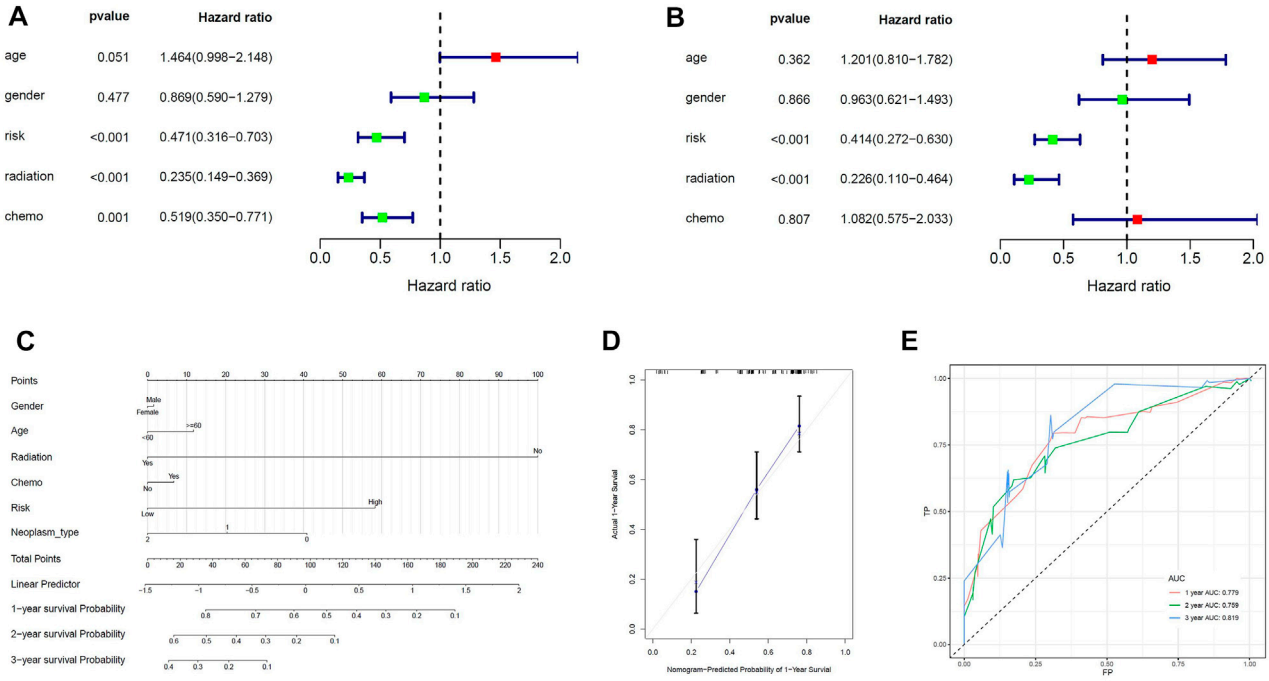

FIGURE 4
Construction of the nomogram model. **(A)** Univariate Cox analyses indicated that MPS was significantly associated with OS. **(B)** Multivariate Cox analyses indicated that MPS was significantly associated with OS. **(C)** Nomogram model for predicting the probability of 1- and 3-year OS in GBMs. **(D)** Calibration plots of the nomogram for predicting the probability of OS at 1 year. **(E)** ROC curve analysis of the nomogram.

mean-square deviation (RMSD), potential energy, and structural parameters using the original complex configuration as a reference.

3 Results

3.1 Immunogenomic analysis between MCL-1_H and MCL-1_L

A total of 168 glioblastoma patients were included in this study. According to the expression level of MCL-1, they were divided into 2 groups: MCL-1_H (n = 84) and MCL-1_L (n = 84). Firstly, the expression levels of 29 groups of immune-related genes representing different immune cell types, functions, and pathways in glioblastoma samples were investigated. According to the ssGSEA score, we found that the enrichment levels of immune cells, functions, and pathways in the MCL-1_H and MCL-1_L groups were not significantly different (Figure 1A). The ESTIMATE results show that (Figure 1B), The MCL-1_H group had immune score (Kruskal–Wallis test, $p < 0.001$), stromal score (Kruskal–Wallis test, $p < 0.001$), and ESTIMATE score (Kruskal–Wallis test, $p < 0.05$) were higher than those of MCL-1_L group, but tumor purity (Kruskal–Wallis test, $p < 0.001$) was higher than that of MCL-1_H group. These results indicated that MCL-1_H contained more immune cells and stromal cells, and MCL-1_L contained more tumor cells.

The expression of HLA genes and immune checkpoint genes was next analyzed in the two groups. In the analysis of 24 HLA genes (ANOVA test, $p < 0.05$) (Figure 1C), the expression of 15 HLA genes was higher in MCL-1_H than in MCL-1_L. Including HLA-DRA, HLA-A, HLA-C, HLA-E, HLA-DOA, HLA-B, HLA-DQA1, HLA-L, HLA-DPB1, HLA-F, HLA-DRB1, HLA-H, HLA-J, HLA-DMA, HLA DQB1. Among the six immune checkpoint gene assays (Figure 1D), gene expression levels were higher in the MCL-1_H group than that in the MCL-1_L group, with significantly higher expression of CD274 and TIMP3 in the MCL-1-H group than in the MCL-1_L group. These results suggested that patients in the MCL-1_H group were immunosuppressed, and the use of immune checkpoint inhibitors, especially inhibitors of CD274 and TIMP3, had a positive effect on the treatment of MCL-1_H patients. In addition, when grouped according to MCL1 expression levels, there was no significant difference in prognosis between the two groups (p = 0.59) (Figure 1E).

3.2 Differentially expressed genes analysis

R software was used to analyze the information of 168 patients to determine the differentially expressed gene (DEG) data set. To FDR <0.05 and log2 fold change (FC) < 1 or more for the standard, there were 449 genes identified, of which 274 genes downregulated, 175 genes upregulated (Figure 2A). Importing 449 differentially expressed genes into the metascape website, it was found that these genes were mainly enriched in these terms: R-HAS-1474244: Extracellular matrix organization, M5884: NABA CODE MATRISOME, GO:0030198: extracellular matrix organization (Figures 2B–D). Where each node represents a cluster item and is colored by cluster ID and p-value.

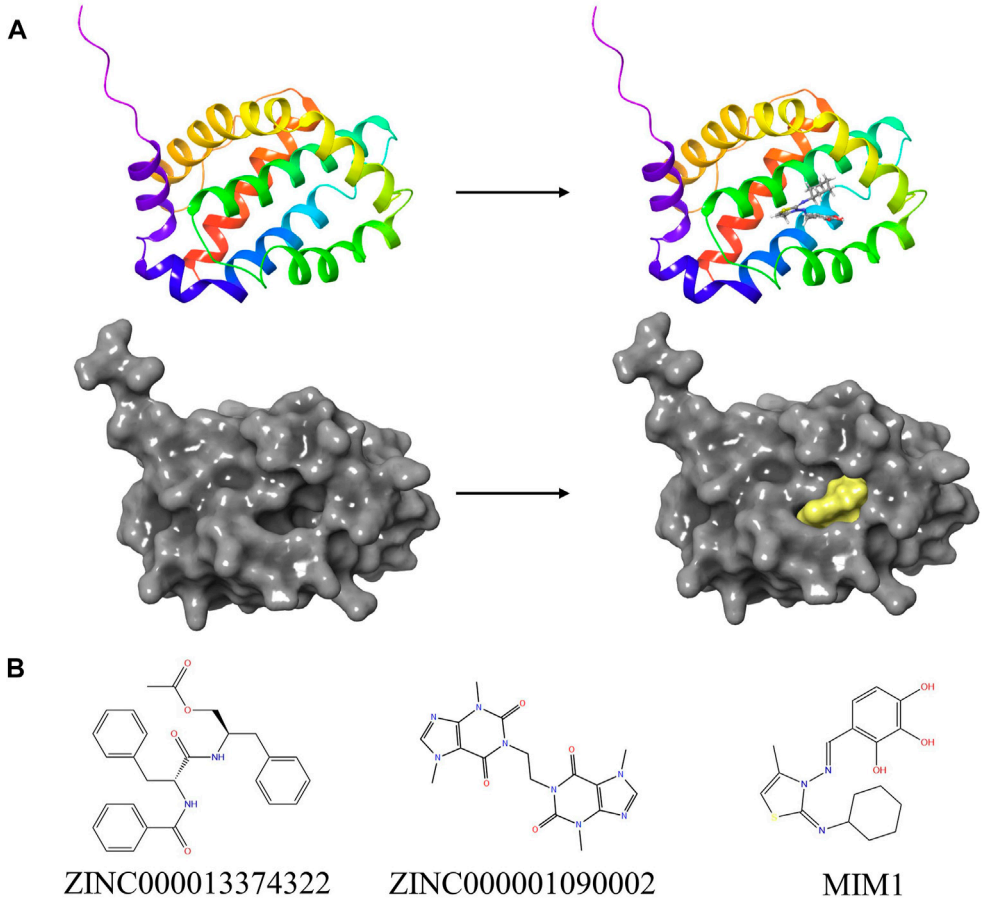

FIGURE 5
(A) The molecular structure of MCL-1 and the complex structure of MCL-1 with MIM1. Initial molecular structure was shown. The surface of the complex was added, yellow for MIM1 and gray for MCL-1. **(B)** The 2D structures of MIM1 and novel compounds were selected from virtual screening.

3.3 The MCL-1 related prognostic signature (MPS) was constructed and validated

MPS were constructed in the training group using lasso cox regression analysis (Figures 3A, B, E) to calculate the risk score for each sample. The survminer package in R software was used to calculate the optimal cut-off value, and the patients in the training group were divided into 2 groups: high-risk group and low-risk group. The results of the Kaplan-Meier analysis indicated that the patients in the low-risk group had a better prognosis (Figure 3C). Figure 3H shows the distribution of risk scores [risk score = (−0.112721)*TSHR + (−0.016743)* HIST3H2A+ 0.030476*ARGE+ 0.046739*OSMR +0.005866*ARHGEF25] and gene expression in the training group. We analyzed the MPS of the training group by ROC curve, which showed high accuracy in predicting 1-year survival and 3-year survival (AUC of 1-year survival = 0.741, AUC of 3-year survival = 0.775) (Figure 3F).

We next validated the prognostic value of MPS using the same formula in the validation set. Similarly, all patients were divided into high-risk and low-risk groups. Figure 3D shows that patients in the high-risk group had a lower survival rate. Figure 3I shows the risk score and gene expression distribution of the validation group. Figure 3G demonstrates that MPS has high accuracy and sensitivity in predicting 1-year survival and 3-year survival (AUC of 1-year survival = 0.71, AUC of 3-year survival = 0.81).

3.4 Construct MPS-based nomogram model

Univariate cox analysis was first used to demonstrate that MPS was significantly associated with OS (Hazard ratio: 0.471%, 95% confidence interval: 0.316–0.703, $p < 0.001$), and then multivariate cox analysis was used to test the accuracy of MPS as an independent prognostic factor (Hazard ratio: 0.414%, 95% confidence interval: 0.272–0.630, $p < 0.001$) (Figures 4A, B). An MPS-based nomogram model was then developed (Figure 4C). A nomogram calibration plot predicting 1-year OS probability showed better agreement (Figure 4D). The AUC of 1-year, 2-year, and 3-year were 0.779, 0.759, and 0.819 (Figure 4E), respectively, which proved that the nomogram had good validity.

3.5 Virtual screening using Libdock, ADME, and TOPKAT of DS 2019

Based on the above results, MCL-1 proved to be a key target for the treatment of glioblastoma and influencing the prognosis of

TABLE 1 Top 30 ranked compounds with higher LibDock scores.

Number	Compounds	Libdock score
1	ZINC000002572533	148.62
2	ZINC000040976869	147.033
3	ZINC000014883350	146.406
4	ZINC000100822245	145.294
5	ZINC000004096910	144.356
6	ZINC000230075702	144.266
7	ZINC000017044426	144.106
8	ZINC000004095521	143.012
9	ZINC000053147179	142.643
10	ZINC000003951623	142.538
11	ZINC000014951634	142.502
12	ZINC000049784088	141.387
13	ZINC000014883354	140.322
14	ZINC000013374322	140.085
15	ZINC000073280937	139.939
16	ZINC000014883346	139.835
17	ZINC000001577210	139.731
18	ZINC000019899011	139.665
19	ZINC000008552019	139.597
20	ZINC000038143593	138.888
21	ZINC000004104845	138.315
22	ZINC000014767590	138.235
23	ZINC000034944434	137.288
24	ZINC000002526388	137.022
25	ZINC000001090002	136.26
26	ZINC000008689960	136.136
27	ZINC000002097863	135.868
28	ZINC000005766341	135.342
29	ZINC000005811273	135.342
30	ZINC000006845904	135.298
	MIM1	106.167

glioblastoma. Therefore, we used MCL-1 as a target for drug screening for the treatment of glioblastoma. The MIM1-MCL-1 complex binding pocket was an essential regulatory region that was chosen as a significant reference site for screening probable MCL-1 inhibitors. Figure 5A shows the 3D structures of MCL-1 (PDB ID: 6UDV) and the MIM1-MCL-1 compound. In accordance with the LibDock score, 4,854 compounds had a higher LibDock score than MIM1 (106.167). The top 30 compounds were chosen for additional investigation based on the LibDock score, and these 30 compounds are described in Table 1.

Then ADME and TOPKAT modules of DS2019 were used to predict the pharmacological and toxicological properties of the top 30 compounds and MIM1. Based on the analysis in Tables 2, 3, ZINC000013374322 and ZINC000001090002 are not inhibitors of CYP2D6 and have a high intestinal absorption level. What's more, these two compounds are weakly bound plasma proteins. More importantly, these two compounds showed no hepatotoxicity and no Ames mutagenicity. Figure 5B shows that these two compounds and MIM1 have similar six-membered and five-membered annular structures, reactive oxygen and nitrogen species atoms, suggesting that they may play similar roles. The compounds ZINC000013374322 and ZINC000001090002, which are expected to be promising candidates, were then investigated.

3.6 Ligand binding analysis

ZINC000013374322 and ZINC000001090002 were accurately connected to the binding pocket of MCL-1, and the mechanism of ligand binding was examined by using CDOCKER module. As shown in Table 4, the interaction energies of ZINC000001577210 (−40.7616 kcal/mol) and ZINC000001090002 (−43.3771 kcal/mol) are both much lower than MIM1 (−35.0968 kcal/mol), indicating that they may have higher binding affinity to MCL-1.

By applying DS2019 and Schrodinger software, we thoroughly analyzed the ligand conformation in the MCL-1 binding pocket and the protein-ligand complex interaction (Figures 6A–C). In these figures, the binding pattern of the two molecules to the MCL-1 binding pocket is visually shown. As shown in Figure 6D, there is a significant overlap between the two molecules and MIM1 in the binding pocket posture. According to Figure 6; Table 5, these two molecules and MIM1 are essentially identical in the way they bind and interact with MCL-1, proving that they have similar inhibitory effects on MCL-1. At the same time, it can be inferred that the two amino acid residues of PHE270 and MET250 play a crucial role in the functional domain of MCL-1.

Through the precise analysis of DS 2019, we showed detailed information on the interaction between ligand and protein, including bond length, bond type, bond atoms, and so on (Tables 5, 6). The results showed that ZINC000013374322 and ZINC000001090002 and MIM1 formed 2, 2, 1 pair of hydrogen bonds with MCL-1, respectively. In addition, ZINC000013374322 and ZINC000001090002, and MIM1 formed 12, 5, 8 pairs of hydrophobic interaction with MCL-1, respectively. Among them, although the hydrophobic interaction formed by ZINC000013374322 and MCL-1 are few, the bond lengths are small. So ZINC000013374322 forms a more stable hydrophobic interaction bonds with MCL-1. In conclusion, these results indicate that ZINC000013374322 and ZINC000001090002 may have better binding affinity to MCL-1 than MIM1, indicating that these two compounds have broad application prospects.

3.7 Pharmacophore analysis and molecular dynamic simulation

We performed pharmacophore analysis on these three molecules (Figure 7A). 9 and 5 hydrogen bond acceptors are

TABLE 2 Adsorption, distribution, metabolism, and excretion properties of compounds.

Number	Compounds	Solubility level	BBB level	CYP2D6	Hepatotoxicity	Absorption level	PPB level
1	ZINC000002572533	2	4	1	0	3	0
2	ZINC000040976869	3	4	0	0	2	1
3	ZINC000014883350	0	4	0	0	3	1
4	ZINC000100822245	2	4	1	0	3	0
5	ZINC000004096910	0	4	1	0	3	1
6	ZINC000230075702	2	4	1	0	2	0
7	ZINC000017044426	2	4	1	0	3	0
8	ZINC000004095521	0	4	0	0	3	1
9	ZINC000053147179	3	4	0	1	3	0
10	ZINC000003951623	2	2	1	1	0	1
11	ZINC000014951634	3	4	0	0	3	0
12	ZINC000049784088	4	4	0	0	3	0
13	ZINC000014883354	0	4	0	0	3	1
14	ZINC000013374322	2	2	0	0	0	0
15	ZINC000073280937	2	4	0	1	2	1
16	ZINC000014883346	0	4	0	0	3	1
17	ZINC000001577210	2	1	0	0	0	1
18	ZINC000019899011	2	2	0	1	0	1
19	ZINC000008552019	2	4	1	0	3	0
20	ZINC000038143593	3	4	0	0	3	0
21	ZINC000004104845	2	3	0	1	0	1
22	ZINC000014767590	0	4	0	0	3	1
23	ZINC000034944434	2	4	1	0	2	0
24	ZINC000002526388	2	4	1	1	0	1
25	ZINC000001090002	3	4	0	0	0	0
26	ZINC000008689960	3	1	0	0	0	0
27	ZINC000002097863	3	4	0	1	3	0
28	ZINC000005766341	1	4	0	0	3	1
29	ZINC000005811273	1	4	0	0	3	1
30	ZINC000006845904	0	4	1	0	3	1
	MIM1	2	2	0	1	0	1

BBB, blood-brain barrier; CYP2D6, cytochrome P-450 2D6; PPB, plasma protein binding.
Aqueous-solubility level: 0, extremely low; 1, very low, but possible; 2, low; 3, good.
BBB, level: 0, very high penetrant; 1, high; 2, medium; 3, low; 4, undefined.
CYP2D6 level: 0, noninhibitor; 1, inhibitor.
Hepatotoxicity: 0, nontoxic; 1, toxic.
Human-intestinal absorption level: 0, good; 1, moderate; 2, poor; 3, very poor.
PPB: 0, absorbent weak; 1, absorbent strong.

displayed on the ZINC000013374322 and ZINC000001090002 respectively. There are 3 hydrophobic centers and 6 aromatic nuclei in ZINC000013374322 meanwhile ZINC000001090002 formed 3 hydrophobic centers and 4 aromatic nuclei. In summary, ZINC000013374322 has 18 characteristic pharmacophores and ZINC000001090002 has 12 characteristic pharmacophores. The characteristic pharmacophore of both molecules is basically the same as that of MIM1.

TABLE 3 Toxicities of compounds.

Number	Compounds	Mouse NTP		Rat NTP		Ames	DTP
		Female	Male	Female	Male		
1	ZINC000002572533	0	1	1	0.051	0.238	1
2	ZINC000040976869	0	1	1	0	0.021	0
3	ZINC000014883350	1	0	0	0.968	0	0
4	ZINC000100822245	0	1	1	0.051	0.238	1
5	ZINC000004096910	0	1	1	0	1	1
6	ZINC000230075702	0	0	1	0.02	0	1
7	ZINC000017044426	0	1	1	0.051	0.238	1
8	ZINC000004095521	0	1	1	0	0.017	0
9	ZINC000053147179	1	1	1	0	0	1
10	ZINC000003951623	0	0.999	1	0.023	0	0.824
11	ZINC000014951634	0.089	0	1	0	0	1
12	ZINC000049784088	0.995	0	0	0.008	1	1
13	ZINC000014883354	1	0	0	0.968	0	0
14	ZINC000013374322	0.002	0	1	0.015	0	0.095
15	ZINC000073280937	0.312	1	0	0.185	0	1
16	ZINC000014883346	1	0	0	0.968	0	0
17	ZINC000001577210	0	0.173	0	0.952	0	0.04
18	ZINC000019899011	0	1	0	1	0.802	0.999
19	ZINC000008552019	0	1	1	0.05	0.265	1
20	ZINC000038143593	0.061	0	0.274	0.088	0	1
21	ZINC000004104845	0.011	0.006	0.102	0.989	0	1
22	ZINC000014767590	0.494	0	0	1	0	0
23	ZINC000034944434	0	0	1	0.02	0	1
24	ZINC000002526388	0.999	0.041	0	0.999	0.999	0.745
25	ZINC000001090002	1	1	0	1	0.005	1
26	ZINC000008689960	0	0	0	0	0	0
27	ZINC000002097863	1	1	0	0	1	0
28	ZINC000005766341	0.917	1	1	0.006	1	0
29	ZINC000005811273	0.917	1	1	0.006	1	0
30	ZINC000006845904	0	1	1	0	0.014	0
	MIM1	0	0	0.163	1	0	1

NTP, U.S., national toxicology program; DTP, developmental toxicity potential.
NTP <0.3 (noncarcinogen); > 0.8 (carcinogen).
Ames <0.3 (nonmutagen); > 0.8 (mutagen).
DTP <0.3 (nontoxic); > 0.8 (toxic).

Molecular dynamics simulations were performed in simulated natural environments to evaluate the stability of ZINC000013374322-MCL-1 and ZINC000001090002-MCL-1complexes. As shown in Figures 7B, C, the potential energy and RMSD of each compound became stable over time, and the trajectory of the complex basically reached equilibrium after 15 ps. Molecular dynamics simulation results show that the interaction between these compounds and MCL-1 is beneficial to the stability of the complex. In conclusion, ZINC000013374322-MCL-1 and ZINC000001090002-MCL-1

TABLE 4 DOCKER potential energy of compounds with MIM1, ZINC000013374322 and ZINC000001090002.

Compounds	-CDOCKER energy (Kcal/mol)	-CDOCKER interaction energy (Kcal/mol)
ZINC000013374322	44.039	40.7616
ZINC000001090002	31.916	43.3771
MIM1	5.95782	35.0968

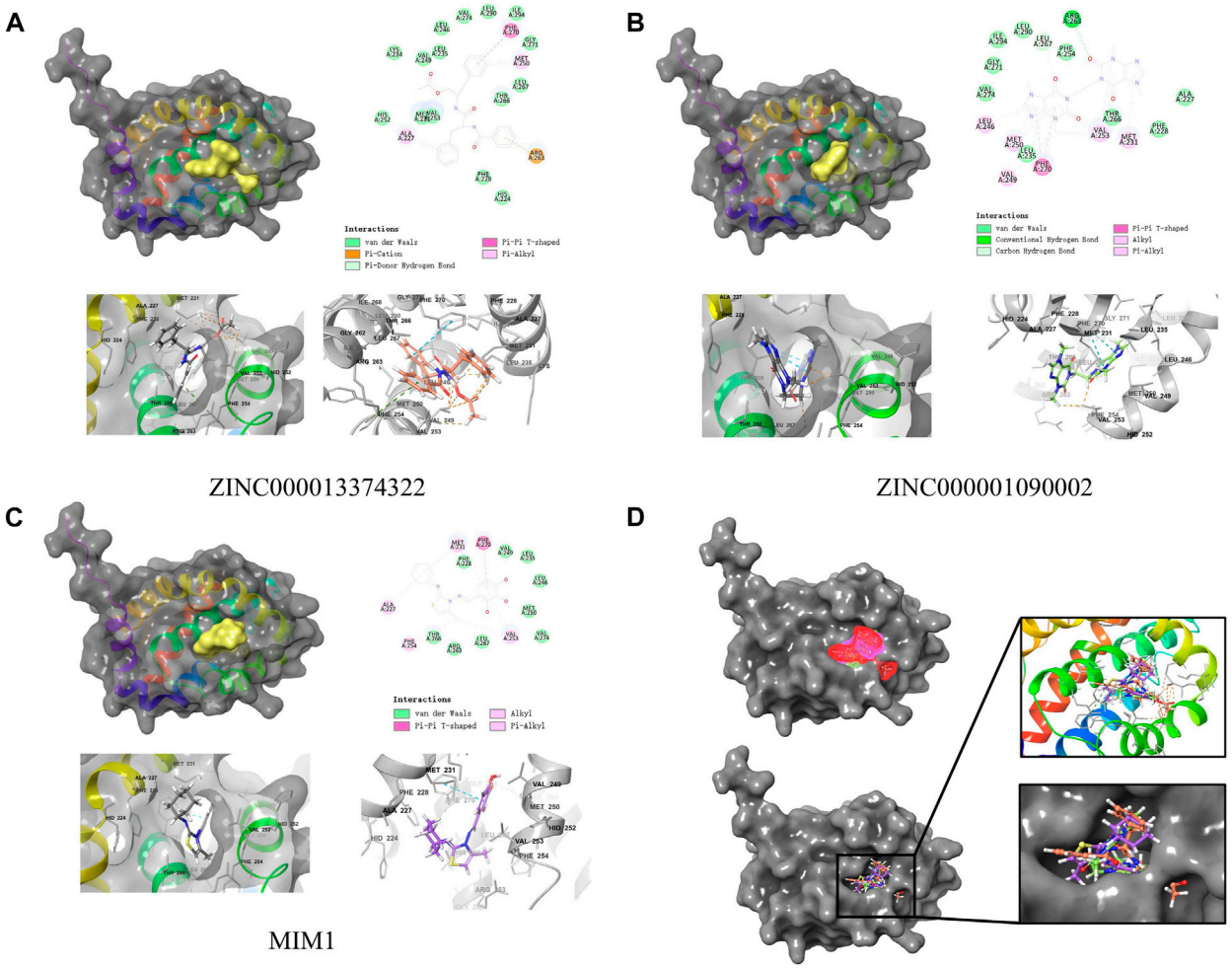

FIGURE 6
Schematic drawing of interactions between ligands and MCL-1 by Schrodinger and schematic of intermolecular interaction of the predicted binding modes. **(A)** ZINC000013374322-MCL-1 complex. **(B)** ZINC000001090002-MCL-1 complex. **(C)** MIM1-MCL-1 complex. **(D)** A comparison of the spatial conformation of small molecules in protein binding pockets and the gray surface of MCL-1 was added.

TABLE 5 Hydrogen bond interaction parameters for each compound with MCL-1 residues.

Receptor	Compound	Donor atom	Receptor atom	Distances (Å)
MCL-1	ZINC000013374322	ARG263:HE	ZINC000013374322	3.01
		ARG263:NH1	ZINC000013374322	4.06
	ZINC000001090002	LEU267:HA	ZINC000001090002:O14	2.59
		ARG263:HH11	ZINC000001090002:O26	3.00
	MIM1	MIM1:H43	A:ALA227:O	1.96

TABLE 6 Hydrophobic interaction related interaction parameters for each compound with MCL-1 residues.

Receptor	Compound	Donor atom	Receptor atom	Distances (Å)
6UDV	ZINC000013374322	ZINC000013374322	MET250	3.98
		PHE270	ZINC000013374322	4.9
		ZINC000013374322	ALA227	3.94
		ZINC000013374322	ZINC000013374322	5.65
		ZINC000013374322	ARG263	5.19
	ZINC000001090002	ZINC000001090002	VAL253	5.38
		ZINC000001090002	MET231	5.08
		PHE270	ZINC000001090002	4.86
		ZINC000001090002:C22	MET231	3.98
		ZINC000001090002	PHE270	4.6
		ZINC000001090002	LEU246	4.8
		ZINC000001090002:C22	VAL249	4.47
		ZINC000001090002	MET250	4.6
		ZINC000001090002	MET250	5.02
		ZINC000001090002:C22	VAL253	4.47
		ZINC000001090002	VAL253	5.14
		ZINC000001090002:C28	VAL253	4.86
	MIM1	MIM1:C1	ARG263	4.44
		MIM1	ARG263	5.49
		MIM1	VAL253	5.33
		MET250	MIM1	5.39
		PHE270	MIM1	5.05
		MIM1	MET231	4.66
		MIM1	ALA227	4.74
		VAL253	MIM1	4.96

complexes can stably exist in a natural environment and inhibit MCL-1 activity.

4 Discussion

Glioblastoma is a common brain tumor with a high degree of malignancy. Most patients have a poor prognosis and a very short survival time. The current conventional treatment methods for brain tumors have no significant improvement in the survival time and quality of life of glioblastoma. The occurrence and development of most tumors, including glioblastoma, are closely related to cell apoptosis. At present, a large number of studies have proved that the induction of apoptosis through a variety of ways can inhibit the progression of glioblastoma, which is the key way of drug treatment for glioblastoma. MCL-1 is a widely studied and potent anti-apoptotic protein that regulates cells by various mechanisms, including interactions with cell cycle regulators to affect cell division, acting as a molecular switch for double-strand break (DSB) DNA repair, regulation of autophagy and mitophagy through BH3-like protein interactions, etc. (Widden and Placzek, 2021). Down-regulating the expression and function of MCL-1 in tumor cells can effectively promote the apoptosis of tumor cells. Among them, the widely studied MCL-1 inhibitor is BH3-mimic, which has good effects on blood system tumors and multiple myeloma and has made great progress in combination with established therapies (Caenepeel et al., 2018). Among them, the widely studied MCL-1 inhibitors are BH3-mimics, including AZD5991, S63845, MIM1, etc. (Tron et al., 2018; Mallick et al., 2019; Moujalled et al., 2019; Wei et al., 2020), which have good effects on hematological tumors and multiple myeloma and have made great progress in combination with established therapies (Caenepeel et al., 2018). In recent years, targeted therapy has been widely used in the treatment of a variety of tumors and has achieved good results. By matching with genetic testing, targeted agents have significantly improved patient outcomes. However, GBM shows strong drug resistance, and the use of targeted drugs is severely limited [21] due to the permeability of the blood-brain barrier that limits drug delivery, low mutation burden, and

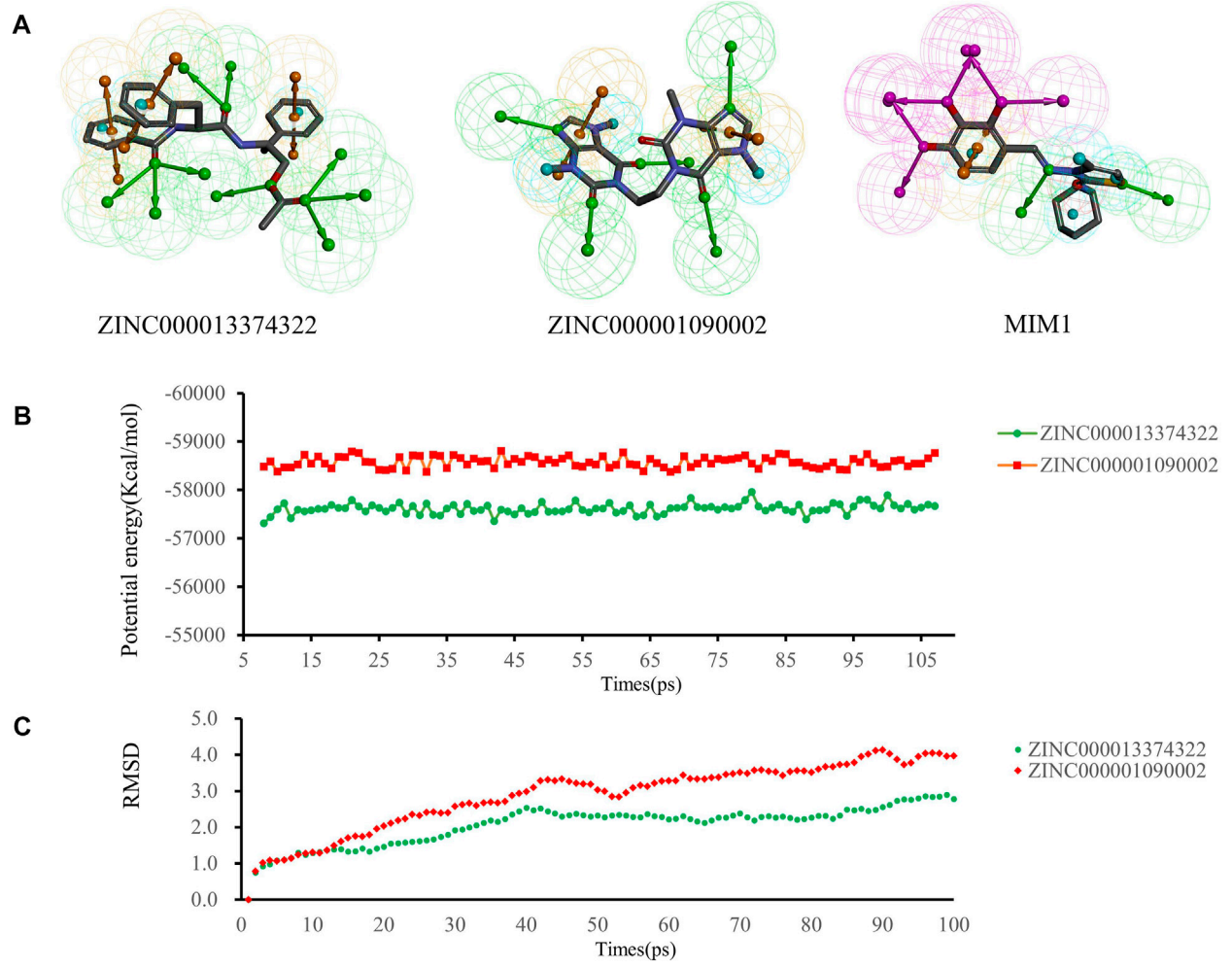

FIGURE 7
(A) Pharmacophore predictions using the 3D-QSAR module of DS2019 Green represents the hydrogen acceptor; blue represents the hydrophobic center; purple represents the hydrogen donor; yellow represents Aromatic Ring. **(B,C)** Results of molecular dynamics simulation of the compounds ZINC000013374322 and ZINC000001090002. **(B)** Potential energy, RMSD, root-mean-square deviation. **(B)** Average backbone root-mean-square deviation.

suppression of the immune microenvironment (Yuan et al., 2022). However, the relatively mature small molecule inhibitors of MCL-1 that have been studied and developed are largely not used in the treatment of glioblastomas, probably due to difficulties in crossing the blood-brain barrier. Therefore, it is essential to study the role of MCL-1 in the prognosis prediction of glioblastoma patients and to develop safer and more effective MCL-1 inhibitors for the treatment of glioblastoma.

The present study aimed to establish an MCL-1-based prognostic model and to screen safe and effective MCL-1 inhibitors. Firstly, GBM samples were divided into two groups according to the expression level of MCL-1, and the immune signal enrichment level and differential gene expression were analyzed. Functional enrichment analysis of differential genes showed that these genes were in the extracellular matrix organization, and the expression level of MCL1_H group is significantly higher than that of MCL1_L group. NABA CORE MATRISOME and other aspects were enriched. Next, the prognostic MPS model was constructed and validated, which had high accuracy and sensitivity in predicting 1-year and 3-year survival rates of patients. By LASSO cox regression analysis, 5 genes were found to be independent prognostic factors: TSHR, HIST3H2A, AREG, OSMR, ARHGEF25. Glioblastoma highly expresses TSHR and TSH in the tumor microenvironment promotes its proliferation, invasion and immune evasion, which limits the T cell killing of glioblastoma. Treatment targeting intracranial TSH may reverse the immunosuppressive state of glioblastoma (Wu et al., 2022). miR-516a-5p downregulates the expression of HIST3H2A, thereby reversing the anti-proliferation effect induced by miR-516a-5p in NSCLC cells. miR-516a-5p may inhibit the proliferation of NSCLC cells by targeting HIST3H2A (Ye et al., 2019). AREG, one of the seven ligands that bind and activate EGFR, can promote the differentiation of T cells into Tregs in the tumor microenvironment, and targeting AREG in the tumor microenvironment may inhibit tumor invasion and immunosuppression (Coniglio and Segall, 2021). OSMR is a cell surface receptor that is a key component of EGFRvIII-STAT3 signaling, which forms a feedforward signaling mechanism with these molecules to drive glioblastoma genesis and progression

(Jahani-Asl et al., 2016). ARHGEF25 promotes tumor cell migration, and serum-induced ARHGEF25 activation plays a key role in chemotactic migration by restricting lamellipodia formation to the direction of cell movement and keeping it at the leading edge (Hayashi et al., 2013).

Next, we chose the crystal structure of MCL-1 (PDB ID: 6UDV) and used MIM1 as the positive reference drug for the entire study. We first used the LibDock module of DS2019 to analyze the LibDock scores of compounds downloaded from the ZINC15 database. The 30 compounds with the highest LibDock scores were selected to analyze their pharmacological and toxicological properties using ADME and TOPKAT modules. In this step, several pharmacological properties of ZINC000013374322 and ZINC000001090002 were found to be superior to MIM1 and less toxic, so these two compounds were selected for further analysis. Next, the binding modes of the compounds and proteins were precisely analyzed using the CDOCKER module, and the results showed that the complex formed by these two compounds with MCL-1 had lower interaction energy, proving that their binding was more stable. Two amino acid residues, PHE270 and MET250 of MCL-1, were found to interact with two compounds and MIM1, indicating that these two amino acid residues were the key sites for inhibiting MCL-1 protein. This is the latest discovery in our study. At present, the specific functions of these two amino acid residues in MCL-1 have not been mentioned in other existing studies. We consider PHE270 and MET250 as the key amino acid residues in the MCL-1 pocket, and through modification and modification of them, the small molecule inhibitor can be more stably bound to the corresponding domain of MCL-1. In the development of more MCL-1 inhibitors, PHE270 and MET250 can be used as effective binding sites to select more reasonable inhibitors. We then analyzed the pharmacophores of the compounds and found that the compounds had similar characteristic pharmacophores. Finally, molecular dynamics simulations were performed for both compounds. In the simulated natural environment, the complex trajectories reached equilibrium after 30 ps, and the potential energy and RMSD of each complex tend to stabilize with time. Based on these results, ZINC000013374322 and ZINC000001090002 can be further modified to make the ligand binding to MCL-1 more reasonable and stable. Furthermore, few studies have been conducted on these two compounds, ZINC000013374322 (Aurantiamide Acetate) and ZINC000001090002 (Bisdionin B), and studies that have shown no effect on cancer, especially in the treatment of glioblastoma by inhibiting MCL-1 function. However, our study did demonstrate that they can effectively inhibit the MCL-1 function, which provides more prodrugs for the treatment of glioblastoma. Through further modification and improvement, these two compounds show excellent development prospects as MCL-1 small molecule inhibitors.

We have to admit that despite accurate measurements and virtual calculations in this study, there are still some limitations. Since there are many changes in the metabolism and transformation of drugs *in vivo*, corresponding experiments will be carried out in the future to verify other safety indexes of these two compounds, such as IC50, AB (aerobic biodegradability) and MTD (maximum tolerated dose), etc., to continuously optimize the structure of compounds and develop more reasonable drugs.

5 Conclusion

This study demonstrated that MCL-1 was a key factor affecting the prognosis of glioblastoma patients, and inhibition of MCL-1 can improve the prognosis of glioblastoma patients. We used lasso cox regression analysis to construct an MCL-1 related prognostic evaluation model and prognostic-related nomogram to predict the survival rate of glioblastoma patients. In addition, we found that TSHR, HIST3H2A, AREG, OSMR, and ARHGEF25 are novel independent factors affecting the diagnosis, treatment, and prognosis of GBM. Based on the role of MCL-1 in glioblastoma development, we used a series of computer-aided techniques to screen safer and more effective MCL-1 small molecule inhibitors from the ZINC15 database. ZINC000013374322 and ZINC000001090002 are safe and ideal drug candidates. In addition, this study also provided 30 candidate drugs and their pharmacological properties, which provided a new idea for the development and study of MCL-1 inhibitors.

Data availability statement

The original contributions presented in the study are included in the article/supplementary material, further inquiries can be directed to the corresponding author.

Author contributions

AZ, HW, and ZG designed experiments; J-XR and HC wrote manuscript; WY, YZ, LP, ZC, and FR carried out experiments; YC, MZ, FP, and WC analyzed experiments results. XW and ZZ revised the manuscript, figures and tables. All authors contributed to the article and approved the submitted version

Conflict of interest

The authors declare that the research was conducted in the absence of any commercial or financial relationships that could be construed as a potential conflict of interest.

The reviewer HC declared a shared parent affiliation with the author(s) JR, ZG, YZ, FR, YC, WC, and ZZ to the handling editor at the time of review.

Publisher's note

References

Allahyarzadeh Khiabani, N., Amin Doustvandi, M., Mohammadnejad, F., Salmani Hassan Kohal, E., Boushehri, N., Jafarlou, M., et al. (2023). Combination of B7H6-siRNA and temozolomide synergistically reduces stemness and migration properties of glioblastoma cancer cells. *Exp. Cell. Res.* 429 (1), 113667. doi:10.1016/j.yexcr.2023.113667

Boongird, A., Lekcharoensombat, N., Jinawath, A., Theparee, T., Jittapiromsak, N., Shuangshoti, S., et al. (2023). Glioblastoma with novel EGFR mutations (T790M and exon 20 insertion) yet unresponsive to osimertinib: A case report. *Genes. Chromosom. Cancer* 62 (7), 423–429. doi:10.1002/gcc.23143

Caenepeel, S., Brown, S. P., Belmontes, B., Moody, G., Keegan, K. S., Chui, D., et al. (2018). AMG 176, a selective MCL1 inhibitor, is effective in hematologic cancer models alone and in combination with established therapies. *Cancer Discov.* 8 (12), 1582–1597. doi:10.1158/2159-8290.Cd-18-0387

Coniglio, S. J., and Segall, J. E. (2021). Microglial-stimulation of glioma invasion involves the EGFR ligand amphiregulin. *PLoS One* 16 (11), e0260252. doi:10.1371/journal.pone.0260252

Denis, C., Sopková-de Oliveira Santos, J., Bureau, R., and Voisin-Chiret, A. S. (2020). Hot-spots of mcl-1 protein. *J. Med. Chem.* 63 (3), 928–943. doi:10.1021/acs.jmedchem.9b00983

Finch, A., Solomou, G., Wykes, V., Pohl, U., Bardella, C., and Watts, C. (2021). Advances in research of adult gliomas. *Int. J. Mol. Sci.* 22 (2), 924. doi:10.3390/ijms22020924

Gratas, C., Séry, Q., Rabé, M., Oliver, L., and Vallette, F. M. (2014). Bak and Mcl-1 are essential for Temozolomide induced cell death in human glioma. *Oncotarget* 5 (9), 2428–2435. doi:10.18632/oncotarget.1642

Hayashi, A., Hiatari, R., Tsuji, T., Ohashi, K., and Mizuno, K. (2013). p63RhoGEF-mediated formation of a single polarized lamellipodium is required for chemotactic migration in breast carcinoma cells. *FEBS Lett.* 587 (6), 698–705. doi:10.1016/j.febslet.2013.01.043

Hotchkiss, K. M., Batich, K. A., Mohan, A., Rahman, R., Piantadosi, S., and Khasraw, M. (2023). Dendritic cell vaccine trials in gliomas: Untangling the lines. *Neuro Oncol.*, noad088. doi:10.1093/neuonc/noad088

Jahani-Asl, A., Yin, H., Soleimani, V. D., Haque, T., Luchman, H. A., Chang, N. C., et al. (2016). Control of glioblastoma tumorigenesis by feed-forward cytokine signaling. *Nat. Neurosci.* 19 (6), 798–806. doi:10.1038/nn.4295

Jane, E. P., Premkumar, D. R., Cavaleri, J. M., Sutera, P. A., Rajasekar, T., and Pollack, I. F. (2016). Dinaciclib, a cyclin-dependent kinase inhibitor promotes proteasomal degradation of mcl-1 and enhances ABT-737-mediated cell death in malignant human glioma cell lines. *J. Pharmacol. Exp. Ther.* 356 (2), 354–365. doi:10.1124/jpet.115.230052

Jatyan, R., Sahel, D. K., Singh, P., Sakhuja, R., Mittal, A., and Chitkara, D. (2023). Temozolomide-fatty acid conjugates for glioblastoma multiforme: *In vitro* and *in vivo* evaluation. *J. Control Release* 359, 161–174. doi:10.1016/j.jconrel.2023.05.012

Juric, V., Hudson, L., Fay, J., Richards, C. E., Jahns, H., Verreault, M., et al. (2021). Transcriptional CDK inhibitors, CYC065 and THZ1 promote Bim-dependent apoptosis in primary and recurrent GBM through cell cycle arrest and Mcl-1 downregulation. *Cell. Death Dis.* 12 (8), 763. doi:10.1038/s41419-021-04050-7

Li, H., Yang, W., Wang, Z., Wang, X., Hao, Y., Xi, J., et al. (2021). Computational research of mTORC1 inhibitor on cerebral ischemia-reperfusion injury. *Aging (Albany NY)* 13 (15), 19598–19613. doi:10.18632/aging.203371

Li, L., Yin, Y., Zhang, J., Wu, X., Liu, J., Chai, J., et al. (2023). USP18 regulates the malignant phenotypes of glioblastoma stem cells. *Pathol. Res. Pract.* 247, 154572. doi:10.1016/j.prp.2023.154572

Li, S., Guo, W., and Wu, H. (2021). The role of post-translational modifications in the regulation of MCL1. *Cell. Signal* 81, 109933. doi:10.1016/j.cellsig.2021.109933

Liu, T., Lam, V., Thieme, E., Sun, D., Wang, X., Xu, F., et al. (2021). Pharmacologic targeting of mcl-1 induces mitochondrial dysfunction and apoptosis in B-cell lymphoma cells in a TP53- and BAX-dependent manner. *Clin. Cancer Res.* 27 (17), 4910–4922. doi:10.1158/1078-0432.Ccr-21-0464

Mallick, D. J., Soderquist, R. S., Bates, D., and Eastman, A. (2019). Confounding off-target effects of BH3 mimetics at commonly used concentrations: MIM1, UMI-77, and A-1210477. *Cell. Death Dis.* 10 (3), 185. doi:10.1038/s41419-019-1426-3

Moujalled, D. M., Pomilio, G., Ghiurau, C., Ivey, A., Salmon, J., Rijal, S., et al. (2019). Combining BH3-mimetics to target both BCL-2 and MCL1 has potent activity in pre-clinical models of acute myeloid leukemia. *Leukemia* 33 (4), 905–917. doi:10.1038/s41375-018-0261-3

Ostrom, Q. T., Bauchet, L., Davis, F. G., Deltour, I., Fisher, J. L., Langer, C. E., et al. (2014). The epidemiology of glioma in adults: A "state of the science" review. *Neuro Oncol.* 16 (7), 896–913. doi:10.1093/neuonc/nou087

Ostrom, Q. T., Cioffi, G., Gittleman, H., Patil, N., Waite, K., Kruchko, C., et al. (2019). CBTRUS statistical report: Primary brain and other central nervous system tumors diagnosed in the United States in 2012-2016. *Neuro Oncol.* 21 (5), v1–v100. doi:10.1093/neuonc/noz150

Premkumar, D. R., Jane, E. P., Agostino, N. R., DiDomenico, J. D., and Pollack, I. F. (2013). Bortezomib-induced sensitization of malignant human glioma cells to vorinostat-induced apoptosis depends on reactive oxygen species production, mitochondrial dysfunction, Noxa upregulation, Mcl-1 cleavage, and DNA damage. *Mol. Carcinog.* 52 (2), 118–133. doi:10.1002/mc.21835

Respondek, M., Beberok, A., Rok, J., Rzepka, Z., Wrześniok, D., and Buszman, E. (2018). MIM1, the Mcl-1 - specific BH3 mimetic induces apoptosis in human U87MG glioblastoma cells. *Toxicol Vitro* 53, 126–135. doi:10.1016/j.tiv.2018.08.007

Sancho, M., Leiva, D., Lucendo, E., and Orzáez, M. (2021). Understanding MCL1: From cellular function and regulation to pharmacological inhibition. *Febs J.* 289, 6209–6234. doi:10.1111/febs.16136

Tron, A. E., Belmonte, M. A., Adam, A., Aquila, B. M., Boise, L. H., Chiarparin, E., et al. (2018). Discovery of Mcl-1-specific inhibitor AZD5991 and preclinical activity in multiple myeloma and acute myeloid leukemia. *Nat. Commun.* 9 (1), 5341. doi:10.1038/s41467-018-07551-w

Wei, A. H., Roberts, A. W., Spencer, A., Rosenberg, A. S., Siegel, D., Walter, R. B., et al. (2020). Targeting MCL-1 in hematologic malignancies: Rationale and progress. *Blood Rev.* 44, 100672. doi:10.1016/j.blre.2020.100672

Widden, H., and Placzek, W. J. (2021). The multiple mechanisms of MCL1 in the regulation of cell fate. *Commun. Biol.* 4 (1), 1029. doi:10.1038/s42003-021-02564-6

Wu, B., Yang, W., Fu, Z., Xie, H., Guo, Z., Liu, D., et al. (2021). Selected using bioinformatics and molecular docking analyses, PHA-793887 is effective against osteosarcoma. *Aging (Albany NY)* 13 (12), 16425–16444. doi:10.18632/aging.203165

Wu, Z., Xi, Z., Xiao, Y., Zhao, X., Li, J., Feng, N., et al. (2022). TSH-TSHR axis promotes tumor immune evasion. *J. Immunother. Cancer* 10 (1), e004049. doi:10.1136/jitc-2021-004049

Xiang, W., Yang, C. Y., and Bai, L. (2018). MCL-1 inhibition in cancer treatment. *Onco Targets Ther.* 11, 7301–7314. doi:10.2147/ott.S146228

Xu, S., Tang, L., Li, X., Fan, F., and Liu, Z. (2020). Immunotherapy for glioma: Current management and future application. *Cancer Lett.* 476, 1–12. doi:10.1016/j.canlet.2020.02.002

Yang, W., Wang, S., Zhang, X., Sun, H., Zhang, M., Chen, H., et al. (2022). New natural compound inhibitors of PDGFRA (platelet-derived growth factor receptor α) based on computational study for high-grade glioma therapy. *Front. Neurosci.* 16, 1060012. doi:10.3389/fnins.2022.1060012

Ye, X. Y., Xu, L., Lu, S., and Chen, Z. W. (2019). MiR-516a-5p inhibits the proliferation of non-small cell lung cancer by targeting HIST3H2A. *Int. J. Immunopathol. Pharmacol.* 33, 2058738419841481. doi:10.1177/2058738419841481

You, W. C., Lee, H. D., Pan, H. C., and Chen, H. C. (2023). Re-Irradiation combined with bevacizumab for recurrent glioblastoma beyond bevacizumab failure: Survival outcomes and prognostic factors. *Sci. Rep.* 13 (1), 9442. doi:10.1038/s41598-023-36290-2

Yuan, B., Wang, G., Tang, X., Tong, A., and Zhou, L. (2022). Immunotherapy of glioblastoma: Recent advances and future prospects. *Hum. Vaccin Immunother.* 18 (5), 2055417. doi:10.1080/21645515.2022.2055417

Zhong, S., Wu, B., Yang, W., Ge, J., Zhang, X., Chen, Z., et al. (2021). Effective natural inhibitors targeting poly ADP-ribose polymerase by computational study. *Aging (Albany NY)* 13 (2), 1898–1912. doi:10.18632/aging.103986

Zhong, S., Zhang, Z., Guo, Z., Yang, W., Dou, G., Lv, X., et al. (2022). Identification of novel natural inhibitors targeting AKT Serine/Threonine Kinase 1 (AKT1) by computational study. *Bioengineered* 13 (5), 12003–12020. doi:10.1080/21655979.2021.2011631

frontiers | Frontiers in Oncology

TYPE Original Research
PUBLISHED 21 August 2023
DOI 10.3389/fonc.2023.1185466

OPEN ACCESS

EDITED BY
Wei Wang,
Massachusetts General Hospital and Harvard Medical School, United States

REVIEWED BY
Feng Lin,
Jilin University, China
Jorge Matias-Guiu,
Complutense University of Madrid, Spain
Xu-zhao Li,
Guizhou University of Traditional Chinese Medicine, China

*CORRESPONDENCE
Jiajun Dong
dongjiajun408@126.com

†These authors have contributed equally to this work and share first authorship

RECEIVED 13 March 2023
ACCEPTED 01 August 2023
PUBLISHED 21 August 2023

CITATION
Dong J, Wang S, Xie H, Mou Y, Zhu H, Peng Y, Xi J, Zhong M, Xie Z, Jiang Z, Wang K, Chen H, Yang W, Zhu M, Wen Y and Wu Y (2023) COVID–19 hospitalization increases the risk of developing glioblastoma: a bidirectional Mendelian-randomization study.
Front. Oncol. 13:1185466.
doi: 10.3389/fonc.2023.1185466

COVID–19 hospitalization increases the risk of developing glioblastoma: a bidirectional Mendelian-randomization study

Jiajun Dong[1†*], Shengnan Wang[2†], Haoqun Xie[3], Yanhao Mou[4], Hao Zhu[5], Yilong Peng[1], Jianxin Xi[6], Minggu Zhong[1], Zhengyuan Xie[1], Zongyuan Jiang[1], Kang Wang[1], Hongyu Chen[3], Wenzhuo Yang[3], Mingqin Zhu[2], Yufeng Wen[7] and Yi Wu[1]

[1]Department of Neurosurgery, Jiangmen Central Hospital, Jiangmen, China, [2]Department of Neurology, The First Hospital of Jilin University, Changchun, China, [3]Department of Neurosurgery, Cancer Hospital of Sun Yat sen University, Guangzhou, China, [4]Department of Neurosurgery, State Key Laboratory of Oncology in South China, Collaborative Innovation Center for Cancer Medicine, Sun Yat-sen University Cancer Center, Guangzhou, China, [5]Department of Hepatology, The First Hospital of Jilin University, Changchun, China, [6]Clinical College, Jilin University, Changchun, China, [7]Department of Bioengineering, University of Texas at Arlington, Arlington, TX, United States

Background: As a result of the COVID-19 pandemic, patients with glioblastoma (GBM) are considered a highly vulnerable population. Despite this, the extent of the causative relationship between GBM and COVID-19 infection is uncertain.

Methods: Genetic instruments for SARS-CoV-2 infection (38,984 cases and 1,644,784 control individuals), COVID-19 hospitalization (8,316 cases and 1,549,095 control individuals), and COVID-19 severity (4,792 cases and 1,054,664 control individuals) were obtained from a genome-wide association study (GWAS) from European populations. A total of 6,183 GBM cases and 18,169 controls from GWAS were enrolled in our study. Their associations were evaluated by applying Mendelian randomization (MR) including IVW meta-analysis, MR-Egger regression, and weighted-median analysis. To make the conclusions more robust and reliable, sensitivity analyses were performed.

Results: Our results showed that genetically predicted COVID–19 hospitalization increases the risk of GBM (OR = 1.202, 95% CI = 1.035–1.395, p = 0.016). In addition, no increased risk of SARS-CoV-2 infection, COVID-19 hospitalization and severity were observed in patients with any type of genetically predicted GBM.

Conclusion: Our MR study indicated for the first time that genetically predicted COVID–19 hospitalization was demonstrated as a risk factor for the development of GBM.

KEYWORDS

Mendelian randomization, COVID-19, SARS-CoV-2, glioblastoma, genome-wide association study

1 Introduction

In Coronavirus disease 2019 (COVID-19), the severe acute respiratory syndrome Coronavirus 2 (SARS-CoV-2) is responsible for the illness (1). Since January 1, 2023, more than 661 million people have died from COVID-19, which has caused the tragic loss of over 6 million lives. Coronavirus infections may cause acute cardiac or kidney injury, acute respiratory distress syndrome, shock, secondary infection, cancer, and high mortality risk (2). According to epidemiological studies, cancer is an independent adverse prognostic factor for COVID-19 outcomes, including admission to the intensive care unit and invasive ventilation (3–5). It is especially true for patients suffering from glioblastoma (GBM), which is one of the most aggressive and common types of primary brain tumor. Several factors make GBM patients one of the most fragile and vulnerable cancer populations. Firstly, GBM patients tend to be old age and have multiple age-related comorbidities. Additionally, their large use of steroid medications further increases immunosuppression. Furthermore, there is an increased risk of tumor and/or chemotherapy-related thromboembolic events due to the patient's loss of autonomy. These result in a greater susceptibility to infection (6).

Besides, the role of COVID-19 in GBM was also a topic of interest. Angiotensin-converting enzyme 2 (ACE2) receptor molecules on the cell membrane interact with the viral spike (S) glycoprotein to allow viral entry (7). According to several studies, the viral S protein binds to the VEGFR (Vascular Endothelial Growth Factor Receptor) and the EGFR (Epidermal Growth Factor Receptor) more frequently in GBM cells than in other types of cancer cells, contributing to their development (8). It has been suggested that COVID-19 infections are associated with a unique brain predisposition to thrombosis caused by cytokine storms (9), which is correlated with faster GBM development. Poor prognosis is associated with tumor thrombus in GBM (10).

Several studies have shown a close relationship between GBM and COVID-19 susceptibility and severity, and traditional observational studies are biased by unmeasured confounding factors, making it difficult to speculate on their causal relationship (6, 11–13). However, observational studies are susceptible to unmeasured confounding or reverse causality. Single-nucleotide polymorphisms (SNPs) are used as instrumental variables (IVs) in Mendelian randomization (MR) studies to examine causal relationships between risk factors and outcomes (14, 15). We used the MR method to evaluate the causal associations between GBM and COVID-19 outcomes, given the limitations of the current research.

2 Methods

2.1 Study design

The overall design of our MR study exploring the causal relationships between GBM and COVID-19 outcomes can be seen in Figure 1. The study was conducted on a bidirectional two-sample univariable design. To estimate the causal effects of GBM on COVID-19, a genetically predicted GBM risk is used as an exposure and COVID-19 severity, hospitalization, or susceptibility is used as an outcome (16, 17). Based on genetically predicted COVID-19 severity, hospitalization, and susceptibility risks, we estimate the causal effects of COVID-19 on GBM. MR analysis is based on three critical assumptions: (i) There is a strong association between exposure and IVs; (ii) Confounders should not affect IVs due to exposure and outcome; and (iii) Only exposure mediates IV-outcome associations.

2.2 Data sources and instruments selection

We obtained summary-level GWAS data for the datasets of genetically predicted COVID-19 risk (38,984 cases and 1,644,784 control individuals for SARS-CoV-2 infection, 8,316 cases and 1,549,095 control individuals for COVID-19 hospitalization, and 4,792 cases and 1,054,664 control individuals for COVID-19 severity) (18). Participants in this GWAS were from the COVID-19 Host Genetics Initiative, which is publicly available (19). Those with very severe respiratory confirmed COVID-19 were defined as those hospitalized for lab confirmed SARS-CoV-2 infection and

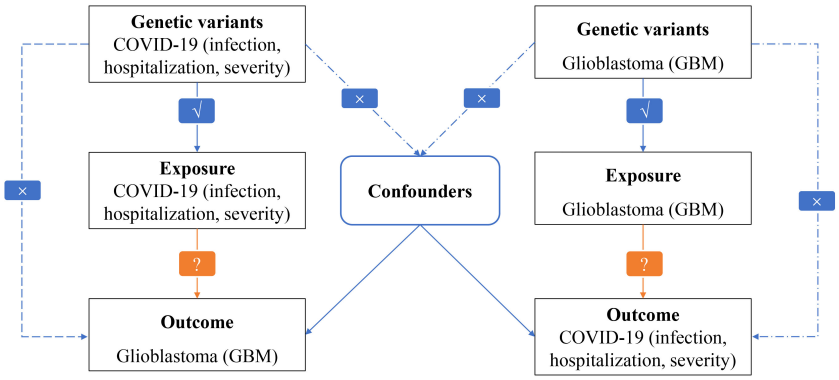

FIGURE 1
Flowchart of MR analysis in this study.

dying or requiring respiratory support (20). GBM is defined as glioblastoma (World Health Organization grade IV). GBM genotyping data were derived from a meta-analysis of GWAS, which included 6183 cases and 18169 controls (21). We provided comprehensive details of the genotyping and quality control of COVID-19 and GBM's GWASs (Supplementary Table 1). We used 1000-Genome imputed GWAS data from the European GWAS (22). The mean sample size was larger for COVID-19 and GBM traits, so the genome-wide significance threshold ($p < 5\times10^{-9}$) was used to avoid selecting false positive instruments. In the European 1000G reference panel, SNPs with the lowest p-values were retained as independent SNPs after pruning all SNPs in linkage disequilibrium (LD; $r^2 < 0.0001$) (23).. We cross-checked the Phenoscanner database (http://www.phenoscanner.medschl.cam.ac.uk/) to identify SNPs associated with the exposure that could potentially be linked to confounding variables or outcomes. We calculated the F-statistic for each SNP to evaluate the strength of the IVs (24, 25). Instruments with an F-statistic below 10 are considered weak (26). Supplementary Table 2 showed the characteristics of all the SNPs included in our analysis.

2.3 Statistical analysis

Several MR analytical methods were used to assess the causal effects and evaluate the potential pleiotropic effects of genetic variants. The main analysis was conducted using inverse-variance weighted (IVW) regression, which assumes no directional pleiotropic effects of individual instrumental variables (27). Weighted median and MR-Egger regression methods were used in complementary analyses (28). Additionally, we conducted sensitivity analyses using the Mendelian Randomization Pleiotropy RESidual Sum and Outlier (MR-PRESSO) global test, MR-Egger intercept, and leave-one-out sensitivity analysis. The sensitivity analysis was tested using a leave-one-out sensitivity analysis by removing each SNP from the analysis and re-estimating its causal effect (29). The horizontal pleiotropy of IVs was assessed by MR-PRESSO and MR-Egger intercept methods ($p< 0.05$ was considered significant) (30). SNPs with outliers are investigated in the MR-PRESSO global test (31). To test heterogeneity, IVW, and MR-Egger in Cochran's Q statistic were used ($p< 0.05$ was considered significant) (32, 33). If the results of the IVW method are significant ($p< 0.05$), and no pleiotropy and heterogeneity were found, even if the results of other methods were not significant, as long as the beta values of other methods were in the same direction, they could be considered as positive results (34). In R (version 4.2.1), MRPRESSO (version 1.0) and TwoSampleMR (version 0.5.6) were used for the analyses.

3 Results

A comparison of MR estimates obtained from different methods of determining whether COVID-19 causes GBM is presented in Table 1. The IVW analysis revealed that the genetically determined COVID-19 hospitalized patients were at higher risk of developing GBM than the general population (OR = 1.202, 95% CI = 1.035–1.395, p = 0.016) (Figure 2). According to the MR-Egger intercept, there was no evidence of horizontal pleiotropy (p=0.918). Additionally, there was no obvious heterogeneity (all p-values were >0.05). In leave-one-out analysis, the effect of COVID-19 SNPs on GBM was robust. For sensitivity analysis, leave-one-out

TABLE 1 Association of COVID-19 genetic IVs with GBM GWAS.

Exposure	Outcome	Method	Number of snps	Beta	P	OR (95% CI)	P for heterogeneity test	P for MR-Egger intercept
SARS-CoV-2 infection	GBM	IVW	4	-0.016	0.934	0.984 (0.676-1.434)	0.184	
		MR Egger	4	-0.553	0.418	0.575 (0.197-1.677)	0.210	0.404
		Weighted median	4	-0.096	0.610	0.908 (0.627-1.314)		
COVID-19 severity		IVW	6	0.089	0.125	1.093 (0.976-1.225)	0.194	
		MR Egger	6	-0.384	0.139	0.681 (0.453-1.024)	0.750	0.080
		Weighted median	6	0.082	0.181	1.086 (0.962-1.225)		
COVID-19 hospitalization (significant)		IVW	5	0.184	0.016	1.202 (1.035-1.395)	0.271	
		MR Egger	5	0.288	0.778	1.334 (0.213-8.364)	0.162	0.918
		Weighted median	5	0.127	0.168	1.135 (0.948-1.360)		

OR, Odds Radio; IVs, Instrumental variables.

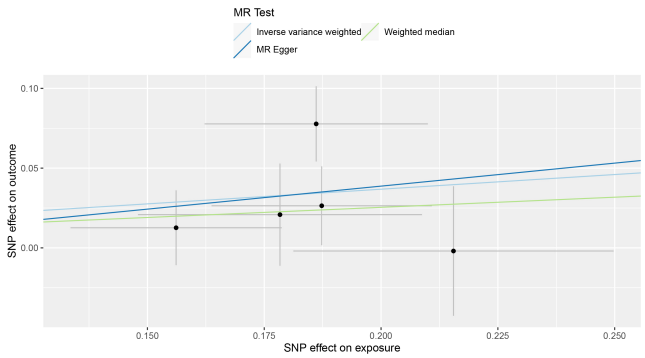

FIGURE 2
Individual estimates about the putative causal effect of COVID-19 hospitalization on the risk of GBM.

studies were used and showed no influence (Figure 3). Furthermore, no significant association was found between severe COVID-19, SARS-CoV-2 infection, and the risk of GBM.

With the same approach, we predicted the association between genetically predicted GBM and COVID-19 risk. All MR methods did not indicate an association between genetically predicted GBM and SARS-CoV-2 infection, COVID-19 hospitalization, or severity. MR, heterogeneity, pleiotropy, and sensitivity analyses of all methods associated with genetically predicted GBM and COVID-19 risk are summarized in Table 2.

4 Discussion

According to epidemiological studies, cancer is an independent adverse prognostic factor for COVID-19 (3). Due to a higher incidence of GBM in the elderly population, frequent hospitalizations, and treatment-related immunosuppression, COVID-19 is a pandemic that affects many patients with GBM (35, 36). The treatment of patients with high-grade gliomas has already been recommended by several expert groups (6, 37). Some preliminary cross-sectional studies have also supported the hypothesis that patients with GBM are biologically vulnerable to COVID-19 (38, 39). Methodological biases and unmeasured confounders prevented the causality of the association from being established. We investigated the causal relationship between GBM and COVID-19 susceptibility, hospitalization, and severity using public GWAS data.

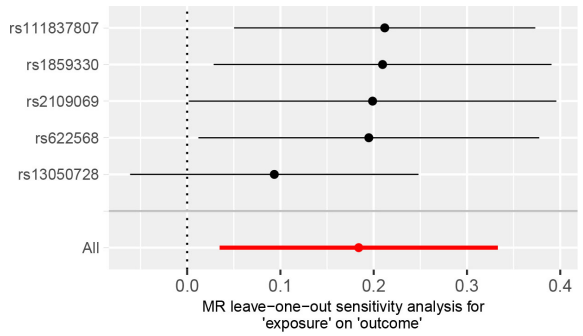

FIGURE 3
MR leave-one-out sensitivity analysis for the effect of COVID-19 hospitalization SNPs on the risk of GBM.

The results of our MR analyses showed that genetically predicted COVID-19 hospitalization risk significantly increased the risk of GBM in the European population (OR = 1.202, 95% CI = 1.035–1.395, p = 0.016). The following mechanism might explain our results. As a receptor for human Coronavirus-229E (40), Alanyl aminopeptidase (ANPEP) plays an important role in the entry of SARS-CoV-2 into cells (41, 42). Based on its co-expression with ACE2, glutamyl aminopeptidase (ENPEP) has been identified as a candidate co-receptor for SARS-CoV-2 (42, 43). COVID-19 infection results in increased distribution of ENPEP and ANPEP in endothelial cells of the blood-brain barrier, providing the place for SARS-CoV-2 cell entry into the brain. Six receptors were analyzed for survival in GBM cells in a study, and it was found that ANPEP and ENPEP have a beneficial effect on survival. This increases the susceptibility of SARS-CoV-2 to GBM (44).

Healthy human lungs contain large amounts of 27-hydroxycholesterol (27-OHC) produced by macrophages in the alveoli (45). 27-OHC prevents the virus's lipid envelope from fusing with the host cell membrane, making it difficult for the virus to enter the cell (46). Concentrations of 27-OHC will increase during the presence of COVID-19 infection in lung tissue and blood (47). At the same time, 27-OHC can also promote the growth of glioblastoma tumor cells *in vitro* by stimulating cell division, promoting cell migration and invasion (48). High levels of oxysterols found in glioblastoma tumors isolated from patients were associated with a poorer prognosis. Moreover, the findings confirmed that COVID-19 promotes the malignant behavior of GBM cells. Additionally, there is a possibility that COVID-19-associated coagulopathy could affect long-term tumor behavior and disease progression in GBM in a manner that has not yet been recognized.

According to our MR analyses, genetically predicted GBM risk is not associated with COVID-19 susceptibility, hospitalization, or severity in the European population. This differs from the findings of several preliminary cross-sectional studies (5, 49). Examples of possible confounding factors include the following: the severe

TABLE 2 Association of GBM genetic IVs with COVID-19 GWAS.

Outcome	Exposure	Method	Number of snps	Beta	P	OR (95%CI)	P for heterogeneity test	P for MR-Egger intercept
GBM	SARS-CoV-2 infection	IVW	7	-0.017	0.213	0.983 (0.958-1.047)	0.543	
		MR Egger	7	0.020	0.591	1.020 (0.954-1.050)	0.599	0.299
		Weighted median	7	-0.018	0.269	0.982 (0.952-0.987)		
	COVID-19 severity	IVW	7	-0.045	0.370	0.956 (0.867-1.186)	0.246	
		MR Egger	7	0.073	0.612	1.075 (0.826-1.295)	0.243	0.390
		Weighted median	7	-0.005	0.922	0.995 (0.892-1.068)		
	COVID-19 hospitalization	IVW	7	-0.044	0.171	0.957 (0.899-1.066)	0.745	
		MR Egger	7	0.001	0.988	1.001 (0.851-1.111)	0.677	0.581
		Weighted median	7	-0.057	0.138	0.954 (0.876-1.078)		

OR, Odds Radio; IVs, Instrumental variables.

lymphopenia often associated with disease or treatment (e.g., alkylating agents like nitrosourea and temozolomide), a frequent presence of neurological deficits resulting in a loss of autonomy in daily living activities and an increased risk of thromboembolic events, an increase in infection susceptibility as a result of chronic use of steroids to treat brain edema, and finally comorbidities and frailties associated with aging. Additionally, since most patients with GBM are hospitalized patients, the detection rate of COVID-19 in this situation may be higher than that in the non-hospitalized population. As a result, the COVID-19 incidence can appear to be higher in cancerous populations when the detection rate is confused with the actual incidence.

Our study has significant clinical implications. First, it has not been clear in the past whether COVID-19 increases the risk of GBM in patients without prior malignancies. In this study, we used Mendelian randomization to reveal that COVID−19 hospitalization increases the risk of developing glioblastoma. This suggests that cancer development is one such foreseeable COVID-19 sequelae since chronic inflammation is long-established to be a fertile ground for oncogenesis, especially for hospitalized patient. Better prevention of COVID-19 and possibly better evidence-based treatment of COVID-19 is warranted in these patients. Second, in our study, genetically predicted GBM risk is not associated with COVID-19 susceptibility, hospitalization, or severity in the European population. This will help us better allocate medical resources.

Our study, however, has several limitations. First, the results of other MR methods showed a consistent but nonsignificant direction. The best results would be obtained if all three methods were significant. The IVW approach, however, is statistically significantly more powerful than the other MR approaches, including MR-Egger (50). The requirement for MR approaches to follow a consistent beta direction has also been strengthened by research. We used this requirement in our study as well (51, 52). In addition, although our data did not show that a genetic predisposition to GBM is associated with COVID-19 susceptibility or severity, it is not appropriate for patients to assume that these patients can be treated at the same level as the general population for medical surveillance management. The third issue is that the sample is of mixed European ancestry. More studies should be carried out on other ethnic groups or immigrants to prove that the same relationship exists. Fourth, we don't know what percentage of COVID-19 patients already have symptoms that may be related to glioblastoma. We are also unable to analyze the period after COVID-19 when risk arises, and the information provided for control groups remains incomplete.

In conclusion, even though our analysis suggests a causal link between genetically increased COVID-19 and increased risk of GBM, further studies are needed to determine the mechanism behind this association. To optimize the allocation of healthcare resources, it is crucial to identify those who are susceptible to SARS-CoV-2 and those who are prone to severe illness (53).

Data availability statement

Human data used in this study are publicly available. The database of Genotypes and Phenotypes (dbGaP) contains genotype data from the GWAS for the Glioma International Case-Control Consortium Study under accession phs001319.v1.p1. GWAS Data on

COVID-19 is available for download from the website: COVID19-hg GWAS meta-analyses round 5 (covid19hg.org).

Author contributions

SW and JD drafted the article and contributed to its editing and revision. A bioinformatic analysis was conducted by HX, HZ, MQZ, and WY. JX, YP, MGZ, ZX, ZJ, KW, YW, YM and HC was responsible for the collation and analysis of the data. The manuscript was substantively edited by JD, and all authors have approved the final version.

Funding

This study was supported by the Digital Medicine and Additive Manufacturing Engineering Technology Research Center of Jiangmen Engineering Technology Research Center.

Acknowledgments

We thank Melin BS et al. for uploading the GBM Public GWAS, and Andrea Ganna et al. for founding the COVID-19 Host Genetics Project.

Conflict of interest

The authors declare that the research was conducted in the absence of any commercial or financial relationships that could be construed as a potential conflict of interest.

The reviewer, FL, declared a shared parent affiliation with the authors SW, JX, HZ and MQZ to the handling editor at the time of review.

Publisher's note

Supplementary material

The Supplementary Material for this article can be found online at: https://www.frontiersin.org/articles/10.3389/fonc.2023.1185466/full#supplementary-material

References

1. Ismail II, Salama S. Association of CNS demyelination and COVID-19 infection: an updated systematic review. *J Neurol* (2022) 269(2):541–76. doi: 10.1007/s00415-021-10752-x

2. Huang C, Wang Y, Li X, Ren L, Zhao J, Hu Y, et al. Clinical features of patients infected with 2019 novel coronavirus in Wuhan, China. *Lancet* (2020) 395(10223):497–506. doi: 10.1016/s0140-6736(20)30183-5

3. Zhang H, Han H, He T, Labbe KE, Hernandez AV, Chen H, et al. Clinical characteristics and outcomes of COVID-19-infected cancer patients: A systematic review and meta-analysis. *J Natl Cancer Inst* (2021) 113(4):371–80. doi: 10.1093/jnci/djaa168

4. Tian Y, Qiu X, Wang C, Zhao J, Jiang X, Niu W, et al. Cancer associates with risk and severe events of COVID-19: A systematic review and meta-analysis. *Int J Cancer* (2021) 148(2):363–74. doi: 10.1002/ijc.33213

5. Liang W, Guan W, Chen R, Wang W, Li J, Xu K, et al. Cancer patients in SARS-CoV-2 infection: a nationwide analysis in China. *Lancet Oncol* (2020) 21(3):335–7. doi: 10.1016/s1470-2045(20)30096-6

6. Mohile NA, Blakeley JO, Gatson NTN, Hottinger AF, Lassman AB, Ney DE, et al. Urgent considerations for the neuro-oncologic treatment of patients with gliomas during the COVID-19 pandemic. *Neuro Oncol* (2020) 22(7):912–7. doi: 10.1093/neuonc/noaa090

7. Paules CI, Marston HD, Fauci AS. Coronavirus infections-more than just the common cold. *Jama* (2020) 323(8):707–8. doi: 10.1001/jama.2020.0757

8. Khan I, Hatiboglu MA. Can COVID-19 induce glioma tumorogenesis through binding cell receptors? *Med Hypotheses* (2020) 144:110009. doi: 10.1016/j.mehy.2020.110009

9. Coolen T, Lolli V, Sadeghi N, Rovai A, Trotta N, Taccone FS, et al. Early postmortem brain MRI findings in COVID-19 non-survivors. *Neurology* (2020) 95(14):e2016–27. doi: 10.1212/wnl.0000000000010116

10. Reichard RR, Kashani KB, Boire NA, Constantopoulos E, Guo Y, Lucchinetti CF. Neuropathology of COVID-19: a spectrum of vascular and acute disseminated encephalomyelitis (ADEM)-like pathology. *Acta Neuropathol* (2020) 140(1):1–6. doi: 10.1007/s00401-020-02166-2

11. Zlotnik Y, Gadoth A, Abu-Salameh I, Horev A, Novoa R, Ifergane G. Case report: anti-LGI1 encephalitis following COVID-19 vaccination. *Front Immunol* (2021) 12:813487. doi: 10.3389/fimmu.2021.813487

12. Liu X, Guo C, Leng T, Fan Z, Mai J, Chen J, et al. Disease, Differential regulation of H3K9/H3K14 acetylation by small molecules drives neuron-fate-induction of glioma cell. *Cell Death Dis* (2023) 14(2):142. doi: 10.1038/s41419-023-05611-8

13. Zhong S, Ren J-X, Yu Z-P, Peng Y-D, Yu C-W, Deng D, et al. Predicting glioblastoma molecular subtypes and prognosis with a multimodal model integrating convolutional neural network, radiomics, and semantics. *J Neurosurg.* (2022) 1–10. doi: 10.3171/2022.10.JNS22801

14. Hartwig FP, Borges MC, Horta BL, Bowden J, Davey Smith G. Inflammatory biomarkers and risk of schizophrenia: A 2-sample mendelian randomization study. *JAMA Psychiatry* (2017) 74(12):1226–33. doi: 10.1001/jamapsychiatry.2017.3191

15. Sekula P, Del Greco MF, Pattaro C, Köttgen A. Mendelian randomization as an approach to assess causality using observational data. *J Am Soc Nephrol* (2016) 27(11):3253–65. doi: 10.1681/asn.2016010098

16. Zhang Z, Wang S, Ren F, Yang L, Xie H, Pan L, et al. Inflammatory factors and risk of meningiomas: a bidirectional mendelian-randomization study. *Front Neurosci* (2023) 17:1186312. doi: 10.3389/fnins.2023.1186312

17. Wang S, Pan L, Wu R, Shao Y, Xue M, Zhu H, et al. Oily fish and raw vegetable consumption can decrease the risk of AQP4-positive neuromyelitis optica spectrum disorders: a Mendelian-randomization study. *Sci Rep* (2023) 13(1):9372. doi: 10.1038/s41598-023-36372-1

18. A first update on mapping the human genetic architecture of COVID-19. *Nature* (2022) 608(7921):E1–e10. doi: 10.1038/s41586-022-04826-7

19. The COVID-19 Host Genetics Initiative, a global initiative to elucidate the role of host genetic factors in susceptibility and severity of the SARS-CoV-2 virus pandemic. *Eur J Hum Genet* (2020) 28(6):715–8. doi: 10.1038/s41431-020-0636-6

20. Yoshikawa M, Asaba K, Nakayama T. Estimating causal effects of genetically predicted type 2 diabetes on COVID-19 in the East Asian population. *Front Endocrinol (Lausanne)* (2022) 13:1014882. doi: 10.3389/fendo.2022.1014882

21. Melin BS, Barnholtz-Sloan JS, Wrensch MR, Johansen C, Il'yasova D, Kinnersley B, et al. Genome-wide association study of glioma subtypes identifies specific differences in genetic susceptibility to glioblastoma and non-glioblastoma tumors. *Nat Genet* (2017) 49(5):789–94. doi: 10.1038/ng.3823

22. Bentham J, Morris DL, Graham DSC, Pinder CL, Tombleson P, Behrens TW, et al. Genetic association analyses implicate aberrant regulation of innate and adaptive immunity genes in the pathogenesis of systemic lupus erythematosus. *Nat Genet* (2015) 47(12):1457–64. doi: 10.1038/ng.3434

23. Georgakis MK, de Lemos JA, Ayers C, Wang B, Björkbacka H, Pana TA, et al. Association of circulating monocyte chemoattractant protein-1 levels with

cardiovascular mortality: A meta-analysis of population-based studies. *JAMA Cardiol* (2021) 6(5):587–92. doi: 10.1001/jamacardio.2020.5392

24. Shim H, Chasman DI, Smith JD, Mora S, Ridker PM, Nickerson DA, et al. A multivariate genome-wide association analysis of 10 LDL subfractions, and their response to statin treatment, in 1868 Caucasians. *PloS One* (2015) 10(4):e0120758. doi: 10.1371/journal.pone.0120758

25. Yarmolinsky J, Bonilla C, Haycock PC, Langdon RJQ, Lotta LA, Langenberg C, et al. Circulating selenium and prostate cancer risk: A mendelian randomization analysis. *J Natl Cancer Inst* (2018) 110(9):1035–8. doi: 10.1093/jnci/djy081

26. Burgess S, Small DS, Thompson SG. A review of instrumental variable estimators for Mendelian randomization. *Stat Methods Med Res* (2017) 26(5):2333–55. doi: 10.1177/0962280215597579

27. Burgess S, Scott RA, Timpson NJ, Davey Smith G, Thompson SG. Using published data in Mendelian randomization: a blueprint for efficient identification of causal risk factors. *Eur J Epidemiol* (2015) 30(7):543–52. doi: 10.1007/s10654-015-0011-z

28. Larsson SC, Scott RA, Traylor M, Langenberg CC, Hindy G, Melander O, et al. Type 2 diabetes, glucose, insulin, BMI, and ischemic stroke subtypes: Mendelian randomization study. *Neurology* (2017) 89(5):454–60. doi: 10.1212/wnl.0000000000004173

29. Burgess S, Davey Smith G, Davies NM, Dudbridge F, Gill D, Glymour MM, et al. Guidelines for performing Mendelian randomization investigations. *Wellcome Open Res* (2019) 4. doi: 10.12688/wellcomeopenres.15555.2

30. Aung N, Khanji MY, Munroe PB, Petersen SE. Causal inference for genetic obesity, cardiometabolic profile and COVID-19 susceptibility: A mendelian randomization study. *Front Genet* (2020) 11:586308. doi: 10.3389/fgene.2020.586308

31. Verbanck M, Chen CY, Neale B, Do R. Detection of widespread horizontal pleiotropy in causal relationships inferred from Mendelian randomization between complex traits and diseases. *Nat Genet* (2018) 50(5):693–8. doi: 10.1038/s41588-018-0099-7

32. Greco MF, Minelli C, Sheehan NA, Thompson JR. Detecting pleiotropy in Mendelian randomisation studies with summary data and a continuous outcome. *Stat Med* (2015) 34(21):2926–40. doi: 10.1002/sim.6522

33. Liu G, Zhang S, Cai Z, Ma G, Zhang L, Jiang Y, et al. PICALM gene rs3851179 polymorphism contributes to Alzheimer's disease in an Asian population. *Neuromol Med* (2013) 15(2):384–8. doi: 10.1007/s12017-013-8225-2

34. Chen X, Hong X, Gao W, Luo S, Cai J, Liu G, et al. Causal relationship between physical activity, leisure sedentary behaviors and COVID-19 risk: a Mendelian randomization study. *J Transl Med* (2022) 20(1):216. doi: 10.1186/s12967-022-03407-6

35. Ostrom QT, Cioffi G, Gittleman H, Patil N, Waite K, Kruchko C, et al. CBTRUS statistical report: primary brain and other central nervous system tumors diagnosed in the United States in 2012-2016. *Neuro Oncol* (2019) 21(Suppl 5):v1–v100. doi: 10.1093/neuonc/noz150

36. Gatson NTN, Barnholtz-Sloan J, Drappatz J, Henriksson R, Hottinger AF, Hinoul P, et al. Tumor treating fields for glioblastoma therapy during the COVID-19 pandemic. *Front Oncol* (2021) 11:679702. doi: 10.3389/fonc.2021.679702

37. Bernhardt D, Wick W, Weiss SE, Sahgal A, Lo SS, Suh JH, et al. Neuro-oncology management during the COVID-19 pandemic with a focus on WHO grade III and IV gliomas. *Neuro Oncol* (2020) 22(7):928–35. doi: 10.1093/neuonc/noaa113

38. Dai M, Liu D, Liu M, Zhou F, Li G, Chen Z, et al. Patients with cancer appear more vulnerable to SARS-coV-2: A multicenter study during the COVID-19 outbreak. *Cancer Discovery* (2020) 10(6):783–91. doi: 10.1158/2159-8290.Cd-20-0422

39. Moujaess E, Kourie HR, Ghosn M. Cancer patients and research during COVID-19 pandemic: A systematic review of current evidence. *Crit Rev Oncol Hematol* (2020) 150:102972. doi: 10.1016/j.critrevonc.2020.102972

40. Millet JK, Jaimes JA, Whittaker GR. Molecular diversity of coronavirus host cell entry receptors. *FEMS Microbiol Rev* (2021) 45(3). doi: 10.1093/femsre/fuaa057

41. Tang D, Comish P, Kang R. The hallmarks of COVID-19 disease. *PloS Pathog* (2020) 16(5):e1008536. doi: 10.1371/journal.ppat.1008536

42. Qi F, Qian S, Zhang S, Zhang Z. Single cell RNA sequencing of 13 human tissues identify cell types and receptors of human coronaviruses. *Biochem Biophys Res Commun* (2020) 526(1):135–40. doi: 10.1016/j.bbrc.2020.03.044

43. Tripathi SC, Deshmukh V, Creighton CJ, Patil A. Renal carcinoma is associated with increased risk of coronavirus infections. *Front Mol Biosci* (2020) 7:579422. doi: 10.3389/fmolb.2020.579422

44. Chen A, Zhao W, Li X, Sun G, Ma Z, Peng L, et al. Comprehensive oncogenic features of coronavirus receptors in glioblastoma multiforme. *Front Immunol* (2022) 13:840785. doi: 10.3389/fimmu.2022.840785

45. Kikuchi T, Sugiura H, Koarai A, Ichikawa T, Minakata Y, Matsunaga K, et al. Increase of 27-hydroxycholesterol in the airways of patients with COPD: possible role of 27-hydroxycholesterol in tissue fibrosis. *Chest* (2012) 142(2):329–37. doi: 10.1378/chest.11-2091

46. Cagno V, Civra A, Rossin D, Calfapietra S, Caccia C, Leoni V, et al. Inhibition of herpes simplex-1 virus replication by 25-hydroxycholesterol and 27-hydroxycholesterol. *Redox Biol* (2017) 12:522–7. doi: 10.1016/j.redox.2017.03.016

47. Marcello A, Civra A, Milan Bonotto R, Nascimento Alves L, Rajasekharan S, Giacobone C, et al. The cholesterol metabolite 27-hydroxycholesterol inhibits SARS-CoV-2 and is markedly decreased in COVID-19 patients. *Redox Biol* (2020) 36:101682. doi: 10.1016/j.redox.2020.101682

48. Liu L, Li MY, Xing Y, Wang XY, Wang Y. The oncogenic roles of 27-hydroxycholesterol in glioblastoma. *Oncol Lett* (2019) 18(4):3623–9. doi: 10.3892/ol.2019.10690

49. Zhang Y, Mao Q, Li Y, Cheng J, Xia Q, Chen G, et al. Cancer and COVID-19 susceptibility and severity: A two-sample mendelian randomization and bioinformatic analysis. *Front Cell Dev Biol* (2021) 9:759257. doi: 10.3389/fcell.2021.759257

50. Lin Z, Deng Y, Pan W. Combining the strengths of inverse-variance weighting and Egger regression in Mendelian randomization using a mixture of regressions model. *PloS Genet* (2021) 17(11):e1009922. doi: 10.1371/journal.pgen.1009922

51. Bowden J, Del Greco MF, Minelli C, Davey Smith G, Sheehan NA, Thompson JR. Assessing the suitability of summary data for two-sample Mendelian randomization analyses using MR-Egger regression: the role of the I2 statistic. *Int J Epidemiol* (2016) 45(6):1961–74. doi: 10.1093/ije/dyw220

52. Venkatesh SS, Ferreira T, Benonisdottir S, Rahmioglu N, Becker CM, Granne I, et al. Obesity and risk of female reproductive conditions: A Mendelian randomisation study. *PloS Med* (2022) 19(2). doi: 10.1371/journal.pmed.1003679

53. Li Z, Wei Y, Zhu G, Wang M, Zhang L. Cancers and COVID-19 risk: A mendelian randomization study. *Cancers (Basel)* (2022) 14(9). doi: 10.3390/cancers14092086

frontiers | Frontiers in Pharmacology

TYPE Original Research
PUBLISHED 02 November 2023
DOI 10.3389/fphar.2023.1247812

OPEN ACCESS

EDITED BY
Dianwen Ju,
Fudan University, China

REVIEWED BY
Joseph Paul McElroy,
The Ohio State University, United States
Xinmao Song,
Fudan University, China

*CORRESPONDENCE
Jian Gong,
gongjian88@tom.com

RECEIVED 26 June 2023
ACCEPTED 19 October 2023
PUBLISHED 02 November 2023

CITATION
Li X and Gong J (2023), Survival nomogram for medulloblastoma and multi-center external validation cohort. *Front. Pharmacol.* 14:1247812. doi: 10.3389/fphar.2023.1247812

Survival nomogram for medulloblastoma and multi-center external validation cohort

Xiang Li[1] and Jian Gong[1,2]*

[1]Department of Pediatric Neurosurgery, Beijing Tiantan Hospital, Capital Medical University, Beijing, China, [2]Beijing Neurosurgical Institute, Capital Medical University, Beijing, China

Background: Medulloblastoma (MB) is a highly malignant neuroepithelial tumor occurring in the central nervous system. The objective of this study was to establish an effective prognostic nomogram to predict the overall survival (OS) of MB patients.

Materials and methods: The nomogram was developed using data from a retrospective cohort of 280 medulloblastoma patients (aged 3–18 years) identified from Beijing Tiantan Hospital between 2016 and 2021 as the training cohort. To validate the performance of the nomogram, collaborations were formed with eight leading pediatric oncology centers across different regions of China. A total of 162 medulloblastoma patients meeting the inclusion criteria were enrolled from these collaborating centers. Cox regression analysis, best subsets regression, and Lasso regression were employed to select independent prognostic factors. The nomogram's prognostic effectiveness for overall survival was assessed using the concordance index, receiver operating characteristic curve, and calibration curve.

Results: In the training cohort, the selected variables through COX regression, best subsets regression, and Lasso regression, along with their clinical significance, included age, molecular subtype, histological type, radiotherapy, chemotherapy, metastasis, and hydrocephalus. The internally and externally validated C-indexes were 0.907 and 0.793, respectively. Calibration curves demonstrated the precise prediction of 1-, 3-, and 5-year OS for MB patients using the nomogram.

Conclusion: This study developed a nomogram that incorporates clinical and molecular factors to predict OS prognosis in medulloblastoma patients. The nomogram exhibited improved predictive accuracy compared to previous studies and demonstrated good performance in the external validation cohort. By considering multiple factors, clinicians can utilize this nomogram as a valuable tool for individualized prognosis prediction and treatment decision-making in medulloblastoma patients.

KEYWORDS

medulloblastoma, training cohort, validation cohort, overall survival, nomogram, end results

1 Introduction

Medulloblastoma, a malignant brain tumor primarily affecting children, remains a significant challenge in pediatric oncology (Gajjar and Robinson, 2014). Despite advancements in treatment modalities, including surgery, radiation therapy, and chemotherapy, the overall prognosis for patients with medulloblastoma varies widely due to tumor heterogeneity and the complex interplay of genetic and clinical factors (Bouffet, 2021). Consequently, accurate prediction of individual patient outcomes is essential for tailoring treatment strategies and improving survival rates. In recent years, the development of prognostics has emerged as a valuable tool in oncology (Iasonos et al., 2008). These predictive models combine various clinical and pathological variables to estimate the likelihood of specific outcomes for patients. Nomograms provide clinicians with a visual representation of the probability of survival or recurrence, facilitating personalized treatment decisions and enhancing patient care.

Building upon this approach, a group of researchers has recently developed a novel Survival Nomogram specifically tailored for medulloblastoma patients (Dasgupta et al., 2019; Zhu et al., 2020; Liu and Sun, 2022). The nomogram incorporates crucial prognostic factors, such as age at diagnosis, histological subtype, resection extent, and molecular subgroup classification. Recent research has found that pathological classification is not strongly correlated with clinical prognosis (Entz-Werle et al., 2008). For medulloblastoma, molecular classification plays a significant role in determining patient outcomes (Northcott et al., 2019). However, studies are scarce that incorporate molecular subtyping into prognostic models. This study introduces a novel approach by integrating molecular subtyping into a clinical prognostic model. By integrating these variables, the nomogram generates a risk score that enables accurate predictions of individual patient survival probabilities.

To validate the efficacy and reliability of the Survival Nomogram, the research team has embarked on a groundbreaking multi-center external validation study. Collaborating with leading pediatric oncology centers across different geographical regions, the study aims to assess the nomogram's performance using an independent cohort of medulloblastoma patients. This approach ensures the generalizability and robustness of the nomogram in diverse clinical settings, enhancing its potential as a practical tool for oncologists worldwide. The multi-center external validation cohort consists of a large sample of medulloblastoma patients spanning various demographics, treatment protocols, and follow-up durations. By comparing the predicted survival probabilities generated by the nomogram with the observed patient outcomes, the researchers will evaluate the nomogram's accuracy, discrimination, and calibration. These analyses will confirm the nomogram's validity and provide insights into its potential limitations and areas for further refinement.

The implications of a validated Survival Nomogram for medulloblastoma are profound. By enabling accurate individualized predictions, this predictive model can guide treatment decisions, helping clinicians strike a delicate balance between aggressive interventions and minimizing long-term treatment-related complications. Moreover, the nomogram promises to optimize clinical trial designs, stratify patients for targeted therapies, and facilitate long-term survivorship planning.

In conclusion, the development and validation of a Survival Nomogram for medulloblastoma represent a significant advancement in pediatric oncology. By harnessing the power of prognostic modeling, this nomogram offers a personalized approach to patient management and prognosis prediction. The ongoing multi-center external validation study aims to provide robust evidence supporting the nomogram's clinical utility and establish it as a valuable tool in the battle against medulloblastoma.

2 Patients and methods

2.1 Study design

This study was designed to develop a Survival Nomogram for medulloblastoma patients and validate its performance using a multi-center external validation cohort.

2.1.1 Nomogram development

a. Patient Selection: A retrospective cohort of 280 medulloblastoma patients (Ages 3–18 years) was identified from Beijing Tiantan Hospital between 2016 and 2021. Only patients with confirmed medulloblastoma diagnosis and complete clinical and molecular data were included. b. Data Collection: Relevant clinical information such as age at diagnosis, histological subtype, metastasis, tumor texture, hydrocephalus, resection extent, and adjuvant therapy details were collected from patient medical records. Genetic profiling obtained molecular subtyping information, including WNT, SHH, Group 3, and Group 4. c. We have employed three methods for variable selection. Method 1: Univariable Cox and multivariable Cox analysis regression analysis were conducted to screen for potential prognostic variables. Each variable was assessed individually for its association with the survival outcome. Method 2: Best subsets regression (BSR) was performed to screen for variables that showed significant associations with the survival outcome. Different combinations of variables were evaluated, starting with subsets containing only one variable and gradually increasing the size of the subsets. The BSR was used to determine the optimal variable combination by maximizing the adjusted R^2 value. Method 3: Lasso regression, combined with cross-validation, was employed in the variable selection process. This method utilized regularization techniques to shrink the coefficients of irrelevant variables and select the most relevant ones. Lasso regression with cross-validation was used to determine the variable combination by selecting the λ value that corresponds to the minimum mean squared error (MSE).

2.1.2 Final variable selection

After constructing three models through variable selection using the methodologies, we proceeded with a comprehensive analysis. Consequently, a final model, referred to as the "Summary model," was formulated. To determine the most optimal model, we conducted a rigorous comparison of the Akaike information criterion (AIC) and area under the curve (AUC) values among the four models (COX, BSR, Lasso, Summary). This meticulous evaluation allowed us to identify the model with superior predictive performance and robustness, culminating in the selection of the most suitable and reliable model for our study.

2.1.3 External validation cohort

a. Collaboration with Multiple Centers: To validate the nomogram's performance, collaborations were established with eight leading pediatric oncology centers across different regions. b. Patient Enrollment: A total of 162 medulloblastoma patients who met the inclusion criteria were enrolled from the collaborating centers. Detailed clinical and molecular data were collected, including age at diagnosis, histological subtype, metastasis, tumor texture, hydrocephalus, extent of resection, and adjuvant therapy and molecular subtyping. c. Comparative Analysis: The developed nomogram was applied to the external validation cohort. The predicted survival probabilities generated by the nomogram were compared with the observed survival outcomes of the validation cohort. Calibration plots and Harrell's concordance index were performed to assess the nomogram's accuracy and discrimination in the independent patient population. d. The final model compared with the model built using only clinical factors.

Ethical approvals were obtained from the institutional review boards of all participating centers, ensuring patient privacy and data protection. Informed consent was obtained from patients or their legal guardians.

2.1.4 Statistical analyses

Statistical analyses were performed using R software, and the nomogram was constructed using the "rms" package in R software (version 4.2.3). In addition, to build the model in R language, we also used the following packages: "survival," "plyr," "MASS," "leaps," "glmnet," "riskRegression," "ggplot2," "pec" and "ggDCA". A novel nomogram including all the independent prognostic factors was developed to predict 1-, 3- and 5-year OS for medulloblastoma patients. Statistical analysis categorical variables are expressed as percentages and continuous variables as the mean ± standard deviation (SD). All p-values were two-sided, and $p < 0.05$ was considered statistically significant.

3 Results

3.1 Patient baseline characteristics

A total of 280 eligible patients with medulloblastoma were enrolled from Beijing Tiantan Hospital as the training cohort. They had an average age of 7.74 years (SD 3.25). Classic histology was the most common subtype at 68.57%, followed by desmoplastic/nodular at 23.21%, and large cell/anaplastic at 2.86%. Metastasis was present in 17.50% at diagnosis. Hydrocephalus occurred in 88.21% of patients. Gross total resection was achieved in 43.93%, while 56.07% had subtotal resection. Most patients received adjuvant therapy, including chemotherapy (89.29%) and radiotherapy (95.36%). Molecular subtyping revealed Group 3 10.36% and Group 4 50.00% in training cohort, WNT in 14.64%, and SHH-activated subtypes in 25.00%. Apart from molecular subtyping, there were no significant differences observed between males and females in the other variables (chi-square tests). Additionally, 162 cases of patients with medulloblastoma from eight other centers were selected and utilized as the external validation cohort. In the external validation cohort, the patients had an average age of 8.24 years (standard deviation 3.51). Classic histology was the most common subtype, accounting for 77.16%, followed by desmoplastic/nodular at 14.81%, and large cell/anaplastic at 3.70%. Metastasis was present in 14.81% at the time of diagnosis. Hydrocephalus was observed in 76.54% of the patients. Gross total resection was achieved in 80.25% of cases, while 19.75% underwent subtotal resection. The majority of patients received adjuvant therapy, including chemotherapy (81.48%) and radiotherapy (87.65%). Molecular subtyping revealed that 12.35% belonged to Group 3 and 42.59% to Group 4 in the training cohort, 17.90% were classified as WNT subtype, and 27.16% as SHH-activated subtypes. The clinicopathological characteristics of the patients are summarized in Table 1. Some of the risk factors of medulloblastoma previous referenced (Rieken et al., 2011; Guo et al., 2020; Zhu et al., 2020; Liu and Sun, 2022) research utilized included age, gender, tumor size, histological type, extent of surgical resection, radiation therapy, chemotherapy, and metastasis. In our study, we added some significant important variables, including hydrocephalus, tumor texture, and most importantly, molecular subtyping.

3.2 The relationship between pathological classification and molecular classification

The Sankey diagram displays the heterogeneity of pathological classification and molecular subtyping between the training group and the external validation group (Figures 1A, B). Indeed, it is evident that a single pathological classification can correspond to multiple molecular subtypes. Multiple studies have consistently demonstrated a significant correlation between molecular subtypes of medulloblastoma and prognosis (Schwalbe et al., 2017). This represents the complex relationship between pathological classification and molecular classification.

3.3 Feature selection and nomogram construction

A total of nine clinical parameters were included in the training cohort. **Method 1:** In the univariate Cox regression analysis, Molecular subtype, Radiotherapy, Chemotherapy, and Metastasis were associated with OS ($p < 0.05$) (Figure 2A). And the variables selected were then included in the multivariable Cox analysis. The final Cox model included four variables: Molecular subtype, Radiotherapy, Chemotherapy, and Metastasis. The AIC value for this model was 305.7054. **Method 2:** In the BSR analysis, the goal was to identify the best combination of variables based on evaluation criteria, such as minimizing Mallows' Cp, maximizing adjusted R^2, and minimizing the Bayesian information criterion. The analysis aimed to determine the most informative subset of variables for predicting survival in medulloblastoma patients. The results of the best subset regression revealed that a combination of six variables was selected for inclusion in the model. These variables are Molecular subtype, Histological, Radiotherapy, Chemotherapy, Metastasis, and Hydrocephalus. This subset regression analysis

TABLE 1 Patient baseline characteristics.

Characteristics	Training cohort				External validation cohort			
	Male (*N* = 184)	Female (*N* = 96)	Total (*N* = 280)	*p*-value	Male (*N* = 105)	Female (*N* = 57)	Total (*N* = 162)	*p*-value
Age								
Mean ± SD	7.65 ± 3.27	7.91 ± 3.23	7.74 ± 3.25		8.22 ± 3.44	8.28 ± 3.67	8.24 ± 3.51	
Median [min-max]	7.00 [3.00, 18.00]	7.00 [3.00, 15.00]	7.00 [3.00, 18.00]		7.00 [3.00, 17.00]	8.00 [3.00, 17.00]	8.00 [3.00, 17.00]	
Molecular				3.40E−05				0.96
G3	21 (7.50%)	8 (2.86%)	29 (10.36%)		13 (8.02%)	7 (4.32%)	20 (12.35%)	
G4	104 (37.14%)	36 (12.86%)	140 (50.00%)		44 (27.16%)	25 (15.43%)	69 (42.59%)	
SHH	45 (16.07%)	25 (8.93%)	70 (25.00%)		28 (17.28%)	16 (9.88%)	44 (27.16%)	
WNT	14 (5.00%)	27 (9.64%)	41 (14.64%)		20 (12.35%)	9 (5.56%)	29 (17.90%)	
Histological				0.54				0.4
Classic	122 (43.57%)	70 (25.00%)	192 (68.57%)		83 (51.23%)	42 (25.93%)	125 (77.16%)	
Desmoplastic	44 (15.71%)	21 (7.50%)	65 (23.21%)		16 (9.88%)	8 (4.94%)	24 (14.81%)	
Large cell/anapla-stic histology	6 (2.14%)	2 (0.71%)	8 (2.86%)		2 (1.23%)	4 (2.47%)	6 (3.70%)	
Medulloblastoma with extensive nodularity	12 (4.29%)	3 (1.07%)	15 (5.36%)		4 (2.47%)	3 (1.85%)	7 (4.32%)	
Radiotherapy				0.98				0.79
No	8 (2.86%)	5 (1.79%)	13 (4.64%)		14 (8.64%)	6 (3.70%)	20 (12.35%)	
Yes	176 (62.86%)	91 (32.50%)	267 (95.36%)		91 (56.17%)	51 (31.48%)	142 (87.65%)	
Chemotherapy				0.37				0.38
No	17 (6.07%)	13 (4.64%)	30 (10.71%)		22 (13.58%)	8 (4.94%)	30 (18.52%)	
Yes	167 (59.64%)	83 (29.64%)	250 (89.29%)		83 (51.23%)	49 (30.25%)	132 (81.48%)	
Metastasis				0.67				0.62
No	150 (53.57%)	81 (28.93%)	231 (82.50%)		91 (56.17%)	47 (29.01%)	138 (85.19%)	
Yes	34 (12.14%)	15 (5.36%)	49 (17.50%)		14 (8.64%)	10 (6.17%)	24 (14.81%)	
Resection				0.55				0.92
GTR	78 (27.86%)	45 (16.07%)	123 (43.93%)		85 (52.47%)	45 (27.78%)	130 (80.25%)	
STR	106 (37.86%)	51 (18.21%)	157 (56.07%)		20 (12.35%)	12 (7.41%)	32 (19.75%)	
Texture				0.14				0.12
Soft	127 (45.36%)	75 (26.79%)	202 (72.14%)		44 (27.16%)	32 (19.75%)	76 (46.91%)	
Tone	57 (20.36%)	21 (7.50%)	78 (27.86%)		61 (37.65%)	25 (15.43%)	86 (53.09%)	
Hydrocephalus				0.64				0.66
No	20 (7.14%)	13 (4.64%)	33 (11.79%)		23 (14.20%)	15 (9.26%)	38 (23.46%)	
Yes	164 (58.57%)	83 (29.64%)	247 (88.21%)		82 (50.62%)	42 (25.93%)	124 (76.54%)	

GTR, gross total resection; STR, subtotal resection.

10.3389/fphar.2023.1247812

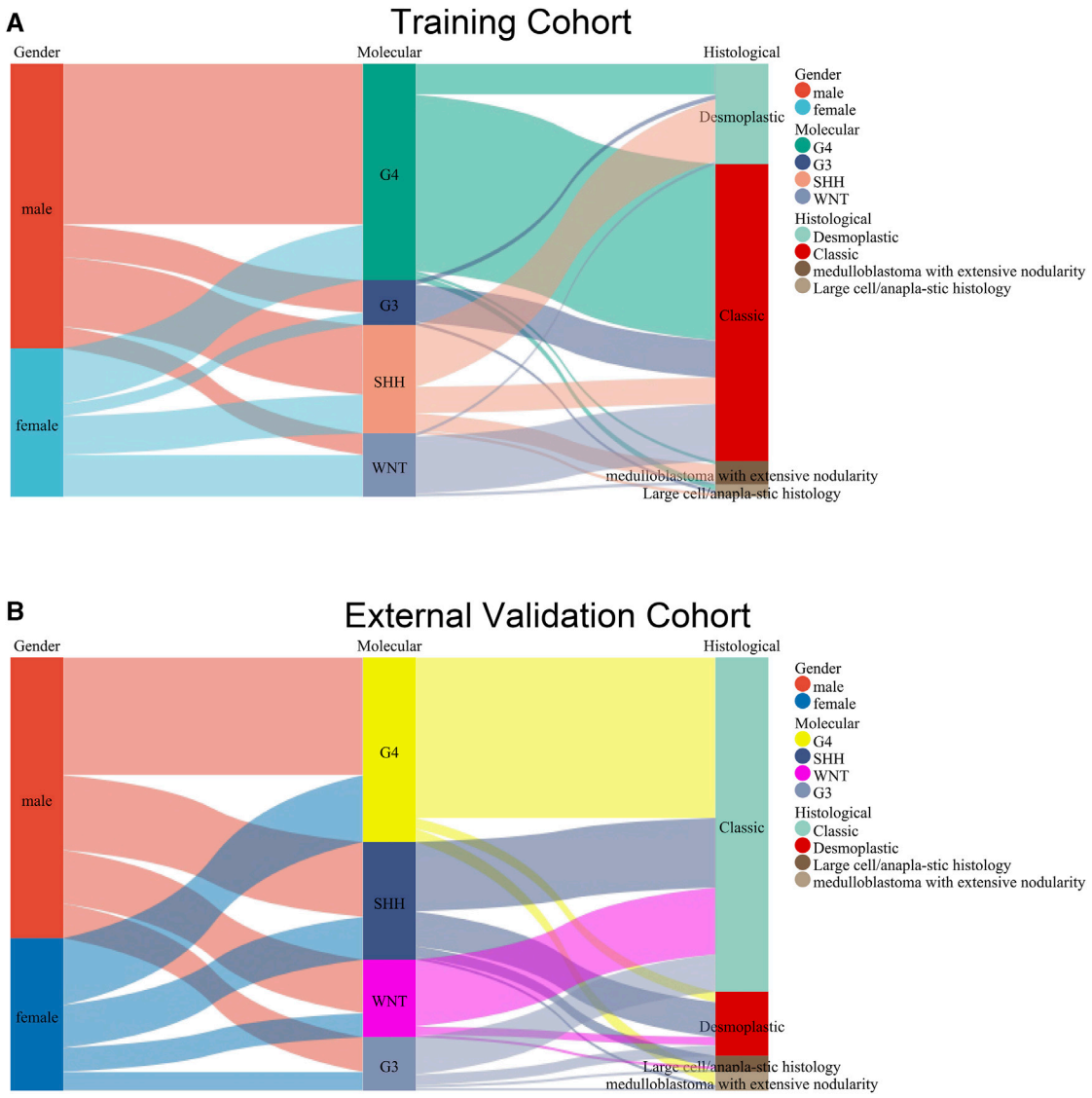

FIGURE 1
Sankey diagram displaying the relationship between pathological classification and molecular subtyping in the training group **(A)** and the external validation group **(B)**.

considered all possible combinations of variables and evaluated their performance based on adjusted R^2. The selected combination of variables demonstrated the highest adjusted R^2 among all evaluated combinations, indicating its strong association with the survival outcome in medulloblastoma patients (Figure 2B). This subset regression analysis provides valuable insights into the significant predictors of survival in medulloblastoma, incorporating both molecular and clinical factors. The AIC value for this model was 298.9553. **Method 3:** LASSO regression is a technique used to address overfitting and severe multicollinearity in regression models by introducing a penalty function that shrinks the regression coefficients of variables. The choice of the λ value determines which variables contribute to an optimal model, and cross-validation is employed to find the best λ value. The λ value corresponding to the minimum mean squared error (MSE) determines the variables included in the model. The graph illustrates the partial-likelihood deviance as a function of log(λ) (Figures 2C, D). The selected variables for the LASSO regression model are Age, Histological, Radiotherapy, Chemotherapy, Metastasis, Tumor Texture, and Hydrocephalus. The AIC value for this model was 303.3649.

After comparison, it was determined that the model constructed with the variables Age + Molecular + Histological + Radiotherapy + Chemotherapy + Metastasis + Hydrocephalus, obtained through comprehensive analysis (Summary model), performed better. The variable of tumor texture was excluded because adding this variable made only a minimal contribution to the model, and the resulting AIC value was not the lowest. Summary model had the highest AUC value and the lowest AIC value (Figures 3A, B). Therefore, based on the data, the final selection was to construct a nomogram using these seven factors: Age, Molecular subtype, Histological, Radiotherapy,

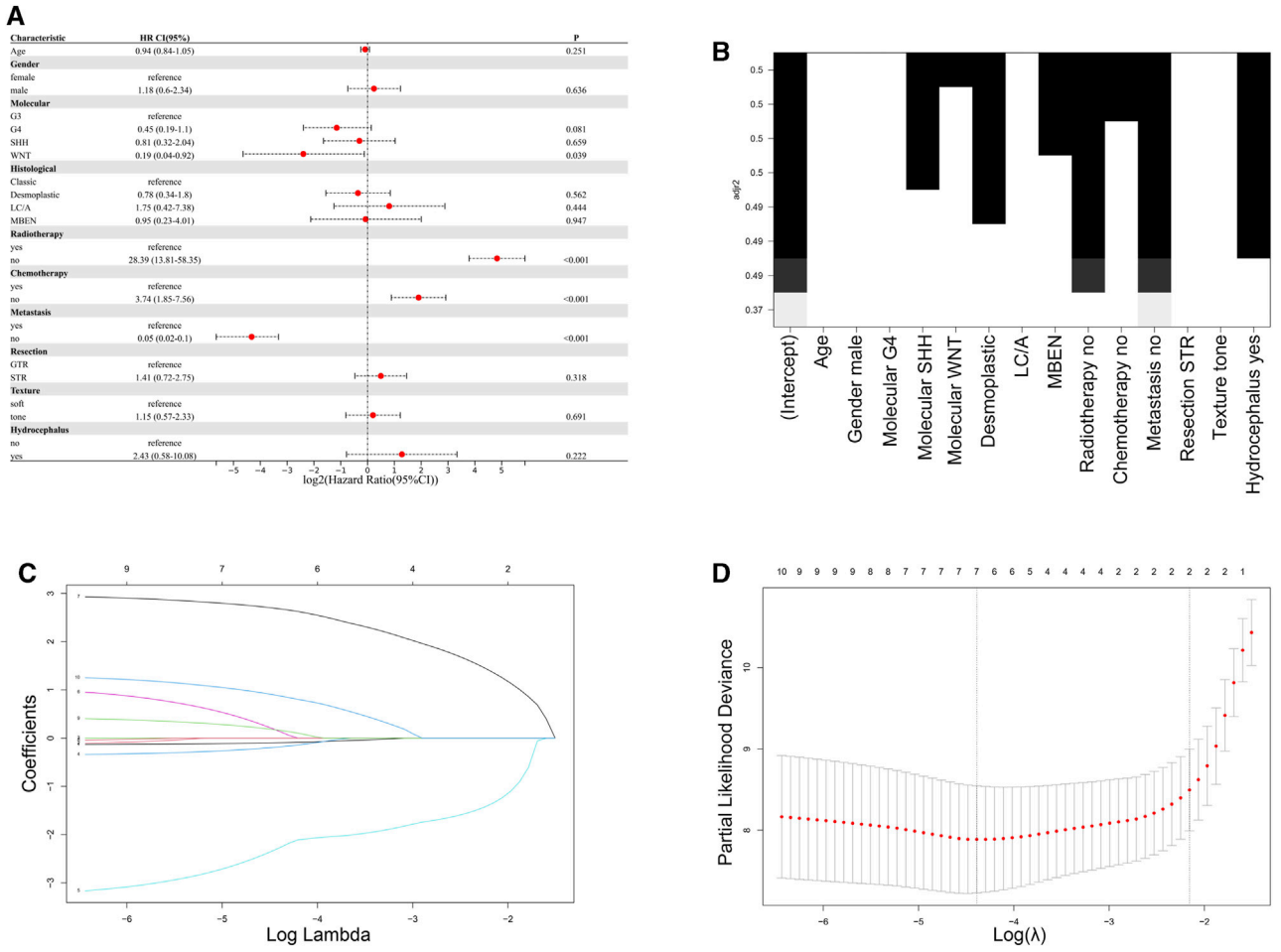

FIGURE 2
Comparison of feature selection methods for the development of the nomogram. **(A)** Results of univariate Cox regression analysis. **(B)** Results of best subset regression analysis. **(C,D)** LASSO regression variable selection process.

Chemotherapy, Metastasis, and Hydrocephalus (Figure 3C). The calibration curves of the nomogram showed high uniformity between the predicted and actual probabilities of 1-,3- and 5-year OS in the training cohort (Figures 3D–F). The continuous calibration curve also demonstrates the model's strong predictive capability of summary model (Supplementary Figure S1). The DCA curve of the Summary model mostly lies above the curves of the other three models. This indicates that, at most patient probability thresholds, the Summary model achieves the highest net benefit. Along this curve, the Summary model performs well within the threshold range of 0.3–0.9 and demonstrates a stronger advantage compared to the other three models (Supplementary Figure S2).

3.4 Performance and validation of the nomogram

The C-index values obtained from the nomogram were higher in both the training cohort (0.907) and the external validation cohort (0.793) compared to a previous study (Guo et al., 2020) (training cohort, 0.681; external validation cohort, 0.644). Furthermore, the nomogram demonstrated good performance in predicting the overall survival prognosis in the external validation cohort, as evidenced by the time-dependent ROC curves (Figure 4A). Additionally, the calibration curves of the nomogram exhibited a high level of agreement between the predicted probabilities and the actual probabilities of 1-, 3-, and 5-year OS in the external validation cohort (Figures 4B–D). In the validation set, continuous calibration curves demonstrate the predictive capability of the model (Supplementary Figure S3).

3.5 The comparison between the final nomogram and the model using only clinical factors

Several studies have indicated that age, histological subtype, extent of surgical resection, radiotherapy, chemotherapy, and metastatic status are prognostic risk factors for medulloblastoma (Packer et al., 2006; Rieken et al., 2011; Thompson et al., 2016; Huang et al., 2017; Guo et al., 2020;

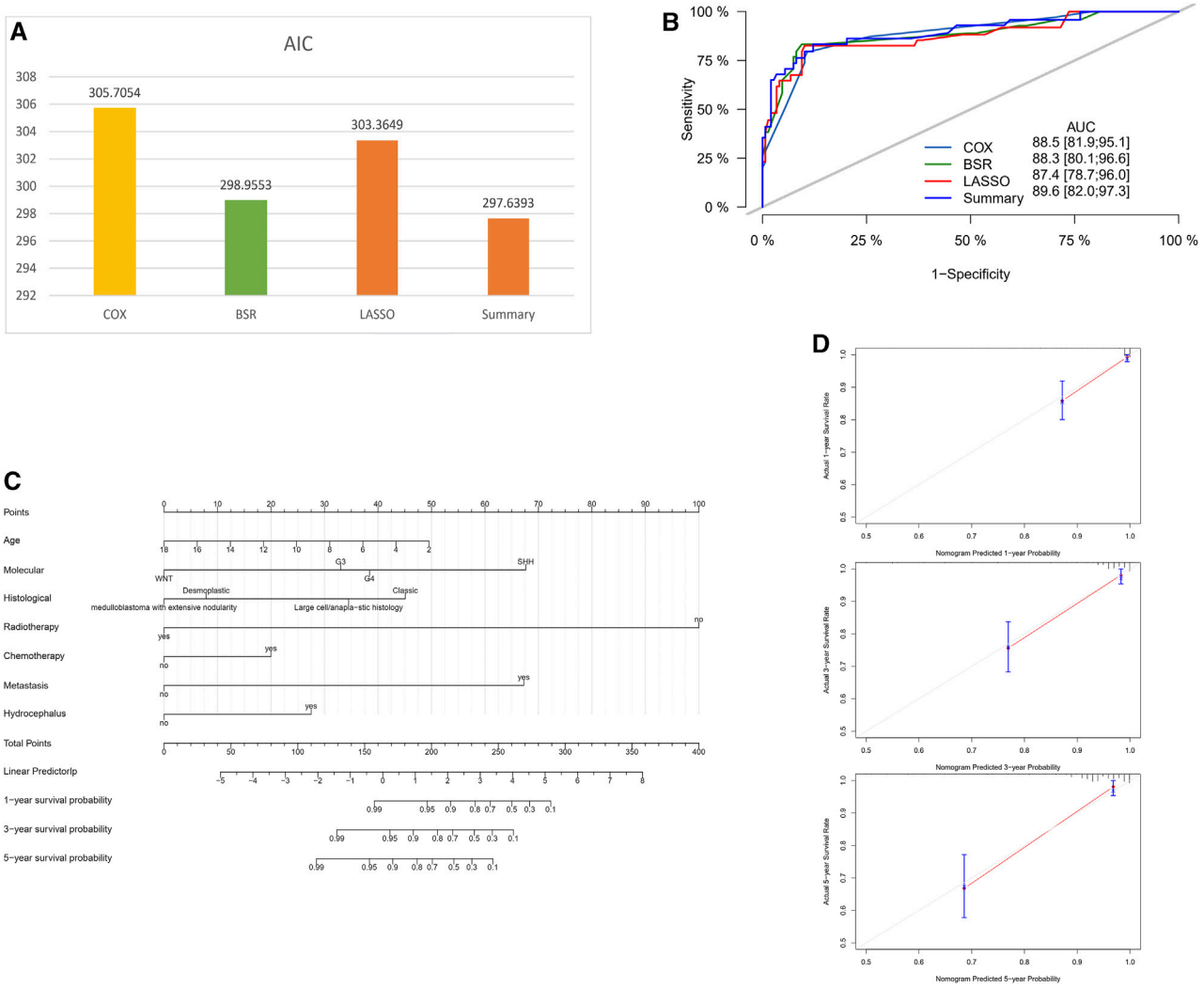

FIGURE 3
Comparison of different models for nomogram construction. **(A)** Comparison of AIC values for different models. **(B)** Comparison of AUC values for different models. **(C)** Final selection of variables for the summary model. **(D–F)** Calibration curves for the nomogram in the training cohort (1-, 3-, and 5-year OS).

Zhu et al., 2020; Liu and Sun, 2022). We compared the final model constructed using our own data with the model using only clinical factors. The results showed that the model we constructed had a higher C-index, lower AIC value, and a larger area under the ROC curve (Figures 5A–D).

4 Discussion

In this study, we aimed to develop a predictive model for overall survival prognosis in patients with medulloblastoma by incorporating both clinical and molecular factors. Based on their histopathological features, medulloblastomas can be classified into four subtypes: classic medulloblastoma, large cell/anaplastic medulloblastoma, desmoplastic/nodular medulloblastoma, and medulloblastoma with extensive nodularity (Louis et al., 2007). The heterogeneity of pathological classification and molecular subtyping was evident between the training and external validation groups, indicating that the prognosis varied greatly in different cases, emphasizing the importance of incorporating molecular subtyping into predictive models. Previous studies have shown a significant correlation between molecular subtypes of medulloblastoma and prognosis, further justifying the inclusion of this factor in the predictive model (Archer et al., 2017), but currently, there is limited research that incorporates molecular subtyping as a variable in predictive models. We utilized three different methods for variable selection: univariate Cox regression analysis, Best Subsets Regression, and LASSO regression. These three methods can effectively screen out variables that are significantly associated with clinical prognosis (Emura et al., 2019; Kwong et al., 2020; McEligot et al., 2020). By innovatively applying these three methods to screen variables associated with

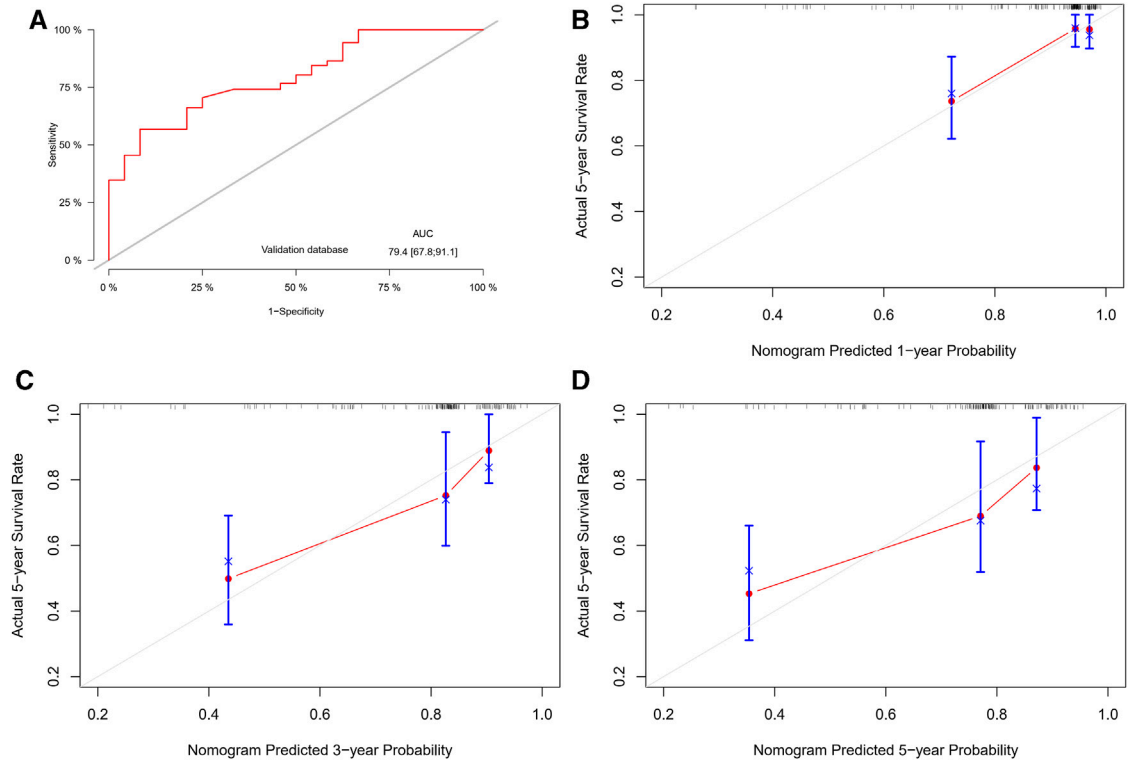

FIGURE 4
Performance and validation of the nomogram. **(A)** ROC curves for the nomogram in the external validation cohort. **(B–D)** Calibration curves for the nomogram in the external validation cohort (1-, 3-, and 5-year OS).

medulloblastoma prognosis, we enhance the accuracy of the final predictive model. After comparing the results, we constructed a nomogram using seven factors: Age, Molecular subtype, Histological, Radiotherapy, Chemotherapy, Metastasis, and Hydrocephalus. The summary model had the highest AUC value and the lowest AIC value. This also confirms the credibility and effectiveness of the model we constructed.

The univariate Cox regression analysis revealed that Molecular subtype, Radiotherapy, Chemotherapy, and Metastasis were associated with OS. BSR identified a combination of six variables: Molecular subtype, Histological, Radiotherapy, Chemotherapy, Metastasis, and Hydrocephalus. LASSO regression, on the other hand, selected Age, Histological, Radiotherapy, Chemotherapy, Metastasis, Tumor texture, and Hydrocephalus. The variables screened through these three methods have been previously validated to be associated with prognosis in existing research on medulloblastoma (Archer et al., 2017; Guo et al., 2020; Aras et al., 2021; Franceschi et al., 2021). This aligns with our study findings. Considering the clinical significance and variables selected by all three methods, a comprehensive approach was adopted, resulting in a model with seven variables. First, different pathology subtypes of MB may indicate distinct biological behaviors that can influence treatment strategies. Large-cell and anaplastic MB are considered high-risk diseases, indicating poorer survival rates, and requiring more aggressive chemotherapy and higher radiation doses. On the other hand, desmoplastic nodular MB may exhibit better outcomes. In our study, Large-cell and anaplastic MB showed the highest risk factor among the histopathological subtypes, which aligns with previous research findings (Huang et al., 2017). Second, Chang staging for MB was introduced in the 1960s, which classified MB patients into M0, M1, M2, M3, or M4 and T1, T2, T3a, T3b, or T4 according to their clinical features. Tumor metastasis indicates a poor prognosis, which is consistent with our research findings (Dufour et al., 2012). Third, for medulloblastoma, postoperative adjuvant therapy is crucial, especially radiation therapy. Previous studies also support our findings (Menyhárt and Győrffy, 2020). It is worth noting that the tumor resection extent did not show a clear correlation with prognosis in our experimental and validation datasets. The prognostic benefit of increased resection extent for patients with medulloblastoma is attenuated after molecular subgroup affiliation is considered. Although maximum safe surgical resection should remain the standard of care, surgical removal of small residual portions of medulloblastoma is not recommended when the likelihood of neurological morbidity is high because there is no definitive benefit to gross total resection compared with near-total resection (Thompson et al., 2016). This suggests that when the tumor adheres to the brainstem or some important neurovascular structure, it is not necessary to aggressively pursue complete tumor resection to avoid catastrophic consequences.

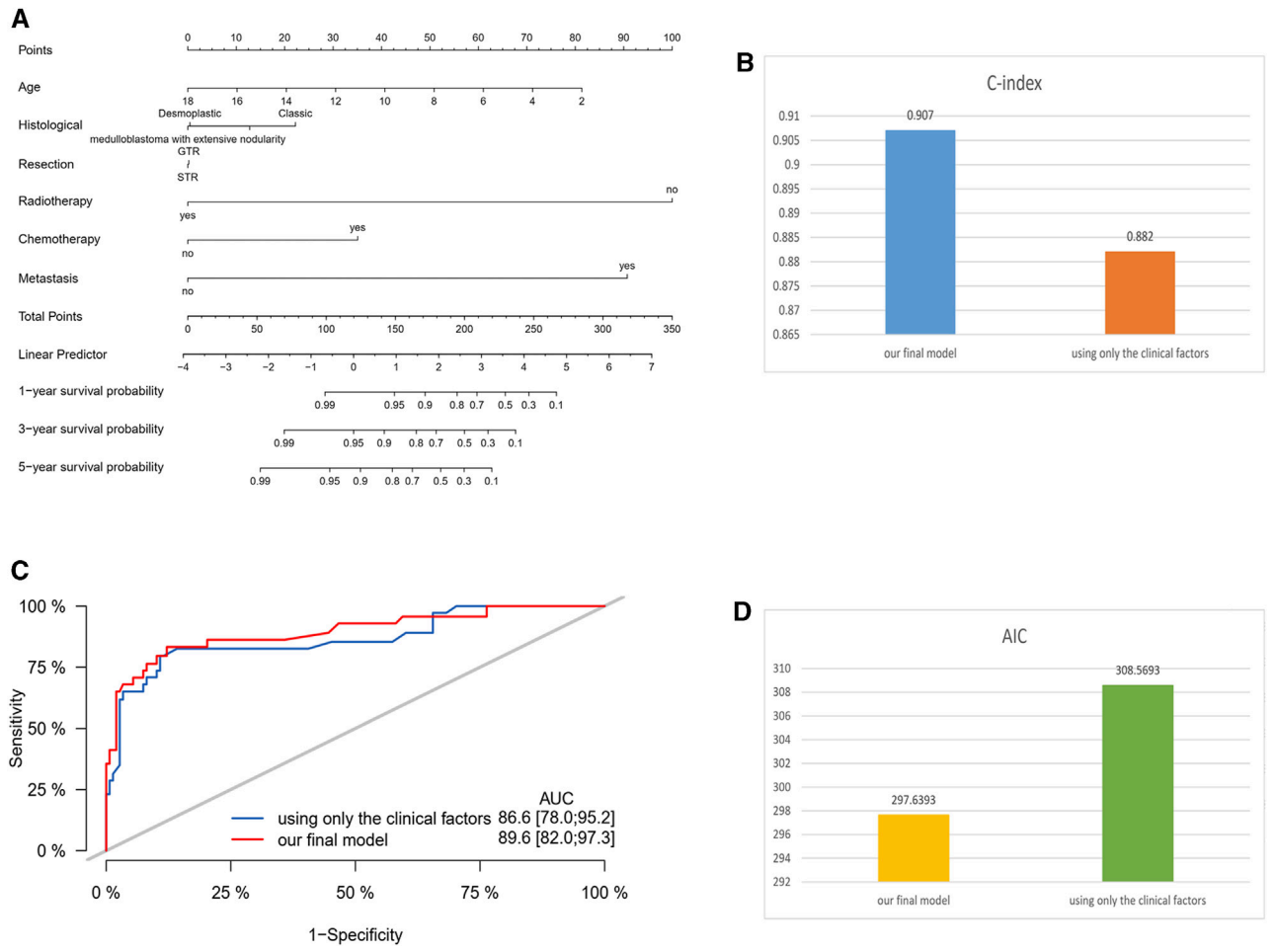

FIGURE 5
Comparison between the final nomogram and the model using only clinical factors. **(A)** Nomogram of the model using only clinical factors. **(B)** C-index comparison. **(C)** ROC curve comparison. **(D)** AIC value comparison.

The performance of the nomogram constructed using the seven selected factors was evaluated using the C-index and compared to a previous study (Guo et al., 2020). The C-index values obtained from the nomogram were higher in both the training cohort and the external validation cohort, indicating improved predictive accuracy. The nomogram demonstrated good performance in predicting the OS prognosis, as supported by the ROC and calibration curves in both the training and external validation cohorts.

The incorporation of both clinical and molecular factors in the nomogram provides a more comprehensive and accurate prediction of the OS prognosis in medulloblastoma patients. By considering variables such as age, treatment modalities (radiotherapy and chemotherapy), metastasis status, molecular subtype, histological classification, and the presence of hydrocephalus, clinicians can make more informed decisions regarding patient management and treatment strategies.

It is important to note that this study has certain limitations. The data used for model development and validation were collected from a single institution and eight external centers, which may introduce bias and limit the generalizability of the findings. Further external validation in larger and more diverse patient populations is necessary to validate the performance of the nomogram. Additionally, the study did not consider other potential prognostic factors such as genetic mutations or gene expression profiles, which could further enhance the predictive accuracy of the model.

5 Conclusion

In conclusion, this study developed a nomogram incorporating clinical and molecular factors for predicting the OS prognosis in medulloblastoma patients. The nomogram demonstrated improved predictive accuracy compared to a previous study and exhibited good performance in the external validation cohort. By considering multiple factors, clinicians can utilize this nomogram as a valuable tool for individualized prognosis prediction and treatment decision-making in medulloblastoma patients. Further research and validation are warranted to refine and optimize the predictive model.

Data availability statement

The original contributions presented in the study are included in the article/Supplementary Material, further inquiries can be directed to the corresponding author.

Ethics statement

The studies involving humans were approved by Ethics committee of Beijing Tiantan Hospital, Ethics committee of Qilu Children's Hospital, Ethics committee of Xijing Hospital, Ethics committee of Xiangya Hospital, Ethics committee of Qilu Hospital, Ethics committee of Children's Hospital of Chongqing Medical University, Ethics committee of Huashan Hospital, Ethics committee of Sanbo Brain Hospital, Ethics committee of Zhengzhou Children's Hospital. The studies were conducted in accordance with the local legislation and institutional requirements. Written informed consent for participation in this study was provided by the participants' legal guardians/next of kin.

Author contributions

XL and JG conceived the study and collected and analyzed the data. XL wrote the manuscript. JG provided technical guidance. All authors contributed to the article and approved the submitted version.

Funding

This research is funded by the National Natural Science Foundation of China (Nos 81870834 and 62276027).

Acknowledgments

The authors thank all patients and institutions involved in this study. Thanks to the following physicians for collating and collecting clinical data. Guangyu Wang, Department of Neurosurgery, Qilu Children's Hospital of Shandong University, Jinan, 250022, Shandong, China. Xiaosheng He, Department of Neurosurgery, Xijing Hospital, Fourth Military Medical University, Xi'an 710032, China. Jie Zhao, Department of Neurosurgery, Xiangya Hospital, Central South University, Changsha, 410008, Hunan, China. Jie Gong, Department of Neurosurgery, Qilu Hospital of Shandong University and Institute of Brain and Brain-Inspired Science, Shandong University, Jinan, 250012, Shandong, China. Ping Liang, Department of Neurosurgery, Children's Hospital of Chongqing Medical University, Chongqing, 400014, China. Rong Zhang, Department of Neurosurgery, Huashan Hospital, Fudan University, 12 Wulumuqi Zhong Road, Shanghai, China. Junping Zhang, Department of Neuro-Oncology, Sanbo Brain Hospital, Capital Medical University, Beijing 100093, China.

Conflict of interest

The authors declare that the research was conducted in the absence of any commercial or financial relationships that could be construed as a potential conflict of interest.

Publisher's note

All claims expressed in this article are solely those of the authors and do not necessarily represent those of their affiliated organizations, or those of the publisher, the editors and the reviewers. Any product that may be evaluated in this article, or claim that may be made by its manufacturer, is not guaranteed or endorsed by the publisher.

Supplementary material

The Supplementary Material for this article can be found online at: https://www.frontiersin.org/articles/10.3389/fphar.2023.1247812/full#supplementary-material

References

Aras, Y., Dölen, D., İribas Çelik, A., Kılıç, G., Kebudi, R., Ünverengil, G., et al. (2021). Effects of different molecular subtypes and tumor biology on the prognosis of medulloblastoma. *Child's Nerv. Syst.* 37 (12), 3733–3742. ChNS : official journal of the International Society for Pediatric Neurosurgery. doi:10.1007/s00381-021-05350-1

Archer, T. C., Mahoney, E. L., and Pomeroy, S. L. (2017). Medulloblastoma: molecular classification-based personal therapeutics. *Neurother. J. Am. Soc. Exp. Neurother.* 14 (2), 265–273. doi:10.1007/s13311-017-0526-y

Bouffet, E. (2021). Management of high-risk medulloblastoma. *Neuro-Chirurgie.* 67 (1), 61–68. doi:10.1016/j.neuchi.2019.05.007

Dasgupta, A., Gupta, T., Pungavkar, S., Shirsat, N., Epari, S., Chinnaswamy, G., et al. (2019). Nomograms based on preoperative multiparametric magnetic resonance imaging for prediction of molecular subgrouping in medulloblastoma: results from a radiogenomics study of 111 patients. *Neuro-oncology* 21 (1), 115–124. doi:10.1093/neuonc/noy093

Dufour, C., Beaugrand, A., Pizer, B., Micheli, J., Aubelle, M. S., Fourcade, A., et al. (2012). Metastatic medulloblastoma in childhood: chang's classification revisited. *Int. J. Surg. Oncol.* 2012, 245385. doi:10.1155/2012/245385

Emura, T., Matsui, S., and Chen, H. Y. (2019). compound.Cox: univariate feature selection and compound covariate for predicting survival. *Comput. methods programs Biomed.* 168, 21–37. doi:10.1016/j.cmpb.2018.10.020

Entz-Werle, N., Carli, E. D., Ducassou, S., Legrain, M., Grill, J., and Medulloblastoma, D. C. (2008). What is the role of molecular genetics? *Expert Rev. anticancer Ther.* 8 (7), 1169–1181. doi:10.1586/14737140.8.7.1169

Franceschi, E., Seidel, C., Sahm, F., Pajtler, K. W., and Hau, P. (2021). How we treat medulloblastoma in adults. *ESMO open* 6 (4), 100173. doi:10.1016/j.esmoop.2021.100173

Gajjar, A. J., and Robinson, G. W. (2014). Medulloblastoma-translating discoveries from the bench to the bedside. *Nat. Rev. Clin. Oncol.* 11 (12), 714–722. doi:10.1038/nrclinonc.2014.181

Guo, C., Yao, D., Lin, X., Huang, H., Zhang, J., Lin, F., et al. (2020). External validation of a nomogram and risk grouping system for predicting individual prognosis of patients with medulloblastoma. *Front. Pharmacol.* 11, 590348. doi:10.3389/fphar.2020.590348

Huang, P. I., Lin, S. C., Lee, Y. Y., Ho, D. M., Guo, W. Y., Chang, K. P., et al. (2017). Large cell/anaplastic medulloblastoma is associated with poor prognosis-a retrospective analysis at a single institute. *Child's Nerv. Syst.* 33 (8), 1285–1294. ChNS : official journal of the International Society for Pediatric Neurosurgery. doi:10.1007/s00381-017-3435-9

Iasonos, A., Schrag, D., Raj, G. V., and Panageas, K. S. (2008). How to build and interpret a nomogram for cancer prognosis. *J. Clin. Oncol.* 26 (8), 1364–1370.

official journal of the American Society of Clinical Oncology. doi:10.1200/JCO.2007.12.9791

Kwong, Y. D., Mehta, K. M., Miaskowski, C., Zhuo, H., Yee, K., Jauregui, A., et al. (2020). Using best subset regression to identify clinical characteristics and biomarkers associated with sepsis-associated acute kidney injury. *Am. J. physiology Ren. physiology* 319 (6), F979–f87. doi:10.1152/ajprenal.00281.2020

Liu, H., and Sun, P. (2022). A nomogram model for predicting prognosis of patients with medulloblastoma. *Turk. Neurosurg.* doi:10.5137/1019-5149.JTN.40397-22.3

Louis, D. N., Ohgaki, H., Wiestler, O. D., Cavenee, W. K., Burger, P. C., Jouvet, A., et al. (2007). The 2007 WHO classification of tumours of the central nervous system. *Acta neuropathol.* 114 (2), 97–109. doi:10.1007/s00401-007-0243-4

McEligot, A. J., Poynor, V., Sharma, R., and Panangadan, A. (2020). Logistic LASSO regression for dietary intakes and breast cancer. *Nutrients* 12 (9), 2652. doi:10.3390/nu12092652

Menyhárt, O., and Győrffy, B. (2020). Molecular stratifications, biomarker candidates and new therapeutic options in current medulloblastoma treatment approaches. *Cancer metastasis Rev.* 39 (1), 211–233. doi:10.1007/s10555-020-09854-1

Northcott, P. A., Robinson, G. W., Kratz, C. P., Mabbott, D. J., Pomeroy, S. L., Clifford, S. C., et al. (2019). *Medulloblastoma. Nat. Rev. Dis. Prim.* 5 (1), 11. doi:10.1038/s41572-019-0063-6

Packer, R. J., Gajjar, A., Vezina, G., Rorke-Adams, L., Burger, P. C., Robertson, P. L., et al. (2006). Phase III study of craniospinal radiation therapy followed by adjuvant chemotherapy for newly diagnosed average-risk medulloblastoma. *J. Clin. Oncol.* 24 (25), 4202–4208. official journal of the American Society of Clinical Oncology. doi:10.1200/JCO.2006.06.4980

Rieken, S., Mohr, A., Habermehl, D., Welzel, T., Lindel, K., Witt, O., et al. (2011). Outcome and prognostic factors of radiation therapy for medulloblastoma. *Int. J. Radiat. Oncol. Biol. Phys.* 81 (3), e7–e13. doi:10.1016/j.ijrobp.2010.12.042

Schwalbe, E. C., Lindsey, J. C., Nakjang, S., Crosier, S., Smith, A. J., Hicks, D., et al. (2017). Novel molecular subgroups for clinical classification and outcome prediction in childhood medulloblastoma: a cohort study. *Lancet Oncol.* 18 (7), 958–971. doi:10.1016/S1470-2045(17)30243-7

Thompson, E. M., Hielscher, T., Bouffet, E., Remke, M., Luu, B., Gururangan, S., et al. (2016). Prognostic value of medulloblastoma extent of resection after accounting for molecular subgroup: a retrospective integrated clinical and molecular analysis. *Lancet Oncol.* 17 (4), 484–495. doi:10.1016/S1470-2045(15)00581-1

Zhu, S., Lin, F., Chen, Z., Jiang, X., Zhang, J., Yang, Q., et al. (2020). Identification of a twelve-gene signature and establishment of a prognostic nomogram predicting overall survival for medulloblastoma. *Front. Genet.* 11, 563882. doi:10.3389/fgene.2020.563882

frontiers | Frontiers in Oncology

TYPE Original Research
PUBLISHED 29 November 2023
DOI 10.3389/fonc.2023.1276253

OPEN ACCESS

EDITED BY
Sheng Zhong,
Sun Yat-sen University Cancer Center, China

REVIEWED BY
Felix Mircea Brehar,
Carol Davila University of Medicine and Pharmacy, Romania
Alessandro Consales,
Giannina Gaslini Institute (IRCCS), Italy
Judith Ann Schwartzbaum,
Independent Researcher, United States
Andrea Botturi,
IRCCS Carlo Besta Neurological Institute Foundation, Italy

*CORRESPONDENCE
Licia Iacoviello
licia.iacoviello@neuromed.it

†These authors have contributed equally to this work

RECEIVED 04 September 2023
ACCEPTED 30 October 2023
PUBLISHED 29 November 2023

CITATION
Esposito S, Ruggiero E, Di Castelnuovo A, Costanzo S, Bonaccio M, Bracone F, Esposito V, Innocenzi G, Paolini S, Cerletti C, Donati MB, de Gaetano G, Iacoviello L and Gialluisi A (2023) Identifying brain tumor patients' subtypes based on pre-diagnostic history and clinical characteristics: a pilot hierarchical clustering and association analysis. *Front. Oncol.* 13:1276253. doi: 10.3389/fonc.2023.1276253

Identifying brain tumor patients' subtypes based on pre-diagnostic history and clinical characteristics: a pilot hierarchical clustering and association analysis

Simona Esposito[1†], Emilia Ruggiero[1†], Augusto Di Castelnuovo[2], Simona Costanzo[1], Marialaura Bonaccio[1], Francesca Bracone[1], Vincenzo Esposito[3], Gualtiero Innocenzi[3], Sergio Paolini[3], Chiara Cerletti[1], Maria Benedetta Donati[1], Giovanni de Gaetano[1], Licia Iacoviello[1,4*] and Alessandro Gialluisi[1,4,5] for the MEDICEA Study Investigators

[1]Department of Epidemiology and Prevention, IRCCS Neuromed, Pozzilli, Italy, [2]Mediterranea Cardiocentro, Napoli, Italy, [3]Department of Neurosurgery, IRCCS Neuromed, Pozzilli, Italy, [4]Libera Università Mediterranea (LUM) "Giuseppe Degennaro", Casamassima (Bari), Italy, [5]Department of Medicine and Surgery, LUM University, Bari, Italy

Introduction: Central nervous system (CNS) tumors are severe health conditions with increasing incidence in the last years. Different biological, environmental and clinical factors are thought to have an important role in their epidemiology, which however remains unclear.

Objective: The aim of this pilot study was to identify CNS tumor patients' subtypes based on this information and to test associations with tumor malignancy.

Methods: 90 patients with suspected diagnosis of CNS tumor were recruited by the Neurosurgery Unit of IRCCS Neuromed. Patients underwent anamnestic and clinical assessment, to ascertain known or suspected risk factors including lifestyle, socioeconomic, clinical and psychometric characteristics. We applied a hierarchical clustering analysis to these exposures to identify potential groups of patients with a similar risk pattern and tested whether these clusters associated with brain tumor malignancy.

Results: Out of 67 patients with a confirmed CNS tumor diagnosis, we identified 28 non-malignant and 39 malignant tumor cases. These subtypes showed significant differences in terms of gender (with men more frequently presenting a diagnosis of cancer; $p = 6.0 \times 10^{-3}$) and yearly household income (with non-malignant tumor patients more frequently earning ≥25k Euros/year; $p = 3.4 \times 10^{-3}$). Cluster analysis revealed the presence of two clusters of patients: one (N=41) with more professionally active, educated, wealthier and healthier

patients, and the other one with mostly retired and less healthy men, with a higher frequency of smokers, personal history of cardiovascular disease and cancer familiarity, a mostly sedentary lifestyle and generally lower income, education and cognitive performance. The former cluster showed a protective association with the malignancy of the disease, with a 74 (14-93) % reduction in the prevalent risk of CNS malignant tumors, compared to the other cluster (p=0.026).

Discussion: These preliminary data suggest that patients' profiling through unsupervised machine learning approaches may somehow help predicting the risk of being affected by a malignant form. If confirmed by further analyses in larger independent cohorts, these findings may be useful to create potential intelligent ranking systems for treatment priority, overcoming the lack of histopathological information and molecular diagnosis of the tumor, which are typically not available until the time of surgery.

KEYWORDS

central nervous system tumors, cluster analysis, pre-diagnostic history, clinical characteristics, cognitive performance, cancer diagnosis, risk and protective factors, malignancy

1 Introduction

Central nervous system (CNS) tumors are quite rare forms of tumors, representing about 1.3% of all cancers. They are hypothesized to have distinct cellular origins, which can be discriminated on the basis of anatomical location, expression of cellular markers, and morphological resemblance to normal brain cells (1). According to the World Health Organization (WHO), there are over 120 different types of brain tumors and data suggest that their incidence is further increasing (2). It is estimated that about 1,000 people receive a new cancer diagnosis every day in Italy (3) and, according to estimates by the National Cancer Registry, approximately 5,700 cases of CNS tumors are diagnosed in the Country each year (4).

CNS tumors are linked with a number of risk and protective factors, including both genetic and environmental factors. The main risk factors include family history of the disease, age, exposure to chemical compounds and radiations (5–7).

Levin and colleagues carried out a large case-control study of more than 400 between cases and controls to investigate whether sensitivity to γ radiation was associated with the risk of CNS tumors (8), and observed that this and the consequent inability to repair DNA damage induced by radiation can increase the risk of such tumors (8). A growing number of studies are supporting the importance of healthy eating in cancer prevention. In particular, a high adherence to Mediterranean Diet (MD) reduces the risk of mortality and the incidence of many types of tumors (7, 9). The protective effects of the MD could be attributed to the high concentration of polyphenols contained in olive oil, wine and vegetables, all foods known for their antioxidant and anti-inflammatory capacity (10, 11). Similarly, omega-3 fatty acids, which are abundant in fish, help slowing down cell proliferation, angiogenesis, inflammation and metastasis (12).

A large number of epidemiological studies have also analyzed the relationship between mobile phone use and the incidence of tumors in the CNS (13, 14), but a meta-analysis of these studies did not reveal any robust statistical evidence for an increase in the risk of malignant or benign neoplasms for a prolonged use of the mobile phone (>10 years) (15). Another potential risk factor is cigarette smoking, which represents a major source of exposure to multiple chemical carcinogens, including polycyclic aromatic hydrocarbons (PAHs) and N-nitroso compounds (16). These cancerous agents are associated with permeability of the blood brain barrier in animal models, along with nicotine (16). As for obesity, the relative risk of all CNS cancers – and especially meningiomas increases with increasing body mass index (BMI) (17).

CNS tumors have also been associated with several socioeconomic factors, occupational and environmental exposures. Inskip et al. found a significant positive association with education and income for low-grade glioma, but not for high grade glioma (18). Among the most reported environmental risk factors were also exposure to agricultural chemicals such as pesticides, insecticides and herbicides (19).

Moreover, studies have indicated that psychological and cognitive manifestations can be considered not only symptoms of CNS tumors but also early warning signs (20, 21), or even risk factors. In fact, a systematic review conducted by Ghandour and colleagues on case reports studies on brain tumors and psychiatric symptoms revealed that in some cases, psychiatric and minor neurological symptoms can emerge even months or years prior to the onset of noticeable neurological signs (22).

Overall, the association of these risk factors with the tumors of CNS has been scarcely investigated, especially through machine learning techniques, which allow to potentially identify subtypes of disease by taking into account also more complex and non-linear relationships among risk factors. This would provide a notable contribution to current knowledge in the field, in light of the modern view that each disease - and even more prominently cancer - has different clinical and biological subtypes, and that each patient is a unique combination of biological, clinical, cultural and psychological characteristics (23, 24).

The aim of this study was to preliminarily investigate the link of different known and suspected risk factors with CNS tumor malignancy, in a cohort of patients elected for neurosurgical treatment. This was accomplished through analysis of associations between diverse exposures which could influence the risk of CNS tumors and their diagnosis - including occupational, socioeconomic, psychometric, nutritional and anthropometric variables, cancer familiarity and history of chronic health conditions - and the different type of tumors, including malignant and non-malignant ones. The very final purpose of this approach is that - shall we identify clusters of patients associated with a higher risk of malignancy - this information may turn useful in future clinical practice, e.g. prioritizing patients for treatment, overcoming the lack of histopathological information and molecular diagnosis of the tumor, which are typically not available until the time of surgery.

2 Subjects and methods

2.1 Study design

Between October 2018 and March 2020, 90 consecutive patients were enrolled in the MEDICEA (adherence to the MEditerranean DIet in relation to CancEr of brAin) study. Recruited patients (≥ 18 years) had a suspected diagnosis of CNS tumors based on neuroimaging scan and were eligible for surgery at the Neurosurgery Department of the IRCCS Neuromed. Subjects with metastatic and/or recurrent brain tumors were excluded, as well as subjects with confirmed diagnosis of conditions other than brain tumor or with missing diagnosis (see below). Anthropometric measurements and administration of questionnaires were completed before surgery.

The pilot study, conducted according to the principles of the Helsinki declaration, was approved by the Ethical Committee at the IRCCS Neuromed, Pozzilli, Italy (Protocol number: 01262017). All patients signed a written informed consent to be enrolled in the study.

2.2 Study population

Trained research personnel from the Department of Epidemiology and Prevention at the IRCCS Neuromed carried out recruitment – carried out between 8.00 and 11.00 a.m. in the Neuromed clinical center and anthropometric measurements, using methods that had been standardized beforehand during preliminary training sessions. Primary CNS tumors were validated through medical records and confirmed by histological reports. Patients without histopathological confirmation or with a diagnosis of brain cysts, secondary tumors or other expansive cerebral processes (n= 22) were excluded. Similarly, one participant who did not complete any questionnaire was filtered out before analysis. Histological information was used to identify main CNS tumors types (i.e. meningiomas 29.5%, glioblastomas 18.2%, adenoma 13.6%, astrocytomas 13.6%, other types 25.1%; Supplementary Table 1). Other types of CNS tumors included olygoastrocitoma, chordoma, epidermoid cyst, rolandic tumor, oligodendroglioma, angioma, schwannoma, pituitary adenoma and hemangioblastoma. Additionally, CNS tumors were categorized in malignant (behavior code = 3) and non-malignant (behavior code = 0 or 1) (25).

2.3 Definition of variable analyzed

Education was based on the highest qualification attained and was categorized as up to secondary (≤8 y), upper secondary (≥9 y and ≤13 y) and post-secondary (>13 y). Occupational social class was classified as non-manual occupation, manual occupation, retired, housewife and unemployed/unclassified. Marital status was assessed and classified into married, separated/divorced, single and widowed. Household income, expressed as Euros per year, was classified as a four-level variable (<10,000; 10,000-25,000; ≥25,000 Euros/year), with missing values collapsed into a non-respondent category. Smoking status of participants was classified as never-smoker, current smoker or former smoker (i.e. having quitted smoking at least 1 year before enrollment). For clustering purposes, these classes were condensed into never vs ever smokers. Physical activity level was classified into: sedentary, mildly active or physically active lifestyle.

The study sample was also stratified as living in an urban or rural environment on the basis of the urbanization level of the city of residence, as defined by the European Institute of Statistics (EUROSTAT definition) and obtained by the tool "Atlante Statistico dei Comuni" provided by the Italian National Institute of Statistics (www.istat.it) (26).

Height and weight were measured, and BMI was calculated as weight to squared height ratio (kg/m^2). Waist circumference was measured according to the National Institutes of Health, Heart, Lung, and Blood Guidelines (27), then waist-to-hip ratio was computed as the ratio between waist and hip, both measured in centimeters. Diastolic and systolic blood pressure were also measured during the visit, through three repeated assessments, and the average values of the last two measurements were taken as the final measure. Diagnosis of hypertension, hypercholesterolemia and diabetes were defined by current pharmacological treatments reported, while history of cardiovascular (angina, stroke and myocardial infarction) and peripheral artery disease was based on self-reported diagnosis.

Patients were also asked about family history of tumor disease within their first-degree family (Yes/No). Furthermore, they were asked whether they lived or worked in proximity of industries,

signal relays/repeaters/antennas, sources of asbestos or landfills. The use of mobile phone was also investigated, both asking if patients used to sleep with the mobile phone nearby (Yes/No), and asking how many hours per day they used the phone, with the following potential answers: <2h/day, 2-4h/day and ≥ 4h/day. Finally, patients were asked if they had ever been hospitalized following a head injury due to an accident, a strong bump or a bruise, and if they had undergone previous surgery (Yes/No).

2.4 Dietary assessment

Data on food intake during the year before enrolment was collected by the validated Italian version of the EPIC food frequency questionnaire (28) which includes 188 food items, classified into 75 predefined food groups on the basis of similar nutrient characteristics or culinary usage. Adherence to the traditional MD was evaluated by the Mediterranean Diet Score (MDS) developed by Trichopoulou et al. (29) and ranged from 0 to 9 (the latter reflecting maximal adherence).

2.5 Psychometric assessment

Quality of life of the patients was assessed through a self-administered Functional Assessment of Cancer Therapy -Brain cancer (FACT-Br) questionnaire before the surgery. This includes five subscales that evaluate physical, social life and family, emotional and functional wellbeing, and additional conditions. The total score ranged from 0 to 184 (the latter indicating higher quality of life) (30).

Psychological resilience was tested in the patients through the Connor-Davidson Resilience Scale (CD-RISC), a self-rated assessment based on 25 items and assessing domains of personal competence, trust/tolerance/strengthening effects of stress, acceptance of change, secure relationships, control, humor, patience, and spiritual influences. Since each item is rated on a 5-point scale (0–4), the total score ranges from 0 to 100, with higher score reflecting greater psychological resilience (31). Global cognitive function was assessed via the Montreal Cognitive Assessment (MoCA). The MoCA is a widely used screening tool that assesses cognitive ability through brief evaluation of various cognitive domains, including visuospatial/executive, naming, memory, attention, language, abstraction, delayed recall and orientation (to time and place) (32). This test incorporates an adjustment for participants with ≤12 years of education, by the addition of 1 point to the final score (33). A total score out of 30 is given, with scores <18 indicating dementia, scores between 18 and 26 indicating mild cognitive impairment and scores ≥26 being classified as cognitively normal. This tool is administered in-person and takes ~10 minutes to complete (33). Depressive symptoms were assessed through the Patient Health Questionnaire 9 (PHQ-9) self-administered scale, assessing the nine symptoms most often affected in major depression, namely anhedonia, low mood, alteration of sleeping pattern, altered appetite or eating behavior, feeling of failure/low self-estimate, fatigue, troubles in mental concentration, hypo/hyperactivity behaviors, and suicidal ideation. Each item can receive a score from 0 to 3, depending on how often the relevant domain is affected, with the total PHQ-9 score ranging between 0 (indicating no depressive symptoms at all) to 27 (suggestive of severe depression) (34).

2.6 Statistical analysis

Malignant and non-malignant subtypes were compared for a number of variables, which included demographic (age, gender), socioeconomic (education, annual income, occupation), anthropometric (weight, height, BMI, diastolic and systolic blood pressure) and lifestyle variables (smoking habit, physical activity, adherence to MD, daily alcohol and energy intake), as well as psychometric variables (CD-RISC, MoCA, FACT-Br and PHQ-9 scores), professional and other environmental exposures (proximity to industries, exposure to pesticides, insecticides and herbicides). Descriptive analysis of continuous data included the mean and standard deviation (SD) for each group, while the frequency of each class was compared across groups for categorical variables. Fisher Exact tests were applied on the resulting contingency tables for all categorical variables, while unpaired t-test was used for analyzing continuous variables (Table 1).

Statistical association analyses were carried out at the Department of Epidemiology and Prevention of IRCCS Neuromed, through SAS/STAT software, Version 9.4 of the SAS System for Windows©2009.

2.7 Hierarchical clustering

Pre-diagnostic history and clinical data also underwent a hierarchical clustering analysis among all the patients with clear diagnosis and definition of malignancy (N=67), in R (37). This analysis, which was aimed at identifying subtypes of brain tumor patients in an agnostic way within the analyzed dataset - based only on anthropometric, socioeconomic, psychometric, lifestyle and other environmental information - was carried out as described in the Supplementary Methods, using both a divisive (top-down) and an agglomerative (bottom-up) approach. Briefly, we selected the variables to be included in the analysis, removing collinear features, implemented missing data imputation through a k-nearest neighbor algorithm (see Supplementary Methods) and then computed a pairwise (Gower distance) dissimilarity matrix across 67 patients (Supplementary Figure 1). Through the Average Silhouette method (Supplementary Figure 2), we determined the optimal number of clusters to classify patients based on their clinical and pre-diagnostic characteristics data, then carried out the actual cluster analysis, through which each patient was assigned to one of the clusters. Since divisive clustering has been reported to be more accurate and robust than agglomerative clustering (35) and the two classification methods were significantly homogeneous (Fisher Exact Test $p = 0.004$; Supplementary Table 2; Supplementary Figure 3), we took the divisive cluster

10.3389/fonc.2023.1276253

TABLE 1 Characteristics of the sample according to type of central nervous system tumors.

	All CNS (N=67)	Non-malignant CNS (N= 28)	Malignant CNS (N=39)	*p-value*
Gender, men; N (%)	33 (49.2)	8 (28.6)	25 (64.1)	*0.006*
Age, years; mean (SD)	56.3 (14.1)	57.3 (14.7)	56.2 (13.8)	*0.71*
Educational level; N (%)				*0.78*
Up to secondary	26 (38.8)	11 (39.3)	15 (38.5)	
Upper secondary	24 (35.8)	11 (39.3)	13 (33.3)	
Post-secondary	17 (25.4)	6 (21.4)	11 (28.2)	
Occupation; N (%)				*0.88*
Non-manual	21 (31.3)	9 (32.1)	12 (30.8)	
Manual	10 (14.9)	5 (17.9)	5 (12.8)	
Retired	21 (31.3)	9 (32.1)	12 (30.8)	
Housewife, unemployed and Unclassified	15 (22.4)	5 (17.9)	10 (25.6)	
Place of residence; N (%)				*0.17*
Rural	19 (28.4)	5 (17.9)	14 (35.9)	
Urban	48 (71.6)	33 (82.1)	25 (64.1)	
Marital status; N (%)				*0.71*
Married	38 (56.7)	15 (53.6)	23(60.0)	
Divorced/separated	10 (14.9)	3 (10.7)	7 (17.9)	
Single	10 (14.9)	6 (21.5)	4 (10.3)	
Widowed	4 (6.0)	2 (7.1)	2 (5.1)	
Missing	5 (7.5)	2 (7.1)	3 (7.7)	
Income; N (%)				*0.003*
< 10,000 Euros/y	11 (16.4)	8 (28.6)	3 (7.7)	
10,000-25,000 Euros/y	16 (23.9)	10 (35.7)	6 (15.4)	
≥25,000 Euros/y	24 (35.8)	8 (28.6)	16 (41.0)	
Non responder	16 (23.9)	2 (7.1)	14 (35.9)	
Smoking habit; N (%)				*0. 17*
Never	36 (53.7)	16 (57.1)	20 (51.3)	
Ever	31 (46.3)	12 (42.9)	19 (48.7)	
Diastolic blood pressure, mmHg; mean (SD)	74.1 (19.8)	78.7 (17.5)	70.7 (20.9)	*0.10*
Systolic blood pressure, mmHg; mean (SD)	119.1 (31.9)	124.4 (28.5)	115.4 (33.9)	*0.26*
Body mass index, kg/m^2; mean (SD)	27.1 (4.8)	27.4 (5.5)	26.9 (4.3)	*0.65*
Waist circumference, cm; mean (SD)	100.0 (14.2)	98.8 (17.0)	100.9 (11.8)	*0.58*
Physical activity level (lifestyle); N (%)				*0.29*
Sedentary	40 (59.7)	15 (53.6)	25 (64.1)	
Mildly active	15 (22.4)	9 (32.1)	6 (15.4)	
Physically active	12 (17.9)	4 (14.3)	8 (20.5)	
Hypertension; N (%)				*0.19*
No	39 (58.2)	16 (57.1)	23 (59.0)	
Yes	28 (41.8)	12 (42.9)	16 (41.0)	

(Continued)

10.3389/fonc.2023.1276253

TABLE 1 Continued

	All CNS (N=67)	Non-malignant CNS (N= 28)	Malignant CNS (N=39)	*p-value*
Diabetes; N (%)				*0.36*
No	62 (92.5)	26 (92.9)	36 (92.3)	
Yes	5 (7.5)	2 (7.1)	3 (7.7)	
Dyslipidemia; N (%)				*0.14*
No	52 (77.6)	19 (67.9)	33 (84.6)	
Yes	15 (22.4)	9 (32.1)	6 (15.4)	
Cardiovascular disease; N (%)				*0.82*
No	60 (89.5)	25 (89.3)	35 (89.7)	
Yes	6 (9.0)	3 (10.7)	3 (7.7)	
Missing data	1 (1.5)	0 (0.0)	1 (2.6)	
Cancer familiarity; N (%)				*0.87*
No	53 (79.1)	23 (82.1)	30 (76.9)	
Yes	12 (17.9)	4 (14.3)	8 (20.5)	
Missing data	2 (3.0)	1 (3.6)	1 (2.6)	
Proximity to potential pollution sources; N (%)				*0.13*
No	38 (56.7)	14 (50.0)	24 (61.5)	
Yes	29 (43.3)	14 (50.0)	15 (38.5)	
Time spent using telephone; N (%)				*0.25*
<2h/d	41 (61.2)	18 (64.3)	23 (59.0)	
2-4h/d	15 (22.4)	4 (14.3)	11 (28.2)	
≥4h/d	9 (13.4)	4 (14.3)	5 (12.8)	
Missing	2 (3.0)	2 (7.2)	0 (0.0)	
Sleeping with your phone nearby; N (%)				*0.62*
No	34 (50.7)	13 (46.4)	21 (53.8)	
Yes	33 (49.3)	15 (53.6)	18 (46.2)	
Old Head Injuries; N (%)				*0.23*
No	50 (87.7)	20 (71.4)	30 (76.9)	
Yes	7 (12.3)	5 (17.9)	2 (5.1)	
Missing		3 (10.7)	7 (18.0)	
Previous surgery; N (%)				*0.11*
No	12 (17.9)	3 (10.7)	9 (23.1)	
Yes	75 (84.3)	25 (89.3)	30 (76.9)	
Mediterranean Diet Score; mean (SD)	3.5 (1.4)	3.2 (1.1)	3.7 (1.6)	*0.11*
Energy intake, kcal; mean (SD)	2126 (529)	2034 (515)	2191 (536)	*0.23*
Alcohol, g/d; mean (SD)	5.2 (11.7)	5.5 (12.6)	5.0 (11.1)	*0.88*
CD-RISC; mean (SD)	70.1 (13.4)	69.8 (13.4)	70.2 (13.6)	*0.89*
MoCA; mean (SD)	24.0 (3.1)	24.5 (2.9)	23.7 (3.3)	*0.31*

(Continued)

TABLE 1 Continued

	All CNS (N=67)	Non-malignant CNS (N= 28)	Malignant CNS (N=39)	*p-value*
FACT-Br; mean (SD)	146.0 (28.3)	143.3 (28.7)	148.0 (28.2)	*0.51*
PHQ-9; mean (SD)	6.6 (5.7)	6.6 (5.7)	6.6 (5.80.9)	*0.99*

Summary statistics for the total sample analyzed (N=67) and the two degrees of malignancy of brain tumor are reported. P-values (rounded to the second decimal place, unless statistically significant) refer to comparison across these subtypes, which was performed through Fisher Exact Test for categorical variables, and through unpaired t-test for continuous variables.

classification as main exposure analyzed, as in (35). The two resulting clusters of patients, hereafter called Cluster 1 (green, N = 26) and Cluster 2 (red, N = 41), were then compared for all variables mentioned above, through Fisher's Exact Test (for categorical variables) and through Student's t test (for continuous variables). Moreover, a Fisher Exact Test was applied to compare the distribution of the two clusters of patients for each subtype of brain tumor identified a priori, and an Odds Ratio with 95% Confidence Interval (OR [CI]) was computed, so to detect potential associations between the two classifications and determine whether the agnostic clustering was somehow reflecting tumor diagnosis.

3 Results

Basic characteristics of the 67 patients involved in the analyses are reported in Table 1. Comparing non-malignant vs malignant CNS tumor cases, we observed a difference in gender distributions across the two groups, with men (representing 49.2% of the total sample) being more prevalent in malignant cases (64.1%), compared to non-malignant ones (28.6%; p = 0.006). Age (mean ± SD = 56.3 ± 14.1 y in the total sample) did not show any difference across the two categories, as educational attainment, occupational class and marital status. However, among socioeconomic and demographic variables, household income showed a differential distribution (Fisher Exact Test p = 0.003), with non-malignant tumors showing the highest percentage of subjects in the average income class (10,000-25,000 Euros; 35.7%), and malignant tumors showing a higher prevalence of people declaring ≥25,000 Euros (41.0%) and presenting many non-responders (35.9%). Hierarchical clustering analysis allowed to compute two clusters of patients based on pre-diagnostic history and clinical data (Figure 1), which were compared to analyze their characteristics (Table 2). This comparison revealed differences in several characteristics between the two clusters. Patients in Cluster 1 (N=26) were more frequently men (100% vs 17% in Cluster 2; p<0.0001) and smokers (80.8% vs 24.4%; p<0.0001), generally less educated (up to secondary education level: 46.1% vs 34.1%; p = 0.032) and mostly inactive workers (retired: 53.8% vs 17.1%; p<0.0001), with a lower income (≥25.000 Euros/year: 50.0% vs 26.8%; p = 0.002) and a marginal trend toward an older age (mean (SD) age: 60.7(13.3) vs 54.1(14.8); p = 0.061). Likewise, subjects of Cluster 1 reported more frequently a sedentary lifestyle (65.4% vs 56.1%; p=0.049), a previous diagnosis of cardiovascular disease (19.2% vs 2.4%; p=0.018), and a family history of cancer (30.8% vs 9.8%; p=0.012). From a psychometric perspective, Cluster 1 showed worse cognitive performance compared to Cluster 2: (mean (SD) MoCA score: 22.9 (2.4) vs. 24.7(3.3); p=0.023) (Table 2). No other difference was detected, except for self-reported proximity to potential pollution sources, such as industries, signal relays/repeaters/antennas, sources of asbestos or landfills (23.1% in Cluster 1 vs 56.1% in Cluster 2; p=0.006. When we compared the classification of tumor cases based on their malignancy vs the agnostic classification of patients made applying hierarchical clustering on pre-diagnostic history and clinical data, we observed an association of Cluster 2 with a lower risk of malignant tumor (OR [95% CI] = 0.26 [0.07-0.86], Fisher Exact Test p = 0.026; Table 3).

4 Discussion

In this preliminary study, we aimed to investigate the relationship between environmental and biological risk factors and CNS tumor malignancy. We did this through a cross-sectional association analysis between CNS tumor subtypes - divided into non-malignant and malignant CNS tumor cases - and patients clusters derived from a wealth of pre-diagnostic history

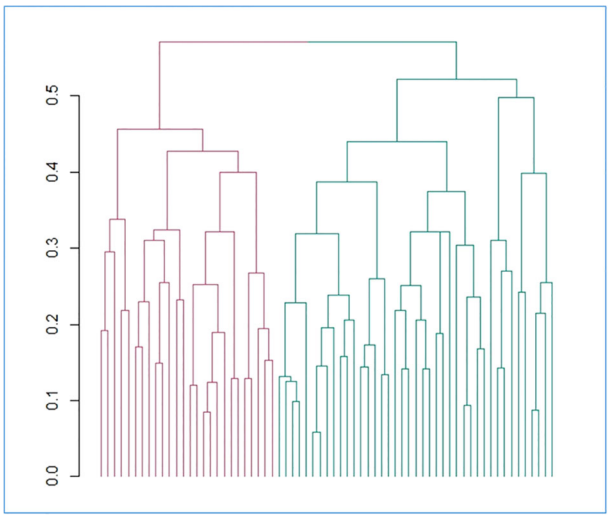

FIGURE 1
Hierarchical divisive clustering of brain tumor patients, based on the collected features. The dendrogram reporting the clusters identified through divisive hierarchical clustering is reported. Gower distance is reported on the y axis and each single unit analyzed (i.e. patients) on the x axis. Vertical lines correspond to groups (or clusters) of units, while connecting (horizontal) lines identify the distance level at which clusters merge. Legend: red = cluster 1; green = cluster 2.

10.3389/fonc.2023.1276253

TABLE 2 Characteristics of the sample according to the two clusters identified.

	Cluster 1 (N=26)	Cluster 2 (N=41)	*p-value*
Gender, men; N (%)	26 (100.0)	7 (17.1)	*<.0001*
Age, years; mean (SD)	60.7 (13.3)	54.1 (14.8)	*0.06*
Educational level; N (%)			*0.032*
Up to secondary	12 (46.1)	14 (34.1)	
Upper secondary	8 (30.8)	16 (39.0)	
Post-secondary	6 (23.1)	11 (26.8)	
Occupation; N (%)			*<.0001*
Non- manual	6 (23.1)	15 (36.6)	
Manual	4 (15.4)	6 (14.6)	
Retired	14 (53.8)	7 (17.1)	
Housewife, unemployed and unclassified	2 (7.7)	13 (13.7)	
Place of residence; N (%)			*0.14*
Rural	9 (34.6)	10 (24.4)	
Urban	17 (65.4)	31 (75.6)	
Marital status; N (%)			*0.004*
Married	14 (53.9)	24 (58.5)	
Divorced/separated	3 (11.5)	7 (17.1)	
Single	5 (19.2)	5 (12.2)	
Widowed	1 (3.9)	3 (7.3)	
Missing	3 (11.5)	2 (4.9)	
Income; N (%)			*0.002*
< 10,000 Euros/y	3 (11.5)	8 (19.5)	
10,000-25,000 Euros/y	6 (23.1)	10 (24.4)	
≥25,000 Euros/y	13 (50.0)	11 (26.8)	
Non responder	4 (15.4)	12 (29.3)	
Smoking habit; N (%)			*<.0001*
Never	5 (19.2)	31 (75.6)	
Ever	21 (80.8)	10 (24.4)	
Diastolic blood pressure, mmHg; mean (SD)	70.2 (23.9)	76.5 (16.6)	*0.20*
Systolic blood pressure, mmHg; mean (SD)	112.3 (39.5)	123.5 (25.5)	*0.16*
Body mass index, kg/m^2; mean (SD)	28.0 (3.4)	26.6 (5.5)	*0.25*
Waist circumference, cm; mean (SD)	105.1 (10.4)	97.2 (15.3)	*0.046*
Physical activity level (life-style); N (%)			*0.049*
Sedentary	17 (65.4)	23 (56.1)	
Mildly active	5 (19.2)	10 (24.4)	
Physically active	4 (15.4)	8 (19.5)	
Hypertension; N (%)			*0.11*
No	13 (50.0)	26 (63.4)	
Yes	13 (50.0)	15 (36.6)	
Diabetes; N (%)			*0.22*
No	23 (88.5)	39 (95.1)	
Yes	3 (11.5)	2 (4.9)	
Dyslipidemia; N (%)			*0.14*
No	22 (84.6)	30 (73.2)	
Yes	4 (15.4)	11 (26.8)	
Cardiovascular disease; N (%)			*0.018*
No	21 (80.8)	39 (95.2)	
Yes	5 (19.2)	1 (2.4)	
Missing	0 (0.0)	1 (2.4)	
Cancer familiarity; N (%)			*0.012*
No	17 (65.4)	36 (87.8)	
Yes	8 (30.8)	4 (9.8)	
Missing	1 (3.8)	1 (2.4)	
Proximity to potential pollution sources; N (%)			*0.006*
No	20 (76.9)	18 (43.9)	
Yes	6 (23.1)	23 (56.1)	
Time spent using telephone; N (%)			*0.018*
<2h/d	16 (61.5)	25 (61.0)	
2-4h/d	7 (26.9)	8 (19.5)	
>4h/d	2 (7.7)	7 (17.1)	
Missing	1 (3.9)	1 (2.4)	
Sleeping with your phone nearby; N (%)			*0.13*
No	15 (57.7)	19 (46.3)	
Yes	11 (42.3)	22 (53.7)	
Old Head Injuries; N (%)			*0.059*
No	19 (73.1)	31 (75.6)	
Yes	2 (7.7)	5 (12.2)	
Missing	5 (19.2)	5 (12.2)	
Previous surgery; N (%)			*0.08*

10.3389/fonc.2023.1276253

TABLE 2 Continued

	Cluster 1 (N=26)	Cluster 2 (N=41)	*p-value*
No	7 (26.9)	5 (12.2)	
Yes	19 (73.1)	36 (87.8)	
Mediterranean Diet Score; mean (SD)	3.9 (1.5)	3.3 (1.3)	*0.09*
Energy intake, kcal; mean (SD)	2234 (588)	2057 (482)	*0.18*
Alcohol, g/d; mean (SD)	7.2 (15.8)	3.9 (8.0)	*0.27*
CD-RISC; mean (SD)	71.5 (14.2)	69.2 (13.0)	*0.50*
MoCA; mean (SD)	22.9 (2.4)	24.7 (3.3)	*0.02*
FACT-Br; mean (SD)	150.2 (29.7)	143.4 (27.4)	*0.34*
PHQ-9; mean (SD)	6.6 (5.7)	6.6 (5.8)	*0.97*

P-values (rounded to the second decimal place, unless statistically significant) refer to the comparison between clusters, which was performed through Fisher Exact Test for categorical variables, and through unpaired t-test for continuous variables.

TABLE 3 Contingency table showing tumor subtype by cluster distribution.

CNS tumors	Cluster 1	Cluster 2
Non-malignant	6	22
Malignant	20	19

and clinical data collected within the MEDICEA study. These included not only classical sociodemographic and anthropometric measures, but also environmental exposures, socioeconomic and lifestyle factors, clinical and psychometric features of the patients. We observed two distinct subtypes of patients: one with more professionally active, educated, wealthier and healthier patients, and the other one with mostly retired and less healthy men, with a family history of the disease and lower cognitive performance. Of note, the former cluster showed a protective association with the malignancy of the disease, showing a 74 (14-93) % reduction in the prevalent risk of CNS malignant tumors, compared to the other cluster (Figure 2). Since we cannot formally compare our findings with previous evidence due to the lack of studies using a cluster approach to pre-diagnostic history and clinical characteristics of brain cancer patients, we will focus below on the comparison of the evidence derived by this analysis with that produced by classical association studies in the field. Indeed, most of the associations and discrepancies observed between the two risk clusters followed the same trend reported by other studies. As for gender, our results revealed a significantly higher number of men among patients affected by cancer, especially among malignancies, and the totality of our putative risk cluster was made up of men. Previous literature reports a clear predominance of some types of brain tumors in males, such as astrocytomas, glioblastomas multiforme, medulloblastomas, ependymomas and oligodendrogliomas (25), while meningiomas occur more commonly in females than in males, a trend thought to be related to hormonal components (36). Another significant association was detected between self-reported yearly household income and tumor malignancy, with a higher income being associated with the putative risk cluster. Moreover, non-malignant tumors showed the highest percentage of subjects in the average income class (10,000-25,000 Euros/year), while patients with malignant tumors showed a higher prevalence of people declaring ≥25,000 Euros/year and presented many non-responders (37). Part of these non-responders may actually represent people who feel ashamed to self-report a low income (which may actually counteract the imbalance between clusters) and are usually treated as a class. In a study including a total of 11,892 patients with meningiomas, low-grade gliomas, and high-grade gliomas, no clear association was observed between income and the risk of developing brain tumors (38).

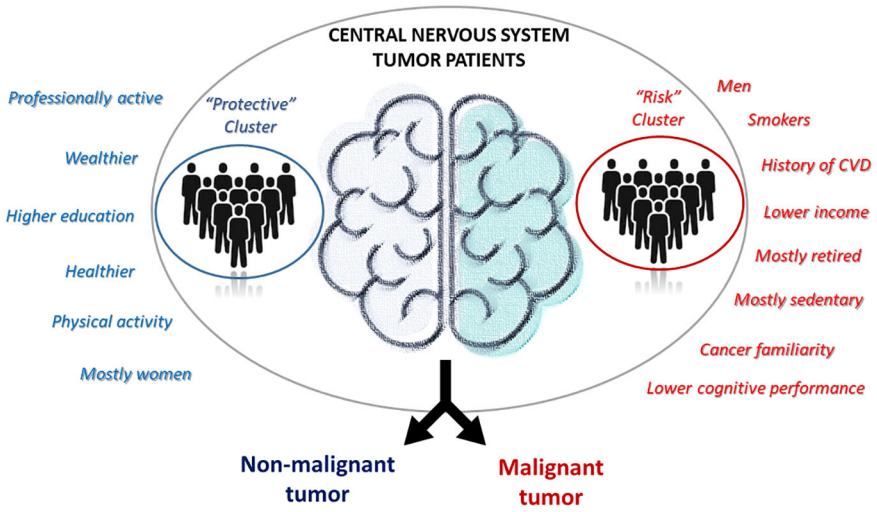

FIGURE 2
Characteristics of the two patients' clusters identified.

While no association was observed between cancer familiarity and tumor malignancy, this was significantly more frequent in the putative risk cluster, in line with previous studies, such as (39), which however reported significant excess of relatedness for astrocytomas, but not for glioblastomas. However, this link is still debated and needs to be clarified, especially with regard to the contribution of shared environmental and genetic factors to the clustering of cases within families (39). Similarly, we observed a higher frequency of ever smokers in the putative risk cluster, in spite of no significant direct association between malignancy and smoking status, but in agreement with previous evidence that active cigarette smoking was associated with an increased risk of CNS tumors in men, but with a reduced risk in women (40), and with gender-differential association between smoking and CNS tumor diagnosis in China (41).

From a more psychological perspective, although none of the psychometric scales assessed revealed direct associations with malignancy degree, the putative risk cluster identified showed a slightly worse cognitive performance. This is in line with the evidence that cognitive deficits are commonly observed in patients with brain tumors (42), and that this could even delay the diagnosis of brain tumor, because these symptoms are often linked to psychiatric diseases (22). However, it remains unclear whether this represents an early marker of brain tumor or a risk factor, a hypothesis which requires long-term longitudinal studies to be tested.

Our pilot study revealed no association with other potential or known risk factors like obesity and use of mobile phone, neither with tumor malignancy nor with risk/protective clusters. While the link with the use of mobile phone is still uncertain and debated (43–45), the lack of associations with obesity is in contrast with previous evidence reported by (17), although this association may be stronger in adolescence, rather than in adulthood (46). Moreover, participants assigned to the putative protective cluster reported more often to live or work in proximity of potential pollution sources like industries, signal relays/repeaters/antennas, sources of asbestos or landfills, which is not in line with a recent review in the field (47). However, this may be partly due to subjects from Cluster 2 more often reporting to live in an urban setting, where there is a higher density of such potential sources of pollution, or simply be a false positive finding.

Overall, we observed here a clear link between patients clinical, lifestyle, psychometric, environmental and socioeconomic profiling and the risk of malignancies, as well as different associations of potential risk factors with the putative risk cluster – in line with previous literature – which we could not always observe when comparing malignant vs non-malignant tumors. This supports the application of machine learning algorithms in stratifying patients based on a combination of risk and protective factors, clinical and biological characteristics, in line with the modern view of cancer epidemiology (23, 24), which represents the essence of personalized medicine and prevention. Should our findings be confirmed by larger independent studies, this information may be useful in the future to create potential intelligent ranking systems for treatment priority, overcoming the lack of histopathological information and molecular diagnosis of the tumor, which are typically not available until the time of surgery. This may ultimately have beneficial implications on timely cancer diagnosis, prognosis and outcomes, possibly increasing survival for patients.

4.1 Strengths and limitations

This preliminary study shows some points of strength, but also limitations. Strengths include the originality and novelty of the approach. Although clustering techniques have been already used in brain tumor classification, these were applied to segment brain tumors (48) and identify transcriptomic/immune subtypes useful for prognosis prediction (49) rather than to classify patients' profiles (49). To our knowledge, the present work is the first report of a cluster analysis based on data other than histological, neuroimaging and molecular characteristics from CNS tumor cases. This may notably improve the power to identify subtypes of disease, by taking into account also potentially complex and non-linear relationships among risk and protective factors. A further novelty consists in comparing CNS tumors based on their malignancy, while they are usually analyzed based on the tissue and cell type affected. The main limitation is represented by the cross-sectional/retrospective approach of the study, due to the current lack of longitudinal prospective data. Indeed, we are still collecting follow-up data after neurosurgery. Also, additional clinical variables like latency, dose-response and tumor localization may have been useful in patients profiling, but were not available at the time of the study due to the limitations imposed to the clinical research activity by the Covid-19 pandemics emergency, which forced us to interrupt recruitment, data collection and assessment. Due to this and to the rarity of the disease, sample size is also relatively small (<100), which may represent a hindrance to statistical power and clustering accuracy. For this reason, these findings warrant further replication in future independent studies on larger sample sizes, possibly including longitudinal data and a wider range of clinical features.

Author's note

MEDICEA Study investigators are listed in Supplementary Materials.

Data availability statement

The datasets presented in this study can be found in online repositories. The names of the repository/repositories can be found below: https://repository.neuromed.it. The password for accessing raw data will be provided upon reasonable request to the corresponding author.

Ethics statement

The studies involving humans were approved by Ethical Committee at the IRCCS Neuromed, Pozzilli, Italy. The studies

were conducted in accordance with the local legislation and institutional requirements. The participants provided their written informed consent to participate in this study.

Author contributions

SE: Conceptualization, Visualization, Writing – original draft, Data curation, Investigation, Project administration. ER: Conceptualization, Data curation, Formal analysis, Investigation, Project administration, Writing – original draft. ADC: Methodology, Writing – review & editing. SC: Data curation, Writing – review & editing. MB: Funding acquisition, Writing – review & editing. FB: Methodology, Writing – review & editing. VE: Data curation, Project administration, Resources, Writing – review & editing. GI: Data curation, Project administration, Resources, Writing – review & editing. SP: Data curation, Project administration, Resources, Writing – review & editing. CC: Conceptualization, Supervision, Writing – review & editing. MD: Conceptualization, Supervision, Writing – review & editing. GdG: Conceptualization, Supervision, Writing – review & editing. LI: Conceptualization, Funding acquisition, Supervision, Writing – review & editing. AG: Conceptualization, Formal analysis, Visualization, Writing – original draft.

Funding

The author(s) declare financial support was received for the research, authorship, and/or publication of this article. The present work has been performed in the context of the Fondazione Umberto Veronesi - IRCCS Neuromed framework agreement. The data analyses were partially supported by the Italian Ministry of Health (Ricerca Corrente 2022-2024). ER was supported by the Fondazione Umberto Veronesi, which is gratefully acknowledged. Funders had no role in study design, collection, analysis, and interpretation of data, nor in the writing of the manuscript or in the decision to submit the article for publication. All Authors were and are independent from funders.

Acknowledgments

We are grateful to the participants of the MEDICEA Study. The present study has been performed in the context of the Fondazione Umberto Veronesi - IRCCS Neuromed framework agreement. ER was supported by a fellowship of the Fondazione Umberto Veronesi, that is gratefully acknowledged. We are grateful to all the Clinical Network Big Data and Personalised Health Project participants who enthusiastically joined the study and to all clinicians who contributed to recruitment, collection, assessment and elaboration of samples.

Conflict of interest

The authors declare that the research was conducted in the absence of any commercial or financial relationships that could be construed as a potential conflict of interest.

The author(s) declared that ER was a review editor, MB, MD, GdG and LI were all Guest associate editors, VE was an associate editor and AG was a Guest Associate Editor and Review Editor and they were all members of the Frontiers, editorial board member of at the time of submission. This had no impact on the peer review process and the final decision.

Publisher's note

Supplementary material

The Supplementary Material for this article can be found online at: https://www.frontiersin.org/articles/10.3389/fonc.2023.1276253/full#supplementary-material

References

1. Bondy ML, Scheurer ME, Malmer B, Barnholtz-Sloan JS, Davis FG, Il'yasova D, et al. Brain Tumor Epidemiology Consortium. Brain tumor epidemiology: consensus from the Brain Tumor Epidemiology Consortium. *Cancer* (2008) 113(7 Suppl):1953–68. doi: 10.1002/cncr.23741

2. Louis DN, Perry A, Reifenberger G, von Deimling A, Figarella-Branger D, Cavenee WK, et al. The 2016 World Health Organization classification of tumors of the central nervous system: a summary. *Acta Neuropathol* (2016) 131(6):803–20. doi: 10.1007/s00401-016-1545-1

3. Busco S, Buzzoni C, Mallone S, Trama A, Castaing M, Bella F, et al. Italian cancer figures–Report 2015: The burden of rare cancers in Italy. *Epidemiol Prev* (2016) 40(1 Suppl 2):1–120. doi: 10.19191/EP16.1S2.P001.035

4. Connelly JM, Malkin MG. Environmental risk factors for brain tumours. *Curr Neurol Neurosci Rep* (2007) 7(3):208–14. doi: 10.1007/s11910-007-0032-4

5. Barnholtz-Sloan JS, Ostrom QT, Cote D. Epidemiology of brain tumours. *Neurol Clin* (2018) 36(3):395–419. doi: 10.1016/j.ncl.2018.04.001

6. Schwingshackl L, Schwedhelm C, Galbete C, Hoffmann G. Adherence to mediterranean diet and risk of cancer: an updated systematic review and meta-analysis. *Nutrients* (2017) 9(10):E1063. doi: 10.3390/nu9101063

7. Levin VA, Leibel SA, Gutin PH. Neoplasms of the central nervous system. In: DeVita VTJ, Hellman S, Rosenberg SA, editors. *Cancer: Principles and Practice of Oncology*. Lippincott-Raven: Philadelphia (2001). p. 2100–60.

8. Praud D, Bertuccio P, Bosetti C, Turati F, Ferraroni M, La Vecchia C. Adherence to the mediterranean diet and gastric cancer risk in Italy. *Int J Cancer* (2014) 134:2935–41. doi: 10.1002/ijc.28620

9. Machowetz A, Poulsen HE, Gruendel S, Weimann A, Fitó M, Marrugat J, et al. Effect of olive oils on biomarkers of oxidative DNA stress in Northern and Southern Europeans. *FASEB J* (2007) 21(1):45–52. doi: 10.1096/fj.06-6328com

10. Castelló A, Boldo E, Pérez-Gómez B, Lope V, Altzibar JM, Martín V, et al. Adherence to the western, prudent and mediterranean dietary patterns and breast cancer risk: MCC-Spain study. *Maturitas* (2017) 103:8–15. doi: 10.1016/j.maturitas.2017.06.020

11. Esposito S, Bonaccio M, Ruggiero E, Costanzo S, Di Castelnuovo A, Gialluisi A, et al. Food processing and risk of central nervous system tumours: A preliminary case-control analysis from the MEditerranean DIet in relation to CancEr of brAin (MEDICEA) study. *Clin Nutr* (2022) 42(2):93–101. doi: 10.1016/j.clnu.2022.11.016

12. Lian W, Wang R, Xing B, Yao Y. Fish intake and the risk of brain tumor: a meta-analysis with systematic review. *Nutr J* (2017) 16(1):1. doi: 10.1186/s12937-016-0223-4

13. Carlberg M, Söderqvist F, Hansson Mild K, Hardell L. Meningioma patients diagnosed 2007–2009 and the association with use of mobile and cordlessphones: a case–control study. *Environ Health* (2013) 12(1):60. doi: 10.1186/1476-069X-12-60

14. Carlberg M, Hardell L. Decreased survival of glioma patients with astrocytoma grade IV (glioblastoma multiforme) associated with long-term use of mobile and cordless phones. *Int J Environ Res Public Health* (2014) 11(10):10790–805. doi: 10.3390/ijerph111010790

15. Leng L. The relationship between mobile phone use and risk of brain tumour: a systematic review and meta-analysis of trails in the last decade. *Leng Chin Neurosurgical J* (2016) 2:38. doi: 10.1186/s41016-016-0059-y

16. Bogovski P, Bogovski S. Animal Species in which N-nitroso compounds induce cancer. *Int J Cancer* (1981) 27(4):471–4. doi: 10.1002/ijc.2910270408

17. Benson VS, Pirie K, Green J, Casabonne DV Beral for the Million Women Study Collaborators. Lifestyle factors and primary glioma and meningioma tumours in the Million Women Study cohort. *Br J Cancer* (2008) 99:185–190. doi: 10.1038/sj.bjc.6604445

18. Inskip PD, Tarone RE, Hatch EE, Wilcosky TC, Fine HA, Black PM, et al. Sociodemographic indicators and risk of brain tumours. *Int J Epidemiol* (2003) 32 (2):225–33. doi: 10.1093/ije/dyg051

19. Provost D, Cantagrel A, Lebailly P, Jaffré A, Loyant V, Loiseau H, et al. Brain tumours and exposure to pesticides: a case-control study in southwestern France. *Occup Environ Med* (2007) 64(8):509–14. doi: 10.1136/oem.2006.028100

20. Giovagnoli AR. Investigation of cognitive impairments in people with brain tumors. *J Neurooncol* (2012) 108(2):277–83. doi: 10.1007/s11060-012-0815-6

21. Kahana MJ. The cognitive correlates of human brain oscillations. *J Neurosci* (2006) 26(6):1669–72. doi: 10.1523/JNEUROSCI.3737-05c.2006

22. Ghandour F, Squassina A, Karaky R, Diab-Assaf M, Fadda P, Pisanu C. Presenting psychiatric and neurological symptoms and signs of brain tumors before diagnosis: A systematic review. *Brain Sci* (2021) 11(3):301. doi: 10.3390/brainsci11030301

23. Dagogo-Jack I, Shaw AT. Tumour heterogeneity and resistance to cancer therapies. *Nat Rev Clin Oncol* (2018) 15(2):81–94. doi: 10.1038/nrclinonc.2017.166

24. Garattini S, Fuso Nerini I, D'Incalci M. Not only tumor but also therapy heterogeneity. *Ann Oncol* (2018) 29(1):13–9. doi: 10.1093/annonc/mdx646

25. Ostrom QT, Cioffi G, Gittleman H, Patil N, Waite K, Kruchko C, et al. CBTRUS statistical report: primary brain and other central nervous system tumors diagnosed in the United States in 2012-2016. *Neuro Oncol* (2019) 21(Suppl 5):v1–v100. doi: 10.1093/neuonc/noz150

26. Luca S. Proposal for a statistical-economic assessment of soil degradation: A national scale approach. *RIV* (2014) 56:312–43. doi: 10.4081/ija.2020.1770

27. Clinical guidelines on the identification, evaluation, and treatment of overweight and obesity in adults–the evidence report. National institutes of health. *Obes Res* (1998) 6 Suppl 2:51S–209S. doi: 10.1002/j.1550-8528.1998.tb00690.x

28. Pisani P, Faggiano F, Krogh V, Palli D, Vineis P, Berrino F. Relative validity and reproducibility of a food frequency dietary questionnaire for use in the Italian EPIC centres. *Int J Epidemiol* (1997) 26 Suppl 1:S152–60. doi: 10.1093/ije/26.suppl_1.s152

29. Trichopoulou A, Costacou T, Bamia C, Trichopoulos D. Adherence to a Mediterranean diet and survival in a Greek population. *N Engl J Med* (2003) 348 (26):2599–608. doi: 10.1056/NEJMoa025039

30. Available at: https://www.facit.org/measures/FACT-Br.

31. Connor KM, Davidson JR. Development of a new resilience scale: the Connor-Davidson Resilience Scale (CD-RISC). *Depress Anxiety* (2003) 18(2):76–82. doi: 10.1002/da.10113

32. Hobson J. The montreal cognitive assessment (MoCA). *Occup Med (Lond)* (2015) 65(9):764–5. doi: 10.1093/occmed/kqv078

33. Nasreddine ZS, Phillips NA, Bédirian V, Charbonneau S, Whitehead V, Collin I, et al. The Montreal Cognitive Assessment, MoCA: a brief screening tool for mild cognitive impairment. *J Am Geriatr Soc* (2005) 53(4):695–9. doi: 10.1111/j.1532-5415.2005.53221.x

34. Kroenke K, Spitzer RL, Williams JB. The PHQ-9: validity of a brief depression severity measure. *J Gen Intern Med* (2001) 16(9):606–13. doi: 10.1046/j.1525-1497.2001.016009606.x

35. R Core Team. *R: A language and environment for statistical computing*. Vienna, Austria: R Foundation for Statistical Computing (2021). Available at: https://www.R-project.org/.

36. Cowppli-Bony A, Bouvier G, Rué M, Loiseau H, Vital A, Lebailly P, et al. Brain tumors and hormonal factors: review of the epidemiological literature. *Cancer Causes Control* (2011) 22(5):697–714. doi: 10.1007/s10552-011-9742-7

37. Bonaccio M, Di Castelnuovo A, Costanzo S, De Curtis A, Persichillo M, Cerletti C, et al. Impact of combined healthy lifestyle factors on survival in an adult general population and in high-risk groups: prospective results from the Moli-sani Study. *J Intern Med* (2019) 286(2):207–20. doi: 10.1111/joim.12907

38. Nilsson J, Holgersson G, Järås J, Bergström S, Bergqvist M. The role of income in brain tumour patients: a descriptive register-based study: No correlation between patients' income and development of brain cancer. *Med Oncol* (2018) 35(4):52. doi: 10.1007/s12032-018-1108-5

39. Blumenthal DT, Cannon-Albright LA. Familiarity in brain tumors. *Neurology* (2008) 71(13):1015–20. doi: 10.1212/01.wnl.0000326597.60605.27

40. Claus EB, Walsh KM, Calvocoressi L, Bondy ML, Schildkraut JM, Wrensch M, et al. Cigarette smoking and risk of meningioma: the effect of gender. *Cancer Epidemiol Biomarkers Prev* (2012) 21(6):943–50. doi: 10.1158/1055-9965.EPI-11-1059

41. Lei H, Jiang J, Liu B, Han W, Wu Y, Zou X, et al. Smoking and adult glioma: a population-based case-control study in China. *Neuro Oncol* (2016) 18(1):105–13. doi: 10.1093/neuonc/nov146

42. Van Kessel E, Baumfalk AE, van Zandvoort MJE, Robe PA, Snijders TJ. Tumor-related neurocognitive dysfunction in patients with diffuse glioma: a systematic review of neurocognitive functioning prior to anti-tumor treatment. *J Neurooncol* (2017) 134 (1):9–18. doi: 10.1007/s11060-017-2503-z

43. Inskip PD, Hoover RN, Devesa SS. Brain cancer incidence trends in relation to cellular telephone use in the United States. *Neuro Oncol* (2010) 12(11):1147–51. doi: 10.1093/neuonc/noq077

44. Hardell L, Carlberg M. Mobile phones, cordless phones and rates of brain tumors in different age groups in the Swedish Na-tional Inpatient Register and the Swedish Cancer Register during 1998-2015. *PloS One* (2017) 12(10):e0185461. doi: 10.1371/journal.pone.0185461

45. Hours M, Bernard M, Montestrucq L, Arslan M, Bergeret A, Deltour I, et al. Téléphone mobile, risque de tumeurs cérébrales et du nerf vestibuloacoustique: l'étude cas-témoins INTERPHONE en France [Cell Phones and Risk of brain and acoustic nerve tumours: the French INTERPHONE case-control study]. *Rev Epidemiol Sante Publique* (2007) 55(5):321–32. doi: 10.1016/j.respe.2007.06.002

46. Moore SC, Rajaraman P, Dubrow R, Darefsky AS, Koebnick C, Hollenbeck A, et al. Height, body mass index, and physical activity in relation to glioma risk. *Cancer Res* (2009) 69(21):8349–55. doi: 10.1158/0008-5472.CAN-09-1669

47. Pagano C, Navarra G, Coppola L, Savarese B, Avilia G, Giarra A, et al. Impacts of environmental pollution on brain tumorigenesis. *Int J Mol Sci* (2023) 24(5):5045. doi: 10.3390/ijms24055045

48. Khan AR, Khan S, Harouni M, Abbasi R, Iqbal S, Mehmood Z. Brain tumor segmentation using K-means clustering and deep learning with synthetic data augmentation for classification. *Microsc Res Tech* (2021) 84(7):1389–99. doi: 10.1002/jemt.23694

49. Shen X, Wang X, Shen H, Feng M, Wu D, Yang Y, et al. Transcriptomic analysis identified two subtypes of brain tumor characterized by distinct immune infiltration and prognosis. *Front Oncol* (2021) 11:734407. doi: 10.3389/fonc.2021.734407

frontiers | Frontiers in Neuroscience

TYPE Review
PUBLISHED 14 December 2023
DOI 10.3389/fnins.2023.1217629

OPEN ACCESS

EDITED BY
Peichen Pan,
Zhejiang University, China

REVIEWED BY
Prateek Pratyasha,
National Institute of Technology Raipur, India
Masamichi Takahashi,
National Cancer Center Hospital, Japan

*CORRESPONDENCE
L. Nicolas Gonzalez Castro
✉ lgonzalez-castro@dfci.harvard.edu

RECEIVED 05 May 2023
ACCEPTED 14 November 2023
PUBLISHED 14 December 2023

CITATION
Nakhate V and Gonzalez Castro LN (2023) Artificial intelligence in neuro-oncology. *Front. Neurosci.* 17:1217629. doi: 10.3389/fnins.2023.1217629

Artificial intelligence in neuro-oncology

Vihang Nakhate[1,2] and L. Nicolas Gonzalez Castro[1,3,4]*

[1]Department of Neurology, Brigham and Women's Hospital, Harvard Medical School, Boston, MA, United States, [2]Massachusetts General Hospital, Harvard Medical School, Boston, MA, United States, [3]Harvard Medical School, Boston, MA, United States, [4]The Center for Neuro-Oncology, Dana–Farber Cancer Institute, Boston, MA, United States

Artificial intelligence (AI) describes the application of computer algorithms to the solution of problems that have traditionally required human intelligence. Although formal work in AI has been slowly advancing for almost 70 years, developments in the last decade, and particularly in the last year, have led to an explosion of AI applications in multiple fields. Neuro-oncology has not escaped this trend. Given the expected integration of AI-based methods to neuro-oncology practice over the coming years, we set to provide an overview of existing technologies as they are applied to the neuropathology and neuroradiology of brain tumors. We highlight current benefits and limitations of these technologies and offer recommendations on how to appraise novel AI-tools as they undergo consideration for integration into clinical workflows.

KEYWORDS

neuro-oncology, Artificial intelligence, brain tumor, glioma, glioblastoma, IDH gliomas mut

Introduction

As Artificial intelligence (AI) continues to shape and reshape various aspects of our physical and virtual lives, its growing impact on and promise in medicine are hard to ignore. One of the first definitions of "artificial intelligence" was formulated in 1956 by Prof. John McCarthy at Dartmouth University, to refer to "making a machine behave in ways that would be called intelligent if a human were so behaving." (Nillson, 2010). In a broad sense, AI signifies machines that can simulate human intelligence with tasks like learning, visual processing, problem-solving, decision-making, and that increasingly can extend the reaches of human intelligence with enhanced classification and prediction. While Artificial General Intelligence (AGI), or "strong AI," refers to systems that can perform a wide range of tasks comparably to humans, most existing systems are considered Artificial Narrow Intelligence (ANI), or "weak AI," signifying systems capable of performing a defined task (Russel and Norvig, 2020). Narrow AI systems can be further classified based on physical (robotic/automation systems) and cognitive applications (machine learning, computer vision, natural language processing). Most AI applications in medicine are comprised of machine learning (ML) applications. ML refers to the ability of algorithms (see Table 1) to derive patterns and rules ("learn") from large sets of data to recognize patterns, perform tasks or make predictions without being explicitly programmed to do so (Kann et al., 2021). Within ML, learning algorithms can be characterized as supervised (using data with labeled input–output pairs), unsupervised (using data without labeled inputs) or reinforcement (using a reinforcement feedback signal for learning). While conventional ML requires manual engineering of raw data to create representations suitable for ML algorithms to learn, deep learning (DL) refers to a subset of ML techniques that can extract and learn features from raw, unstructured and multimodal data (e.g., raw imaging, text, audio-visual data) using

TABLE 1 Glossary of commonly used artificial intelligence terms.

Artificial intelligence (AI)	Computer algorithms that can solve problems, inform decision-making and perform complex tasks that have traditionally required human intelligence
Machine learning (ML)	Discipline in AI involving computers or "machines" as agents that can learn patterns and rules from large sets of data to build predictive models and solve problems, without being explicitly programmed to do so
Algorithm	Set of rules that an agent, in this case a "machine," can follow to complete a set of tasks
Supervised learning	Machine learning in which the agent observes data consisting of input–output pairs with manually assigned labels, and learns a function that predicts output from input
Unsupervised learning	Machine learning in which the agent learns patterns in the input without any explicit manual feedback
Random forest algorithm	Type of supervised learning algorithm used for classification and regression tasks, in which a large number of decision trees operate together as an ensemble to reach a common output result
Support vector machine	Type of supervised learning algorithm used for classification and regression tasks, in which a subset of training points (support vectors) from the decision function are used to complete a given task
Deep learning (DL)	Machine learning techniques in which the computational path between input and output consists of multiple layers of simple, adjustable computing elements. The resulting computational circuit, termed a**neural network**, allows for a large number of input variables to interact in complex ways. Widely used in visual object recognition, speech recognition, image and speech synthesis.
Convolutional neural networks	Type of DL neural network architecture commonly used in analysis of images
Transfer learning	Machine learning method in which knowledge gained by an agent from one domain can be transferred and applied to a new domain, so that learning can proceed faster with less data
Large language model	A neural network-based model trained on large text datasets using self-supervised learning.

Adapted from *Artificial Intelligence: A Modern Approach*, Russel and Norvig (2020).

layered neural networks (LeCun et al., 2015). DL algorithms can be supervised or unsupervised (see Figure 1).

With the advent of increasing computing power in recent decades, DL has achieved remarkable results in areas including image classification, speech recognition, and game playing, among others (LeCun et al., 2015; Silver et al., 2016). Remarkable flexibility of input and output structures coupled with modern computing power have positioned ML and DL well to analyze large data sets that are increasingly being generated in modern medicine and oncology, and to aid in using such data to guide decision making.

The applications of ML to medicine, oncology, and neuro-oncology are myriad, spanning enhanced screening, diagnosis, prognosis, classification, drug discovery, precision medicine, and more (di Nunno et al., 2022). In neuro-oncology, work utilizing ML algorithms has so far predominantly been focused on neuropathology and neuroradiology applications, including tumor diagnosis and grading, prediction of molecular features, and automated assessment of tumor volume (Figure 2).

Neuropathology applications of AI for neuro-oncology

Histopathologic and genomic features

Histopathologic analysis has long been at the heart of diagnosis in oncology. However, it is susceptible to interobserver variability that can impede accurate diagnosis and optimized management (van den Bent, 2010). In neuro-oncology, grading of gliomas based on atypia, mitosis, microvascular proliferation and necrosis entails some degree of subjectivity that is contributory. The introduction of molecular features such as isocitrate dehydrogenase (IDH) mutation and 1p/19q co-deletion status into WHO grading of gliomas, as well as the burgeoning availability of individualized tumor genetic data, leaves AI well-positioned to assist pathologists in interpreting large and multiparametric data to establish diagnoses (see Table 2).

The advent of high quality digitized whole slide images (WSIs) has allowed for the application of DL in histopathologic diagnosis. Broadly in oncology, DL algorithms have been used to detect metastatic breast cancer in lymph node biopsies (Litjens et al., 2016; Ehteshami Bejnordi et al., 2017), assign Gleason scores in prostate cancer biopsies (Litjens et al., 2016; Nagpal et al., 2020), and distinguish lung adenocarcinoma and squamous cell carcinoma from normal lung tissue (Coudray et al., 2018), among others, with high accuracy.

In neuro-oncology, convolutional neural networks (CNNs) trained on WSIs of gliomas have been used to render nonbiased neuropathologic diagnoses of gliomas. Ertosun et al. trained two CNNs on publicly available hematoxylin and eosin (H&E) stained histopathology images of gliomas from The Cancer Genome Atlas (TCGA). One CNN aimed to distinguish glioblastoma (GBM) vs. low-grade glioma (LGG), the other to distinguish grade 2 from grade 3 LGGs. When tested on an independent data set of glioma WSIs, the CNNs determined histopathologic grade with 96% accuracy for GBM vs. LGG and 71% accuracy for grade 2 vs. grade 3 (Ertosun and Rubin, 2015). A similar study by Truong et al. trained multiple CNNs using TCGA WSIs, with the best models achieving 73% mean accuracy in distinguishing GBM from LGG, and 53% accuracy in distinguishing grade 2 from grade 3 LGGs (Truong et al., 2020). Limitations in both included absence of IDH mutant/1p19q codeletion status of the tumors.

Jin et al. developed a platform named "AI Neuropathologist," whereby a CNN was trained on over 79,000 H&E-stained histologic patch WSIs from 267 patients from an institutional biobank to distinguish GBM, anaplastic astrocytoma (AA), anaplastic oligodendroglioma (AO), astrocytoma (A), oligodendroglioma (O), and background glia. The CNN derived histopathologic features and

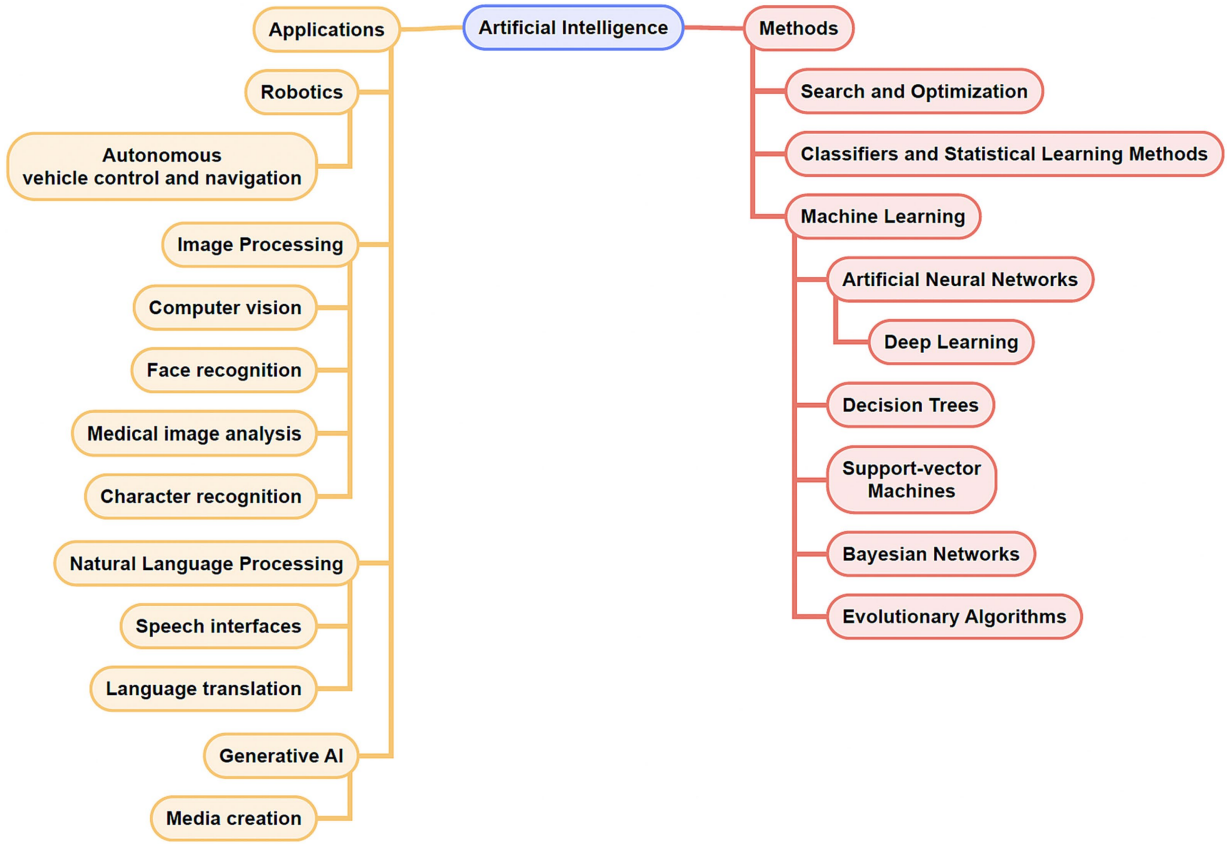

FIGURE 1
Concept map of select artificial intelligence (AI) applications and methods. Note that there exists overlap among some of the applications and methods listed.

classified gliomas from 56 independent patients with over seventeen thousand images into the above categories with an average patch-level accuracy of 86.5%, and patient-level accuracy of 87.5% (Jin et al., 2021). However when the tumors' IDH/1p19q status was assessed, the numbers of patients with each genetically classified tumor subtype in the training sample were in some cases found to be relatively low (e.g., 16 "GBM with IDH mutant" and 39 "GBM with IDH-wild type") (Komori, 2021). Im et al. used deep transfer learning to classify subtypes of gliomas from histopathologic images generated in routine clinical practice from a single institution cohort of 468 patients. Their model distinguished oligodendroglial tumors from non-oligodendroglial tumors with an accuracy of 87.3%, whereas in distinguishing glioma grade 2 vs. 3 vs. 4 the accuracy was 58% (Im et al., 2021). Pie et al. developed a deep learning-based model that fused molecular and histopathologic features to predict glioma grade. They used digital WSIs from 549 patients in the TCGA with molecular information on IDH, 1p/19q, *ATRX*, and O^6-methylguanine-DNA methyltransferase (*MGMT*) promoter alterations. Their model achieved an accuracy of 93.8% in distinguishing high grade glioma (HGG) from LGG, and 74% distinguishing grade 2 vs. grade 3 gliomas, the latter outperforming state-of-the-art methods (Pei et al., 2021). Finally, Hollon et al. developed a DL-based method of rapid automated molecular classification of diffuse glioma from intraoperative tissue samples (Hollon et al., 2023). They trained a CNN using histologic images from 373 diffuse glioma patients, acquired by Stimulated Raman Histology (SRH) imaging. They also trained a genetic embedding model using TCGA and other public glioma genomic databases to learn labels that define molecular subgroups of diffuse gliomas. The SRH and genetic encoders were integrated to predict IDH, 1p19q, and ATRX mutations and thereby achieve molecular classification of gliomas by WHO criteria. When prospectively tested on 153 patients, the model predicted WHO glioma classification with a mean 93.3% accuracy, including IDH mutation (94.7%), 1p19q co-deletion (94.1%), and ATRX mutation (91.0%).

Tumor classification based on DNA methylome profiling

In addition to histopathology and direct genomic alterations, DNA methylome profiling has emerged as a valuable method for classifying CNS tumors. Cancer cells undergo substantial alterations in DNA methylation patterns, which when profiled by epigenome-wide methylation assays may be used to classify tumor types with high specificity (Moran et al., 2016). Seminal work in harnessing the methylome was conducted by Capper et al., who developed a ML algorithm to classify CNS tumors based on DNA methylation profiles (Capper et al., 2018). The authors trained the algorithm with methylation data for 2,801 pre-classified samples of almost every CNS

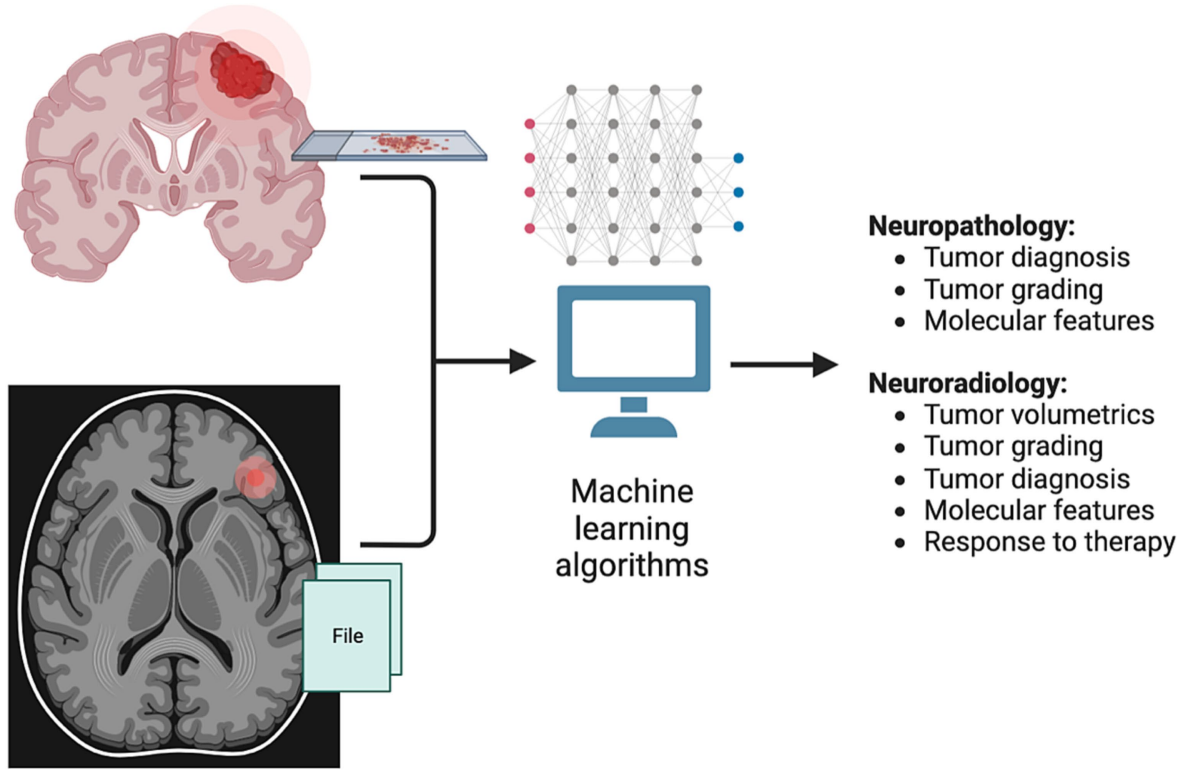

FIGURE 2
Applications of machine learning (ML) in neuro-oncology. Current research applications of ML methods in neuro-oncology have mainly introduced in the fields of neuropathology and neuro-radiology. In neuropathology, ML methods have been developed to establish a tumor diagnosis based on histopathologic and genomic features, as well as to classify tumors based on DNA methylation status. In neuroradiology, ML has been used to generate automated 3D tumor measurements (volumetrics), as well as to help predict tumor diagnosis, grading, molecular features and response to therapy.

TABLE 2 Select studies on the application of AI/ML to neuropathology in neuro-oncology.

Authors and year	Study sample (total n)	Task	ML algorithm	Performance
Ertosun and Rubin (2015)	Gliomas grade 2–4 (44 whole tissue slides)	Glioma grade	CNN	Accuracy 96% GBM vs. LGG; 71% grade 2 vs. grade 3
Jin et al. (2021)	Glioma grade 2–4 (323 patients)	Glioma classification	CNN	Accuracy 87.5%
Pei et al. (2021)	Glioma grade 2–4 (549 patients)	Glioma grade	DNN	Accuracy 93.8% HGG vs. LGG; 74% grade 2 vs. grade 3
Hollon et al. (2023)	Diffuse glioma (373 patients)	Glioma WHO classification	CNN	93.3% accuracy
Capper et al. (2018)	Most WHO-classified CNS tumors (2801)	CNS Tumor WHO classification	Supervised ML (random forest classifier), unsupervised ML	60.4% agree with pathologist; 15.5% better subclass; 12.6% did not match pathologist but most eventually proved accurate; 11.5% unclassified

LGG, low-grade glioma; HGG, high-grade glioma; GBM, glioblastoma; WHO, world health organization; ML, machine learning; CNN, convolutional neural network; DNN, deep neural network.

tumor type. The algorithm used supervised machine learning to recognize methylation patterns based on the known classifications, as well as unsupervised learning to search for patterns to independently assign samples into computer generated categories. In so doing the algorithm assigned the tumors to 82 distinct classes – around one-third matched known WHO tumor types; one-third represented sub-classes of WHO tumor types; notably, the remainder were classifications that did not match WHO groupings, including previously unrecognized tumor types, and those with histologic overlap but distinct methylation profiles. When prospectively tested on 1,104 new samples, the algorithm's classification matched the pathologist's diagnosis in 60.4% of cases; in 15.5%, the two classifications matched but the algorithm classified the tumor into a subgroup that could not be assigned by histopathology alone. In 12.6% of the cases, the algorithm's diagnosis did not match the pathologist's and, remarkably, further analysis (including by gene sequencing)

revealed that 92.8% of these unmatched tumors were reclassified from the pathologists' diagnosis to the algorithm's diagnosis, including a majority that were assigned a new tumor grade. Finally, 11.5% could not be classified by the algorithm (Capper et al., 2018; Machine Learning Improves Diagnosis of CNS Cancers, 2018; Wong and Yip, 2018). Since then, multiple studies have corroborated the algorithm's fidelity, and it has been incorporated into clinical pipelines at centers across the world (Capper et al., 2018; Jaunmuktane et al., 2019; Karimi et al., 2019; Priesterbach-Ackley et al., 2020). It has been especially useful in the classification of tumors with morphology that is heterogeneous or otherwise challenging to distinguish, including ependymomas, medulloblastomas, and diffuse glioneuronal tumors (Capper et al., 2018; Pickles et al., 2020). Its utility in guiding diagnoses for these tumors has been incorporated into the 2021 WHO guidelines for CNS tumor classification (Louis et al., 2021).

Neuroradiology applications of AI for neuro-oncology

MRI imaging is the mainstay of diagnosis, radiographic surveillance, and assessment of treatment response in neuro-oncology. However, MRI interpretation in brain tumor patients can sometimes be challenging – treatment related changes may resemble tumor progression; histologic and molecular features that drive prognosis and guide treatment often lack readily apparent imaging correlates; and determining tumor size can pose a challenge in tumors with heterogeneous and infiltrative components. AI methods including ML, DL, and radiomics have been employed to extract from images clinically relevant information that may not be apparent visually (see Table 3). Radiomics is the process of extracting quantitative and mineable data or "features" (e.g., shape, intensity, texture) from clinical imaging. ML methods are often used to build models using these features that can predict various clinical variables. In neuro-oncology, ML/DL have been used to quantify tumor size and type, predict tumor grade, molecular features, and survival. Typically, MRI data are pre-processed and standardized, labeled/annotated by radiologists to establish ground truth for training of ML algorithms, and then may undergo augmentation, transformation and further pre-processing before being used for the training of ML/DL algorithms (Zhu et al., 2022). Often the performance of these trained algorithms is assessed on a "test" cohort of patient images not encountered in training. Technical aspects of AI in brain tumor imaging have also been reviewed elsewhere (Afridi et al., 2022; Aftab et al., 2022).

Tumor volumetrics

Reliably delineating tumor size and burden on structural MRI brain is necessary to longitudinally assess tumor progression and response to treatment, and is thus critical to both effective clinical care and the assessment of response in clinical trials. However, identifying tumor boundaries manually on MRI per the RANO (Response Assessment in Neuro-Oncology) criteria, which involve quantitative 2D measurements of contrast-enhancing and FLAIR hyperintense lesions, can be challenging for infiltrative tumors like high grade gliomas, and is associated with high interrater variability (Vos et al., 2003; Pope and Hessel, 2011; Ford et al., 2016).

Chang et al. developed a deep learning algorithm to automatically segment T2/FLAIR and T1-post contrast MRI images of adult gliomas to quantify both 2D RANO measurements as well as 3D tumor volumes (Chang et al., 2019). They used MRIs from 800 patients with newly diagnosed LGG and HGGs, and over 700 post-op longitudinal MRIs from 50 patients with newly diagnosed GBMs. Their automated tumor quantification was reproducible in double baseline MRIs (interclass correlation coefficients, or ICCs, > 0.97), with high agreement between manual and automated tumor volumes (ICCs >0.91), and between manually and automatically derived longitudinal changes in tumor burden (ICCs >0.85). Though their automated RANO measurements were reproducible and internally consistent, they were often larger than manual RANO measurements. Taken together with inconsistency of RANO measurements found between the two human raters, these findings suggested that the automated measurements may be more accurate (detecting longer diameters than can be visualized by eye), and more precise. Peng et al. used a similar deep-learning approach to develop an algorithm that determines two dimensional measurements and three-dimensional volume in pediatric high grade gliomas, medulloblastomas, and other leptomeningeal-seeding tumors, with high repeatability and agreement with human raters (Peng et al., 2022).

3D volumetric measurements are not routinely used in response assessment for gliomas, in part due to the labor intensive, time-consuming, and variable nature of segmentation approaches, though they are likely more reliable and accurate than 2D measurements (Sorensen et al., 2001, 2008). Kickingereder et al. trained a DL-based CNN to carry out automated tumor segmentation on MRI data from 455 patients with brain tumors (mostly gliomas), and tested it on over two thousand MRIs from over 500 patients. The algorithm demonstrated high precision with Dice coefficients of 0.91 (T1 post-contrast) and 0.93 (T2/FLAIR) (Barash and Klang, 2019; Kickingereder et al., 2019).

Although a recent evaluation of the RANO criteria suggests that analysis of FLAIR data (when performed by humans) does not add additional information in terms of predicting survival (Youssef et al., 2023), analysis of FLAIR sequences with automated algorithms such as developed by Chang et al. and Kickingereder et al. may enable the incorporation of volumetric assessment of gliomas into research assessments and potentially clinical practice.

Prediction of molecular features

As signified by their growing prominence in the WHO classification of central nervous system tumors in 2016 and 2021, molecular features of CNS tumors are increasingly informing diagnosis, prognosis, and management (Louis et al., 2021; Gritsch et al., 2022). For instance, the presence of an IDH mutation in adult gliomas precludes a diagnosis of glioblastoma, WHO grade 4, regardless of histologic grade given its favorable prognosis compared to IDH wildtype tumors. IDH mutant gliomas with 1p/19q co-deletion are classified as oligodendrogliomas (WHO grade 2–3), and those without 1p/19q co-deletion are classified as astrocytomas (WHO grade 2–4). This highlights the importance of molecular testing, which can be time consuming and requires adequate surgical tissue for histopathologic and genetic analysis, in routine clinical practice. Noninvasive determination of a tumor's molecular features via

TABLE 3 Select studies on the application of AI/ML to neuroradiology in neuro-oncology.

Authors and Year	Study sample (total n)	Task	ML algorithm	Performance
Chang et al. (2019)	Newly diagnosed LGG/HGG (800), longitudinal newly diagnosed GBM (50)	tumor volumes and RANO measurements	DL	Double baseline MRIs ICCs >0.97; manual vs. automated ICC > 0.85
Kickingereder et al. (2019)	Mostly gliomas (1027)	Tumor volumes	ANN	DICE coefficients 0.91 (T1-post), 0.93 (T2/FLAIR)
Zhang et al. (2017)	HGGs (120)	IDH mutation status	Random forest	Accuracy 89%, AUC 0.92
Chang et al. (2018)	LGGs and HGGs (259)	Automated segmentation; IDH, 1p/19q, *MGMT* promoter status	CNN	Accuracy 94% (IDH), 92% (1p/19q), 83% (MGMT promoter)
Akkus et al. (2017)	LGGs (159)	1p/19q status	CNN	Accuracy 87.7%
van der Voort et al. (2019)	Presumed LGG on pre-op MRI (413)	1p/19q status	Support vector machine	AUC 0.72
Yogananda et al. (2020)	LGGs and HGGs (368)	1p/19q status	3D CNN	Accuracy 93.46%
Zhou et al. (2019)	Grade 2–4 glioma (744)	IDH and 1p/19q status	Random forest	AUC 0.92 (IDH status); accuracy 78.2% (3-group classification)
Cluceru et al. (2022)	Grade 2–4 glioma (531)	IDH and 1p/19q status	CNN	Accuracy 85.7% (overall 3-group), 95.2% (IDHwt), 88.9% (IDHmut-intact), 60.0% IDHmut-codel
Korfiatis et al. (2017)	GBM (155)	*MGMT* promoter status	CNN	Accuracy 94.9%
Chen et al. (2022)	Diffuse glioma (111)	*MGMT* promoter status	CNN	Accuracy 91%; AUC 0.90
Sun et al. (2019)	Midline glioma (100)	H3 K27 mutation status	DL	AUC 0.85
Prasanna et al. (2017)	GBM (65)	Survival	Random forest	CI = 0.70 (short term vs. long term survival)
Park et al. (2020)	GBM (216)	Survival	LASSO cox regression	CI = 0.70 (overall survival)
Beig et al. (2018)	GBM (115)	Survival	Random forest	CI = 0.83 (short term vs. long term survival)
Kim et al. (2019)	GBM (95)	Progression vs. Pseudoprogression	Hybrid ML-DL	AUC = 0.85

ICC, interclass correlation coefficient; AUC, area under the curve (referring to receiver operating characteristics curve); ANN, artificial neural network; CNN, convolutional neural network; LGG, low-grade glioma; HGG, high-grade glioma; GBM, glioblastoma; IDH, isocitrate dehydrogenase; MGMT, O^6-methylguanine-DNA methyltransferase; RANO, response assessment in neuro-oncology; CI, concordance index. *n* reflects training and validation cohorts where applicable.

imaging would be valuable not only in cases of inoperable tumors or insufficient surgical samples, but also in all cases to guide early diagnosis or early pre-surgical enrollment into clinical trials (Gonzalez Castro et al., 2023).

Certain qualitative radiographic correlates of molecular features have previously been recognized. For instance, IDH wildtype LGGs have poorer definition of non-enhancing margin and more multifocal distributions than IDH mutant LGGs; IDH wildtype tumors have larger percentage core enhancing component; and the "T2-FLAIR mismatch" sign can identify IDH-mutant 1p19q-intact gliomas with good specificity (Ellingson, 2015; Patel et al., 2017; Park et al., 2018; Lasocki et al., 2021; Miller et al., 2023). IDH mutant gliomas have been shown to have higher ADC and lower relative cerebral blood volume (rCBV) values, though these findings have wide ranging sensitivities (56 to 100%) and specificities (51–100%) depending on the study (Xing et al., 2017; Suh et al., 2019). 2-HG MR spectroscopy has better sensitivity in detecting IDH mutant status, in one analysis sensitivity 96% and specificity 85% (Suh et al., 2019). Additionally, 1p/19q co-deleted tumors are associated with indistinct tumor borders, frontal tumor location, heterogeneous T2 signal intensity, and cortical/subcortical tumor infiltration (Smits and van den Bent, 2017).

ML algorithms developed to predict molecular features based on imaging data offer the promise of automated recognition of these and other features, and have the advantage of being independent of operator experience, more accessible, and more amenable to training on improved data sets. Here we highlight some salient studies among the numerous studies that have employed ML approaches to predict molecular features including IDH mutation, 1p/19q codeletion, *MGMT* promoter methylation status, and other relevant features.

Zhang et al. developed a ML-based model using a random forest classifier to predict IDH mutation status based on patient age and pre-operative MRIs of 90 patients with HGGs. Using T1, T2/FLAIR, and ADC sequences, the model achieved accuracy of 89% (AUC 0.9231) in the validation cohort of 30 HGGs (Zhang et al., 2017). Imaging features contributing the most to IDH genotyping were patient age and MRI parametric intensity, texture and shape features. In a similar study, Chang et al. trained a CNN to predict IDH mutation status from pre-operative MRIs of patients with grade II-IV gliomas, and accuracies improved from 85.7 to 89.1% with incorporation of

patient age into the predictive model (Chang et al., 2018). These models required manual tumor segmentation which limits clinical viability, but automated segmentation approaches (as described in the previous section) may help overcome this. A meta-analysis of 9 studies by Zhao et al. employing ML to radiographically predict IDH mutations in gliomas found pooled sensitivity and specificity of 87 and 88%, respectively, in the training set, and 87 and 90%, respectively, in the validation set (Zhao et al., 2020). Finally, Chang, P et al. used MRI data from 259 patients with low or high grade gliomas from The Cancer Imaging Archive (TCIA) to train a CNN to predict IDH mutation, 1p/19q codeletion, and *MGMT* promoter methylation status simultaneously and using an automated segmentation tool (Chang et al., 2018). They achieved a high accuracy of 94% in IDH mutation status, while accuracies for 1p19q codeletion and *MGMT* promoter methylation were 92 and 83%, respectively.

Codeletion of the 1p/19q chromosome arms in IDH mutant gliomas is characteristic of oligodendroglioma and associated with increased survival and better response to treatment, and is another important part of glioma classification by WHO criteria (Taal et al., 2015; Louis et al., 2021). Fellah et al. used multivariate random forest models to retrospectively predict 1p/19q codeletion status from conventional MRI (cMRI) sequences (T1- and T2-weighted sequences) and from diffusion-weighted imaging (DWI), perfusion-weighted imaging (PWI), and MRI spectroscopy (MRS). Their model had misclassification rate of 48% and established that inclusion of DWI, PWI, and MRS did not help improve the prediction of 1p/19q codeletion relative to cMRI sequences alone (Fellah et al., 2013). Akkus et al. used 159 preoperative cMRIs of LGGs to train and test a CNN to predict 1p/19q codeletion status, and achieved an accuracy of 87.7% (Akkus et al., 2017). Van der woort et al. trained a support vector machine (SVM) algorithm on cMRI images of 284 patients who had undergone biopsy or resection for presumed LGG (rather than histologically confirmed LGG, so as to reflect a more clinically relevant population). Their model, which also incorporated age and sex data, predicted 1p/19q codeletion in 129 patients from an external test cohort from the TCIA, with AUC of 0.72. The authors compared this to predictions by clinical experts, who achieved AUCs of 0.52 (two neurosurgeons) and 0.81 (two neuroradiologists) albeit with wide variability among the clinical experts (AUC 0.45–0.83) (van der Voort et al., 2019). Finally, Yogananda et al. used only T2-weighted MRI sequences from a cohort of 368 patients from the TCIA/TCGA with low and high-grade gliomas, divided into training, validation and testing sets, to predict 1p/19q-codeletion. Their 3D CNN achieved an accuracy of 93.46% (Yogananda et al., 2020). Their exclusive use of T2-weighted images, as well as of automated tumor segmentation, signified a step forward in terms of potential implementation in a clinical setting.

Given the need to identify multiple molecular alterations simultaneously (e.g., IDH and 1p/19q codeletion status) for accurate classification of gliomas, some investigators have worked to develop models for simultaneous classification into one of 3 groups: IDH wild type (IDHwt), IDH mutant and 1p/19q-codeleted (IDHmut-codel), and IDH mutant and 1p/19q non-codeleted (IDHmut-non-codel). Matsui et al. used multi-modal MRI ^{11}C,-methionine PET, and CT images as well as age/gender data from 217 LGG patients to develop a DL model to predict glioma classification, achieving 68.7% accuracy in the test dataset. They noted lower accuracies with only MRI, MRI and PET, and MRI and CT, and reasoned that ^{11}C-methionine-PET increased yield for oligodendrogliomas and IDH wild type astrocytomas, while CT increased yield for oligodendrogliomas by detecting calcification (Matsui et al., 2020). Zhou et al. trained a random forest algorithm on preoperative cMRI in 538 patients with grade 2–4 gliomas from three different institutions. Integrating patient age, they developed two models to sequentially detect IDH mutation status, then 1p/19q status among the IDH mutants. When tested on an external validation cohort from the TCIA of 206 patients with glioma, their model achieved AUC of 0.919 for IDH mutation, and an overall accuracy for glioma classification of 78.2% (Zhou et al., 2019). The authors suggest that a larger sample size may enhance 1p/19q codeletion status prediction in this model. Finally, Cluceru et al. trained a CNN to identify IDH mutation and 1p/19q co-deletion in pre-operative MRIs of newly diagnosed grade 2–4 gliomas, using a cohort of 384 patients from a single institution and 147 patients from the TCGA dataset (Cluceru et al., 2022). They trained multiple CNN classifiers, including using a sequential model (predicting IDH mutation first, then 1p19q codeletion) and a simultaneous 3-group model; they also trained CNNs with or without DWI sequences in addition to cMRI sequences. They found that their best classifier was a 3-group CNN that included DWI as input, predicted molecular features with an overall test accuracy of 85.7%, and correctly classified 95.2% IDHwt, 88.9% IDHmut-intact, and 60.0% IDHmut-codel gliomas. The authors suggested that incorporating susceptibility-weighted imaging (SWI) and rCBV sequences into future algorithms may improve diagnostic accuracy in IDHmut-codel gliomas.

Methylation of the *MGMT* promoter in gliomas predicts longer survival and better response to alkylating chemotherapy agents such as temozolomide, and is thus a clinically vital molecular feature to determine (Stupp et al., 2009). Radiographically, gliomas with *MGMT* promoter methylation have been associated with less vasogenic edema, higher ADC values, and lower cerebral blood flow and blood volume on MR PWI, relative to unmethylated tumors according to a meta-analysis of relevant studies (Suh et al., 2019). Several studies have endeavored to noninvasively assess *MGMT* promoter methylation status via MRI using ML and DL methods.

Li et al. used a cohort of 193 patients with newly diagnosed GBM to build a ML-based random forest classifier for prediction of *MGMT* promoter methylation status in pre-operative cMRIs. Their model selected six features including location, geometry, intensity and texture features; it predicted *MGMT* promoter methylation status with 80% accuracy (AUC 0.88), and the addition of clinical features did not lead to an improvement of this result (Li et al., 2018). Crisi et al. used MR PWI in a cohort of 59 patients with GBM to identify 14 quantitative radiomic features that were used to build a DL model to classify *MGMT* promoter methylation status into three groups: unmethylated (<10% methylated), intermediate-methylated (10–30% methylated), and methylated (>29% methylated). Their model classified *MGMT* promoter methylation status into these three groups with AUC 0.84, sensitivity 75% and specificity 85% (Crisi and Filice, 2020). This lends support to MR PWI as a potential biomarker for *MGMT* promoter methylation status using ML/DL classifiers. Korfiatis et al. used T2 MRI images from 155 patients with newly diagnosed GBM to train and test three different residual CNNs to predict *MGMT* promoter methylation status in each image slice. Their best performing CNN had 50 layers, and predicted MGMT status (methylated, unmethylated, or no tumor) with 94.90% accuracy in the test set. Notably their model eliminated the need for a manual tumor

segmentation step (Korfiatis et al., 2017). Chen et al. built a DL model to assess the predictive value of cMRI and ADC sequences in 111 patients using two regions of interest (ROIs), tumor core and tumor whole (the latter including tumor edema). They found highest predictive value in the tumor core ROI using T1-post contrast combined with ADC sequences, with 91% accuracy and AUC 0.90 (Chen et al., 2022).

A review and meta-analysis of ML-based prediction of molecular features in glioma using MRI by Jian et al. examined 44 studies and found a pooled sensitivity and specificity for IDH mutation of 0.83 and 0.85, respectively. Pooled sensitivities and specificities for 1p/19q codeletion and *MGMT* promoter methylation ranged between 0.76 and 0.83. Of the 44, 7 studies utilized DL, while most used ML-based random forest or SVM classifiers (Jian et al., 2021). Another review and meta-analysis by Bhandari et al. on using MRI radiomics to predict IDH and 1p/19q status in LGGs examined 14 studies. They found that for IDH mutation status prediction, conventional radiomics combined with DL based CNN derived features was the most accurate approach, with 94.4% sensitivity and 86.7% specificity. In contrast, conventional texture-based radiomics performed best in predicting 1p/19q codeletion status, with 90% sensitivity and 96% specificity (Bhandari et al., 2021). These results should be interpreted cautiously, as there was a high degree of heterogeneity among the studies reviewed, with varying radiomic pipelines many of which required manual tumor segmentation, making direct comparisons challenging.

In diffuse midline gliomas, H3 K27 mutation is commonly observed in both pediatric and adult patients, and in pediatric patients portends decreased overall survival regardless of tumor location or histopathological grade (Karremann et al., 2018; Kleinschmidt-DeMasters and Mulcahy Levy, 2018; Ebrahimi et al., 2019). As many of these tumors are located in the brainstem, surgical intervention, including biopsy, can be morbid and is sometimes foregone, increasing the utility of accurate non-invasive H3 K27 mutation status prediction. Su et al. developed deep learning models to predict H3 K27 mutation using only T2 weighted MRI sequences in a cohort of 100 patients with midline gliomas, including 40 mutant and 60 wild type tumors, with three quarters of the cohort reserved for a training set and one quarter for testing. Of ten generated prediction models, accuracies ranged 60 to 84% in the testing cohort, and the best model had a AUC of 0.85 in the test cohort. Larger sample sizes, may help further refine the accuracy of this approach.

Prognostic models

Discussing prognosis is of major importance at the time of brain tumor diagnosis, especially for GBM where the median survival is approximately 16–18 months despite completion of standard-of-care therapy (Wen et al., 2020). Risk factors for poor survival in GBMs include older age and lower Karnofsky Performance Scale (KPS) scores at time of diagnosis, surgery without adjuvant chemoradiation, and absence of *MGMT* promoter methylation (Krex et al., 2007; Thumma et al., 2012). Radiographic MRI features have also been associated with worse overall survival including degree of necrosis and contrast enhancement, multifocality, peritumor edema and higher rCBV (Hammoud et al., 1996; Lacroix et al., 2001; Pope et al., 2005; Jain et al., 2014).

ML and DL-based algorithms have been developed and evaluated to predict survival using a combination of radiographic and clinical features. Sun et al. used a 3D CNN for automated segmentation of cMRI images from 210 HGG and 75 LGG patients, and then used a ML-based random forest classifier to extract radiomics features and predict overall survival. They classified 66 gliomas in a validation cohort into short-term (<10 months), mid-term (10–15 months) and long-term (>15 months) survivors with a modest (61%) accuracy (Sun et al., 2019). Prasanna et al. used cMRI sequences from 65 patients with GBM from the TCIA, manually segmented into enhancing, peritumoral brain zone, and tumor necrosis regions; they extracted 402 radiomics features and used a random forest classifier to isolate features most predictive of short-term (< 7 months) vs. long term (>18 months) survival. They found that peritumoral radiomic features combined with multiparametric MRI sequences performed best at predicting long- vs. short-term survival with a concordance index (CI) of 0.70 (as opposed to combining tumor necrosis features with specific T1 or T2 sequences). When combined with clinical features the model's highest predictive accuracy was achieved at a CI of 0.735 (Prasanna et al., 2017). Lao et al. developed a DL-based model using cMRI combined with clinical data (age and KPS) from 112 patients with GBM from TCIA and institutional cohorts, to predict overall survival with a similar CI of 0.710 (Lao et al., 2017).

Nie et al. used T1 MRI, resting state functional MRI (rs-fMRI), and diffusion tensor imaging (DTI) from 68 HGG patients, and develop a 3D CNN to extract predictive radiomics features. These were combined with clinical features including age, gender, tumor location/size, and WHO grade, and incorporated into a SVM model to predict short vs. long overall survival time, defined as less than, or greater than 650 days, respectively, with 88% accuracy on a 25 patient validation cohort (Nie et al., 2019). Limitations of this study include the its small sample sizes, as well as a binary cutoff of 650 days defining short- vs. long-term survival. Park et al. extracted radiomics features from MRI DWI and PWI in addition to cMRI from 158 patients with newly diagnosed GBM, and combined these with clinical features including age, gender, KPS, *MGMT* promoter methylation status, and extent of surgical resection to develop a ML-based predictive model for survival. On a test set of 58 patients the model predicted OS with a CI of 0.70, performing better than the authors' models that used radiomics features or clinical predictors alone (Park et al., 2020).

As tumor hypoxia is considered an important molecular mechanism driving treatment resistance and poor prognosis, Beig et al. aimed to study radiomics features that predict tumor hypoxia, and utilized these to develop a predictive model for survival in GBM. Radiomics features extracted from cMRI of 115 subjects from the TCIA, coupled with RNA seq data from 21 genes implicated in GBM hypoxia, were used to generate a hypoxia enrichment score (HES). A random forest classifier was then used to stratify patients into short-term (OS <7 months), mid-term (OS 7–16 months) and long-term (OS >16 months) survival based on radiomic markers of hypoxia and clinical features (age, gender, KPS). On a validation subset, the model was able to predict a statistically significant separation between the Kaplan–Meier curves of short-term and long-term survivors, with a CI of 0.83 (Beig et al., 2018). In addition to predicting survival, non-invasive assessment of tumor hypoxia may

guide selection of patients for clinical trials or management with anti-angiogenic therapy (Rahman et al., 2010). Future studies on prognostication may benefit from greater incorporation of molecular features, including IDH mutation, *MGMT* promoter methylation and 1p/19q codeletion status into predictive models.

Differentiating progression from treatment-related radiographic changes (PseudoProgression)

Assessment of true progression (TP) of brain tumors (particularly HGG) on surveillance MRI often presents a significant clinical and radiologic challenge as true progression can appear radiographically similar to pseudoprogression (PsP), i.e., radiation treatment-related inflammatory changes most common 3–6 months after completing radiotherapy (Ellingson et al., 2017). Distinguishing TP from PsP is vital in guiding management and enrollment in (or withdrawal from) clinical trials. In practice, while pathological diagnosis is often considered gold standard to distinguish the two, serial MRI is often used for practical reasons as treatement-related changes regress over time (Youssef et al., 2023). However, this approach can lead to diagnostic delay. Moreover, TP and PsP may co-exist. Studies have suggested that recurrent tumors have lower ADC values than radiation necrosis on DWI sequences, and higher rCBV on PWI can predict PsP with 81.5% sensitivity and 77.8% specificity (Kong et al., 2011; Chu et al., 2013). Approaches utilizing radiomics, ML and DL have ventured to make this distinction noninvasively in the hopes of improving diagnostic fidelity.

Kim et al. studied cMRI, ADC and CBV sequences in 61 patients with GBMs who had undergone resection and standard concurrent chemoradiation therapy (CCRT), and had developed new contrast enhancing lesions within 12 weeks of completion of the latter. Ground truth of TP vs. PsP was based mostly on subsequent serial MRIs, though 8 cases were confirmed with pathology. They extracted radiomics features from the contrast-enhancing portion of the MRIs and used a ML-based classifier to develop a model to distinguish TP vs. PsP. Their multiparametric model (incorporating cMRI, ADC, CBV) performed the best with AUC 0.85 on an external validation cohort of 34 patients (Kim et al., 2019). Jang et al. used a similar cohort of 59 GBM patients to train a hybrid ML-DL model with CNN-LSTM (long short-term memory) on T1 pre- and post-contrast MRI, as well as clinical and molecular features, and were able to distinguish TP from PsP with AUC of 0.83 on an external validation set of 19 patients (Jang et al., 2018). Pathologic confirmation was available for 20 TP and 3 PsP cases. In a similar study employing data from 124 GBM patients with new enhancing lesion after resection and CCRT, Moassefi et al. trained a CNN that achieved AUC 0.75 in distinguishing TP from PsP, with all ground truth determination of TP vs. PSP based on serial imaging (Moassefi et al., 2022).

Discussion

The practice of neuro-oncology is developing at an ever-faster pace, propelled by advances in our understanding of brain tumor biology and technical innovations in allied fields such as neuropathology and neuroradiology. In parallel, advances in AI methods hold increasing promise to optimize workflows in many aspects of neuro-oncology care, as well as to generate new insights regarding tumor biology and therapeutic mechanisms. In neuropathology, to date, AI algorithms have been applied to WSI data to resolve histopathologic features, aiding brain tumor diagnosis and grading. In addition, ML is increasingly being applied to tumor classification on the basis of DNA methylome profiling. In neuroradiology, AI algorithms have been applied to the problem of tumor measurement (volumetrics), to the prediction of grade, molecular features and diagnosis, as well as to the discrimination between progression and treatment-related changes, and the determination of prognosis. As highlighted above, the accuracy of the output of many of these analyses depends on the complexity and diversity of the training datasets, and the AI methods applied to tackle each problem. There is clearly room for improvement, and this is expected through collaboration across centers (leading to more extensive and diverse datasets) and improvements in computational methods and hardware.

Witnessing the current progress, a natural question is if these algorithms will one day come to replace the work of neuropathologists and neuroradiologists in neuro-oncology practice. Although the roles of neuropathologists and neuroradiologists will evolve, we do not expect these specialists to come "out of the loop," as their expertise is irreplaceable, particularly when it comes to diagnosing and evaluating difficult cases. AI will not replace neuropathology or neuroradiology but rather expedite and enhance their workflows. With advances in large language models (LLM; e.g., ChatGPT), which are able to address complex queries with increasing accuracy (Haupt and Marks, 2023), the relevance of the clinical neuro-oncologist also comes into question. Here again, we think that AI will not replace but rather support the role of neuro-oncologists, putting the latest clinical evidence and treatment algorithms at their fingertips, systematizing part of their role but unable to replace the physical touch that enables patient assessment and the development of a relationship that helps guide patients through difficult decisions.

As the field of AI continues to develop and progressively integrate into research and clinical practice, we need to remain aware of the limitations of each method/algorithm, particularly since their underpinnings are often not clearly explained and, more importantly, are difficult to assess by end users. Guidelines for evaluating, validating and approving AI systems for their use in medicine in general, and neuro-oncology specifically, will be fundamental to the safe introduction of these methods into practice. Elements to consider when evaluating novel AI tools include, (1) the characteristics of training datasets (data types and standards, diversity of dataset elements, size of dataset, accuracy of data annotations, if relevant), (2) the specifics of the algorithms involved, (3) the characteristics of the validation dataset (including metrics that are consistent with those of the training dataset), and (4), the performance of the system at the moment of its release as well as over time, including specific warnings regarding blindspots of classification or systematic errors regarding output for specific inputs. Related to this last point, it is important to note that AI systems have the potential to perpetuate clinical and social biases (Larrazabal et al., 2020; Seyyed-Kalantari et al., 2021).

In the end, how AI will continue to integrate into the practice of neuro-oncology remains to be determined. We hope to have updated neuro-oncology clinicians and researchers on current advances in the field of AI to help them inform how to incorporate AI tools into their practice. In the words of the Nobel Prize winning physicist, Dennis Gabor, "the future cannot be predicted, but futures can be invented (Gabor, 1964)."

Author contributions

VN performed the literature review and drafted the manuscript. LG conceived the project, performed the literature review, and drafted the manuscript. All authors contributed to the article and approved the submitted version.

Conflict of interest

The authors declare that the research was conducted in the absence of any commercial or financial relationships that could be construed as a potential conflict of interest.

Publisher's note

All claims expressed in this article are solely those of the authors and do not necessarily represent those of their affiliated organizations, or those of the publisher, the editors and the reviewers. Any product that may be evaluated in this article, or claim that may be made by its manufacturer, is not guaranteed or endorsed by the publisher.

References

Afridi, M., Jain, A., Aboian, M., and Payabvash, S. (2022). Brain tumor imaging: applications of artificial intelligence. *Semin. Ultrasound CT MR* 43, 153–169. doi: 10.1053/j.sult.2022.02.005

Aftab, K., Aamir, F. B., Mallick, S., Mubarak, F., Pope, W. B., Mikkelsen, T., et al. (2022). Radiomics for precision medicine in glioblastoma. *J. Neuro-Oncol.* 156, 217–231. doi: 10.1007/s11060-021-03933-1

Akkus, Z., Ali, I., Sedlář, J., Agrawal, J. P., Parney, I. F., Giannini, C., et al. (2017). Predicting deletion of chromosomal arms 1p/19q in low-grade gliomas from MR images using machine intelligence. *J. Digit. Imaging* 30, 469–476. doi: 10.1007/s10278-017-9984-3

Barash, Y., and Klang, E. (2019). Automated quantitative assessment of oncological disease progression using deep learning. *Ann. Trans. Med.* 7:S379. doi: 10.21037/atm.2019.12.101

Beig, N., Patel, J., Prasanna, P., Hill, V., Gupta, A., Correa, R., et al. (2018). Radiogenomic analysis of hypoxia pathway is predictive of overall survival in glioblastoma. *Sci. Rep.* 8:7. doi: 10.1038/s41598-017-18310-0

Bhandari, A. P., Liong, R., Koppen, J., Murthy, S. V., and Lasocki, A. (2021). Noninvasive determination of IDH and 1p19q status of lower-grade gliomas using MRI Radiomics: a systematic review. *AJNR Am. J. Neuroradiol.* 42, 94–101. doi: 10.3174/ajnr.A6875

Capper, D., Jones, D. T. W., Sill, M., Hovestadt, V., Schrimpf, D., Sturm, D., et al. (2018). DNA methylation-based classification of central nervous system tumours. *Nature* 555, 469–474. doi: 10.1038/nature26000

Capper, D., Stichel, D., Sahm, F., Jones, D. T. W., Schrimpf, D., Sill, M., et al. (2018). Practical implementation of DNA methylation and copy-number-based CNS tumor diagnostics: the Heidelberg experience. *Acta Neuropathol.* 136, 181–210. doi: 10.1007/s00401-018-1879-y

Chang, K., Bai, H. X., Zhou, H., Su, C., Bi, W. L., Agbodza, E., et al. (2018). Residual convolutional neural network for the determination of IDH status in low- and high-grade gliomas from MR imaging. *Clin. Cancer Res.* 24, 1073–1081. doi: 10.1158/1078-0432.CCR-17-2236

Chang, K., Beers, A. L., Bai, H. X., Brown, J. M., Ly, K. I., Li, X., et al. (2019). Automatic assessment of glioma burden: a deep learning algorithm for fully automated volumetric and bidimensional measurement. *Neuro-Oncology* 21, 1412–1422. doi: 10.1093/neuonc/noz106

Chang, P., Grinband, J., Weinberg, B. D., Bardis, M., Khy, M., Cadena, G., et al. (2018). Deep-learning convolutional neural networks accurately classify genetic mutations in gliomas. *AJNR Am. J. Neuroradiol.* 39, 1201–1207. doi: 10.3174/ajnr.A5667

Chen, S., Xu, Y., Ye, M., Li, Y., Sun, Y., Liang, J., et al. (2022). Predicting MGMT promoter methylation in diffuse gliomas using deep learning with Radiomics. *J. Clin. Med.* 11:3445. doi: 10.3390/jcm11123445

Chu, H. H., Choi, S. H., Ryoo, I., Kim, S. C., Yeom, J. A., Shin, H., et al. (2013). Differentiation of true progression from pseudoprogression in glioblastoma treated with radiation therapy and concomitant temozolomide: comparison study of standard and high-b-value diffusion-weighted imaging. *Radiology* 269, 831–840. doi: 10.1148/radiol.13122024

Cluceru, J., Interian, Y., Phillips, J. J., Molinaro, A. M., Luks, T. L., Alcaide-Leon, P., et al. (2022). Improving the noninvasive classification of glioma genetic subtype with deep learning and diffusion-weighted imaging. *Neuro-Oncology* 24, 639–652. doi: 10.1093/neuonc/noab238

Coudray, N., Ocampo, P. S., Sakellaropoulos, T., Narula, N., Snuderl, M., Fenyö, D., et al. (2018). Classification and mutation prediction from non-small cell lung cancer histopathology images using deep learning. *Nat. Med.* 24, 1559–1567. doi: 10.1038/s41591-018-0177-5

Crisi, G., and Filice, S. (2020). Predicting MGMT promoter methylation of glioblastoma from dynamic susceptibility contrast perfusion: a Radiomic approach. *J. Neuroimaging* 30, 458–462. doi: 10.1111/jon.12724

di Nunno, V., Fordellone, M., Minniti, G., Asioli, S., Conti, A., Mazzatenta, D., et al. (2022). Machine learning in neuro-oncology: toward novel development fields. *J. Neuro-Oncol.* 159, 333–346. doi: 10.1007/s11060-022-04068-7

Ebrahimi, A., Skardelly, M., Schuhmann, M. U., Ebinger, M., Reuss, D., Neumann, M., et al. (2019). High frequency of H3 K27M mutations in adult midline gliomas. *J. Cancer Res. Clin. Oncol.* 145, 839–850. doi: 10.1007/s00432-018-02836-5

Ehteshami Bejnordi, B., Veta, M., Johannes van Diest, P., van Ginneken, B., Karssemeijer, N., Litjens, G., et al. (2017). Diagnostic assessment of deep learning algorithms for detection of lymph node metastases in women with breast Cancer. *JAMA* 318, 2199–2210. doi: 10.1001/jama.2017.14585

Ellingson, B. M. (2015). Radiogenomics and imaging phenotypes in glioblastoma: novel observations and correlation with molecular characteristics. *Curr. Neurol. Neurosci. Rep.* 15:506. doi: 10.1007/s11910-014-0506-0

Ellingson, B. M., Chung, C., Pope, W. B., Boxerman, J. L., and Kaufmann, T. J. (2017). Pseudoprogression, radionecrosis, inflammation or true tumor progression? Challenges associated with glioblastoma response assessment in an evolving therapeutic landscape. *J. Neuro-Oncol.* 134, 495–504. doi: 10.1007/s11060-017-2375-2

Ertosun, M. G., and Rubin, D. L. (2015). Automated grading of gliomas using deep learning in digital pathology images: a modular approach with ensemble of convolutional neural networks. *AMIA Annu. Symp. Proc.* 2015, 1899–1908.

Fellah, S., Caudal, D., de Paula, A. M., Dory-Lautrec, P., Figarella-Branger, D., Chinot, O., et al. (2013). Multimodal MR imaging (diffusion, perfusion, and spectroscopy): is it possible to distinguish oligodendroglial tumor grade and 1p/19q codeletion in the pretherapeutic diagnosis? *AJNR Am. J. Neuroradiol.* 34, 1326–1333. doi: 10.3174/ajnr.A3352

Ford, R. R., O'Neal, M., Moskowitz, S. C., and Fraunberger, J. (2016). Adjudication rates between readers in blinded independent central review of oncology studies. *J. Clin. Trials* 6, 1–9. doi: 10.4172/2167-0870.1000289

Gabor, D. (1964) *Inventing the future.* (New York: Alfred A Knopf).

Gonzalez Castro, L. N., Arrillaga-Romany, I. C., and Batchelor, T. T. (2023). Challenges and opportunities for clinical trials in patients with glioma. *JAMA Neurol.* 80, 227–228. doi: 10.1001/jamaneurol.2022.4924

Gritsch, S., Batchelor, T. T., and Gonzalez Castro, L. N. (2022). Diagnostic, therapeutic, and prognostic implications of the 2021 World Health Organization classification of tumors of the central nervous system. *Cancer* 128, 47–58. doi: 10.1002/cncr.33918

Hammoud, M. A., Sawaya, R., Shi, W., Thall, P. F., and Leeds, N. E. (1996). Prognostic significance of preoperative MRI scans in glioblastoma multiforme. *J. Neuro-Oncol.* 27, 65–73. doi: 10.1007/BF00146086

Haupt, C. E., and Marks, M. (2023). AI-generated medical advice-GPT and beyond. *JAMA* 329, 1349–1350. doi: 10.1001/jama.2023.5321

Hollon, T., Jiang, C., Chowdury, A., Nasir-Moin, M., Kondepudi, A., Aabedi, A., et al. (2023). Artificial-intelligence-based molecular classification of diffuse gliomas using rapid, label-free optical imaging. *Nat. Med.* 29, 828–832. doi: 10.1038/s41591-023-02252-4

Im, S., Hyeon, J., Rha, E., Lee, J., Choi, H. J., Jung, Y., et al. (2021). Classification of diffuse glioma subtype from clinical-grade pathological images using deep transfer learning. *Sensors (Basel)* 21:3500. doi: 10.3390/s21103500

Jain, R., Poisson, L. M., Gutman, D., Scarpace, L., Hwang, S. N., Holder, C. A., et al. (2014). Outcome prediction in patients with glioblastoma by using imaging, clinical,

and genomic biomarkers: focus on the nonenhancing component of the tumor. *Radiology* 272, 484–493. doi: 10.1148/radiol.14131691

Jang, B.-S., Jeon, S. H., Kim, I. H., and Kim, I. A. (2018). Prediction of Pseudoprogression versus progression using machine learning algorithm in glioblastoma. *Sci. Rep.* 8:12516. doi: 10.1038/s41598-018-31007-2

Jaunmuktane, Z., Capper, D., Jones, D. T. W., Schrimpf, D., Sill, M., Dutt, M., et al. (2019). Methylation array profiling of adult brain tumours: diagnostic outcomes in a large, single Centre. *Acta Neuropathol. Commun.* 7:24. doi: 10.1186/s40478-019-0668-8

Jian, A., Jang, K., Manuguerra, M., Liu, S., Magnussen, J., and di Ieva, A. (2021). Machine learning for the prediction of molecular markers in glioma on magnetic resonance imaging: a systematic review and Meta-analysis. *Neurosurgery* 89, 31–44. doi: 10.1093/neuros/nyab103

Jin, L., Shi, F., Chun, Q., Chen, H., Ma, Y., Wu, S., et al. (2021). Artificial intelligence neuropathologist for glioma classification using deep learning on hematoxylin and eosin stained slide images and molecular markers. *Neuro-Oncology* 23, 44–52. doi: 10.1093/neuonc/noaa163

Kann, B. H., Hosny, A., and Aerts, H. J. W. L. (2021). Artificial intelligence for clinical oncology. *Cancer Cell* 39, 916–927. doi: 10.1016/j.ccell.2021.04.002

Karimi, S., Zuccato, J. A., Mamatjan, Y., Mansouri, S., Suppiah, S., Nassiri, F., et al. (2019). The central nervous system tumor methylation classifier changes neuro-oncology practice for challenging brain tumor diagnoses and directly impacts patient care. *Clin. Epigenetics* 11:185. doi: 10.1186/s13148-019-0766-2

Karremann, M., Gielen, G. H., Hoffmann, M., Wiese, M., Colditz, N., Warmuth-Metz, M., et al. (2018). Diffuse high-grade gliomas with H3 K27M mutations carry a dismal prognosis independent of tumor location. *Neuro-Oncology* 20, 123–131. doi: 10.1093/neuonc/nox149

Kickingereder, P., Isensee, F., Tursunova, I., Petersen, J., Neuberger, U., Bonekamp, D., et al. (2019). Automated quantitative tumour response assessment of MRI in neuro-oncology with artificial neural networks: a multicentre, retrospective study. *Lancet Oncol.* 20, 728–740. doi: 10.1016/S1470-2045(19)30098-1

Kim, J. Y., Park, J. E., Jo, Y., Shim, W. H., Nam, S. J., Kim, J. H., et al. (2019). Incorporating diffusion- and perfusion-weighted MRI into a radiomics model improves diagnostic performance for pseudoprogression in glioblastoma patients. *Neuro-Oncology* 21, 404–414. doi: 10.1093/neuonc/noy133

Kleinschmidt-DeMasters, B. K., and Mulcahy Levy, J. M. (2018). H3 K27M-mutant gliomas in adults vs. children share similar histological features and adverse prognosis. *Clin. Neuropathol.* 37, 53–63.

Komori, T. (2021). AI neuropathologist: an innovative technology enabling a faultless pathological diagnosis? *Neuro-Oncology* 23, 1–2. doi: 10.1093/neuonc/noaa229

Kong, D.-S., Kim, S. T., Kim, E. H., Lim, D. H., Kim, W. S., Suh, Y. L., et al. (2011). Diagnostic dilemma of pseudoprogression in the treatment of newly diagnosed glioblastomas: the role of assessing relative cerebral blood flow volume and oxygen-6-methylguanine-DNA methyltransferase promoter methylation status. *AJNR Am. J. Neuroradiol.* 32, 382–387. doi: 10.3174/ajnr.A2286

Korfiatis, P., Kline, T. L., Lachance, D. H., Parney, I. F., Buckner, J. C., and Erickson, B. J. (2017). Residual deep convolutional neural network predicts MGMT methylation status. *J. Digit. Imaging* 30, 622–628. doi: 10.1007/s10278-017-0009-z

Krex, D., Klink, B., Hartmann, C., von Deimling, A., Pietsch, T., Simon, M., et al. (2007). Long-term survival with glioblastoma multiforme. *Brain* 130, 2596–2606. doi: 10.1093/brain/awm204

Lacroix, M., Abi-Said, D., Fourney, D. R., Gokaslan, Z. L., Shi, W., DeMonte, F., et al. (2001). A multivariate analysis of 416 patients with glioblastoma multiforme: prognosis, extent of resection, and survival. *J. Neurosurg.* 95, 190–198. doi: 10.3171/jns.2001.95.2.0190

Lao, J., Chen, Y., Li, Z. C., Li, Q., Zhang, J., Liu, J., et al. (2017). A deep learning-based Radiomics model for prediction of survival in glioblastoma Multiforme. *Sci. Rep.* 7:10353. doi: 10.1038/s41598-017-10649-8

Larrazabal, A. J., Nieto, N., Peterson, V., Milone, D. H., and Ferrante, E. (2020). Gender imbalance in medical imaging datasets produces biased classifiers for computer-aided diagnosis. *Proc. Natl. Acad. Sci. U. S. A.* 117, 12592–12594. doi: 10.1073/pnas.1919012117

Lasocki, A., Anjari, M., Örs Kokurcan, S., and Thust, S. C. (2021). Conventional MRI features of adult diffuse glioma molecular subtypes: a systematic review. *Neuroradiology* 63, 353–362. doi: 10.1007/s00234-020-02532-7

LeCun, Y., Bengio, Y., and Hinton, G. (2015). Deep learning. *Nature* 521, 436–444. doi: 10.1038/nature14539

Li, Z.-C., Bai, H., Sun, Q., Li, Q., Liu, L., Zou, Y., et al. (2018). Multiregional radiomics features from multiparametric MRI for prediction of MGMT methylation status in glioblastoma multiforme: a multicentre study. *Eur. Radiol.* 28, 3640–3650. doi: 10.1007/s00330-017-5302-1

Litjens, G., Sánchez, C. I., Timofeeva, N., Hermsen, M., Nagtegaal, I., Kovacs, I., et al. (2016). Deep learning as a tool for increased accuracy and efficiency of histopathological diagnosis. *Sci. Rep.* 6:26286. doi: 10.1038/srep26286

Louis, D. N., Perry, A., Wesseling, P., Brat, D. J., Cree, I. A., Figarella-Branger, D., et al. (2021). The 2021 WHO classification of tumors of the central nervous system: a summary. *Neuro-Oncology* 23, 1231–1251. doi: 10.1093/neuonc/noab106

Machine Learning Improves Diagnosis of CNS Cancers (2018). Machine learning improves diagnosis of CNS cancers. *Cancer Discov.* 8, 523–524. doi: 10.1158/2159-8290.CD-NB2018-040

Matsui, Y., Maruyama, T., Nitta, M., Saito, T., Tsuzuki, S., Tamura, M., et al. (2020). Prediction of lower-grade glioma molecular subtypes using deep learning. *J. Neuro-Oncol.* 146, 321–327. doi: 10.1007/s11060-019-03376-9

Miller, J. J., Gonzalez Castro, L. N., McBrayer, S., Weller, M., Cloughesy, T., Portnow, J., et al. (2023). Isocitrate dehydrogenase (IDH) mutant gliomas: a Society for Neuro-Oncology (SNO) consensus review on diagnosis, management, and future directions. *Neuro-Oncology* 25, 4–25. doi: 10.1093/neuonc/noac207

Moassefi, M., Faghani, S., Conte, G. M., Kowalchuk, R. O., Vahdati, S., Crompton, D. J., et al. (2022). A deep learning model for discriminating true progression from pseudoprogression in glioblastoma patients. *J. Neuro-Oncol.* 159, 447–455. doi: 10.1007/s11060-022-04080-x

Moran, S., Martínez-Cardús, A., Sayols, S., Musulén, E., Balañá, C., Estival-Gonzalez, A., et al. (2016). Epigenetic profiling to classify cancer of unknown primary: a multicentre, retrospective analysis. *Lancet Oncol.* 17, 1386–1395. doi: 10.1016/S1470-2045(16)30297-2

Nagpal, K., Foote, D., Tan, F., Liu, Y., Chen, P. H. C., Steiner, D. F., et al. (2020). Development and validation of a deep learning algorithm for Gleason grading of prostate Cancer from biopsy specimens. *JAMA Oncol.* 6, 1372–1380. doi: 10.1001/jamaoncol.2020.2485

Nie, D., Lu, J., Zhang, H., Adeli, E., Wang, J., Yu, Z., et al. (2019). Multi-Channel 3D deep feature learning for survival time prediction of brain tumor patients using multi-modal Neuroimages. *Sci. Rep.* 9:1103. doi: 10.1038/s41598-018-37387-9

Nillson, N. J. *The quest for artificial intelligence*. Cambridge: Cambridge University Press, (2010).

Park, Y. W., Han, K., Ahn, S. S., Bae, S., Choi, Y. S., Chang, J. H., et al. (2018). Prediction of IDH1-mutation and 1p/19q-Codeletion status using preoperative MR imaging phenotypes in lower grade gliomas. *AJNR Am. J. Neuroradiol.* 39, 37–42. doi: 10.3174/ajnr.A5421

Park, J. E., Kim, H. S., Jo, Y., Yoo, R. E., Choi, S. H., Nam, S. J., et al. (2020). Radiomics prognostication model in glioblastoma using diffusion- and perfusion-weighted MRI. *Sci. Rep.* 10:4250. doi: 10.1038/s41598-020-61178-w

Patel, S. H., Poisson, L. M., Brat, D. J., Zhou, Y., Cooper, L., Snuderl, M., et al. (2017). T2-FLAIR mismatch, an imaging biomarker for IDH and 1p/19q status in lower-grade gliomas: a TCGA/TCIA project. *Clin. Cancer Res.* 23, 6078–6085. doi: 10.1158/1078-0432.CCR-17-0560

Pei, L., Jones, K. A., Shboul, Z. A., Chen, J. Y., and Iftekharuddin, K. M. (2021). Deep neural network analysis of pathology images with integrated molecular data for enhanced glioma classification and grading. *Front. Oncol.* 11:668694. doi: 10.3389/fonc.2021.668694

Peng, J., Kim, D. D., Patel, J. B., Zeng, X., Huang, J., Chang, K., et al. (2022). Deep learning-based automatic tumor burden assessment of pediatric high-grade gliomas, medulloblastomas, and other leptomeningeal seeding tumors. *Neuro-Oncology* 24, 289–299. doi: 10.1093/neuonc/noab151

Pickles, J. C., Stone, T. J., and Jacques, T. S. (2020). Methylation-based algorithms for diagnosis: experience from neuro-oncology. *J. Pathol.* 250, 510–517. doi: 10.1002/path.5397

Pope, W. B., and Hessel, C. (2011). Response assessment in neuro-oncology criteria: implementation challenges in multicenter neuro-oncology trials. *AJNR Am. J. Neuroradiol.* 32, 794–797. doi: 10.3174/ajnr.A2582

Pope, W. B., Sayre, J., Perlina, A., Villablanca, J. P., Mischel, P. S., and Cloughesy, T. F. (2005). MR imaging correlates of survival in patients with high-grade gliomas. *AJNR Am. J. Neuroradiol.* 26, 2466–2474.

Prasanna, P., Patel, J., Partovi, S., Madabhushi, A., and Tiwari, P. (2017). Radiomic features from the peritumoral brain parenchyma on treatment-naïve multi-parametric MR imaging predict long versus short-term survival in glioblastoma multiforme: preliminary findings. *Eur. Radiol.* 27, 4188–4197. doi: 10.1007/s00330-016-4637-3

Priesterbach-Ackley, L. P., Boldt, H. B., Petersen, J. K., Bervoets, N., Scheie, D., Ulhøi, B. P., et al. (2020). Brain tumour diagnostics using a DNA methylation-based classifier as a diagnostic support tool. *Neuropathol. Appl. Neurobiol.* 46, 478–492. doi: 10.1111/nan.12610

Rahman, R., Smith, S., Rahman, C., and Grundy, R. (2010). Antiangiogenic therapy and mechanisms of tumor resistance in malignant glioma. *J. Oncol.* 2010:251231, 1–16. doi: 10.1155/2010/251231

Russel, S., and Norvig, P. *Artificial intelligence: a modern approach*. London: Pearson (2020).

Seyyed-Kalantari, L., Zhang, H., McDermott, M. B. A., Chen, I. Y., and Ghassemi, M. (2021). Underdiagnosis bias of artificial intelligence algorithms applied to chest radiographs in under-served patient populations. *Nat. Med.* 27, 2176–2182. doi: 10.1038/s41591-021-01595-0

Silver, D., Huang, A., Maddison, C. J., Guez, A., Sifre, L., van den Driessche, G., et al. (2016). Mastering the game of go with deep neural networks and tree search. *Nature* 529, 484–489. doi: 10.1038/nature16961

Smits, M., and van den Bent, M. J. (2017). Imaging correlates of adult glioma genotypes. *Radiology* 284, 316–331. doi: 10.1148/radiol.2017151930

Sorensen, A. G., Batchelor, T. T., Wen, P. Y., Zhang, W.-T., and Jain, R. K. (2008). Response criteria for glioma. *Nat. Clin. Pract. Oncol.* 5, 634–644. doi: 10.1038/ncponc1204

Sorensen, A. G., Patel, S., Harmath, C., Bridges, S., Synnott, J., Sievers, A., et al. (2001). Comparison of diameter and perimeter methods for tumor volume calculation. *J. Clin. Oncol.* 19, 551–557. doi: 10.1200/JCO.2001.19.2.551

Stupp, R., Hegi, M. E., Mason, W. P., van den Bent, M., Taphoorn, M. J., Janzer, R. C., et al. (2009). Effects of radiotherapy with concomitant and adjuvant temozolomide versus radiotherapy alone on survival in glioblastoma in a randomised phase III study: 5-year analysis of the EORTC-NCIC trial. *Lancet Oncol.* 10, 459–466. doi: 10.1016/S1470-2045(09)70025-7

Suh, C. H., Kim, H. S., Jung, S. C., Choi, C. G., and Kim, S. J. (2019). Imaging prediction of isocitrate dehydrogenase (IDH) mutation in patients with glioma: a systemic review and meta-analysis. *Eur. Radiol.* 29, 745–758. doi: 10.1007/s00330-018-5608-7

Sun, L., Zhang, S., Chen, H., and Luo, L. (2019). Brain tumor segmentation and survival prediction using multimodal MRI scans with deep learning. *Front. Neurosci.* 13:810. doi: 10.3389/fnins.2019.00810

Taal, W., Bromberg, J. E. C., and van den Bent, M. J. (2015). Chemotherapy in glioma. *CNS Oncologia* 4, 179–192. doi: 10.2217/cns.15.2

Thumma, S. R., Fairbanks, R. K., Lamoreaux, W. T., Mackay, A. R., Demakas, J. J., Cooke, B. S., et al. (2012). Effect of pretreatment clinical factors on overall survival in glioblastoma multiforme: a surveillance epidemiology and end results (SEER) population analysis. *World J. Surg. Oncol.* 10:75. doi: 10.1186/1477-7819-10-75

Truong, A. H., Sharmanska, V., Limbäck-Stanic, C., and Grech-Sollars, M. (2020). Optimization of deep learning methods for visualization of tumor heterogeneity and brain tumor grading through digital pathology. *Neurooncol Adv.* 2, 1–13. doi: 10.1093/noajnl/vdaa110

van den Bent, M. J. (2010). Interobserver variation of the histopathological diagnosis in clinical trials on glioma: a clinician's perspective. *Acta Neuropathol.* 120, 297–304. doi: 10.1007/s00401-010-0725-7

van der Voort, S. R., Incekara, F., Wijnenga, M. M. J., Kapas, G., Gardeniers, M., Schouten, J. W., et al. (2019). Predicting the 1p/19q Codeletion status of presumed low-grade glioma with an externally validated machine learning algorithm. *Clin. Cancer Res.* 25, 7455–7462. doi: 10.1158/1078-0432.CCR-19-1127

Vos, M. J., Uitdehaag, B. M. J., Barkhof, F., Heimans, J. J., Baayen, H. C., Boogerd, W., et al. (2003). Interobserver variability in the radiological assessment of response to chemotherapy in glioma. *Neurology* 60, 826–830. doi: 10.1212/01.WNL.0000049467.54667.92

Wen, P. Y., Weller, M., Lee, E. Q., Alexander, B. M., Barnholtz-Sloan, J. S., Barthel, F. P., et al. (2020). Glioblastoma in adults: a Society for Neuro-Oncology (SNO) and European Society of Neuro-Oncology (EANO) consensus review on current management and future directions. *Neuro-Oncology* 22, 1073–1113. doi: 10.1093/neuonc/noaa106

Wong, D., and Yip, S. (2018). Machine learning classifies cancer. *Nature* 555, 446–447. doi: 10.1038/d41586-018-02881-7

Xing, Z., Yang, X., She, D., Lin, Y., Zhang, Y., and Cao, D. (2017). Noninvasive assessment of IDH mutational status in World Health Organization grade II and III Astrocytomas using DWI and DSC-PWI combined with conventional MR imaging. *AJNR Am. J. Neuroradiol.* 38, 1138–1144. doi: 10.3174/ajnr.A5171

Yogananda, C. G. B., et al. (2020). A novel fully automated MRI-based deep-learning method for classification of 1p/19q co-deletion status in brain gliomas. *Neuro Oncol. Adv.* 2, vdaa066. iv42–iv48.

Youssef, G., Rahman, R., Bay, C., Wang, W., Lim-Fat, M. J., Arnaout, O., et al. (2023). Evaluation of standard response assessment in neuro-oncology, modified response assessment in neuro-oncology, and immunotherapy response assessment in neuro-oncology in newly diagnosed and recurrent glioblastoma. *J. Clin. Oncol.* 41, 3160–3171. doi: 10.1200/JCO.22.01579

Zhang, B., Chang, K., Ramkissoon, S., Tanguturi, S., Bi, W. L., Reardon, D. A., et al. (2017). Multimodal MRI features predict isocitrate dehydrogenase genotype in high-grade gliomas. *Neuro-Oncology* 19, 109–117. doi: 10.1093/neuonc/now121

Zhao, J., Huang, Y., Song, Y., Xie, D., Hu, M., Qiu, H., et al. (2020). Diagnostic accuracy and potential covariates for machine learning to identify IDH mutations in glioma patients: evidence from a meta-analysis. *Eur. Radiol.* 30, 4664–4674. doi: 10.1007/s00330-020-06717-9

Zhou, H., Chang, K., Bai, H. X., Xiao, B., Su, C., Bi, W. L., et al. (2019). Machine learning reveals multimodal MRI patterns predictive of isocitrate dehydrogenase and 1p/19q status in diffuse low- and high-grade gliomas. *J. Neuro-Oncol.* 142, 299–307. doi: 10.1007/s11060-019-03096-0

Zhu, M., Li, S., Kuang, Y., Hill, V. B., Heimberger, A. B., Zhai, L., et al. (2022). Artificial intelligence in the radiomic analysis of glioblastomas: a review, taxonomy, and perspective. *Front. Oncol.* 12:924245. doi: 10.3389/fonc.2022.924245

frontiers | Frontiers in Neuroscience

TYPE Original Research
PUBLISHED 19 December 2023
DOI 10.3389/fnins.2023.1321246

OPEN ACCESS

EDITED BY
Wei Wang,
Massachusetts General Hospital and Harvard Medical School, United States

REVIEWED BY
Alessandro Gialluisi,
Università Lum Jean Monnet, Italy
Jie Lu,
Sun Yat-sen University Cancer Center (SYSUCC), China

*CORRESPONDENCE
Ying Shao
✉ shao_ying@jlu.edu.cn

RECEIVED 13 October 2023
ACCEPTED 29 November 2023
PUBLISHED 19 December 2023

CITATION
Zhang Z, Liu N, Pan X, Zhang C, Yang Y, Li X and Shao Y (2023) Assessing causal associations between neurodegenerative diseases and neurological tumors with biological aging: a bidirectional Mendelian randomization study. *Front. Neurosci.* 17:1321246. doi: 10.3389/fnins.2023.1321246

Assessing causal associations between neurodegenerative diseases and neurological tumors with biological aging: a bidirectional Mendelian randomization study

Zhiyun Zhang[1], Ningfang Liu[2], Xuyang Pan[1], Chuyi Zhang[1], Yifan Yang[3], Xinyun Li[4] and Ying Shao[1]*

[1]Department of Plastic and Reconstructive Surgery, The First Hospital of Jilin University, Changchun, China, [2]Department of Anesthesiology, The First Affiliated Hospital of Xiamen University, School of Medicine, Xiamen University, Xiamen, China, [3]The Second Hospital of Jilin University, Changchun, Jilin, China, [4]Infection Department, The First Bethune Hospital of Jilin University, Changchun, China

Background: Aging is a significant risk factor for many neurodegenerative diseases and neurological tumors. Previous studies indicate that the frailty index, facial aging, telomere length (TL), and epigenetic aging clock acceleration are commonly used biological aging proxy indicators. This study aims to comprehensively explore potential relationships between biological aging and neurodegenerative diseases and neurological tumors by integrating various biological aging proxy indicators, employing Mendelian randomization (MR) analysis.

Methods: Two-sample bidirectional MR analyses were conducted using genome-wide association study (GWAS) data. Summary statistics for various neurodegenerative diseases and neurological tumors, along with biological aging proxy indicators, were obtained from extensive meta-analyses of GWAS. Genetic single-nucleotide polymorphisms (SNPs) associated with the exposures were used as instrumental variables, assessing causal relationships between three neurodegenerative diseases (Alzheimer's disease, Parkinson's disease, amyotrophic lateral sclerosis), two benign neurological tumors (vestibular schwannoma and meningioma), one malignant neurological tumor (glioma), and four biological aging indicators (frailty index, facial aging, TL, and epigenetic aging clock acceleration). Sensitivity analyses were also performed.

Results: Our analysis revealed that genetically predicted longer TL reduces the risk of Alzheimer's disease but increases the risk of vestibular schwannoma and glioma (All Glioma, GBM, non-GBM). In addition, there is a suggestive causal relationship between some diseases (PD and GBM) and DNA methylation GrimAge acceleration. Causal relationships between biological aging proxy indicators and other neurodegenerative diseases and neurological tumors were not observed.

Conclusion: Building upon prior investigations into the causal relationships between telomeres and neurodegenerative diseases and neurological tumors, our study validates these findings using larger GWAS data and demonstrates, for the first time, that Parkinson's disease and GBM may promote epigenetic age acceleration. Our research provides new insights and evidence into the causal relationships between biological aging and the risk of neurodegenerative diseases and neurological tumors.

KEYWORDS

neurodegenerative diseases, neurological tumors, biological aging, bidirectional Mendelian randomization study, genome-wide association study (GWAS)

Introduction

As the global aging process continues to intensify, it is projected that the global elderly population will exceed 2 billion by 2050. Aging is associated with a variety of age-related health issues, among which the risks of neurodegenerative diseases and neurological tumors are particularly prominent, posing a significant threat to healthy life expectancy and quality of life. In older age groups, having a disease-free brain is a rare occurrence. Neurodegenerative diseases such as Alzheimer's disease (AD), Parkinson's disease (PD), and amyotrophic lateral sclerosis (ALS) are closely linked to aging, with their incidence sharply increasing with age (Hou et al., 2019). For instance, the incidence of AD almost doubles every 5 years after the age of 65, and by the ninth decade of life, approximately one in three adults meets the criteria for dementia (Alzheimer's Association, 2015). Similarly, the incidence of PD steadily rises with age on a global scale (Bloem et al., 2021). Furthermore, the prevalence of ALS peaks around the age of 80 (Mehta et al., 2018). In addition to neurodegenerative diseases, in the realm of neurological tumors, particularly glioblastoma (GBM), age has been identified as a clear risk factor for both disease onset and prognosis (Thakkar et al., 2014). The incidence of GBM sharply increases after the age of 54, reaching its peak between the ages of 74 and 85 (Ostrom et al., 2017). However, chronological age alone cannot accurately gauge the extent of biological aging or predict the risks associated with these diseases. Therefore, the assessment of an individual's biological age becomes paramount, as different individuals may exhibit variations in biological age at the same chronological age. When biological age surpasses chronological age, the body enters a state of accelerated aging, resulting in elevated disease risks and reduced quality of life (Jylhävä et al., 2017).

Over the years, researchers have been actively seeking reliable biomarkers to assess an individual's biological age (Jylhävä et al., 2017). Among these, telomere length (TL) is a well-known biological aging marker closely associated with neurodegenerative diseases and neurological tumors (Hou et al., 2019; Saunders et al., 2022). Recently, Blanca et al. successfully demonstrated a causal relationship between shortened TL and an increased risk of AD using Mendelian randomization (MR) (Rodríguez-Fernández et al., 2022a). However, the relationship between TL and other neurodegenerative diseases such as PD and ALS remains unclear. Rodríguez-Fernández and colleagues found that, apart from its association with AD, there is no causal relationship between the length of TL and the risk of other neurodegenerative diseases. Similarly, Chen and colleagues also did not find a causal relationship between TL and the onset of PD (Chen and Zhan, 2021; Rodríguez-Fernández et al., 2022b). Additionally, there is evidence indicating a significant genetic association between leukocyte TL (LTL) increase and glioma risk (Saunders et al., 2022). These findings appear contradictory to the notion that aging increases the risk of neurodegenerative diseases and neurological tumors. Furthermore, these studies have not validated the reverse causal relationship between aging and neurodegenerative diseases or neurological tumors. The true nature of the relationship between these factors remains a subject of considerable controversy. This prompts us to further investigate the intricate relationship between biological aging and the risk of neurodegenerative diseases and neurological tumors.

Therefore, this study aims to comprehensively explore the potential relationships between biological aging and neurodegenerative diseases as well as neurological tumors by integrating multiple biological age proxy indicators (Yu et al., 2020; Duan et al., 2022; Chen et al., 2023). These indicators include molecular biomarkers such as TL and DNA methylation epigenetic age acceleration and phenotypic biomarkers such as frailty index and facial visual aging. Notably, we have selected the latest generation of epigenetic clock acceleration, GrimAge Acceleration, as one of the biological age proxy indicators. Epigenetic age acceleration, where an individual's biological age exceeds their chronological age, has been associated with increased mortality and the risk of age-related diseases, including cancer (Yu et al., 2020). Furthermore, GrimAge utilizes a DNA methylation pattern at specific CpG sites to predict biological age and is considered one of the most robust methods for assessing biological age (Duan et al., 2022). Distinguishing itself from other Epigenetic Clocks, GrimAge stands out for its predictive capabilities of health outcomes and lifespan. GrimAge incorporates data from 1,030 CpGs associated with smoking pack-years and seven plasma proteins (cystatin C, leptin, tissue inhibitor of metalloproteinases 1, adrenomedullin, β-2 microglobulin, growth differentiation factor 15, and plasminogen activator inhibitor 1) (Lu et al., 2019). In various disease contexts, epigenetic age has been found to be greater than chronological age, while in long-lived populations, it tends to be lower than chronological age, providing strong evidence for the reflection of biological age by epigenetic age (Jylhävä et al., 2017; Yu et al., 2020; Tang et al., 2022). Through this multidimensional research approach, we aim to gain a deeper understanding of the relationship between biological age and the risk of neurodegenerative diseases as well as brain tumors, providing a scientific basis for future intervention strategies.

MR is an increasingly popular and effective causal inference method in recent years (Weith and Beyer, 2023). It employs genetic variation (single-nucleotide polymorphisms, SNPs) as instrumental variables (IVs) to infer causal relationships between exposures and outcomes, effectively circumventing confounding biases present in traditional epidemiological studies (Birney, 2022). MR analysis reduces confounding and reverse causality due to the segregation and independent assortment of genes passed from parents to offspring. In the absence of horizontal pleiotropy (i.e., genetic variants being independently associated with the putative exposure and the putative outcome) and population stratification, MR can provide clear estimates of disease risk (Bowden and Holmes, 2019).

In this study, we adopted a two-sample and bidirectional MR analysis aiming to assess the causal relationships between three neurodegenerative diseases (Alzheimer's disease, Parkinson's disease, amyotrophic lateral sclerosis), two benign neurological tumors

(vestibular schwannoma and meningioma), and one malignant neurological tumor (glioma) with four biological age proxies (frailty index, facial aging, TL, and epigenetic aging clock acceleration). Previous research has conducted some MR analyses on the associations between AD, PD, ALS, glioma, meningioma, and TL (Chen and Zhan, 2021; Saunders et al., 2022; Rodríguez-Fernández et al., 2022a,b; Yu et al., 2023), as well as AD and frailty index using MR analysis (Liu et al., 2022). However, some of the findings from these studies are in partial contradiction to the notion that aging is a crucial risk factor for neurodegenerative diseases and the development of neurological tumors. Notably, to date, there has been no MR causal inference analysis conducted on neurodegenerative diseases, benign and malignant neurological tumors, in relation to frailty index and epigenetic aging clock acceleration. Therefore, this study, for the first time, incorporates a variety of biological aging proxy indicators, with special attention to the epigenetic aging clock acceleration. We also employ larger sample GWAS data in the hope of ultimately elucidating the direction and magnitude of the causal relationships between biological aging and the risk of neurodegenerative diseases and neurological tumors, providing new insights and understanding to this field of research.

Methods

Data sources

Neurodegenerative disease

For the investigation of AD, we utilized recently published summary statistics data from the GWAS Catalog (Schwartzentruber et al., 2021). This comprehensive meta-analysis data pertains to a large-scale GWAS conducted on European populations, incorporating data from the UK Biobank (53,042 cases and 355,900 controls), the AD GWAS meta-analysis by Kunkle et al. (21,982 cases and 41,944 controls), the GR@ACE project (4,120 cases and 3,289 controls), and the FinnGen biobank (3,697 cases and 131,941 controls), among others. These datasets ultimately unveiled 13 risk loci (p-value $<5\times10^{-8}$), including 10 loci previously reported in studies. Genome-wide association study (GWAS) summary statistics data for PD patients were obtained from the International Parkinson's Disease Genomics Consortium,[1] encompassing 33,674 cases and 449,056 controls of European descent (Nalls et al., 2019). Large-scale European ancestry ALS GWAS summary data, including 12,577 ALS patients and 23,475 controls, were acquired from a recent study (van Rheenen et al., 2016). All patients were diagnosed by specialized neurologists following the (revised) El Escorial criteria.

Benign neurological tumor

To obtain GWAS summary statistics data for vestibular schwannoma, we retrieved data from Wouter et al., who conducted a GWAS using 911 sporadic vestibular schwannoma cases from the Type 2 Neurofibromatosis Gene Testing Service in Northwest England and 5,500 control samples from the UK Biobank resource (Sadler et al., 2023). Summary statistics data for meningioma were obtained from the UK Biobank, comprising 307 cases and 456,041 controls of European ancestry. The data were analyzed using the fastGWA-GLMM method with adjustments for relevant variables (Jiang et al., 2021).

Malignant neurological tumor

The glioma GWAS data were sourced from a recent meta-analysis of 12,488 glioma cases and 18,169 control samples of European ancestry available on the European Genome-Phenome Archive (EGA). Gliomas encompass various subtypes, some of which are defined by their malignant grade (e.g., pilocytic astrocytoma - World Health Organization [WHO] grade I, diffuse "low-grade" glioma - WHO grade II, anaplastic glioma - WHO grade III, glioblastoma multiforme [GBM] - WHO grade IV). In this study, gliomas were categorized into two subtypes: GBM ($n=6,183$) and non-GBM ($n=5,820$) (Melin et al., 2017).

Molecular aging biomarkers

We utilized the open GWAS[2] database, which is the largest repository of genetic variation to date. This database comprises a sizable population-based cohort collected by the UK Biobank between 2006 and 2010, with participants aged between 40 and 69 years. These individuals underwent comprehensive profiling through questionnaires, physical examinations, plasma biomarkers, whole-genome analyses, and other investigations. Codd et al. (2022) conducted an analysis of 489,092 peripheral blood leukocyte DNA samples obtained from the UK Biobank, reporting measurements and initial characterizations of LTL for 472,174 UK Biobank participants. The GWAS summary statistics for genetic association estimates of epigenetic age acceleration measures, specifically GrimAge, were derived from a recent meta-analysis of biological aging, encompassing 34,467 participants of European ancestry. Among the participants included in the analysis from 28 European ancestry studies, 57.3% were female. Detailed descriptions of the methods employed can be found in McCartney et al.'s publication (McCartney et al., 2021).

Phenotypic aging biomarkers

A questionnaire-based survey was conducted to investigate non-subjective perception of facial aging and explore the relationship between participants' biological age and their subjectively perceived age. A total of 8,630 participants reported appearing older than their actual age, 103,300 participants reported appearing their actual age, and 312,062 participants reported appearing younger. These observations were made by independent third parties unaware of the participants' actual ages. Participants were coded as 1 for appearing younger, 0 for appearing older, and 0.5 for appearing their actual age. Subsequently, mixed-effects linear models were employed, considering covariates such as age, gender, and study participation center, to transform perceived age (FA) into an ordered categorical variable. Log odds ratios (OR) were derived from linear scale statistical data using a Taylor expansion series, where an $OR>1$ indicates a greater chance of appearing younger (Jiang et al., 2021). The study also associated

1 https://pdgenetics.org/

2 https://gwas.mrcieu.ac.uk/

frailty index (FI) and genetic variants, sourced from a GWAS meta-analysis of 164,610 UK Biobank participants and 10,616 TwinGene participants. The frailty index is based on an accumulation of deficits model, where each individual's FI is calculated as the number of deficits they possess divided by a total of 49 possible deficits. Results revealed that the average deficit proportion for UK Biobank participants was 0.129 ± 0.075, while TwinGene participants exhibited an average deficit proportion of 0.121 ± 0.080 (Atkins et al., 2021).

MR design

We conducted a two-sample bidirectional MR study based on extensive GWAS research. Specifically, we incorporated four biological aging proxy indicators, including molecular biomarkers (such as TL and DNA methylation epigenetic age) and phenotypic biomarkers (such as frailty index and facial visual aging), to investigate the causal relationship between chronological aging and age-related neurodegenerative diseases (including AD, PD, and ALS) as well as benign and malignant neurological tumors (vestibular schwannoma, meningioma, and glioblastoma).

Reliable MR analysis requires adherence to three core assumptions: (1) genetic variants are strongly associated with the exposure factor; (2) genetic variants are independent of any potential confounding factors; (3) genetic variants are independent of the outcome and affect the outcome solely through the exposure factor. Additionally, certain other assumptions need to be met, including the absence of linear relationships and statistical interactions (Birney, 2022). Furthermore, we selected single-nucleotide polymorphism (SNP) sites that demonstrated a genome-wide significance level (p-value $<5\times10^{-8}$). However, due to the limited sample sizes in the GWAS summary statistics for meningioma and vestibular schwannoma, we relaxed the genome-wide significance levels for both to identify an adequate number of SNPs for causal relationship inference (p-value $<5\times10^{-6}$). If there is linkage disequilibrium (LD) present in the single nucleotide polymorphisms (SNPs) of the genetic instrumental variable, it could lead to misleading results. To mitigate this impact, we employed the clustering procedure within the two-sample MR package, clustering SNPs based on their LD relationships within a given genomic region. In this clustering process, we utilized a threshold of $r^2<0.001$ and a window size of 10,000 kb to identify independent SNPs. Additionally, we calculated the phenotype variance explained by the genetic instrumental variables (R^2) and the F-statistics of these variable regression analyses to assess the reliability of these genetic instrumental variable SNPs. The formulas for calculating R^2 and F-statistics are as follows: $R^2 = 2\times(1-MAF)\times MAF\times\frac{BETA}{SE\times\sqrt{N}}$ and $F=\frac{N-K-1}{K}\times\frac{R^2}{1-R^2}$, where MAF denotes the minor allele frequency for the SNP, BETA represents the magnitude of the SNP's impact on the phenotype, SE represents the standard error of the SNP's impact on the phenotype, N denotes the sample size of the GWAS, and K represents the number of SNPs selected for MR analysis after filtering. SNPs with strong instrumentation were identified as having an F-statistic > 10 (Lawlor et al., 2008).

Statistical analysis

We initiated our analysis by assessing the causality of each SNP through the application of the Wald ratio. In instances where more than one SNP could potentially be employed as an instrumental variable, we utilized the inverse variance weighted (IVW) method to conduct a meta-analysis of Wald estimates. The meta-analysis of Wald estimates for each individual SNP was computed using the IVW method in the following formulas: $\beta=\sum X_kY_k\sigma_{Y_k}^{-2}/\sum X_k^2\sigma_{Y_k}^{-2}$ with $\sigma_{MR}=\sqrt{1/\sum X_k^2\sigma_{Y_k}^{-2}}$ where X_k represents the association of SNP_k with the exposure, and Y_k corresponds to the association of SNP_k with the outcome, both accompanied by their respective standard errors. IVW is recognized as the most robust method with the highest statistical power available, although it assumes the effectiveness of all instrumental covariates and may deviate when the mean multifactor effect deviates from zero. Furthermore, we complemented our analysis with the use of MR-Egger and weighted median methods alongside IVW (Atkins et al., 2021). The weighted median method yields consistent causal estimates under the assumption that at least 50% of SNPs are effective. In cases of substantial heterogeneity, we applied a random effects model.

Furthermore, we executed MR-Egger intercept analysis (Bowden et al., 2015) and MR-PRESSO (Verbanck et al., 2018) tests to scrutinize the potential presence of horizontal pleiotropy and outlier SNPs in our study. A MR-Egger intercept value of p exceeding 0.05 signifies the absence of horizontal pleiotropic effects. In cases where we detected outliers, we reported the MR causal estimate recalculated using the MR-PRESSO method as our primary outcome; otherwise, we relied on the IVW method. To ensure the resilience of our MR analysis, we harnessed Cochran Q statistics to gauge heterogeneity among SNPs (Hemani et al., 2018). To pinpoint possibly influential SNPs, we conducted a "leave-one-out" sensitivity analysis, systematically excluding one SNP at a time and performing an IVW-random method on the remaining SNPs to assess the potential impact of outlying variants on our estimates (Supplementary Figures S1–S65). Forest and scatter plots were generated for further scrutiny of heterogeneity. To rectify the bias from multiple comparisons, we used a Benjamini–Hochberg false discovery rate (FDR). A causal relationship was concluded if the direction and estimates of the causal effects of the IVW and weighted median methods were consistent and the p value with the FDR was less than 0.05 after correction for heterogeneity and horizontal polymorphism. A $p<0.05$ but with an FDR >0.05 was interpreted as a suggestive causal relationship. Our analysis was conducted utilizing the "Two-Sample MR" and "MR-PRESSO" packages within R 4.2.3 software.

Results

The sources, sample sizes, and population information for the GWAS summary statistics data used in our study are presented in Table 1. Following the selection of instrumental variables, the number of SNPs used for two-sample bidirectional MR analyses ranged from 7 to 144, with the explained variance (R^2) ranging from 0.19 to 22.8%

TABLE 1 Data sources used in the Mendelian randomization for the current study.

Phenotype				Source	PMID	Total or cases/controls	Ancestry
Neurodegenerative diseases		Alzheimer's disease		GWAS Catalog	33,589,840	75,024/397,844	European
		Parkinson's disease		International Parkinson's Disease Genomics Consortium	31,701,892	33,674/ 449,056	European
		Amyotrophic lateral sclerosis		Project MinE	27,455,348	12,577/ 23,475	European
Benign brain tumor		Vestibular schwannomas		GWAS Catalog	36,546,557	911/5,500	European
		Meningioma		GWAS Catalog	34,737,426	307 /456,041	European
Malignant brain tumor		All-glioma		European genome-phenome archive (EGA)	28,346,443	12,488/18,169	European
		GBM				6,183/18,169	
		Non-GBM				5,820/18,169	
Biological aging proxy indicators	Molecular biomarkers	Telomere length		MRC-IEU	37,117,760	472,174	European
		Epigenetic aging clock	DNA methylation Hannum age	GWAS catalog	34,187,551	34,449	European
	Phenotypic biomarkers	Frailty index		MRC-IEU	34,431,594	175,226	European
		Facial aging		UK Biobank	31,768,069	423,999	European

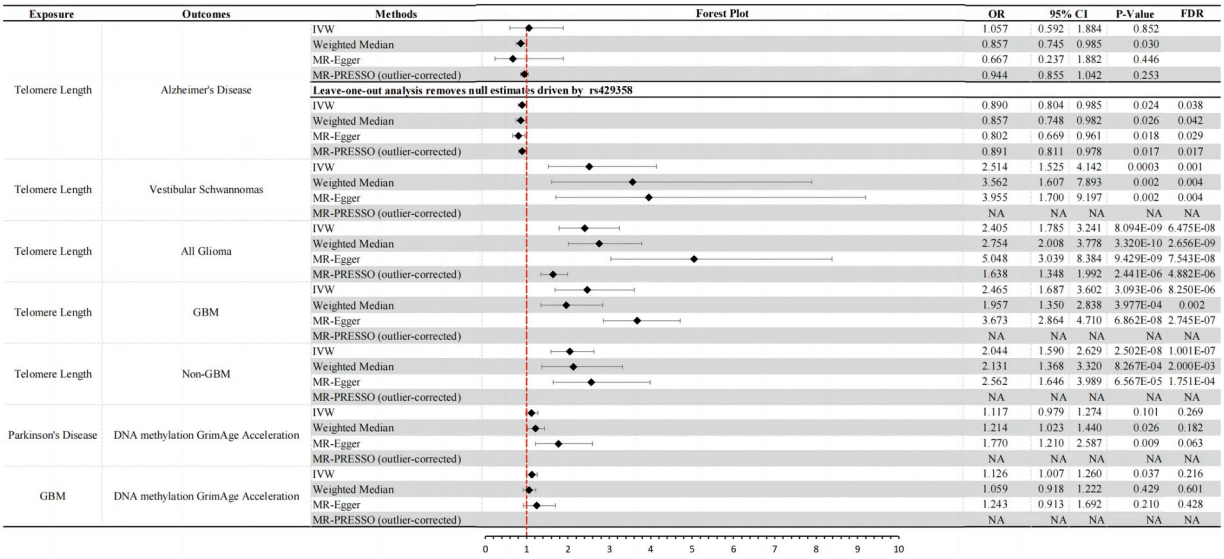

FIGURE 1
Significant results and forest plots from IVW, weighted-median, MR-Egger regression, and outlier-corrected MR-PRESSO.

(Supplementary Tables S3–S14). Additionally, after calculating the F-statistics, values ranged from 36.05 to 712.83, indicating sufficient instrument strength and mitigating the risk of weak instrument bias (F-statistics >10) (Lawlor et al., 2008).

Neurodegenerative disease

Alzheimer's disease

AD to biological aging: we did not find evidence of a causal impact of genetically predicted AD on biological aging (Supplementary Table S1).

Biological aging to AD: in reverse causal inference analysis, we excluded the ineffective genetic instrument rs429358 through leave-one-out analysis (Supplementary Figure S1A). Consistently across three MR analysis methods, genetically predicted longer TL was associated with a decreased risk of AD [IVW: OR = 0.890, 95% CI = 0.804 ~ 0.985, p-value (corrected) = 0.038; weighted median: OR = 0.857, 95% CI = 0.748 ~ 0.982, p-value (corrected) = 0.042; MR-Egger: OR = 0.802, 95% CI = 0.669 ~ 0.961, p-value (corrected) = 0.029] (Figure 1). Furthermore, we conducted tests for pleiotropy and MR-PRESSO analysis, which indicated that this result was not influenced by horizontal pleiotropy (Supplementary Tables S1, S2). Although heterogeneity tests showed

some degree of heterogeneity in the results (heterogeneity test: $p < 0.05$), it did not affect our causal inference regarding the relationship between the two (Supplementary Table S2). Additionally, our study did not find that other biological aging proxy indicators had an impact on the risk of AD (Supplementary Table S1).

Parkinson's disease

PD to biological aging: although MR analysis using the IVW method did not provide definitive evidence that an increased genetic risk for PD leads to epigenetic aging acceleration (DNA methylation GrimAge acceleration) (IVW: OR = 1.117, 95% CI = 0.979 ~ 1.274, $p = 0.101$), the other two analysis methods both indicated a causal relationship between them. All three methods consistently showed a direction of causality suggesting an increased risk (OR > 1) (weighted median: OR = 1.214, 95% CI = 1.023 ~ 1.440, $p = 0.026$; MR-Egger: OR = 1.770, 95% CI = 1.210 ~ 2.587, $p = 0.009$) (Figure 1). Importantly, MR-PRESSO analysis results indicated that this association was not influenced by horizontal pleiotropy (MR-PRESSO test: $p > 0.05$; Supplementary Table S1), and there was no apparent heterogeneity or confounding effects (heterogeneity test: $p > 0.05$; Supplementary Table S2). However, after further adjustment using Benjamini–Hochberg false discovery rate (FDR), we found that the corrected p-values were all >0.05 (Supplementary Table S1). In summary, our results suggest a suggestive causal relationship between PD and DNA methylation GrimAge acceleration. An increase in PD risk may promote DNA methylation acceleration. However, we did not find evidence that an increased risk for PD has a significant impact on other biological aging proxy indicators.

Biological aging to PD: in reverse MR analysis, we did not find that genetically predicted biological aging proxy indicators significantly affect the risk of PD (Supplementary Table S1).

Amyotrophic lateral sclerosis

There is no evidence of a causal relationship between ALS and biological aging in the current results of this study (Supplementary Table S1).

Benign neurological tumor

Vestibular schwannomas

Vestibular schwannomas to biological aging: we did not find that genetically predicted risk of vestibular schwannomas significantly affect biological aging (Supplementary Table S1).

Biological aging to vestibular schwannomas: by employing three different MR analysis methods, including IVW, Weighted Median, and MR-Egger, we consistently observed a significant positive association between genetically predicted longer TL and an increased risk of vestibular schwannoma [IVW: OR = 2.514, 95% CI = 1.525 ~ 4.412, p-value (corrected) = 0.001; weighted median: OR = 3.562, 95% CI = 1.607 ~ 7.893, p-value (corrected) = 0.004; MR-Egger: OR = 3.955, 95% CI = 1.700 ~ 9.197, p-value (corrected) = 0.004] (Figure 1). It's noteworthy that our results were further validated through MR-PRESSO and heterogeneity tests, demonstrating that this causal relationship is not influenced by horizontal pleiotropy ($P > 0.05$; Supplementary Tables S1, S2) and is not disrupted by heterogeneity confounding factors (heterogeneity test: $p > 0.05$; Supplementary Table S2). Furthermore, our study did not find any significant causal relationships between other genetically predicted biological aging proxy indicators and the risk of vestibular schwannoma (Supplementary Table S1).

Meningioma

In the current findings of this study, there is no evidence to suggest causal relationship between meningioma and biological aging (Supplementary Table S1).

Malignant neurological tumor

All glioma

All glioma to biological aging: we did not find that genetically predicted risk of glioma significantly affects biological aging (Supplementary Table S1).

Biological aging to all glioma: consistent with previous research findings (Saunders et al., 2022), we observed a positive association between genetically predicted longer TL and the risk of glioma. We employed various causal inference methods to validate this association, including IVW, Weighted Median, and MR-Egger analysis. The results of these analyses all indicate a significant causal relationship between TL and glioma risk [IVW: OR = 2.405, 95% CI = 1.785 ~ 3.241, p-value (corrected) = 6.475E-08; weighted median: OR = 3.562, 95% CI = 1.607 ~ 7.893, p-value (corrected) = 2.656E-09; MR-Egger: OR = 3.955, 95% CI = 1.700 ~ 9.197, p-value (corrected) = 7.543E-08] (Figure 1). It is worth noting that we conducted tests for horizontal pleiotropy and heterogeneity, which revealed some degree of influence on this causal inference due to pleiotropy (pleiotropy test: $p = 0.001$) and heterogeneity (heterogeneity test: $p < 0.001$; Supplementary Table S2). However, after correction using the MR-PRESSO Outlier Corrected method, the impact of horizontal pleiotropy was eliminated, and the results still demonstrated a significant causal relationship between TL and glioma risk [MR-PRESSO (outlier-corrected): OR = 1.638, 95% CI = 1.348 ~ 1.992, p-value (corrected) = 4.882E-06] (Figure 1). Other biological aging proxy indicators with All Glioma yielded negative results (Supplementary Table S1).

GBM

GBM to biological aging: we found that there is a suggestive casual relationship between increased risk of GBM and epigenetic age acceleration (DNA methylation GrimAge acceleration) (IVW: OR = 1.126, 95% CI = 1.007 ~ 1.260, p-value = 0.037, p-value (corrected) = 0.216). The other two MR analysis methods yielded consistent causal effect directions with IVW (Figure 1), and they were not affected by horizontal pleiotropy (pleiotropy test: $p > 0.05$) and heterogeneity (heterogeneity test: $p > 0.05$; Supplementary Table S2).

Biological aging to GBM: similar to the results observed in All Glioma, we also found a significant causal relationship between genetically predicted TL and the risk of GBM (glioblastoma) [IVW: OR = 2.465, 95% CI = 1.687 ~ 3.602, p-value (corrected) = 8.250E-06; weighted median: OR = 1.957, 95% CI = 1.350 ~ 2.838, p-value (corrected) = 0.002; MR-Egger: OR = 3.673, 95% CI = 2.864 ~ 4.710, p-value (corrected) = 2.745E-07] (Figure 1). Similarly, we conducted tests for horizontal pleiotropy and heterogeneity, which indicated some heterogeneity interference with the current causal inference (heterogeneity test: $p < 0.05$), but no influence from horizontal pleiotropy (Supplementary Table S2). MR-PRESSO results also confirmed the absence of horizontal pleiotropy impact (Figure 1). Apart from these two findings above, bidirectional MR analysis results

of other biological aging proxy indicators with GBM were negative (Supplementary Table S1).

Non-GBM

Non-GBM to biological aging: we did not find that genetically predicted risk of Non-GBM significantly affects biological aging (Supplementary Table S1).

Biological aging to non-GBM: longer telomeres also increase the risk of Non-GBM (non-Glioblastoma) [IVW: OR = 2.044, 95% CI = 1.590 ~ 2.629, *p*-value (corrected) = 1.001E-07; Weighted Median: OR = 2.131, 95% CI = 1.368 ~ 3.320, *p*-value (corrected) = 2.000E-03; MR-Egger: OR = 2.562, 95% CI = 1.646 ~ 3.989, *p*-value (corrected) = 1.751E-04] (Figure 1). It is worth noting that we conducted tests for horizontal pleiotropy and heterogeneity, and the results indicated that this causal relationship inference was influenced by heterogeneity (heterogeneity test: $p < 0.001$) but not affected by horizontal pleiotropy (Supplementary Table S2). Bidirectional MR analysis results of other biological aging proxy indicators with Non-GBM were negative (Supplementary Table S1).

Discussion

In this bidirectional MR study examining the association between biological aging and neurodegenerative diseases and neurological tumors, we found that TL influences the risk of AD, Vestibular Schwannoma, All Glioma, GBM, and Non-GBM. Notably, telomere shortening, typically considered a hallmark of biological aging, was only found to increase the risk of AD while reducing the risk of the latter four conditions. It is worth mentioning that we observed there is a suggestive causal relationship between some diseases (PD and GBM) and DNA methylation GrimAge acceleration, suggesting that these two diseases might, to some extent, accelerate biological aging. Ultimately, for the two key characteristics of biological aging, namely frailty index and facial aging, we did not find any evidence of a positive or negative causal relationship with the neurodegenerative diseases and neurological tumors considered in this study.

Our MR estimates regarding the causal inference between TL and the risk of AD align with the findings of Blanca et al.'s MR study (Rodríguez-Fernández et al., 2022b). Utilizing a larger sample size from GWAS studies for MR analysis, we corroborated that shorter telomeres are associated with an increased risk of AD, further underscoring the significance of TL in AD pathology. Surprisingly, aside from TL, other physiological aging proxy measures, including frailty index, facial aging, and DNA methylation GrimAge acceleration, did not exhibit causal associations with the risk of AD. This outcome prompts significant discussions and reflections. Firstly, it is essential to recognize that different physiological aging proxy measures may reflect aging processes at various biological levels. TL is commonly regarded as a cellular-level marker of aging, and its shortening may be linked to biological processes such as decreased cellular function, increased inflammation, and apoptosis, which might play crucial roles in the pathogenesis of AD (Rodríguez-Fernández et al., 2022a). Conversely, phenotypic measures like the frailty index and facial aging are more likely to reflect the overall decline in physical health and function, influenced by multiple factors, including lifestyle, nutrition, environment, and genetics (Atkins et al., 2021). Thus, while these indicators play crucial roles in the overall manifestation of aging, their direct causal relationship with AD might be weaker or more complex. Secondly, DNA methylation GrimAge acceleration, as an epigenetic aging clock, has been closely associated with overall mortality and age-related health conditions (Duan et al., 2022). However, its causal relationship with the risk of AD remains inconclusive. Some studies suggest there is currently no evidence of an association between epigenetic aging and dementia/mild cognitive impairment, while others provide evidence of an association, particularly concerning GrimAge acceleration (Zhou et al., 2022).

In prior research, TL has similarly been demonstrated to have no causal association with other neurodegenerative diseases (PD and ALS) (Rodríguez-Fernández et al., 2022b). Furthermore, although frailty index and facial aging are both important proxies of physiological aging, and frailty may impact the clinical presentation and progression of neurodegenerative diseases, the relationship between these factors and PD remains unclear in most current studies. Only a few studies have found that PD patients may be more prone to frailty or that frailty is associated with motor and non-motor features of PD (Belvisi et al., 2022; Borda et al., 2022). There is almost no research on the relationship between frailty index and ALS, with only a few studies focusing on the frailty status of ALS patients (Larson and Wilbur, 2020). In addition to the findings mentioned above, it is noteworthy that we have, for the first time, discovered that PD may accelerate DNA methylation GrimAge. Previous research has predominantly focused on understanding how aging impacts PD, with some studies illustrating a connection between DNAm-age acceleration and the age of PD onset (Tang et al., 2022). However, there has been limited investigation into the influence of PD on DNAm age (Salvioli et al., 2023). A case–control analysis revealed that PD patients exhibit a higher DNAm age based on different epigenetic clocks (Horvath and Ritz, 2015; Paul et al., 2021). Some of these associations are also correlated with a more rapid decline in cognitive abilities and the progression of motor symptoms in patients (Paul et al., 2021). Nevertheless, another longitudinal study of PD patients did not observe such a correlation (Tang et al., 2022). Due to the constraints of traditional observational studies and ethical considerations in clinical research, exploring the impact of neurodegenerative diseases on aging has been nearly impractical. We employed the MR method, marking the first instance, to demonstrate that PD may contribute to the acceleration of GrimAge.

In exploring the causal associations between physiological aging proxies and benign neurological tumors, we have, for the first time, employed MR analysis to reveal that genetically predicted longer TL is associated with an elevated risk of vestibular schwannoma. Furthermore, our results have been validated through sensitivity analyses, including tests for heterogeneity and horizontal pleiotropy, confirming the robustness of our findings. To the best of our knowledge, no prior studies have investigated the relationship between TL and vestibular schwannoma. However, it should be noted that the GWAS study sample size for vestibular schwannoma used in our analysis is relatively small, and we plan to validate our results in the future using larger GWAS summary statistics datasets. Additionally, we did not find any causal relationship between physiological aging and benign neurological tumors (vestibular schwannoma and meningioma).

Finally, our results are consistent with previous MR studies, confirming that genetically predicted longer TL is associated with an increased risk of glioma (All-Glioma, GBM, Non-GBM) (Saunders

et al., 2022). Additionally, for the first time, we utilized MR analysis to confirm that an elevated genetic risk of GBM is associated with accelerated DNA methylation GrimAge. Although a prior study by Liao et al. demonstrated that epigenetic age is generally accelerated in glioma patients and is an important independent predictor of survival, they did not establish a causal relationship between the two (Liao et al., 2018). In our analysis, we not only used GWAS summary statistics for glioma with the largest available sample size, but we also examined the causal relationship between glioma subtypes (All-Glioma, GBM, non-GBM) and DNA methylation GrimAge acceleration separately. Ultimately, our findings clarify that GBM, the most malignant subtype of glioma, promotes epigenetic aging.

In this study, various neurodegenerative and neurological tumor diseases included are typically found to be more prevalent in the elderly population. However, whether this association is truly linked to aging remains largely unclear (Thakkar et al., 2014; Alzheimer's Association, 2015; Mehta et al., 2018; Hou et al., 2019; Bloem et al., 2021). MR methods have a strong capacity for uncovering potential causal relationships, and in this study, we utilized the bidirectional two-sample MR approach along with a larger sample size of GWAS data to unveil causal relationships among PD, glioblastoma multiforme (GBM), epigenetic aging, and TL for the first time, laying a theoretical foundation for further research on the relationship between aging and neurodegenerative diseases and neurological tumors. However, there are some limitations in this study that should be noted, including the absence of gender or age stratification in the GWAS data and the lack of genetic data, as we were restricted to using whole-genome association data from individuals of European ancestry. In addition, the GWAS meta-analysis sample size for meningiomas and vestibular schwannomas is limited. We relaxed the genome-wide significance thresholds for both to identify a sufficient number of SNPs for causal inference (p-value $<5\times10^{-6}$). This adjustment may, to some extent, impact the inference of causal relationships. Ideally, our future objective is to expand the scope of analysis, including as many diverse populations as possible, and to further analyze using larger GWAS datasets.

Data availability statement

The original contributions presented in the study are included in the article/Supplementary material, further inquiries can be directed to the corresponding author.

Author contributions

ZZ: Conceptualization, Data curation, Formal analysis, Investigation, Methodology, Project administration, Software, Supervision, Validation, Visualization, Writing – original draft, Writing – review & editing. NL: Writing – review & editing, Data curation, Methodology, Validation, Investigation. XP: Data curation, Supervision, Validation, Visualization, Writing – review & editing. CZ: Investigation, Methodology, Software, Writing – review & editing. YY: Investigation, Software, Writing – review & editing. XL: Writing - review & editing, Data curation, Investigation. YS: Conceptualization, Data curation, Investigation, Project administration, Software, Supervision, Writing – original draft, Writing – review & editing.

Funding

The author(s) declare that no financial support was received for the research, authorship, and/or publication of this article.

Conflict of interest

The authors declare that the research was conducted in the absence of any commercial or financial relationships that could be construed as a potential conflict of interest.

Publisher's note

Supplementary material

The Supplementary material for this article can be found online at: https://www.frontiersin.org/articles/10.3389/fnins.2023.1321246/full#supplementary-material

References

Alzheimer's Association (2015). Alzheimer's disease facts and figures. *Alzheimers Dement.* 11, 332–384. doi: 10.1016/j.jalz.2015.02.003

Atkins, J. L., Jylhävä, J., Pedersen, N. L., Magnusson, P. K., Lu, Y., Wang, Y., et al. (2021). A genome-wide association study of the frailty index highlights brain pathways in ageing. *Aging Cell* 20:e13459. doi: 10.1111/acel.13459

Belvisi, D., Canevelli, M., Costanzo, M., Giangrosso, M., Fabbrini, A., Borraccino, A., et al. (2022). The role of frailty in Parkinson's disease: a cross-sectional study. *J. Neurol.* 269, 3006–3014. doi: 10.1007/s00415-021-10873-3

Birney, E. (2022). Mendelian randomization. *Cold Spring Harb. Perspect. Med.* 12:a041302. doi: 10.1101/cshperspect.a041302

Bloem, B. R., Okun, M. S., and Klein, C. (2021). Parkinson's disease. *Lancet* 397, 2284–2303. doi: 10.1016/S0140-6736(21)00218-X

Borda, M. G., Pérez-Zepeda, M. U., Jaramillo-Jimenez, A., Chaudhuri, K. R., Tovar-Rios, D. A., Wallace, L., et al. (2022). Frailty in Parkinson's disease and its association with early dementia: a longitudinal study. *Parkinsonism Relat. Disord.* 99, 51–57. doi: 10.1016/j.parkreldis.2022.05.004

Bowden, J., Davey Smith, G., and Burgess, S. (2015). Mendelian randomization with invalid instruments: effect estimation and bias detection through egger regression. *Int. J. Epidemiol.* 44, 512–525. doi: 10.1093/ije/dyv080

Bowden, J., and Holmes, M. V. (2019). Meta-analysis and Mendelian randomization: a review. *Res. Synth. Methods* 10, 486–496. doi: 10.1002/jrsm.1346

Chen, Z., Chen, Z., and Jin, X. (2023). Mendelian randomization supports causality between overweight status and accelerated aging. *Aging Cell* 22:e13899. doi: 10.1111/acel.13899

Chen, R., and Zhan, Y. (2021). Association between telomere length and Parkinson's disease: a Mendelian randomization study. *Neurobiol. Aging* 97, 144.e9–144.e11. doi: 10.1016/j.neurobiolaging.2020.07.019

Codd, V., Denniff, M., Swinfield, C., Warner, S. C., Papakonstantinou, M., Sheth, S., et al. (2022). Measurement and initial characterization of leukocyte telomere length in

474,074 participants in UK Biobank. *Nat Aging* 2, 170–179. doi: 10.1038/s43587-021-00166-9

Duan, R., Fu, Q., Sun, Y., and Li, Q. (2022). Epigenetic clock: a promising biomarker and practical tool in aging. *Ageing Res. Rev.* 81:101743. doi: 10.1016/j.arr.2022.101743

Hemani, G., Zheng, J., Elsworth, B., Wade, K. H., Haberland, V., Baird, D., et al. (2018). The MR-base platform supports systematic causal inference across the human phenome. *elife* 7:7. doi: 10.7554/eLife.34408

Horvath, S., and Ritz, B. R. (2015). Increased epigenetic age and granulocyte counts in the blood of Parkinson's disease patients. *Aging* 7, 1130–1142. doi: 10.18632/aging.100859

Hou, Y., Dan, X., Babbar, M., Wei, Y., Hasselbalch, S. G., Croteau, D. L., et al. (2019). Ageing as a risk factor for neurodegenerative disease. *Nat. Rev. Neurol.* 15, 565–581. doi: 10.1038/s41582-019-0244-7

Jiang, L., Zheng, Z., Fang, H., and Yang, J. (2021). A generalized linear mixed model association tool for biobank-scale data. *Nat. Genet.* 53, 1616–1621. doi: 10.1038/s41588-021-00954-4

Jylhävä, J., Pedersen, N. L., and Hägg, S. (2017). Biological age predictors. *EBioMedicine* 21, 29–36. doi: 10.1016/j.ebiom.2017.03.046

Larson, S. T., and Wilbur, J. (2020). Muscle weakness in adults: evaluation and differential diagnosis. *Am. Fam. Physician* 101, 95–108.

Lawlor, D. A., Harbord, R. M., Sterne, J. A. C., Timpson, N., and Davey, S. G. (2008). Mendelian randomization: using genes as instruments for making causal inferences in epidemiology. *Stat. Med.* 27, 1133–1163. doi: 10.1002/sim.3034

Liao, P., Ostrom, Q. T., Stetson, L., and Barnholtz-Sloan, J. S. (2018). Models of epigenetic age capture patterns of DNA methylation in glioma associated with molecular subtype, survival, and recurrence. *Neuro-Oncology* 20, 942–953. doi: 10.1093/neuonc/noy003

Liu, W., Zhang, L., Fang, H., Gao, Y., Liu, K., Li, S., et al. (2022). Genetically predicted frailty index and risk of stroke and Alzheimer's disease. *Eur. J. Neurol.* 29, 1913–1921. doi: 10.1111/ene.15332

Lu, A. T., Quach, A., Wilson, J. G., Reiner, A. P., Aviv, A., Raj, K., et al. (2019). DNA methylation GrimAge strongly predicts lifespan and healthspan. *Aging* 11, 303–327. doi: 10.18632/aging.101684

McCartney, D. L., Min, J. L., Richmond, R. C., Lu, A. T., Sobczyk, M. K., Davies, G., et al. (2021). Genome-wide association studies identify 137 genetic loci for DNA methylation biomarkers of aging. *Genome Biol.* 22:194. doi: 10.1186/s13059-021-02398-9

Mehta, P., Raymond, J., Zhang, Y., Punjani, R., Han, M., Larson, T., et al. (2018). Prevalence of amyotrophic lateral sclerosis in the United States. *Amyotroph Lateral Scler Frontotemporal Degener.* 2023, 1–3. doi: 10.1080/21678421.2023.2264922

Melin, B. S., Barnholtz-Sloan, J. S., Wrensch, M. R., Johansen, C., Il'yasova, D., Kinnersley, B., et al. (2017). Genome-wide association study of glioma subtypes identifies specific differences in genetic susceptibility to glioblastoma and non-glioblastoma tumors. *Nat. Genet.* 49, 789–794. doi: 10.1038/ng.3823

Nalls, M. A., Blauwendraat, C., Vallerga, C. L., Heilbron, K., Bandres-Ciga, S., Chang, D., et al. (2019). Identification of novel risk loci, causal insights, and heritable risk for Parkinson's disease: a meta-analysis of genome-wide association studies. *Lancet Neurol.* 18, 1091–1102. doi: 10.1016/S1474-4422(19)30320-5

Ostrom, Q. T., Gittleman, H., Liao, P., Vecchione-Koval, T., Wolinsky, Y., Kruchko, C., et al. (2017). CBTRUS statistical report: primary brain and other central nervous system tumors diagnosed in the United States in 2010-2014. *Neuro-Oncology* 19, v1–v88. doi: 10.1093/neuonc/nox158

Paul, K. C., Binder, A. M., Horvath, S., Kusters, C., Yan, Q., Rosario, I. D., et al. (2021). Accelerated hematopoietic mitotic aging measured by DNA methylation, blood cell lineage, and Parkinson's disease. *BMC Genomics* 22:696. doi: 10.1186/s12864-021-08009-y

Rodríguez-Fernández, B., Gispert, J. D., Guigo, R., Navarro, A., Vilor-Tejedor, N., and Crous-Bou, M. (2022b). Genetically predicted telomere length and its relationship with neurodegenerative diseases and life expectancy. *Comput. Struct. Biotechnol. J.* 20, 4251–4256. doi: 10.1016/j.csbj.2022.08.006

Rodríguez-Fernández, B., Vilor-Tejedor, N., Arenaza-Urquijo, E. M., Sánchez-Benavides, G., Suárez-Calvet, M., Operto, G., et al. (2022a). Genetically predicted telomere length and Alzheimer's disease endophenotypes: a Mendelian randomization study. *Alzheimers Res. Ther.* 14:167. doi: 10.1186/s13195-022-01101-9

Sadler, K. V., Bowes, J., Rowlands, C. F., Perez-Becerril, C., van der Meer, C. M., King, A. T., et al. (2023). Genome-wide association analysis identifies a susceptibility locus for sporadic vestibular schwannoma at 9p21. *Brain* 146, 2861–2868. doi: 10.1093/brain/awac478

Salvioli, S., Basile, M. S., Bencivenga, L., Carrino, S., Conte, M., Damanti, S., et al. (2023). Biomarkers of aging in frailty and age-associated disorders: state of the art and future perspective. *Ageing Res. Rev.* 91:102044. doi: 10.1016/j.arr.2023.102044

Saunders, C. N., Kinnersley, B., Culliford, R., Cornish, A. J., Law, P. J., and Houlston, R. S. (2022). Relationship between genetically determined telomere length and glioma risk. *Neuro-Oncology* 24, 171–181. doi: 10.1093/neuonc/noab208

Schwartzentruber, J., Cooper, S., Liu, J. Z., Barrio-Hernandez, I., Bello, E., Kumasaka, N., et al. (2021). Genome-wide meta-analysis, fine-mapping and integrative prioritization implicate new Alzheimer's disease risk genes. *Nat. Genet.* 53, 392–402. doi: 10.1038/s41588-020-00776-w

Tang, X., Gonzalez-Latapi, P., Marras, C., Visanji, N. P., Yang, W., Sato, C., et al. (2022). Epigenetic clock acceleration is linked to age at onset of Parkinson's disease. *Mov. Disord.* 37, 1831–1840. doi: 10.1002/mds.29157

Thakkar, J. P., Dolecek, T. A., Horbinski, C., Ostrom, Q. T., Lightner, D. D., Barnholtz-Sloan, J. S., et al. (2014). Epidemiologic and molecular prognostic review of glioblastoma. *Cancer Epidemiol. Biomark. Prev.* 23, 1985–1996. doi: 10.1158/1055-9965.EPI-14-0275

van Rheenen, W., Shatunov, A., Dekker, A. M., McLaughlin, R. L., Diekstra, F. P., Pulit, S. L., et al. (2016). Genome-wide association analyses identify new risk variants and the genetic architecture of amyotrophic lateral sclerosis. *Nat. Genet.* 48, 1043–1048. doi: 10.1038/ng.3622

Verbanck, M., Chen, C.-Y., Neale, B., and Do, R. (2018). Detection of widespread horizontal pleiotropy in causal relationships inferred from Mendelian randomization between complex traits and diseases. *Nat. Genet.* 50, 693–698. doi: 10.1038/s41588-018-0099-7

Weith, M., and Beyer, A. (2023). The next step in Mendelian randomization. *elife* 12:e86416. doi: 10.7554/eLife.86416

Yu, M., Hazelton, W. D., Luebeck, G. E., and Grady, W. M. (2020). Epigenetic aging: more than just a clock when it comes to Cancer. *Cancer Res.* 80, 367–374. doi: 10.1158/0008-5472.CAN-19-0924

Yu, W., Mei, Y., Lu, Z., Zhou, L., Jia, F., Chen, S., et al. (2023). The causal relationship between genetically determined telomere length and meningiomas risk. *Front. Neurol.* 14:1178404. doi: 10.3389/fneur.2023.1178404

Zhou, A., Wu, Z., Zaw Phyo, A. Z., Torres, D., Vishwanath, S., and Ryan, J. (2022). Epigenetic aging as a biomarker of dementia and related outcomes: a systematic review. *Epigenomics.* 14, 1125–1138. doi: 10.2217/epi-2022-0209

frontiers | Frontiers in Oncology

TYPE Case Report
PUBLISHED 12 March 2024
DOI 10.3389/fonc.2024.1264926

OPEN ACCESS

EDITED BY
Peichen Pan,
Zhejiang University, China

REVIEWED BY
Parackrama Karunathilake,
Anuradhapura Teaching Hospital, Sri Lanka
Lei Wen,
Southern Medical University, China

*CORRESPONDENCE
Yihua Sun
600611@hrbmu.edu.cn

RECEIVED 21 July 2023
ACCEPTED 19 February 2024
PUBLISHED 12 March 2024

CITATION
Guo T, Liu Z, Chen Y, Cheng Y, He K, Lin X, Wang M and Sun Y (2024) Hemophagocytic lymphohistiocytosis during treatment of intracranial multifocal germinoma: a case report and literature review.
Front. Oncol. 14:1264926.
doi: 10.3389/fonc.2024.1264926

Hemophagocytic lymphohistiocytosis during treatment of intracranial multifocal germinoma: a case report and literature review

Ting Guo[1], Zichun Liu[1], Yixin Chen[2], Yangyang Cheng[2], Kaitong He[2], Xin Lin[2], Mingzhu Wang[2] and Yihua Sun[2]*

[1]Department of Clinical Laboratory, Fengcheng Hospital of Fengxian District, Shanghai, China, [2]Department of Clinical Laboratory, Harbin Medical University Cancer Hospital, Harbin, China

Hemophagocytic lymphohistiocytosis (HLH), also known as hemophagocytic syndrome (HPS), is a benign histiocytosis with hyperreactive proliferation of the mononuclear phagocyte system caused by immune function abnormalities, which often occurs under the background of genetic mutations, inflammation, infection or tumors. Because the research on malignancy-associated HLH (M-HLH) is focused on hematological malignancies, reports on HLH secondary to solid tumors are rare. In this case, we report a 14-year-old girl who developed HLH during treatment for intracranial multifocal germinoma, and the disease was controlled after hormone combined with etoposide(VP-16) and other related treatments. To our knowledge, there have been no documented cases of HLH caused by intracranial multifocal germinoma.

KEYWORDS

hemophagocytic lymphohistiocytosis, hemophagocytic syndrome, malignancy, intracranial multifocal germinoma, case report

Introduction

Hemophagocytic lymphohistiocytosis (HLH) is a severe and even life-threatening syndrome of excessive inflammatory response due to impaired activity of cytotoxic T lymphocytes and natural killer cells (1). It is characterized by unregulated activation and proliferation of macrophages in all reticuloendothelial organs (e.g., bone marrow, spleen, liver, and lymph nodes), leading to a persistent cytokine storm and histiocytosis, with clinical symptoms such as persistent fever, pancytopenia, and hepatosplenomegaly, and rapid progression to disseminated intravascular coagulation and multiple organ failure (2). HLH can be divided into Primary HLH(P-HLH) and Secondary HLH(S-HLH). P-HLH mainly occurs in children aged 0-2 years with poor prognosis,which is autosomal or sex

chromosome recessive genetic disease (2). However, S-HLH usually occurs in adults without genetic factors, which often induced by infection, malignancy, hematopoietic stem cell transplantation, autoimmune diseases, immunodeficiency diseases, and drug hypersensitivity reactions. The number of reports on Malignancy associated hemophagocytic syndrome(M-HLH) has been increasing year by year. However, the current known studies of M-HLH are still focused on hematological malignancies, such as lymphoma, acute leukemia, myelodysplastic syndrome, etc., while S-HLH in malignant solid tumors is rarely mentioned.

Here, we give a report of a secondary HLH case in a 14-year-old girl during her treatment of intracranial multifocal germinoma. The patient developed severe intracranial infection after craniotomy. During her chemoradiotherapy, there were pancytopenia, transient liver injury, persistent fever, exfoliative dermatitis, and bone marrow hemophagocytosis, etc. But the final prognosis was good after early diagnosis and early therapy. According to the onset time of HLH in this case, it is suggested that tumor cell destruction induced by chemoradiotherapy drugs and secondary infection after immunosuppression may be the trigger factors of HLH. At the same time, we review the relevant literatures on malignant tumor-associated hemophagocytic syndrome and give the report of this case.

Case description

A 14-year-old girl came to Harbin Medical University Cancer Hospital due to intermittent headache for 10 days without obvious incentive on December 28, 2020. On admission, she denied special life history, family history of previous diseases or genetic diseases and any accompany symptoms of nausea, vomiting, dizziness. She had stable vital signs, dysplasia, and not yet menarche. The height of the patient was 150cm, the weight was 29kg, and the BMI was only 12.89kg/m^2. The rest of the patient's medical and neurological examinations showed no abnormalities. Imaging examination (December 24, 2020): Head enhanced Magnetic Resonance Imaging (MRI) (Figure 1) showed irregular nodular shadows in the intracranial pineal region, septum pellucidum, lateral ventricle and suprasellar cistern, the larger one was about 16 ×16 mm in size, and the lesion grew cast along the ventricular wall; the bilateral ventricle and third ventricle revealed hydrops; the septum pellucidum showed dilatation. Due to the multiple periventricular masses in this patient, ependymoma was considered as a possibility, and germ cell tumor could not be ruled out. Electrocardiogram, chest CT and echocardiography displayed no abnormalities. Serological tests: sodium 153 mmol/L (reference range:137 ~ 147 mmol/L), chlorine 112 mmol/L (99 ~ 110 mmol/L), high-density lipoprotein cholesterol1.83 mmol/L (1.04 ~ 1.74 mmol/L), homocysteine 27.5 ummol/L (1.5 ~ 15 ummol/L), prolactin 97.73 ng/ml (female: 5.18-29.53 ng/ml), alpha-fetoprotein 2.16 ng/ml (0-7 ng/ml), carcinoembryonic antigen 1.29 ng/ml (0-5 ng/ml), human chorionic gonadotropin β subunit 0.69 mIU/ml (0-5 mIU/ml); Other laboratory parameters [three infectious disease antibodies (human immunodeficiency virus, hepatitis C virus, treponema pallidum), five hepatitis B, and coagulation function] were in the normal range. Urine routine: urine specific gravity 1.003 (1.015-1.025). Cerebrospinal fluid (CSF) examination: lateral decubitus pressure 180 mmH_2O, colorless and transparent, protein (+), white blood cell count 10 × 10^6/L, monocyte percentage 4.9%, lymphocytes 90.2%, AFP < 0.61 ng/ml (reference range:0-7 ng/ml), β-HCG 15 mIU/ml (0-5 mIU/ml), and no atypical cells on cytology. On January 4, 2021, the patient underwent craniotomy with tumor resection near the intercompartment hole area of the septum pellucidum, posterior part of the third ventricle, and quadrigeminal region, as well as third subventricular fistula. Postoperative pathological immunohistochemical markers (Figure 2): SALL4 (+), CD117 (+), OCT4 (+), D2-40 (+), CD30, GFAP, S-100, Syn, LCA, AFP and CYP-3 were all negative, and Ki67 labeling index was about 80%, which was diagnosed as germinoma. MRI of the whole spine showed that the physiological curvature of the patient's cervical spine was straightened, and there was no abnormality in the rest. After surgery, the patient was given etoposide combined with carboplatin regimen chemotherapy for 1 cycle, during which she developed bone marrow suppression, severe intracranial infection and transient liver injury (ALT: 166U/L, AST: 422U/L, LDH: 4575U/L). After a series of symptomatic treatments, the patient 's condition was improved and underwent sequential IMRT radiotherapy in February 2021. Combined with image-guided techniques, irradiation was performed for the whole brain spinal cord and tumor bed to complete the whole spinal cord DT: 1600 cGy/10f, whole brain DT: 3600 cGy/20f, and tumor bed area boost DT: 1400 cGy/7f. During radiotherapy, the patient developed grade IV bone marrow suppression, which had reached the indication of blood transfusion, and the patient's hemogram recovered after multiple treatments of leukocyte-elevating platelets and blood transfusion. Then the patient could not tolerate whole brain and spinal cord radiotherapy, so the plan was changed to continue radiotherapy for the whole brain and tumor bed area.

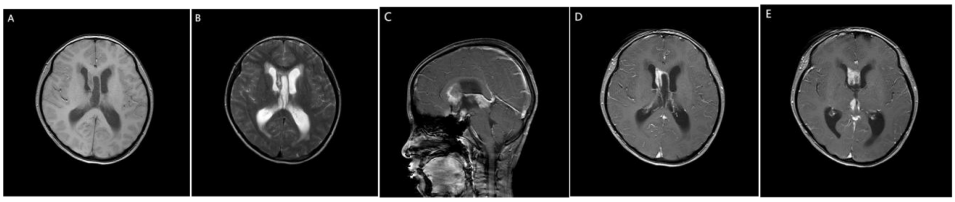

FIGURE 1
MRI of the patient's brain. **(A)** Slightly hypo signal on T1WI. **(B)** Slightly higher signal intensity on T2WI. **(C)** sagittal view. **(D, E)** On enhanced scan, the nodules were significantly enhanced, and the lesions grew along the ventricular wall casting.

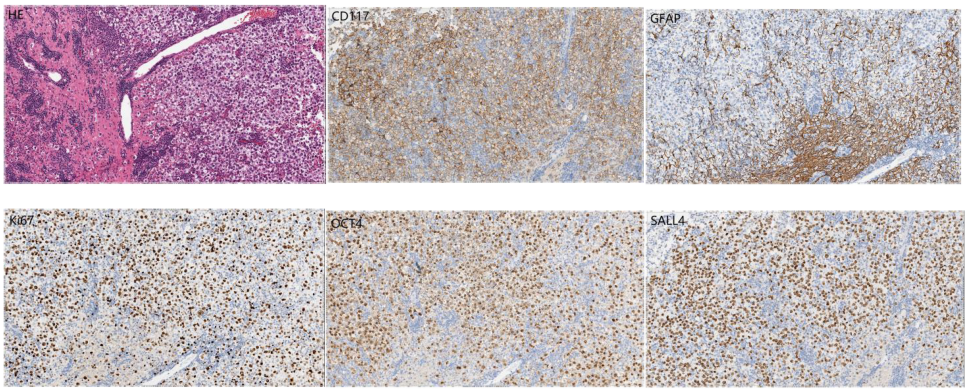

FIGURE 2
Postoperative pathological images of the tumor ×200.

The patient was readmitted on 21 May 2021 with pancytopenia. Laboratory tests: pancytopenia (white blood cell (WBC)2.12 × 10^9/L, red blood cell count(RBC) 2.69 × 10^{12}/L, hemoglobin (HB)89 g/L, platelet count(PLT) 20 × 10^9/L); ion disturbance (potassium 3.1 mmol/L, sodium 184 mmol/L, chlorine 144 mmol/L, magnesium 1.26 mmol/L); mild liver dysfunction (lactate dehydrogenase 322 U/L), decreased serum total protein 63.7 g/L, urine routine white blood cell 20.9/ul, normal coagulation, and no tumor metastasis or recurrence on brain MRI. The patient's peripheral blood was extremely reduced, which was considered to be related to bone marrow suppression after chemoradiotherapy, and bone marrow invasion was not excluded. The patient was given WBC-elevating needle, transfusion of leukocyte-depleted platelets and suspended red blood cells. On May 25, the platelet increased to 91 × 10^9/L and bone marrow aspiration was performed immediately to determine whether there was bone marrow infiltration. Bone marrow aspiration (Figure 3): grade III myelodysplasia, a few cells of multiple lineage abnormal development, easy to see hemophagocytic cells. We highly suspected that the patient had secondary hemophagocytic syndrome and immediately performed relevant tests: ferritin 351.8 ng/ml on May 27. According to experience, we immediately gave the patient intravenous dexamethasone (10 mg/d × 13 days) combined with etoposide (50 mg/d × 3 days) regimen, and transfused red blood cells and leukocyte-depleted platelets, subcutaneous thrombopoietin and granulocyte colony-stimulating factor and other supportive treatment, closely monitored the hemogram and timely adjusted the treatment regimen. On June 2, the patient had persistent fever up to 38.4deg;C, perfected relevant infection tests (G test, blood culture, sputum and urine bacterial culture were negative, procalcitonin 0.681 ng/ml), and was given intravenous meropenem (1.5 g/d × 14 d) and fluconazole (100 ml/d × 13 d) for anti-infective treatment. On June 17, blood routine (WBC 7.96 × 10^9/L, RBC 2.68 × 10^{12}/L, Hb 85 g/L, Plt 86 × 10^9/L) and ions (potassium 3.4 mmol/L, sodium 166 mmol/L, chloride 127 mmol/L) were reexamined, and the patient strongly requested to be discharged. Within the following 6 months, the patient was admitted several times due to pancytopenia, and hemophilic cells was still observed in the bone marrow three times successively. Fortunately, intravenous VP16 (50 mg/d × 3 days) combined with steroids (10 mg/d × 3 days) kept the patient 's condition under good control. During this time, the patient presented with subcutaneous bleeding, coagulation abnormalities (fibrinogen 4.88g/L, elevated D-dimer 1.11mg/L), keratolysis exfoliative of both hands, and persistent hypersodium, hyperchloride, and hypokalemia. At the time of discharge from hospital on January 23, 2022 to the last follow-up on August 30, 2022, the patient was in good condition and had not received any further treatment.

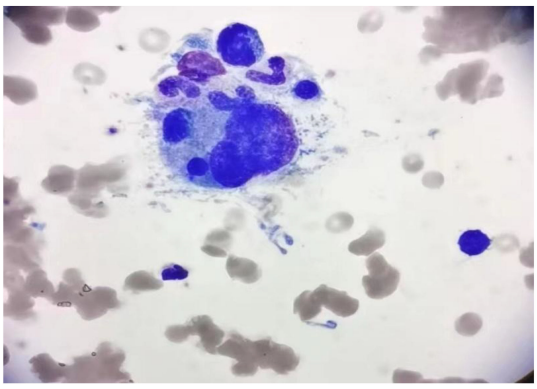

FIGURE 3
Bone marrow aspirate smear showed the evidence of hemophagocytosis; original magnification ×1000.

Discussion

Intracranial germ cell tumors (GCTs) are rare malignant brain tumors derived from primitive embryonic cell, accounting for 1% to 2% of primary intracranial tumors in North America and Europe, while Asians have a higher incidence compared with Westerners (3). GCTs is more common in children and young adults, with a male to female ratio of approximately 2:1, which often appears in the form of solitary nodules or multiple lesions[3]. Different histological types of GCTs often occur on midline structures of

the central nervous system, particularly in the pineal gland (48%) and suprasellar (neurohypophysis) region (37%). GCTs away from the midline, such as the basal ganglia, thalamus, cerebellar vermis, ventricular system, and optic chiasm, may be caused by the migration of ectopic germ cell from the midline during ventricular development, but no studies have yet revealed its etiology (3, 4). Germinomas are the most common type of GCTs, with about 10% of GCTs presenting as bifocal tumors (involving both the pineal gland and neurohypophyseal region), and multifocality is even rarer (5). No studies have clearly demonstrated whether this phenomenon is caused by tumor metastasis along the cerebrospinal fluid or synchronous tumor growth. American scholars believed that it is metastatic disease, but it was considered to be a localized disease in Europe (6). When germinoma is disseminated and metastasized in the ventricular system, it usually presents as nodular abnormally enhanced lesions along the ependyma, which should be differentiated from ependymoma (7). In this case, no dysmorphic cells were observed in preoperative cerebrospinal fluid liquid-based smear, and imaging examination could not confirm the diagnosis so surgical treatment was adopted. In addition, as for the pathogenesis of germinoma, some studies have shown from the molecular biological level that primary intracranial multifocal germinoma has multiple chromosome imbalances, and almost all of them have manifested hypomethylation and active X chromosomes, which indicates that the occurrence of Intracranial multifocal germ cell tumors (IMGCTs) is related to chromosomal changes (8). In this case, due to the patient's young age and multiple lesions, even if no abnormal cells were found in the cerebrospinal fluid, we were unable to completely rule out metastasis. For long-term prognosis considerations, we initially administered craniospinal radiation therapy. However, for the entire spinal cord, we only used low-dose prophylactic radiation (1600cGy/10f). When the patient later found it difficult to tolerate craniospinal radiation and developed IV degree bone marrow suppression, we changed the plan to only continue irradiation for the entire brain and tumor bed.

The various clinical manifestations of germinoma are related to the size, the site, and the invasion extent of the tumor. Tumors located in the pineal region often block the midbrain corpora quadrigemina and cause hydrocephalus due to tumor protruding to the back of the third ventricle or invading the tetras downward, thus leading to headache, vomiting and other symptoms of elevated intracranial pressure, which can also be manifested as binocular hyperopia (Parinaud syndrome) (9). Germinoma in sellar region or suprasellar region is often accompanied by diabetes insipidus, precocious puberty or delay, hypothyroidism, growth hormone deficiency, adrenal insufficiency and other endocrine disorders, which may invade optic chiasma and cause vision loss or visual field defect (10). In this case, the patient was admitted with intermittent headache as the first symptom, without obvious symptoms of polyuria and polydipsia. Examination showed a decreased urine proportion, accompanied by hypernatremia and abnormal neuroendocrine hormones. Oral DDAVP was effective, hence central diabetes insipidus was considered. The tumor invaded the anterior inferior wall of the third ventricle of the patient, damaging the vascular endplate in the anterior hypothalamus, namely the osmotic pressure receptor in the AV3V region and the thirst center. The supraoptic nucleus was damaged and the hypothalamic-pituitary axis was destroyed, resulting in reduced vasopressin secretion and increased PRL secretion. Meanwhile, the repeated existence of low potassium, high Na and high K during the course of the disease is also related to the treatment of cranial pressure reduction by dehydration. In addition, the patient presented with intermittent headache as the first symptom, which may be caused by hydrocephalus or GCT in the septum pellucidum. Besides connecting two cerebral hemispheres, the pellucidum has no other clear function. Studies have shown that tumors here often take the symptoms and signs of headache and epilepsy as the first symptom (11). At present, there are only individual reports on septum pellucidum germ cell tumor, which needs further exploration.

Hemophagocytic lymphohistiocytosis (HLH) is a rare and serious inflammatory disorder characterized by excessive activation of immune cells, resulting in impaired pathogen clearance, sustained activation of the immune system, and massive production of cytokines (interleukin (IL) -1-β, IL-2, IL-6, IL-10, IL-18, and tumor necrosis factor (TNF), etc.) (12). Depending on the trigger, HLH can be classified as primary or hereditary and secondary. Primary or hereditary HLH is characterized by a number of different genetically heterogeneous diseases caused by mutations in high-permeability genes that affect cytolytic function, lymphocyte survival, or inflammasome activation, including familial HLH (pathogenic alterations in PRF1, UNC13D, STXBP2, and STX11 lead to severe impairment of NK and CD8+ cell cytotoxic function), certain dyschromic immunodeficiency diseases (RAB27A, LYST, AP3B1 mutations resulting in degranulation disorders, such as Griscelli syndrome type II and Chediak-Higashi syndrome), X-linked lymphoproliferative disorders (SH2D1A and XIAP gene defects), and other diseases such as NLRC4, CDC42, and eb virus susceptibility (12–14). Secondary HLH does not have any obvious genetic tendency of HLH, and is often induced by infection, malignant tumor, and autoimmune diseases. Interestingly, HLHs in different disease contexts have different terminologies. It is commonly called macrophage activation syndrome (MAS) when it occurs in the context of rheumatic or autoinflammatory diseases, and cytokine release syndrome is commonly caused by bispecific T-cell engager (BiTE) or chimeric antigen receptor (CAR) therapy (14, 15). Infection-associated HLH is common with DNA viruses (Epstein-Barr virus, cytomegalovirus, and adenovirus) and intracellular pathogens (leishmaniasis), and there have been reports of HLH caused by brucellosis and COVID-19 infection, as well as cases of HLH caused by COVID-19 vaccination (16–19). M-HLH is common in hematologic tumors, such as T-cell or NK-cell lymphomas or leukemias, followed by B-cell lymphomas, and HLH caused by solid tumors is rare (20). There have been numerous previous reports on M-HLH, such as gastric cancer (21), glioblastoma (22), prostate cancer (23), and pembrolizumab in the treatment of head and neck squamous cell carcinoma to induce HLH (24). Here we report a case of intracranial germinoma causing HLH.

Malignancy plays a pathogenic role in approximately 50% of adult HLH. HLH may emerge as a consequence of malignancy, occurring before or during cancer therapy and can complicate malignancy in 1% of adults with very high mortality (25). At present, the pathological mechanism of M-HLH is still unclear, and inflammation, as a hallmark of cancer, may play an important role (26). M-HLH is considered to be associated with sustained antigenic stimulation of tumor cells and secretion of large amounts of cytokines, causing excessive inflammatory responses (27, 28). It's worth noting that chemotherapy-associated HLH(Ch-HLH) occurs well during cancer treatment, including induction, consolidation, and maintenance phases, and is associated with secondary infections caused by immunosuppression caused by chemotherapy (27, 29). Because of the low incidence of M-HLH and the substantial overlap between HLH and tumor characteristics, it makes it challenging to identify HLH in the context of malignancy. The widely adopted pediatric HLH-2004 guideline has strict diagnostic criteria, including positive gene/mutation detection, or in the absence of genetic testing, at least 5 of 8 clinical laboratory tests can confirm the diagnosis (see Table 1 for details) (30). However, HLH-2004 guidelines have limited diagnosis in adult HLH, and the HLH probability score (H-score, Table 2) [http://saintantoine.aphp.fr/score/] can assist in the diagnosis of HLH] (31, 32). Furthermore, the study have shown that HLH-2004 criteria (meeting at least five items) has 91% sensitivity and 93% specificity for predicting HLH, while H-score cut-off value ≥ 169 has 96% sensitivity and 71% specificity for HLH diagnosis (33). Some scholars have also proposed that HLH that cannot be diagnosed but has supportive features including elevated liver transaminases, bilirubin, lactate dehydrogenase (LDH), and D-dimer, while most HLH with seizures as the main clinical manifestation have cerebrospinal fluid leukocytosis and peripheral blood mononucleosis (2). HLH should be highly suspected when patients present with pancytopenia, elevated ferritin, hepatosplenomegaly, and hemophagocytosis in bone marrow or lymph nodes (34). In this patient, the whole blood cells decreased during postoperative chemoradiotherapy for intracranial germinoma, accompanied by persistent fever, elevated ferritin, easy to see hemophagocytosis in bone marrow aspiration and other manifestations, so the occurrence of HLH was rapidly highly suspected. Given the rapid progression of HLH, we can be sure that the patient had HLH even if the test results at that time met only 3 of the 8 diagnostic criteria of HLH-2004 (see Table 1). The effectiveness of the subsequent VP-16 combination steroid regimen for HLH and the presence of hemophagocytes in three bone marrow aspirates for three consecutive months also confirmed the accuracy of this diagnosis. Unfortunately, the detailed examination of HLH was not perfect due to the patient 's family economy, and serum ferritin, plasma fibrinogen, and fasting triglycerides, which were slightly changed at the initial stage of HLH, were not continuously monitored subsequently. During chemoradiotherapy, the patient developed recurrent pancytopenia, while bone marrow aspiration showed no tumor infiltration, which reflected the destruction of tumor cells by chemoradiotherapy and the inhibition of bone marrow hematopoiesis. It is worth thinking that the tumor burden is relatively small due to tumor resection,

TABLE 1 Diagnostic criteria for HLH.

HLH-2004 Diagnostic criteria[3] (Patients need to be greater than or equal to five of the eight diagnostic criteria)	Patient's early symptoms and laboratory findings
Fever (Temperature>38.5°C for>7 day)	*
Splenomegaly /hepatomegaly/ lymphadenopathy	–
Cytopenia (affecting≥2 lineages in peripheral blood)	* (Hemoglobin 89g/l Platelets 16×10^9/l Neutrophil 1.06×10^9/l)
Hypertriglyceridemia (>3 mmol/1) and/or hypofibrinogenemia (<1.5g/l)	Triglyceride 1.17 mmol/l Fibrinogen2.55 g/l
Hemophagocytosis (in bone marrow or spleen or liver or lymph node or other tissues)	* (Hemophagocytosis in bone marrow)
Hyperferritinemia (>500μg/l)	351.8 ng/ml
Elevated soluble CD25 (>2400 U/ml)	–
Reduced or absent NK cytotoxicity	–
Supportive evidence	
Elevated transaminases and bilirubin	* (transient)
Elevated lactate dehydrogenase	*
Elevated d-dimers	*
Elevated cerebrospinal fluid cells and/or protein	*

Diagnostic criteria for HLH (-:Untested experimental items for patients, *: The patient met this diagnostic criteria).

TABLE 2 HScore (probability score) in diagnosis of HLH.

HScore (probability score) in diagnosis of HLH[4].	
Judge item	Scoring criteria
Known underlying immunodepression	0 (N) or 18(Y)
Maximal Temperature(°C)	0 (< 38.4), 33 (38.4–39.4), or 49 (> 39.4)
Hepatomegaly/ Splenomegaly	0 (N), 23 (either), or 38 (both)
Reduction level of Hemoglobin/ Leucocytes/ Platelets count	0 (1 lineage), 24 (2 lineages), or 34 (3 lineages)
Higher Ferritin level (ng/ml)	0 (< 2000), 35 (2000–6000), or 50 (> 6000)
Higher Triglyceride level (mmol/l)	0 (< 1.5), 44 (1.5–4), or 64 (> 4)
Lower Fibrinogen level (g/l)	0 (>2.5), or 30 (≤2.5)
Higher serum glutamate oxaloacetate transferase (SGOT) level (UI/L)	0 (<30), or 19 (≥30)
Hemophagocytosis features on bone marrow aspirate	0 (N) or 35 (Y)

N, (No); Y, (Yes).

and based on the time of onset of HLH, we highly suspect that HLH is caused by secondary infection due to chemoradiotherapy-induced IV bone marrow hematopoietic suppression and immunosuppression. However, the influence of surgical stress and the modulation of cytokines by the primary lesion cannot be completely ruled out. Although infection caused by immunosuppression was considered to cause HLH, the relevant laboratory tests failed to find microbiological evidence. The patient's condition improved after initial treatment with meropenem combined with fluconazole to cover gram-negative and fungal conditions, suggesting that the infected microorganism was not common, but direct evidence could not be obtained. For GCTs with malignant cell burden, HLH should be considered as a serious adverse event during chemoradiotherapy. Unfortunately, there have been no reports and studies on HLH associated with intracranial germinoma. It has not been confirmed whether it is germinoma itself, or activated immune cells responding to tumor antigens or infection. Even which kind of cell is the main cells that releases cytokines leading to high inflammatory response is a mystery.

HLH has diverse clinical manifestations and high mortality, and early diagnosis and treatment are essential. Current treatment goals for HLH are to measure disease severity while taking prompt control of inflammation and addressing any identified triggers based on the underlying etiology or trigger (35). P-HLH is usually treated with steroids and chemotherapy to suppress the systemic immune system, and cure can only be achieved by allogeneic hematopoietic stem cell transplantation (HSCT) (36). MAS was treated with high-dose intravenous corticosteroids (CS) and targeted IL-1 blockade. It is inconclusive whether M-HLH therapy is mainly to inhibit cytokine storm or to treat tumors, or both, and specific analysis is required according to the patient 's clinical condition. In the active stage of HLH, especially in patients with organ dysfunction, standard chemotherapy regimens for malignant tumors do not improve disease status at this time, but may increase mortality (37). For patients with M-HLH, dexamethasone/etoposide based HLH-94 regimen/HLH-2004 or DEP regimen is recommended before tumor-specific treatment (30, 38). If the central nervous system is involved, dexamethasone is preferred to better cross the blood-brain barrier, or in combination with methotrexate (39). In this case, dexamethasone combined with etoposide (VP16) was used to control HLH, which was effective and the patient's condition was significantly controlled. Currently, there is no recognized salvage therapy for refractory HLH, in addition to HLH-94 regimen, and currently effective tentative treatment regimens include the combined use of JAK1/2 inhibitor lusoritinib (40), monoclonal anti-CD52 antibody alemtuzumab (41), neutralizing antibody against INFγ epavatinib (42), and plasma exchange (43). However, the exact location of these regimens in the treatment of HLH remains to be determined.

In summary, we report a case of HLH following surgical, chemoradiotherapy for intracranial multifocal germinoma. Early diagnosis and treatment of HLH significantly inhibited the dramatic deterioration of the disease. In the future, further studies are needed to clarify the pathogenesis of HLH in cancer patients. Simultaneously, it is imperative to find appropriate treatment options for refractory HLH.

Data availability statement

The datasets presented in this article are not readily available because requests to access the datasets should be directed to Ting Guo,guot202206@163.com.

Ethics statement

The studies involving humans were approved by the ethics committee of the Harbin Medical University Cancer Hospital (Harbin, China). The studies were conducted in accordance with the local legislation and institutional requirements. Written informed consent for participation was not required from the participants or the participants' legal guardians/next of kin in accordance with the national legislation and institutional requirements. Written informed consent was obtained from the individual(s), and minor(s)' legal guardian/next of kin, for the publication of any potentially identifiable images or data included in this article.

Author contributions

SYH designed the study. GT gathered the clinical information and drafted the manuscript. LZC, CYX, CYY, and HKT confirm the authenticity of all raw data. LX and WMZ revised the manuscript. All authors contributed to the article and approved the submitted version.

Funding

The author(s) declare that no financial support was received for the research, authorship, and/or publication of this article.

Acknowledgments

We thank the pathologists, technicians, clinicians, nurses, and administrative employers who have provided support for the study.

Conflict of interest

The authors declare that the research was conducted in the absence of any commercial or financial relationships that could be construed as a potential conflict of interest.

Publisher's note

References

1. Birndt S, Schenk T, Heinevetter B, Brunkhorst FM, Maschmeyer G, Rothmann F, et al. Hemophagocytic lymphohistiocytosis in adults: collaborative analysis of 137 cases of a nationwide German registry. *J Cancer Res Clin Oncol*. (2020) 146:1065–77. doi: 10.1007/s00432-020-03139-4

2. Sarangi R, Pathak M, Padhi S, Mahapatra S. Ferritin in hemophagocytic lymphohistiocytosis (HLH): current concepts and controversies. *Clin Chim Acta*. (2020) 510:408–15. doi: 10.1016/j.cca.2020.07.053

3. Ostrom QT, Cioffi G, Gittleman H, Patil N, Waite K, Kruchko C, et al. CBTRUS statistical report: primary brain and other central nervous system tumors diagnosed in the United States in 2012-2016. *Neuro Oncol*. (2019) 21:v1–v100. doi: 10.1093/neuonc/noz150

4. Caro-Osorio E, Alcazar-Felix RJ, Martinez HR, Figueroa-Sanchez JA, Herrera-Castro JC, Barbosa-Quintana A. Ectopic germinoma in the corpus callosum with severe restrictive anorexia: case report and review of literature. *World Neurosurg*. (2019) 124:256–8. doi: 10.1016/j.wneu.2019.01.026

5. Schneider DT, Zahn S, Sievers S, Alemazkour K, Reifenberger G, Wiestler OD, et al. Molecular genetic analysis of central nervous system germ cell tumors with comparative genomic hybridization. *Mod Pathol*. (2006) 19:864–73. doi: 10.1038/modpathol.3800607

6. Rogers SJ, Mosleh-Shirazi MA, Saran FH. Radiotherapy of localised intracranial germinoma: time to sever historical ties? *Lancet Oncol*. (2005) 6:509–19. doi: 10.1016/S1470-2045(05)70245-X

7. Yang P, Li L, Kuang W, Li B, Zhou B, Yang J, et al. Intracranial multiple germ cell tumors: a case report and review of literature. *Int J Clin Exp Pathol*. (2014) 7:9002–7.

8. Thakkar JP, Chew L, Villano JL. Primary CNS germ cell tumors: current epidemiology and update on treatment. *Med Oncol*. (2013) 30:496. doi: 10.1007/s12032-013-0496-9

9. Kabashi S, Ahmetgjekaj I, Harizi E, Hyseni F, Kola E, Vokshi V, et al. Mixed germ cell tumor of the pineal gland in a pediatric patient. *Radiol Case Rep*. (2022) 17:2940–5. doi: 10.1016/j.radcr.2022.05.024

10. Crawford JR, Santi MR, Vezina G, Myseros JS, Keating RF, LaFond DA, et al. CNS germ cell tumor (CNSGCT) of childhood: presentation and delayed diagnosis. *Neurology*. (2007) 68:1668–73. doi: 10.1212/01.wnl.0000261908.36803.ac

11. Ghani Zghair MA. Corpus callosum disorders and associated malformations in paediatric epilepsy: MRI analytic study. *J Pak Med Assoc*. (2021) 71:S190.

12. Carter SJ, Tattersall RS, Ramanan AV. Macrophage activation syndrome in adults: recent advances in pathophysiology, diagnosis and treatment. *Rheumatol (Oxford)*. (2019) 58:5–17. doi: 10.1093/rheumatology/key006

13. Griffin G, Shenoi S, Hughes GC. Hemophagocytic lymphohistiocytosis: An update on pathogenesis, diagnosis, and therapy. *Best Pract Res Clin Rheumatol*. (2020) 34:101515. doi: 10.1016/j.berh.2020.101515

14. Canna SW, Marsh RA. Pediatric hemophagocytic lymphohistiocytosis. *Blood*. (2020) 135:1332–43. doi: 10.1182/blood.2019000936

15. Hines MR, Keenan C, Maron Alfaro G, Cheng C, Zhou Y, Sharma A, et al. Hemophagocytic lymphohistiocytosis-like toxicity (carHLH) after CD19-specific CAR T-cell therapy. *Br J Haematol*. (2021) 194:701–7. doi: 10.1111/bjh.17662

16. Retamozo S, Brito-Zerón P, Sisó-Almirall A, Flores-Chávez A, Soto-Cárdenas MJ, Ramos-Casals M. Haemophagocytic syndrome and COVID-19. *Clin Rheumatol*. (2021) 40:1233–44. doi: 10.1007/s10067-020-05569-4

17. Wiseman D, Lin J, Routy JP, Samoukovic G. Haemophagocytic lymphohistiocytosis in an adult with postacute COVID-19 syndrome. *BMJ Case Rep*. (2021) 14:e245031. doi: 10.1136/bcr-2021-245031

18. Al Noumani J, Al Busaidi I, Al Hajri M. Brucellosis-induced hemophagocytic lymphohistiocytosis. *Cureus*. (2021) 13:e15677. doi: 10.7759/cureus.15677

19. Tang LV, Hu Y. Hemophagocytic lymphohistiocytosis after COVID-19 vaccination. *J Hematol Oncol*. (2021) 14:87. doi: 10.1186/s13045-021-01100-7

20. Al-Samkari H, Berliner N. Hemophagocytic lymphohistiocytosis. *Annu Rev Pathol*. (2018) 13:27–49. doi: 10.1146/annurev-pathol-020117-043625

21. Zhou YS, Cui YC, Yin MJ, Xie QW, Shen ZL, Shi HX, et al. Gastric cancer complicated with hemophagocytic lymphohistiocytosis: case report and a brief review. *J Gastrointest Oncol*. (2021) 12:892–9. doi: 10.21037/jgo-20-432

22. Kumar V, Eulitt PJ, Bermudez A, Khagi S. Hemophagocytic lymphohistiocytosis in a patient with glioblastoma: a case report. *CNS Oncol*. (2019) 8:CNS45. doi: 10.2217/cns-2019-0013

23. Rajapakse P, Shrestha SD, Bakirhan K. Hemophagocytic lymphohistiocytosis secondary to prostatic adenocarcinoma. *Cureus*. (2021) 13:e12798. doi: 10.7759/cureus.12798

24. Kalmuk J, Puchalla J, Feng G, Giri A, Kaczmar J. Pembrolizumab-induced Hemophagocytic Lymphohistiocytosis: an immunotherapeutic challenge. *Cancers Head Neck*. (2020) 5:3. doi: 10.1186/s41199-020-0050-3

25. Daver N, McClain K, Allen CE, Parikh SA, Otrock Z, Rojas-Hernandez C, et al. A consensus review on Malignancy-associated hemophagocytic lymphohistiocytosis in adults. *Cancer*. (2017) 123:3229–40. doi: 10.1002/cncr.30826

26. Diakos CI, Charles KA, McMillan DC, Clarke SJ. Cancer-related inflammation and treatment effectiveness. *Lancet Oncol*. (2014) 15:e493–503. doi: 10.1016/S1470-2045(14)70263-3

27. La Rosée P, Horne A, Hines M, von Bahr Greenwood T, Machowicz R, Berliner N, et al. Recommendations for the management of hemophagocytic lymphohistiocytosis in adults. *Blood*. (2019) 133:2465–77. doi: 10.1182/blood.2018894618

28. Vick EJ, Patel K, Prouet P, Martin MG. Proliferation through activation: hemophagocytic lymphohistiocytosis in hematologic Malignancy. *Blood Adv*. (2017) 1:779–91. doi: 10.1182/bloodadvances.2017005561

29. Wang H, Xiong L, Tang W, Zhou Y, Li F. A systematic review of Malignancy-associated hemophagocytic lymphohistiocytosis that needs more attentions. *Oncotarget*. (2017) 8:59977–85. doi: 10.18632/oncotarget.19230

30. Henter JI, Horne A, Aricó M, Egeler RM, Filipovich AH, Imashuku S, et al. HLH-2004: Diagnostic and therapeutic guidelines for hemophagocytic lymphohistiocytosis. *Pediatr Blood Cancer*. (2007) 48:124–31. doi: 10.1002/pbc.21039

31. Fardet L, Galicier L, Lambotte O, Marzac C, Aumont C, Chahwan D, et al. Development and validation of the HScore, a score for the diagnosis of reactive hemophagocytic syndrome. *Arthritis Rheumatol*. (2014) 66:2613–20. doi: 10.1002/art.38690

32. Debaugnies F, Mahadeb B, Ferster A, Meuleman N, Rozen L, Demulder A, et al. Performances of the H-score for diagnosis of hemophagocytic lymphohistiocytosis in adult and pediatric patients. *Am J Clin Pathol*. (2016) 145:862–70. doi: 10.1093/ajcp/aqw076

33. Bilston L, Croden J, Taparia M, Karkhaneh M, Grossman J, Sun HL. Validation of the HScore and the HLH-2004 diagnostic criteria for the diagnosis of hemophagocytic lymphohistiocytosis in a multicenter cohort. *Eur J Haematol*. (2022) 109:129–37. doi: 10.1111/ejh.13779

34. Martínez-Romera I, Villa M, Areal P, Rodrigo E, Herrero B, López-Ibor B. Hemophagocytic lymphohistiocytosis: A dangerous intruder in pediatric acute lymphoblastic leukemia. *J Pediatr Hematol Oncol*. (2018) 40:e108–10. doi: 10.1097/MPH.0000000000000932

35. Yasin S, Schulert GS. Systemic juvenile idiopathic arthritis and macrophage activation syndrome: update on pathogenesis and treatment. *Curr Opin Rheumatol*. (2018) 30:514–20. doi: 10.1097/BOR.0000000000000526

36. Nepesov S, Yaman Y, Elli M, Bayram N, Özdilli K, Kıykım A, et al. Clinical, genetic, and outcome characteristics of pediatric patients with primary hemophagocytic lymphohistiocytosis. *Turk Arch Pediatr*. (2022) 57:398–405. doi: 10.5152/TurkArchPediatr.2022.21314

37. Lehmberg K, Nichols KE, Henter JI, Girschikofsky M, Greenwood T, Jordan M, et al. Consensus recommendations for the diagnosis and management of hemophagocytic lymphohistiocytosis associated with Malignancies. *Haematologica*. (2015) 100:997–1004. doi: 10.3324/haematol.2015.123562

38. Henter JI, Aricò M, Egeler RM, Elinder G, Favara BE, Filipovich AH, et al. HLH-94: a treatment protocol for hemophagocytic lymphohistiocytosis. HLH study Group of the Histiocyte Society. *Med Pediatr Oncol*. (1997) 28:342–7. doi: 10.1002/(sici)1096-911x(199705)28:5<342::aid-mpo3>3.0.co;2-h

39. Horne A, Wickström R, Jordan MB, Yeh EA, Naqvi A, Henter JI, et al. How to treat involvement of the central nervous system in hemophagocytic lymphohistiocytosis? *Curr Treat Options Neurol*. (2017) 19:3. doi: 10.1007/s11940-017-0439-4

40. Wang H, Gu J, Liang X, Mao X, Wang Z, Huang W. Low dose ruxolitinib plus HLH-94 protocol: A potential choice for secondary HLH. *Semin Hematol*. (2020) 57:26–30. doi: 10.1053/j.seminhematol.2018.07.006

41. Wegehaupt O, Wustrau K, Lehmberg K, Ehl S. Cell versus cytokine - directed therapies for hemophagocytic lymphohistiocytosis (HLH) in inborn errors of immunity. *Front Immunol*. (2020) 11:808. doi: 10.3389/fimmu.2020.00808

42. Burn TN, Weaver L, Rood JE, Chu N, Bodansky A, Kreiger PA, et al. Genetic deficiency of interferon-γ Reveals interferon-γ-independent manifestations of murine hemophagocytic lymphohistiocytosis. *Arthritis Rheumatol*. (2020) 72:335–47. doi: 10.1002/art.41076

43. Nusshag C, Morath C, Zeier M, Weigand MA, Merle U, Brenner T. Hemophagocytic lymphohistiocytosis in an adult kidney transplant recipient successfully treated by plasmapheresis: A case report and review of the literature. *Med (Baltimore)*. (2017) 96:e9283. doi: 10.1097/MD.0000000000009283

Frontiers in Neuroscience

Provides a holistic understanding of brain function from genes to behavior

Part of the most cited neuroscience journal series which explores the brain - from the new eras of causation and anatomical neurosciences to neuroeconomics and neuroenergetics.

Discover the latest Research Topics

See more →

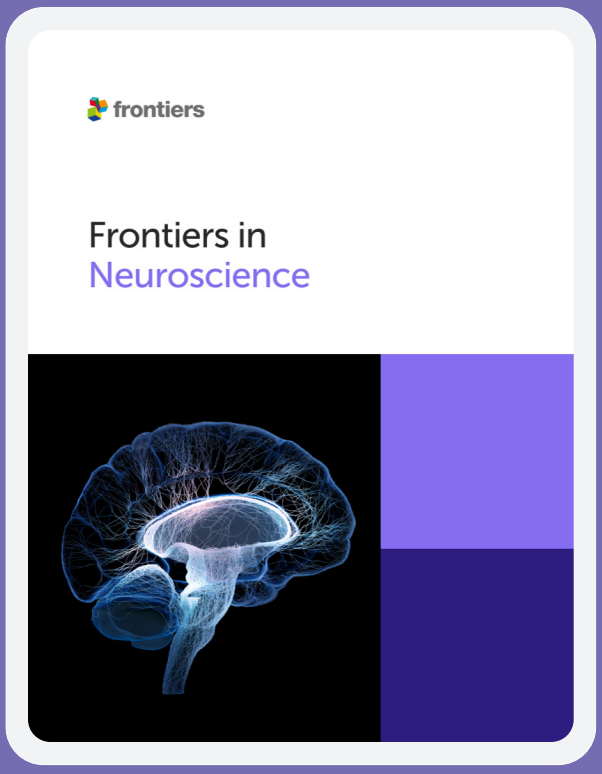

Frontiers

Avenue du Tribunal-Fédéral 34
1005 Lausanne, Switzerland
frontiersin.org

Contact us

+41 (0)21 510 17 00
frontiersin.org/about/contact